

CONFIDENTIAL – Property of GSK – Do Not Copy

University of Strathclyde
Department of Pure and Applied Chemistry

Design and Synthesis of Dimethylisoxazole Quinolines as BET Inhibitors

Thesis submitted to the University of Strathclyde in fulfilment of the
requirements for the degree of Doctor of Philosophy

Christopher Roland Wellaway



Declaration of Copyright

This thesis is the result of the author's original research. It has been composed by the author and has not been previously submitted for examination which has led to the award of a degree.

The copyright of this thesis belongs to the author under the terms of the United Kingdom Copyright Acts as qualified by University of Strathclyde Regulation 3.50. Due acknowledgement must always be made of the use of any material contained in, or derived from, this thesis.

Signed:

Date:

Acknowledgments

Foremost, I would like to thank my academic supervisor, Professor William Kerr. His impact on my overall development as a chemist has been immense, especially regarding my ability to direct science. Also, my approach to science and problem solving has become more rigorous as a result of his supervision. I also thank Professor Kerr for his huge impact on my written communication. His meticulous review of my interim reports, and subsequent advice, has highlighted the attention-to-detail required by skilled chemists and the importance of thorough consideration and clear communication of scientific strategy. The skills he has bestowed upon me have been invaluable in my ability to draft a journal manuscript. Finally, I wish to thank Professor Kerr for his generosity with his time and for providing me with this fantastic opportunity by setting up collaborative PhD programme.

Next, I wish to thank my industrial supervisor, Robert Watson. I am particularly grateful for his scientific guidance, synthetic and technical advice, generous supply of intermediates, proof-reading and for his understanding and advice during challenging stages of these studies.

I am indebted to Harry Kelly for his personal support as well as his overarching role as the programme coordinator and providing the opportunity to carry out these studies. I wish to thank the administrative and support staff at both the University of Strathclyde and GlaxoSmithKline for their assistance in various aspects of this programme.

I would especially like to recognise my line managers over the years I have participated on the PhD programme. Specifically, Mark Bamford, Gordon Bruton, Duncan Holmes and Jerry Siu for their sponsorship at the outset, Nigel Parr, Jason Witherington, Kevin Lee, Rab Prinjha and Vipul Patel for backing throughout the remainder of my studies. I am also most grateful for the support received from senior managers Dave Allen and Patrick Vallance. In particular, I wish to thank Matthew Lindon for his continued understanding and support, and for providing me with exciting scientific opportunities.

Fellow team members have also played an important role in over the years by facilitating my scientific creativity and engaging in helpful scientific discussion. In addition, I wish to also express my gratitude to Dominique Amans and Dr. Allan Watson for their helpful advice and encouragement, and to Richard Horan for providing tuition. Also, I am indebted to David Hirst for his tremendous proof-reading of my reports and thesis, and Dr. Allan Watson for review of my 18 month report.

I warmly acknowledge the many people who have provided research assistance in my studies. Specifically, James Woolven and Paul Bamborough for additional computational

support related to my studies, Chun-wa Chung for her persistence in solving key crystal structures and assisting with figures, Pete Soden for his time and patience in answering my biology questions and conducting cell proliferation experiments, Pete Craggs for biochemistry instruction, Laurie Gordon and Davina Angell for assistance in producing figures, Steve Richards and Sean Lynn for their significant NMR assistance, Shenaz Bunally for physicochemical property profiling, David Dixon for SPR discussion, Eric Hortense for conducting chiral HPLC analysis, David Hemming and Abigail Lucas for laboratory assistance, and DiscoverX Corporation for *BROMOscan* data.

I want to acknowledge the valuable contribution of friends and family who have been at my side throughout my studies. In particular, my beloved and now departed canine friend, Ollie, who provided company and comfort during many late nights. I want to thank my wife Natalie, for her unwavering support, advice, and most of all, for providing a sympathetic ear. Also, thank you to my young daughter Katie, who provided motivation and, through her dependable sleep regime, facilitated the writing of this thesis in a timely manner.

Abstract

Gene regulation is governed by the assembly of protein complexes capable of reading post-translational modifications (PTMs) on chromatin. Bromodomains read acetyl-lysine PTMs on histone tails and are important determinants of epigenetic memory. Dysregulation of epigenetic processes has been shown to contribute to human disease and inhibitors of bromodomains, in particular, represent an emerging class of potential treatments and investigational tools. This thesis describes the research completed towards the design and synthesis of inhibitors of Bromodomain Extraterminal (BET) proteins, a family of bromodomain-containing proteins characterised by their tandem bromodomain modules.

In the first section, compounds from a series of dimethylisoxazole quinoline BET inhibitors were investigated for their potential as *intravenous*-administered drug pre-candidates. A detailed account of improving compound solubility and efforts to overcome a human ether-a-go-go related gene (hERG) developability issue is provided. Building on results gathered in the early stage of this research, a pyridine ring was used to lower lipophilicity compared to a phenyl ring and, in the case of an *N*-methylpiperazine substituted aryl ring, this transformation successfully abolished hERG activity. These encouraging data, combined with those obtained from biochemical, phenotypic and aqueous solubility assays, established the *N*-methylpiperazine substituted pyridine as the lead compound within this programme of research at that point in time.

The second section details the development of a small molecule probe selective for the first bromodomains (BD1s) of the BET proteins. Here, a programme of research to enhance the selectivity and potency of the dimethylisoxazole quinoline series of inhibitors towards the BD1 domains is described. Using both data-driven and structure-based design, a dimethylisoxazole imidazolquinoline was developed and, upon screening, was found to exceed the programme requirements regarding potency and domain-selectivity. This molecule was used as a probe in biological studies alongside pan-BET inhibitors and demonstrated that the anti-inflammatory and antiproliferative phenotype typical of pan-BET inhibition was retained upon selective BD1-inhibition. With increasing interest in scientific community for the development of domain-selective BET inhibitors and their use in biological experiments, these studies provide an important foundation for further research in this specific arena.

Abbreviations

Å	Angstrom
Ac	Acetyl
AcOH	Acetic acid
ADME	Absorption Distribution Metabolism Excretion
Ala/A	Alanine
ALPHA	Amplified Luminescence Proximity Homogeneous Assay
AML	Acute Myeloid Leukaemia
AMP	Artificial Membrane Permeability
ApoA1	Apolipoprotein A1
aq	Aqueous
Ar	Aromatic
Arg/R	Arginine
Asn/N	Asparagine
Asp/D	Aspartic Acid
ATAD2	Adenosine Triphosphatases Associated with Diverse Cellular Activities Domain-containing Protein 2
AUC	Area Under Curve
BAZ2B	Bromodomain Adjacent to Zinc Finger Domain 2B
BCP	Bromodomain-containing Protein
BD	Bromodomain
BET	Bromodomain Extraterminal
Bn	Benzyl
Boc	<i>t</i> -Butyloxycarbonyl
BRCT	Breast Cancer Gene 1 Carboxy Terminus Domain
BRD	Bromodomain-containing Protein
Bu	Butyl
ⁿ Bu	Normal Butyl
^t Bu	<i>tert</i> -Butyl
BzD	Benzodiazepine
BzT	Benzotriazepine
CDK9	Cyclin-dependent Kinase 9
cHex	Cyclohexyl
ChIP	Chromatin Immunoprecipitation
CLND	Chemiluminescent Nitrogen Detection

CREBBP	Cyclic Adenosine Monophosphate Response Binding Element Binding Protein
CSD	Cambridge Structural Database
CTD	Carboxyl Terminal Domain
CYP	Cytochrome P450
Cys/C	Cysteine
DAD	Diode Array Detection
dba	Dibenzylideneacetone
DCE	Dichloroethane
DCM	Dichloromethane
DEAD	Diethylazodicarboxylate
DIBAL-H	Diisobutylaluminium Hydride
DIPEA	Diisopropylethylamine
DMA	<i>N,N</i> -Dimethylacetamide
DMAP	4-Dimethylaminopyridine
DME	1,2-Dimethoxyethane
DMF	<i>N,N</i> -Dimethylformamide
DMSO	Dimethylsulfoxide
DNA	Deoxyribonucleic Acid
DPPA	Diphenylphosphoryl Azide
dppf	1,1'-Bis(diphenylphosphino)ferrocene
DSF	Differential Scanning Fluorimetry
EDCI	1-Ethyl-3-(3-dimethylaminopropyl)carbodiimide
e.e.	Enantiomeric Excess
ESI	Electrospray Ionisation
ET	Extraterminal
Et	Ethyl
EtOAc	Ethyl Acetate
EtOH	Ethanol
equiv	Equivalents
FA	Fluorescence Anisotropy
FBDD	Fragment-based Drug Discovery
FHT	Fixed Hold Time
Fmoc	Fluorenylmethyloxycarbonyl
FP	Fluorescence Polarisation

FRAP	Fluorescence Recovery After Photobleaching
FRET	Fluorescence Resonance Energy Transfer
FW	Free-Wilson
g	Gas
g	Grammes
GABA	γ -Aminobutyric Acid
Gcn5	General Control of Amino Acid Synthesis 5
GFP	Green Fluorescent Protein
Glu/E	Glutamic Acid
Gln/Q	Glutamine
Gly/G	Glycine
GPCR	G Protein-coupled Receptor
h	Hour
HATU	2-(7-Aza-1 <i>H</i> -benzotriazol-1-yl)-1,1,3,3-tetramethyluronium Hexafluorophosphate
HBA	Hydrogen Bond Acceptor
HBD	Hydrogen Bond Donor
HBTU	<i>O</i> -(Benzotriazol-1-yl)- <i>N,N,N',N'</i> -tetramethyluronium Hexafluorophosphate
HCTU	2-(6-Chloro-1 <i>H</i> -benzotriazole-1-yl)-1,1,3,3-tetramethylaminium Hexafluorophosphate
HDAC	Histone Deacetylase
HDL	High-Density Lipoprotein
HDM	Histone Demethylase
hERG	Human Ether-a-go-go Related Gene
His/H	Histidine
HIV	Human Immunodeficiency Virus
HMBC	Heteronuclear Multiple Bond Correlation
HMT	Histone Methyltransferase
HOBt	1-Hydroxybenzotriazole
HPLC	High-performance Liquid Chromatography
HRMS	High Resolution Mass Spectroscopy
HTRF	Homogeneous Time Resolved Fluorescence
HTS	High-throughput Screening
IL	Interleukin
Ile/I	Isoleucine

<i>i.p.</i>	<i>Intra-peritoneal</i>
IPA	Isopropylalcohol
IR	Infrared
ITC	Isothermal Titration Calorimetry
<i>i.v.</i>	<i>Intravenous</i>
<i>J</i>	Coupling Constant
KAc	Acetyl-Lysine
kg	Kilogrammes
LCMS	Liquid Chromatography Mass Spectroscopy
LDL	Low-Density Lipoprotein
LE	Ligand Efficiency
Leu/L	Leucine
LiHMDS	Lithium Hexamethyldisilazide
LPS	Lipopolysaccharide
Lys/K	Lysine
<i>m</i>	<i>Meta</i>
MBT	Malignant Brain Tumour
MCP-1	Monocyte Chemotactic Protein-1
MDAP	Mass-Directed AutoPreparative High-performance Liquid Chromatography.
Me	Methyl
MeOH	Methanol
Met/M	Methionine
mg	Milligrammes
MHz	Megahertz
min	Minutes
mL	Millilitre
mM	Millimolar
mm	Millimetre
mmol	Millimols
MMP	Matched Molecular Pair
MOA	Mode of Action
mol	Moles
m.p.	Melting Point
mRNA	Messenger Ribonucleic Acid

Mwt	Molecular Weight
MYC	Myelocytomatosis Oncogene
NFκB	Nuclear Factor κB
ng	Nanogrammes
nM	Nanomolar
nm	Nanometre
NMC	Nuclear Protein in Testis Midline Carcinoma
NMP	<i>N</i> -Methylpyrrolidinone
NMR	Nuclear Magnetic Resonance; s-singlet d-doublet t-triplet q-quartet quin-quintet m-multiplet br-broad
NOE	Nuclear Overhauser Effect
NT	Not Tested
NUT	Nuclear Protein in Testis
OTf	Trifluoromethanesulfonyloxy
PAFc	Polymerase-Associated Factor Complex
<i>p</i>	<i>Para</i>
PB1	Polybromodomain 1
PBMC	Peripheral Blood Mononuclear Cell
PCAF	p300/CBP Associated Factor
PDB	Protein Data Bank
PDE4	Phosphodiesterase 4
Ph	Phenyl
PHD	Plant Homeodomain
Phe/F	Phenylalanine
Php	Phosphorylation
PIFA	Phenylodine Bis(trifluoroacetate)
PK	Pharmacokinetic
PMB	<i>Para</i> -methoxybenzyl
<i>p.o.</i>	<i>Per Os</i>
ppm	Parts Per Million

Pr	Propyl
ⁱ Pr	<i>Iso</i> -propyl
Pro/P	Proline
PyBOP	(Benzotriazol-1-yloxy)tripyrrolidinophosphonium
P-TEFb	Positive Transcription Elongation Factor b
PTM	Post-Translational Modification
qPCR	Quantitative Polymerase Chain Reaction
QSAR	Quantitative Structure Activity Relationship
RFC	Replication Factor C
RNA	Ribonucleic Acid
RNAPII	Ribonucleic Acid Polymerase II
ROESY	Rotating-frame Overhauser Effect Spectroscopy
RuPhos	2-Dicyclohexylphosphino-2',6'-diisopropoxybiphenyl
r.t.	Room Temperature
Rt	Retention Time
s	Seconds
SAR	Structure Activity Relationship
<i>s.c.</i>	<i>Sub-cutaneous</i>
SEC	Super Elongation Complex
SEED	Serine-Glutamic Acid-Aspartic Acid-rich Region
Ser/S	Serine
SGC	Structural Genomics Consortium
siRNA	Small Interfering Ribonucleic Acid
SMILES	Simplified Molecular Input Line Entry System
S _N Ar	Nucleophilic Aromatic Substitution
SP140	SP140 Nuclear Body Protein
SPE	Solid Phase Extraction
SPR	Surface Plasmon Resonance
<i>t/tert</i>	Tertiary
TFA	Trifluoroacetic Acid
THF	Tetrahydrofuran
THP	Tetrahydropyran
THQ	Tetrahydroquinoline
Thr/T	Threonine
TMS	Trimethylsilyl

TNF	Tumour Necrosis Factor
Trp/W	Tryptophan
TSA	Trichostatin A
TSS	Transcriptional Start Site
Tyr/Y	Tyrosine
UPLC	Ultra Performance Liquid Chromatography
UV	Ultra Violet
Val/V	Valine
V_{ss}	Volume of Distribution at Steady State
v/v	Volume/volume
WB	Whole Blood
WPF	Tryptophan-Proline-Phenylalanine
WT	Wild Type
μL	Microlitre
μm	Micrometre
μM	Micromolar
μs	Microseconds
μwave	Microwave
$^{\circ}\text{C}$	Degrees Centigrade

Notes on Nomenclature

In keeping with standard convention,¹ gene names and symbols are italicised throughout this thesis, while the proteins encoded by these genes are written in plain text. In addition, human gene symbols and human protein abbreviations are displayed in upper case, whereas gene symbols and protein abbreviations for other species, such as mice, are written with only the first letter capitalised. Only abbreviations pertaining to human proteins have been provided above, but these may equally refer to non-human proteins or the corresponding gene encoding them.

Contents

Declaration of Copyright	i
Acknowledgments	ii
Abstract	iv
Abbreviations	v
Notes on Nomenclature	xi
Contents	xii
1. Introduction	1
1.1. <i>Epigenetics</i>	1
1.2. <i>Chromatin Structure, Modifications and Remodelling</i>	1
1.3. <i>Bromodomains and Reading of the Histone Code</i>	4
1.4. <i>The BET Family of Bromodomain-containing Proteins</i>	6
1.5. <i>Triazolodiazepine and Related BET Inhibitors</i>	11
1.6. <i>3,5-Dimethylisoxazole BET Inhibitors</i>	25
1.7. <i>Other BET Inhibitors</i>	46
2. Quinoline BET Inhibitors for Intravenous Administration	61
2.1. <i>Medicinal Chemistry Strategy and Project Aims</i>	61
2.2. <i>3-Methylamine Exploration</i>	65
2.3. <i>4-Amino Substituent Exploration and Molecular Budgeting</i>	68
2.4. <i>4-C Linked Aryls</i>	79
2.5. <i>Further 4-Amino Substituent Exploration</i>	83
2.6. <i>Conclusions and Future Work</i>	89
3. Imidazoquinolinones as Bromodomain-Selective BET Probes	91
3.1 <i>Medicinal Chemistry Strategy and Project Aims</i>	92
3.1.1 <i>SAR Review</i>	96
3.2. <i>Imidazoquinolinone 8-Position Investigation</i>	105
3.3. <i>Pyridine 6-Position Chemistry</i>	118
3.4. <i>Rigidification Strategy to Improve Activity and Selectivity</i>	120
3.6. <i>Investigation of Overlap with BDI-Selective Thienopyridones</i>	129

3.7.	<i>A Shift Towards a More BDI-potent Scaffold</i>	135
3.8.	<i>Conclusions</i>	155
4.	Experimental	158
4.1.	<i>General</i>	158
4.2.	<i>Notes on NMR Spectra</i>	161
4.3.	<i>Synthetic Procedures and Compound Characterisation</i>	164
4.4.	<i>Racemisation Study</i>	278
4.5.	<i>Computational Procedures</i>	278
5.	Appendix	280
5.1.	<i>Structures of Histone Peptides</i>	280
5.2.	<i>BET WT FP Assays</i>	282
5.3.	<i>BET WT HTRF Assays</i>	283
5.4.	<i>Solubility Measurements by CLND</i>	284
5.5.	<i>Solubility Measurements from Solid</i>	284
5.6.	<i>hERG Inhibition</i>	285
5.7.	<i>ChromLogD and ChromLogP Measurements</i>	287
5.8.	<i>Inhibition of IL-6 Production in LPS-Stimulated Human WB</i>	288
5.9.	<i>Mutant FRET Assays</i>	289
5.10.	<i>AMP Assay</i>	292
5.11.	<i>qPCR Bromodomain Binding Assay Panel</i>	292
5.12.	<i>Inhibition of IL-6 Production in LPS-Stimulated Human PBMCs</i>	294
5.13.	<i>MV-4-11 Growth Inhibition Assay</i>	296
6.	References	297

1. Introduction

The research presented in this thesis details the design and development of Bromodomain Extraterminal (BET) inhibitors. The four proteins which comprise the BET family each contain two conserved modules, known as bromodomains, which recognise acetyl-lysine (KAc) post-translational modifications (PTMs) on chromatin. Through this mechanism, the BET proteins serve as epigenetic regulators of gene transcription and aberrant control of their function make BET bromodomains highly valued therapeutic targets.

To provide greater understanding of the research presented, brief overviews of epigenetic and chromatin remodelling biological concepts are first presented, and these are followed by descriptions of bromodomains and the BET family of bromodomain-containing proteins, and their involvement in these areas of biology and in disease. To place the research described in this thesis into broader context, a review of BET inhibitors published in the literature is then presented in the final section of this introduction.

1.1. Epigenetics

Epigenetics refers to heritable changes in gene function which are not caused by changes in the underlying deoxyribonucleic acid (DNA) sequence. While all cells within any one human carry the same DNA sequence, each cell type expresses different genes. The selective activation and/or silencing of gene expression gives rise to cellular differentiation and can be governed by epigenetic control. Diseases which have a genetic component may be modified by epigenetic mechanisms through their role in gene activation and silencing.²

1.2. Chromatin Structure, Modifications and Remodelling

A number of mechanisms of epigenetic control have been discovered, one of which is chromatin remodelling.³ Within the cell, DNA is wrapped around histone protein octamers to form nucleosomes, the basic unit of chromatin (Figure 1). The role of chromatin is to package and strengthen DNA and control gene expression and DNA replication. Chromatin is a highly dynamic material mainly existing in two forms: heterochromatin - the closed and silent configuration consisting of densely packed chromatin; and euchromatin - the open and active configuration consisting of less densely packed chromatin.⁴

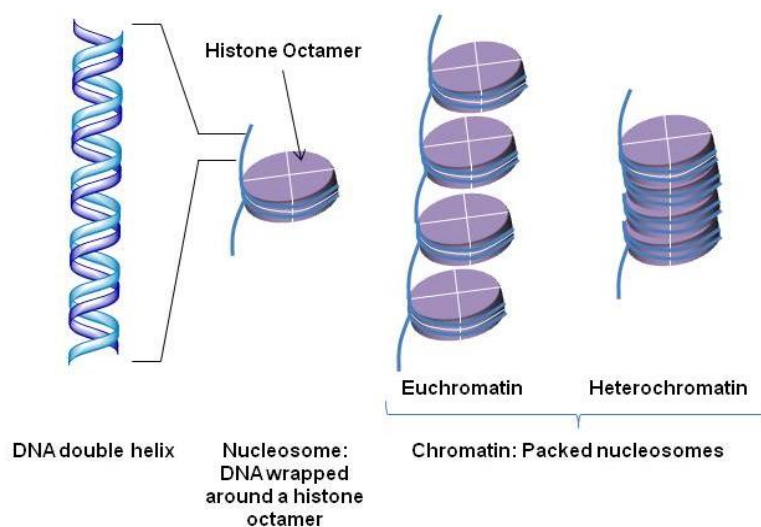


Figure 1. Structure of chromatin.

Heterochromatin may be remodelled into euchromatin to allow access to DNA and facilitate gene transcription. A number of mechanisms control the dynamics of this remodelling, including cytosine methylation of DNA and post-translational modifications (PTMs) of histones.⁵ Numerous modifications are made in the flexible *N*-terminal tails of histone proteins and, to a lesser extent, with the *C*-terminal tails and globular domains.³ Only a subset of amino acids contained in the histone tails are known to be covalently modified, including lysine (Lys/K), arginine (Arg/R), serine (Ser/S), threonine (Thr/T), glutamic acid (Glu/E), proline (Pro/P), tyrosine (Tyr/Y) and histidine (His/H). A range of modifications to these amino acids may occur; a selection is shown in Table 1.^{6,7}

Modification	Residue Modified	Functions Regulated
Acetylation (Ac)	K	Transcription, Repair, Replication, Condensation
Methylation (Me)	K	Transcription, Repair
	R	Transcription
Phosphorylation (Php)	S, T	Transcription, Repair, Condensation
Ubiquitylation	K	Transcription, Repair
Sumoylation	K	Transcription
Adenosine diphosphate ribosylation	E	Transcription
Deimination	R	Transcription
Proline isomerisation	P	Transcription

Table 1. A selection of histone PTMs.

The majority of modifications include the addition or removal of small, yet chemically and structurally distinct, moieties. These modifications provide a histone code which can be written, read and erased.

A range of protein domains read the histone code by binding to PTMs in a specific manner, facilitating chromatin remodelling and gene transcription. Reader modules are structurally engineered to recognise:

- the type of PTM;
- a specific histone tail;
- the position on the histone tail; and
- the valency of the PTM.

Also, combinations of PTMs may be read in parallel and the timing of the ‘reading’ can contribute to transcriptional activation. Reader modules grouped by domain family and the PTM marks they recognise are shown in Table 2.⁷

Reader Module	PTM mark
Bromodomain	KAc
<i>Royal Superfamily</i>	
Chromodomain	KMe
Double chromodomain	KMe
Chromo barrel	KMe
Tudor	KMe, RMe
Double/tandem tudor	KMe
Malignant Brain Tumour (MBT)	KMe
Plant Homeodomain (PHD) finger	KMe
WD40 repeat	KMe
14-3-3	SPhp
Breast Cancer Gene 1 Carboxy Terminus Domain (BRCT)	SPhp

Table 2. Histone reader modules and their associated PTM marks.

1.3. Bromodomains and Reading of the Histone Code

Bromodomains are an important class of reader module consisting of approximately 110 amino acids which recognise acetyl-lysine (KAc) PTM marks on histone tails. They were first discovered in 1992 as evolutionary and structurally conserved modules in six human genes, *Drosophila* Brahma and yeast.⁸ Bromodomain-containing proteins (BCPs) have crucial roles in transcriptional regulation through KAc recognition. They function as a scaffold for assembly of macromolecular complexes through protein-protein interactions and can remodel chromatin allowing recruitment or activation of ribonucleic acid (RNA) polymerases.⁹ Bromodomains are often found in combination with other epigenetic modifying domains, such as methyl and acetyl transferases, and other reader modules, such as PHD and tudor domains. Furthermore, multiple bromodomains can be found within the same protein such as in polybromodomain-1 (PB1) and the Bromodomain Extraterminal (BET) family, highlighting the complex and specific recognition of multiple PTMs. As such, the human genome encodes 42 BCPs encompassing 61 unique bromodomains (Figure 2).¹⁰

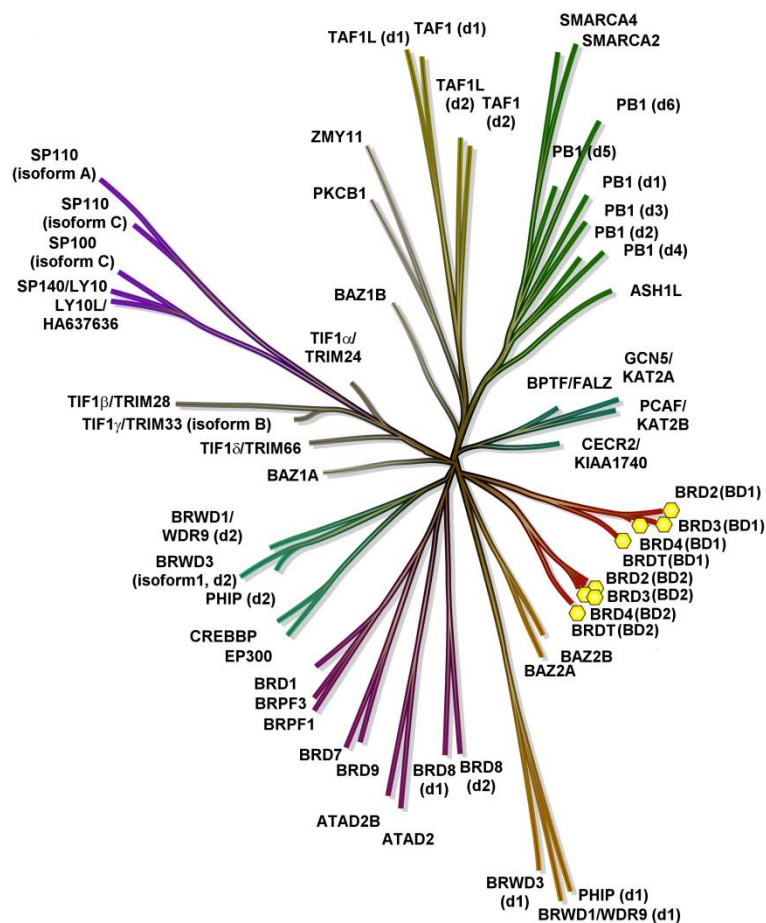


Figure 2. Phylogenetic tree displaying structural homology between BCPs.¹¹

The first three-dimensional structure of a bromodomain, transcriptional co-activator p300/CBP associated factor (PCAF), was solved by nuclear magnetic resonance (NMR) spectroscopy revealing an anti-parallel bundle of four left-handed α -helices (α_Z , α_A , α_B and α_C) with a left-handed twist (Figure 3a).¹² From structure-based sequence alignment, the authors predicted that the entire bromodomain family shared a similar helix bundle. These original findings were confirmed when a high resolution crystal structure of the PCAF-related bromodomain general control of amino acid synthesis 5 (Gcn5) was obtained in complex with histone H4 peptide, residues 15–29, acetylated at K16 (H4_{15–29}K16Ac)^{13,14} (Figure 3b). Since then, the structures of over half the bromodomain family have been solved with all members found to contain a conserved fold.^{15,16} Loops linking each of the helices (ZA and BC loops) pack against each other creating a surface accessible hydrophobic depression into which the histone peptide binds. Shallow surface grooves and high residue variation within the loops on the rim of the KAc binding site are thought to contribute to the specificity of KAc peptide recognition.

The acetyl-lysine segment of a histone tail inserts into a deep and narrow cavity lined with hydrophobic and uncharged residues (Figure 3c). The carbonyl of the acetyl group is anchored into this cavity through a direct hydrogen bond to the NH bond of a highly conserved asparagine (Asn/N) residue and through a water-bridged interaction with a highly conserved tyrosine residue. The bridging water molecule is part of a larger water network at the base of the recognition site which generally remains unchanged upon ligand binding. The methyl substituent of the acetyl group resides in a small hydrophobic pocket which can also tolerate larger propionylated and butyrylated lysine groups.¹⁷

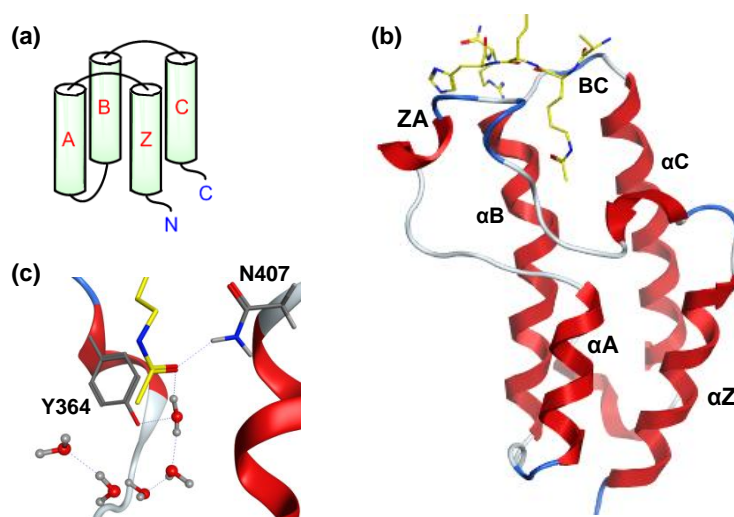


Figure 3. (a) Topology of the bromodomain fold. (b) Structure of H4_{15–29}K16Ac¹⁴ (carbon = yellow) in complex with Gcn5 (pdb 1E6I). (c) Recognition of KAc by conserved asparagine and tyrosine residues.

More recently, the druggability of bromodomains was assessed using the extensive structural knowledge of this area.¹⁸ Accordingly, the bromodomain extraterminal (BET) family of BCPs have ranked highly in the subsequent analysis and these indications have been supported by the disclosure of various small molecule BET inhibitors (*vide infra*). Intense research into this family has led the way for bromodomain drug discovery and provided insight into the therapeutic potential of this target class.

1.4. The BET Family of Bromodomain-containing Proteins

The BET family is a subgroup of the bromodomain superfamily consisting of bromodomain-containing protein 2, 3 and 4 (BRD2, BRD3 and BRD4) and bromodomain testis-specific protein (BRDT). This protein family share similar gene arrangements, domain architecture (Figure 4) and functional properties, and are widely expressed in humans (except the testis and ovary localised BRDT).

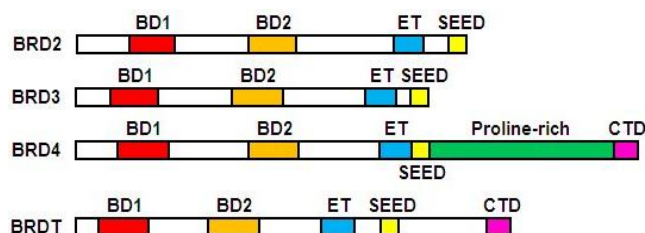


Figure 4. Domain architecture of BET proteins.

The BET proteins are characterised by their two tandem bromodomains, which bind acetylated chromatin, and an extraterminal (ET) domain. The first bromodomain (BD1) is found closer to the *N*-terminus while the second bromodomain (BD2) is situated nearer the *C*-terminus. The serine-glutamic acid-aspartic acid-rich region (SEED) is a conserved domain across the BET proteins, while the carboxyl terminal domain (CTD) is only found in BRD4 and BRDT. Both BRD2 and BRD4 mediate transcriptional elongation through recruitment of positive transcription elongation factor b (P-TEFb).¹⁹ This protein complex is composed of a cyclin-dependent kinase 9 (CDK9) which, in its active form, phosphorylates RNA polymerase II (RNAPII), stimulating productive elongation and synthesis of messenger ribonucleic acid (mRNA).

With a central role in normal cell cycle progression^{20,21} and cell growth,²² dysregulation of BET protein function is especially important in oncology. For example, translocation of the BRD4 gene (and, more rarely, BRD3) to the nuclear protein in testis (NUT) protein, results in an aggressive form of human squamous carcinoma termed NUT midline carcinoma (NMC).²³ Inhibition of BRD4 as a treatment strategy for NMC was

validated after reduced proliferation and differentiation of tumour cells was found upon RNA silencing of BRD4 in NMC cell lines.²⁴ A separate RNA interference screen identified *Brd4* as a critical requirement for acute myeloid leukaemia (AML) disease maintenance. Suppression of BRD4 led to cell-cycle arrest and apoptosis of leukaemia cells through downregulation of the myelocytomatosis oncogene (*MYC*).²⁵ Additionally, a *BRD4* transcriptional signature has been shown to be a robust predictor of breast cancer progression and/or survival.²⁶ In addition to cancer, BET family members have been implicated in inflammatory disease^{27,28,29} with one notable study establishing the role of Brd4 in the activation of nuclear factor κ B (NF κ B)-dependant inflammatory genes in response to bacteria-derived endotoxin lipopolysaccharide (LPS) or tumour necrosis factor α (TNF α) stimulation.³⁰ A number of studies have also suggested a role of the BET proteins in infectious diseases such as human immunodeficiency virus (HIV), herpes, and human papillomavirus.³¹⁻³³

Taken together, these studies clearly demonstrate the involvement of BET proteins in a variety of pathological conditions and make these BCPs desirable targets for pharmacological intervention. In particular, inhibition of bromodomain-KAc binding is an attractive strategy for probing BET biology further and as the basis of therapy, due to the importance of the reader module in transcriptional control. The weak interaction of the BET bromodomains with their substrates¹⁰ suggests that competitive displacement with small molecules would be favourable with rational design of such inhibitors facilitated by the availability of appropriate X-ray crystal structures.

Human BET bromodomains are well characterised with 7 apo structures publicly available. The overall structures are shown in Table 3, with the conserved four helical bromodomain fold being evident. Similar loop lengths are apparent within the family, although BRDT has an extended helix within the ZA loop.

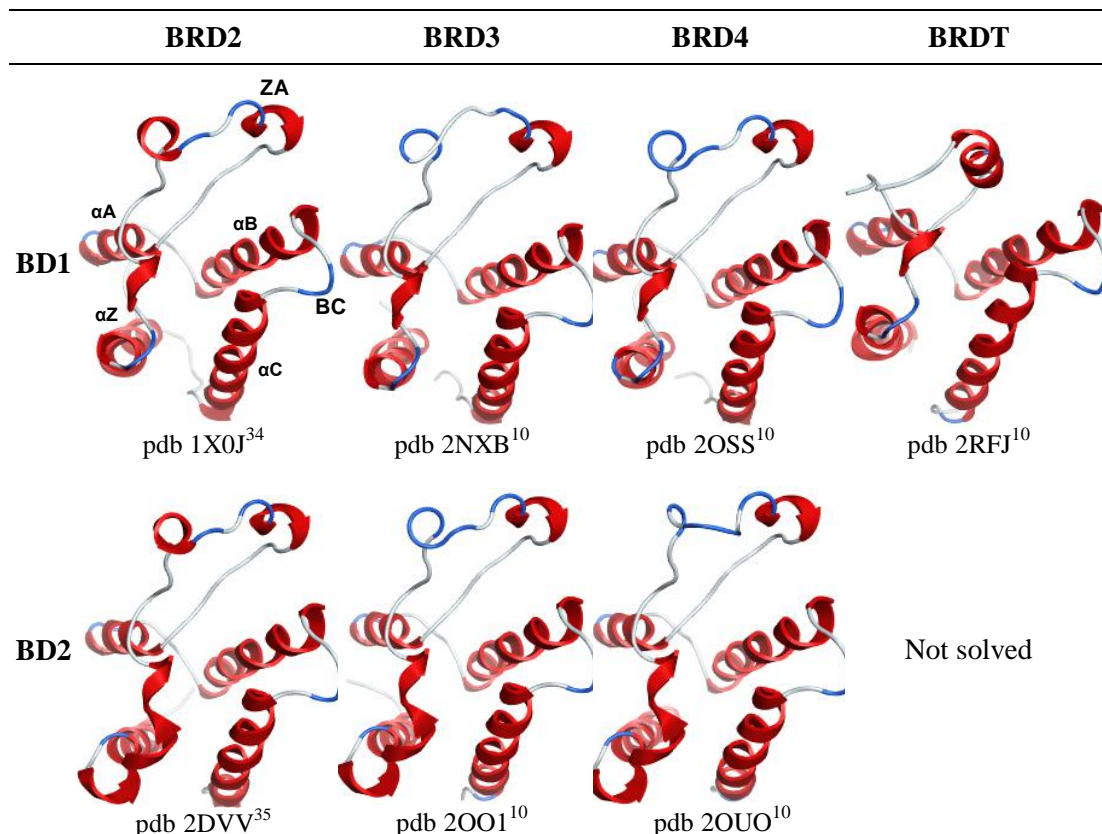


Table 3. Apo structures of human BET bromodomains.

In contrast to the structural features noted above, noticeable differences are apparent in the electrostatic potential around the KAc binding site (Table 4) and these may give rise to selective histone tail recognition.¹⁰ However, the key asparagine and tyrosine KAc recognition residues at the base of the binding site are conserved across the BET bromodomains (Figure 5); the X-ray crystal structure of histone peptide H4₇₋₁₇K8AcK12Ac¹⁴ bound to BRD4 BD1¹⁰ highlights the importance of these residues in KAc binding (Figure 6). Either valine (Val/V) or isoleucine (Ile/I) ‘gatekeeper’ residues are present in all the BET bromodomains and allow access to a hydrophobic region of the ZA loop termed the tryptophan-proline-phenylalanine (TrpProPhe/WPF) shelf. A nearby methionine (Met/M) on the C-helix influences the position of the tryptophan shelf residue creating a relatively enclosed hydrophobic pocket not present in other bromodomains. Additionally, extended ZA loops are found in the BET family compared to other bromodomains.

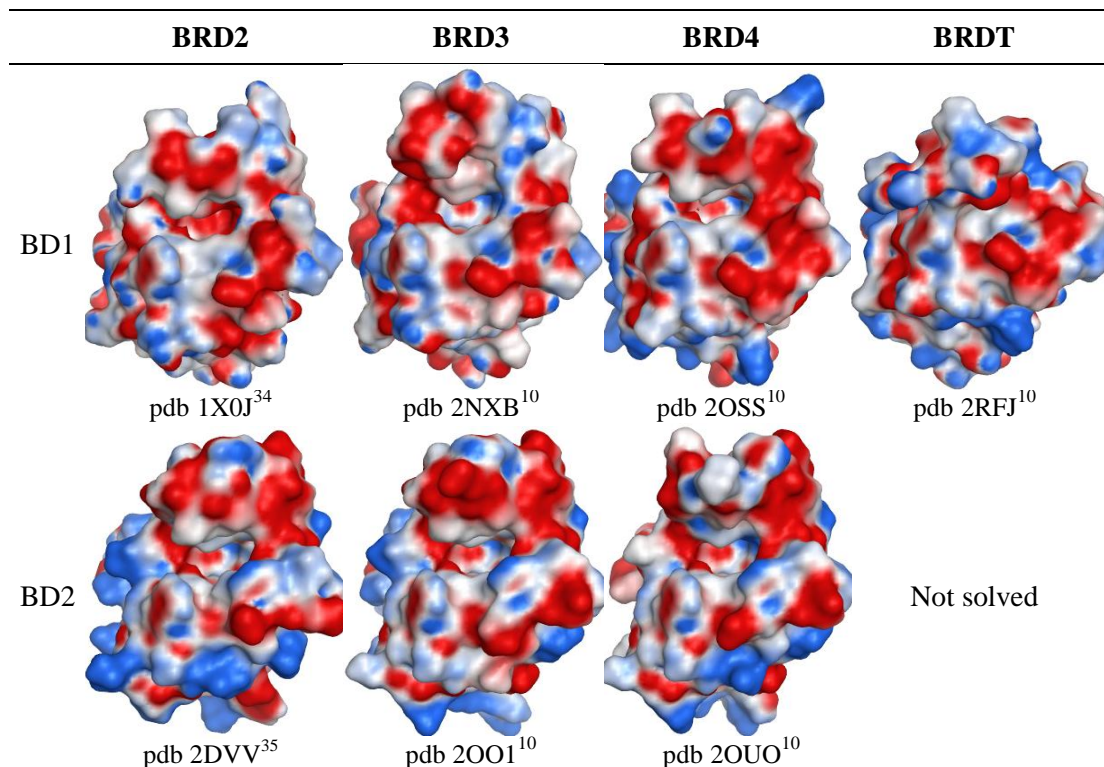


Table 4. Electrostatic surface potentials of human BET bromodomains.



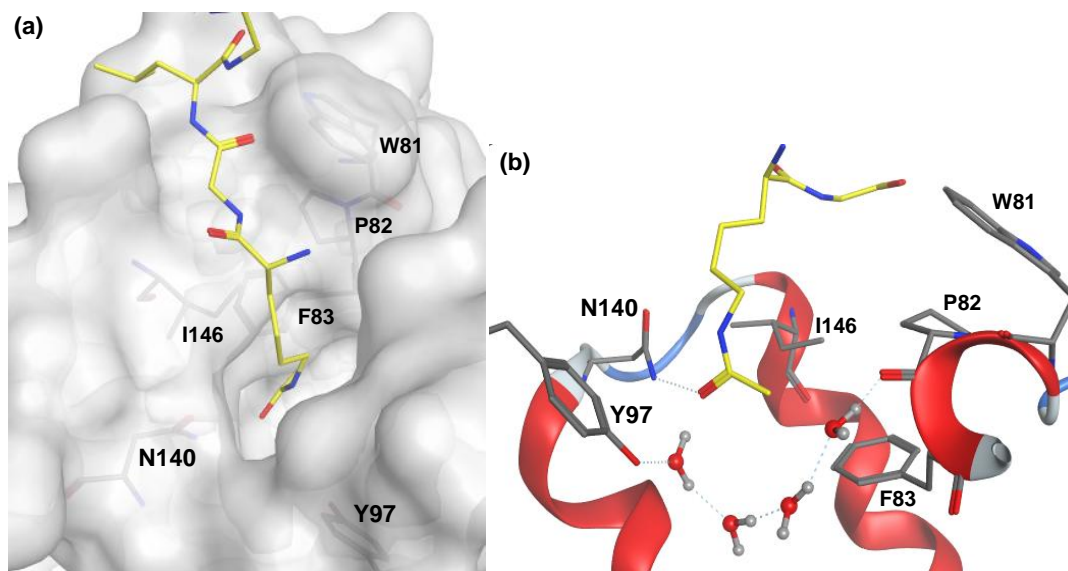


Figure 6. Crystal structure of H4₇₋₁₇-K8AcK12Ac¹⁴ (carbon = yellow) in BRD4 BD1 (pdb 3UW9). (a) Molecular surface representation of the binding site. (b) Ribbon representation with KAc interactions highlighted.

These structural features make the BET bromodomains attractive targets for interaction with small molecules. A sufficiently large and enclosed surface area presents opportunity for high affinity binding, while architectural differences over other bromodomains make selectivity for the BET bromodomains achievable. Furthermore, as the BET proteins contain multiple domains, the identification of small molecules which are specific for the bromodomains are important to establish an understanding of the effects of inhibiting KAc binding without affecting the other roles of the BCP. This is an area of research which was, until recently, relatively under-explored, and over the course of the studies presented in this thesis, a number of BET bromodomain inhibitors have been discovered. Several of these molecules have been reviewed in the context of epigenetic modifiers,² bromodomain ligands,³⁶⁻⁴² and, more specifically, BET bromodomain inhibitors.⁴³ An up-to-date BET bromodomain-focused review of small molecule inhibitors will now be presented with emphasis on the development and application of these molecules.

1.5. Triazolodiazepine and Related BET Inhibitors

Over recent years, BET inhibitors from a variety of structural classes have been discovered. The first potent and selective structures disclosed were the benzodiazepines (BzDs) GW841819X and I-BET762, and the thienodiazepine (+)-JQ1 (Figure 7).

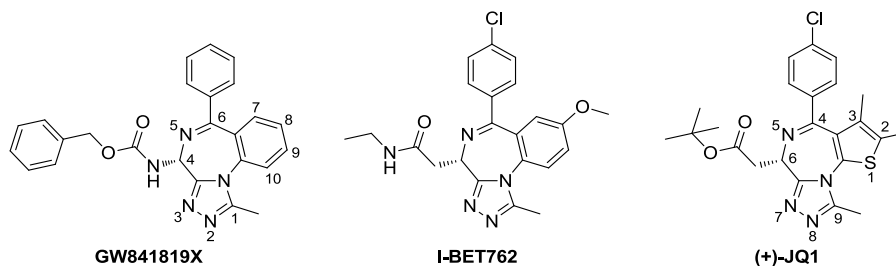
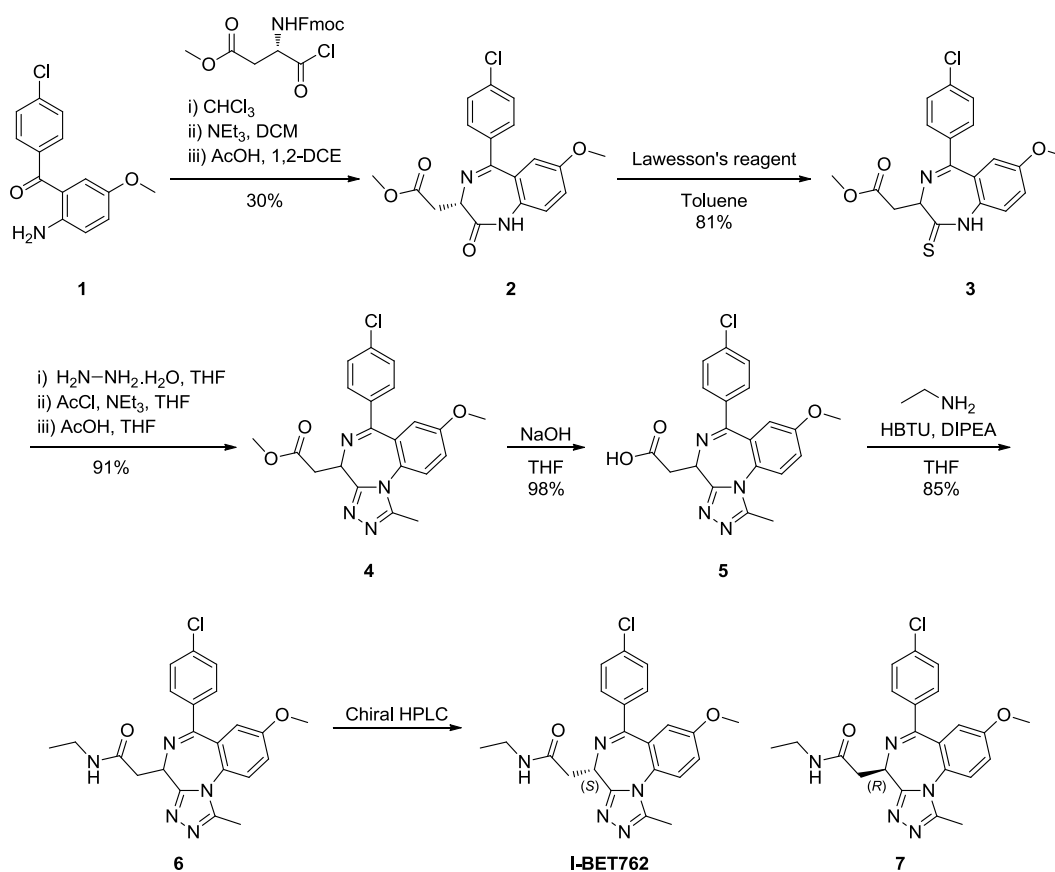


Figure 7. First generation BET inhibitors and their associated numbering systems.

Importantly, studies with these first generation molecules have provided greater understanding of the relevance of BET bromodomains in disease. In fact, the mode of action (MOA) of the triazolobenzodiazepines GW841819X and I-BET762 was unknown at the point of identification.⁴⁴ These compounds were discovered as part of a drug discovery programme targeting the Apolipoprotein A1 protein (ApoA1) as a treatment for atherosclerosis. A cell reporter phenotypic screen identified compounds belonging to the BzD structural class as specific activators of *ApoA1* and, upon minimal optimisation, GW841819X was discovered.⁴⁴ This compound exhibited an EC_{50} of 440 nM in the ApoA1 reporter gene assay and its specificity as an ApoA1 upregulator was confirmed in a subsequent experiment. A medicinal chemistry programme to optimise physicochemical and pharmacokinetic (PK) properties led to the synthesis of I-BET762 (Scheme 1) which displayed similar activity to GW841819X with an $EC_{50} = 700$ nM.⁴⁴ The *S*-enantiomer (I-BET762) was confirmed as the active stereoisomer, with the *R*-enantiomer (**7**) producing no effect on ApoA1 induction. Further details regarding the lead optimisation effort towards I-BET762 have only recently been disclosed.⁴⁵



Scheme 1. Synthetic route to I-BET762 and its enantiomer 7.

Synthesis of I-BET762 commenced with amidation of (2-amino-5-methoxyphenyl)(4-chlorophenyl)methanone **1** with the acid chloride derived from fluorenylmethyloxycarbonyl (Fmoc)-aspartic acid methylester.⁴⁴ The benzodiazepine scaffold was then constructed by Fmoc-deprotection, followed by acid-promoted cyclisation furnishing lactam **2** in 30% overall yield. Conversion into the thiolactam **3** with Lawesson's reagent was achieved in high yield (81%) but with loss of stereochemical integrity. Reaction with hydrazine monohydrate followed by acetylation and cyclisation gave the annulated triazole **4** in 91% yield over the three steps. Straightforward saponification and *O*-(benzotriazol-1-yl)-*N,N,N',N'*-tetramethyluronium hexafluorophosphate (HBTU)-mediated amide formation gave the racemate **6**, which upon separation by chiral high-performance liquid chromatography (HPLC) gave I-BET762 and its inactive stereoisomer **7**.

With this compound in hand, efforts to identify the molecular target ensued but screening against a panel of diverse targets failed to provide any insight.⁴⁴ Accordingly, a chemoproteomics approach was taken using the I-BET762 derivative **8** (Figure 8) attached to an agarose matrix.

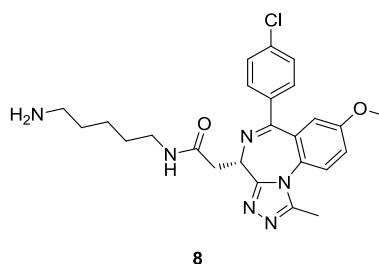


Figure 8. I-BET762 derivative **8** used for chemoproteomic studies.

After incubation of the BzD **8**-matrix in cell lysates, the BET family members were identified as the interacting proteins.⁴⁴ Subsequent immunoprecipitation experiments revealed that the BzD **8**-matrix interacted with an *N*-terminal truncate of BRD2 (containing BD1 and BD2), so isothermal titration calorimetry (ITC) was used to define the binding constants within this region of BRD2, 3 and 4 (Table 5).

	K_d (nM)	
	GW841819X	I-BET762
BRD2	80	61.3
BRD3	19	50.5
BRD4	24	55.2

Table 5. Summary of ITC results for BzDs GW841819X and I-BET762.

High affinities were determined for both GW841819X and I-BET762 and, interestingly, BzD:protein binding stoichiometries of 2:1 were measured in each experiment indicating that the BzDs bound to both bromodomains in each protein.⁴⁴ Further ITC experiments were then carried out using BRD2 protein constructs containing individual bromodomains and revealed similar dissociation constants for BD1 and BD2 (46.0 and 52.5 nM, respectively).

Next, the ability of GW841819X and I-BET762 to interfere with KAc recognition by BET bromodomains was demonstrated using fluorescence resonance energy transfer (FRET) assay technology.⁴⁴ Inhibition of acetylated-lysine histone peptide binding to tandem bromodomain constructs of BRD2, 3 and 4, resulted in IC₅₀ values ranging from 16 to 42 nM (Table 6).

	IC ₅₀ (nM)	
	GW841819X	I-BET762
BRD2	29.9	32.5
BRD3	28.4	42.4
BRD4	15.5	36.1

Table 6. BzD inhibition constants of an acetylated-lysine histone peptide using FRET technology.

While chemoproteomics from cell lysates retrieved only BET proteins, differential scanning fluorimetry (DSF) experiments were conducted to precisely determine the bromodomain selectivity now that binding to the BET family of BCPs was confirmed.⁴⁴ Negligible binding was observed for I-BET762 against Adenosine Triphosphatases Associated with Diverse Cellular Activities Domain-containing Protein 2 (ATAD2), cyclic adenosine monophosphate response binding element binding protein (CREBBP), bromodomain adjacent to zinc finger domain 2B (BAZ2B), PCAF, and SP140 nuclear body protein (SP140).

Insight into how the BzDs bound to the BET bromodomain fold and achieved selectivity over other BCPs was realised through X-ray crystallography.⁴⁴ High resolution cocrystal structures were solved in BRD2 BD1 and showed both molecules binding in a similar manner to the KAc binding site (Figure 9a).

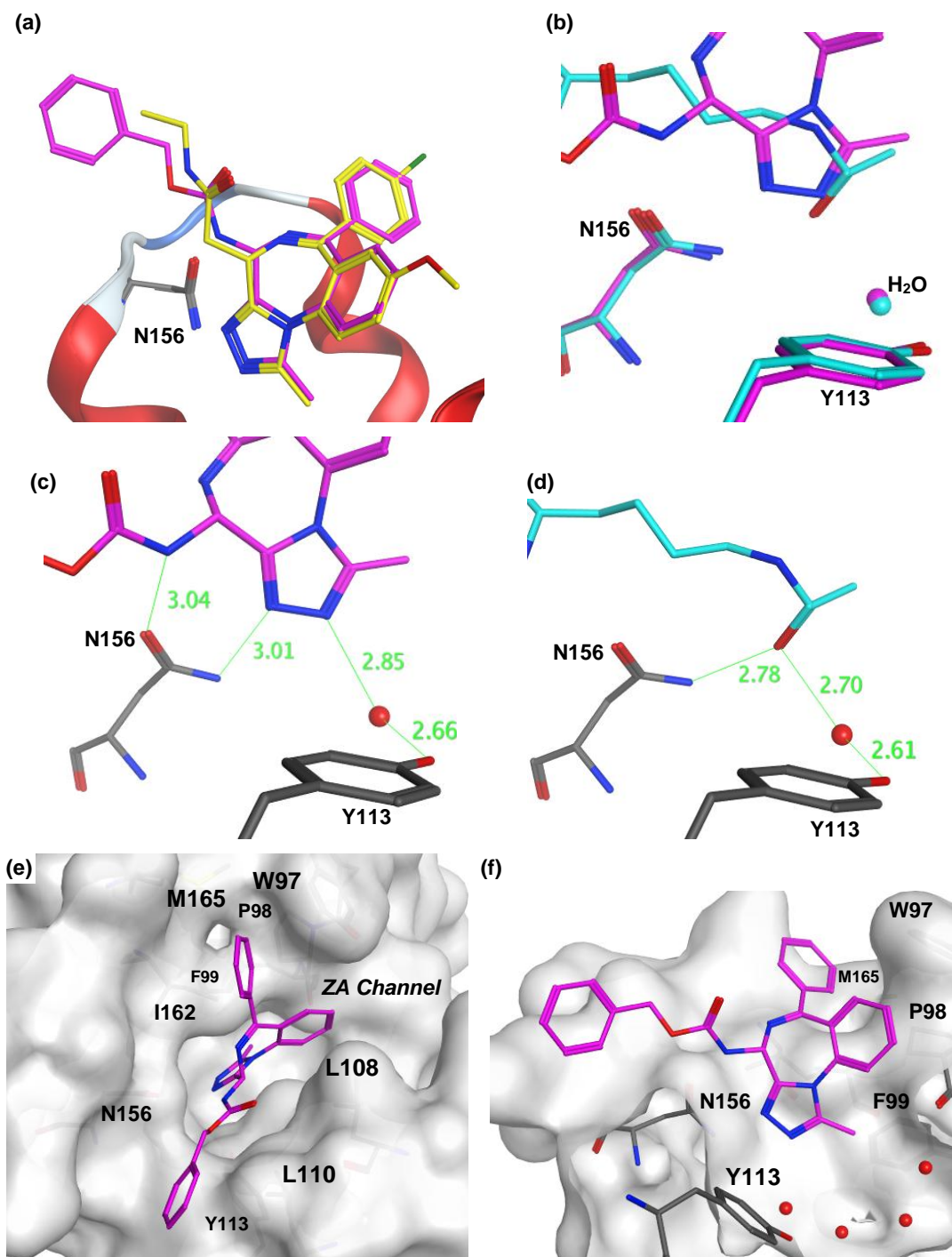


Figure 9. (a) X-ray crystal structure overlay of GW841819X (carbon = magenta, pdb 2YDW) and I-BET762 (carbon = yellow, pdb 2YEK) in BRD2 BD1. (b) Superimposed complexes of GW841819X (carbon = magenta, pdb 2YDW) and histone peptide H₄₁₋₁₅K12Ac¹⁴ (carbon = cyan, pdb 2DVQ) in BRD2 BD1. (c and d) Distances (Å) of key hydrogen bonds of GW841819X (carbon = magenta, pdb 2YDW) and histone peptide H₄₁₋₁₅K12Ac¹⁴ (carbon = cyan, pdb 2DVQ) in BRD2 BD1. (e and f) Alternative surface representations of GW841819X (carbon = magenta) in BRD2 BD1 (pdb 2YDW).

The triazole rings of GW841819X and I-BET762 directly hydrogen-bonded to the NH₂ group of Asn156 through the N2 atom while a water-bridged hydrogen bond to the hydroxyl group of Tyr113 was made through N3. The triazole ring therefore mimicked KAc-binding and this was confirmed by superimposition of a published structure of the histone peptide H4₁₋₁₅K12Ac¹⁴ bound to BRD2 BD1⁴⁶ with the GW841819X-BRD2 BD1 structure (Figure 9b). It was evident that the N2 of the triazole ring was in a similar position to the KAc carbonyl of the histone peptide but the smaller KAc group sat slightly deeper in the binding site and with two lone pairs available to accept hydrogen bonds, bound to both Asn156 and through-water to Tyr113. The triazole, however, had to make the key hydrogen bonds through separate nitrogen atoms, the distances of which were marginally greater than for those measured for the acetylated peptide (Figure 9c and d) (it should be noted that the KAc amide of histone peptide appeared non-planar through erroneous fitting in the published structure⁴⁶). Both the acetyl methyl group of H4₁₋₁₅K12Ac peptide¹⁴ and the C1-methyl of GW841819X pointed towards the small hydrophobic pocket formed by Phe99 which was adjacent to the conserved water network.

In addition to the features described above, a direct hydrogen bond donor (HBD) interaction was made by the carbamate NH of GW841819X to the side chain carbonyl oxygen of Asn156. A methylene group occupied the corresponding position in I-BET762, which instead hydrogen bonded through the amide NH *via* a water molecule (not shown). It was clear from the crystal structure of GW841819X that the stereogenic centre substituted with the benzyl carbamate possessed the same configuration of groups (albeit with different priority assignment) as I-BET762. The authors suggest the opposite stereoisomers would sterically clash with leucine (Leu/L)108 and Leu110 resulting in weakened activity.⁴⁴

The high activity of the BzDs was partly attributed to their curved nature which neatly complemented the binding site architecture (Figure 9e). The benzodiazepine fused phenyl ring occupied a cleft between Pro98 (of the WPF motif) and Leu108 located on the ZA loop, which was termed the ZA channel. Interactions in this region were expected to contribute to the notable selectivity over other BCPs. The other important determinant of selectivity was the WPF shelf on the ZA loop. This hydrophobic region of the bromodomain, created by the WPF motif and the adjacent Ile162 and Met165 residues, was occupied by the pendant 6-position phenyl of GW841819X (Figure 9e and f). Access to the WPF shelf was afforded by the small Ile162 gatekeeper which is replaced by larger residues in some other BCPs (e.g. a tyrosine in the closely related Gcn5), and, consequently, afforded selectivity for BET BCPs. The high conservation of the ZA channel and WPF shelf within the BET family explained the lack of selectivity measured for each BET protein subtype. For example, the

researchers demonstrated similar binding interactions for GW841819X in BRD4 BD1 when compared to the same compound complexed in BRD2 BD1. Moreover, despite a lower sequence identity between BRD2 BD1 and BRD2 BD2, conservation of key binding residues afforded comparable binding modes accounting for the similar measured affinities against the isolated domains.⁴⁴

With the mode of action of these BzDs clearly established, small interfering ribonucleic acid (siRNA) knockdown experiments were performed in order to clarify that inhibition of the BET transcriptional regulators increased ApoA1 expression.⁴⁴ Accordingly, it was shown that knockdown of BRD2 and BRD3 had no effect, while progressive knockdown of BRD4 resulted in ApoA1 upregulation.

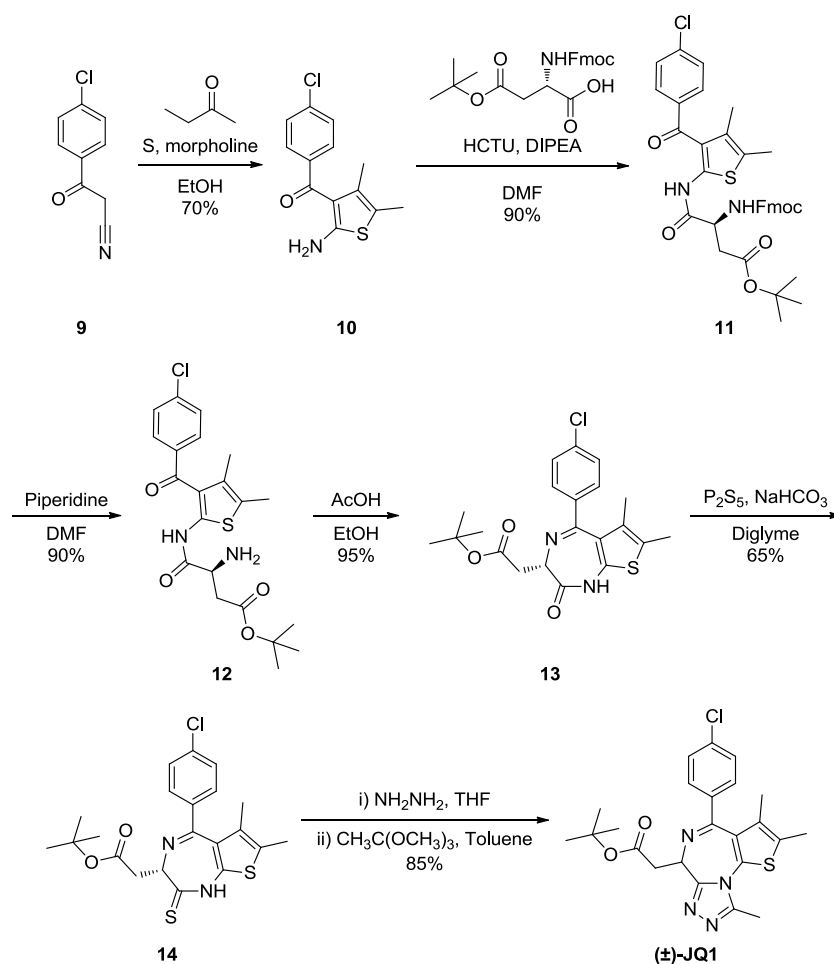
Further biological studies demonstrated the ability of I-BET762 to disrupt chromatin complexes required for expression of inflammatory genes.⁴⁷ In a gene array study, stimulation of bone-marrow derived mouse macrophages with LPS resulted in upregulation of numerous inflammatory genes. However, pre-treatment with I-BET762 suppressed 38 and 151 of the LPS-inducible genes at 1 and 4 h, respectively. Expression of key inflammatory chemokines and cytokines, including *Il-6*, were inhibited by I-BET762 with similar effects observed in response to siRNA-mediated knockdown of BET. Reduced recruitment of BET to the promoter of the *Il-6* gene was revealed as the mechanism for observed anti-inflammatory effects of I-BET762.

These results suggested inflammatory conditions could be treated with I-BET762. Accordingly, in an *in vivo* model of sepsis and endotoxic shock, mice pre-treated with I-BET762 were afforded protection against lethal doses of LPS or heat killed *Salmonella typhimurium*.⁴⁷ The molecule also showed efficacy even when dosed after LPS injection, curing the developing symptoms of inflammatory disease and preventing death.

Through these studies, the first generation pan-BET inhibitors GW841819X and I-BET762 were discovered, and the potential of I-BET762 as an immunomodulatory drug was established. It was shown how phenotypic screening identified a cell permeable molecule with the desired phenotype at an early stage.⁴⁴ Subsequently, chemoproteomic experiments were conducted and identified the BET proteins as the biological targets and subsequent profiling demonstrated high binding affinities to BET bromodomains but limited structure activity relationship (SAR) was presented (more detailed SAR data has only recently been released⁴⁵). Although specific data were not reported, the physicochemical and PK profiles of I-BET762 were suitable for *in vivo* studies in mice. Demonstration that this molecule possessed anti-inflammatory properties highlighted the exciting potential of bromodomain inhibitors in the treatment of disease.⁴⁷ Indeed, our laboratories have now

progressed I-BET762 into a phase I/II clinical trial in NMC patients.⁴⁸ In the future, expansion into different indications and development of alternative administration methods would be of value to the scientific community. Since both I-BET762 and GW841819X induced pan-BET inhibition, further research to deconvolute the role of specific bromodomains within the family with selective inhibitors would also be desirable.

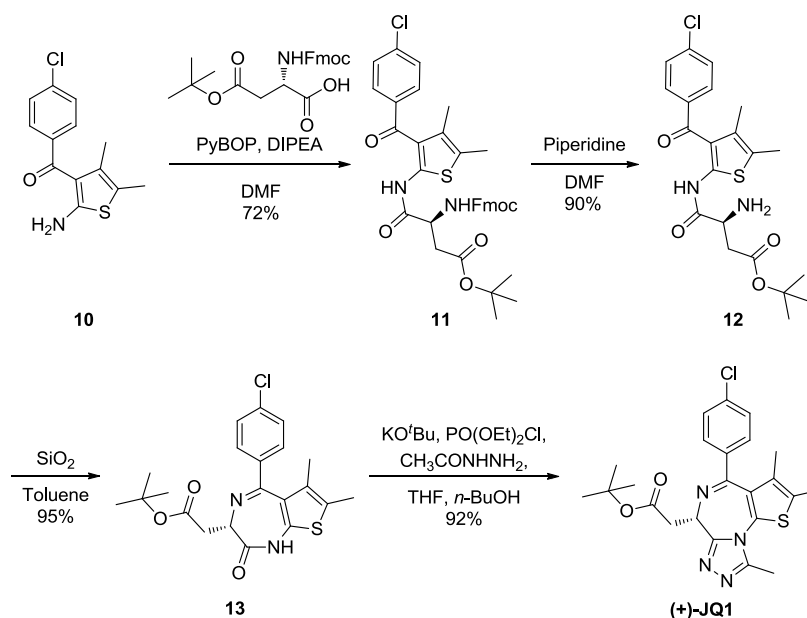
At the same time as the immunomodulatory properties of I-BET762 were disclosed, a report was published highlighting the anti-tumour properties of a related BET inhibitor (+)-JQ1.⁴⁹ Using information contained within a patent from Mitsubishi Pharmaceuticals disclosing a series of triazolothienodiazepines with binding activity for BRD4,⁵⁰ molecular modelling experiments in BRD4 BD1 were conducted and the *t*-butyl ester (+)-JQ1 was designed as a putative ligand.⁴⁹ This molecule was subsequently synthesised according to Scheme 2.



Scheme 2. Synthesis of triazolothienodiazepine (\pm)-JQ1.

The first step in the synthesis involved formation of the 2-aminothiophene **10** by reaction of 4-chlorobenzoyl acetonitrile **9** with sulfur and 2-butanone (70% yield). Amidation with Fmoc-Asp(O^{*t*}Bu)-OH using 2-(6-chloro-1*H*-benzotriazole-1-yl)-1,1,3,3-

tetramethylammonium hexafluoro-phosphate (HCTU) gave the coupling product **11** (90% yield) and subsequent deprotection gave the free amine **12** in 90% yield. Over the course of these steps, the stereochemical integrity was compromised with the enantiomeric purity of amine **12** determined as 75%. Further racemisation occurred when forming the thienodiazepine scaffold. Heating amine **12** with acetic acid induced cyclisation to the lactam **13** in an efficient manner (95% yield) but with decreased enantiomeric purity (67%). Reaction with phosphorus pentasulfide formed the thioamide **14** in moderate yield (65%) with the remaining mass balance being comprised of starting material. With the thioamide in hand, triazole ring formation was effected by reaction with hydrazine followed by trimethyl orthoacetate in 85% yield. The enantiomeric purity was further diminished over the course of these final steps providing (\pm)-JQ1. Based on all of this, the researchers executed a modified route which attenuated racemisation (Scheme 3).⁴⁹



Scheme 3. Optically-enriched synthesis of triazolothienodiazepine (+)-JQ1.

Starting from the 2-aminothiophene **10**, (benzotriazol-1-yl)oxytripyrrolidinophosphonium (PyBOP) was used to form amide **11** in 72% yield, which was followed by Fmoc-removal to afford the amine **12** (90% yield). With identical deprotection conditions used as in the synthesis of (\pm)-JQ1, it was the switch from HCTU to PyBOP which reduced racemisation in the enantio-enriched synthesis (enantiomeric purity = 91%). Another step important in determining the stereochemical outcome was cyclisation to the thienodiazepine **13**. Use of silica gel as a reagent to effect this reaction resulted in negligible loss of enantiomeric purity (90%). Finally, conditions were modified for the triazole annulation. The sequential addition of potassium *tert*-butoxide, diethyl

chlorophosphate, acetic hydrazide, and 1-butanol, and careful control of temperature, resulted in a 92% yield without further degradation of the enantiomeric purity (90%). After preparative chiral HPLC, the *S*-enantiomer was obtained in >99% enantiomeric excess (e.e.) and labelled (+)-JQ1. Synthesis and chiral HPLC purification of the *R*-enantiomer was completed in a similar fashion to give (-)-JQ1 (>99% e.e.).

Like BzDs GW841819X and I-BET762, the configuration of the stereogenic centre of JQ1 was critical for activity. In DSF assays, (+)-JQ1 showed thermal stabilisation of the BET proteins, while (-)-JQ1 did not demonstrate any measurable stabilisation.⁴⁹ Furthermore, (+)-JQ1 was highly selective for the BET family in a panel of thirty other BCPs. Precise determination of binding constants was carried out using ITC with K_d values correlating well with thermal shift data. Nanomolar affinities for individual BET bromodomains resulted after protein titration into (+)-JQ1 with comparable K_d values found for BRD3 BD1, BRD3 BD2, BRD4 BD1, and BRD4 BD2 (Table 7).

	K_d (nM)	
	BD1	BD2
BRD2	128.4	NT
BRD3	59.5	82.0
BRD4	49.0	90.1
BRDT	190.1	NT

Table 7. ITC-determined K_d values for (+)-JQ1 in single BET bromodomain protein constructs.

Amplified luminescence proximity homogeneous assay (ALPHA) technology was used to verify that (+)-JQ1 competitively displaced KAc from BET bromodomains.⁴⁹ Indeed, acetylated histone peptide binding to BRD4 BD1 and BRD4 BD2 was inhibited by (+)-JQ1 with nanomolar potencies ($IC_{50} = 77$ nM and 33 nM, respectively). The specificity of (+)-JQ1 for the BET bromodomains was further confirmed after screening against a panel of 55 human recombinant ligand receptors, ion channels and transport proteins, which revealed no significant off-target activity. A PK study of (+)-JQ1 in mice revealed a moderate clearance (33 mL/min/kg), a short half life (1.4 h), and high oral bioavailability (F = 49%).

The inhibitory properties of (+)-JQ1 were assessed in a cellular environment using fluorescence recovery after photobleaching (FRAP) experiments.⁴⁹ Cells transfected with green fluorescent protein (GFP)-labelled BRD4 were treated with (+)-JQ1 and, upon photobleaching, immediate recovery of fluorescence was observed when compared to vehicle control, indicating (+)-JQ1 had displaced BRD4 from nuclear chromatin liberating

freely diffusing fluorescent protein. A FRAP experiment in cells transfected with GFP–BRD4–NUT also showed accelerated fluorescence recovery upon (+)-JQ1 treatment, demonstrating direct displacement of the oncoprotein from nuclear chromatin.

Next, Filippakopoulos *et al.* examined the impact of BRD4–NUT inhibition in a patient-derived NMC cell line.⁴⁹ Immunohistochemistry analysis showed that (+)-JQ1 induced squamous differentiation and growth arrest, a phenotype equivalent to that observed by RNA knockdown of BRD4 in a previous study.²⁴ Finally, three mice xenograft models of NMC were developed to assess the efficacy of (+)-JQ1 *in vivo*. Mice treated with (+)-JQ1 showed induction of squamous differentiation, reduction in tumour growth, and enhanced survival *versus* vehicle-treated mice.⁴⁹

This study has inspired application of (+)-JQ1 as a probe molecule in other oncological settings including AML,²⁵ various multiple myelomas,⁵¹ Burkitt's lymphoma,⁵² B-cell acute lymphoblastic leukaemia⁵³ and lung cancer.⁵⁴ In addition, (+)-JQ1 has shown promise as a therapy for viral disease,^{55–57} inflammatory disorders,⁵⁸ and idiopathic pulmonary fibrosis,⁵⁹ while its utility as a male contraceptive⁶⁰ has also been explored.

The seminal Nature publication detailing studies with (+)-JQ1⁴⁹ has generated huge interest in the bromodomain arena. Using knowledge of the patent literature, members of the Bradner laboratory and the Structural Genomics Consortium (SGC) devised this first generation pan-BET inhibitor possessing high affinity and selectivity for the BET bromodomains. Moreover, (+)-JQ1 was suitably permeable and metabolically stable allowing studies in cellular systems and *in vivo*. These properties, combined with its commercial availability, have seen the application of (+)-JQ1 in a range of studies by academic and industrial laboratories. Up until recently, the attention of the scientific community has predominantly focused on its use in cancer, but results from explorations into other disease areas are starting to emerge. While the utility of (+)-JQ1 as a probe molecule is undisputed, it is unknown whether it possesses a suitable safety profile as a therapy for humans. In relation to this, future generations of BET inhibitor with prolonged exposures would be beneficial, as well as molecules exhibiting bromodomain selectivity within the BET family.

Structurally related analogues of I-BET762 and (+)-JQ1 have also been investigated. In work by Filippakopoulos *et al.*, the triazolo-BzD and triazolo-benzotriazepine (BzT) scaffolds were validated as privileged structures for BET inhibition.⁶¹ BzDs in particular are important in small molecule therapy with many approved for clinical use in the treatment of sleeping disorders, seizures, muscle spasms, and anxiety *via* action through the γ -aminobutyric acid (GABA) receptor (Figure 10). The disclosure of triazolo-BzD I-BET762

prompted these researchers to investigate whether marketed BzDs interacted with the BET proteins.

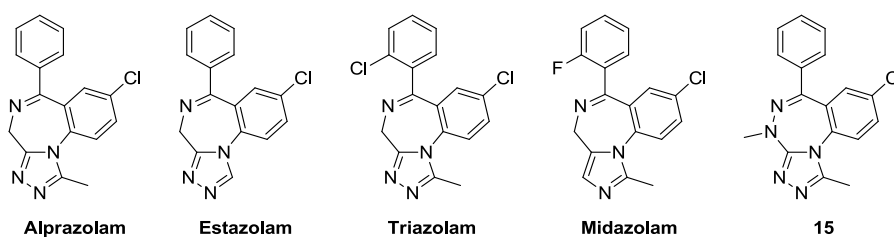


Figure 10. BzDs approved for clinical use and novel BET inhibitor BzT 15.

DSF screening of clinical BzDs revealed interesting SAR. Alprazolam demonstrated large increases in thermal stability of BET proteins over selected BCPs from other families of the bromodomain phylogenetic tree, indicating specificity for the BET family.⁶¹ The methyl group of the triazole ring in alprazolam was determined important for BET binding with estazolam displaying significantly lower T_m shifts. Only slight protein stabilisation was observed with triazolam indicating *ortho*-substitution of the 6-phenyl was unfavourable. Finally, reduced thermal shifts were found with midazolam revealing a poor tolerance for an imidazole over a triazole ring.

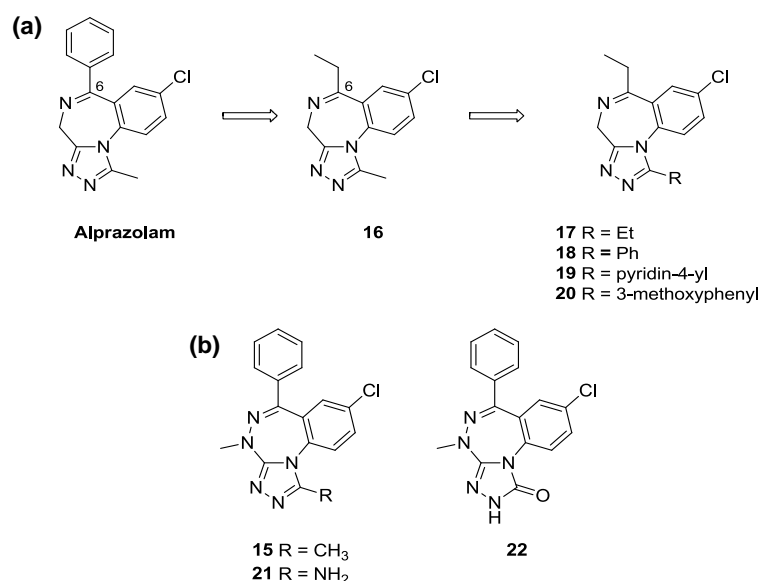


Figure 11. SAR investigations of BzDs (a) and BzTs (b).

A number of BzD analogues (17–20) containing larger substituents on the triazole ring were prepared to explore SAR and attempt to displace postulated conserved waters in the KAc binding site (Figure 11a).⁶¹ However, this SAR investigation was performed with a suboptimal 6-ethyl group and, consequently, none of the triazole ring substituents, including the baseline methyl BzD 16, displayed appreciable binding. More valuable insight into triazole ring SAR was achieved in the more active BzT series with a 6-phenyl group. Here,

the primary amine **21** showed reduced thermal shifts relative to its methyl congener **15**, while the triazolone **22** displayed negligible shifts (Figure 11b).⁶¹

Confirmation that alprazolam bound to the bromodomain fold of BET was obtained by X-ray crystallography in BRD4 BD1 (Figure 12a).⁶¹ A similar binding mode compared to I-BET762 and (+)-JQ1 was observed with the triazolo ring mimicking KAc recognition by forming a hydrogen bond with Asn140 (Figure 12b). The good shape complementarity with the binding site and occupation of the WPF shelf by the 6-phenyl substituent were cited as being contributors to the high activity. A complex of midazolam in BRD4 BD1 was also solved and both crystal structures used to rationalise SAR for the clinical BzDs. It was apparent that midazolam, lacking a heterocyclic nitrogen atom compared to alprazolam, was unable to make the key interaction to Asn140 resulting in outward displacement of this ligand from the KAc binding site (Figure 12c), contributing to lowered ΔT_m measurements.

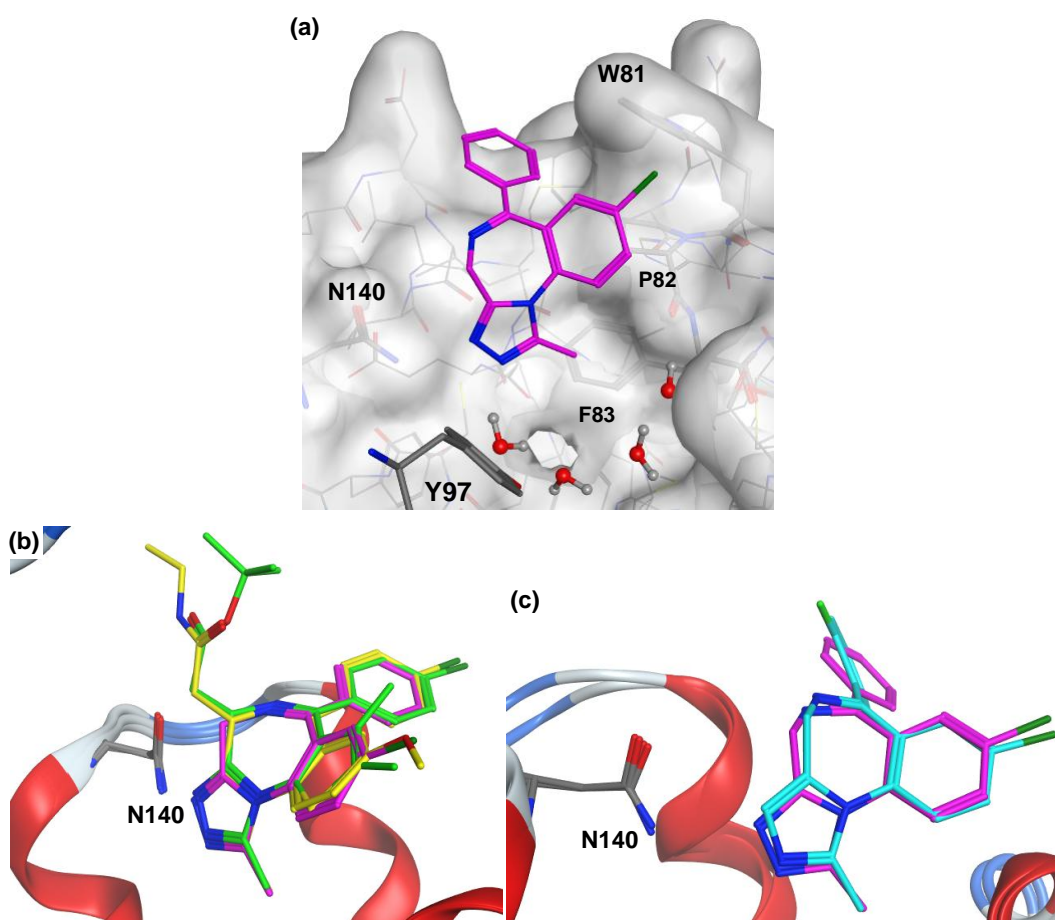


Figure 12. (a) Crystal structure of alprazolam (carbon = magenta) bound to BRD4 BD1 (pdb 3U5J). A protein molecular surface was applied. (b) Overlay of alprazolam (carbon = magenta, pdb 3U5J), I-BET762 (carbon = yellow, pdb 3P50) and (+)-JQ1 (carbon = green, pdb 3MXF) in BRD4 BD1; solvent was omitted for clarity. (c) Overlay of alprazolam (carbon = magenta, pdb 3U5J) and midazolam (carbon = cyan, pdb 3U5K) in BRD4 BD1; solvent was omitted for clarity.

The authors also found that the dihedral angle of the 2-fluorophenyl group in midazolam (45°) was larger than that measured for the phenyl group in alprazolam (29°).⁶¹ This latter observation was used to rationalise the poor activity of triazolam which contains a 2-chlorophenyl and was therefore expected to be rotated to a greater extent. A structure of BzT-7 in BRD4 BD1 (not shown here) was also solved verifying binding at the KAc recognition site in a similar manner to the clinical BzDs.

ITC measurements were conducted for alprazolam and triazolo-BzT **15** in BRD4 BD1 and the resulting binding constants compared to those published for (+)-JQ1, along with thermal shift data (Table 8).⁶¹ Only moderate ΔT_m values were measured for alprazolam and triazolo-BzT **15** in comparison to (+)-JQ1 and these translated into lower K_d values. The modest result for alprazolam highlighted the importance of the *t*-butyl ester functionality in (+)-JQ1 for high affinity binding. The triazolo-BzT **15** still bound to BRD4 BD1 with good affinity (0.64 μ M) but was almost an order of magnitude less potent than (+)-JQ1.

	ΔT_m (° C)	K_d (μ M)
Alprazolam	4.7	2.46
15	4.2	0.64
(+)-JQ1	9.3	0.049

Table 8. Biophysical measurements for alprazolam and triazolo-BzT **15** in BRD4 BD1.

The structural requirements for binding to the BET proteins with BzDs and BzTs were established in this work through SAR exploration and structural studies. Although clinically-approved BzDs were found to bind to the BET bromodomains, only weak activity was observed suggesting that BET-mediated transcriptional control side-effects were unlikely to occur during therapy. Novel BzDs and BzTs were also designed and prepared but did not show potency improvements over I-BET762 or (+)-JQ1. Interestingly, results from DSF experiments indicated that certain analogues preferentially bound to BD2 but accurate quantification was not carried out.⁶¹ Overall, the SAR generated for triazolo-BzDs and their further validation as privileged BET bromodomain ligands represent the foremost contributions to this research field to date.

More recently, a letter describing the discovery of an isoxazole azepine BET inhibitor was published by Constellation Pharmaceuticals.⁶² Inspired by crystallographic data obtained for the fragment hit **23** (Figure 13), an isoxazole motif was incorporated into an azepine scaffold to mimic the shape of (+)-JQ1 and synthetic explorations conducted at the 4- and 6-positions to determine SAR with regard to BRD4 BD1 binding affinity and activity in a MYC-dependant cancer cell line (Raji).

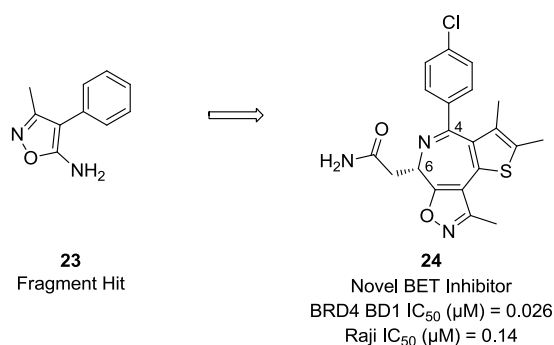


Figure 13. Structure-based design of an isoxazole azepine BET inhibitor from Gehling and co-workers.

Upon *in vitro* ADME profiling of a number of cell active analogues, isoxazole azepine **24** was progressed for PK studies where suitable oral exposure in mouse was achieved to warrant investigation *in vivo*.⁶² Here, dose-dependent decrease of MYC expression was observed upon oral administration to mice xenografted with Raji tumour cells. A time course experiment showed inhibition out to 8 h after which MYC expression recovered.

This work⁶² demonstrated the fusion of two privileged KAc mimetics, the triazolothienodiazepine and the isoxazole, a class of BET inhibitor discussed in more detail in the following section. The resulting isoxazole azepines provided entry into novel chemical space, but did not provide any other clear benefits. In fact, the direct isoxazole azepine analogue of (+)-JQ1 showed reduced BRD4 BD1 and cellular activity, and marginally reduced exposure following oral dosing in mouse. Aqueous solubility and suitability for alternative dosing methods were not reported. While negligible binding at other selected BCPs was confirmed, the selectivity over other BET family members or BRD4 BD2 was not determined.

1.6. 3,5-Dimethylisoxazole BET Inhibitors

The 3,5-dimethylisoxazole unit has also proven to be a privileged motif for bromodomain inhibition. Several groups have published BET inhibitors containing this structure, with the most advanced compound being a dimethylisoxazole imidazoquinolinone I-BET151 (*vide infra*), which, similarly to I-BET762, originated as an upregulator of ApoA1.⁶³ In this regard, a high-throughput screening (HTS) campaign, using a reporter gene assay, identified the 3,5-dimethylisoxazole quinoline GW694481 (Figure 14) as a hit molecule with an EC₁₇₀ = 0.5 μM.

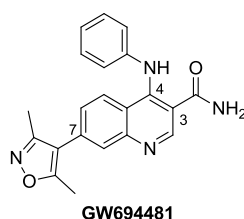
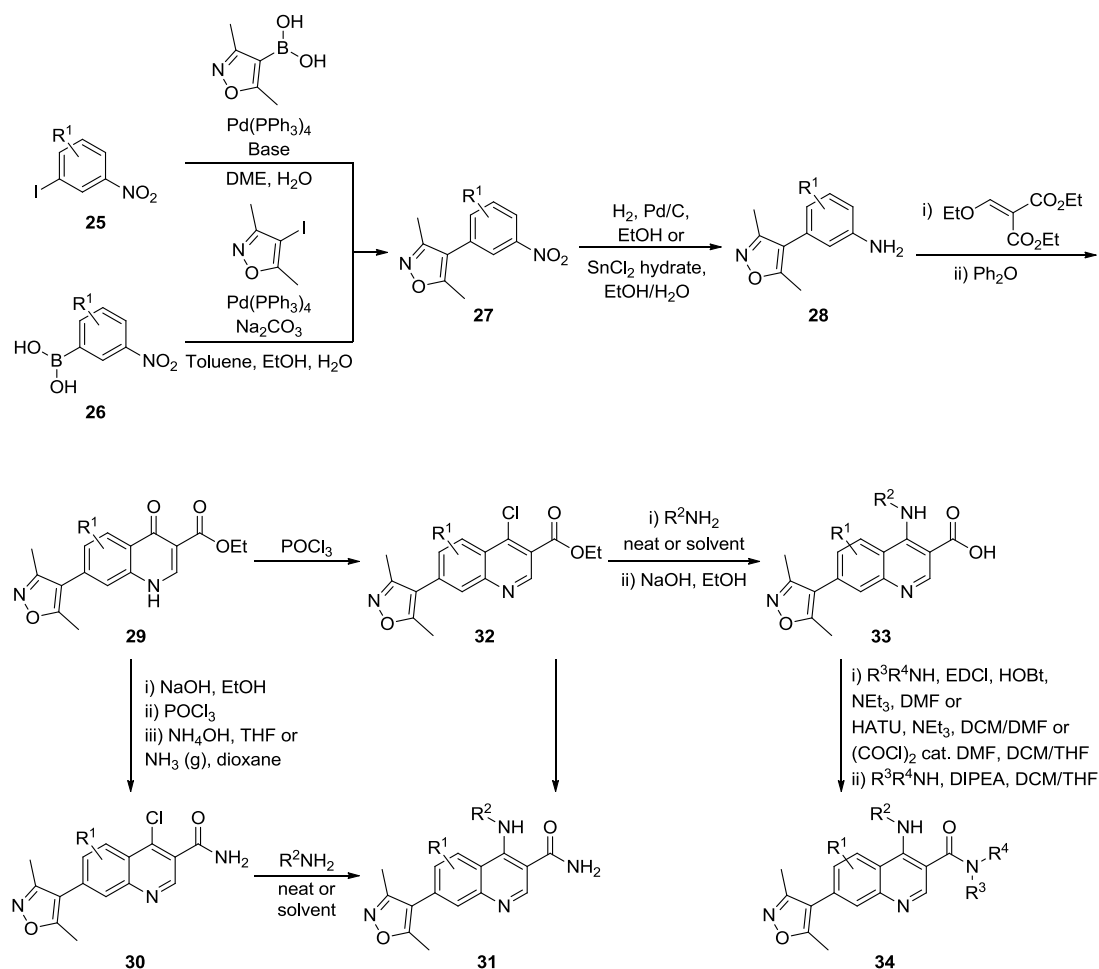


Figure 14. 3,5-Dimethylisoxazole quinoline hit GW694481 identified from a HTS.

Testing of analogues identified from substructure searching demonstrated the dimethylisoxazole as critical for activity, while the 3- and 4-positions were suitable areas for optimisation.⁶³ In particular, overcoming a cytochrome P450 (CYP) inhibition issue was necessary to minimise potential drug–drug interactions, as ApoA1 upregulator therapy was expected to be in combination with statins.

The synthesis outlined in Scheme 4 allowed the authors to explore a number of positions in this compound series.⁶³

Scheme 4. Synthetic routes used by Mirguet and co-workers for SAR exploration of dimethylisoxazole quinolines.⁶³

The first stage of the preparative sequence employed complementary Suzuki-Miyaura coupling strategies using either the iodide **25** or the boronic acid **26** to give the nitro-containing compounds **27**, with subsequent reduction affording anilines **28**. Condensation with diethyl 2-(ethoxymethylene)malonate, followed by cyclisation in refluxing diphenylether gave quinolinone esters **29**. Altering the order of transformations from these intermediates allowed for diversification. Saponification, chlorination then amidation gave the late stage intermediates **30**. This sequence allowed modification at the 4-position while retaining a 3-primary carboxamide to give dimethylisoxazole quinolines **31**. Alternatively, a chlorination followed by an S_NAr -saponification sequence gave the 3-carboxylic acids **33**, which allowed final stage variation of the amide moiety resulting in dimethylisoxazole quinolines **34**.

A comprehensive SAR investigation at the 4-position was reported with various substituted aliphatic, aromatic, and benzyl groups being tolerated; *ortho*-substitution with large groups afforded high activity when R^2 was a homoaryl unit.⁶³ A limited number of changes were made at the 6-position revealing a preference for OMe over Me or H (Table 9). Substitution of the 2- and 8-positions with a methyl group was shown to reduce activity by 5-fold and 4-fold, respectively (not shown). With regard to the 3-position, carboxylic acids showed a beneficial reduction of P450 inhibition but also lowered ApoA1 expression *versus* their carboxamide congeners.

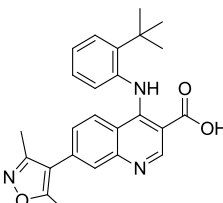
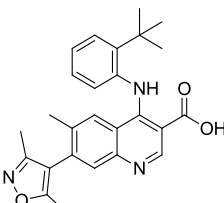
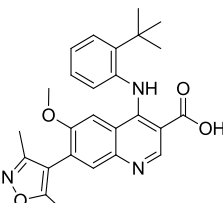
			
	35	36	37
ApoA1 EC₁₇₀ (μM)	0.32	1.99	0.28

Table 9. Dimethylisoxazole quinoline 6-position SAR.

A cyclisation strategy was employed to remove the 3-carboxamide, which was the suspected cause of the CYP inhibition.⁶³ This also had the effect of freezing a postulated intramolecular hydrogen bond between the 3-carboxamide and the 4-NH, thus rigidifying the molecular conformation (Figure 15).

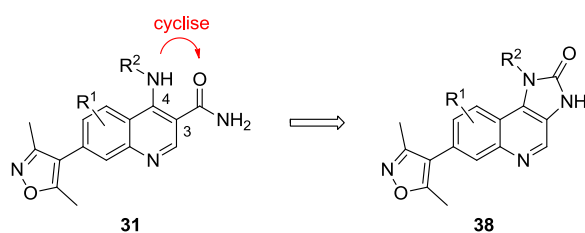
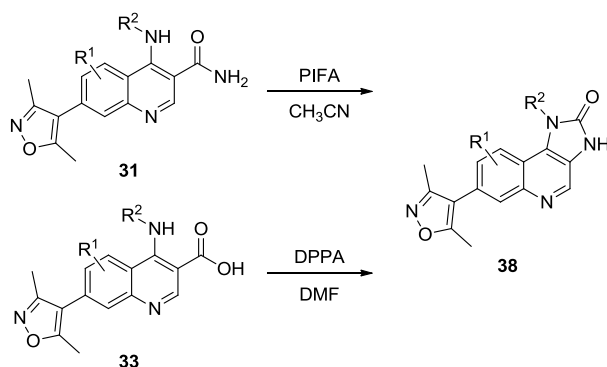


Figure 15. Rigidification of quinolines to imidazoquinolinones.

The key synthetic transformation to allow access to imidazoquinolinones **38** was accomplished using a modification of the Hofmann rearrangement from primary amides **31** or *via* a Curtius rearrangement from carboxylic acids **33** (Scheme 5).⁶³



Scheme 5. Rearrangement reactions used for imidazoquinolinone synthesis.

When R^2 was a substituted phenyl unit, the cyclisation strategy did not improve ApoA1 activity or reduce CYP inhibition. When R^2 = benzyl (**39**), high ApoA1 potency was achieved but CYP inhibition was still apparent (Table 10). Introduction of a nitrogen atom in the ring (**40**) attenuated this with only a slight decrease in ApoA1 activity. Substitution of the benzylic centre with a methyl group (**41**) improved activity further and upon chiral HPLC separation, the *R*-enantiomer (**R**)-**41** was found to be the more active stereoisomer. Combining the favourable pyridine-2-ylmethyl and (*R*)-1-phenylethyl substituents resulted in the (*R*)-1-(pyridin-2-yl)ethyl I-BET151, which exhibited high ApoA1 activity and an acceptable level of P450 activity.⁶³ The PK profile of this compound was evaluated in rat revealing a short half life (1.7 h), moderate clearance (18 mL/min/kg), and high oral bioavailability (66%).

		$R^2 =$						
			39	40	41	(R)-41	(S)-41	I-BET151
ApoA1 EC₁₇₀ (μM)			0.06	0.38	0.03	0.01	0.47	0.09
CYP Inhibition IC₅₀ (μM)	2C9		1.2	9.8	1.3	1.0	-	9.9
	3A4		3.7	12.9	2.0	1.5	-	9.7

Table 10. SAR of a selection of imidazoquinolinones.

Upon *in vitro* profiling of compounds active in the ApoA1 assay, Mirguet *et al.* observed cellular anti-inflammatory effects with TNF α production correlating with ApoA1 expression, suggesting a common pharmacology.⁶³ With dose-dependant inhibition of TNF α and IL-6 production in LPS-stimulated human peripheral blood mononuclear cells (PBMCs) determined, I-BET151 was assessed in an acute inflammation model in mice. After LPS stimulation, oral administration of I-BET151 reduced plasma cytokine levels in a comparable manner to known anti-inflammatory agents such as prednisolone. With previous demonstration that the ApoA1 upregulator I-BET762 functioned by inhibition of the BET proteins, Seal and co-workers postulated that dimethylisoxazole quinolines also exerted phenotypic effects through this mechanism.⁶⁴ Therefore, a number of dimethylisoxazole quinolines were tested in BRD2, 3 and 4 wild type (WT) fluorescence polarisation (FP) assays revealing submicromolar IC₅₀s which broadly correlated with ApoA1 activity. Similar SAR trends were observed, such as increased activity with a methoxy group at the 6-position and a reduction in activity upon switching from a 3-carboxamide to a 3-carboxylic acid (Table 11).

	42	43	44	45
ApoA1 pEC₁₇₀	6.3	6.5	5.7	6.7
BRD2, 3, 4 WT FP pIC₅₀	4.9, 5.5, 5.1	6.3, 6.5, 6.2	5.8, 6.2, 5.9	6.0, 6.3, 6.1

Table 11. Selected BRD2, 3 and 4 SAR of dimethylisoxazole quinolines.⁶⁴

Activities in the BET WT FP assays were also reported for the imidazoquinolinones with principle SARs shown in Table 12.⁶⁴ Inhibition of IL-6 production in LPS-stimulated human PBMCs was also examined with I-BET151 demonstrating high activity.

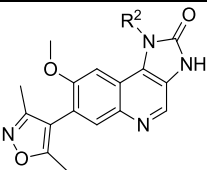
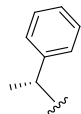
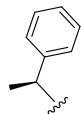
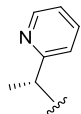
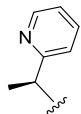
 $R^2 =$	 (R)-41	 (S)-41	 I-BET151	 46
	ApoA1 pEC₁₇₀	8.0	6.3	7.0
BRD2, 3, 4 WT FP pIC₅₀	6.4, 6.7, 6.6	5.7, 6.2, 5.9	6.3, 6.6, 6.1	5.8, 6.2, 5.4
PBMC pIC₅₀	7.0	-	6.7	6.1

Table 12. SAR of a selection of imidazoquinolinones.

The encouraging results for I-BET151 meant this molecule was progressed for further studies. A high resolution X-ray crystal structure in BRD2 BD1 was solved to determine its binding mode and showed the 3,5-dimethylisoxazole moiety positioned at the KAc binding site (Figure 16a).⁶⁴ In a similar manner to the triazole ring of BzD BET inhibitors, the dimethylisoxazole ring mimicked KAc binding as seen by superimposition with complex of histone peptide H4₁₋₁₅K12Ac¹⁴ in BRD2 BD1⁴⁶ (Figure 16b). A polar interaction was made between the isoxazole oxygen to the side chain NH₂ of the conserved asparagine at a distance of 3.25 Å (Figure 16c); this was marginally longer than those of the triazolo-BzDs GW841819X and I-BET762 (both 3.0 Å). The methyl groups of the isoxazole meanwhile, occupied lipophilic pockets adjacent to Phe99 and Leu110. The quinoline ring bound in a hydrophobic cleft between Trp97 and Pro98 on one side of the fused ring system, and Leu108 on the other, while the quinoline nitrogen accepted a hydrogen bond from an adjacent water molecule (Figure 16d and e).⁶⁵ The WPF shelf was occupied by the pyridine ring which was believed to impart BET bromodomain selectivity.

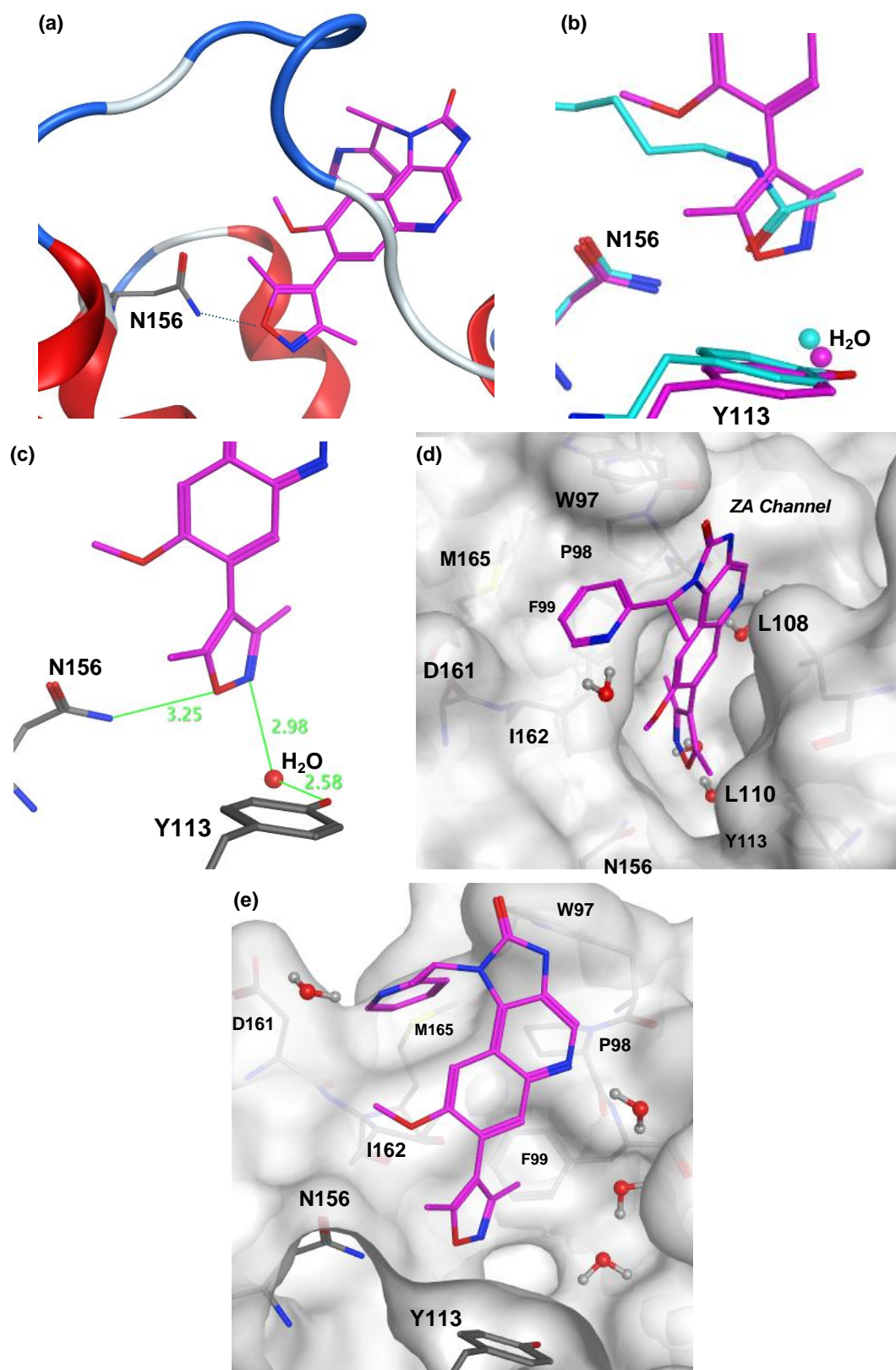


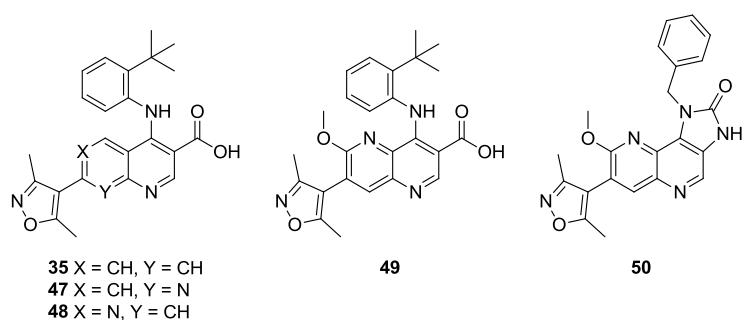
Figure 16. (a) X-ray crystal structure of I-BET151 (carbon = magenta) in BRD2 BD1 at 1.6 Å resolution (pdb 4ALG). (b) Superimposed complexes of I-BET151 (carbon = magenta, pdb 4ALG) and histone peptide H4₁₋₁₅K12Ac¹⁴ (carbon = cyan, pdb 2DVQ) in BRD2 BD1. (c) Hydrogen bond distances of I-BET151 (carbon = magenta) bound to BRD2 BD1 (pdb 4ALG). (d and e) Alternative protein surface representations of I-BET151 (carbon = magenta) in BRD2 BD1 (pdb 4ALG).

Developability assay data were disclosed in this same published report⁶⁴ and revealed lowered P450 inhibition, a negative Ames result, and reduced phosphodiesterase 4 (PDE4) inhibition for I-BET151 when compared to its close analogues. Generally, high *in vitro* metabolic stability was found for this compound and this translated *in vivo* with low blood clearance, and good oral bioavailability in both rat and mini-pig. Suitably low blood clearance and a moderate half-life in the mouse allowed *intravenous* (*i.v.*)-dosing of I-BET151 in the same endotoxaemia model used to assess I-BET762. In fact, a similar profile to I-BET762 was observed with I-BET151-pretreated mice showing reduced Il-6 levels after LPS challenge. In addition, mice treated prophylactically and therapeutically with I-BET151 showed a 100% survival rate after lethal injection with LPS; a result similarly achieved by I-BET762.⁴⁷

Advanced biological studies were conducted with I-BET151 demonstrating its potential in leukaemia treatment.⁶⁶ After members of the polymerase-associated factor complex (PAFc) and super elongation complex (SEC), complexes crucial for malignant transformation by mixed-lineage leukaemia (MLL) fusions, were identified to be associated with BRD3 and 4, the authors postulated that displacement of the BET proteins from chromatin using I-BET151 would provide therapeutic benefit. The efficacy of I-BET151 was then demonstrated in MLL-fusion leukaemic cell lines and in a mouse xenotransplant model of human MLL leukaemia, where mice treated with I-BET151 showed enhanced survival and reduced tumour size compared to an untreated group.

Overall, compelling evidence for use of I-BET151 as a therapeutic agent in specific leukaemias and inflammation was presented. By perturbing the recognition of histone tails by chromatin modifiers, I-BET151 provided further confirmation that small molecule BET inhibitors have utility in epigenetic therapy. Like I-BET762, further benefit would be gained by broadening the disease indications beyond the acute and aggressive diseases studied, as well as the investigation of alternative dosing methods. Also, no comparable data in BD1- and BD2-specific assays was presented and consequently the domain selectivity of I-BET151 is unknown.

More recently, a series of related 3,5-dimethylisoxazole naphthyridines were reported as novel BET inhibitors.⁶⁷ These analogues were synthesised to expand chemical diversity and improve aqueous solubility compared to their quinoline counterparts. Using similar chemistry to that previously reported by the same group,⁶³ the 1,6- and 1,8-naphthyridines (**47** and **48**, respectively) were synthesised and tested in BET WT FP and PMBC assays, and revealed lower activity relative to the quinoline analogue **35** (Figure 17).

Figure 17. 3,5-Dimethylisoxazole naphthyridines reported by Mirguet *et al.*⁶⁷

Comparison of the crystal structures of quinoline **35** and 1,6-naphthyridine **47** in BRD4 (not shown) did not provide an explanation for the difference in activity, so analysis of the minimum energy conformations in the unbound state was conducted.⁶⁷ Quantum mechanical calculations of the naphthyridine–isoxazole torsion angles showed that both naphthyridine isomers **47** and **48** possessed flatter conformations compared to quinoline **35**. It was therefore concluded that introduction of nitrogen atoms next to the aryl-aryl bond reduced activity by disfavoring the nonplanar conformation required for binding to the BET bromodomain. 1,5-Isomers were next explored and this allowed the incorporation of a beneficial methoxy group at the 6-position giving naphthyridine **49**, which displayed comparable binding activity to quinoline **35**. Using the same strategy reported for the quinoline series,⁶³ carboxamide then imidazolinone analogues were prepared resulting in compounds with improved cellular activity, such as imidazolinone naphthyridine **50**. With a PK profile in rat suitable for chronic oral administration, this compound was progressed into an acute inflammation mouse model where 60% reduction of plasminogen activator inhibitor-1 mRNA was observed upon dosing post LPS challenge.

These 3,5-dimethylisoxazole naphthyridines provided increased chemical diversity over the 3,5-dimethylisoxazole quinolines and offered the potential for fine-tuning of physicochemical properties. Good developability properties and PK profiles resulted from this exploration⁶⁷ and *in vivo* efficacy was demonstrated. However, one of the aims of this investigation was to improve solubility over quinoline derivatives but no comparison of data was made to allow assessment of this goal. Furthermore, as with the 3,5-dimethylisoxazole quinoline studies, no data was reported to establish the domain selectivity of these compounds.

A number of 3,5-dimethyl-4-phenylisoxazole derivatives were identified by the SGC as ligands for the BET protein family.^{68–70} Acquisition of dihydroquinazolinone isoxazole **51** (Figure 18a) and subsequent testing in a peptide-displacement ALPHA revealed low IC₅₀ values against BRD2 BD1 and BRD4 BD1 (~3 μM and ~7 μM, respectively).⁶⁸ With two

possible KAc mimetics in this molecule, an X-ray crystal structure in BRD4 BD1 unambiguously confirmed the 3,5-dimethylisoxazole as the Asn140-interacting moiety (Figure 18b). Electron density was unexpectedly found extending from the dihydroquinazolinone 4-position and this was determined to be an ethylene glycol unit resulting from oxidation under the crystallisation conditions giving the dihydroquinazolinone isoxazole structure **52**.

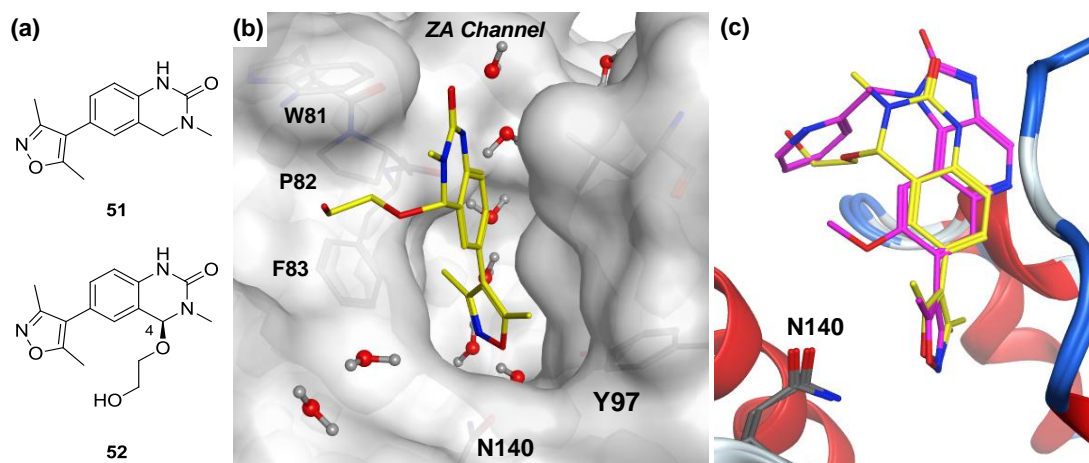
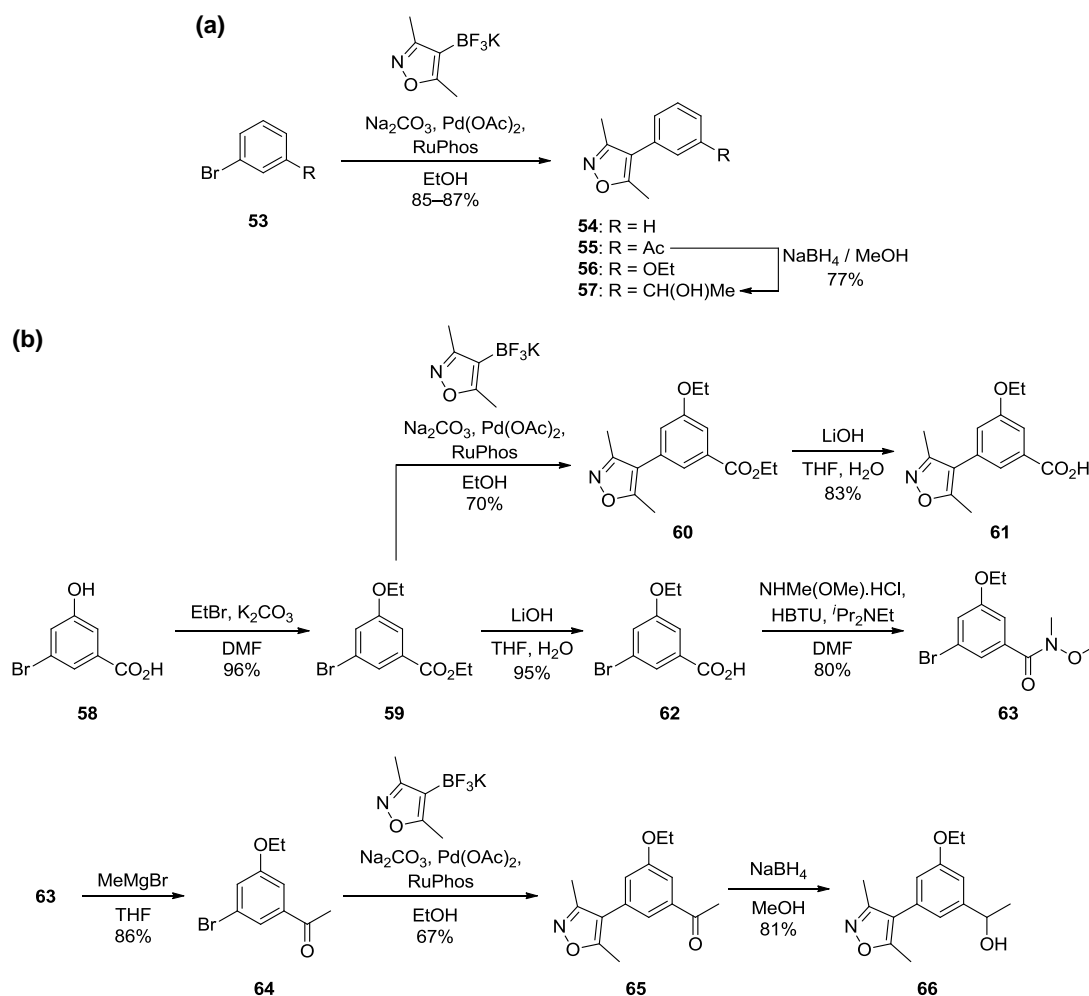


Figure 18. (a) Chemical structures of dihydroquinazolinone **51** containing the 3,5-dimethylisoxazole motif and its oxidation product **52**. (b) Crystal structure of dihydroquinazolinone **52** (carbon = yellow) in BRD4 BD1 at 1.98 Å resolution (pdb 3SVF). (c) Overlay of dihydroquinazolinone **52** (carbon = yellow, pdb 3SVF) and I-BET151 (carbon = magenta, pdb 3ZYU) in BRD4 BD1; solvent was omitted for clarity.

The dimethylisoxazole moiety of **52** made the same interactions to the bromodomain as I-BET151. The isoxazole oxygen accepted a hydrogen bond from Asn140, while the nitrogen made a through-water interaction to Tyr97. The methyl substituents made lipophilic contacts with Phe99 and Leu110. The dihydroquinazolinone ring was positioned in the hydrophobic cleft with the urea carbonyl and NH extending towards the ZA channel. Only the *S*-enantiomer of the oxidation by-product was resolved, with the ethylene glycol positioned in a hydrophobic groove on the WPF shelf. This substituent was expected to afford BET subfamily selectivity over other BCPs such as CREBBP. Therefore, compounds that lacked a readily oxidizable centre but possessed functionality to interact with the WPF shelf were synthesised.⁶⁸ In addition to the 3'-substituted 3,5-dimethyl-4-phenylisoxazole target compounds **54–57**, the 3',5'-disubstituted 3,5-dimethyl-4-phenylisoxazole analogues **60**, **61**, **65** and **66** were also synthesised to occupy the ZA channel as achieved by I-BET762, (+)-JQ1, and I-BET151 (Scheme 6).



Scheme 6. Synthesis of phenyl dimethylisoxazole analogues designed to occupy the WPF shelf and/or the ZA channel. (a) Preparation of 3-substituted compounds **54–57**. (b) Preparation of 3,5-disubstituted derivatives **60**, **61**, **65** and **66**.

Single step cross couplings with potassium (3,5-dimethylisoxazol-4-yl)trifluoroborate gave the 3-substituted compounds **54–56**, and in turn **57**, while 3,5-disubstituted targets **60**, **61**, **65** and **66**, were accessed using straightforward chemistry from 3-bromo-5-hydroxybenzoic acid **58**.

All 3,5-dimethylisoxazole derivatives were found to displace acetylated histone from BRD2 BD1 and BRD4 BD1 with reasonable activities (<50 μM).⁶⁸ Several substituents were tolerated with the secondary alcohol proving optimal, while additional substitution with an ethoxy group enhanced activity further, with 3,5-disubstituted **66** displaying IC₅₀ values of 4.8 μM and 1.6 μM against BRD2 BD1 and BRD4 BD1, respectively. Unlike dihydroquinazolinone **51**, the dimethylisoxazole **66** exhibited selectivity over CREBBP and confirmation of its specificity for the BET family was obtained upon DSF screening against a wide panel of other bromodomains but no selectivity was observed within the BET family. The BRD4 BD1 ligand efficiency (LE)⁷¹ of dimethylisoxazole **66** was 0.39, which compared

favourably with (+)-JQ1 (0.32), indicating that this low molecular weight structure made appreciably positive interactions with the protein. Indeed, this was confirmed by X-ray crystallography in BRD4 BD1 where key regions of the binding site occupied by (+)-JQ1 were also occupied by dimethylisoxazole **66** (Figure 19).⁶⁸

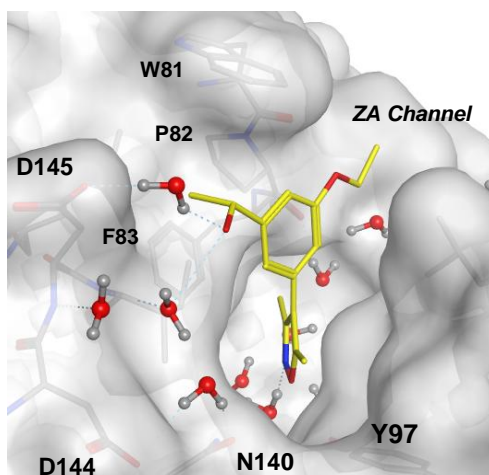
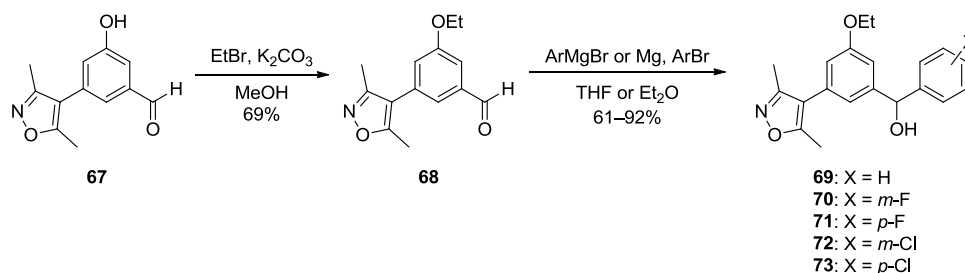


Figure 19. X-ray crystal structure of dimethylisoxazole **66** (carbon = yellow) bound to BRD4 BD1 at 1.68 Å resolution (pdb 3SVG).

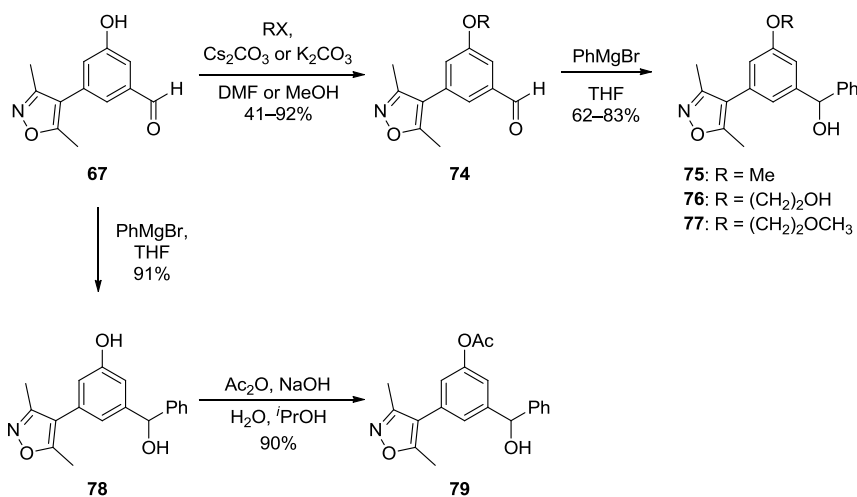
This compound made characteristic interactions of dimethylisoxazole-BET binding *i.e.* the oxygen accepted a hydrogen bond from the conserved asparagine and the nitrogen made a through-water hydrogen bond to Tyr97. While the secondary alcohol was synthesised in racemic form, only density for the *R*-enantiomer was observed.⁶⁸ In this configuration the methyl group was placed onto the WPF shelf and the alcohol directed into a water network interacting with Asp144 and Asp145.

A second publication from this group described the structure-driven optimisation of isoxazole **66** into more potent BET inhibitors with cellular activity.⁶⁹ Further exploration of the methyl and ethoxy groups, which occupied the WPF shelf and ZA channel, respectively, was conducted to enhance affinity with the BRD4 bromodomain. Inspired by the observed interaction of aryl groups with the WPF shelf in the crystal structures of I-BET762, (+)-JQ1, and I-BET151, the methyl group was replaced with halogenated phenyls by alkylation of intermediate phenol **67** followed by Grignard addition to the aldehyde **68** affording the target 3,5-dimethylisoxazoles **69–73** (Scheme 7).



Scheme 7. Synthesis of substituted aryls designed to enhance interaction with the WPF shelf.

Upon ALPHA screening, all diarylmethanols displayed higher BRD4 BD1 potency than the ethanol **66** with the unsubstituted phenyl **69** determined as the most potent (640 nM).⁶⁹ Attention then turned to displacing, or interacting with, water molecules present in the ZA channel, where phenol, acetate, methoxy, ethylene glycol and *O*-ethylmethoxy groups were introduced in place of the ethoxy group (Scheme 8).



Scheme 8. Modification of the ethoxy group occupying the ZA channel.

Testing in the BRD4 ALPHA revealed highest affinities for the acetate **79** (IC₅₀ = 371 nM) and phenol **78** derivatives.⁶⁹ Chiral resolution of phenol **78** was conducted and comparable activities of the individual enantiomers (*S*)-**78** and (*R*)-**78** were found upon testing in the ALPHA (IC₅₀ = 386 nM and 382 nM, respectively) and by SPR (*K_D* = 0.36 and 0.39 μM, respectively). To further understand this SAR, crystal structures were obtained which revealed identical binding modes for each enantiomer (Figure 20).

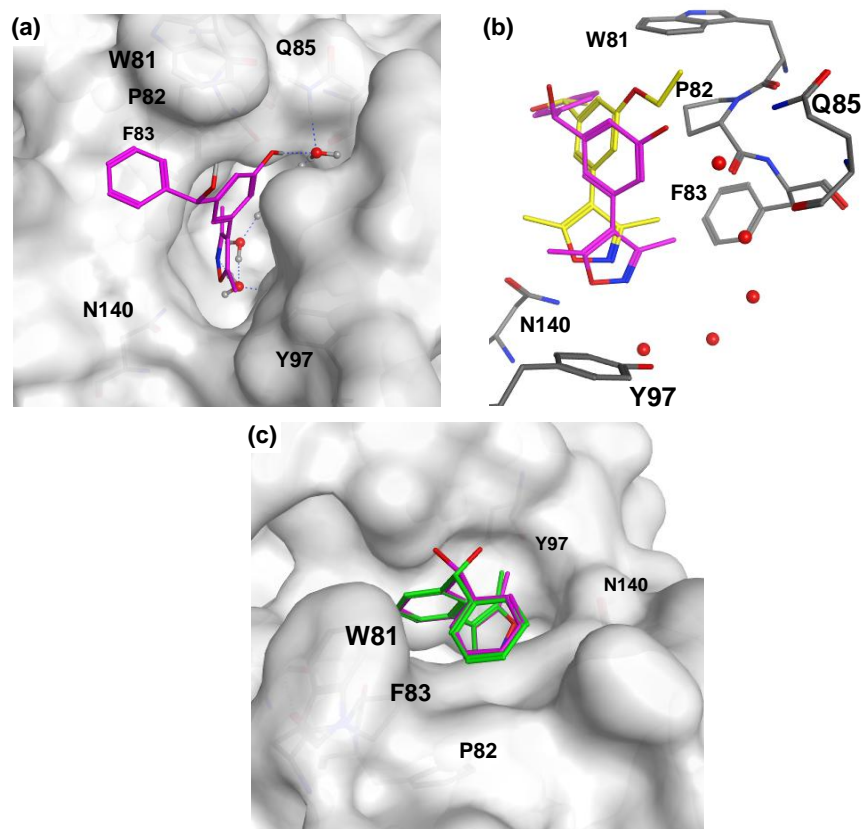


Figure 20. (a) Binding mode of phenol (*S*)-**78** (carbon = magenta) in BRD4 BD1 (pdb 4J0S). (b) Superposition of the BRD4 BD1 X-ray crystal structures of phenol (*S*)-**78** (carbon = magenta, pdb 4J0S) and ethoxy **66** (carbon = yellow, pdb 3SVG). (c) Structural overlay of the enantiomeric phenols (*S*)-**78** (carbon = magenta, pdb 4J0S) and (*R*)-**78** (carbon = green, pdb 4J0R) bound to BRD4 BD1.

The dimethylisoxazole moiety of phenol (*S*)-**78** interacted with Asn140 and Tyr97 in the usual manner but deeper binding was observed compared to the ethoxyphenyl **66**. The phenyl rings of both (*S*)-**78** and (*R*)-**78** occupied the WPF shelf and directed the alcohol groups towards solvent; this provided an explanation for the similar activities measured for each stereoisomer. The phenol hydroxyl groups of both enantiomers successfully formed hydrogen bonds to a tightly bound water molecule in the ZA channel.

With the wider bromodomain screening indicating a selective profile for phenol (*S*)-**78**, assessment in cancer cell lines followed.⁶⁹ Cytotoxicity in MV4;11 cells, an AML cell line, was observed at an IC₅₀ value of 794 nM, but was reduced with respect to (+)-JQ1. Lowered cytotoxicity in lung adenocarcinoma cell lines was also found but this was consistent with the weak growth inhibition of I-BET151 in solid tumour lines.

These investigations by Hewings *et al.* have provided further examples of dimethylisoxazole-containing BET inhibitors with novel SAR and have resulted in promising leads.^{68,69} Additional experiments such as determining the developability characteristics (e.g. solubility, PK) and assessing efficacy in non-oncologic settings would be

required to elevate the utility of these compounds to match that of I-BET151. Determination of domain selectivity within the BET family of BCPs would also be of interest to the scientific community.

The 3,5-dimethylisoxazole KAc mimetic also featured in a series of simple 5- and 6-benzimidazoles developed as potential BET inhibitor leads.⁷⁰ In this study, previously unexplored vectors were accessed from 5-membered rings fused to 4-aryl-3,5-dimethylisoxazole units. From the initially prepared scaffolds **80–83** (Figure 21), benzimidazole **81** showed the highest BRD4 BD1 activity ($pIC_{50} = 5.2$) using an ALPHA, but exhibited almost equal activity against CREBBP ($pIC_{50} = 5.4$). Despite the indanone **82** showing the weakest BRD4 BD1 activity ($pIC_{50} = 4.2$), this scaffold was used as the basis for further chemistry-development.

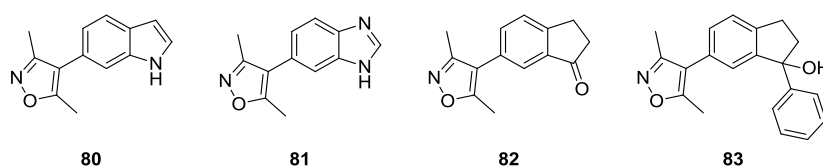


Figure 21. 5,6-Fused aryl-dimethylisoxazoles.

The carbonyl oxygen was used as a handle to append basic functionality in an effort to interact with Asp145 at the beginning of the C-helix.⁷⁰ However, no appreciable activity was gained. Reminiscent of the favourable secondary alcohol moiety present in the previously reported BET ligand **66**,⁶⁸ the authors incorporated a tertiary alcohol moiety by reaction of ketone **82** with phenylmagnesium bromide. The resulting nucleophilic addition product **83** displayed increased activity at BRD4 BD1 ($pIC_{50} = 5.9$) and increased selectivity against CREBBP ($pIC_{50} = 4.7$) relative to indanone **82**. An X-ray crystal structure of the tertiary alcohol **83** was solved in BRD4 BD1 with an *R*-configuration determined at the benzyl position (Figure 22a).

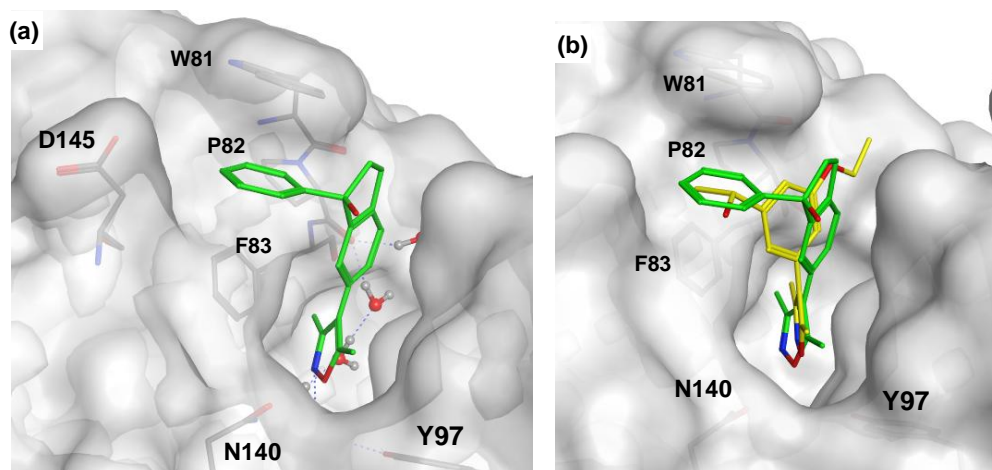
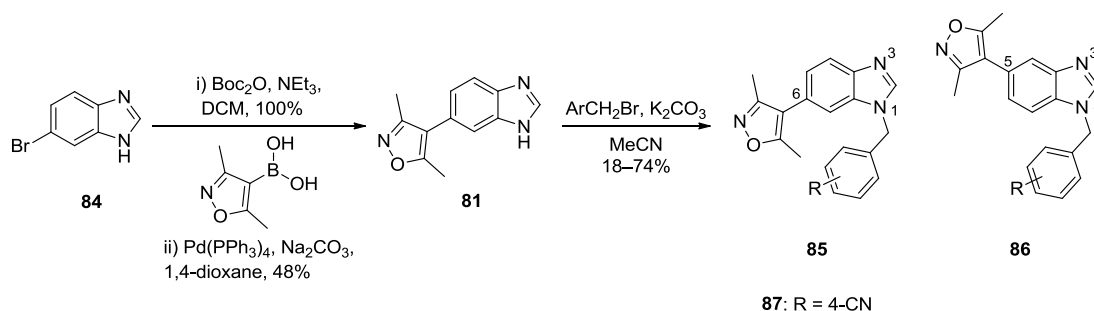


Figure 22. (a) Tertiary alcohol **83** (carbon = green) crystal structure in BRD4 BD1 (pdb 4GPJ). (b) Overlay of tertiary alcohols **83** (carbon = green, pdb 4GPJ) and **66** (carbon = yellow, pdb 3SVG) bound to BRD4 BD1.

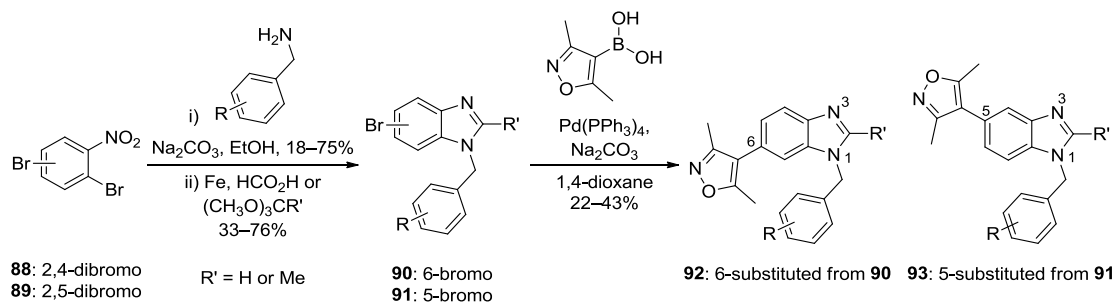
This compound displayed the usual dimethylisoxazole binding mode, with hydrogen bonding to Asn140 and through-water hydrogen bonding to Tyr97. The phenyl group sat in the hydrophobic pocket on the WPF shelf but unlike the secondary alcohol in **66**, the tertiary alcohol here did not make any interactions. In fact, when the crystal structures of indenol **83** and phenylethanol **66** were aligned, the OH groups were positioned over 3 Å apart due to the accommodation of the larger phenyl group of **83** on the WPF shelf (Figure 22b).

Unfortunately, during the attempted synthesis of further indenols, dehydration of the doubly benzylic alcohols occurred affording the corresponding indenenes.⁷⁰ Further chemistry was therefore conducted on the more stable benzimidazole 5,6-system, but mixtures of regioisomers were obtained with reactions of the azole. Ullmann arylation products gave weaker activity than their benzylated counterparts, with the benzyl unit being incorporated at the last stage in the synthesis, as outlined in Scheme 9. Initial *t*-butyloxycarbonyl (Boc)-protection of the bromobenzimidazole **84** improved yields of the Suzuki-Miyaura coupling with 3,5-dimethylisoxazolylboronic acid. *In situ* deprotection followed by alkylation gave mixtures of 6-substituted (**85**) and 5-substituted (**86**) regioisomers.



Scheme 9. Preparation of substituted benzimidazoles **85** and **86**.

While the products were separable, their identity was assumed from their chromatographic elution order by comparison of compounds prepared *via* both the unselective-separation route and the regioselective route shown in Scheme 10.⁷⁰



Scheme 10. Regioselective synthesis of benzimidazoles **92** and **93**.

Based on all of this, the most potent compound **87** (Scheme 9) was identified as the 6-isoxazolyl isomer.⁷⁰ This molecule demonstrated 180 nM activity for BRD4 BD1 and excellent selectivity over CREBBP as determined in an ALPHA. Wider selectivity over other BCPs was confirmed with DSF studies.

This work further demonstrates the utility of the 3,5-dimethylisoxazole as an effective KAc mimetic. The 5,6-fused benzimidazole scaffold presented differentiated vectors for growth but further verification of substitution patterns would be preferable when preparing analogues of this fused ring system. Also, the developability characteristics of these compounds were not determined, hindering their evaluation as suitable leads for further optimisation. Further assessment of bromodomain selectivity within the BET family for this series of compounds would also be valuable to the research community.

Complementing the studies described to this stage, our laboratories have reported the fragment-based discovery of phenylisoxazole sulfonamides as BET inhibitors in a proof-of-principle study.⁷² A fragment approach was attractive as a number of crystal structures had been solved in multiple chemical series revealing a sufficiently large and deep binding site to facilitate fragment binding. Screening of a focused fragment set targeting the KAc pocket was carried out in a FA assay format in BRD2, 3 and 4 WT proteins. From these screens, 3,5-dimethyl-4-phenylisoxazole **54** was identified as a hit and was selected for optimisation (Figure 23).

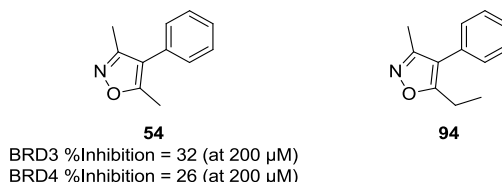


Figure 23. Structure of 3,5-dimethyl-4-phenylisoxazole hit **54** and its 5-ethyl congener **94**.

A crystal structure in BRD2 BD1 was obtained and showed a binding mode analogous to other dimethylisoxazoles by mimicking KAc recognition (Figure 24a and b).⁷² The phenyl ring was sandwiched in a cleft between Pro98 and Leu108 and was rotated relative to the 3,5-dimethylisoxazole ring with torsion angles ranging between 51–59° within the asymmetric unit. These values were slightly greater than that of the minimised conformer determined by the quantum mechanical calculations (44°), although the energy difference was deemed negligible.

The isoxazole methyl groups occupied hydrophobic pockets while the nitrogen and oxygen ring atoms were bisected by the KAc carbonyl upon superimposition with the structure of diacetylated histone peptide H4_{1–20}K5AcK8Ac¹⁴ in mouse Brdt⁷³ (Figure 24c).

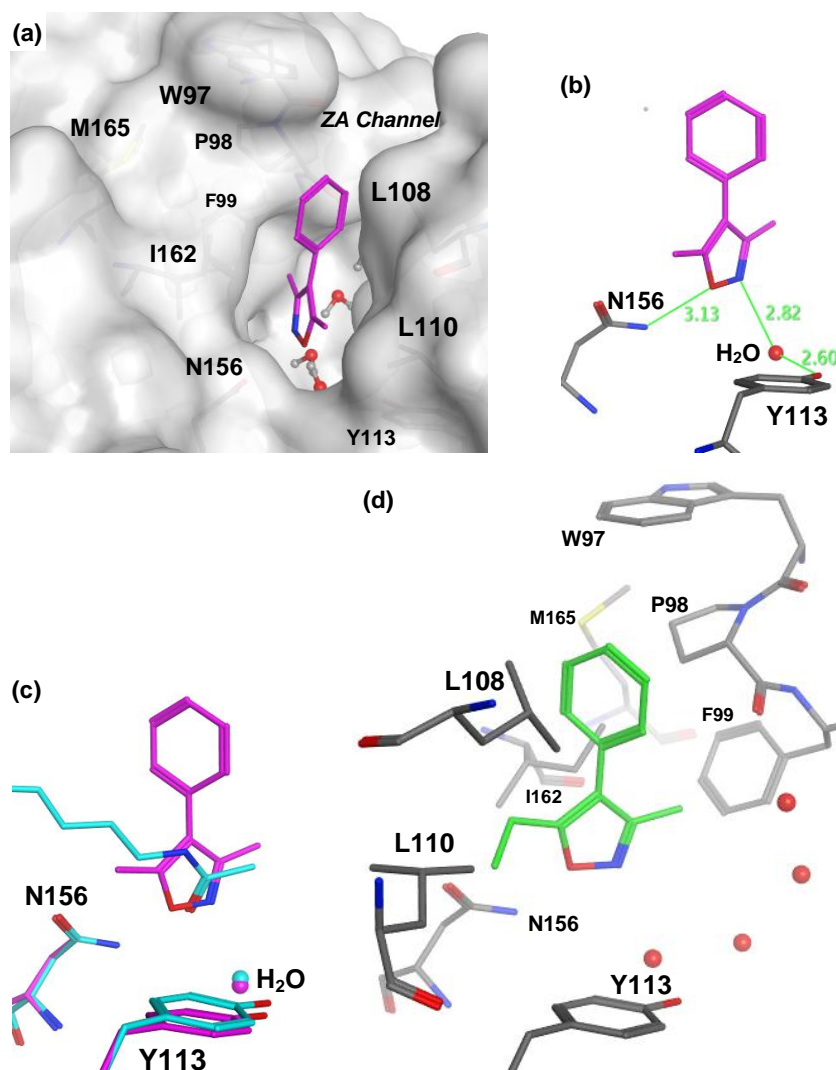


Figure 24. (a) X-ray structure of 3,5-dimethyl-4-phenylisoxazole **54** (carbon = magenta) in complex with BRD2 BD1 (pdb 4ALH). (b) Polar interactions of the isoxazole unit with BRD2 BD1 (pdb 4ALH). (c) Superimposition of the isoxazole **54** BRD2 BD1 complex (carbon = magenta, pdb 4ALH) with the H4_{1–20}K5AcK8Ac¹⁴ mouse Brdt BD1 complex (carbon = cyan, pdb 2WP2). (d) Structure of the 5-ethyl-3-methyl isoxazole **94** (carbon = green) in BRD2 BD1 determining the orientation of heteroaromatic ring (pdb 4A9O).

These observations prompted investigation into the orientation of the isoxazole ring, which appeared essentially symmetrical with electron density unable to differentiate the position of the heteroatoms unambiguously.⁷² The angle of interaction to the water deviated by 50° from that of an ideal electron lone pair, and the interaction distances to water and Asn156 through each atom were similar (2.7–2.9 Å) casting further uncertainty. By incorporation of a larger ethyl substituent at the 5-position of the isoxazole ring, the orientation of the heterocycle was determined as shown in the crystal structure of **94** (Figure 24d). However, the possibility that the 5-ethyl substituent could induce a switch in the isoxazole binding mode, swapping the positions of the nitrogen and oxygen atoms, was not considered.

A 3D pharmacophore was generated based upon a number of ligand-BET X-ray structures and this was used to search a database of commercial compounds resulting in the identification of a series of sulfonamide isoxazoles **95** (Figure 25).⁷² Improved activities and LEs over the original fragment hit **54** were realised with the tolylsulfonamide **96** displaying 100-fold increased activity.

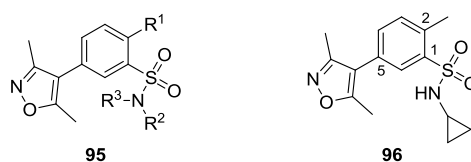


Figure 25. Sulfonamide isoxazoles identified from pharmacophore searching.

A crystal structure of **96** in BRD2 BD1 was obtained and confirmed the pharmacophoric features (Figure 26).⁷² The binding mode was similar to the hit compound **54** but with additional water interactions from the sulfonamide moiety and occupation of cyclopropyl substituent on the WPF shelf.

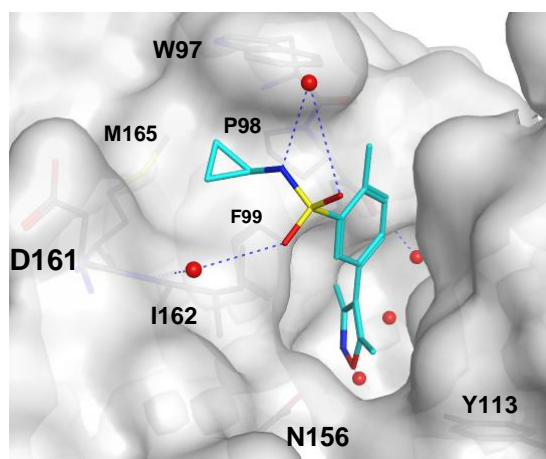
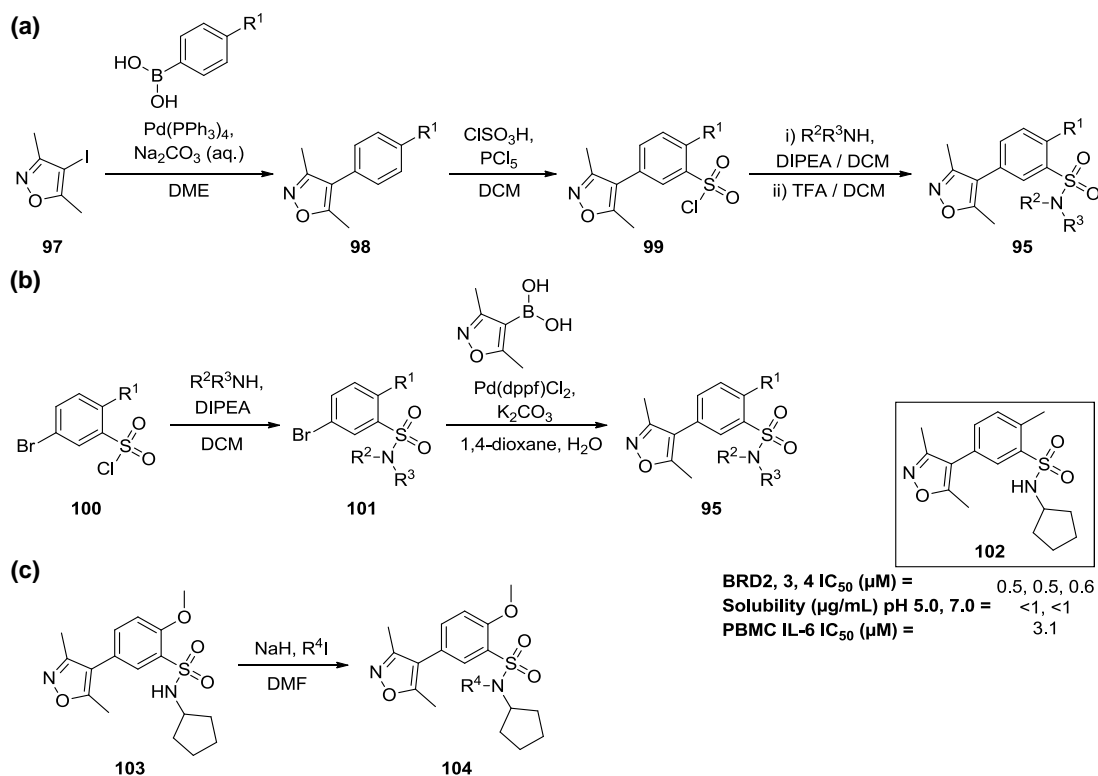


Figure 26. Complex of sulfonamide **96** (carbon = cyan) in BRD2 BD1 (pdb 4A9N).

To investigate the SAR, chemistry was carried out to synthesise analogues that were unavailable from commercial suppliers (Scheme 11).⁷² Compounds containing either a methyl or methoxy group at the 2-position (R^1) were targeted.

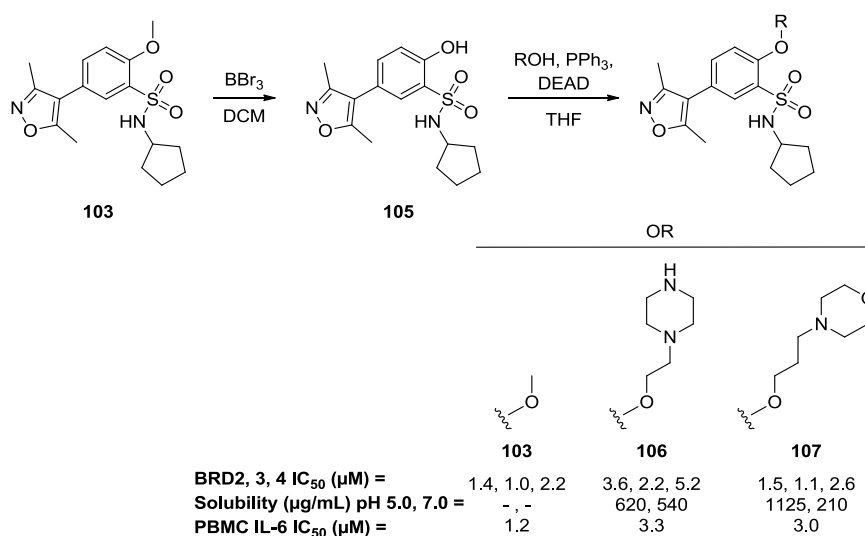


Scheme 11. Routes used to access sulfonamide isoxazole analogues.

A Suzuki-Miyaura coupling of 4-iodo-3,5-dimethylisoxazole **97** with the appropriately substituted phenyl boronic acid followed by sulfonylation and chlorination gave the sulfonyl chloride **99**, which was used to form the target compounds **95** (Scheme 11a).⁷² Alternatively, the sequence could be reversed by firstly condensing 5-bromo-2-substituted phenylsulfonyl chlorides **100** with amines to give sulfonamides **101**, followed by cross-coupling with (3,5-dimethylisoxazol-4-yl)boronic acid (Scheme 11b). Tertiary sulfonamide target compounds **104** were obtained by simple deprotonation and alkylation of the secondary sulfonamide **103** (Scheme 11c).

An SAR investigation was conducted and the results rationalised using structural information.⁷² The preferred compound identified from this investigation, cyclopentyl analogue **102**, exhibited LEs equivalent to cyclopropyl sulfonamide **96** but poor aqueous solubility was an issue. Utilising structural insight, the 2-position was identified as a vector to incorporate solubilising groups. Accordingly, the piperazine **106** and morpholine **107** were prepared from the 2-methoxy sulfonamide **103** (Scheme 12). These compounds significantly improved aqueous solubility but are likely to incur a significant LE cost (LE data were not

presented). Encouragingly, inhibition of IL-6 production in LPS-stimulated PBMCs was observed at micromolar IC_{50} s.⁷²



Scheme 12. Synthesis of analogues designed to improve solubility.

This research nicely demonstrated the tractability of BET BCPs towards fragment-based drug discovery (FBDD). X-ray crystallography was used to confirm the binding modes of hits and guide selection for focused screening. Through compound acquisition and synthesis, extensive SAR was developed with many examples showing desirable LE values. One limitation of these compounds was the inherent low solubility. FBDD optimisation principles were forsaken to overcome this by incorporation of poorly ligand-efficient solubilising groups. Nevertheless, morpholine **107** exhibited sufficient activity to show efficacy in human PBMCs and aqueous solubility to be suitable for *i.v.* administration, if required. Unfortunately, whole blood and domain-selectivity data were not reported for the optimised compounds.

From the array of dimethylisoxazole BET inhibitors discussed, I-BET151 stands out as the most developed compound with PK properties suitable for assessment within *in vivo* disease models.^{63,64,66} Other dimethylisoxazoles, such as the phenyl dimethylisoxazoles by Hewings *et al.*^{68,69} and the benzimidazole dimethylisoxazoles by Hay *et al.*,⁷⁰ are less developed but show promise as lead molecules for further optimisation while the phenylsulfonamide dimethylisoxazoles from Bamborough *et al.*⁷² demonstrated that optimisation of a weakly-active dimethylisoxazole fragment was possible. However, in all of these studies, data pertaining to properties required for *i.v.* administration, such as aqueous solubility or whole blood activity, were either unreported or revealed incompatibility for this dosing method. Furthermore, determinations of domain selectivities within the BET family

were not carried out in these studies; this constitutes data which is of considerable interest to the research community in this arena.

1.7. Other BET Inhibitors

Fragment-based screening has been particularly fruitful in the identification of BET inhibitors with orthogonal KAc mimetics.⁷⁴ In this study by Chung *et al.*, a focused set of fragments containing a hydrogen bond acceptor (HBA) and a small alkyl group to mimic KAc was created. Screening at single concentrations yielded 132 fragments and hits were confirmed in full dose-response curve mode. Forty fragment-protein complexes were obtained after soaks in apo BRD2 BD1 crystals and the most frequent ligand-interacting residues were determined to be the conserved asparagine and tyrosine, Asn156 and Tyr113, the gatekeeper Ile162, and the WPF motif. The detailed binding modes of representative fragments were revealed and are shown in Figure 27.

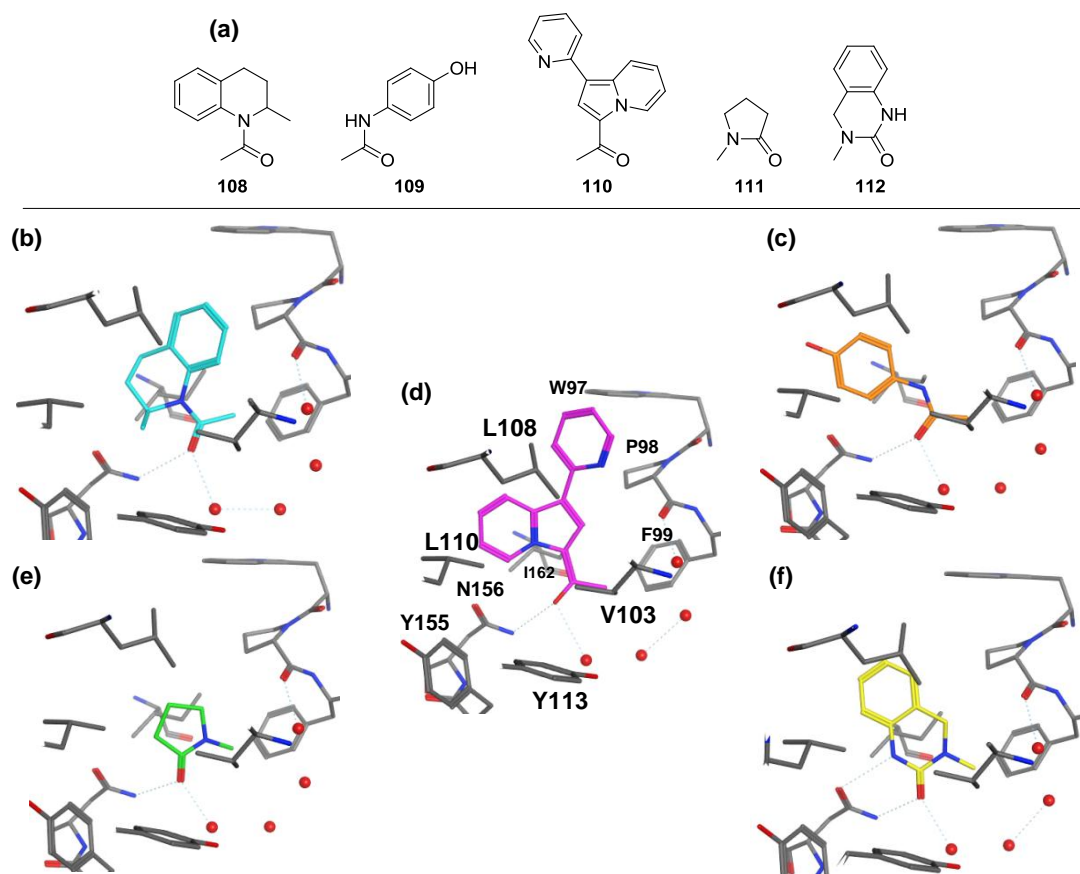


Figure 27. (a) Chemical structures of representative fragments. (b–f) X-ray crystal structures in BRD2 BD1. (b) THQ **108** (carbon = cyan, pdb 4A9H). (c) Paracetamol **109** (carbon = orange, pdb 4AJ). (d) Indolizine methylketone **110** (carbon = magenta, pdb 4A9I). (e) NMP **111** (carbon = green, pdb 4A9F). (f) 3-Methyl-3,4-dihydroquinazolinone **112** (carbon = yellow, pdb 4A9E).

Racemic *N*-acetyl-2-methyltetrahydroquinoline (THQ) **108** was soaked into apo BRD2 BD1 resulting in a crystal complex of only the *S*-enantiomer (Figure 27b).⁷⁴ The *N*-acetyl functionality successfully mimicked KAc by interaction of the carbonyl oxygen with Asn156 and through-water to Tyr113, and occupation of the pocket adjacent to Phe99 by the methyl group. The THQ ring was sandwiched between the hydrophobic residues Pro98 and Leu108, as well as the gatekeeper Ile162. The 2-methyl group occupied another lipophilic pocket and the preference for the *S*-enantiomer was rationalised by an expected clash between Asn156 and the C2-methyl of the *R*-enantiomer.

Despite its weak binding in the FA assays, a crystal structure of acetaminophen (Paracetamol) **109** in BRD2 BD1 was obtained after a high concentration soak and resulted in a binding mode analogous to that of THQ **108** (Figure 27c).⁷⁴ The acetamide oxygen interacted with Asn156 and water as expected, while the phenyl ring was flanked by the lipophilic residues Ile162 on one side, and Leu108 and Leu110 on the other. As the MOA of paracetamol is unclear, the possibility that it may exert its analgesic and anti-inflammatory effects through BCPs was discussed. Although activities at BRD2, 3 and 4 were weak, its small size and propensity to bind to other bromodomains, such as CREBBP (an X-ray structure was obtained confirming this), and probable cumulative bromodomain-engagement *in vivo*, was suggested as a possible mechanism for Paracetamol's physiological effects.

The structure of indolizine methylketone **110** showed that this fragment mimicked KAc by interactions through the ketone oxygen atom (Figure 27d).⁷⁴ The fused ring system sat in the lipophilic pocket between Ile162 and Leu108. The pyridyl substituent occupied the WPF shelf but the orientation of the ring was ambiguous as no water binding to the pyridine nitrogen was observed. Due to its larger size, the IC₅₀s of this fragment in the FA assays were measurable giving values in the range 2.6–6.31 μM for BRD2, 3 and 4 and subsequent testing in LPS-stimulated PBMCs showed respectable IL-6 inhibition (IC₅₀ = 14 μM).

Crystallisation experiments were conducted on another weakly active fragment from the FA screen, *N*-methylpyrrolidinone (NMP) **111**, resulting in the structure shown in Figure 27e.⁷⁴ The binding modes of ligands discussed in this manuscript up until this point made the key KAc-interactions through an acceptor and methyl group separated by one atom. With NMP however, two atoms separate the acceptor (the carbonyl oxygen) and the methyl group (substituted on the amide nitrogen). This result expanded understanding of the requirements for BET bromodomain binding and provided opportunity for discovery of new KAc-mimetics.

Finally, 3-methyl-3,4-dihydroquinazolinone **112** was successfully crystallised in BRD2 BD1 and a X-ray structure solved (Figure 27f).⁷⁴ Like NMP, the KAc binding features

were incorporated within a ring and the HBA and methyl group were separated by two atoms. The acceptor functionality was provided by the carbonyl oxygen and the *N*-methyl substituent occupied the Phe99 subpocket. An additional HBD interaction was made by the urea NH to Asn156 affording an overall bidentate interaction between the urea and the conserved asparagine.

Further exploration of fragment **112** was conducted through analogue searching within the GSK screening collection and subsequent testing in the FA assays.⁷⁴ The sulfonamide derivative **113** showed higher potencies ($IC_{50} = 14\text{--}40\ \mu\text{M}$) than the parent compound and possessed LEs in the range 0.25–0.27 (Figure 28a). Notably, this compound possessed an *N*1-methyl group which was not present in fragment **112** and therefore could not participate in a similar bidentate interaction to the conserved asparagine. The precise binding mode was determined in BRD4 BD1 and was found to be very similar to that of the parent compound **112** (Figure 28b and c). Interestingly, the additional *N*-methyl group was accommodated by puckering of the fused ring system. The expected loss of binding energy resulting from this movement may have been recovered by additional interactions of the morpholine sulfonamide on the WPF shelf.

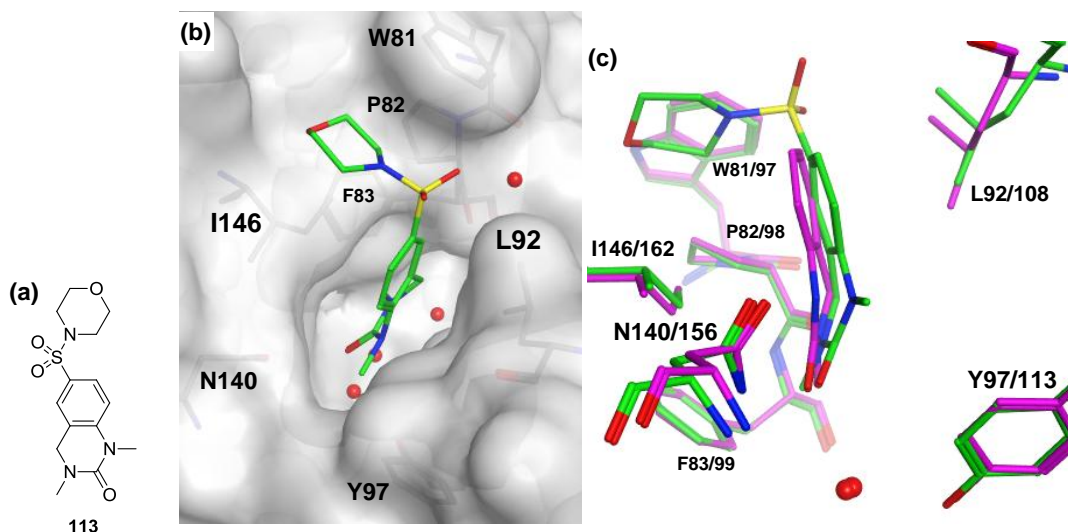


Figure 28. (a) Chemical structure of sulfonamide **113**. (b) Complex of sulfonamide **113** (carbon = green) with BRD4 BD1 (pdb 4A9L). (c) Structural overlay of 1,3-dimethyl dihydroquinazolinone **113** in BRD4 BD1 (carbon = green, pdb 4A9L) with 3-methyl-3,4-dihydroquinazolinone **112** in BRD2 BD1 (carbon = magenta, pdb 4A9E).

The X-ray complexes presented in this paper significantly expanded the scope of KAC-mimetics known at the time and demonstrated that BET bromodomains were attractive targets for FBDD and prompted further investigation by other groups.

For example, the promising activities and high LEs determined for dihydroquinazolin-2(1*H*)-one **112**,⁷⁴ stimulated optimisation of this fragment by Fish and co-workers into a potent and selective BET probe molecule.⁷⁵ Firstly, the binding mode of the 6-bromo

substituted dihydroquinazolin-2(1*H*)-one **114** (Figure 29) was determined by solving a cocrystal structure in BRD4 BD1.

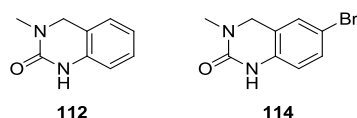


Figure 29. Fragments screened at Pfizer and the SGC.

In contrast with Conway's studies with the dihydroquinazolinone dimethylisoxazole **51**,⁶⁸ no oxidative reactivity was seen during the crystallisation process.⁷⁵ The binding mode matched that determined by Chung *et al.* in BRD2 BD1⁷⁴ with the cyclic urea located in the KAc recognition pocket with the additional bromine directed towards solvent.⁷⁵ From here, substituted sulfonamides were introduced to generate a structural kink to access the WPF shelf in the pursuit of selectivity. Synthesis of these sulfonamides involved sulfonylation of 3-methyl-3,4-dihydroquinazolin-2(1*H*)-one **112** to the 6-sulfonylchloride **115**, followed by reaction with various amines, while the reverse sulfonamides were obtained through nitration of 3-methyl-3,4-dihydroquinazolin-2(1*H*)-one **112** and subsequent reduction to the 6-amine **120**, which was used for sulfonamide library synthesis (Figure 30).⁷⁵

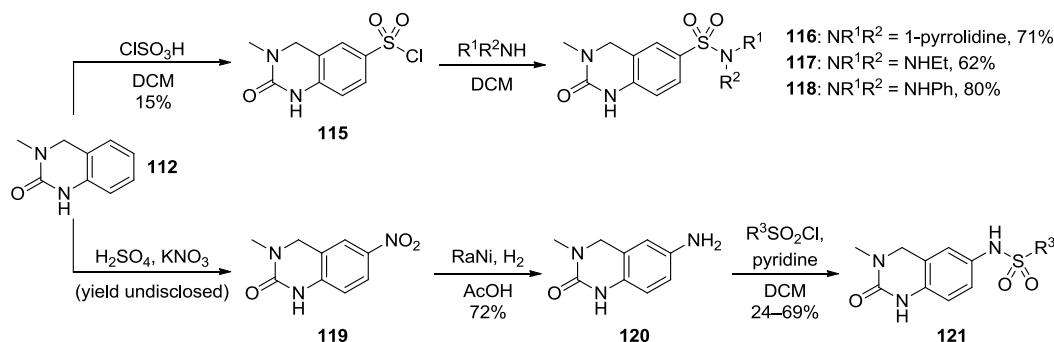


Figure 30. Synthesis of sulfonamide dihydroquinazolin-2(1*H*)-ones.

Coupling products (**116–118**) derived from the 6-sulfonylchloride **115** were tested in the BRD4 BD1 peptide-displacement ALPHA.⁷⁵ Activities (1.9–4.8 μM) and LEs (0.33–0.40) were lower than the parent unsubstituted or 6-bromo compounds with aryl sulfonamides being worse than alkyl sulfonamides.

Improved activities were obtained with the reversed sulfonamides **121** linked to aryl groups.⁷⁵ A variety of substituents on the aryl ring were tolerated with *ortho*-substitution being preferred. In particular, the 2-methoxyphenyl (PFI-1, Figure 31a) inhibited BRD4 BD1-peptide binding with an $\text{IC}_{50} = 0.22 \mu\text{M}$ resulting in a LE = 0.38. Although this LE value was reduced compared to the starting fragments, and was comparable to the unpreferred alternative sulfonamides **116** and **117**, the potency met the probe criteria of 100–

300 nM and thus, PFI-1 was crystallised in BRD4 BD1 to investigate the binding mode of this compound (Figure 31).⁷⁵

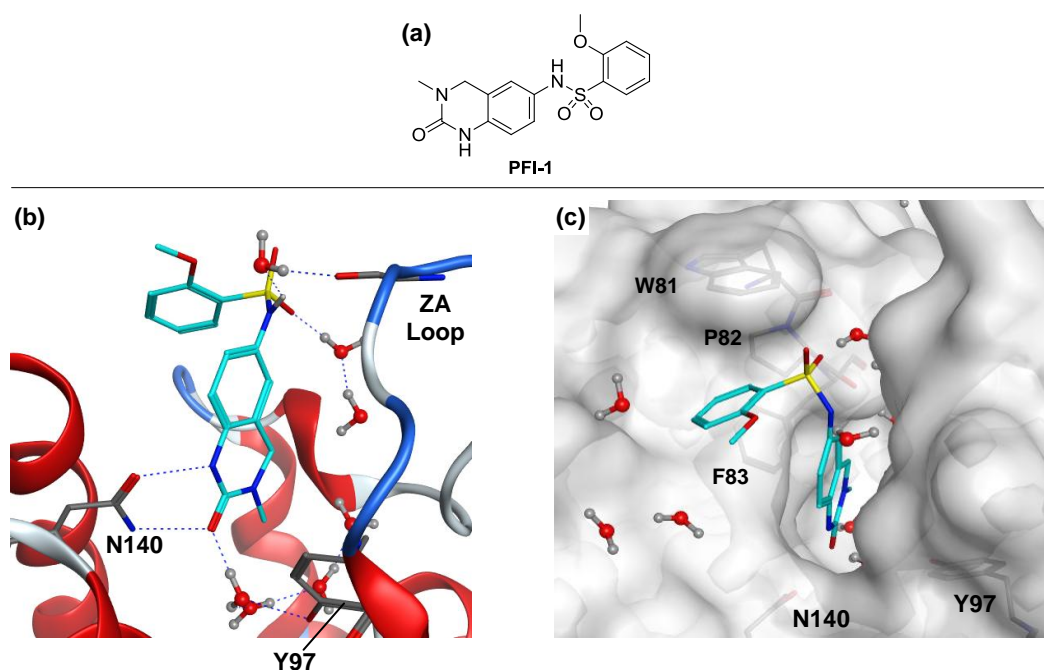


Figure 31. (a) Structure of 3-methyl-3,4-dihydroquinazolin-2(1*H*)-one PFI-1. (b and c) High resolution crystal structure of PFI-1 (carbon = cyan) in BRD4 BD1 (pdb 4E96).

Consistent with the fragment structure, PFI-1 interacted with the conserved asparagine in a complementary manner and formed a through-water hydrogen bond to the conserved tyrosine. The aryl group of the sulfonamide occupied the hydrophobic pocket on the WPF shelf while the NH of the sulfonamide made contact with a water molecule bound to the carbonyl of Leu92 on the ZA loop.

In addition to improving potency over the parent fragment hits **112** and **114**, the 6-sulfonamide moiety also enhanced BET family selectivity.⁷⁵ DSF measurements revealed a low ΔT_m value for CREBBP (1.7 °C) and negligible shifts ($\Delta T_m < 1.0$ °C) for other representative bromodomains PCAF, BAZ2B, and PB1. These values were all less than those obtained for the BET proteins (ΔT_m 2.1–6.5 °C) where little selectivity between BD1 and BD2 within a single protein was observed. Screening of PFI-1 against a panel of kinases, enzymes, ion channels, and G protein-coupled receptors (GPCRs) showed no significant activity and therefore results from testing in a LPS-stimulated PBMC assay could solely be attributed to BET bromodomain inhibition. In this regard, PFI-1 inhibited IL-6 production with an $EC_{50} = 1.89$ μ M, demonstrating cell membrane permeability and efficacy in prevention of inflammation. In rat PK studies with this compound, inconsistency between the low clearance (18 mL/min/kg) and only moderate oral bioavailability (32%) was explained by limited solubility providing low but steady concentrations till 7 h after dosing.

While this compound presents a complementary probe, I-BET151 and (+)-JQ1 are more potent, exhibit superior PK properties, and have proven efficacy in models of disease. No aqueous solubility data for PFI-1 was presented but interpretation of PK data led the authors to suggest the compound was poorly soluble,⁷⁵ which could be a limiting factor for further development. Furthermore, the authors note in the reference section that PFI-1 was unstable with respect to C-4 oxidative insertion of nucleophiles (e.g. DMSO) when stored for extended periods. Also, accurate measurement of affinities for individual bromodomains within the BET family was not performed in this study. The demonstration that a fragment hit can be optimised into a ligand efficient and selective BET inhibitor is perhaps the foremost contribution from this individual body of research.⁷⁵

The FBDD approach was also used in the identification of a series of 2-thiazolidinone inhibitors of BRD4.⁷⁶ Here, a fragment library was constructed from a free database of commercially-available compounds using a range of molecular descriptor filters. Computational dockings in BRD4 BD1 were then used to identify fragments with the ability to bind Asn140, and 41 of these molecules were selected for crystallisation attempts. Out of the nine crystal structures solved, only those corresponding to the fragments shown within Figure 32 were revealed in this published report.⁷⁶

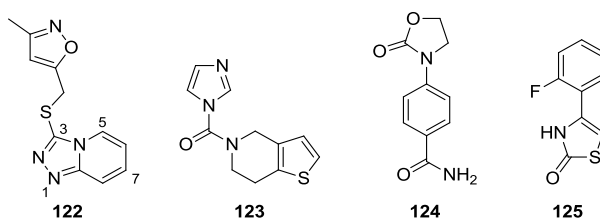
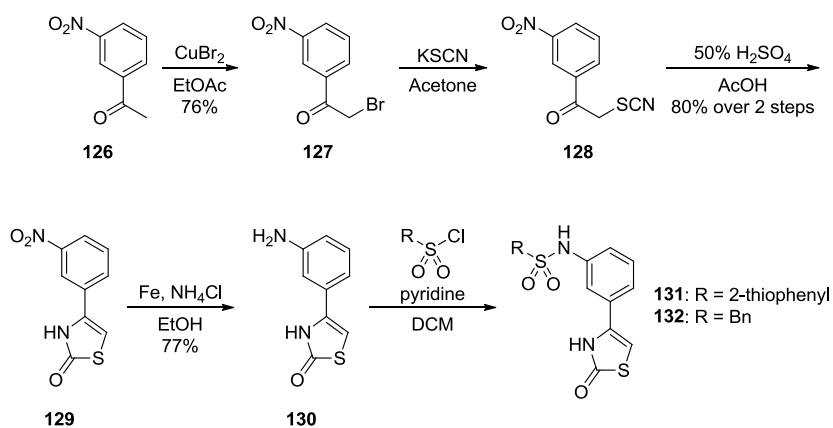


Figure 32. Chemical structures of disclosed fragments

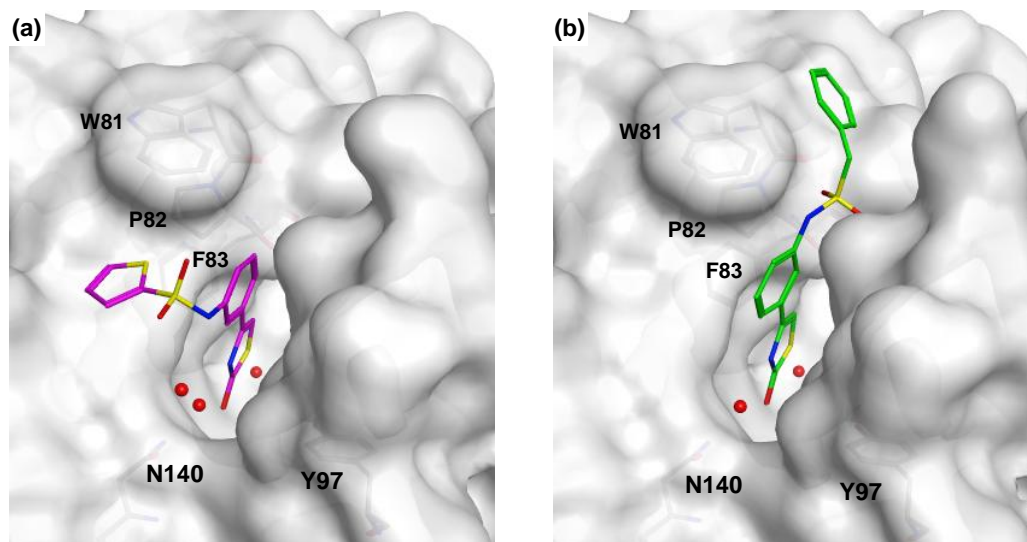
All fragments were found to bind at the KAc recognition site but, intriguingly, none of the compounds possessed a methyl group for a lipophilic contact next to Phe83. Comparisons of the crystal structure of phenylthiazolidinone **125** and those of (+)-JQ1 and 3,5-dimethyl-4-phenylisoxazole **54** indicated the *meta*- and *para*-positions of the phenyl ring as suitable vectors to gain further protein interactions.⁷⁶ In particular, sulfonamides and amides were incorporated to provide access to the WPF shelf using the preparative sequence shown in Scheme 13, with an additional regioisomer of the starting nitrophenylethanone also being employed in order to explore *para*-substitution.



Scheme 13. Synthesis of the 3-substituted phenylthiazolidinone sulfonamides.

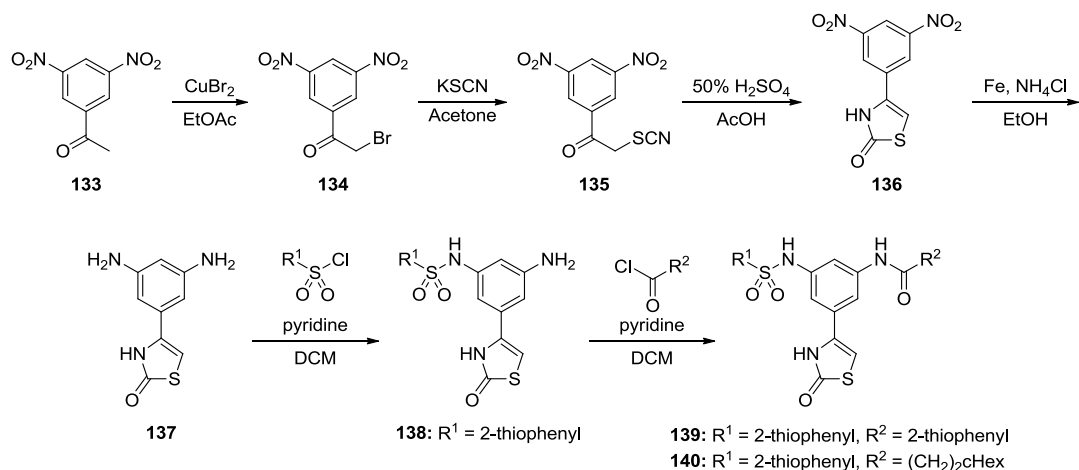
Bromination of the methylketone **126** to α -bromoketone **127** was followed by thiocyanation to **128**. Acid-promoted cyclisation formed the thiazolidinone ring of **129** and nitro group reduction gave intermediate amine **130**, which was amenable to condensation with various sulfonyl chlorides.

In general, *meta*-substitution was preferred delivering submicromolar potency with both the thiophene sulfonamide **131** and the benzyl sulfonamide **132** displaying IC_{50} values = 4.1 μM . X-ray crystal structures of these compounds bound to BRD4 BD1 were obtained and revealed alternative binding modes (Figure 33).⁷⁶

Figure 33. X-ray crystal structures of (a) thiophene sulfonamide **131** (carbon = magenta, pdb 4HXS) and (b) benzyl sulfonamide **132** (carbon = green, pdb 4HXR) in complex with BRD4 BD1.

The thiophene sulfonamide group of **131** was positioned on the WPF shelf as expected but, surprisingly, the benzyl sulfonamide group of **132** occupied the ZA channel with the oxygen atoms forming hydrogen bond interactions with a water network in this region. Using this information, disubstituted analogues were prepared to occupy both the WPF shelf

and ZA channel simultaneously to further increase potency.⁷⁶ In the design of these compounds, it was rationalised that a sulfonamide was not required to direct a substituent into the ZA channel and an amide was used as a bioisosteric replacement. Synthesis of these compounds was achieved using similar chemistry to that used for the monosubstituted compounds (Scheme 14). Additional use of 3,4-dinitrophenyl methylketone gave access to an alternative substitution pattern, and variation of the sulfonyl and acid chlorides allowed SAR exploration.



Scheme 14. Synthesis of the 3,5-substituted phenylthiazolidinones (yields undisclosed).

Higher binding affinities were observed with the disubstituted phenylthiazolidinones compared to the monosubstituted analogues. A 3,5-substitution pattern was preferred over 3,4-substitution, with bithiophene **139** displaying the highest activity at IC₅₀ = 0.23 μM.⁷⁶ X-ray crystallography of another disubstituted phenylthiazolidinone **140** (IC₅₀ = 2.2 μM) in BRD4 BD1 confirmed occupation of both the WPF shelf and the ZA channel by the sulfonamide thiophene and amide cyclohexylethyl groups, respectively (Figure 34).

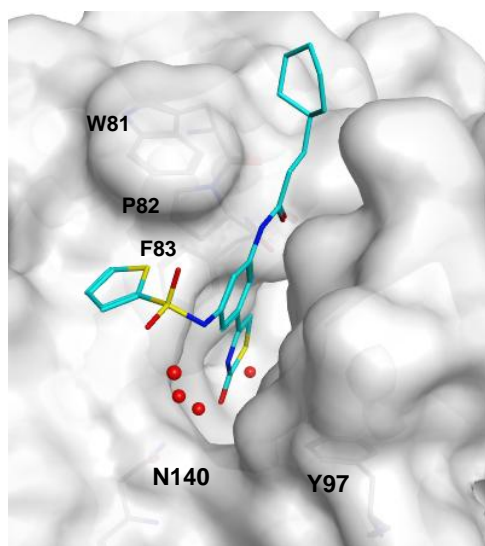


Figure 34. Binding mode of phenylthiazolidinone **140** (carbon = cyan) in BRD4 BD1 (pdb 4HXL).

The lead compounds **131** and **139** were assessed for their stability to human and mouse liver microsomes, revealing generally low clearances.⁷⁶ Additionally, low inhibition of P450 enzymes was observed for both compounds. Finally, testing in a cancer cell proliferation assay and for MYC mRNA expression was conducted. Results from 13 examples in the HT-29 human colon cancer cell assay poorly correlated with data from the binding assays. This was attributed to ineffective membrane permeability of a number of compounds resulting from non-ideal physicochemical properties. The best activity was achieved by the 3-amino-5-sulfonamide **138** ($GIC_{50} = 37.3 \mu\text{M}$) but this was weaker than with the previously disclosed dimethylisoxazole sulfonamide **102** used as the positive control ($GIC_{50} = 22.5 \mu\text{M}$). Compound activities in this assay did correlate with data obtained in MYC expression assay, with 3-amino-5-sulfonamide **138** displaying >50% inhibition at 10 μM , but this was again weaker than dimethylisoxazole sulfonamide **102**.

These studies, again, demonstrated that a BET bromodomain was amenable to FBDD. Screening a fragment set generated a number of hits including a 2-thiazolidinone as a novel KAc mimetic. Knowledge from previous publications was successfully used in compound design to increase potency but came at the expense of membrane permeability for a number of examples. While the authors claim the 2-thiazolidinones represent a reasonable starting point for optimisation, the disubstituted phenyl derivatives, such as bithiophene **139**, are already large ($M_{wt} = 433 \text{ g/mol}$) and aqueous solubility was not disclosed. Before embarking on a programme of optimisation, determination of compound affinities at other BET family member bromodomains and BCPs, and members of other target classes is essential to link cellular phenotype to a mechanism.

During the development of a fluorescent probe to visualise acetylation of histone peptide in living cells, the small molecule BIC1 (Figure 35) was identified as an inhibitor of BRD2.⁷⁷

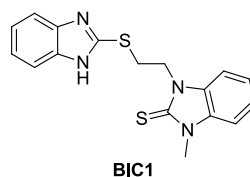


Figure 35. BRD2 BD1 inhibitor BIC1 identified using a fluorescent probe.

Computational docking screens of compound libraries filtered using Lipinski's rules, were conducted in BRD2 BD1 to identify molecules for SPR screening.⁷⁷ Four compounds were taken forward for screening in cells expressing a fluorescent probe and BIC1 was found to bind BRD2. This was confirmed with an X-ray crystal structure of BIC1 bound to BRD2 BD1 (Figure 36).

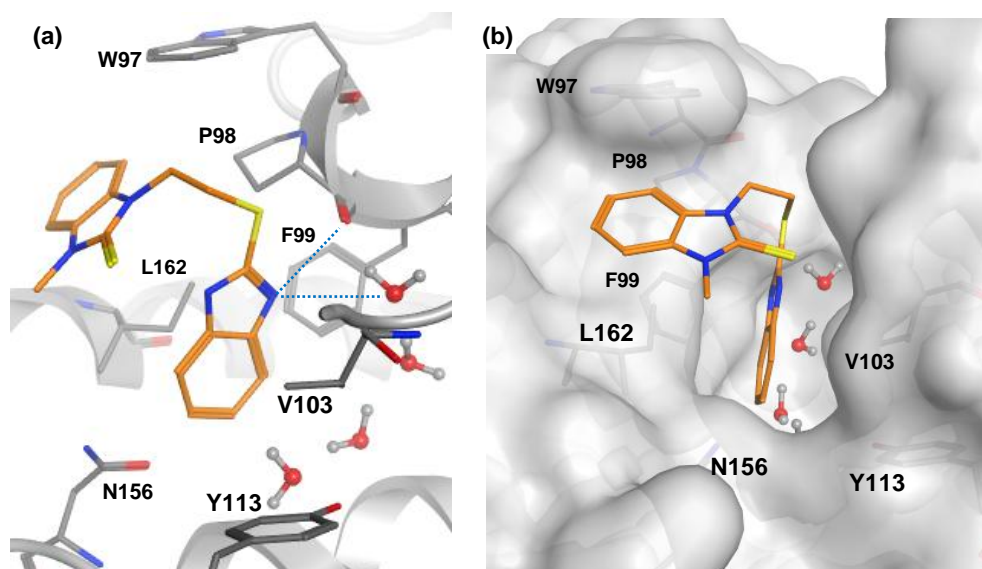


Figure 36. X-ray crystal structure of BIC1 (carbon = orange) in BRD2 BD1 (pdb 3AQA). (a) Ribbon representation with key residues highlighted. (b) Molecular surface representation.

A distinctive binding mode was observed with no apparent hydrogen bond interaction with Asn156 or any through-water interaction to Tyr113 (Figure 36a). This was perhaps compensated by the formation of hydrogen bonds from a benzimidazole nitrogen to the backbone carbonyl of Pro98 and an adjacent water molecule. Like most other BET inhibitors, the lipophilic pocket between Val103 and Ile162, and the WPF shelf was occupied, in this case by the benzimidazole and benzoimidazole-thione rings, respectively (Figure 36b). Based on these observations, inhibition of BRD2 BD1 was determined as the mechanism for blocking BRD2-dependant transcriptional activity in human cells.⁷⁷

In these studies, a fluorescent probe expressed in cells was used to screen for BRD2 inhibitors and therefore automatically identified compounds possessing good cellular permeability, an important property not accounted for in a binding assay approach. While Lipinski's rules were used to filter the screening set, measurement of other physicochemical properties would be desirable to determine the suitability of the hit molecule, BIC1, for optimisation into a potent BET inhibitor. Further investigation into the broader bromodomain selectivity of BIC1 would be required before it could be considered as a useful probe molecule of BET bromodomains.

The discovery of novel BRD4 inhibitors using structure-based virtual screening has very recently been disclosed.⁷⁸ Identification of chemotypes able to mimic KAc was carried out using two distinct methods. In the first method, a library was created from the substructures of published bromodomain inhibitors and their potential bioisosteric replacements. In the second method, shape, pharmacophoric and 2D fingerprint similarity searches were performed using (+)-JQ1 as a probe compound. Only compounds able to fit the tight geometric constraints of the KAc binding pocket, as determined from dockings into BRD4 BD1, were retained in the set. Novel KAc mimetics were then extracted through visual inspection and combined with the library generated from the first method before substructure searching in a database of commercially available compounds was carried out. These compounds were docked into BRD4 BD1, purchased, and tested in a BRD4 BD1 AlphaScreen to identify the six hit compounds shown in Figure 37.

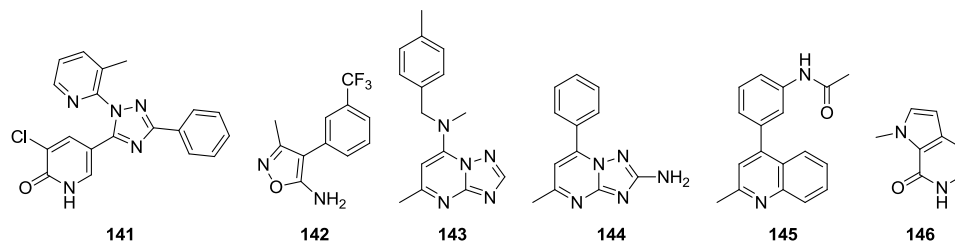


Figure 37. Hits identified from virtual screening.

Crystal structures of hit compounds **141**, **143**, **144** and **145** in BRD4 BD1 were obtained and revealed close overlap with predicted poses from the docking studies.⁷⁸ Further searching, purchasing and/or synthesis and testing, was conducted for each hit compound resulting in derivatives exhibiting greater activity.

This study successfully demonstrated structure-based virtual screening as a tool to discover new KAc mimetics. BRD4 was selected as model target, but the approach could be extended to other bromodomains. Four novel scaffolds suitable for further chemical exploration were identified, but no selectivity or developability data were reported to guide prioritisation of templates.

Further examples of BET inhibitors can be found in the patent literature. While most of these chemotypes have also been published in journal articles, there are some important exceptions which are now discussed. For example, elaborated variants of the THQ fragment first reported by Chung⁷⁴ are included in several patents from GSK with generic structures **147** and **148** (Figure 38).^{79,80}

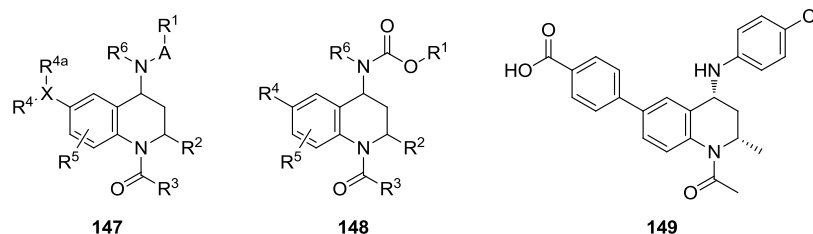


Figure 38. Patented THQ BET inhibitors.

Most examples included in these patents were reported to be active in BRD2, 3 and 4 WT FA assays with a number also demonstrating inhibition of inflammatory mediator production (TNF α and IL-6) in human whole blood following LPS-stimulation. One example, THQ **149**, showed profound efficacy in an *in vivo* model of sepsis.⁸⁰ In a control group, only 6% of mice treated with lethal doses of LPS survived while in the group treated with THQ **149** 90 minutes later, 58% of the animals were rescued. In addition, this compound was screened in a panel of cancer cell lines showing GIC₅₀ values in the range 40–9200 nM in breast cancer cell lines and 35–844 nM in heme lines.⁸⁰

It should be noted that in the latter stages of preparing this thesis, an article emerged describing the ability of the THQ **149** (or I-BET726 as named in the paper) to inhibit growth and induce cytotoxicity in neuroblastoma solid tumour.⁸¹ High binding affinities upon displacement of a tetra-acetylated histone peptide from tandem bromodomain BRD2, 3 and 4 constructs were reported (22–41 nM), as well as DSF data which highlighted the selectivity of THQ **149** for the BET family. In addition, similar thermal shifts were found for individual bromodomain constructs of BRD4 ($\Delta T_m = 13.6^\circ \text{C}$ and 12.5°C for BD1 and BD2, respectively) indicating no domain selectivity. Finally, inhibition of cell growth and cytotoxic effects of THQ **149** were demonstrated in neuroblastoma cell lines and its therapeutic potential established *in vivo* using a mouse xenograft model of neuroblastoma.

Abbott laboratories and Abbvie have recently published patents on BET inhibitors containing a pyrrolopyridone KAc-mimetic, such those shown in Figure 39.^{82,83} Within these manuscripts, data from FRET assays of individual BRD4 bromodomains were reported. Nanomolar potencies were achieved with a number of examples, such as the pyrrolopyridone **150**, while, perhaps more interestingly, several examples displayed bias for BRD4 BD1 or

BRD4 BD2 with the *N*-methylpiperazine **151** in particular showing considerable selectivity for BRD4 BD1.

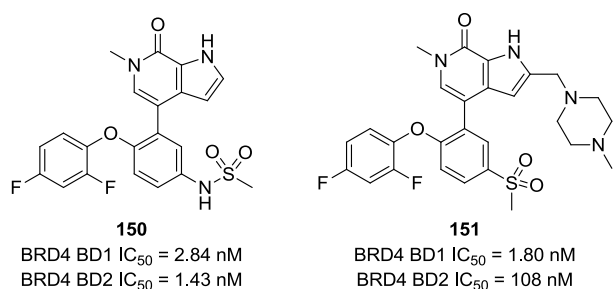


Figure 39. Examples of pyrrolopyridone BET inhibitors from Abbot Laboratories

Dose-dependent effects upon breast cancer cell proliferation were determined with pyrrolopyridone **150** giving an EC₅₀ = 17.4 nM. Two examples were also screened in a panel of cancer cell lines with notable potent effects in reducing AML proliferation. Metabolic stabilities in human, rat, and mouse microsomes were reported, with pyrrolopyridone **150** displaying prolonged stabilities in all species. Finally, data from *in vivo* studies in inflammation and cancer models were reported. After oral dosing to LPS-stimulated immunodeficient mice, high inhibition of Il-6 production was observed for a number of compounds including example **150**. Pyrrolopyridone **150** also inhibited paw swelling in a rat collagen-induced arthritis model in a dose dependant manner and showed comparable efficacy with prednisolone at a third of the dose (1 mg/kg). The ability of example **150** to inhibit growth of tumour xenografts in mice was also disclosed. Oral dosing at 3 mg/kg/day over 14 days reduced growth of an OPM-2 myeloma xenograft by 90% and exhibited dose-dependant inhibition of MX-1 breast cancer growth. Efficacy in a number of additional cancer cells was also established and, when dosed in combination with the established treatments cytarabine, azacitidine and bortezomib, beneficial additive effects were observed.

The compounds covered in these patents represent a new class of KAc mimetic but details on the development of these BET inhibitors are unknown at the present time. Based on the encouraging results in the mouse inflammation and tumour models, considerable potential exists for effective human therapy.

In addition to reports of BET inhibitors found in the journal and patent literature, company websites are another source of valuable information. Of particular note was the emergence that an ApoA1 upregulator, developed by ResVerlogix (RVX-208), functions by inhibiting BET proteins (Figure 40).⁸⁴

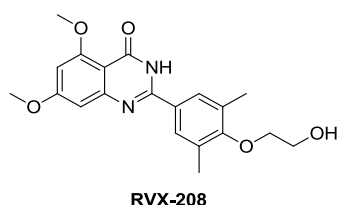


Figure 40. ResVerlogix first-in-class BET inhibitor.

RVX-208 entered phase I clinical trials in the USA in 2007 and is currently being assessed in a phase IIb study for the treatment of both coronary atherosclerotic plaque and atherosclerotic coronary disease. RVX-208 is therefore a first-in-class BET inhibitor despite its MOA only being announced recently.⁸⁴ As a consequence, details on BET affinity and binding mode remained unpublished until very recently.^{85,86} Studies conducted by researchers at ResVerlogix demonstrated that RVX-208 bound preferentially to BD2 over BD1.⁸⁵ The degree of selectivity was dependant on the method of measurement, but based on dissociation constants determined by ITC, BD2 selectivities of 82-fold and 29-fold for BRD2 and BRD4, respectively, were reported. Independent ITC measurements from the SGC laboratories also determined preferential binding of RVX-208 to BD2, albeit with a reduced magnitude (23-fold for BRD2 and 8-fold for BRD4).⁸⁶ Here, gene-expression studies with RVX-208 showed that selective inhibition of BD2 only modestly affected BET-mediated transcription and suggested a dominant role of BD1 in transcriptional control.

The clinical progression of RVX-208 provides increased confidence in BET inhibition as a viable strategy for treatment of non-oncologic indications. As development of RVX-208 was directed towards atherosclerotic disease, limited data has been presented outside this therapeutic area and a wider investigation of the biological effects of this compound is awaited. However, caution would be required in attributing results from such studies to inhibition of BD2 as the modest selectivity of RVX-208 means that contributory effects from engagement of BD1 towards the biological response cannot be ruled out.

It is apparent from this review that much progress has been made in the identification and development of small molecule BET inhibitors in recent years by both industrial and academic institutions. These molecules span a range of KAc mimetics and often exhibit high affinity and selectivity for the BET family of BCPs. After pioneering work by Chung and co-workers in the identification of the BET bromodomains as the molecular targets of ApoA1 upregulators,⁴⁴ a more focused mechanistic approach has been adopted to elucidate the biological effects upon BET bromodomain inhibition. The abundance of structural information has allowed rapid development of small molecule ligands and has facilitated the use of modern methods such as FBDD. A range of assay formats have been developed for

the identification of ligands, including label-free methods and biochemical technologies, as well as assays studying the outcome of BET inhibition in whole cells. Many of the compounds identified have been used as tools to probe the biological consequences upon blocking interaction of KAc with BET bromodomains. Notably, several examples are currently in clinical trials, the outcomes of which will determine the viability of BET inhibition as a therapeutic strategy.

At the start of the work contained within this thesis, no small molecule BET inhibitors had been published in the journal literature. Furthermore, as the above literature review reveals, a strategy to specifically develop compounds suitable for *i.v.* administration had not been described, an aspect of small molecule BET inhibition which remains unpublished up to the present day. When commencing these studies, several programmes of research were underway within our laboratories to discover and optimise BET inhibitors as potential therapeutics. In particular, we aimed to develop molecules from different structural classes and optimise these for routes of administration appropriate for different disease indications. The first section of this research describes the optimisation of a dimethylisoxazole quinoline series of BET inhibitor designed for *i.v.* administration towards drug pre-candidates. Novel SAR and developability data is included and expands the knowledge base of the scientific community concerning small molecule BET inhibition.

It was apparent from examination of the literature that small molecule inhibition of the BET bromodomains elicits profound biological responses, but their potential as therapeutics beyond acute inflammation and cancer is limited. Furthermore, there was a distinct lack of selectivity data for the individual bromodomains within the BET proteins and, where data did exist, indiscriminate binding was generally observed. To enable further understanding of the broad phenotype characteristic of pan-BET inhibition, development of inhibitors selective for individual, or sets of, bromodomains within the family is required. The second section of this research describes the effort towards this goal through the development of a dimethylisoxazole quinoline probe molecule which selectively inhibited the first bromodomain of the BET proteins.

2. Quinoline BET Inhibitors for *Intravenous Administration*

2.1. Medicinal Chemistry Strategy and Project Aims

As described in a research paper which was published following the initiation of this project, the 3,5-dimethylisoxazole quinoline GW694481 (Figure 41) was identified as a hit compound in an ApoA1 upregulation assay within our laboratories.⁶³

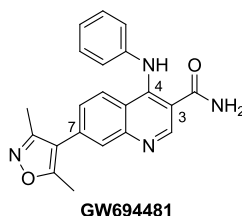


Figure 41. 3,5-Dimethylisoxazole quinoline hit GW694481 identified from a HTS.

The 3-, 4- and 6-positions of the quinoline ring were explored by the authors to optimise ApoA1 activity and attenuate CYP inhibition.⁶³ The discovery that these ApoA1 upregulators were inhibitors of the BET bromodomains was disclosed in a separate publication released at the same time.⁶⁴ Other studies within our laboratories revealed that small molecule BET inhibition suppressed LPS-induced inflammation and sepsis in a mouse endotoxaemia model, which was also published during the programmes of study described in this thesis.^{47,66} With promising biological results achieved with several dimethylisoxazole quinolines, a programme of work to develop drug pre-candidates for human sepsis was pursued.

Sepsis is an acute inflammatory condition affecting millions of people around the globe with the number of cases growing each year.⁸⁷ Of those affected, 25% ultimately die making sepsis one of the most common causes of death in the world. A key feature of this condition is a hyperinflammatory immune response upon invasion by bacteria, fungi, parasites or viruses in the blood, lungs, urinary tract or other tissues. An inability to regulate this response leads to septic shock, organ failure and, potentially, death. Potent pro-inflammatory mediators, including IL-6, are released during the onset of sepsis and many therapeutic strategies have targeted such mediators but, unfortunately, these have been met with limited success in clinic trials.⁸⁸ Therefore, new mechanisms through which anti-inflammatory agents may act, such as inhibition of BET bromodomains, would be of high value for the research community and sepsis patients.

Although I-BET762 demonstrated profound effects in a mouse sepsis model, this molecule, and other BET inhibitors published subsequently, have not, apparently, been developed specifically as treatments for human sepsis despite the huge unmet need in this area. The reasons for this are unknown, but it is likely that these molecules do not possess the very high aqueous solubility required for *i.v.* administration, a method to rapidly deliver drug to the systemic circulation which is likely to positively affect patient response after severe sepsis develops. Even in the case of oral administration, where the level of aqueous solubility required is lower, the poor aqueous solubility of the BET inhibitor PFI-1 was attributed as non-ideal property discovered during an oral PK study.⁷⁵ Therefore, the discovery of a highly soluble drug pre-candidate presented both a novel and challenging approach in the field of BET inhibition.

The specific requirements in this programme of research to develop dimethylisoxazole quinolines suitable for *i.v.* administration were:

- potent BET bromodomain inhibition ($pIC_{50} > 6.0$) determined using FP assays;
- high aqueous solubility:
 - $> 50 \mu\text{g/mL}$ determined using a high throughput DMSO precipitative solubility method using Chemiluminescent Nitrogen Detection (CLND) and then;
 - $> 1000 \mu\text{g/mL}$ (at pH 5.0 or 7.0) determined using a more accurate lower throughput solubility method, using solid compound and visual inspection;
- potent inhibition of pro-inflammatory cytokine production in LPS-stimulated human whole blood (WB) ($pIC_{50} > 6.0$); and
- inactivity ($pIC_{50} < 4.2$) of the human ether-a-go-go related gene (hERG) ion channel determined using an electrophysiology assay.

Detailed information for these assays can be found in the Appendix.

A number of dimethylisoxazole quinolines were synthesised as part of the existing programmes of work focused on oral administration. However, no previously synthesised molecules possessed the high WB activity combined with aqueous solubility required for *i.v.* drug delivery, and the focus of the research described here was to address these limitations. A data-driven approach towards optimisation of WB activity was taken, while structural information guided the optimisation of solubility. In this regard, a high resolution crystal structure of the dimethylisoxazole quinoline **152** bound to BRD2 BD1 (solved within our laboratories⁸⁹) was examined (Figure 42). This structure showed that the quinoline was positioned at the KAc binding pocket of the bromodomain. Like the published structures of dimethylisoxazole-containing BET inhibitors discussed in the introduction, the dimethylisoxazole unit of quinoline **152** formed key hydrogen bond interactions to Asn156 and to the water molecule contacting Tyr113 (Figure 42b) (the hydrogen bond distances of I-BET151 were later found to be in close accordance with those of the quinoline **152**⁶⁴). The quinoline ring occupied the lipophilic cleft between Leu108 on one side, and Trp97 and Pro98 on the other, while the 4-aniline substituent made hydrophobic contacts with the WPF shelf. The 3-amide was positioned in the ZA channel and, to avoid placing a hydrophobic aryl ring into bulk solvent, the pyridin-2-ylmethyl substituent bent round to form hydrophobic interactions with Leu108 and the hydrocarbon section of Lys107.

From this structure, a number of vectors from quinoline **152** were identified for the introduction of polar chemical functionality (termed solubilising groups) such as basic moieties and alcohols, to modify the physicochemical properties and improve aqueous solubility (Figure 42d and e). Accordingly, positions on the quinoline amide template which were attractive for substitution included the 3-amide, the 4-NH bond and the *ortho*- and *meta*-positions on the 4-aniline ring, all of which pointed towards solvent exposed areas. Modifications to the 3-position were conducted in the initial chemistry investigations and are now discussed in detail.

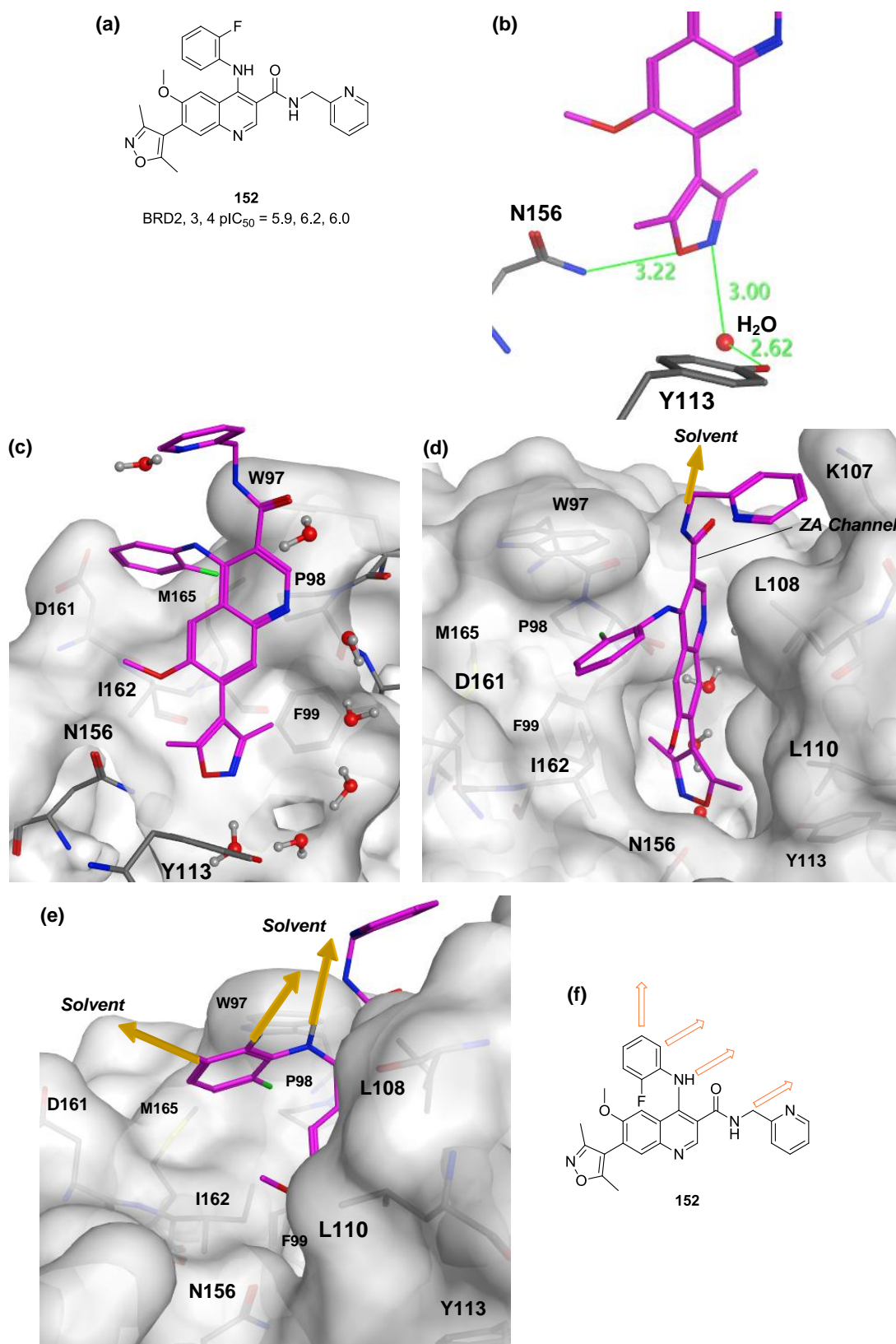


Figure 42. (a) Structure of quinoline **152** and corresponding BET activity. (b–e) X-ray crystal structures of quinoline **152** (carbon = magenta) bound to BRD2 BD1. (b) Hydrogen bond distances (Å) of the dimethylisoxazole unit to Asn156 and Tyr113. (c) Molecular surface of BRD2 BD1 with conserved waters highlighted. (d and e) Vectors from quinoline **152** directed towards solvent are highlighted with orange arrows, from the 3-amide (d) and from the 4-NH and 4-aniline ring (e). (f) Summary of vectors directed towards solvent.

2.2. 3-Methylamine Exploration

Using structural insight, the 3-position of the dimethylisoxazole quinoline template was identified as an attractive vector to alter the physicochemical properties to improve aqueous solubility. To assist in this endeavour, data for the extensive number of amides synthesised at this position as part of the existing programme targeting oral administration was considered, and a selection of these data are shown in Table 13.

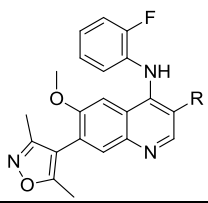
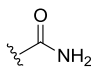
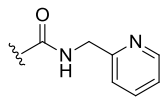
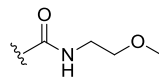
	R =		
	 43 ⁹⁰	 152 ⁸⁹	 153 ⁹¹
BRD2, 3, 4 pIC₅₀	6.3, 6.5, 6.2	5.9, 6.2, 6.0	5.5, 6.0, 5.7
WB pIC₅₀	<4.5 ^a , 4.7 ^a	<5.0	<4.5
Solubility CLND (µg/mL)	46	26 ^b	110
Solubility pH 5.0, 7.0 (µg/mL)	13, 1	21 ^b , <1 ^b	>1000, 130

Table 13. A selection of historical amides and corresponding data. ^aThese individual values resulted from two test occasions and do not represent mean values. ^bThese data were obtained on the dihydrochloride salt.

Both the carboxamide **43**⁹⁰ and the pyridin-2-ylmethanamide **152**⁸⁹ displayed good activities in the BET FP assays but also possessed poor solubilities. Like the pyridin-2-ylmethanamide **152**⁸⁹ most of the pre-existing amides contained an aromatic ring which was suspected to contribute to the poor solubility. The 2-methoxyethanamide **153**⁹¹ was differentiated in terms of structure and displayed very good solubility at pH 5.0 achieving the desired target solubility of >1000 µg/mL. Unfortunately, this particular compound was only moderately active in the BET FP assays and inactive in the WB assay.

Whilst on-going work within the laboratory focused on exploring further amides at the 3-position for solubility improvements,⁹² the objective of the following research was to investigate an alternative functional group to improve solubility and determine the effect of this modification upon BET and WB activity. Specifically, removal of the carbonyl-possessing (amide) unit and the replacement of this group with methylamine functionality was expected to improve solubility through incorporation of a basic centre. A workplan was devised to incorporate different functional groups appended to methylamine and *in silico*⁹³ solubility calculations were conducted. These predictions showed the *N*-methylpiperazine to be highly soluble at pH 4.5, while alcohol-containing functional groups also met the

solubility criteria (Table 14). Ethers were estimated to be less soluble but were included based on previous SAR demonstrating favourable activity when incorporated as part of an amide group such as in the methoxyethylamide **153**.⁹¹

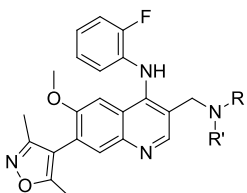
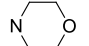
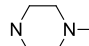
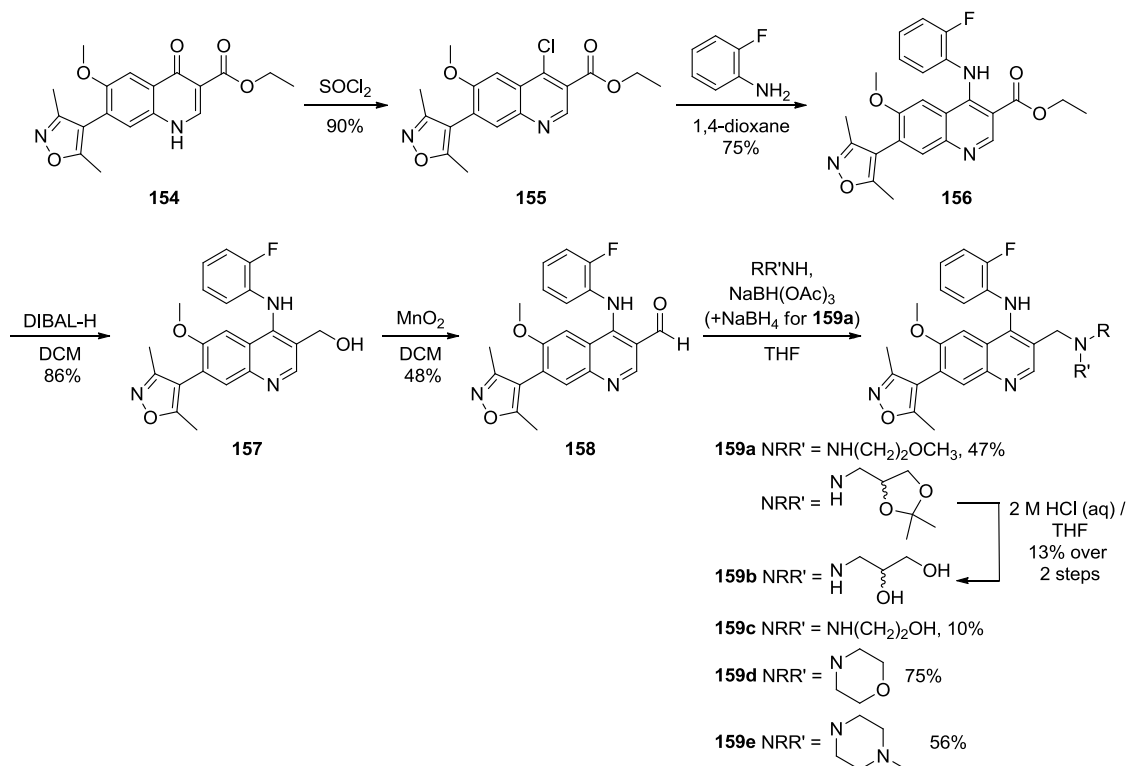
	NRR'	Predicted solubility at pH = 4.5 (mg/mL)
	NH(CH ₂) ₂ OCH ₃	4
	NH(CH ₂)CH(OH)CH ₂ OH	11
	NH(CH ₂) ₂ OH	20
		0.06
		82

Table 14. Solubility predictions for methylamine analogues.

The synthetic strategy for this area of work was to produce a late stage intermediate for amine diversification using robust reductive amination chemistry. Also, an intermediate incorporating a 2-fluoroaniline 4-substituent was desirable to allow direct SAR comparisons to be made with previously synthesised amides. Accordingly, the aldehyde **158** was identified as the desired intermediate for the synthesis of the target methylamine compounds (Scheme 15).



Scheme 15. Synthesis of quinoline 3-position methylamines.

The first step in the synthetic sequence involved chlorination of quinolinone **154**⁹⁴ to give 4-chloroquinoline **155** in high yield (90%). A nucleophilic

aromatic substitution reaction with 2-fluoroaniline provided *N*-(2-fluorophenyl)quinolin-4-amine **156** in 75% yield and this was subsequently reduced to primary alcohol **157** in high yield (86%). Manganese dioxide-mediated oxidation to aldehyde **158** was achieved in 48% yield, which set the stage for amine synthesis. Reductive amination with a range of amines furnished the target amine compounds **159a–e**. These were then screened in the BET FP assays with results displayed in the left hand side of Table 15 (data for analogous amides, where available, are displayed on the right hand side).

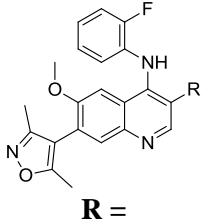
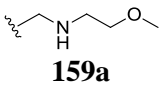
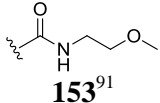
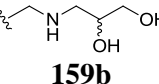
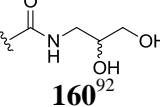
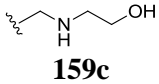
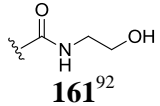
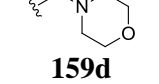
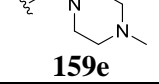
 R =	BRD2, 3, 4 pIC ₅₀	WB pIC ₅₀	CLND (μg/mL)	R =	BRD2, 3, 4 pIC ₅₀	WB pIC ₅₀	CLND (μg/mL)
 159a	6.0, 6.2, 5.8	<4.5, ^a 4.7 ^a	99	 153 ⁹¹	5.5, 6.0, 5.7	<4.5	110
 159b	6.0, 6.4, 5.6	<4.5, ^a 5.3 ^a	146	 160 ⁹²	6.0, 6.1, 5.7	4.8 ^b	221
 159c	6.0, 6.4, 5.6	<4.5, ^a 4.7	143	 161 ⁹²	5.9, 6.1, 5.8	<4.5	189
 159d	6.0, 6.2, 5.8	<4.5, ^a 4.4	8				
 159e	5.9, 6.3, 5.6	5.1	122				

Table 15. Results for 3-position methylamines and comparison to their 3-amide analogues where appropriate. ^aThese individual values resulted from two test occasions and do not represent mean values. ^bpIC₅₀ values of <4.5 were determined on two test occasions out of four and were excluded from the reported mean value.

These data showed that the methylamine unit was well tolerated and that removal of the amide carbonyl retained, or slightly improved activity. As substituents on the methylamine unit were designed to occupy solvent exposed region, little difference in BET FP activity between the congeners was expected and this was confirmed by these data with all methylamines displaying similar (1.6–2.5 μM) BRD4 activity. Interestingly, the methylamine-containing compounds displayed enhanced WB activity over their amide counterparts but it should be noted that methylamines **159a–159d** were determined inactive on another test occasion. The methylamine **159b** showed 3-fold increased WB activity *versus* the amide **160**⁹² when taking the active (pIC₅₀ = 5.3) result. With the exception of the

morpholine **159e**, the methylamines exhibited high CLND solubility but, disappointingly, values were lower than their corresponding amides. However, it was expected that aqueous solubility at pH = 5.0 would have been higher for the methylamines due to their expected positive ionisation state at this pH. Despite the encouraging increases in WB activities achieved through the design and synthesis of the methylamines, the WB activity did not meet the micromolar threshold required for progression into resource-intensive solubility measurements from solid. However, exploration of this vector for incorporating amine solubilising groups demonstrated encouraging results, particularly with the (methylamine)propane-1,2-diol **159b**, and this area was identified for reinvestigation at a later date if the associated exploration of the 4-position boosted WB activity sufficiently.

Attention then turned to vectors on the 4-amino substituent identified from X-ray crystallography for incorporation of solubilising groups.

2.3. 4-Amino Substituent Exploration and Molecular Budgeting

To determine a strategy for incorporation of solubilising groups on the 4-amino substituent, data from the previous programmes of chemistry directed towards oral administration were considered. Accordingly, the compounds shown in Table 16 were highlighted as being of particular interest.

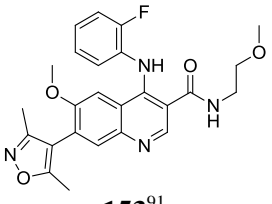
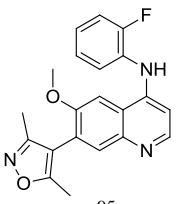
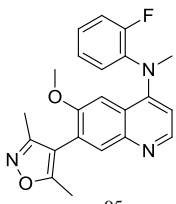
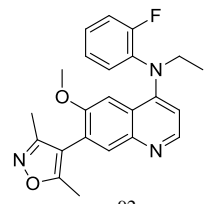
				
	153 ⁹¹	162 ⁹⁵	163 ⁹⁵	164 ⁹²
BRD2, 3, 4	5.5, 6.0, 5.7	5.5, 5.8, 5.2	6.4, 6.8, 6.5	6.1, 6.5, 6.2
pIC₅₀	<4.5	<4.5	NT	NT
WB pIC₅₀	<4.5	<4.5	NT	NT
Solubility				
CLND	110	12	43	12
(µg/mL)				
Solubility pH				
5.0, 7.0	>1000, 130	17, 0	NT	NT
(µg/mL)				

Table 16. SAR table of 4-*N* substituent analogues.

The role of the 3-amide was first considered and upon comparison of dimethylisoxazole quinolines **153**⁹¹ and **162**,⁹⁵ it was concluded that the amide substituent did not play a particularly important role in BET FP activity but it did provide enhanced

solubility. Dimethylisoxazole quinolines lacking a 3-amide substituent were next considered and these data showed that BET FP activity could be increased by substituting the 4-position amine with methyl and ethyl substituents (compounds **163**⁹⁵ and **164**,⁹² respectively). Given the importance of attenuating molecular weight in achieving cell permeability,⁹⁶ an important requirement for interaction with BET proteins in human WB, a molecular budgeting approach was used at this stage of the project and is outlined in Figure 43.

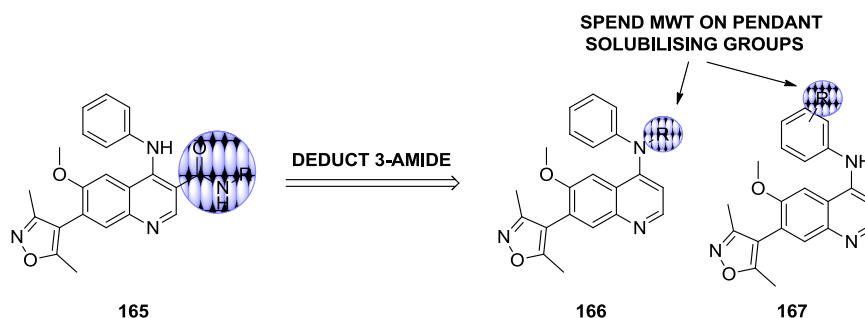


Figure 43. Molecular budget approach to ‘deduct’ the 3-amide molecular weight and ‘spend’ on 4-aniline substituents.

In general, a molecular budgeting approach involves removal of a substituent and its molecular weight ‘spent’ by the addition of another, more optimal group elsewhere in the molecule ensuring minimal net gain of molecular weight. When applied in the context of this area of research, the 3-amide substituent (which, so far, enhanced solubility but not WB activity) was removed from quinoline **165**, and the molecular weight ‘spent’ on a pendant solubilising group on the 4-aniline substituent, ensuring minimal overall increase in molecular weight when exploring different areas of the molecule and to increase the likelihood for achieving high WB activity.

Possible substitution points for the solubilising group were then considered and included the 4-*N* atom as in quinoline **166** or on the 4-aniline ring as in quinoline **167**. Both substitution methods were to be explored within our laboratory with the aim of:

- retaining or improving BET activity, compared to the 3-amide quinolines **165** — the SAR shown in Table 16 suggested this was achievable; and
- exploring new vectors for incorporating solubilising groups — the 4-NH bond vector, and the *ortho*- and *meta*-positions on the 4-aniline ring, pointed towards solvent exposed regions in the crystal structure (Figure 42d).

In addition to this molecular budget approach, one area of interest was to lower the lipophilicity in an attempt to improve solubility. SAR previously explored within our laboratory revealed that only aromatic groups were tolerated at the 4-position of the quinoline (data not shown).⁹² Therefore, the tactic employed was to introduce polarity in the form of a pyridine ring to give target compounds of the type **168** (Figure 44).

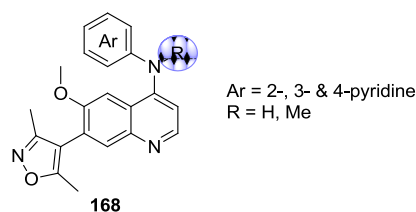
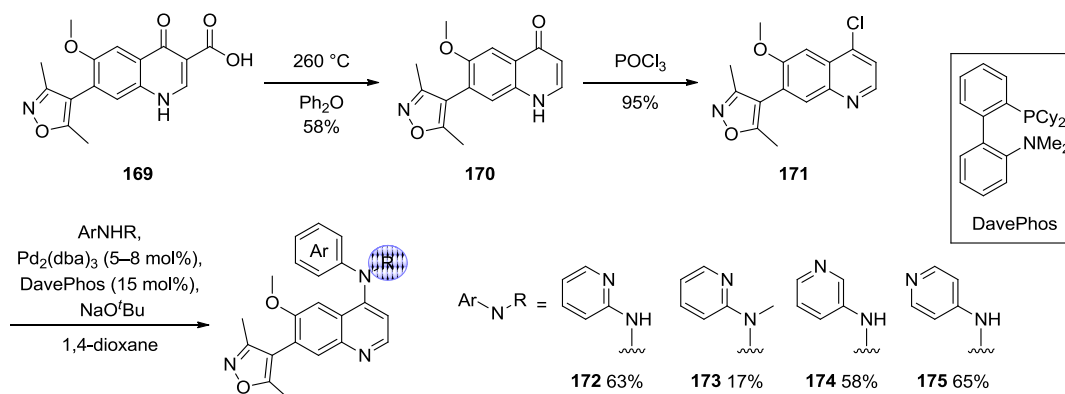


Figure 44. Incorporation of basic pyridine rings for enhanced solubility.

All aminopyridine isomers were targeted to find the optimal position for the new basic centre on the WPF shelf. Additionally, *N*-methyl or *N*-ethyl pyridinamines available from commercial suppliers were desirable for inclusion as a tertiary nitrogen atom at the quinoline 4-position was expected to enhance activity based on previous SAR (Table 16). Synthesis of these target compounds was carried out according to Scheme 16.



Scheme 16. Synthesis of 4-aminopyridines.

Firstly, thermal decarboxylation of the carboxylic acid **169**⁹⁴ (available within our laboratory) at 260 °C afforded the quinolinone **170** in 58% yield. Chlorination to the chloroquinoline **171** was achieved in refluxing POCl₃ in excellent yield (95%) furnishing the required partner for C–N cross-coupling with appropriate aminopyridines. The only commercially available *N*-methyl or *N*-ethyl pyridinamine available was *N*-methylpyridin-2-amine and this was included to provide an example of a tertiary 4-nitrogen analogue. The amination reactions were conducted using typical Buchwald-Hartwig conditions (Pd₂dba₃, DavePhos, NaO^tBu, 1,4-dioxane) in a microwave reactor. This catalytic system comprising of the air stable Pd(0) source and one of the original dialkylbiaryl phosphine ligands successfully generated pyridines **172–175** albeit with varying degrees of coupling efficiency. These compounds were then profiled in our screens with the data being shown in Table 17.

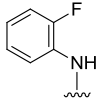
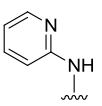
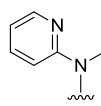
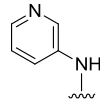
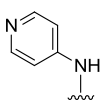
					
	162⁹⁵	172	173	174	175
BRD2, 3, 4 pIC₅₀	5.5, 5.8, 5.2	5.5, 5.7, 5.2	6.4, 6.6, 6.1	5.4, 5.7, 5.1	5.5, 5.9, 5.3
WB pIC₅₀	<4.5	<4.5	5.2	<4.5 ^a , 4.8 ^a	5.1
chromLogD_{7.4}	4.8	4.2	4.8	3.2	3.0
Solubility CLND (µg/mL)	12	74	145	74	149

Table 17. Data for 4-aminopyridines isomers. ^aThese individual values resulted from two test occasions and do not represent mean values.

These results showed that each pyridine isomer from the secondary amines **172**, **174** and **175**, was similarly active in the BET FP assays demonstrating a tolerance for different electron distributions on the WPF shelf. In terms of WB activity however, the *para*-isomer was most active with a pIC₅₀ = 5.1. Encouragingly, lipophilicity was lowered by the introduction of a basic pyridine and this translated into improved CLND solubility compared to the 2-fluorophenyl **162**.⁹⁵

Data for the tertiary amine **173** were particularly interesting. As predicted from previous SAR, a 10-fold increase in activity was achieved when the 4-*N* was substituted with a methyl group (comparing secondary amine **172** to tertiary amine **173**). Although lipophilicity was comparable with the 2-fluorophenyl **162**,⁹⁵ this compound possessed good CLND solubility and the best WB activity in this set of compounds.

Although encouraging results were achieved with these pyridine-containing dimethylisoxazole quinolines, the WB activity was not sufficient to warrant their progression into solubility measurements from solid. However, this initial data package provided valuable information that a pyridine ring was tolerated at the 4-position of the quinoline. Also, the encouraging BET activity and CLND solubility achieved with the tertiary amine **173** provided confidence that tertiary amines were worthwhile targets for further exploration to enhance WB activity and further increase solubility. In this regard, 4-tertiary amines of the type **176** were targeted for synthesis (Figure 45).

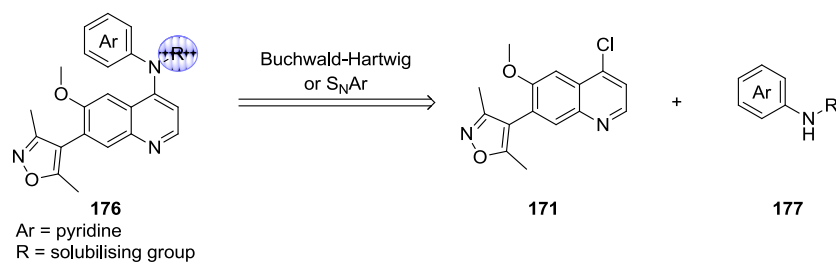


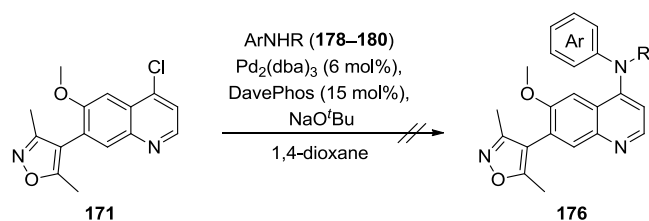
Figure 45. Initial chemistry strategy for synthesis of 4-tertiary amines **176** via Buchwald-Hartwig amination or S_NAr .

Both Buchwald-Hartwig amination and S_NAr chemistry had previously been used in this research to install 4-amino substituents onto the quinoline ring. Therefore, a search for appropriate secondary aminopyridines available within our laboratories was performed and this yielded the three monomers (**178–180**) shown in Figure 46.

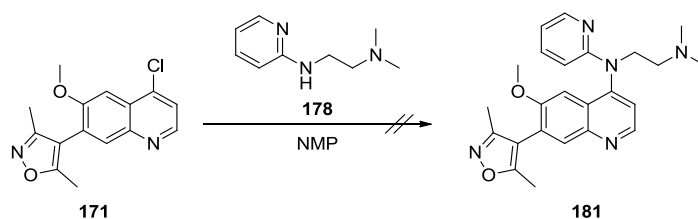
Amines	NH-coupling product	Predicted solubility of NH-coupling product at pH = 4.5 (μM)
 178	 181	>200
 179	 182	30–200
 180	 183	30–200

Figure 46. Predicted solubilities of tertiary 4-aminoquinolines.

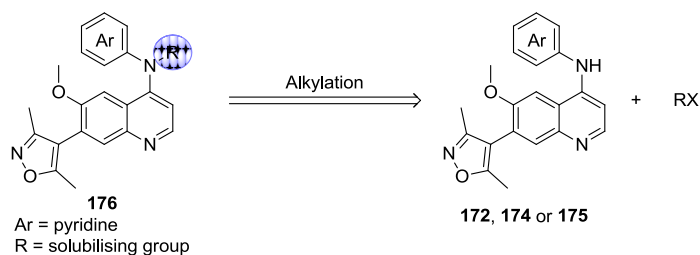
The solubilities of their coupling products (**181–183**) were calculated *in silico*⁹⁷ with the *N,N*-dimethyl-*N'*-2-pyridinyl-1,2-ethanediamine **181** predicted to have high solubility while the 2-(pyridin-2-ylamino)ethanol-4-pyridine **182** and 2-(pyridin-4-ylamino)ethanol-4-pyridine **183** were estimated to have moderate solubility. Therefore, the corresponding secondary amines were subjected to the previously successful Pd-catalysed amination conditions (125 °C, μwave , 15 min) (Scheme 17).

Scheme 17. Attempted synthesis of tertiary 4-aminoquinolines *via* Buchwald-Hartwig aminations.

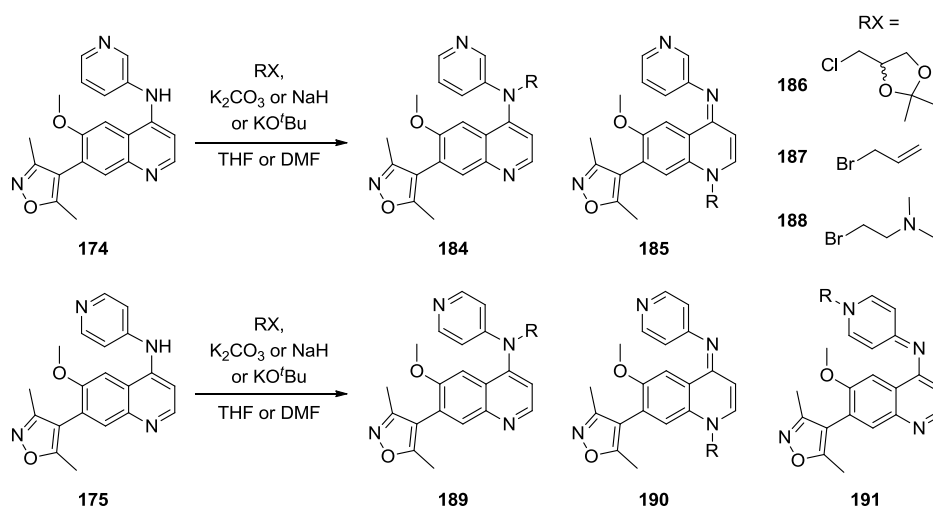
Disappointingly, no product was formed from any of the aminopyridines, with only starting 4-chloroquinoline **171** remaining or inseparable degradation products being observed by liquid chromatography mass spectroscopy (LCMS). An attempt at S_NAr chemistry (150 °C, μ wave, 20 min) with the aminopyridine **178** (Scheme 18) also failed to provide the desired product.

Scheme 18. Attempted synthesis of tertiary 4-aminoquinoline **181** *via* S_NAr .

Alternative amination conditions could have been attempted (e.g. alternative phosphine ligands and/or bases) but given the lack of success so far, an alternative chemistry strategy towards the tertiary 4-aminoquinoline target compounds was sought to meet the demands of this high priority project. One option was to *N*-alkylate the previously synthesised pyridines (**172**, **174** or **175**) to introduce the solubilising group as depicted in Figure 47.

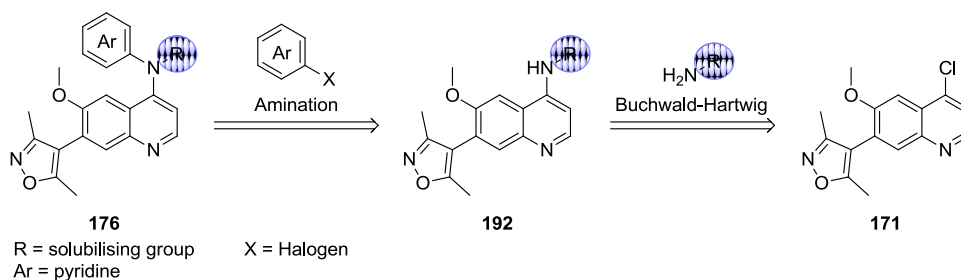
Figure 47. Revised chemistry strategy for synthesis of 4-tertiary amines *via* alkylation.

Accordingly, attempts at alkylation chemistry were made on the secondary 4-aminoquinolines where suitable quantities of material were available (**174** and **175**, Scheme 19).

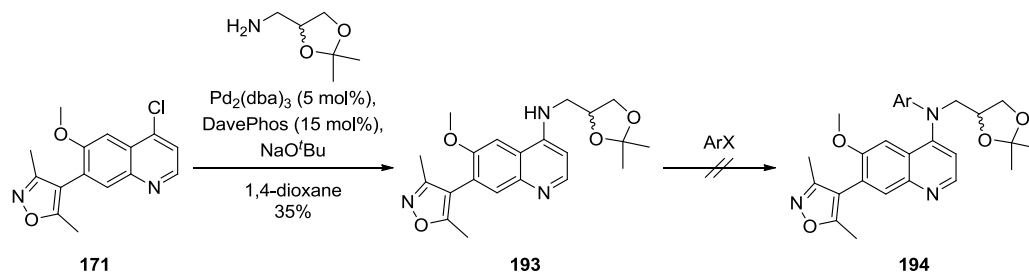
Scheme 19. Attempted synthesis of tertiary 4-aminoquinolines *via* *N*-alkylation chemistry.

The alkyl chloride **186** bearing the acetonide protected diol was examined first and was found to be particularly unreactive, probably due to the poor polarisability of the C–Cl bond, and steric and electronic resistance caused by the acetonide. Therefore, the highly electrophilic allyl bromide **187** was used with a view to subsequently derivatise to the diol *via* dihydroxylation. Several bases were explored (K_2CO_3 , KO^tBu and NaH) and different temperatures (room temperature and $75\text{ }^\circ\text{C}$) were examined. In all cases, either no conversion was observed, or mixtures of regioisomers were formed with the desired 4-aminoquinoline alkylation products **184** and **189** often the minor isomers, which proved difficult to separate from their respective regioisomers **185** and **190** by normal and reverse phase chromatography. The 4-aminopyridine **175** was also, unsurprisingly, activated towards alkylation on the 4-pyridine nitrogen giving the additional regioisomer **191**.

This exercise showed that the inherent reactivity of 4-aminoquinolines is through the quinoline nitrogen and is consistent with literature examples.^{98,99} Accordingly, an alternative approach to synthesising tertiary 4-aminoquinolines **176** was implemented and involved initial installation of the solubilising substituent to secondary 4-aminoquinolines **192** followed by incorporation of the aryl ring (Figure 48).

Figure 48. Alternative chemistry strategy for synthesis of 4-tertiary amines **176** *via* tandem amination reactions.

It was anticipated that this approach may potentially still suffer from poor reactivity of the 4-aminoquinoline NH in **192** but still had merit as there was some precedent for amination reactions of secondary 4-aminopyridines when using the XANTPHOS phosphine ligand.¹⁰⁰ A diol moiety was selected as the solubilising group as a test bed for this chemistry exploration (Scheme 20).



Scheme 20. Installation of the protected solubilising group to give **193**, followed by attempted introduction of an aryl substituent towards **194**.

Firstly, chloroquinoline **171** was subjected to the favoured Buchwald-Hartwig amination conditions to give the secondary 4-aminoquinoline **193** with a protected diol in 35% yield. Next, a range of amination conditions were investigated to prepare compounds of type **194** (Table 18). Despite varying the substitution pattern of the pyridine coupling partner, the ligand (including XANTPHOS), base and solvent (entries **1–4**), no product formation occurred with mainly starting material and multiple small by-products being formed. Attempts at $\text{S}_{\text{N}}\text{Ar}$ chemistry using 2-fluoropyridine also failed to yield any product under neutral or strongly basic conditions (entries **5** and **6**, respectively). Replacing the pyridine coupling partner with 1-bromo-2-fluorobenzene (a historically favoured aryl group) in Buchwald-Hartwig amination attempts (entries **7–11**) did not lead to productive coupling. Finally, an attempt at arylation using catalytic copper (I) iodide failed to give any conversion.

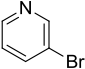
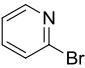
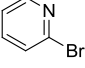
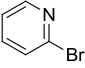
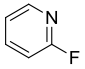
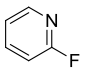
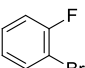
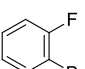
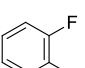
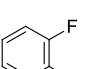
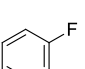
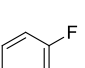
Entry	ArX	Catalyst	Ligand	Base	Solvent	Method
1		Pd ₂ dba ₃ (6 mol%)	DavePhos (12 mol%)	K ₃ PO ₄	toluene	125 °C μwave 20 min
2		Pd ₂ dba ₃ (6 mol%)	DavePhos (12 mol%)	K ₃ PO ₄	toluene	125 °C μwave 20 min
3		Pd ₂ dba ₃ (8 mol%)	DavePhos (15 mol%)	NaO ^t Bu	1,4-dioxane	125 °C μwave 20 min
4		Pd ₂ dba ₃ (8 mol%)	XANTPHOS (15 mol%)	NaO ^t Bu	1,4-dioxane	140 °C μwave 30 min
5		-	-	-	NMP	150 °C μwave 20 min
6		-	-	LiHMDS (1 M in THF)	THF	150 °C μwave 20 min
7		Pd ₂ dba ₃ (7 mol%)	dppf (15 mol%)	NaO ^t Bu	1,4-dioxane	100 °C thermal 22 h
8		Pd ₂ dba ₃ (7 mol%)	S-PHOS (15 mol%)	NaO ^t Bu	1,4-dioxane	100 °C thermal 22 h
9		Pd ₂ dba ₃ (7 mol%)	BINAP (15 mol%)	NaO ^t Bu	1,4-dioxane	100 °C thermal 22 h
10		Pd ₂ dba ₃ (7 mol%)	X-PHOS (15 mol%)	NaO ^t Bu	1,4-dioxane	100 °C thermal 22 h
11		Pd ₂ dba ₃ (7 mol%)	triisobutylphosphatane (15 mol%)	NaO ^t Bu	1,4-dioxane	100 °C thermal 22 h
12		CuI (10 mol%)	ethylene glycol	K ₃ PO ₄	IPA	90 °C thermal 16 h

Table 18. Conditions attempted for introduction of an aryl onto secondary amine **193**.

The many methods attempted at this stage suggested that either the 4-nitrogen atom of **193** was electronically deactivated towards further reaction and/or the reaction site was too sterically encumbered to allow further substitution at the 4-*N* position. To explore the latter possibility, attention turned to synthesis of tertiary anilines at the 4-position of the type **195** (Figure 49), which contained a smaller *N*-methyl substituent and a potential solubilising group on the 2-benzamide unit. Compounds of this type were of interest due to the good WB activity observed for the 4-anilino amide **196**⁸⁹ (Figure 49). However, despite the encouraging solubility for this compound as determined by CLND (196 µg/mL), the measured solubility at pH 5.0 and 7.0 was poor (97 and 10 µg/mL, respectively). Following the molecular budget approach described at the beginning of this section, the 3-amide substituent was ‘deducted’ and the molecular weight ‘spent’ on a 4-*N*-methyl aryl substituent to give the tertiary aniline targets of type **195**. The solubilising group in compounds of type **195** could be included as part of the amide functionality.

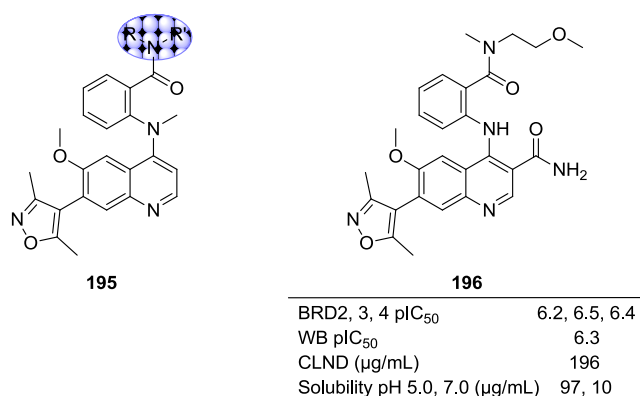
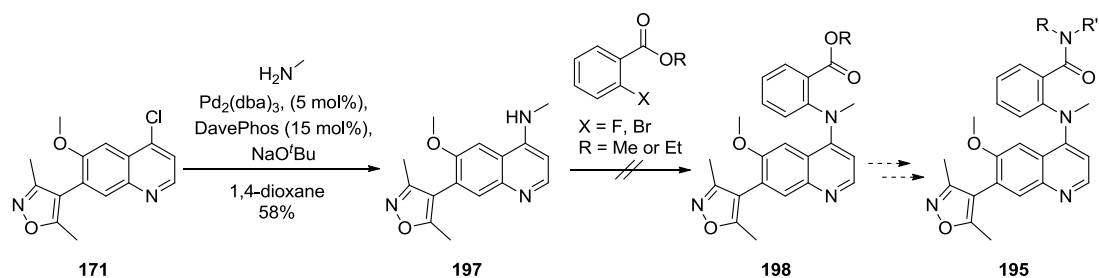


Figure 49. Desirable area of the 4-tertiary amine **195** where a solubilising group could be incorporated; and data for 4-anilino amide **196**.

A chemistry strategy to first install the small *N*-methyl substituent followed by *N*-arylation was pursued (Scheme 21). Formation of the secondary 4-aminoquinoline **197**, containing the *N*-Me substituent, proceeded smoothly using Pd-mediated amination in 58% yield. In turn, several attempts to install an aryl group to give compound **198** were executed either *via* S_NAr or using Buchwald-Hartwig amination conditions (Table 19).



Scheme 21. Attempted synthesis of 4-tertiary amine **198**.

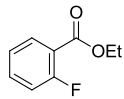
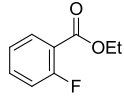
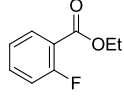
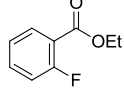
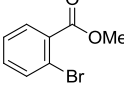
Entry	ArX	Catalyst	Ligand	Base	Solvent	Method
1		-	-	DIPEA	NMP	140 °C μwave 20 min
2		-	-	KO ^t Bu	DMF	120 °C μwave 20 min
3		-	-	LiHMDS (1 M in THF)	THF	120 °C μwave 20 min
4		-	-	NaH (60% in mineral oil)	THF	140 °C μwave 20 min
5		Pd ₂ dba ₃ (6 mol%)	DavePhos (14 mol%)	NaO ^t Bu	1,4-dioxane	125 °C μwave 20 min

Table 19. Reactions conducted in an attempt to install an *N*-aryl substituent.

Firstly, S_NAr reactions using ethyl 2-fluorobenzoate and a variety of bases were attempted (entries 1–4). Disappointingly, no product formed in any reaction with only minor by-product formation and starting material observed according to LCMS analysis. In the case of LiHMDS, a major by-product was observed by LCMS with a mass corresponding to an amide derived from nucleophilic substitution of the ethylester with the secondary 4-amino group on quinoline **197**. An attempt at Buchwald-Hartwig amination chemistry with methyl 2-bromobenzoate also failed to provide the desired product **198**.

The work in this section to this stage had progressively built a body of evidence indicating that tertiary 4-aminoquinolines were not viable targets based on poor synthetic tractability. It was hypothesised that any *N*-substituted 4-aminoquinoline, represented as **192** in Figure 50, was deactivated towards reaction at the 4-NH. Delocalisation of the 4-nitrogen lone pair into the electron-deficient quinoline ring would render the 4-nitrogen atom less nucleophilic and unable to participate both in Buchwald-Hartwig and S_NAr reactions.

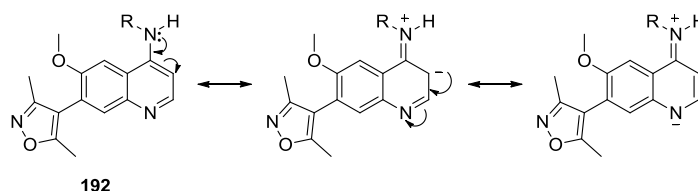


Figure 50. Resonance forms of 4-tertiaryamines.

This evidence, combined with that from elsewhere in our laboratory which also failed to deliver 4-tertiary amines *via* alternative routes,⁹² forced a revision of chemistry strategy. As 4-tertiary amines were not accessed in a robust and time efficient manner, other areas of the molecule and alternative chemistry were explored to increase both potency and solubility. More specifically, a proof of concept investigation was made into the incorporation of 4-*C* linked aryls, which would not be reliant upon the amination or *N*-alkylation chemistry which had proved to be challenging so far.

2.4. 4-*C* Linked Aryls

Given the difficulties encountered in accessing 4-tertiary amines, a review of SAR was conducted for the design of alternative target molecules and chemistries to access them. Accordingly, an exploration to replace the 4-nitrogen atom was pursued.

A search for quinolines containing atoms other than a nitrogen at the 4-position revealed that both the *O*-linked phenyl **199**¹⁰¹ and *C*-linked phenyl **200**¹⁰² had been synthesised as part of the pre-existing ApoA1 programme. These compounds were submitted for testing in the BET FP assays alongside their *N*-linked counterpart GW694481,⁶³ with the results shown in Table 20.

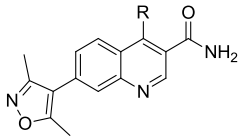
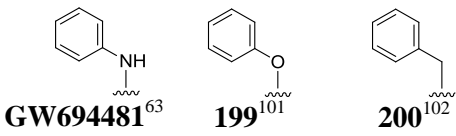
			
	BRD2, 3, 4 pIC₅₀	5.3, 5.9, 5.5	4.7, 5.2, 4.9

Table 20. BET activity of *N*-, *O*- and *C*-linked phenyls.

Although replacement of the 4-nitrogen atom resulted in lowered activity, a carbon atom was still tolerated. Since tertiary substitution on the 4-*N* atom was known to increase activity over secondary substitution (Table 16), then introducing a tertiary 4-*C* atom was predicted to also provide increased activity over the secondary substituted 4-*C* atom **200**. Furthermore, replacing a nitrogen atom with a carbon atom would provide several benefits at the 4-position:

- by providing greater valency, allowing for an additional vector for substitution;
- a differentiated geometry; and
- a stereogenic centre, which can have advantages in drug discovery.¹⁰³

To evaluate if a 4-*C* substituent might improve interaction with BET, computational docking experiments were conducted.¹⁰⁴ A range of molecules of type **201** (Figure 51) were

docked into BRD2 BD1 and an empirical docking score produced. The various contributors to protein–ligand affinity were incorporated into the calculation and included: displacement of waters by a ligand from hydrophobic regions of the binding site, electrostatic, hydrogen bond and lipophilic interactions, desolvation effects, and entropic effects arising from protein and ligand flexibility. The results from this analysis were used to rank virtual compounds against the baseline *N*-ethyl compound **164**,⁹² with lower negative scores indicating more favourable free energy upon binding.

The results revealed two trends: *S*-enantiomers were preferred over *R*-enantiomers and a chain length of $n = 1$ gave improved scores over $n = 2$. The ethylamine (*S*)-**202** displayed the best overall score of -8.5 kcal/mol, superior to that of its *N*-ethyl isomer **164**⁹² (-7.2 kcal/mol).

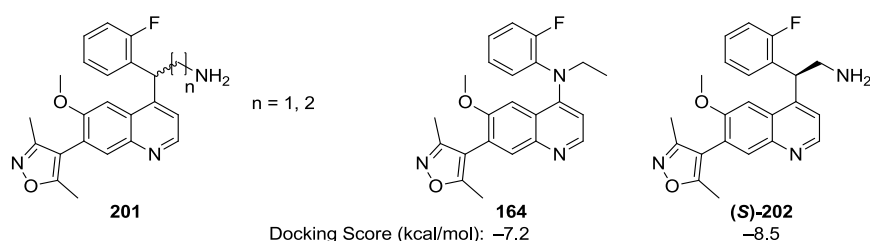


Figure 51. Comparison of docking scores of the 4-*N* ethyl **164** and the 4-*C* ethylamine (*S*)-**202**.

The improvement in estimated free binding energy of ethylamine (*S*)-**202** was rationalised by increased hydrophobic contact of the 4-*C* and ethylamine carbon atom with the adjacent Leu108 and/or closer contact of the 2-fluoroaniline with Trp97 of the WPF motif, as seen in Figure 52.

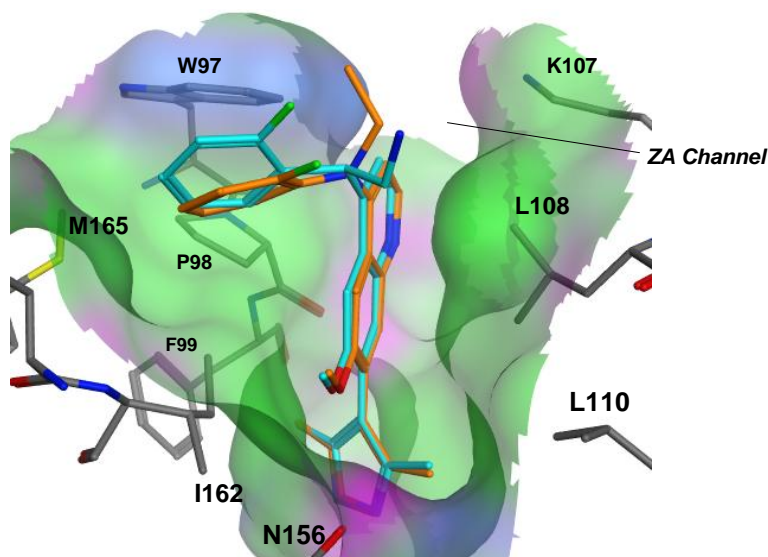


Figure 52. Docking model of *C*-linked (*S*)-**202** (carbon = cyan) into the crystal structure of *N*-linked **164** (carbon = orange) in BRD2 BD1. A molecular surface indicating hydrophobic (green), mildly polar (blue) and hydrogen bonding regions (magenta) was applied.

Substituents on the ethylamine (**S**)-**202** also looked attractive in terms of their predicted solubilities at pH 4.5⁹⁷ when profiled *versus* the *N*-ethyl compound **164**, with some examples shown in Figure 53.

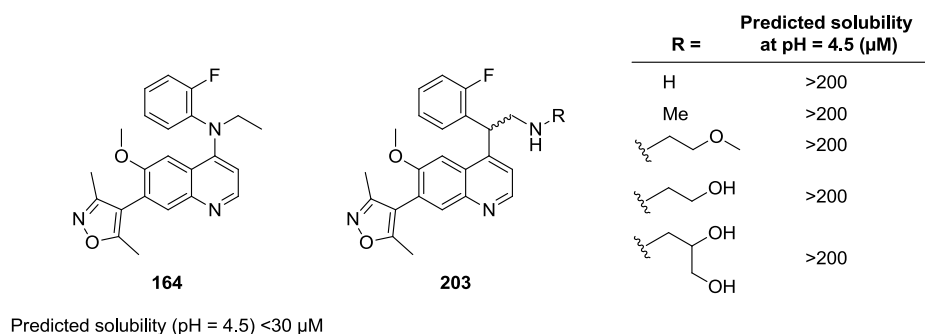
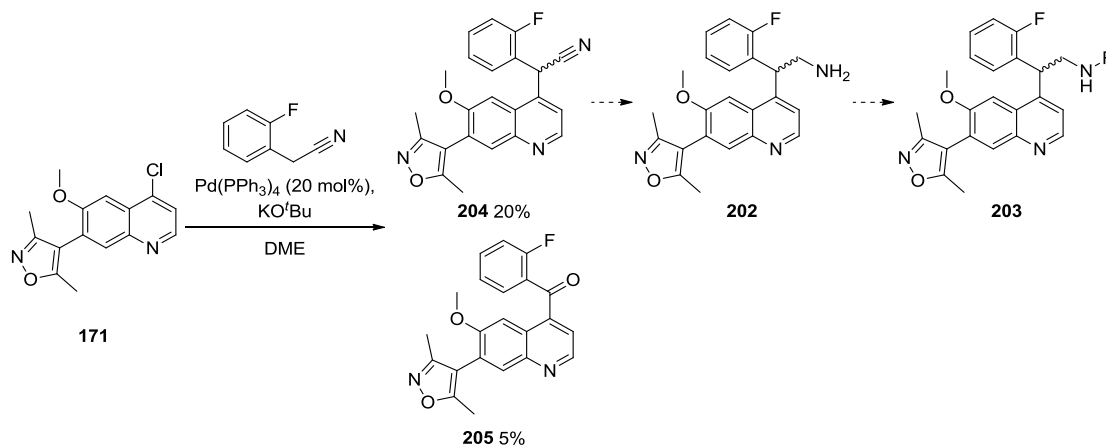


Figure 53. Predicted solubilities of a range of *C*-linked compounds at pH 4.5.

Access to racemic ethylamines of type **203** could be achieved by arylation of 2-(2-fluorophenyl)acetonitrile with the chloroquinoline intermediate **171**, reduction of the nitrile **204** and final stage reductive amination, as outlined in Scheme 22. An attempt to form the C–C bond using S_NAr conditions failed, so a palladium-catalysed arylation with (2-fluorophenyl)acetonitrile was performed, affording the desired nitrile **204** in 20% yield, as well as an unexpected by-product, the ketone **205**.



Scheme 22. Arylation and reduction route to ethylamines **203**.

Miura and co-workers first reported the arylation of phenylacetonitrile by palladium catalysis in 1998.¹⁰⁵ A catalytic cycle for this reaction was subsequently proposed by Hartwig and Culkin and is depicted in Figure 54.^{106,107} The aryl halide **207** first undergoes oxidative addition with the active catalytic species **206** to give the Pd(II) complex **208**. The aryl acetonitrile **209** is deprotonated by a strong base to give **210**, which undergoes ligand

substitution to an intermediate complex **211**, which may exist in a number of coordination modes. Reductive elimination then gives the arylation product **212**, regenerating Pd(0).

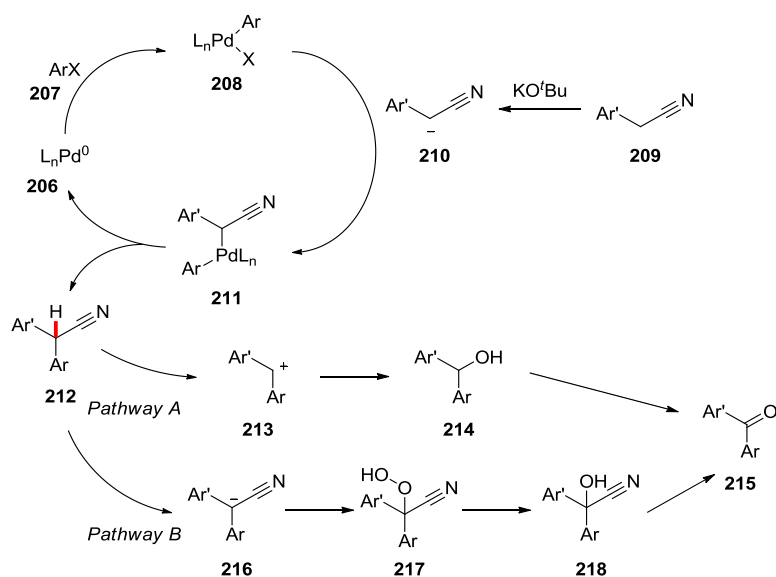


Figure 54. Mechanism of the palladium-catalysed arylation by an aryl acetonitrile and a possible pathway to by-product formation

The structure of by-product ketone **205** was confirmed using NMR analysis. A diagnostic ^{13}C shift at 194.0 ppm for the carbonyl carbon (C-11) and key Heteronuclear Multiple Bond Correlations (HMBCs) to quinoline (H-9) and aryl (H-27) hydrogen atoms were observed (Figure 55).

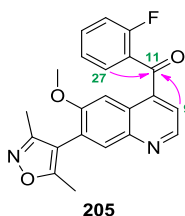


Figure 55. Diagnostic HMBCs of ketone **205**.

Formation of this by-product was postulated to occur *via* the pathways shown in Figure 54. A common contaminant of KO^tBu is KOH ¹⁰⁸ and this provided a potential oxygen atom source for incorporation (Pathway A). Nucleophilic attack of a hydroxide anion on the arylation product **212** could occur in an $\text{S}_{\text{N}}1$ fashion *via* the stabilised cation **213** to give the alcohol **214**. Benzylic oxidation may occur in the presence of Pd(II) and molecular oxygen¹⁰⁹ to give the ketone **215**. Some molecular oxygen may have been present in the reaction mixture, as the solvent was not degassed prior to irradiation. In Pathway B, the stabilised anion **216** may be formed from the slight excess of base in the reaction and subsequent trapping of molecular oxygen would generate the α -cyanohydroperoxide **217**. Reduction

with Pd to the cyanohydrin **218** followed by a base-induced oxidative-decyanation would afford ketone **215**.¹¹⁰

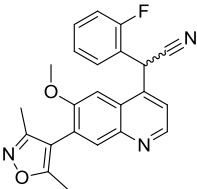
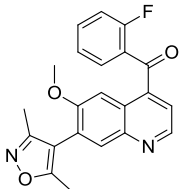
		
	204	205
BRD2, 3, 4 pIC₅₀	6.4, 6.5, 6.1	5.8, 6.2, 5.8
WB pIC₅₀	5.0	5.7
Solubility CLND (µg/mL)	11	11

Table 21. SAR table of C-linked aryls.

This brief foray into C-linked quinolines was suspended as emerging data meant that 4-amino exploration was reprioritised and reduction of the nitrile **204** to the ethylamine **202** was not optimised. The biological data for the C-linked aryls shown in Table 21 showed great potential for further investigation where BET activity was retained and WB activity achieved, even with by-product ketone **205**. Further work on the C-linked aryls would be warranted as a new vector for a solubilising group was created and new chemistry for introducing 4-substituents was established.

Continued exploration of 4-amino substituents was being pursued elsewhere in the laboratory,⁹² and in a concerted effort to build on encouraging WB activity and solubility, synthetic chemistry focus was diverted to further investigation of 4-amino substituents.

2.5. Further 4-Amino Substituent Exploration

The exploration of the 4-amino substituent in Section 2.3 described the molecular budget approach whereby the 3-amide substituent was deducted and the molecular weight ‘saved’ was ‘spent’ on pendant solubilising groups on the 4-aniline substituent. This approach was used to attenuate increases in molecular weight of the target compounds and optimise their physicochemical properties when exploring different areas of the molecule. However, a 4-tertiary amine was crucial to this approach as this would retain or improve BET activity when the 3-amide substituent was removed. Unfortunately, attempts to synthesise 4-tertiary amines were met with limited success and a new strategy to identify potent, soluble compounds was required.

Research ongoing within the laboratory used a strategy to retain the 3-amide substituent while incorporating a *secondary* amine at the 4-position with appropriate substitution on the anilino-aryl unit, giving quinolines of the type **219** shown in Figure 56.⁹²

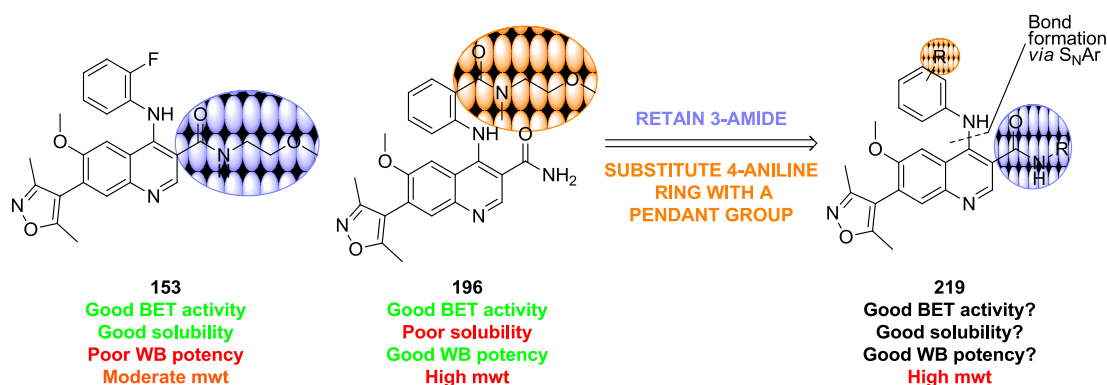
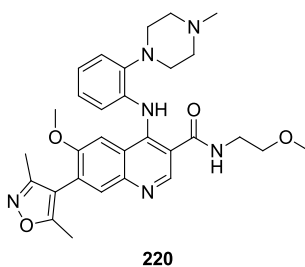
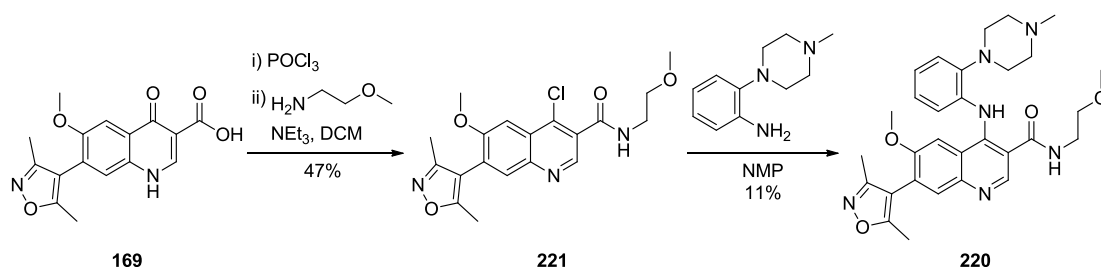


Figure 56. New chemistry strategy retaining the 3-amide substituent.

In some cases, this combination of substituents gave good BET activity and solubility (see compound **153**⁹¹ in Table 13). Such compounds were postulated to be more chemically tractable than 4-tertiary amines, as an electron-withdrawing 3-amide substituent would facilitate a S_NAr reaction of a primary aniline with a 4-chloroquinoline. As part of this strategy, pendant groups were to be incorporated into the 4-aniline ring which, in the case of compound **196**, afforded good WB potency despite the high molecular weight. The vector at the 2-position of the aniline was directed toward solvent and introduction of a solubilising group such as an *N*-methylpiperazine was anticipated to increase solubility. When combined with a favoured 3-methoxyethyl amide giving quinoline **220** (Figure 57), high solubility at pH 4.5⁹³ (130 mg/mL) was predicted and this compound was therefore selected for synthesis. It was recognised that an increase in molecular weight would result from this strategy but previous efforts to attenuate molecular weight did not provide the desired activity and solubility profile. With encouraging results found with related compounds and encouraging predicted properties, synthesis of these analogues continued.

Figure 57. Target dimethylisoxazole quinoline containing an *N*-methylpiperazine on the 4-aryl ring.

Synthesis of dimethylisoxazole quinoline **220** commenced with the chlorination of the quinolinone acid **169**⁹⁴ (available within the laboratory) and subsequent amidation to the chloroquinoline intermediate **221** in 47% yield over two steps (Scheme 23). The *N*-methylpiperazine solubilising group was incorporated by S_NAr reaction with the commercially available 2-(4-methylpiperazin-1-yl)aniline to give the target compound **220** in 11% yield.

Scheme 23. Synthesis of *N*-methylpiperazine **220**.

Upon screening, the *N*-methyl piperazine **220** displayed excellent BET activity (although an unusually high pIC_{50} value for BRD3 was obtained, Table 22). This compound also demonstrated high WB potency ($pIC_{50} = 6.5$) as well as good CLND solubility. The morpholines **222**⁹² and **223**,⁹² synthesised elsewhere within our laboratory, also displayed encouraging results with micromolar WB potency and, in the case of the hydroxyethyl amide **222**, displayed the solubility level required for *i.v.* administration at pH 5.0.

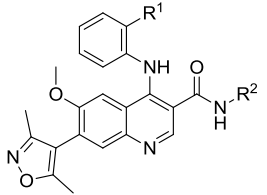
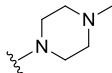
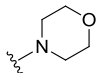
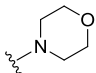
	$R^1 =$	$R^2 =$	
			
	220	222⁹²	223⁹²
BRD2, 3, 4 pIC₅₀	6.7, 7.8, 6.7	6.7, 6.7, 6.2	6.7, 6.7, 6.3
WB pIC₅₀	6.5	5.9	6.0
chromLogD_{7,4}/chromLogP	3.6/5.1	3.9/4.0	5.1/5.4
Solubility CLND (μg/mL)	186	151	86
Solubility pH 5.0 (μg/mL)	NT	>1000, <5000	<1000

Table 22. SAR table of 4-anilines with pendant solubilising groups.

Until this point, obtaining compounds with greater than micromolar WB activity had presented a challenge, particularly when trying to combine with good aqueous solubility required for *i.v.* administration. The synthesis of these compounds made considerable progress towards achieving these goals.

As part of the screening strategy towards developing pre-candidate molecules, quinolines **220**, **222** and **223** were tested in a hERG electrophysiology assay (Table 23).

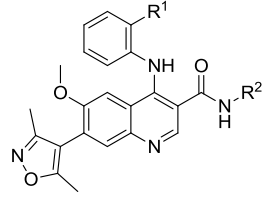
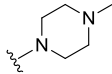
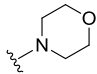
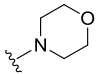
	$R^1 =$	$R^2 =$	
			
	220	222⁹²	223⁹²
hERG pIC₅₀	5.9	5.0	5.0
chromLogD_{7,4}/chromLogP	3.6/5.1	3.9/4.0	5.1/5.4

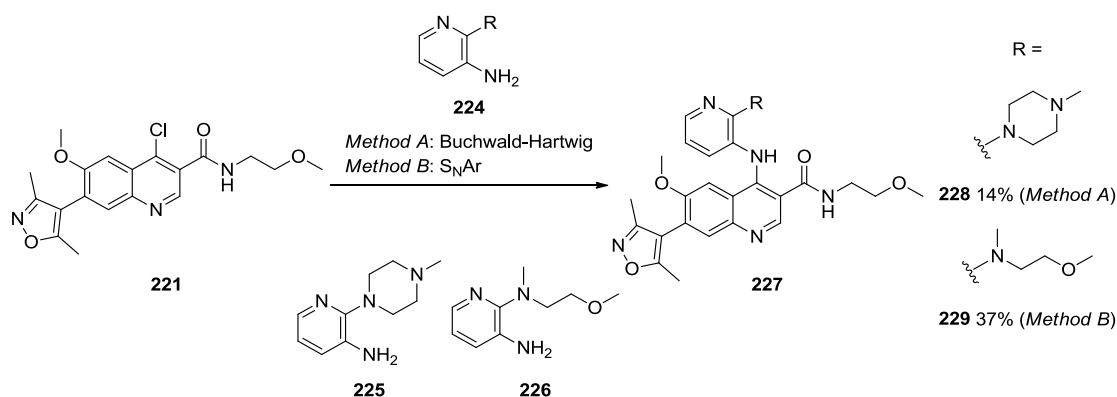
Table 23. hERG activity and chromLogP/D measurements for 4-anilines with pendant solubilising groups.

Inhibition of the hERG ion channel can lead to increases in the cardiac QT interval and thus poses a serious risk for further compound development.¹¹¹ Unfortunately, data from this assay revealed unacceptable inhibition levels for all compounds, and particularly for the *N*-methyl piperazine **220** which displayed a pIC₅₀ = 5.9. With analyses demonstrating the strong contribution of both lipophilicity and positive

ionisation state upon hERG inhibition,¹¹² these compounds were submitted for chromLogP and chromLogD measurements¹¹³ (Table 23).

In a study published by our laboratories, values determined from these chromatographic measurements of lipophilicity were shown to correlate with hERG inhibition.¹¹³ A particularly strong relationship was found for chromLogP and highlighted the importance of the intrinsic lipophilicity on hERG binding. Based on these findings, the additional intrinsic lipophilicity (estimated by chromLogP) of the methoxyethyl amide in **220** compared to the hydroxyethyl amide in **222**, and the strongly basic centre present in the *N*-methyl piperazine moiety in **220** but absent in the morpholine analogue **223**, were proposed to contribute to the increased hERG inhibition. Nevertheless, quinolines **222** and **223** still inhibited the ion channel with unacceptably high potencies and this was attributed to their relatively high intrinsic lipophilicities.

A strategy was therefore devised to reduce the lipophilicity of the 4-aryl group in an attempt to prevent hERG inhibition but still retain high solubility at pH 5.0. This could be achieved by introducing a nitrogen atom into the 4-aniline ring. Using the information gathered from the 4-aminopyridine exploration in Section 2.3, where a *meta*-pyridine was well tolerated, 2,3-disubstituted pyridines of the type **227** (Scheme 24) were targeted for synthesis. These could be accessed from 3-aminopyridines **224** using Buchwald-Hartwig aminations or S_NAr chemistry.



Scheme 24. Synthesis of 3-aminopyridines **228** and **229**.

The aminopyridines **228** and **229** were synthesised from the commercially available 3-aminopyridine **225** and the in-house synthesised 3-aminopyridine **226**¹¹⁴ in 14% and 37% yields, respectively. These compounds, combined with **230**¹¹⁴ (synthesised elsewhere within the laboratory) showed promising results which are displayed in Table 24.

	R =	230 ¹¹⁴	228	229
BRD2, 3, 4 pIC₅₀		5.6, 6.5, 5.5	6.6 ^a , 6.7 ^a , 6.6 ^a	6.1, 6.5, 5.6
WB pIC₅₀		6.1	6.4	5.9
chromLogD_{7.4}/chromLogP		3.8/3.9	2.5/3.1	4.2/4.3
Solubility CLND (µg/mL)		290	176	231
Solubility pH 5.0 (µg/mL)		>1000, <5000	NT	NT
hERG pIC₅₀		4.4	<4.2 ^b	4.9

Table 24. SAR table of 4-aminopyridines with pendant solubilising groups. ^aThese data were obtained from Homogeneous Time Resolved Fluorescence assays. ^bThis data was obtained from a more recent hERG electrophysiology assay (see Appendix for details).

The 2-methoxy-*N*-methylethanamine **229** displayed good activity in the BET FP assays and respectable WB activity with pIC₅₀ = 5.9 but, disappointingly, exhibited hERG inhibition. The pyridinemorpholine **230** also showed good BET binding activity and WB activity (pIC₅₀ = 6.1). With high solubility determined by CLND, pyridinemorpholine **230** was progressed to solubility measurements from solid where the desired solubility of >1000 µg/mL was achieved. However, upon testing in the hERG assay, measurable inhibition was found albeit at a very weak level. The *N*-methylpiperazine **228** displayed high potency in the BET Homogeneous Time Resolved Fluorescence (HTRF) assays (see Appendix) and was the most potent in the WB assay from this set of aminopyridines. The introduction of the additional nitrogen in the aryl ring (compare phenyl **220** in Table 23 with pyridine **228** in Table 24) successfully lowered lipophilicity with a 100-fold reduction in chromLogP observed. Excitingly, this transformation ablated hERG activity and, consequently, piperazine **228** possessed the best profile obtained from the synthetic efforts on this programme of chemistry. Unfortunately, a change in project priorities meant that this compound was not progressed for solubility measurement from solid. If solid solubility matched the encouraging solubility level from DMSO precipitation then this compound would meet the desired criteria and be a candidate for *in vivo* PK studies.

From these data, it was evident that replacement of the 4-phenyl ring with a pyridine successfully decreased hERG inhibition. However, the extent of this effect varied depending on the substituent. In the case of the morpholine substituted rings, the pyridine **230** (Table

24) lowered the hERG pIC₅₀ 2.5-fold when compared to the phenyl **223** (Table 23). When substituted with a piperazine, a pyridine ring (**228**, Table 24) lowered hERG inhibition 25-fold when compared to a phenyl ring (**220**, Table 23). These data demonstrated that in addition to lowering lipophilicity of the 4-aryl ring, subtle effects such as distribution of electron density may account for the reduction in inhibition of the hERG ion channel.

The efforts described in this section made significant progress towards achieving the project objectives. The anilinopiperazine **220** showed promise by achieving the best WB activity observed within the quinoline series so far. However, a drug development issue in the form of hERG inhibition was found for this compound. Accordingly, a strategy was devised to attenuate this risk. Success was achieved by the introduction of a pyridine ring where, for the morpholinopyridine **230**, hERG activity was lowered compared to its phenylmorpholine analogue **223** while retaining micromolar WB activity. The *N*-methylpiperazine **228** exhibited the best profile for this programme of research at that point in time. Potent BET inhibition was achieved, and coupled with high WB activity, *N*-methylpiperazine **228** met the programme requirements. Notably, this compound did not inhibit the hERG ion channel and therefore overcame a serious barrier to further drug development which had previously hindered programme progression. Resource-permitting, the encouraging data achieved with dimethylisoxazole quinoline **228** warranted further progression including solubility measurements from solid.

2.6. Conclusions and Future Work

The research described on the quinoline series of BET inhibitors was carried out in order to quickly identify a drug pre-candidate suitable for *i.v.* administration, targeting immuno-inflammatory disorders. Building on a pre-existing programme of research conducted within our laboratories, compounds from the quinoline series were developed towards pre-candidate drugs with good WB activity and aqueous solubility. The contribution within this specific programme focused on the following different areas.

Firstly, an investigation of quinoline 3-methylamines allowed a comparison of an alternative solubilising substituent compared to previously used amides. Good solubility levels were demonstrated with 3-position amines combined with fair WB activity, but the 3-amines did not display significantly superior values compared to their corresponding amides. This exercise warranted further investigation after exploration of other areas of the dimethylisoxazole quinoline series.

A range of pyridine isomers were synthesised as part of a molecular budget approach to 4-amino substituent exploration, and a data package was built to stimulate future work. An improvement in WB activity and solubility was sought by attempting to substitute the 4-nitrogen with alternative pendant groups. A significant chemistry effort was invested to try and achieve this objective but was unsuccessful.

A revision of the chemistry strategy was made by seeking opportunities to use arylations of alkylnitriles. This initial exploration highlighted the potential for C-linked aryls to achieve high WB activity and solubility.

Lastly, exploration of a 4-amino substituent while retaining a 3-amide substituent achieved valuable progress towards project objectives. An anilinopiperazine substituent displayed the best WB activity observed from the quinoline series to date within this overarching endeavour but, also, displayed hERG ion channel inhibition. The strategy employed to attenuate this risk was to replace the 4-phenyl ring with a pyridine to lower lipophilicity. In the case of the *N*-methylpiperazine **228**, this strategy successfully overcame the hERG liability. With potent BET inhibition and high whole blood activity, this dimethylisoxazole met the programme requirements. Disappointingly, due to a change in project priorities, *N*-methylpiperazine **228** was not progressed for solubility measurement from solid. The high solubility determined by the high-throughput CLND measurements provided evidence that a similarly positive result was likely in the low-throughput solubility measurement from solid. If this was the case, *N*-methylpiperazine **228** would have fully met the project objectives and been progressed into *in vivo* PK studies.

3. Imidazoquinolinones as Bromodomain-Selective BET Probes

The first generation BET inhibitors I-BET762 and (+)-JQ1 show great potential as novel pharmaceuticals. However, to date, these molecules have mainly been studied in aggressive cancers and acute inflammation models. Encouraging studies with (+)-JQ1 as a potential male contraceptive has expanded the therapeutic scope beyond terminal conditions⁶⁰ but translation of spermatogenic effects from mice into humans has yet to be carried out and a testicular shrinkage side effect may affect compliance. The long term safety implications of epigenetic modification by these BET inhibitors are uncertain, especially considering the importance of BET family members in normal cellular function. While these molecules were selective for the BET family over other BCPs, they displayed similar affinities for each of the bromodomains within the BET family. The biological significance of this pan-selectivity is not well understood but affecting such a range of gene expression patterns could give rise to undesired effects.

There have been a limited number of investigations into the specific roles of the individual bromodomains in the BET family, mainly through deleting sections of BET protein. An *in vitro* investigation of cell growth regulation revealed that interaction of Brd4 with replication factor C (RFC) is dependant only on BD2 and not BD1.¹¹⁵ Studies by Alsarraj *et al.* showed that deletion of BD2 had a greater suppressive effect on tumour growth compared to deletion of BD1 in Brd4.¹¹⁶ In another study, mutant mice lacking BD1 of the testis-specific BET protein Brdt implicated the first bromodomain module as essential for sperm chromatin organisation.¹¹⁷ These experiments demonstrated that each individual bromodomain within BET proteins exhibited interesting distinct functions. Small molecules interacting with only a subset of the BET bromodomains would be desirable for biological profiling and may narrow the phenotypes observed compared to pan-BET inhibitors. Accordingly, and as part of this programme, a targeted, small molecule probe approach was taken to identify pan-BD1 and pan-BD2 selective BET inhibitors, with the aim of investigating any differentiated phenotypes compared to pan-BET inhibitors.

3.1 Medicinal Chemistry Strategy and Project Aims

The ultimate goal of this research was to compare *in vitro* phenotypic data of a domain-selective BET inhibitor to a pan-BET inhibitor. Thus, a normal drug discovery strategy was not required for the discovery of a domain-selective molecule but, instead, a chemical probe strategy was undertaken. Accordingly, a number of criteria for probe discovery were set with the objective of clearly understanding the biological outcomes from phenotypic studies:

- at least 100-fold selectivity for either BD1 or BD2 and 100 nM activity for the higher affinity bromodomain determined using mutant FRET assays;
- good cell permeability determined using an artificial membrane permeability (AMP) assay; and
- high specificity for the BET bromodomains over other BCPs determined using a binding assay panel at DiscoverX Corporation.

Detailed information for these assays can be found in the Appendix. Once a compound met these requirements it could then be progressed into *in vitro* phenotypic studies.

A comparison of the amino acid sequence between the bromodomain modules (BD1 and BD2) in the BET proteins, revealed high sequence identity (73–88%) between the bromodomains across the different BET proteins, e.g. BRD2 BD1 *versus* BRD4 BD1 and BRD2 BD2 *versus* BRD4 BD2.⁴⁴ Lower sequence identity (37–43%) was observed between the two bromodomain modules within a BET protein, e.g. between BD1 and BD2 of BRD2 and between BD1 and BD2 of BRD4. The alignment in Figure 58 clearly identified residue differences between the tandem domains. In particular, the residue variation at the terminus of the BC loop (Asp in BD1 and His in BD2), was significant due to the difference in charge, and size, between these amino acids. A small molecule forming a charged interaction with Asp in BD1 would potentially form a charge clash with His in BD2 and afford a BD1-selective inhibitor. Conversely, forming a charged interaction with His in BD2 would potentially form a charge clash with Asp in BD1 affording a BD2-selective inhibitor. However, it should be noted that the key amino acid residues important for small molecule binding, such as the conserved Asn and the WPF motif, are present in both BD1 and BD2. These observations provided confidence that a small molecule chemical probe could distinguish between the BD1 and BD2 bromodomains, but achieving a large selectivity window may be challenging.



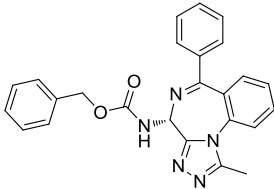
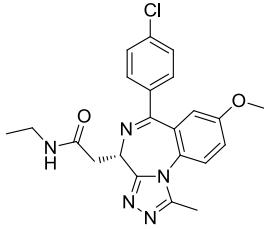
BRD2 BD1	77	NQLQYLHKVVMKALWK . . . HQFAWPFQRPVDAVKLGLPD Y HKKI IKQPMD	122
BRD3 BD1	37	NQLQYMQNVVVKTLWK . . . HQFAWPFYQPVDAIKLNLDP Y HKKI IKNPMD	82
BRD4 BD1	61	NQLQYLLRVVLKTLWK . . . HQFAWPFQQPVDAVKLNLDP Y YKIIKTPMD	106
BRDT BD1	30	NQLQYLQKVVLKDLWK . . . HSFSWPFQRPVDAVKLKLDP Y YTI IKNPMD	75
BRD2 BD2	347	SEQLKHCNGILKELLSKKHAAYAWPFYKPVDAALGLHD Y HDI IKHPMD	395
BRD3 BD2	309	SEHLRYCDSILREMLSKKHAAYAWPFYKPVDAEALGLHD Y HDI IKHPMD	357
BRD4 BD2	351	SEQLKCCSGILKEMFAKKHAAYAWPFYKPV DVEALGLHD Y CDI IKHPMD	399
BRDT BD2	268	TEQLRHCEILKEMLAKKHFSYAWPFYNPVDVNALGLHN Y DVVKNPMD	317



BRD2 BD1		MGTIKRRELENNYYWAASECMQDFNTMFTNCYIY N KPT D DIVLMAQTLEKIFLQKVA	178
BRD3 BD1		MGTIKRRELENNYYWSASECMQDFNTMFTNCYIY N KPT D DIVLMAQALEKIFLQKVA	138
BRD4 BD1		MGTIKRRELENNYYWNAQECIQDFNTMFTNCYIY N KPG D DIVLMAEAELEKLFQKIN	162
BRDT BD1		LNTIKRLENKYAKASECIEDFNTMFSNCYLY N KPG D DIVLMAQALEKLFMQKLS	131
BRD2 BD2		LSTVKKRMENRDYRDAQEFAADVRLMFSNCYKY N PPD H EVVAMARKLQDVFEFRYA	451
BRD3 BD2		LSTVKKRMDGREYPDAQGFAADVRLMFSNCYKY N PPD H EVVAMARKLQDVFEMRFA	413
BRD4 BD2		MSTIKSKLEAREYRDAQEFGADVRLMFSNCYKY N PPD H EVVAMARKLQDVFEMRFA	455
BRDT BD2		LGTIKEKMDNQEYKDAYKFAADVRLMFMNCYKY N PPD H EVVVTMARMLQDVFETHFS	372

Figure 58. Amino acid sequence alignment of human BET proteins. The conserved tyrosine and asparagine KAc recognition residues are highlighted in bold. An important residue difference between BD1 and BD2 is coloured.

Advanced BET inhibitors published in the literature at the outset of this programme of research included the first generation molecules GW841819X, I-BET762 and (+)-JQ1, as well as the more recently disclosed dimethylisoxazole I-BET151. In order to find a start point for probe discovery, these molecules were screened in the BET mutant assays to establish their activity at BD1 and BD2, and determine their suitability for optimisation into domain-selective variants (Table 25).

	 GW841819X			 I-BET762		
	pIC₅₀			pIC₅₀		
	BD1	BD2	BD1–BD2	BD1	BD2	BD1–BD2
BRD2	6.8	6.8	0	6.9	7.3	–0.4
BRD3	7.0	7.3	–0.3	7.2	7.5	–0.3
BRD4	7.1	7.1	0	7.2	7.5	–0.3
BRDT	7.1	6.8	0.3	7.3	6.9	0.4

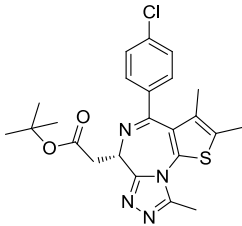
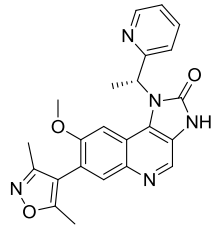
	 (+)-JQ1			 I-BET151		
	pIC₅₀			pIC₅₀		
	BD1	BD2	BD1–BD2	BD1	BD2	BD1–BD2
BRD2	7.3	NT	NT	7.3	6.7	0.6
BRD3	7.1	7.2	–0.1	7.5	7.1	0.4
BRD4	7.3	7.2	0.1	7.5	6.5	1.0
BRDT	7.0	6.5	0.5	6.9	5.8	1.1

Table 25. BET mutant assay results for selected literature BET inhibitors.

The BzD GW841819X showed similar 100 nM activity for all eight BET bromodomains and corroborated the data from Chung *et al.*,⁴⁴ demonstrating that this molecule was unselective. Results for both I-BET762 and (+)-JQ1 showed minimal domain selectivity which varied according the individual BET family member, resulting in an overall unselective binding profile. Taken together, these data confirmed compounds from the BZD structural class possessed no inherent preference for either BD1 or BD2. Intriguingly, I-BET151 exhibited a preference for binding to BD1. In particular, 10-fold selectivity for BRD4 BD1 over BRD4 BD2 was observed while values ranging from 2.5-fold for BRD3 to 12.6-fold for BRDT were found for the other BET mutants.

With a number of residue differences identified in the sequence comparison of the tandem bromodomains, the X-ray crystal structure of I-BET151 in BRD4 BD1⁶³ was superimposed with the apo structure of BRD4 BD2¹⁰ (Figure 59) and the resulting structure examined to provide insight into these initial screening data, and to assess the potential for designing compounds with improved domain selectivity.

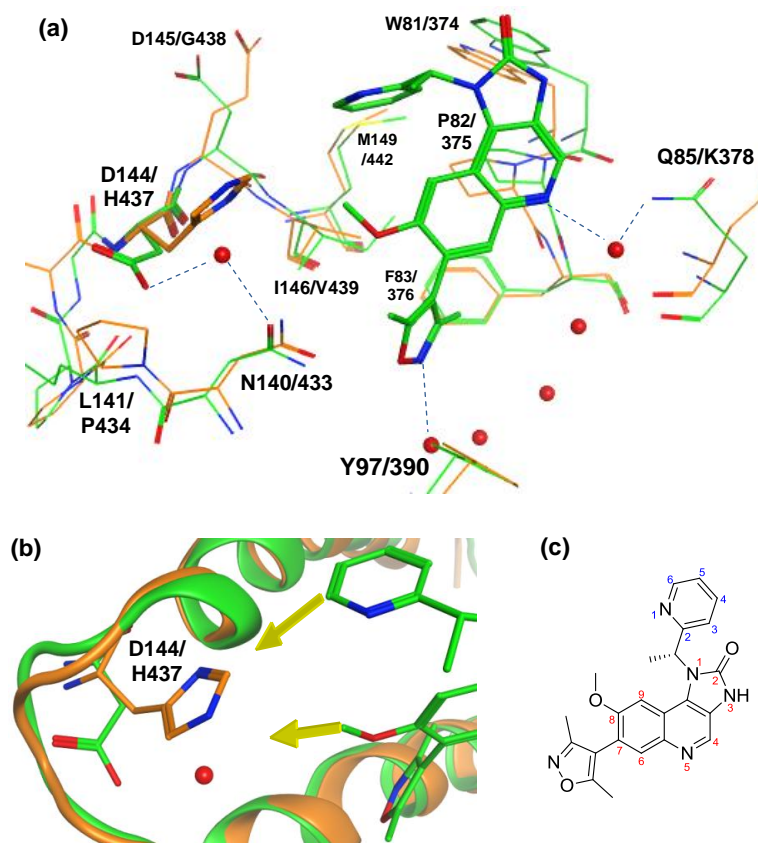


Figure 59. Complex of imidazoquinolinone I-BET151 in BRD4 BD1⁶³ (carbon = green, pdb 3ZYU) superimposed with apo BRD4 BD2¹⁰ (carbon = orange, pdb 2OUO). (a) Side view. (b) Vectors from I-BET151 directed towards Asp144 and His437 are highlighted with yellow arrows. (c) Numbering system of I-BET151.

As highlighted in the introduction, key ligand-protein interactions included hydrogen bonding of the isoxazole to Asn140 and through-water to Tyr97, lipophilic sandwiching of the quinoline by Leu108 and residues of the WPF motif, and occupation of the WPF shelf by the pyridine ring. It was also noted that the quinoline nitrogen accepted a hydrogen bond from a nearby water molecule. Closer examination revealed that this water interacts with Gln85 in BRD4 BD1; a residue replaced by lysine in BD2 and, thus, provided tentative rationale for the inherent BD1-bias of I-BET151. Inspection of the key Asp/His residue difference revealed that the BD1-conserved aspartic acid (Asp144) interacted with a nearby water molecule which has previously been identified as conserved in corresponding structures of fragments bound to BRD2 BD1.⁷⁴ This water hydrogen-bonded to Asn140 and

is replaced by the BD2-conserved histidine (His437) in the corresponding apo BD2 structure. Due to these structural differences, it was posited that small molecules interacting directly or through-water to the Asp residue of BD1 and/or clashing with the histidine of BD2 would display selective binding for BD1. In particular, the imidazoquinolinone 8-position and the pyridine 6-position were identified as preferred vectors for chemical modification to target these residues (Figure 59b).

Synthetic explorations at these positions were therefore prioritised to rapidly assess the potential for attaining greater domain selectivity. Moreover, as significant chemistry effort had been invested in the development of I-BET151, it was preferable that significant alterations to the molecule were avoided and, consequently, a focused plan of work was initially designed. However, before a programme of chemistry was formulated, a thorough assessment of SAR was required to confirm key features required for activity and selectivity.

3.1.1 SAR Review

While some structure activity relationships of I-BET151 have been disclosed,^{63,64} the activities reported were obtained from a cellular phenotypic assay measuring ApoA1 upregulation and from biochemical BRD2, 3 and 4 WT FP assays which could not distinguish selective BD1 or BD2 binding. Consequently, a more in-depth understanding was gained by mining historical data, analysing structural information and testing previously synthesised dimethylisoxazole quinolines available within our in-house compound collection in the new mutant FRET assays.

Firstly, the importance of the 3,5-dimethylisoxazole moiety of I-BET151 was considered. As the sequence alignment in Figure 58 showed residues involved in KAc recognition were highly conserved between BD1 and BD2, alterations to the KAc mimetic were therefore unlikely to modulate selectivity. Moreover, there was a lack of published SAR around the 3,5-dimethylisoxazole moiety. Only reports from our own laboratories provide any comment: Mirguet *et al.* noted that the 3,5-dimethylisoxazole was crucial for ApoA1 activity⁶³ but did not provide supporting SAR data and Bamborough *et al.* synthesised a 5-ethyl-3-methylisoxazole fragment to confirm the binding mode of 3,5-dimethylisoxazole in BRD2 BD1⁷² but did not publish any activity data. Mutant assay results from screening 3,5-dimethylisoxazole analogues available in our in-house collection did not provide any evidence that changes to the KAc mimetic of I-BET151 would enhance domain selectivity (data not shown). Therefore, the 3,5-dimethylisoxazole was retained for the design of domain-selective analogues.

This restraint was also applied to the core quinoline structure. Inspection of crystal structures showed that the fused ring system was beneficially positioned in the binding site and optimising selectivity for BD1 or BD2 by modification of this structural feature would be challenging. Additionally, the limited published SAR and slightly more expansive SAR generated in-house, suggested alteration of the quinoline was a not an immediate priority.

The importance of the stereogenic centre within I-BET151 for BET activity has been highlighted by Seal and co-workers using WT FP assays.⁶⁴ To establish if SAR were replicated in the mutant FRET assays, data for the stereoisomer of I-BET151 (**46**⁶⁴) and the analogue lacking the benzylic methyl **40**⁶³ was obtained in the BRD4 BD1 and BD2 assays and, for completeness, the racemate **231** was synthesised (*vide infra*) and also tested (Table 26).

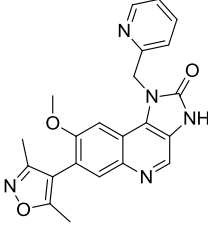
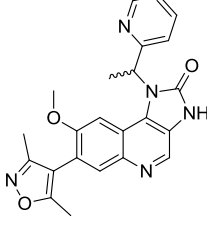
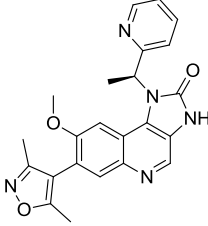
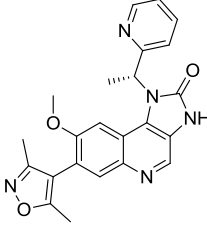
				
	40 ⁶³	231	46 ⁶⁴	I-BET151
BRD4 BD1, BD2 pIC₅₀	6.7, 6.3	7.2, 6.2	6.3, 5.8	7.5, 6.5
BD1–BD2	0.4	1.0	0.5	1.0

Table 26. Profile of a selection of imidazoquinolinones.

As with previous SAR,⁶⁴ the stereochemistry greatly influenced potency, with the *R*-enantiomer showing 16 times greater activity than the *S*-enantiomer at BD1. Intriguingly, the configuration of the stereocentre also appeared to affect selectivity with I-BET151 affording 3 times greater BD1 selectivity than its stereoisomer **46**.⁶⁴ In the above discussion of the I-BET151–BRD4 BD1 crystal structure, it was hypothesised that a through-water interaction of the quinoline nitrogen to Gln85 gave rise to the inherent BD1 selectivity. However, as this structural feature was common to I-BET151 and **46**,⁶⁴ additional factors must be contributing to the magnitude of the selectivity. The racemate **231** was 2-fold less active than I-BET151 in both bromodomains but retained the same 10-fold selectivity, while the unsubstituted pyridine-2-ylmethyl **40**⁶³ was considerably less active and selective.

It was suspected that the additional activity observed with the introduction of the benzylic methyl group was caused by locking the molecular conformation into a bioactive form. Indeed, NMR analysis of most compounds synthesised in this section indicated reduced free rotation about the N1 bond (see Section 4.2 for further details).

These data confirmed the importance of the stereocentre with respect to activity and selectivity and, therefore, this chemical functionality was included in design of domain-selective analogues where appropriate. Also, the identical selectivities of the racemate **231** and I-BET151 allowed selectivity comparisons between compounds which were not enantiomerically pure.

The potential key vectors for modulating selectivity identified from the X-ray crystal structure overlays were considered next. As discussed previously, structural information identified the imidazoquinolinone 8-position as an ideal vector to access the Asp/His amino acid variation between BD1 and BD2. Before a chemistry plan was formulated, the contribution of the 8-position towards BET activity was evaluated to inform design of domain-selective analogues.

During previous programmes of research on dimethylisoxazole imidazoquinolinone BET inhibitors, only few analogues had been prepared to explore the 8-position. More SAR information was available from the uncyclised dimethylisoxazole quinoline series where some alterations had been made to the methoxy substituent (examples of these have been published^{63,64} and are discussed in the introduction section of this thesis). These compounds were tested in the BRD4 WT FP assay but, due to a lack of material, were unavailable for assaying against the mutant proteins. However, it was observed that WT potency was affected by alterations at this position. A quantitative structure activity relationship (QSAR) analysis using the Free-Wilson (FW) linear regression approach,¹¹⁸ was carried out to evaluate the activity contribution of substituents at the quinoline 6-position/imidazoquinolinone 8-position (Figure 60). To include both these structural types, the quinoline structure **232** was used for substructure searching at the positions labelled with R¹ and asterisks. The compound structure and the corresponding BRD4 WT FP data were retrieved from the internal biological database. Compounds were grouped according to the R¹ substituent and the difference in average activity measured, allowing comprehensive SAR analysis over a large number of compounds.

All activity data points for each R¹ group were clustered (or binned) and coloured according to the activity ranges depicted in the legend. The size of the sectors in a pie chart correlated with the percentage of the total number of compounds within each activity range and was termed: Sector size by count(RG-R1). The size of the pie chart signified the total number of quinoline templates containing the corresponding R¹ substituent (termed: COUNT(RG-R1)) with the absolute figure labelled against each pie chart. In the scatter diagram, the R¹ substituent – described by Simplified Molecular Input Line Entry System

(SMILES) nomenclature¹¹⁹ – was plotted against the FW score *i.e.* the activity contribution relative to the average activity ($pIC_{50} = 5.8$).

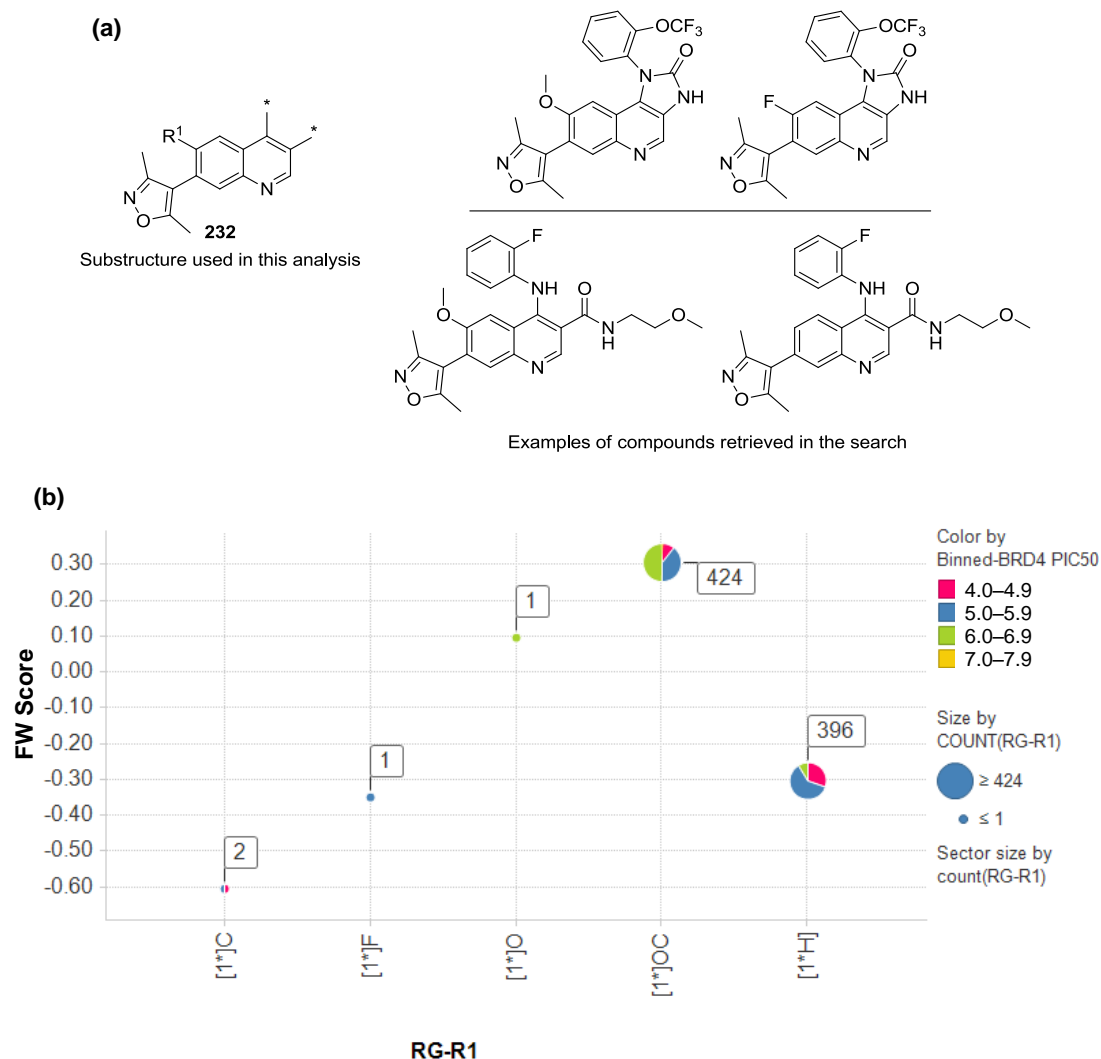


Figure 60. (a) Examples of compounds contained within the substructure **232**; (b) FW analysis of R^1 substituents in the quinoline template.

These data showed that the methoxy substituent ($[1^*]OC$) was the most common R^1 group and was present in 424 different dimethylisoxazole quinolines. The next most common group was $R^1 = H$ ($[1^*]H$) with 396 different dimethylisoxazole quinolines found. The high numbers of compounds for these R^1 groups provided confidence in the output of the analysis which showed that the methoxy substituent contributed to a pIC_{50} increase of 0.6 compared to unsubstituted compounds. Only one example contained a hydroxyl-substituent ($[1^*]O$) and this gave a small positive contribution (+0.1 log units) relative to the average value. The fluorine R^1 group ($[1^*]F$), present in one example, was detrimental to activity with a decrease of 0.4 log units compared to the average pIC_{50} . The methyl group ($[1^*]C$)

was the worst performing substituent with a negative contribution of 0.6 log units, although only two examples existed for comparison.

Drawing conclusions for the latter substituents, for which only one or two examples were available, should be treated with caution as the results may be strongly skewed by error in the biological data. However, it was concluded with confidence that the methoxy substituted compounds showed a 4-fold increase in activity compared to their unsubstituted congeners. Having established that a methoxy group was important for BET activity, insight into how this substituent exerted its beneficial effects was required to establish whether its modification would be tolerated in the design of domain-selective analogues. In view of this, dimethylisoxazole quinoline and dimethylisoxazole imidazoquinolinone crystal structures were examined.

Upon inspection of the structure of I-BET151 bound to BRD4 BD1⁶³ (Figure 59), it was apparent that the 8-methoxy group did not make any interactions with the protein and therefore, the possibility that the increase in activity afforded by a methoxy substituent was due to steric and electronic effects was explored.

Due to the close proximity of the 8-position methoxy group relative to the 7-position dimethylisoxazole ring, it was initially postulated that the OMe perturbed the dimethylisoxazole-quinoline dihedral angle. To investigate this, all in-house crystal structures of dimethylisoxazole quinolines substituted with R = H or OMe (Table 27) bound to any BET protein were examined and the ligand dihedral angles measured. For R = H, one crystal structure had been solved in BRD2 BD1 and the dihedral angle determined to be 59°. With R = OMe, 8 complexes were available in BRD2 BD1, 2 complexes in BRD4 BD1, and none in BD2 of any BET protein. The mean torsion angle for these 10 structures was found to be 56° (standard deviation = 2.5); this value is comparable to those reported for the phenylisoxazoles (lacking *ortho*-substituents) **66**⁶⁸ and **54**,⁷² when bound to BRD4 BD1 and BRD2 BD1, respectively.

	R = H	OMe
Dihedral angle (°)	59	56

Table 27. Mean measured dihedral angles of bonds highlighted in red.

The difference between the two values measured for R = H and R = OMe was negligible and it was therefore concluded that the methoxy substituent did not affect the dihedral angle between the dimethylisoxazole and quinoline rings when bound to a BET bromodomain module. However, it was recognised that these measured angles may be induced through binding to the protein and may not necessarily be the lowest energy conformations in the unbound state. If the methoxy group induced a more favourable conformation prior to binding than an unsubstituted congener, a lower entropic penalty would be incurred upon interaction with the bromodomain compared to R = H. Therefore, a molecular mechanical evaluation was conducted in the absence of protein to identify any differences between the dihedral angles of the lowest energy conformations of R = H and R = OMe.

Dihedral angles ranging from -180° to $+180^\circ$ were scanned using MacroModel (see Section 4.5 for details) and the energy relative to the lowest energy conformer calculated (Figure 61). The absolute energies of the two molecules, however, should not be compared (this would require *ab initio* methods) but insight into the lowest energy conformer angles could be derived from this approach, as well as the relative energy barriers to rotation around the aryl-aryl axis.

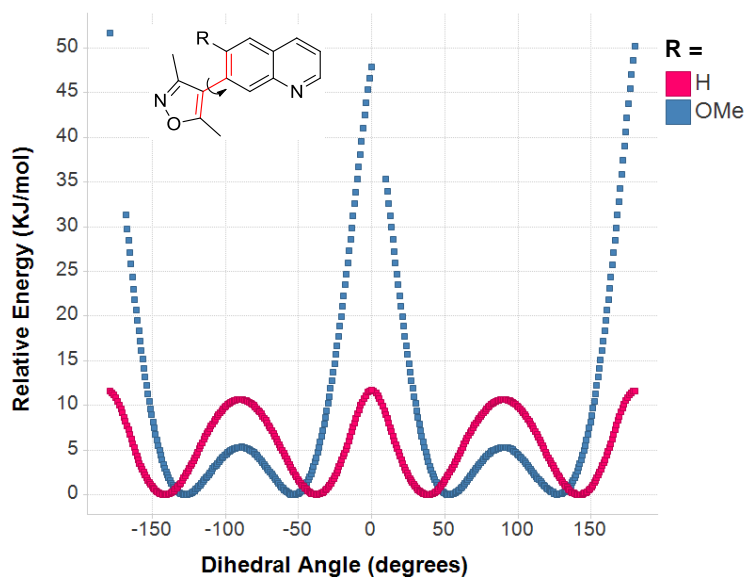


Figure 61. Torsion angle scan of 8-H and 8-OMe substituted dimethylisoxazole quinolines.

Predominantly symmetrical plots were observed for both substituents when scanning from -180° to $+180^\circ$, due to the pseudo symmetrical isoxazole ring. Interestingly, the plot indicated energy minima at slightly different dihedral angles for the two substituents. For the unsubstituted quinoline, the energy minima were found at $\pm 38^\circ$ and $\pm 141^\circ$, values similar to those reported for the phenylisoxazoles (lacking *ortho*-substituents) **66**⁶⁸ and **54**.⁷² For the methoxy substituted quinoline, the energy minima were found at $\pm 52^\circ$ and $\pm 127^\circ$. These data suggested that the bioactive conformations of the methoxy-substituted quinolines were close to their calculated low energy conformation in their unbound state, whereas for the unsubstituted quinoline this was not the case. This could be explained by the fact that only one crystal structure for R = H was available and basing conclusions on such a limited sample set may be misleading, especially since only a quinoline substructure is being considered and that other groups on the quinoline may be making interactions with the protein and also altering the aryl-aryl dihedral angle. Moreover, these data indicated that only a relatively small energy penalty would be required for rotation from the energy minimum 38° to the bioactive dihedral angle of 59° .

In conclusion, it appeared that a methoxy substituent only slightly increased the dihedral angle between the dimethylisoxazole and the quinoline ring when compared to an unsubstituted analogue when calculated *in silico*. As no difference in dihedral angle between compounds containing R = H and OMe was determined upon examination of in-house crystal structures, it was concluded the beneficial activity gained with an methoxy substituent could not be wholly attributed to perturbation of the torsion angle between the dimethylisoxazole and quinoline aryl rings. Therefore, an alternative theory based on electronic effects was investigated.

To explore the possibility that the methoxy substituent improved BET activity through altering the electronics of the quinoline ring system, a more detailed examination of the ligand-receptor interactions between I-BET151 and BRD4 BD1 was conducted (Figure 62).

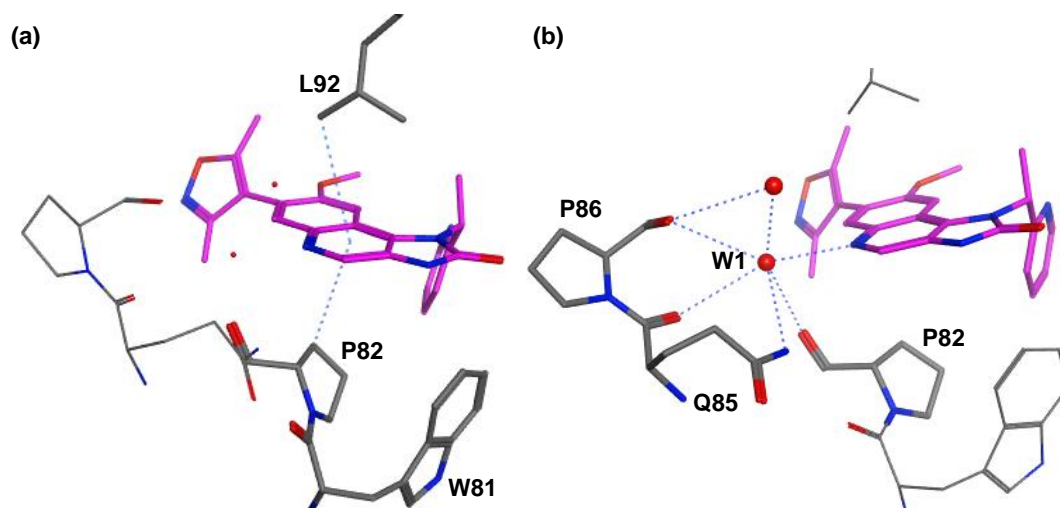


Figure 62. Ligand-receptor interactions of imidazoquinolinone I-BET151 (carbon = magenta) in BRD4 BD1 (pdb 3ZYU).⁶³ (a) Aryl-alkyl interactions with Leu92 and Pro82. (b) Contacts of the conserved water molecule.

As discussed previously, the quinoline ring occupied a hydrophobic cleft between Trp81 and Pro82 of the WPF shelf on one side of the quinoline ring and with Leu92 on the other (Figure 62a). As aryl-alkyl interactions can be influenced by the electronic effects,¹²⁰ it was possible that the increase in activity gained through the incorporation of a methoxy substituent was due to enhanced electron-density in the quinoline ring system.

The high resolution structure also revealed a water molecule (W1) situated within 3.2 Å of several protein residues (Pro82, Gln85 and Pro86), another water molecule, and to the quinoline nitrogen (Figure 62b). Moreover, inspection of all in-house quinoline-BET complexes revealed this water was positioned in a similar manner although subtle differences in the bond angles were apparent. Therefore, W1 was considered an important structural feature and further investigation was conducted to determine if the methoxy group exerted its beneficial effects by improving ligand interaction to this water.

All contacts of W1 as drawn in Figure 62b would over-saturate its hydrogen bonding coordination sites even if some were multifurcated. It was not clear which of these contacts were hydrogen bonds and whether the water molecule participated as a HBD to the quinoline nitrogen. Therefore, a GRID Molecular Interaction Field (MIF) for a water probe was generated for this structure to determine the relative energies for each molecule of solvent at their optimised positions (Figure 63).¹²¹ The calculated energies are displayed and the water molecules coloured accordingly, green for favourable energy and red for unfavourable energy.

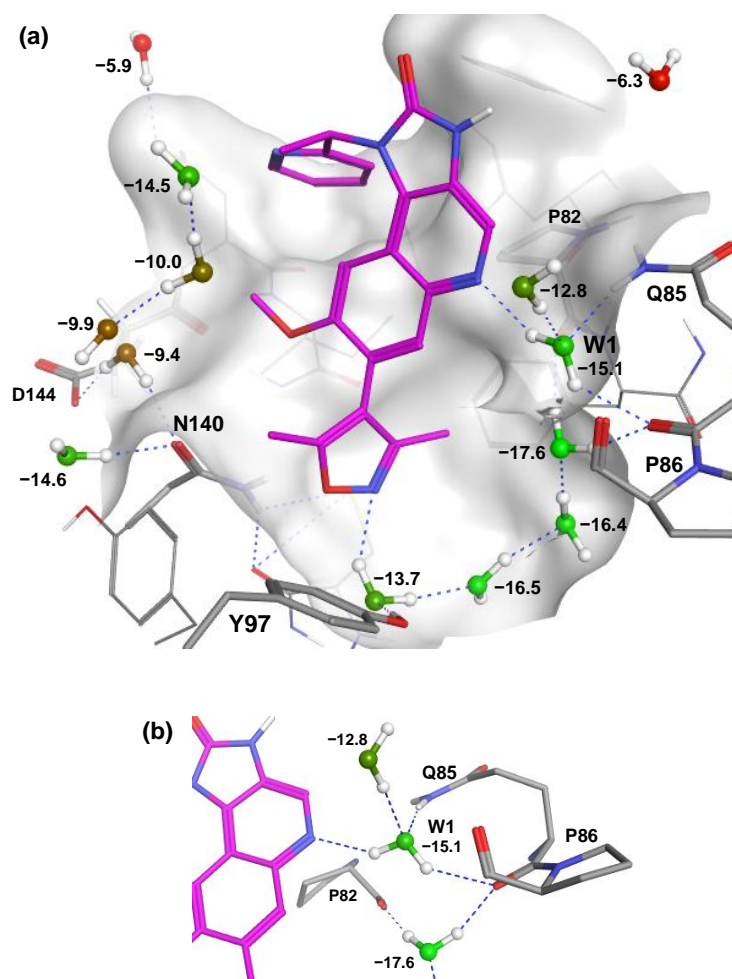


Figure 63. GRID MIF for a water probe in the crystal structure of imidazoquinolinone I-BET151 (carbon = magenta) in BRD4 BD1 (pdb 3ZYU). Water molecules are coloured according to their relative energies (green for favourable energy and red for unfavourable energy). (a) Overview structure including relevant water molecules. (b) Magnified view of water binding to the quinoline nitrogen.

The results confirmed that the water molecule of interest was energetically favourable water with a relative energy of -15.1 kcal/mol and therefore interactions with the ligand might be quite important. This value compares well to four conserved waters at the base of the KAc binding pocket: -13.7 , -16.5 , -16.4 and -17.6 kcal/mol. These calculations revealed that W1 interacted with an adjacent water molecule, a side chain NH of Gln85, the backbone carbonyl of Pro86 and with the quinoline nitrogen. Therefore, the beneficial effects upon BET activity of a methoxy group substituted onto the quinoline ring may have been through increasing the hydrogen bond basicity of the quinoline nitrogen which accepted a hydrogen bond from W1. Indeed, electron-donating substituents on pyridine rings have been shown to increase hydrogen bond basicity of the pyridine nitrogen.¹²² By extension, electron-donating substituents on quinoline rings were also expected to show a similar increase in hydrogen bond basicity, especially since the pK_{BHX} values of unsubstituted pyridine and quinoline are similar; 1.86 and 1.89, respectively.¹²³

To test if the electronic contribution of substituents at the 6-position affected potency, the *meta* sigma constants from the Hammett equation¹²⁴ were plotted against their FW scores obtained from the previous QSAR analysis (Figure 64). A trend existed up to a point, with increasing sigma *meta* values correlating with increased activity contribution for a particular substituent. However, the fluorine substituent was an outlier; although it should be reiterated that the FW score for this substituent was based on only one compound and therefore was prone to over-interpretation.

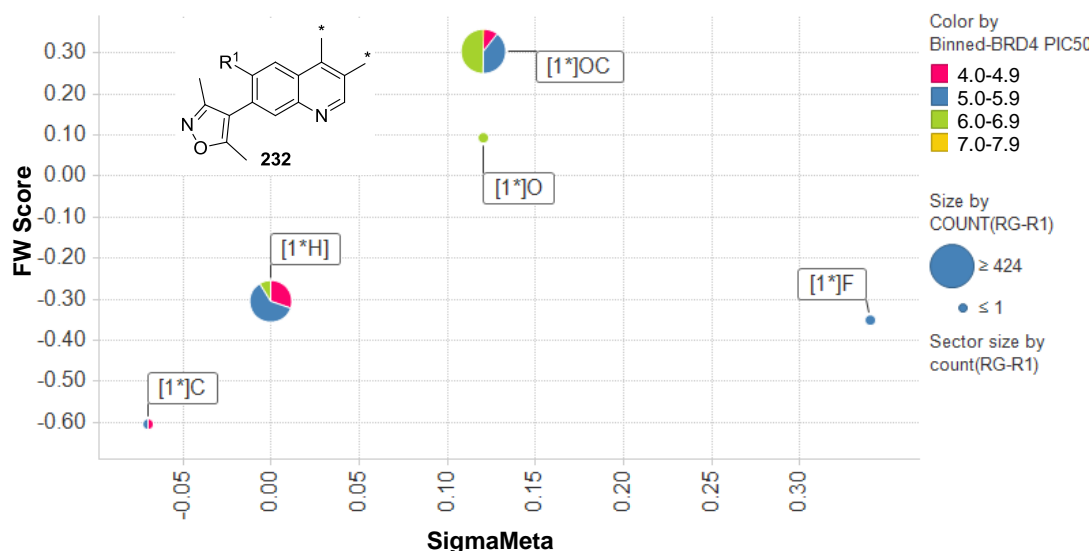


Figure 64. FW scores of 6-substituents plotted against their Hammett sigma *meta* constants.

Despite only a limited number of data points for different R¹ groups, and one outlier being found, this analysis suggested that R¹ substituents electronically influenced activity with methoxy groups providing the most activity. Two interaction modes (quinoline-alkyl interactions and HBA ability of the quinoline nitrogen) were identified from a crystal structure that would benefit from increased electron density afforded by a methoxy substituent. It was also shown that the methoxy group slightly perturbed the quinoline-dimethylisoxazole dihedral angle in the unbound state which also might contribute to improved activity. In view of these results, a chemistry plan retaining an *O*-linked alkyl group at the 8-position of I-BET151 was preferred to retain the high activity and domain selectivity.

3.2. Imidazoquinolinone 8-Position Investigation

Based on all of the data interrogation, as laid out above, a medicinal chemistry plan was devised to incorporate *O*-linked substituents at the imidazoquinolinone 8-position. From here, functionality capable of interacting or clashing with the Asp residues (or bound waters)

in BD1 and His residues in BD2 could be explored. The measured distance from the 8-O atom of I-BET151 to Asp144 in the complex shown in Figure 59, was measured to be 7.5 Å. Therefore, functional groups capable of forming charged and hydrogen bonding interactions that were separated by two or three carbon atoms from the 8-O linking atom, would provide the preferred distance – allowing for some amino acid or ligand mobility – to form an interaction with the conserved Asp (or a surrounding water) of BD1 and give a BD1-selective compound. In particular, alkyl groups, amines, alcohols and ethers of the type shown in Figure 65 were identified for synthesis. Overlay of the BRD4 BD2 protein structure with the I-BET151–BRD4 BD1 complex (Figure 59), showed the distance from the imidazoquinolinone 8-O atom to the C-2 of His437 was 4.6 Å. A functional group directly linked to the imidazoquinolinone or separated by one carbon would provide the preferred distance to form an interaction with the conserved His of BD2 and provide a BD2-selective compound, while allowing for some amino acid and ligand mobility or error in BD1 and BD2 protein alignment in Figure 59. However, target compounds with functional groups directly attached to the imidazoquinolinone *i.e.* those without an *O*-linker, were expected to be less potent – as predicted from the earlier analysis – but may afford desirable BD2 selectivity, which had not been observed from testing of historical compounds (data not shown).

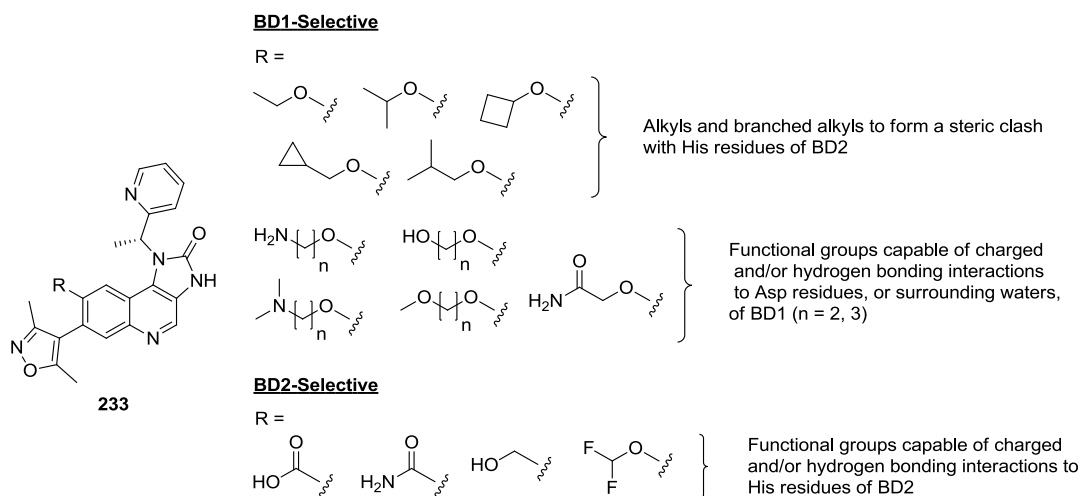


Figure 65. Imidazoquinolinone 8-position analogues identified for synthesis.

The initial synthetic strategy was to make expedient use of supplies of I-BET151 within our laboratories. Target compounds **233** were expected to be obtained from *O*-alkylation of the quinolinol **234** which would result from cleavage of the I-BET151 methylether (Figure 66).

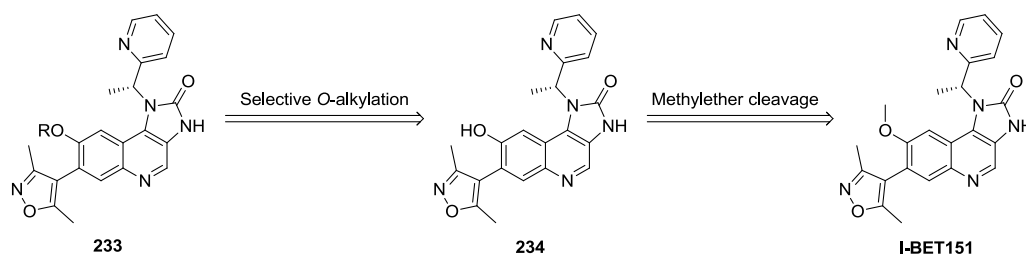
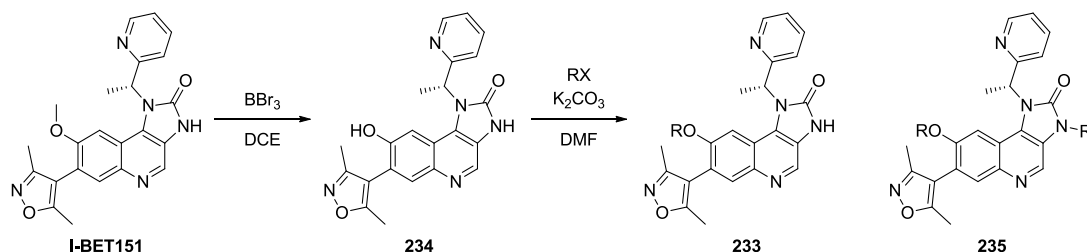


Figure 66. Outline of preliminary chemistry strategy to modify the imidazoquinolinone 8-position.

Preliminary synthetic investigations conducted within the laboratory¹²⁵ used boron tribromide to remove the *O*-methyl group from I-BET151 providing the quinolinol **234** (Scheme 25). However, reactions with appropriate alkyl halides gave mixtures of the desired mono *O*-alkylated **233** and *N,O*-bis-alkylated **235** compounds.¹²⁵ In order to prevent bis-alkylation, attempts were made to install a suitable protecting group on the imidazolinone NH of I-BET151, but were unsuccessful.¹²⁵ Mitsunobu reactions of quinolinol **234** with the appropriate alcohols were also attempted but failed.¹²⁵

Scheme 25. Mixtures of mono- and bis-alkylation products were obtained with the quinolinol imidazolinone **234**.

Therefore, a strategy to block the NH of the imidazolinone with a methyl group was pursued for synthesis of future target compounds as depicted in Figure 67. *N*-Methylation of I-BET151 followed by *O*-demethylation would provide the quinolinol **237** as the intermediate for 8-position diversification.

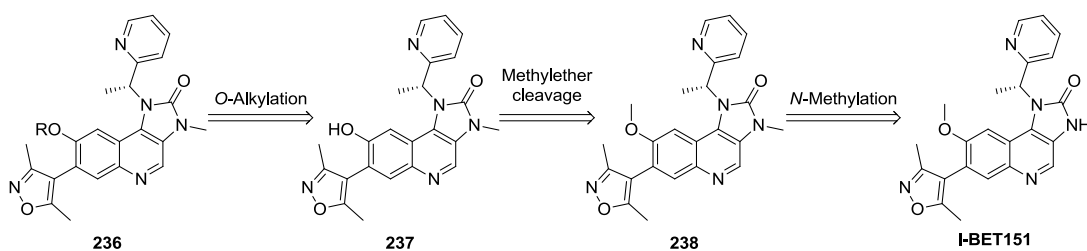
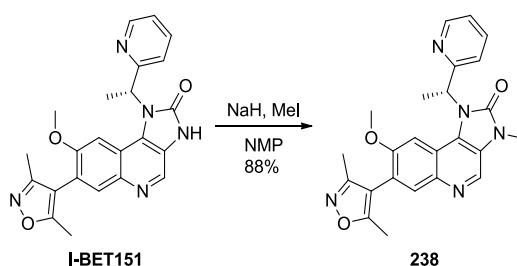


Figure 67. Revised chemistry strategy to modify the imidazoquinolinone 8-position.

Inspection of the crystal structure of I-BET151 in BRD4 BD1⁶³ (Figure 59) showed the imidazolone NH vector pointed towards solvent and a methyl substituent here was not expected to greatly affect activity or selectivity. To confirm this, the NH of I-BET151 was

deprotonated with sodium hydride and subsequent methylation gave the alkylation product **238** in high yield (88%) (Scheme 26).



Scheme 26. Masking the imidazolone NH with a methyl group.

Screening of this compound in the mutant assays revealed that the *N*-methyl imidazolone **238** displayed little difference in activity and/or selectivity over the unalkylated imidazolone I-BET151 (Table 28).

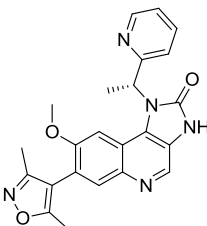
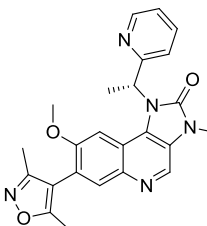
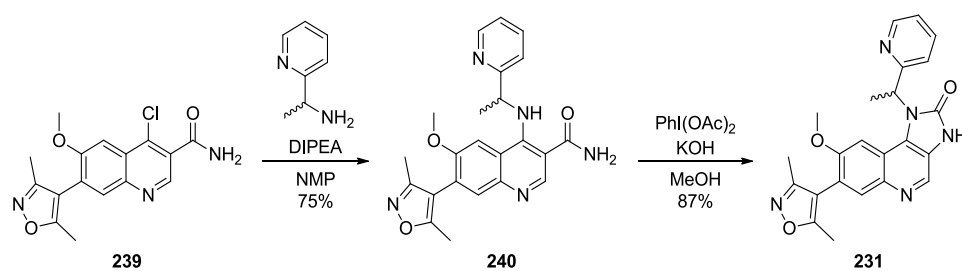
	 I-BET151	 238
BRD4 BD1, BD2 pIC₅₀	7.5, 6.5	7.3, 6.3
BD1–BD2	1.0	1.0

Table 28. BRD4 mutant data for unalkylated imidazolone I-BET151 and *N*-methyl imidazolone **238**.

Therefore, capping the NH to allow exclusive *O*-alkylation could be achieved without affecting SAR by incorporation of the imidazolone NMe group and validated the synthetic chemistry strategy. However, it was recognised that the integrity of the stereogenic centre could be compromised under the strongly basic conditions used in this first step in the synthetic sequence. The benzylic centre was expected to be acidic, especially with an adjacent electron-deficient pyridine ring. Moreover, the particular batch of I-BET151 available within our laboratories for this programme of work was not enantiomerically pure with an e.e. determined as 88%. To establish the degree to which this level of optical purity affected activity and selectivity, the racemate **231** was synthesised (Scheme 27). This material was also to be used in subsequent steps to provide standards for e.e. measurements using HPLC.

Scheme 27. Synthesis of the racemate **231**.

Racemic I-BET151 (**231**) was prepared using similar conditions described for the synthesis of I-BET151.⁶³ Firstly, nucleophilic substitution of the 4-chloroquinoline **239**, available within our laboratories,⁹⁴ using 1-(pyridin-2-yl)ethanamine was accomplished in good yield (75%). A modification of the Hofmann rearrangement was used to convert the primary amide **240** to the imidazolidinone **231** using the iodine (III) species $\text{PhI}(\text{OAc})_2$.¹²⁶ The biological data for the racemate **231** was compared alongside the different batches of I-BET151 and the *S*-enantiomer **46**⁶⁴ (Table 29).

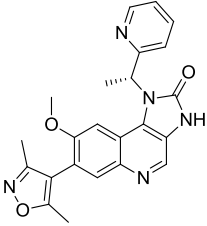
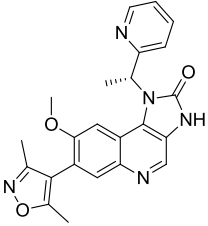
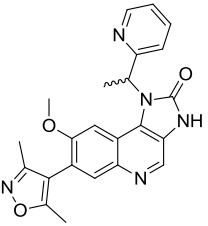
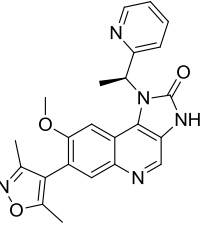
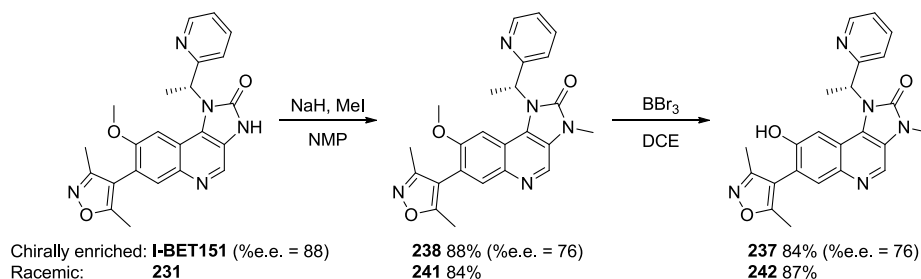
				
	I-BET151	I-BET151	231	46 ⁶⁴
%e.e.	>99	88	0	>99
BRD4 BD1, BD2 pIC₅₀	7.5, 6.5	7.5, 6.5	7.2, 6.2	6.3, 5.8
BD1–BD2	1.0	1.0	1.0	0.5

Table 29. BRD4 mutant assay data for varying %e.e. batches of I-BET151, the racemate **231** and the *S*-enantiomer **46**.⁶⁴

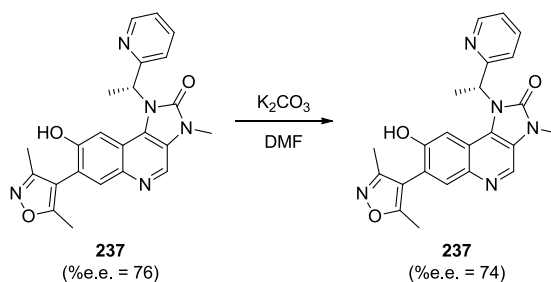
These data showed that the 88% e.e. batch of I-BET151 showed equal activity, and thus selectivity, in the BRD4 mutant assays compared to the enantiomerically-pure batch. The racemate **231** displayed 2-fold lower activity for both bromodomains compared to the >99% e.e. batch, while the *S*-enantiomer **46**⁶⁴ significantly reduced potency and narrowed the domain selectivity. As a consequence, the 88% e.e. batch of I-BET151 was suitable for derivitisation into domain-selective analogues as the 10-fold selectivity was retained. As degradation of optical purity during the following steps in the synthetic sequence was possible, the 10-fold selectivity window retained by the racemate **231** meant that ranking of domain-selective analogues could be accomplished fairly.

To determine if racemisation occurred in subsequent steps, the racemate **231** was subjected to the same *N*-methylation procedure as used for the enantiomerically-enriched batch in Scheme 26, giving the racemic *N*-methyl **241** which was used as a standard for chiral HPLC analysis (Scheme 28). Next, both the racemate **241** and the enantiomerically-enriched batch **238** were subjected to a BBr_3 -mediated *O*-demethylation to provide the corresponding quinolinols **242** and **237**, respectively.

Scheme 28. *N*-Methylation and *O*-demethylation sequence.

As suspected, the highly basic conditions used for *N*-methylation caused partial racemisation at the benzylic centre providing **238** with an e.e. = 76%. The subsequent *O*-demethylation to **237** proceeded in high yield (84%) without any further degradation of enantiomeric purity.

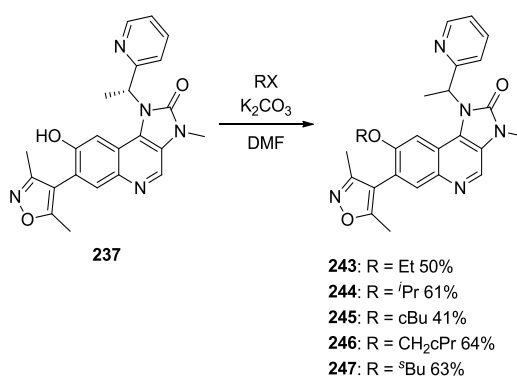
To investigate if the alkylation protocol used to append substituents onto the 8-oxygen caused further racemisation, the quinolinol **237** was subjected to typical reaction parameters in the absence of alkylating agent (100 °C, 1.5 equiv. K_2CO_3 , DMF) but with significantly extended heating time (24 h, Scheme 29; see Section 4.4). Under these conditions, minimal racemisation occurred with the e.e. of the recovered quinolinol **237** being determined as 74%.

Scheme 29. Racemisation study performed on quinolinol **237** under typical alkylation conditions.

These studies showed that conditions used to mask the NH of I-BET151 with a methyl group induced partial racemisation. Encouragingly, the subsequent *O*-demethylation step and simulated *O*-alkylation conditions did not cause further loss of optical purity. Although partial racemisation was observed in the *N*-methylation step, no difference in selectivity was found between the racemate of I-BET151 (**231**) and for enantiomerically pure I-BET151

(Table 29). Therefore, use of the plentiful supply of the 88% e.e. batch of I-BET151, and its 76% e.e. quinolinol **237** derivative was deemed suitable as selectivity data obtained for all compounds synthesised from these intermediates could be compared fairly without the need for chiral purification or %e.e. determination.

Having established the suitability of the enantiomerically-enriched quinolinol **237** as an intermediate for derivitisation, a synthetic exploration was carried out to append alkyl substituents designed to fill space within the BD1 KAc recognition site and sterically clash with His residues of BD2 (Scheme 30).



Scheme 30. The *N*-Me masked imidazolone allowed exclusive quinolinol alkylation

Straightforward *O*-alkylation of quinolinol **237** afforded the target alkyl compounds in yields ranging from 41 to 64%. Results from screening these compounds in the BRD4 mutant assays are shown in Table 30.

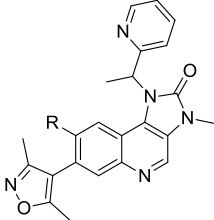
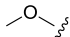
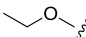
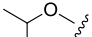
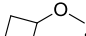
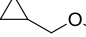
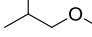
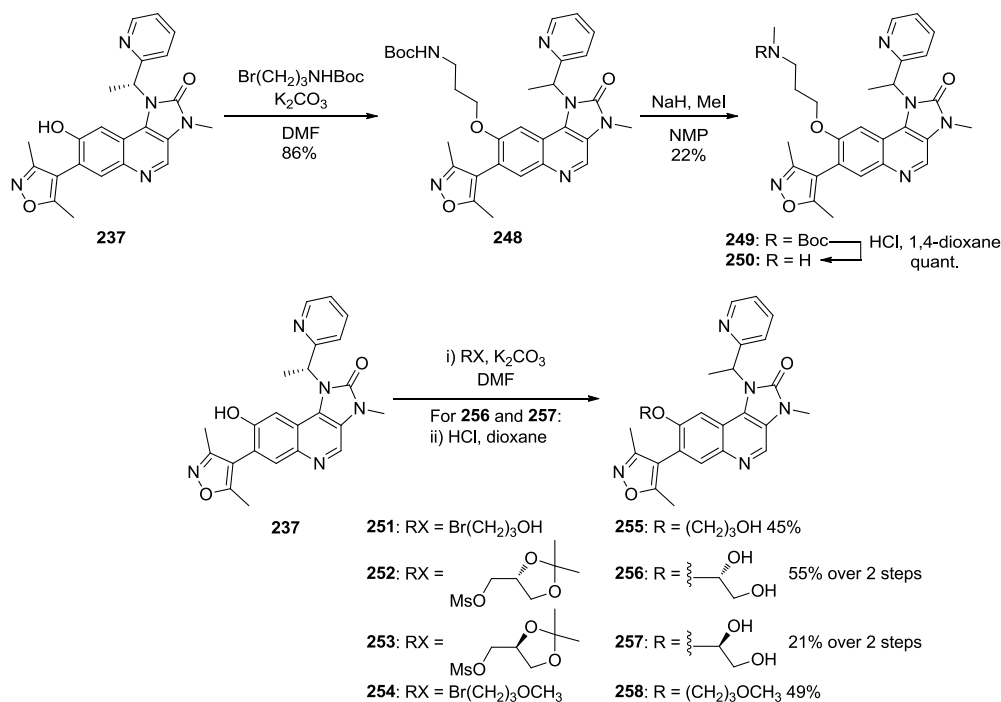
		BRD4 BD1, BD2	
R =	Entry	pIC₅₀	BD1–BD2
	238	7.3, 6.3	1.0
	243	6.7, 5.8	0.9
	244	6.8, 6.1	0.7
	245	6.7, 5.7	1.0
	246	6.8, 6.1	0.7
	247	6.0, 5.1	0.9

Table 30. Results from screening of alkyl substituted quinolines.

The 10-fold selectivity of the imidazoquinolinone **238** was taken as the baseline against which all analogues were compared. As can be seen from these data, no improvement in selectivity was attained with larger alkyl substituents and most examples retained the 10-fold selectivity observed with the methyl **238**. One important observation with these data was the loss of BRD4 BD1 activity as the size of the 8-substituent increased beyond a methyl group. The addition of only one extra carbon atom was sufficient to lower potency, with the ethyl **243** losing 2-fold activity *versus* the methyl **238**. The isopropyl **244**, cyclobutyl **245** and cyclopropyl methyl **246** displayed similar activities but extending a large group further away from the quinoline in the form of an *s*-butyl (**247**) reduced BRD4 BD1 significantly.

These data demonstrated that extending aliphatic bulk towards Asp144 and His437 of BRD4 did not improve domain selectivity. As BRD4 BD1 and BD2 activities were reduced to the same extent for each compound, attempts to mediate a steric clash with His437 alone was, seemingly, not possible without also affecting binding in BD1. Therefore, a range of substituents containing heteroatoms were synthesised to enhance interaction with Asp residues of BD1 (or an associated water molecule), and cause a dipole clash with His residues of BD2 to give enhanced BD1 selectivity.

These heteroatom-containing functional groups were incorporated in a similar manner as the alkyl substituents *i.e. via* alkylation of quinolinol **237** followed by deprotection and derivatisation where appropriate (Scheme 31). Data from screening in the BRD4 mutant assays is shown in Table 31.



Scheme 31. Synthesis of heteroatom-containing substituents.

	238	259 ¹²⁵	260 ¹²⁵	261 ¹²⁵	250	262 ¹²⁵
BRD4 BD1, BD2	7.3, 6.3	5.9, 4.5	5.7, <4.3	6.2, 4.8	6.0, 4.6 ^a	6.2, 5.5
pIC₅₀						
BD1-BD2	1.0	1.4	>1.4	1.4	1.4	0.7

	263 ¹²⁵	255	256 ¹²⁷	257 ¹²⁷	258	264 ¹²⁵
BRD4 BD1, BD2	6.3, 5.2	6.3, 5.2	5.9, 4.6 ^b	5.9, 4.5	6.2, 5.2	6.0, 4.6
pIC₅₀						
BD1-BD2	1.1	1.1	1.3	1.4	1.0	1.4

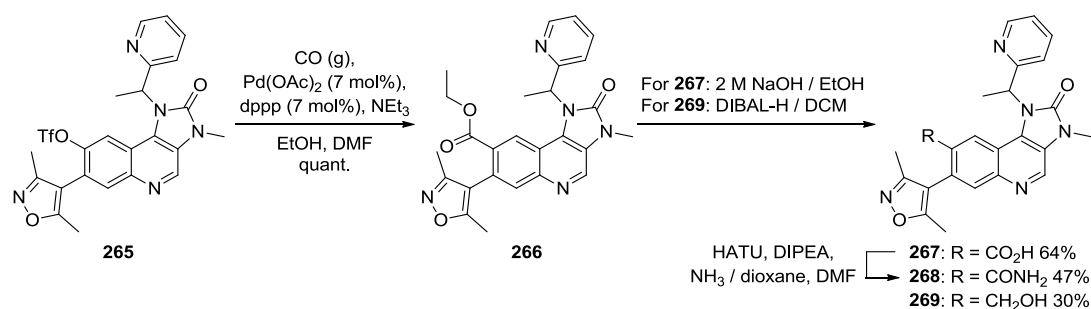
Table 31. Assay results of amines, amides, alcohols and ethers. ^aA pIC₅₀ value of <4.3 was determined on one test occasion out of five and was excluded from the reported mean value. ^bA pIC₅₀ value of <4.3 was determined on one test occasion out of four and was excluded from the reported mean value.

These data revealed that heteroatom-containing substituents enhanced selectivity compared to imidazoquinolinone **238**. For example, the ethylamine **259**¹²⁵ and propylamine **261**¹²⁵ displayed 25-fold greater activity at BD1 compared to BD2, with the longer chain demonstrating slightly increased BD1 activity. Substitution of the amines with methyl groups was marginally unfavourable for BD1 activity as exemplified by the 1.6-fold reduced activities of the *N,N*-dimethylethylamine **260**¹²⁵ and the *N*-methylpropylamine **250** relative to their respective primary amine congeners, ethylamine **259** and propylamine **261**.¹²⁵ However, *N*-methylation appeared to maintain the 25-fold selectivities and, in the case of the *N,N*-dimethylethylamine **260**,¹²⁵ the selectivity may well be larger as the BD2 activity was below the limit of detection of the assay. In addition to the encouraging data achieved with these amines, alcohols and ethers also exhibited enhanced selectivity profiles. However, contrary to the amine SAR, the chain length did not affect BD1 potency greatly, with the ethyl alcohol **262**¹²⁵ and propylalcohol **255** displaying equal activity, although greater selectivity was observed with the longer chain. Attempts to make additional protein interactions with the diols **256**¹²⁷ and **257**¹²⁷ resulted in reduced activity relative to the mono-alcohols but, interestingly, gave enhanced selectivity without any stereochemical preference for the specific 2-alcohol moiety. The methoxyethyl **263**¹²⁵ and methoxypropyl **258** ethers did not show any significant benefit over their alcohol counterparts. Inserting a carbonyl group to give the carboxamide **264**¹²⁵ displayed similar BD1 activity and selectivity to the amine analogue **259**.

The overall package of data from these chemistry explorations was very promising. Although, aliphatic substituents at the 8-position did not improve domain selectivity *versus* imidazoquinolinone **238**, substituents containing heteroatoms gave significantly enhanced selectivity with several compounds displaying 25-fold selectivity for BRD4 BD1 — the highest degree of selectivity achieved at this stage of the programme. Before a further iteration of chemistry to build on these results was devised, attention turned to exploring functionality which may afford BD2 selectivity as part of these initial medicinal chemistry investigations.

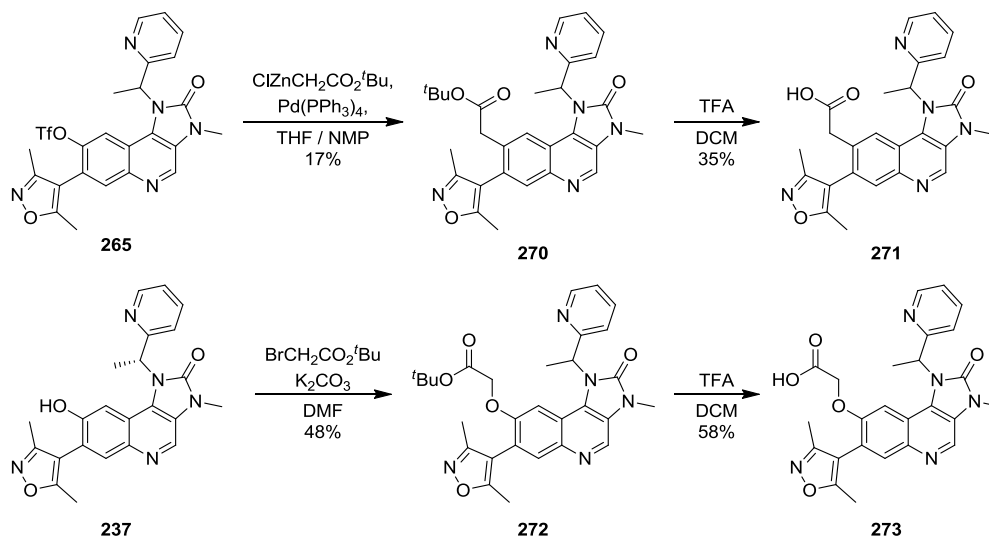
As mentioned previously, the close proximity of His437 to the imidazoquinolinone 8-position, determined from the superimposition of I-BET151 with apo BRD4 BD2 (Figure 59), meant that functional groups directly linked, or linked through a minimal number of atoms, were preferred. In particular, a carboxylic acid and alcohol appended to the quinoline were expected to favourably bind to His residues and afford selectivity for BD2. These functional groups were accessed from the triflate **265**⁹⁴ (Scheme 32). Firstly, Pd-catalysed carbonylation was used to form the ethyl ester intermediate **266** in quantitative yield.

Saponification of the ester gave the target carboxylic acid **267** in a yield of 64%. A HATU-mediated amide coupling gave the carboxamide target compound **268** in moderate yield (47%), while reduction of the ester **266** with DIBAL-H gave the methyl alcohol target compound **269** in 30% yield.



Scheme 32. Pd-catalysed carbonylation followed by functional group transformation.

To maximise the likelihood for the interaction of a pendant carboxylic acid with the His of BD2, additional linking atoms were introduced compared to the directly linked carboxylic acid **267**. In this regard, both the directly linked acetic acid **271** and the *O*-linked acetic acid **273** were prepared as depicted in Scheme 33. Negishi coupling of [2-(*tert*-butoxy)-2-oxoethyl]zinc (II) chloride with triflate **265** gave the *tert*-butyl acetate **270**, and upon treatment with TFA, acetic acid **271** was obtained. For the *O*-linked acetic acid **273**, quinolinol **237** was alkylated with *tert*-butyl 2-bromoacetate to afford *O*-linked *tert*-butyl acetate **272** and subsequent reaction with TFA gave the target compound **273**.



Scheme 33. Preparation of acetic acids **271** and **273**.

Also in this exploration, it was postulated that His residues of BD2 were close enough to form a dipolar interaction with a fluorine atom substituted onto the methoxy group of imidazoquinolinone **238**. A trifluoromethoxy group was not considered as it would have

been likely to adopt an orthogonal conformation to the quinoline ring, whereas the methoxy group prefers a near planar arrangement;¹²⁸ this was confirmed upon examination of the structure of I-BET151 in BRD4 BD1 where the methoxy-quinoline torsion angle was measured to be 8° (Figure 68a).

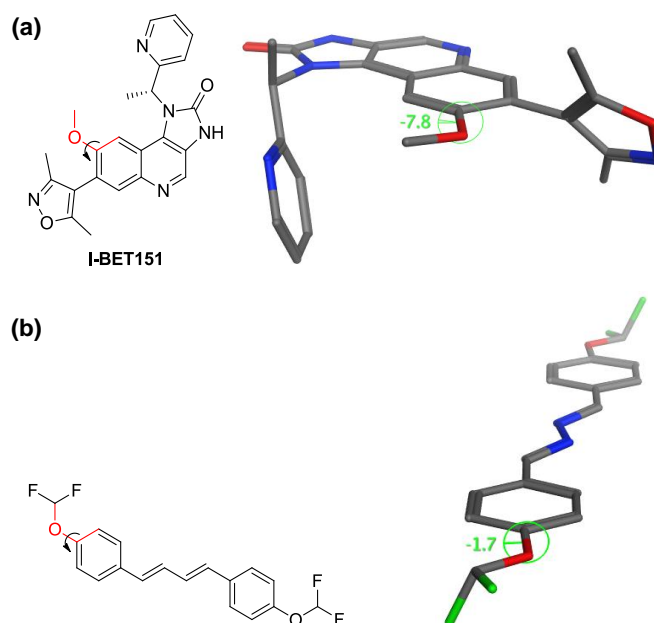
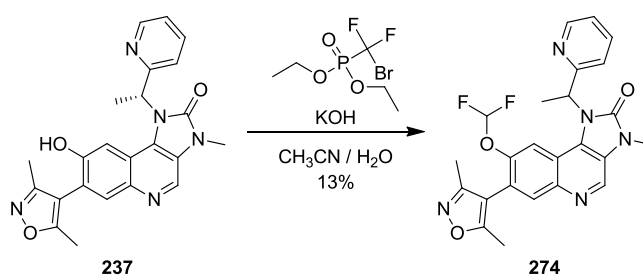


Figure 68. (a) Methoxy-quinoline dihedral angle of I-BET151 in BRD4 BD1 (pdb 3ZYU); solvent and protein were omitted for clarity. (b) Difluoromethoxy-phenyl dihedral angle of an exemplar structure retrieved from the Cambridge Structural Database (CSD), entry code VAYHEI.

Therefore, in order to mimic the planar methoxy substituent, a difluoromethoxy analogue was targeted for synthesis; this substituent has been observed to adopt conformations close to planarity¹²⁹ (one example is shown in Figure 68b). The quinolinol **237** was subjected to conditions reported by Segali *et al.*¹³⁰ using a difluorocarbene precursor and gave the desired difluoromethylether **274** in 13% yield (Scheme 34).



Scheme 34. Synthesis of difluoromethoxy **274**.

Results from the testing of compounds designed to give BD2 selectivity are shown in Table 32.

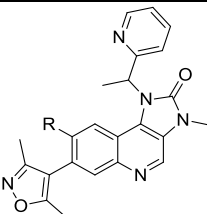
 BRD4 BD1, BD2 pIC₅₀	238	267	268	269	271	273	274
		7.3, 6.3	4.9, <4.3	<4.3, <4.3	4.8, <4.3	<4.3, <4.3	5.7, 4.9
BD1–BD2	1.0	>0.6	0	>0.5	0	0.8	0.4

Table 32. Screening data of compounds designed for BD2 selectivity.

Overall, the data for these modifications was disappointing. Low BD1 activity was observed for the carboxylic acid **267**, the carboxamide **268**, the methyl alcohol **269** and the acetic acid **271**, probably due to the lack of a linking oxygen atom. The difluoromethoxy compound **274** showed significantly reduced selectivity *versus* the parent methoxy compound **238**, as well as reduced BD1 activity, which was consistent with the QSAR-FW analysis discussed earlier. The *O*-linked acetic acid **273** did not show a switch in affinity to BD2 possibly due to the limited space available within the binding site to interact with the His residue.

This first iteration of chemistry at the imidazoquinolinone 8-position revealed a number of important aspects which would be important in the future chemistry strategy. Firstly, alkyl substituents designed to clash with His437 of BD2 were found not to increase selectivity and attempting to achieve selectivity by this mechanism was deemed unfeasible. The alkyl-substituent data demonstrated that increasing the size of the pendant group beyond a methyl reduced BD1 activity and that extending a large group further away from the quinoline ring reduced activity further. It was evident from this initial data that substituents containing heteroatoms afforded the best selectivity windows for BD1 over BD2, with amines in particular performing well. Indeed, selectivity could be enhanced by 2.5-times with amines **259**, **260**, **261** and **250** when compared to the methoxy-substituted imidazoquinolinone **238**. However, an issue was identified with incorporation of these groups where BD1 activity decreased by a maximum of 40-fold relative to methoxy-substituted imidazoquinolinone **238**. This was a feature consistent with the alkyl-substituent results and presented a challenge for design of future BD1-potent compounds. Nevertheless, the 25-fold selectivity for BD1 over BD2 observed for several analogues was the largest selectivity window accomplished at this stage of the overall programme and supported the theory that biologically relevant differences in selectivity between BD1 and BD2 could be achieved. The encouraging results achieved with the amine-containing compounds prepared

in this section provided inspiration for design of further analogues at the imidazoquinolinone 8-position. Accordingly, a second phase of chemistry was conducted and is discussed in Section 3.4.

3.3. Pyridine 6-Position Chemistry

In parallel to modifications at the imidazoquinolinone 8-position, an exploration of the pyridine 6-position was undertaken. As mentioned previously, the vector from this position also pointed towards the Asp/His residue variation. A small focused set of analogues were designed to interact with the Asp (or surrounding waters) of BD1 and maximise chemical diversity, and one example was included to enhance interactions with His residues of BD2 (Figure 69).

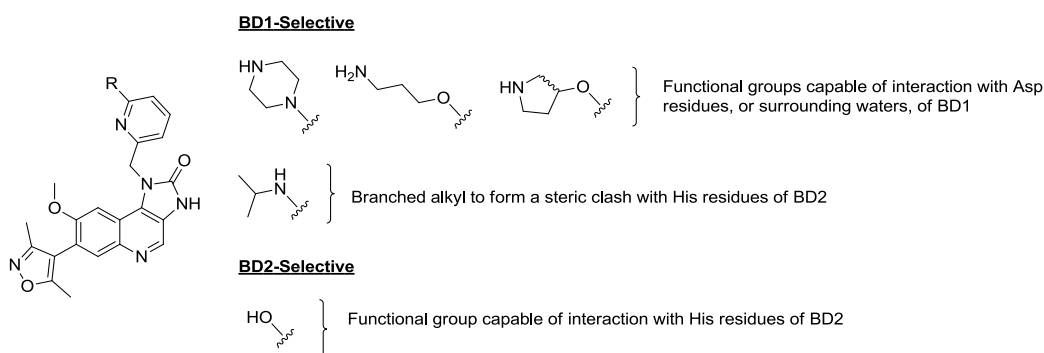
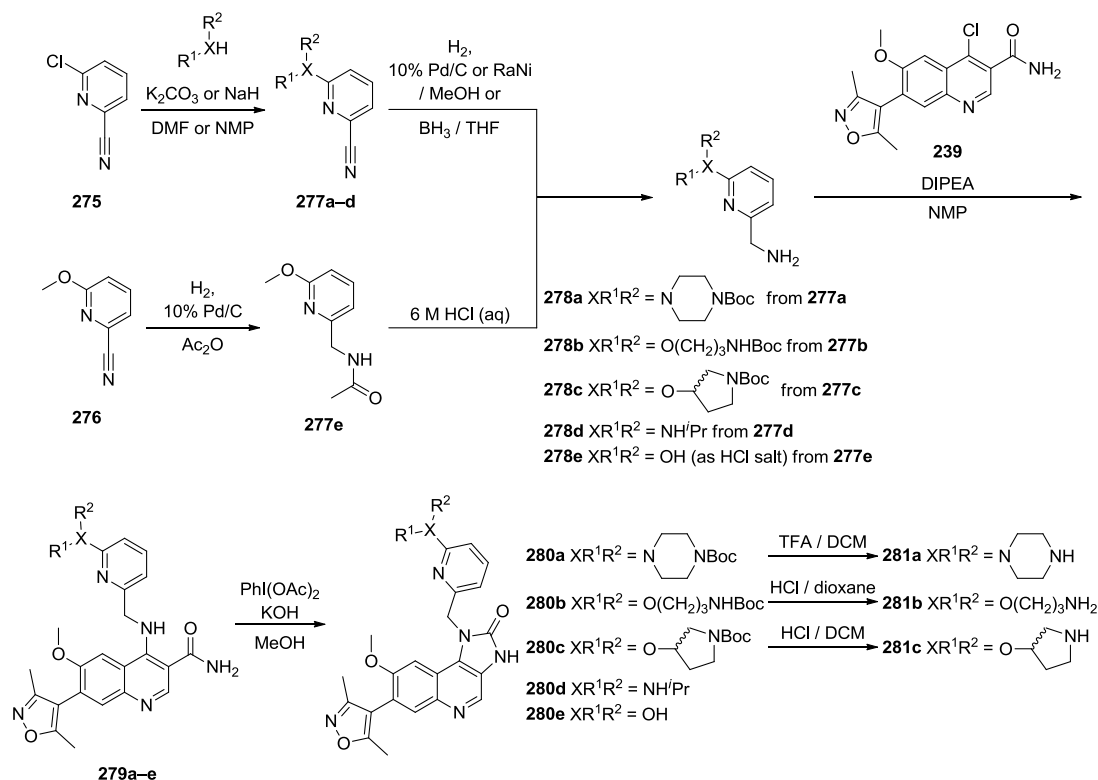


Figure 69. 6-Pyridine modifications targeted for synthesis.

In order to simplify the synthesis of these compounds, the methyl group at the benzylic position was omitted. As seen in Table 26, the benzylic methyl group of I-BET151 was important for activity and selectivity and provided significant improvement over the unsubstituted congener **40**⁶³ and its enantiomer **46**.⁶⁴ Despite this, omission of the methyl group circumvented lengthier and more resource-intensive synthesis. The unsubstituted congener **40**⁶³ still provided a baseline compound for data comparison and interesting demethyl compounds could be synthesised as their methyl-substituted congeners at a later date.

Synthesis of the target compounds was carried out using the generalised route shown in Scheme 35. For target compounds designed to interact with BD1, commercially available 6-chloropicolinonitrile **275** was reacted in an S_NAr fashion with various nucleophiles to give the 6-substituted pyridines **277a–d**. The nitrile groups were then reduced over palladium on charcoal or Raney-Nickel, or with borane, to give the corresponding methyl amines **278a–d**. For the pyridone target compound designed to interact with His residues of BD2, commercially available 6-methoxypicolonitrile **276** was reduced over palladium on charcoal in acetic anhydride to give the methylacetamide **277e**. Simultaneous hydrolysis of

the methylether and the acetamide in aqueous acid gave the pyridonamine **278e**. With all methylamines in hand, reactions were performed with the chloroquinoline intermediate **239** available within our laboratories⁹⁴ to give the S_NAr products **279a–e**. Conversion of the primary amides to the imidazolidinones **280a–e** was achieved using the aforementioned PhI(OAc)₂ conditions. Where appropriate, *N*-Boc protecting groups were removed giving the final target molecules **281a–c**.



Scheme 35. Synthetic route used for 6-substituted pyridine targets.

The results from biological assaying of these compounds are shown in Table 33.

 R =	40 ⁶³	281a	281b	281c	280d	280e
BRD4 BD1, BD2	6.7, 6.3	5.7 ^a , 5.2 ^a	7.0, 7.0	6.1, 6.0	6.4, 6.6	6.8, 6.1
pIC₅₀						
BD1–BD2	0.4	0.5	0	0.1	-0.2	0.7

Table 33. Biological data for pyridine 6-position modifications. ^aData generated in FP assay format.

This focused exploration revealed that substituents at the pyridine 6-position conferred a range of effects upon selectivity and activity. A piperazine substituent **281a** decreased activity by 10-fold compared to the parent compound **40**,⁶³ perhaps because of its steric bulk. The flexible *O*-propylamine **281b** marginally increased activity at BRD4 BD1 and significantly increased activity at BRD4 BD2 resulting in no selectivity for either bromodomain. Conformationally restraining the propylamine to its *O*-pyrrolidine **281c** congener resulted in 10-times decreased activity with a comparable lack of selectivity. The bulky *N*-isopropyl **280d** also gave a reduction of activity at BD1 and, unexpectedly, increased activity at BD2. This result gave an indication that selectivity could be altered from a different vector other than the 8-position in the imidazoquinolinone template. However, the reason for the increase in BD2 activity for this compound could not be rationalised from structural modelling (not shown) and the lack of selectivity for either BD1 or BD2 warranted no further exploration. The most interesting analogue was the pyridone **280e** which showed a similar BD1 activity compared to pyridine **40**⁶³ but decreased BD2 activity resulting in a 5-fold selectivity window.

Interesting SAR was demonstrated from this exploration where some compounds actually reversed selectivity with respect to the baseline pyridine compound **40**.⁶³ However, due to a lack of significant selectivity at either bromodomain, no further chemistry was conducted at this position. These results, combined with those from previous explorations within this research, demonstrated that significant selectivity for BD2 was challenging and efforts were concentrated on furthering the initial positive results for improving selectivity for BD1. Additional optimisation was therefore carried out at the imidazoquinolinone 8-position.

3.4. Rigidification Strategy to Improve Activity and Selectivity

While the first iteration of chemistry (Section 3.2) showed that substituents containing heteroatoms at the imidazoquinolinone 8-position enhanced selectivity for BD1, none of the synthesised compounds met the probe criteria of 100 nM potency and 100-fold selectivity. In order to boost the BD1 activity and selectivity over BD2, a strategy to decrease molecular flexibility was employed.

Molecular flexibility is an important concept in ligand binding with favourable increases in binding often observed through rigidification of a flexible ligand.¹³¹ Preorganisation of a flexible ligand into its active conformer through conformational restraint results in a lower entropic cost to the overall free energy of binding. It was therefore posited that constraining the pendant amine-containing chains at the 8-position into heterocyclic amines would improve BD1 activity and selectivity (Figure 70a). Thus, a workplan was devised to synthesise a number of heterorings as rigidified analogues of both the ethyl **259** and propyl **261** amines (Figure 70b).

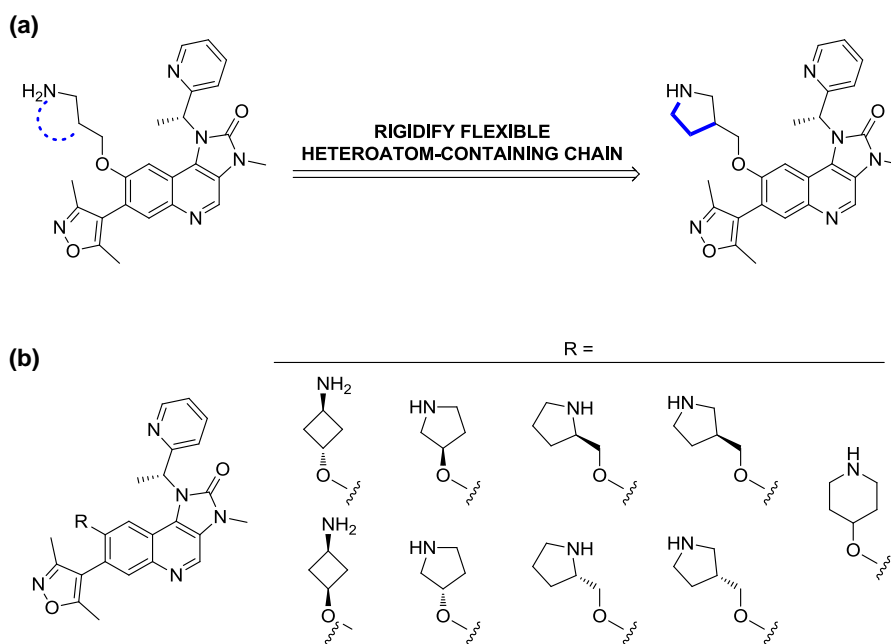
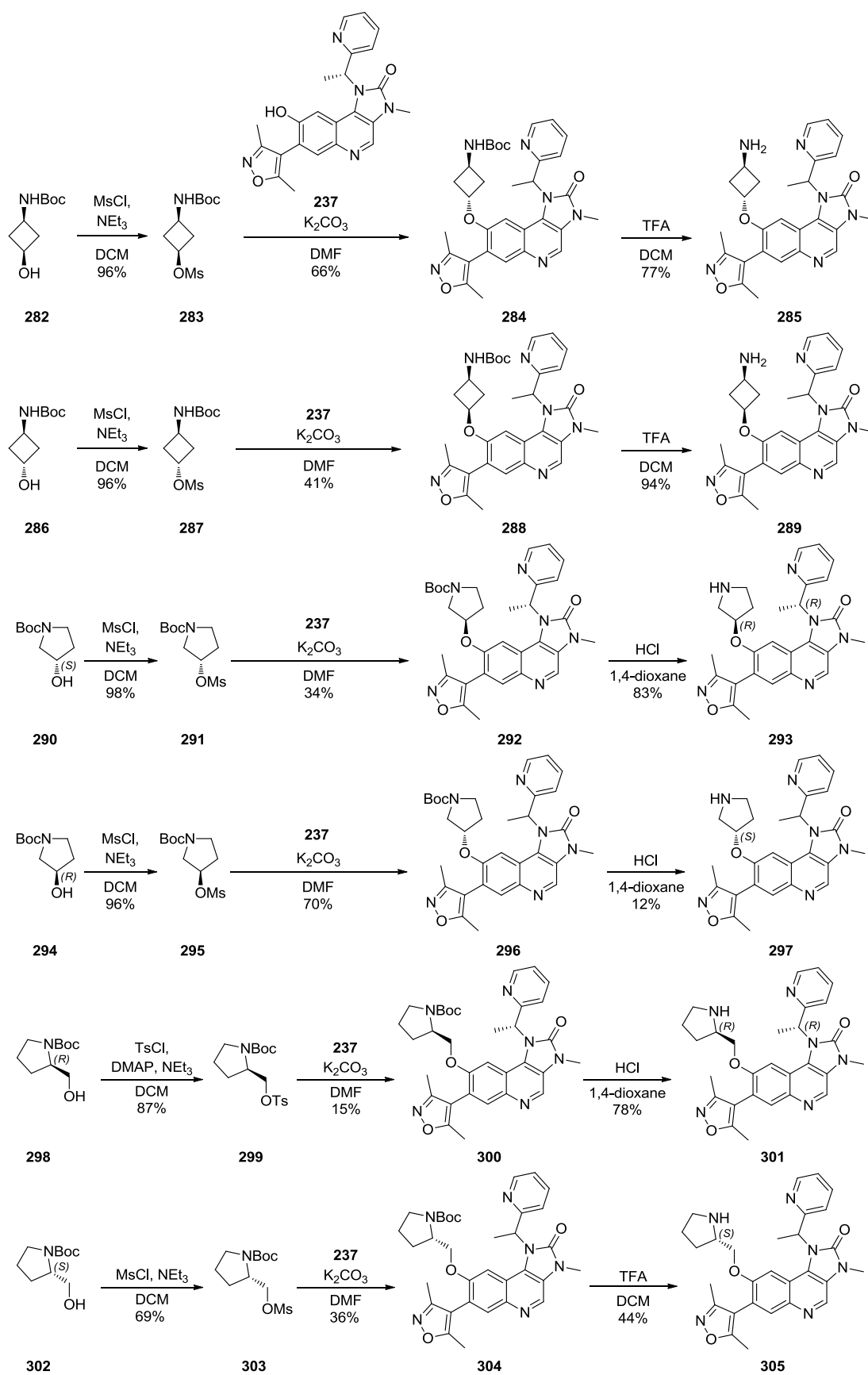
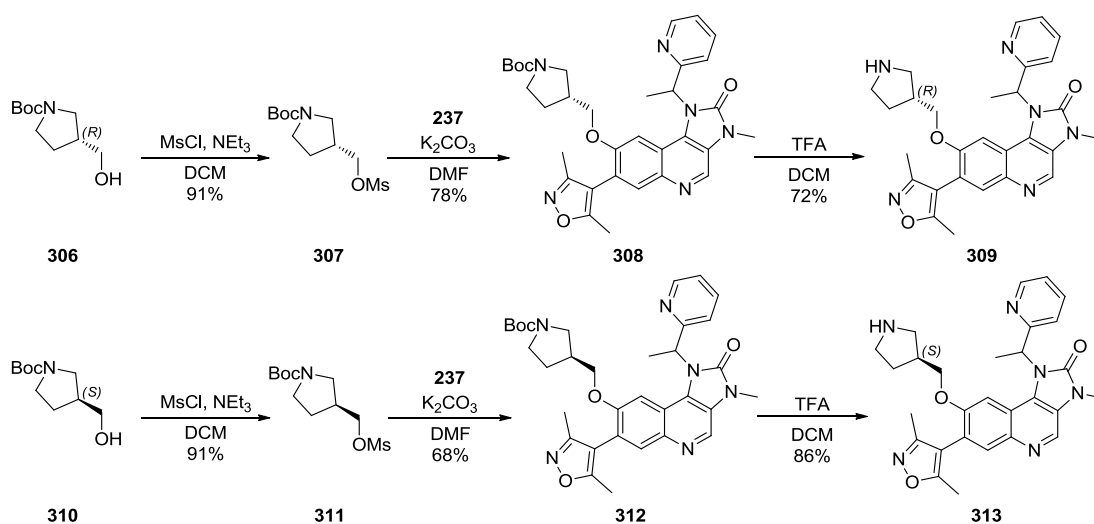


Figure 70. (a) Rigidification strategy to improve activity and selectivity. (b) Rigidified target compounds.

Synthesis of these heterorings was executed using the same sequence used previously, *i.e.* alkylation of the quinolinol **237** followed by Boc hydrolysis (Scheme 36). Although, as the requisite alkyl halides were unavailable for these targets, *N*-Boc protected amino alcohols were first converted into appropriate leaving groups before nucleophilic substitution.

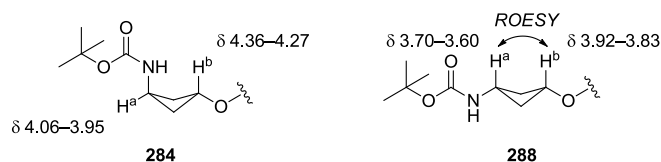


Scheme 36. Synthesis of rigidified amines.



Scheme 36 (continued). Synthesis of rigidified amines.

In the case of the cyclobutylamine targets, the *cis*-**282** and *trans*-**286** building blocks were converted into their corresponding mesylates **283** and **287**, respectively (Scheme 36). Full Walden inversion of the *trans*-mesylate to the *cis*-*N*-Boc cyclobutylamino ether **288** at the alkylation stage was confirmed by rotating-frame Overhauser effect spectroscopy (ROESY). A correlation was observed for the signals corresponding to H^a and H^b indicating a *cis* arrangement in the cyclobutyl ring (Figure 71). The chemical shifts of these protons differed significantly in the ¹H NMR spectra of the two isomers and, by inference, confirmed the *trans* relative stereochemistry of **284**.

Figure 71. Relative stereochemistry confirmation of cyclobutylamines **284** and **288**.

Results from assaying the rigidified amines in the BRD4 mutant assays are shown in Table 34.

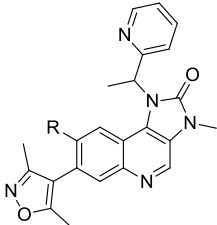
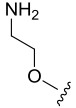
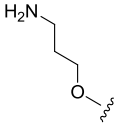


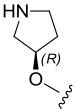
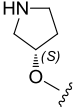
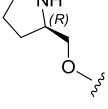
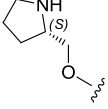
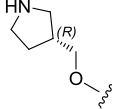
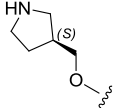
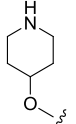
	Entry	BRD4 BD1, BD2 pIC ₅₀	BD1–BD2
	259 ¹²⁵	5.9, 4.5	1.4
	261 ¹²⁵	6.2, 4.8	1.4
	285	7.1, 5.5	1.6
	289	6.6, 5.0	1.6
	293 ¹³²	5.9, 4.3 ^a	1.6
	297 ¹³³	5.2, <4.3	>0.9
	301 ¹³²	5.6, <4.3 ^b /4.6 ^b	1.0
	305 ¹³³	4.9, <4.3	0.6
	309 ¹³³	6.1, 4.5	1.6
	313 ¹³³	6.3, 4.6	1.7
	314 ¹²⁵	5.5, 4.5	1.0

Table 34. BRD4 mutant assay data for rigidified amines. ^apIC₅₀ values of <4.3 were determined on two test occasions out of six and were excluded from the reported mean value. ^bpIC₅₀ values of <4.3 and 4.6 were determined on two test occasions each.

It was evident from these results that BRD4 BD1 activity and selectivity was improved upon rigidification of flexible amine chains but these properties were sensitive to the size of the heteroring and the positioning of the amine. Constraint of the propylamine **261**¹²⁵ into small 4-membered rings gave the cyclobutylamines **285** and **289**, resulting in improved activity and selectivity. The *trans*-isomer **285** displayed above 100 nM BRD4 BD1 activity with 40-fold selectivity over BRD4 BD2, while the *cis*-isomer **289** was 3-times less active at BRD4 BD1 but was equally selective. Rigidification to the slightly larger 3-substituted pyrrolidine **293**,¹³² resulted in improved selectivity (40-fold) compared to the ethylamine **259**¹²⁵ and propylamine **261**¹²⁵ without increased BRD4 BD1 activity. The importance of stereochemistry was highlighted when comparing 3-substituted pyrrolidine diastereoisomers **293**¹³² and **297**¹³³ with 5-fold increased BRD4 BD1 activity observed for the *R*-isomer.

Constraining the propylamine **261**¹²⁵ into a six-membered ring gave the piperidine **314**,¹²⁵ resulting in lower BRD4 BD1 activity and selectivity and suggested that a large heteroring close to the imidazoquinolinone was not well tolerated.

Extending the pyrrolidine ring further towards the Asp/His residues through the introduction of a methylene unit *versus* **293**¹³² and **297**¹³³ gave the 2-methylpyrrolidines **301**¹³² and **305**.¹³³ The data for these compounds demonstrated that stereochemistry was again important with the *R*-isomer showing greater BRD4 BD1 activity and selectivity over the *S*-isomer. However, even the preferred isomer **301**¹³² did not exhibit any improvement in activity over its flexible counterparts ethylamine **259**¹²⁵ and propylamine **261**.¹²⁵

The data for the 3-methylpyrrolidines **309**¹³³ and **313**¹³³ highlighted the importance of the positioning of the nitrogen atom within the pyrrolidine ring as both these compounds showed enhanced BRD4 BD1 activity and selectivity over the 2-methylpyrrolidines **301**¹³² and **305**.¹³³ Unlike their 2-substituted congeners, the 3-methylpyrrolidines did not display a significant stereochemical preference with only marginal greater BRD4 BD1 potency and selectivity observed for **313**¹³³ over **309**.¹³³

With 50-fold greater activity at BD1 over BD2 measured, both the methylpyrrolidine **313**¹³³ and the *cis*-cyclobutylamine **289** were the most selective imidazoquinolinones produced to this stage within this programme and demonstrated a notable increase in selectivity over the unconstrained analogues ethylamine **259**¹²⁵ and propylamine **261**.¹²⁵

Initial screening results in the previous FP assay configuration (see Appendix) indicated that the cyclobutylamine **289** exhibited 100-fold selectivity. Encouraged by these initial data, this compound was progressed for further investigational studies. Unfortunately, upon subsequent retesting in the FP assay configuration and then FRET, the selectivity

window narrowed to 50-fold and 40-fold, respectively (only FRET data are reported in Table 34), but progression of this compound continued.

To rationalise the increase in selectivity observed by appending basic heterorings onto the imidazoquinolinone 8-position, the *cis*-cyclobutylamine **289** was cocrystallised into BRD4 BD1 and an X-ray structure solved at 1.35 Å resolution (Figure 72).⁸⁹

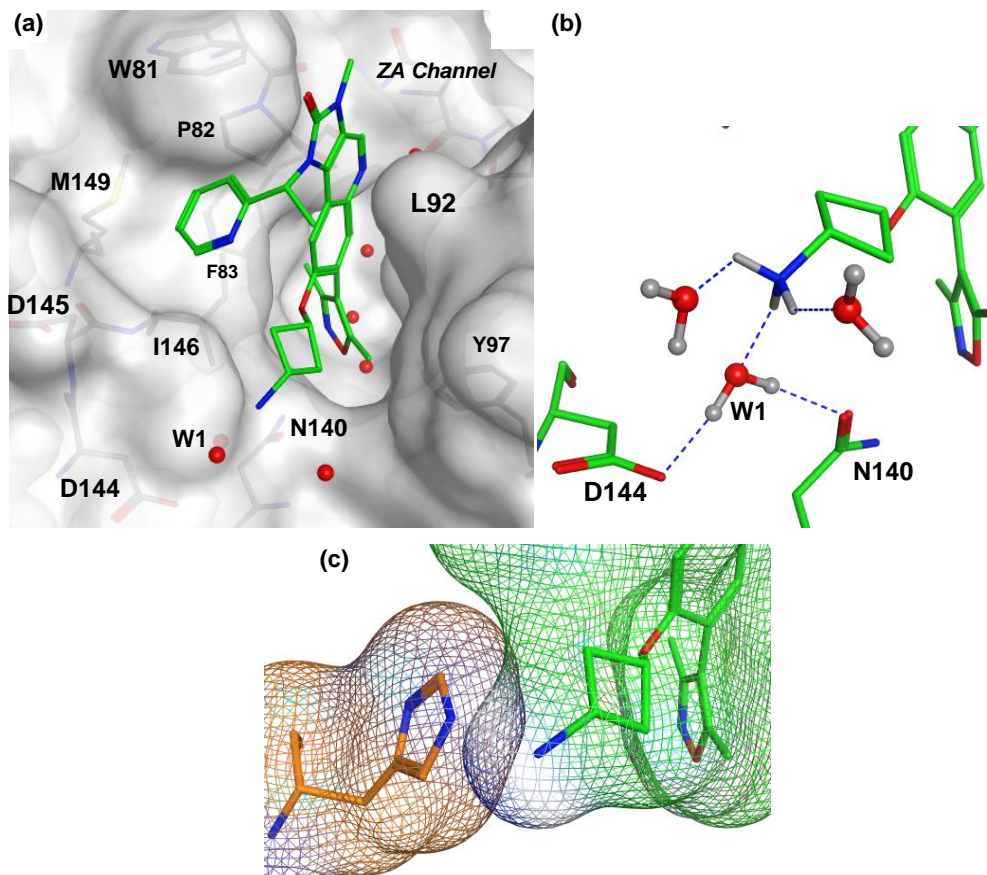


Figure 72. (a) Molecular surface representation of cyclobutylamine **289** (carbon = green) bound in BRD4 BD1. (b) Interactions of the pendant cyclobutylamine in BRD4 BD1 (ionisation state and hydrogen positioning was determined using the Protonate 3D function in MOE). (c) Crystal structure of cyclobutylamine **289** (carbon = green) bound to BRD4 BD1 superimposed with apo BRD4 BD2¹⁰ (carbon = orange, pdb 2OUO); solvent and BD1 protein were omitted for clarity and molecular surfaces applied.

The imidazoquinolinone motif bound to the protein as expected showing a hydrogen bond interaction from the dimethylisoxazole to Asn140 and contact of the pyridine to the WPF shelf (Figure 72a). With regard to the 8-position, the cyclobutylamine comfortably occupied space within the binding site and, due to the rigid nature of the ring, caused the amine to point directly into the water network surrounding Asp144. Notably, the amine interacted with a water molecule (W1) which formed a hydrogen bond to the carbonyl of Asn140, effecting favourable binding to BRD4 BD1 (Figure 72b). This provided interesting evidence that interaction with this water — and not direct interaction with Asp144 — was sufficient to impart selectivity over BRD4 BD2 (note that results from the GRID MIF using

a water probe shown in Figure 63 revealed that this water possessed a binding energy -9.4 kcal/mol, indicating that its displacement by a ligand would require suitably high binding energy compensation). Furthermore, this water was not present in the apo BRD4 BD2 structure as its site was occupied by an imidazole nitrogen atom of His437. The complex was superimposed onto an apo BRD4 BD2 structure¹⁰ and the BD1 protein removed for clarity (Figure 72c). This overlay showed the primary amine well within the van der Waals radius of the His437 side chain and in close proximity to a His nitrogen inducing both a steric and charge clash and, thus, providing a rationale for the observed selectivity.

Intrigued by the interaction of the primary amine functionality of **289** to the water molecule of BRD4 BD1, two analogues of this compound were designed to understand its precise nature (Figure 73). Also, slight adjustment of this interaction might provide the increase in activity and selectivity required to achieve a probe molecule for phenotypic studies.

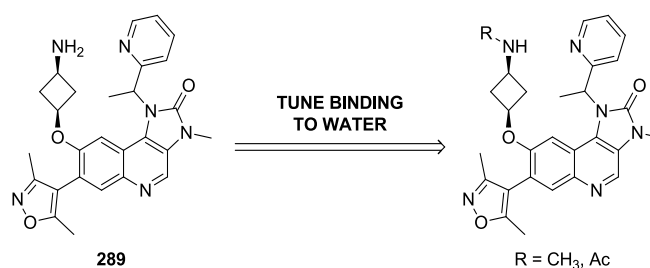
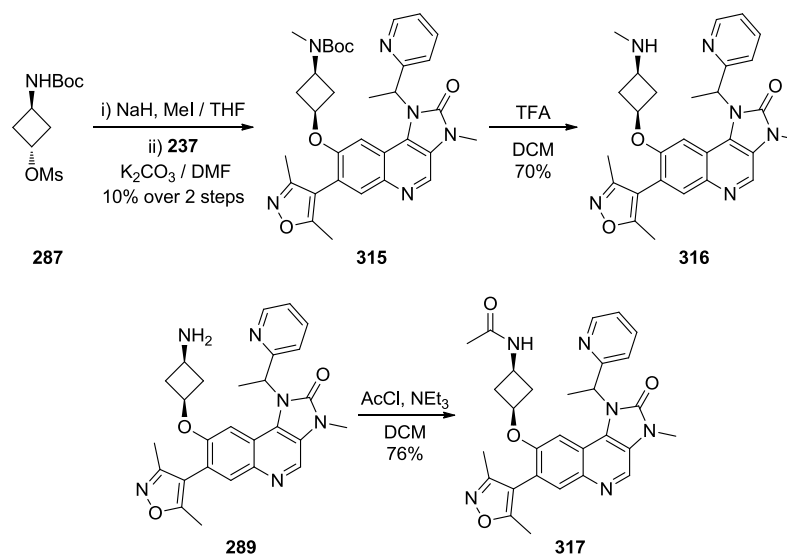


Figure 73. Focused exploration of cyclobutylamine derivatives.

An *N*-methylated derivative was targeted to explore the effect of increased basicity on the interaction with the water molecule bridging Asp144 and Asn140. Conversely, an acetamide derivative was also identified for synthesis to explore the effect of removing basicity while retaining hydrogen bond donating capability. Preparation of these target molecules was executed as shown in Scheme 37.



Scheme 37. Synthesis of cyclobutylamine derivatives.

The *N*-methyl cyclobutylamine **316** was obtained by methylation of the *N*-Boc cyclobutylamine mesylate **287**, reaction with quinolinol **237** followed by TFA treatment, while synthesis of the acetamide **317** was achieved by acetylation of cyclobutylamine **289**. Screening results for these compounds are shown in Table 35.

	R =		
	289	316	317
BRD4 BD1, BD2 pIC₅₀	6.6, 5.0	6.4, 4.8	6.8, 6.1
BD1–BD2	1.6	1.6	0.7

Table 35. BRD4 mutant FRET data for cyclobutylamine derivatives.

The effect of increasing the basicity of the amine by introduction of an *N*-methyl group to secondary amine **316** resulted in a slight loss of BD1 activity and a marginal reduction of selectivity compared to the primary amine **289** (this was consistent with SAR generated in the initial medicinal chemistry plan as detailed in Section 3.2). Examination of the crystal structure of cyclobutylamine **289** showed that a methyl substituent could occupy a vector pointing towards solvent. However, the hydrophobic nature of the methyl group may preclude this conformation and the extra basicity afforded by the methyl group did not give an overall improvement in free energy of binding. Interestingly, removal of the basic centre

with the acetamide **317** slightly improved activity at BD1 as desired. Unfortunately, this modification also significantly increased activity at BD2 and narrowed the selectivity window by 10-fold.

Overall, this iteration of chemistry demonstrated that rigidification of flexible pendant amines into heterocyclic amines increased BRD4 BD1 activity and/or selectivity. Compared to their flexible counterparts, ethylamine **259**¹²⁵ and propylamine **261**,¹²⁵ the cyclobutylamine **289** and methylpyrrolidine **313** markedly increased selectivity for BRD4 BD1 and afforded the largest selectivity achieved in this programme of research so far. X-ray crystallography was used to support the hypothesis that binding to a water molecule contacting the Asp of BD1 and/or clashing with His of BD2 resulted in domain selectivity. Further understanding of the binding interaction was gained through synthesis of close analogues of cyclobutylamine **289** and highlighted the preference for a basic amine.

While encouraging selectivities were achieved with the cyclobutylamine **289** and methylpyrrolidine **313**, they did not meet the 100-fold required threshold. At these selectivity levels, ligand occupancy at BD2 could still have been significant and the phenotype observed not solely attributed to inhibition of BD1. Also, it was evident from the SAR generated so far that BD1 activity decreased when a substituent larger than a methoxy group was appended to the imidazoquinolinone 8-position. While some of the constrained amines made progress towards addressing this issue, BD1 activity comparable to lead pan-BET compounds (IC₅₀ ~100 nM) still had not been reached. Therefore, further optimisation of the imidazoquinolinones was necessary, building on the promising package of data created for this chemotype so far. Other sources of data to inform design efforts were next explored.

3.6. Investigation of Overlap with BD1-Selective Thienopyridones

As part of a wider effort to discover BD1-selective compounds within our laboratories, a series of thienopyridones was being investigated and is exemplified by the structures in Table 36.

	318 ¹³⁴	319 ¹³⁵
BRD4 BD1, BD2 pIC₅₀	6.3, 4.8	6.7, 4.7 ^a
BD1–BD2	1.5	2.0

Table 36. BRD4 mutant assay data for thienopyridones. ^aA pIC₅₀ value of <4.3 was determined on one test occasion out of seven and was excluded from the reported mean value.

The piperazine **318**¹³⁴ displayed 30-fold selectivity for BRD4 BD1 over BRD4 BD2 while the piperazine sulfonamide **319**¹³⁵ displayed an excellent selectivity window of 100-fold. SAR within this series showed that the piperidine sulfonamide was important for selectivity and this was rationalised by X-ray crystallography (Figure 74).

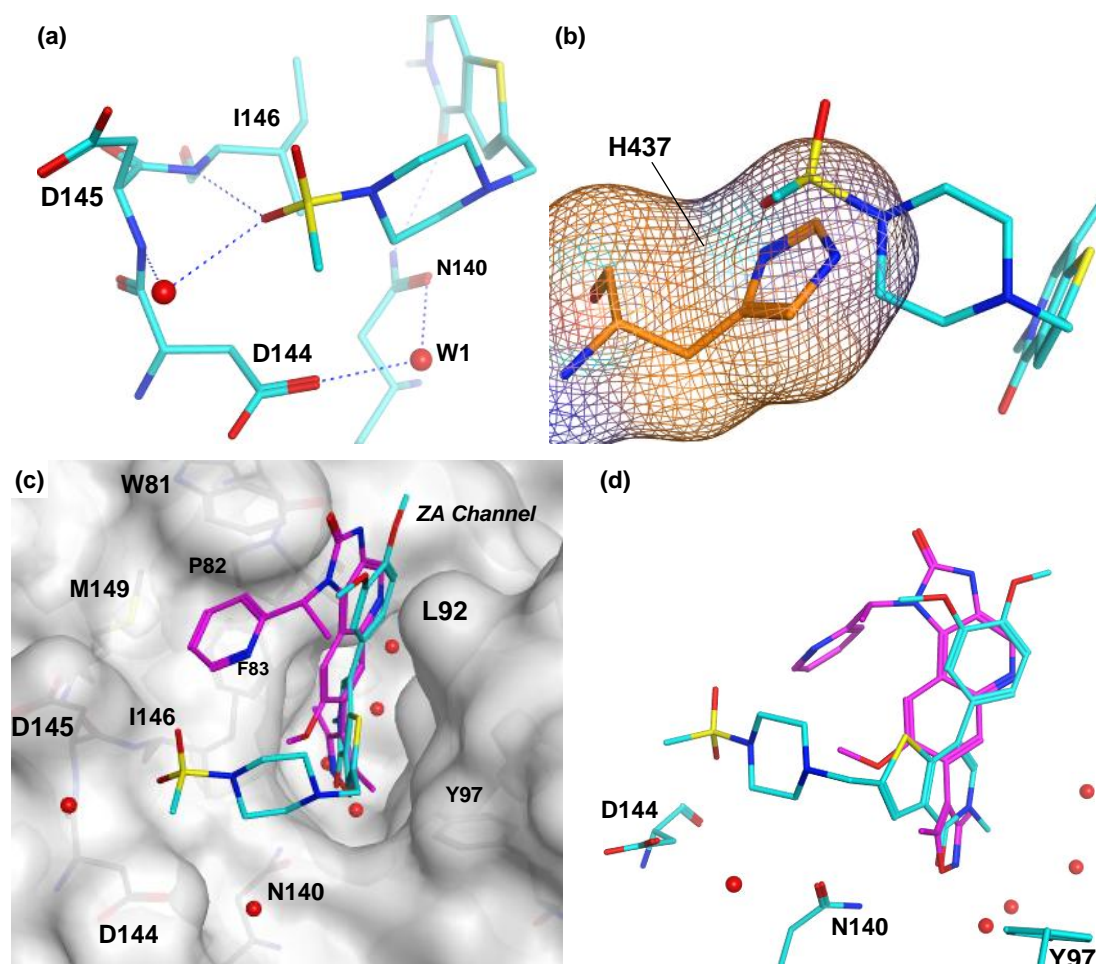


Figure 74. (a) X-ray crystal structure of thienopyridone **319** in BRD4 BD1 (carbon = cyan). (b) Overlay of apo BRD4 BD2 crystal structure¹⁰ (carbon = orange, pdb 2OUO) onto the BRD4 BD1–thienopyridone **319** (carbon = cyan) complex; solvent and BRD4 BD1 protein were omitted for clarity and a BRD4 BD2 molecular surface applied. (c & d) Overlay of the I-BET151–BRD4 BD1 complex (carbon = magenta, (pdb 3ZYU)⁶³ with the structure of thienopyridone **319** bound to BRD4 BD1 (carbon = cyan).

A structure of the sulfonamide **319** in BRD4 BD1 was solved within our labs⁸⁹ and revealed that the oxygen of the sulfonamide displaced a water molecule surrounding Asp144 and interacted with the backbone NH of Ile146 (Figure 74a). Interestingly, the corresponding water in BRD2 BD1 was found to be conserved across a range of ligand-complexes.⁷² Another notable observation was the lack of interaction to the conserved water bridging Asp144 and Asn140 (W1). This was postulated to be an important interaction observed for the cyclobutylamine imidazoquinolinone **289** to achieve 40-fold BD1 selectivity. To investigate if selectivity was achieved by clash with BD2 protein alone, an overlay of apo BRD4 BD2 protein¹⁰ with this crystal structure was examined (Figure 74b). This structure showed the piperidine significantly protruded the van der Waal radius of His437 thus causing a clash and providing a rationale for the observed BD1 selectivity. It was proposed that this SAR in the thienopyridone series could be used to enhance the BD1 activity and selectivity in the imidazoquinolinone series. Accordingly, a superimposition of the BRD4 BD1 structures of I-BET151 and the thienopyridone **319** was carried out (Figure 74c). The resulting structure suggested that appending a piperazine sulfonamide from the 8-position of the imidazoquinolinone would mimic the piperazine sulfonamide in the thienopyridone series. Thus, imidazoquinolinone ‘hybrid’ molecules, such as those shown in Figure 75, were postulated to improve BD1 activity and selectivity. It should be noted that extra flexibility in the form of methylene and ethylene spacers was designed into the targets as this appeared preferable from the crystal structure overlays. Also, SAR had shown previously that the directly *O*-linked piperidine **314** was weakly active at BRD4 BD1 (Table 34).

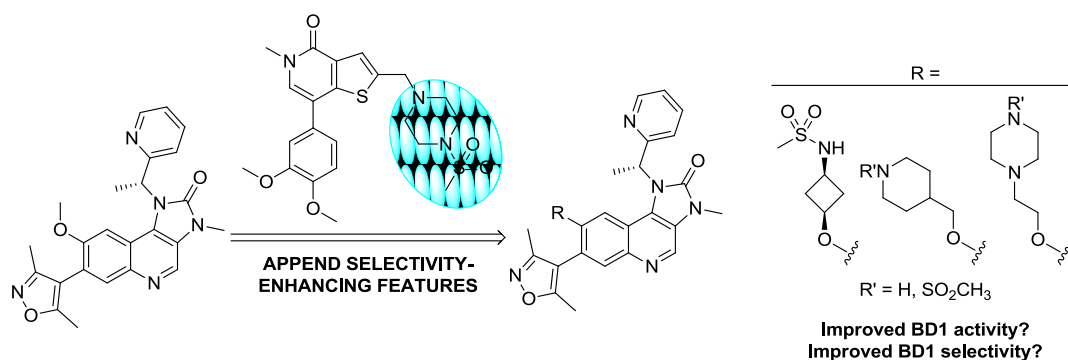
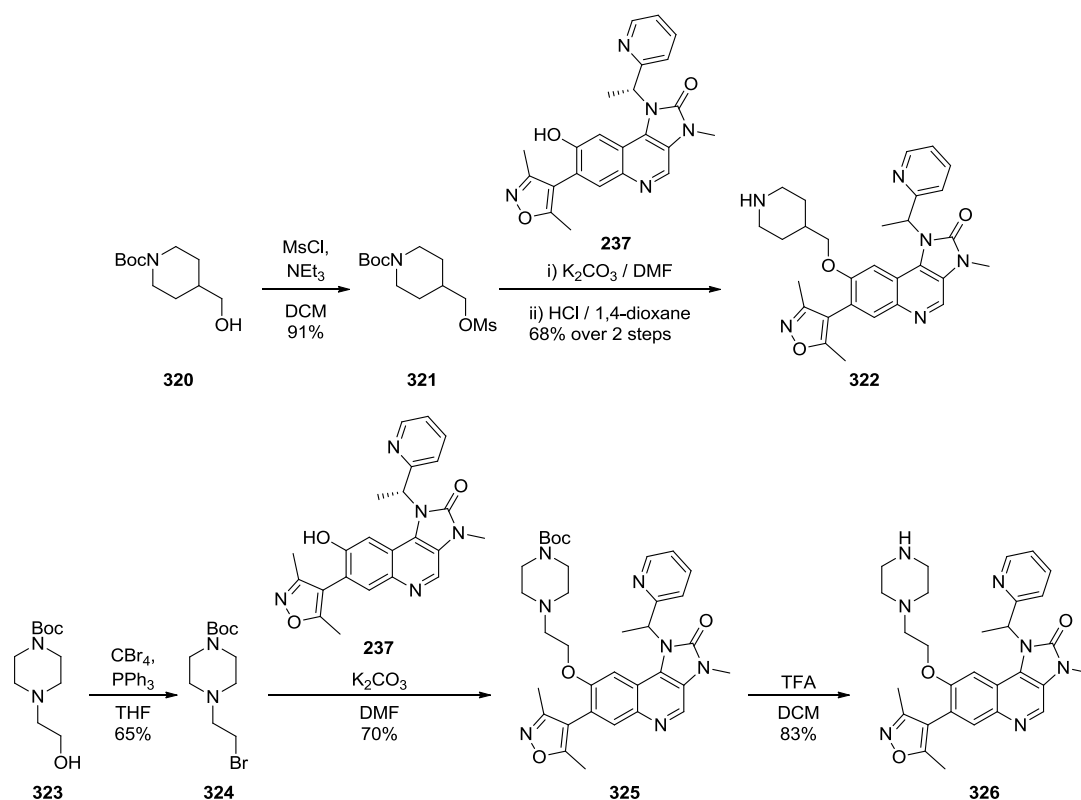


Figure 75. Strategy to use SAR from thienopyridones in the imidazoquinolinones.

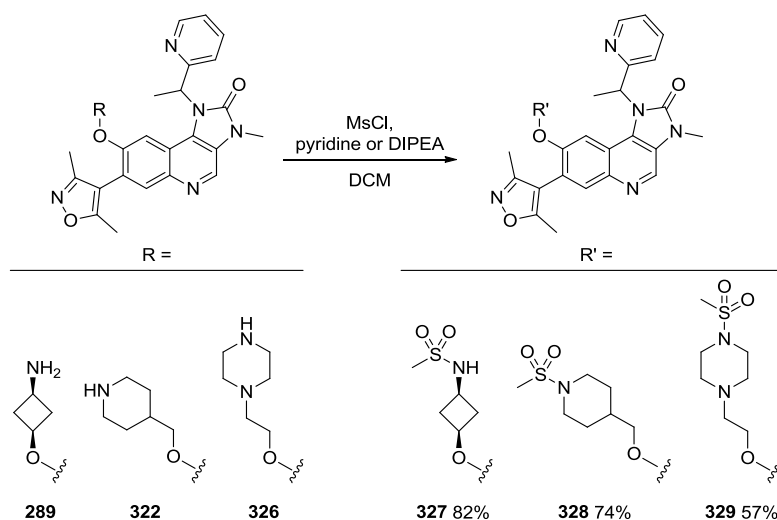
Synthesis of these hybrid targets was completed in a straightforward manner with initial preparation of the free amines as shown in Scheme 38. Using the standard mesylation-alkylation-deprotection sequence, the methylpiperidine **322** was synthesised in 62% overall yield. For the *N*-ethylpiperazine **326** however, activation of the alcohol **323** to its corresponding mesylate failed. Instead, Appel conditions were used successfully to obtain

the alkylbromide **324** in good yield and a subsequent alkylation-deprotection procedure gave the piperazine **326**.



Scheme 38. Preparation of hybrid imidazoquinolinones, piperidine **322** and piperazine **326**.

To obtain the sulfonamide targets, the previously described cyclobutylamine **289** was sulfonylated along with the piperidine **322** and piperazine **326** using mesyl chloride in yields ranging from 57 to 82% (Scheme 39).



Scheme 39. Final step towards hybrid targets.

Screening results of the hybrid molecules in the BRD4 mutant assays are shown in Table 37.

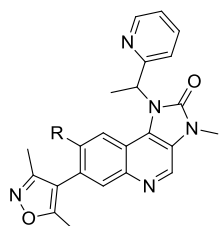
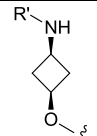
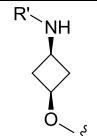
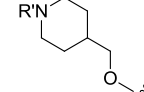
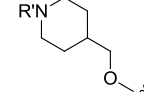
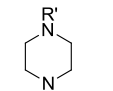
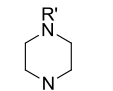
	R =	R' =	Entry	BRD4 BD1, BD2	
				pIC ₅₀	BD1–BD2
	H	H	289	6.6, 5.0	1.6
	SO ₂ CH ₃	H	327	6.6, 5.5	1.1
	H	H	322	6.1, 4.4 ^a	1.7
	SO ₂ CH ₃	H	328	5.6, 4.4 ^b	1.2
	H	H	326	6.4, 4.4	2.0
	SO ₂ CH ₃	H	329	6.1, <4.3	>1.8

Table 37. Results from screening of hybrid molecules. ^apIC₅₀ values of <4.3 were determined on two test occasions out of four and were excluded from the reported mean value. ^bA pIC₅₀ value of <4.3 was determined on one test occasion out of two and was excluded from the reported mean value.

In general, the inclusion of a sulfonamide moiety did not afford the desired BRD4 BD1 activity or selectivity increase that was observed in the thienopyridone series. With the cyclobutylsulfonamide **327**, a 3-fold increase of activity at BRD4 BD2 was observed relative to the cyclobutylamine **289** and, as a result, the selectivity margin narrowed to 13-fold. The 4-methylpiperidine **322** was 50-fold selective for BRD4 BD1 over BRD4 BD2 but its sulfonyl derivative **328** was 3-fold less potent at BRD4 BD1 therefore lowering the selectivity. Pleasingly, the *N*-ethylpiperazine **326** displayed 100-fold greater activity at BD1 over BD2 and was the first imidazolquinolinone to achieve this level of selectivity. Consistent with the methylpiperidine hybrid molecules, the sulfonamide derivative **329** lowered activity relative to its amine counterpart **326**. To verify if the piperidine **322** and piperazine **326** conferred their selectivity in a similar manner to the cyclobutylamine **289**, samples were crystallised in BRD4 BD1 and X-ray structures solved at 1.90 and 1.55 Å resolutions, respectively (Figure 76).⁸⁹

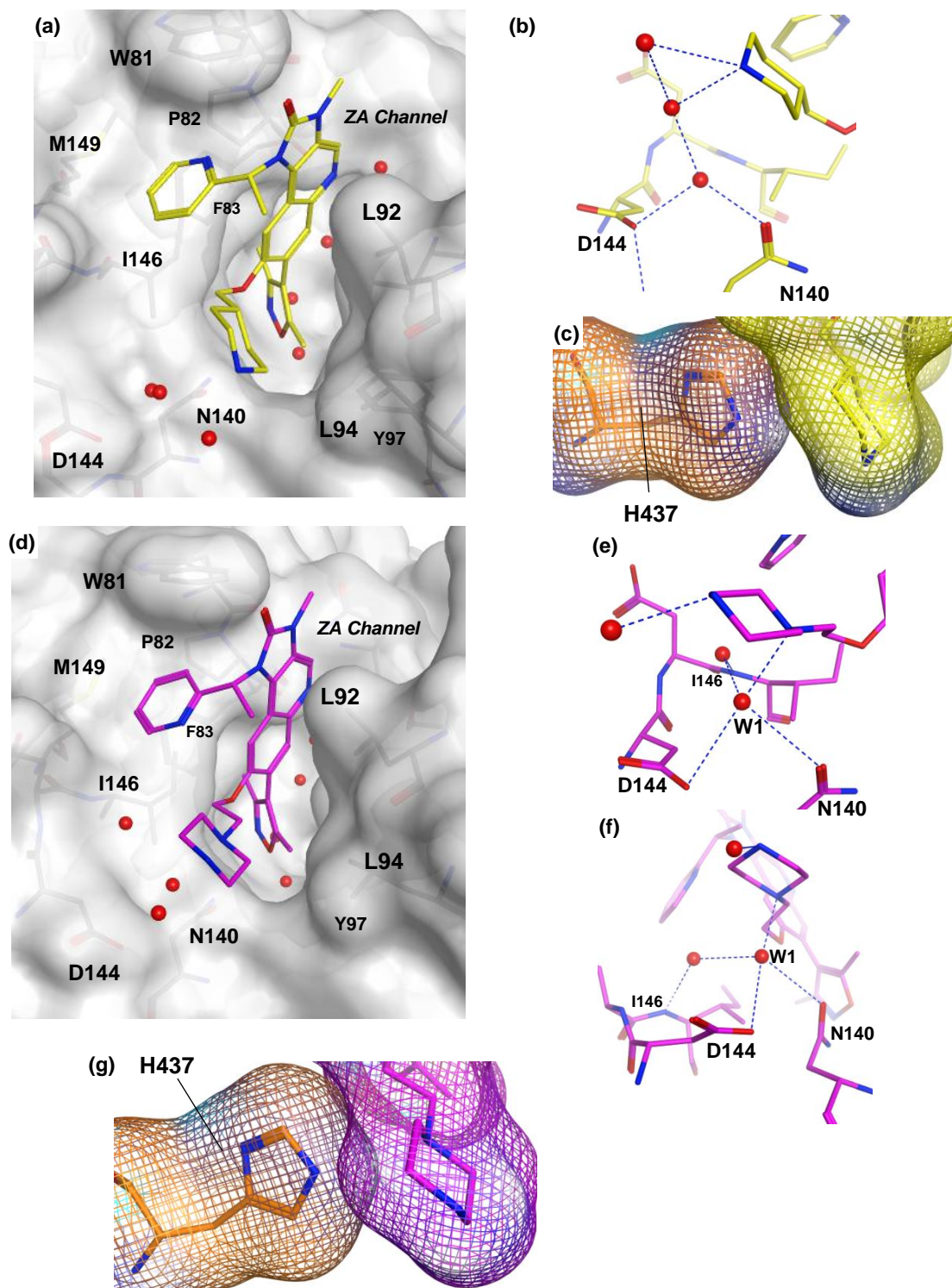


Figure 76. Complexes of hybrid molecules in BRD4 BD1, (a–c) piperidine **322**, (d–g) piperazine **326**. (a) Molecular surface representation of piperidine **322** (carbon = yellow) in BRD4 BD1. (b) Interactions of the piperidine moiety of **322** with BRD4 BD1 (carbon = yellow). (c) Overlay of apo BRD4 BD2 crystal structure¹⁰ (carbon = orange, pdb 2OUO) onto the BRD4 BD1–piperidine **322** (carbon = yellow) complex; solvent and BRD4 BD1 protein were omitted for clarity and molecular surfaces applied. (d) Molecular surface representation of piperazine **326** (carbon = magenta) in BRD4 BD1. (e and f) Interactions of the piperazine moiety of **326** with BRD4 BD1 (carbon = magenta). (g) Overlay of apo BRD4 BD2 crystal structure¹⁰ (carbon = orange, pdb 2OUO) onto the BRD4 BD1–piperazine **326** (carbon = magenta) complex; solvent and BRD4 BD1 protein were omitted for clarity and molecular surfaces applied.

Unexpectedly, the NH of the piperidine moiety in **322** pointed more towards solvent than into protein, perhaps due to space constraints caused by the large heteroring (Figure 76a). However, the amine still interacted with the water network surrounding Asp144 providing BD1 selectivity (Figure 76b), albeit through two water molecules rather than the single through-water interaction seen with cyclobutylamine **289**. The structure of the piperazine **326** revealed a similar feature with the NH directed towards solvent (Figure 76d) although, in this case, it did not interact with any water molecules surrounding Asp144. Instead, the tertiary amine made a single through-water interaction to Asp144 (Figure 76e). It is interesting to note that this heteroring imparts further activity and selectivity benefits when compared to the *N,N*-dimethylethylamine **260**. The pendant amines of both imidazoquinolinones **322** and **326** were found to protrude the van der Waal radius of His437 upon supersition of each crystal structure with apo BRD4 BD2 protein¹⁰ (Figure 76c and g, respectively) which also rationalised the observed selectivity.

It was surmised that straightforward transfer of SAR from the thienopyridones to the imidazoquinolinone series could not be made. Subtle differences in positioning of the different molecules in the BRD4 BD1 binding site would account for this and, thus, vectors extending to the Asp/His selectivity residues were distinct. In addition, previous work within this research programme demonstrated that selectivity was not solely driven by functionality probing of these residues alone and, thus, different chemical series have different intrinsic selectivity preferences. Regardless of this, several heterocyclic amines with almost 100-fold selectivity were discovered in this exploration and these were considered in future work to increase BRD4 BD1 activity while maintaining 100-fold selectivity over BRD4 BD2. Chemistry at another location in the quinoline template was now investigated aiming to achieve the desired selectivity and activity goals.

3.7. A Shift Towards a More BD1-potent Scaffold

An exhaustive chemistry exploration at the 8-position of the imidazoquinolinone has been described and, while 100-fold activity had been achieved, BD1 activity was still suboptimal. To establish if changes to other parts of the quinoline scaffold could enhance BD1 activity, a review of SAR was conducted.

As part of a historical chemistry programme on the isoxazole quinolines, other scaffold modifications had been made in addition to the imidazolinone described previously in Figure 15 and included the introduction of the imidazolquinoline template (Figure 77).



Figure 77. Quinoline isoxazole templates and the substructure used for SAR analysis.

An SAR analysis was carried out on these isoxazole quinolines to determine any differences in BD1 activity between the three scaffolds. BRD4 assay data for compounds containing any of the three scaffold substructures depicted in Figure 77 were displayed as box plots in Figure 78. Tukey-Kramer confidence circles¹³⁶ were also generated with results deemed statistically significant ($P < 0.05$) when these did not overlap.

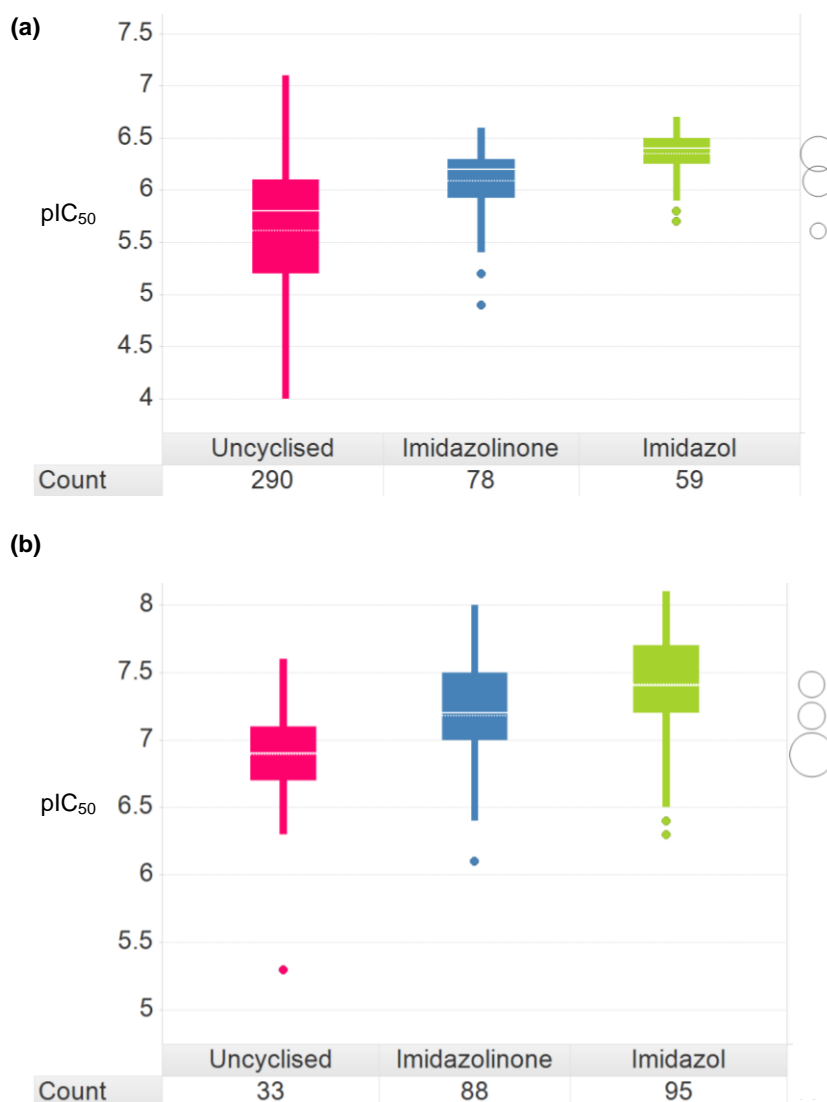


Figure 78. Data for compounds containing quinoline scaffolds in the (a) BRD4 WT FP and (b) BRD4 BD1 FRET assays. The boxes represent the interquartile range and the solid white line the median. Bars extending from the boxes denote the highest and lowest non-outlier values with single points corresponding to outliers.

Data for compounds tested in the historical BRD4 WT FP assay (which correlated with BRD4 BD1 FRET mutant assay) are shown in Figure 78a. It was apparent that, in general, the imidazoquinolinones were more active than the uncyclised quinolines. The most potent scaffold was the imidazolquinoline although this result was not considered statistically significant. However, it should be noted that the low tight binding limit of this assay restricted pIC_{50} measurement of the most potent compounds and, therefore, the imidazolquinolines may have appeared less active than in reality. For quinolines tested in the BRD4 BD1 assay (which were all selective for BRD4 BD1 over BRD4 BD2) the same trend existed and this time all results were determined to be statistically significant (Figure 78b). Not all compounds were tested in each assay and therefore some bias would have been introduced into the analysis. Further evidence that the imidazolquinoline was the more active quinoline scaffold was apparent from the matched molecular pair (MMP) analysis between two closely related examples from each template (Figure 79).

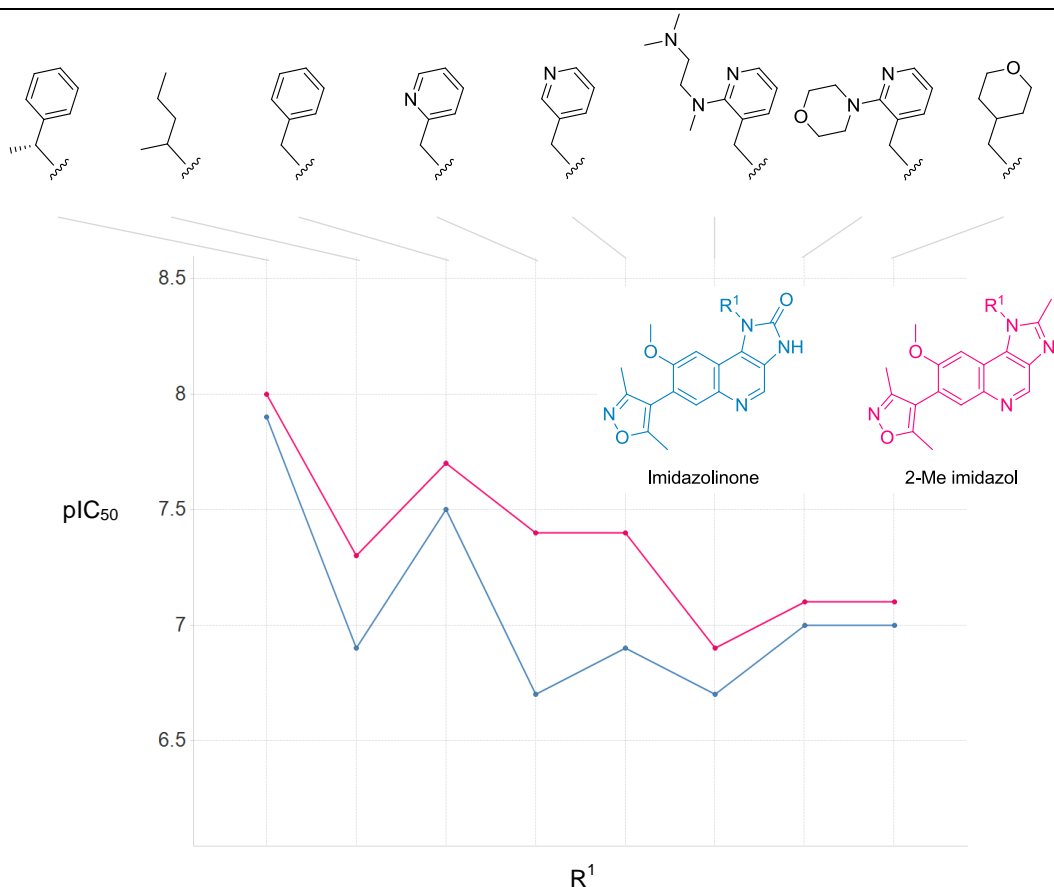


Figure 79. MMP analysis comparing BRD4 BD1 FRET activity of imidazol-2-ones *versus* 2-Me imidazoles.

Pairs of compounds from the imidazoquinolinone and 2-methyl imidazolquinoline templates with matched R¹ groups were identified and data in the BRD4 BD1 assay plotted. These data reaffirmed that the imidazoles were more active than the imidazolinones but

showed that the difference in activity between the two scaffolds varied with each R¹ group suggesting that SAR was not independent.

Based on these SAR analyses, a strategy to switch to a substituted imidazolquinoline template and diversify other positions of the molecule was formulated with the aim of increasing BD1 activity and maintaining or increasing selectivity over BD2 (Figure 80).

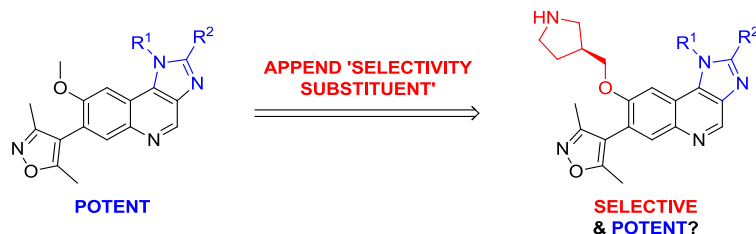


Figure 80. Strategy to switch to the more potent imidazolquinoline scaffold.

Therefore, a number of imidazolquinolines were submitted to the BRD4 mutant FRET assays to identify examples from this class of quinolines for derivitisation into BD1-selective variants. Two imidazolquinolines **330**⁹² and **331**¹⁰² were of particular interest (Table 38).

	330 ⁹²	331 ¹⁰²
BRD4 BD1, BD2 pIC₅₀	7.4, 6.9	8.0, 7.4
BD1–BD2	0.5	0.6

Table 38. Non-selective imidazolquinolines of interest.

The 1-methoxypropan-2-ylimidazolquinoline **330**⁹² was a lead molecule within our laboratories which had been optimised as an orally bioavailable pan-BET inhibitor.⁹² Chemical alteration of this molecule into a BD1-selective variant by appendage of a selectivity substituent at the 8-position of the quinolinol derivative **332** (Figure 81), was of considerable interest for potential phenotypic studies.

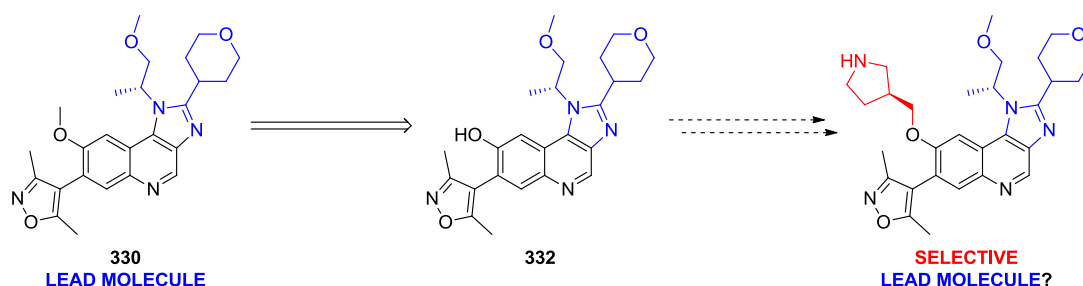


Figure 81. Strategy to append a selectivity substituent to the quinolinol derivative of lead molecule **330**.⁹²

However, considering the BRD4 BD1 activity of the 8-methoxy **330**⁹² and the SAR demonstrated previously, it was recognised this modification could lower the BRD4 BD1 activity to a level similar to the lead BD1-selective imidazoquinolinone **326**. Despite this, synthesis of a pan-BD1 selective analogue of an imidazolquinoline lead molecule was still attractive for biological assessment.

Screening of various imidazolquinolines also identified the 1-phenethyl-imidazolquinoline **331**¹⁰² as a highly potent compound with BRD4 BD1 activity of 10 nM (Table 38). Thus, attaching a selectivity-enhancing group in this instance was expected to achieve the target BD1 activity combined with selectivity over BD2 (Figure 82).

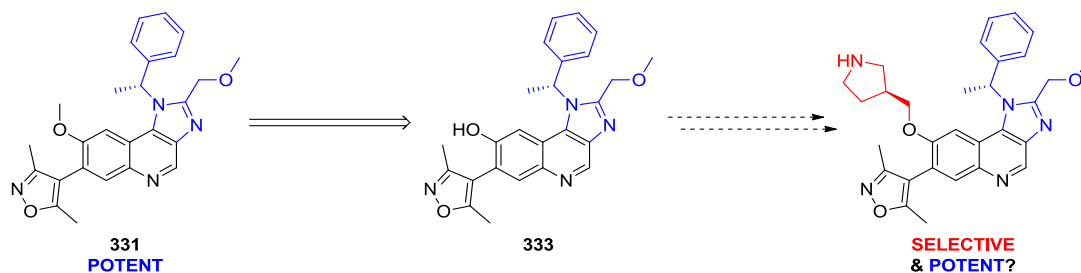
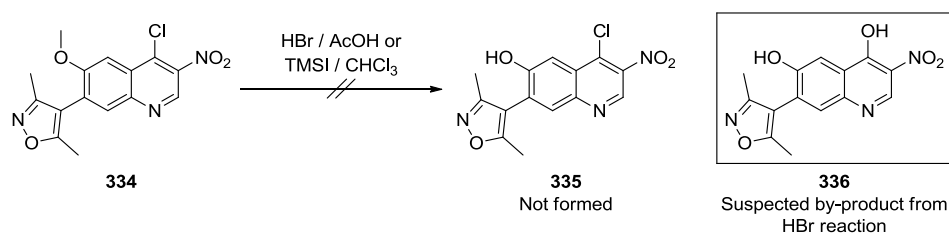


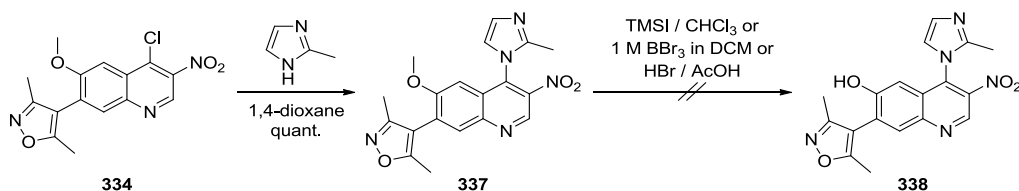
Figure 82. Strategy to append a selectivity substituent to the imidazoquinolinol derivative of the BD1 potent imidazolquinoline **331**.¹⁰²

The chemistry strategy used for installing selectivity-enhancing substituents at the 8-position of the imidazoquinolinones was to *O*-demethylate the 8-methoxy group and alkylate the resulting quinolinol. However, as both **330** and **331** contained two methyl ethers, and in the case of **330**, an additional tetrahydropyran (THP) ether, regioselective 8-OMe cleavage to the corresponding quinolinols **332** and **333** (Figure 81 and 82) was expected to be problematic. Moreover, only limited supplies of the imidazoquinolines **330** and **331** were available within our laboratories at the time. Therefore, attempts were made to effect the demethylation earlier in the reaction sequence and prior to installation of the imidazole 2-position ether functionality.

The 6-methoxy-4-chloroquinoline intermediate **334**, a precursor of **330** and **331**, was readily available within our laboratories (Scheme 40). Demethylation of this material was attempted using both HBr and TMSI. Unfortunately, mainly by-products were observed which, in the case of the HBr reaction, included the hydrolysis by-product quinolin-4-ol **336**, as determined by LCMS analysis. This result was unsurprising since the high reactivity of the chloroquinoline has already been exploited within this research.

Scheme 40. Attempted methylether cleavage of 4-chloroquinoline **334**.

Based on the above synthetic outcomes, a strategy to temporarily mask the 4-position was explored based upon methodology developed previously within our laboratories.¹³⁷ Here, 2-methylimidazole was used as a nucleophile to substitute chloride giving the intermediate **337** protected at the 4-position (Scheme 41). Attempted methyl ether cleavage on this substrate with TMSI or BBr_3 resulted in the formation of multiple by-products, while treatment with HBr induced displacement of the 4-imidazole with water without effecting methylether cleavage.



Scheme 41. Masking the quinoline 4-position followed by demethylation conditions.

Based on the results of these experiments, an alternative strategy to synthesise domain-selective imidazolquinolines was devised. The 8-OMe demethylation of I-BET151 and subsequent alkylation was a convenient method for synthesis of domain-selective imidazoquinolinones but a methyl protecting group for imidazolquinolinols **330** and **331** containing additional ether groups was unattractive as ether cleavage was expected to be unselective. Therefore, the incorporation of a specifically designed quinolinol protecting group was considered in a retrosynthetic analysis shown in Figure 83.

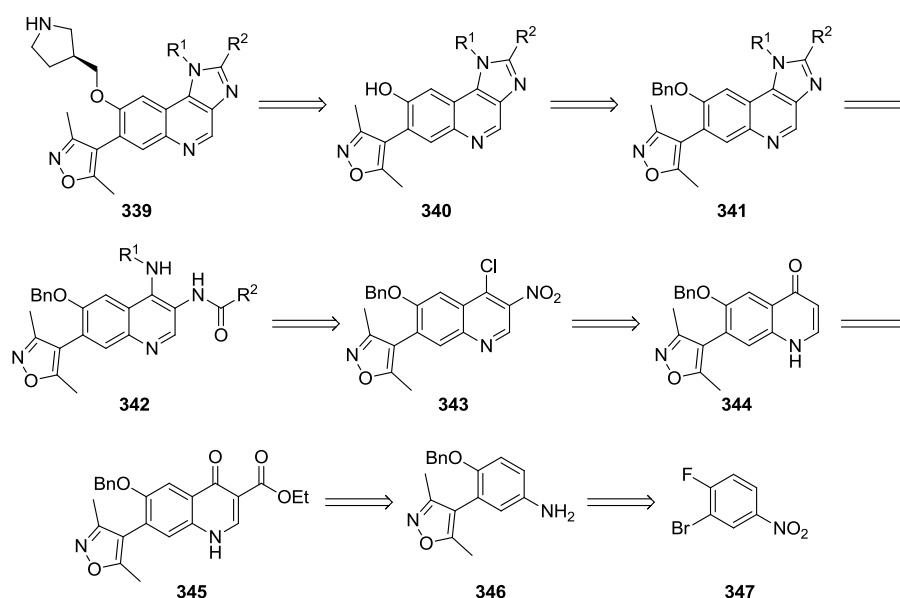
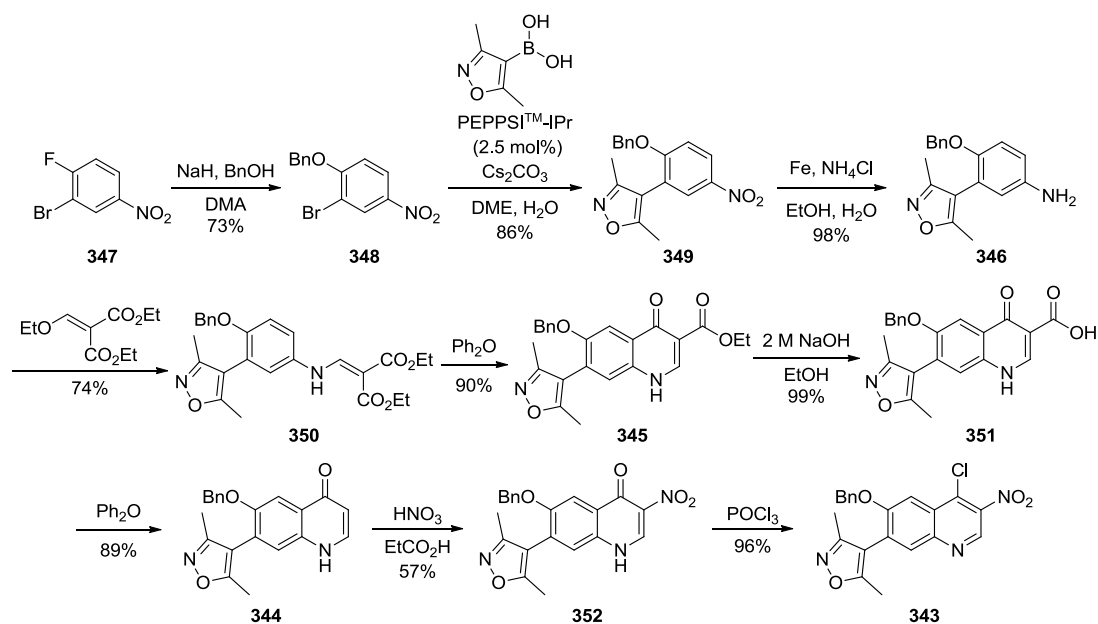


Figure 83. Retrosynthetic analysis of 8-substituted imidazolquinolines.

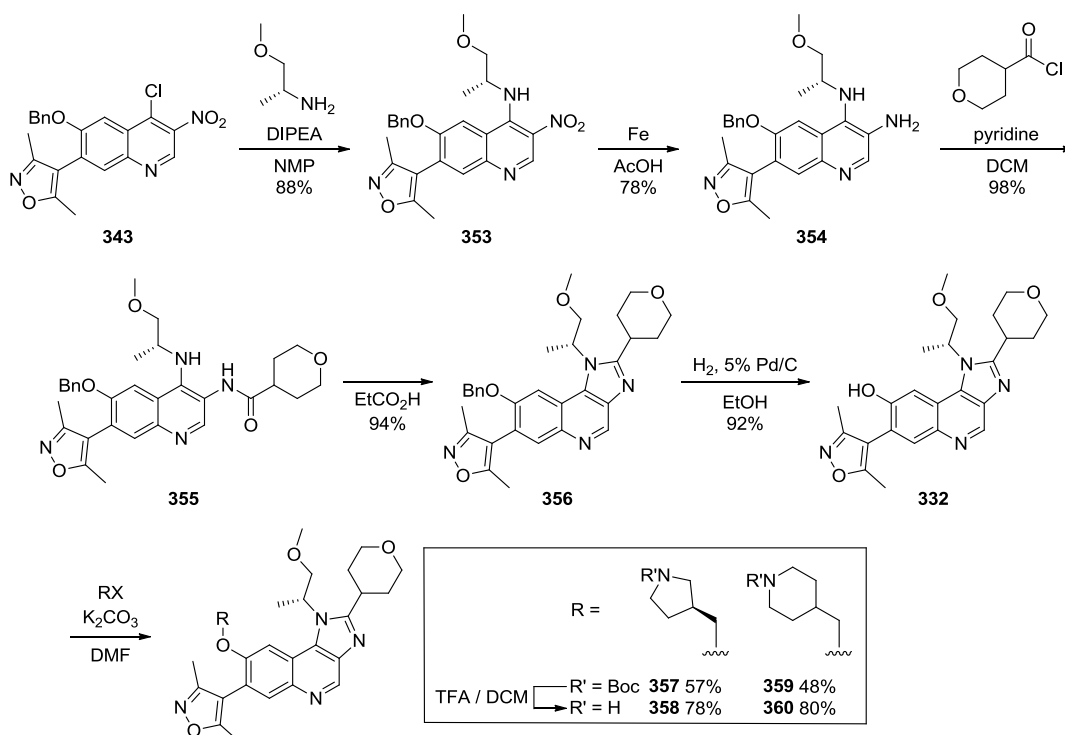
To obtain imidazolquinoline targets of type **339**, imidazolquinolinols **340** were required for appendage of selectivity-enhancing substituents *via* alkylation chemistry in a manner analogous to that carried out for the imidazoquinolinones. A benzyl (Bn) group was selected for protection of the quinolinols as it was expected to be stable to the harsh reaction conditions (strong acid and base, high temperature) throughout the synthetic route and was expected to be removed selectively over *N*-benzyl groups at R^1 due to the reluctance of benzylamines to undergo hydrogenolysis.¹³⁸ Imidazole ring formation required condensation of the 4-amino and the 3-amide groups of **342**. The key intermediate allowing introduction of substituents on the imidazole ring was the 4-chloro-3-nitroquinoline **343** which could be obtained from the nitration and chlorination of quinolin-4(1*H*)-one **344**. This molecule would be derived from the hydrolysis and decarboxylation of ester **345** which is the cyclisation product of aniline **346**. The trisubstituted 2-bromo-1-fluoro-4-nitrobenzene **347** allows for appropriate elaboration at the start of the synthetic route. Based on this, synthesis of the 4-chloro-3-nitroquinoline intermediate **343** was carried out according to the route shown in Scheme 42.



Scheme 42. Synthetic route to access the imidazolquinoline template.

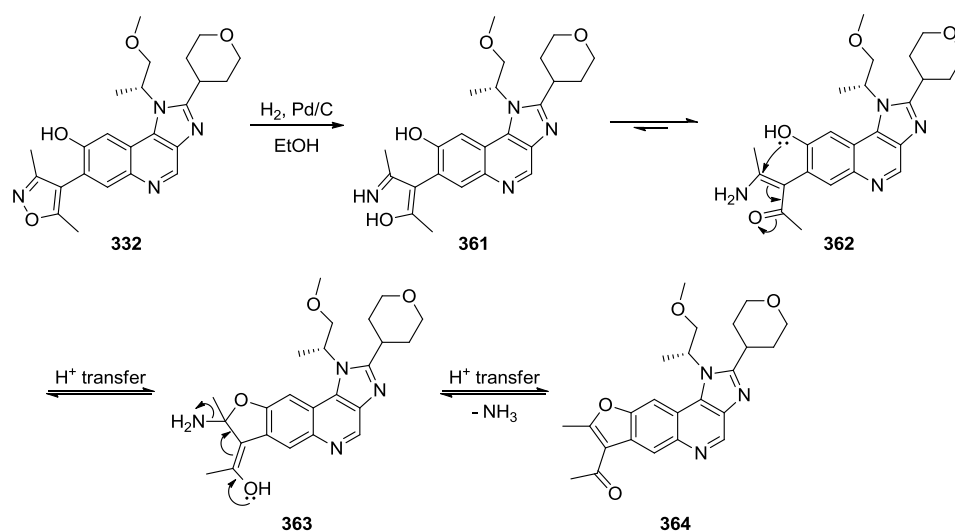
First, the protected phenol moiety was introduced by S_NAr reaction of benzyl alcohol with commercially available 2-bromo-1-fluoro-4-nitrobenzene **347** furnishing the benzylether **348** in good yield (73%). A Suzuki-Miyaura reaction of this material with (3,5-dimethylisoxazol-4-yl)boronic acid using the *N*-heterocyclic carbene Pd-precatalyst PEPPSITM-IPr, formed the cross-coupling product **349** in high yield (86%). Reduction of the nitro group with iron at room temperature gave the aniline **346** in excellent yield (98%) while keeping the benzylether intact. Performing the reaction at elevated temperature resulted in suspected reduction and opening of the isoxazole ring as indicated by LCMS. Attempts to isolate a pure sample of the assumed 4-aminopent-3-en-2-one failed, however, the propensity of the isoxazole to undergo reductive ring opening was confirmed at a later a stage (*vide infra*). The aniline **346** was subjected to Gould-Jacobs conditions¹³⁹ where conjugate substitution with diethyl-2-(ethoxymethylene)malonate proceeded to give the aminomethylene malonate **350** in 74% yield and was followed by cyclisation in refluxing diphenylether giving the 3-ethyl[quinolin-4(1*H*)-one]carboxylate **345** in 90% yield. Saponification to the acid **351** occurred in near quantitative yield and subsequent decarboxylation at 260 °C gave the quinolin-4(1*H*)-one **344** in high yield (89%). Nitration at the activated 3-position to **352** was accomplished in 57% yield and subsequent chlorination furnished the requisite 4-chloro-3-nitroquinoline late stage intermediate **343**. From here, access to the imidazolquinoline scaffold could be achieved straightforwardly and diversity embedded readily at several positions in the molecule.

Firstly, analogues of the lead imidazolquinoline **330** were prepared using the sequence shown in Scheme 43.



Scheme 43. Synthesis of 1-methoxypropan-2-ylimidazolquinoline **330** analogues.

The chloroquinoline intermediate **343** was reacted with (*R*)-1-methoxypropan-2-amine in S_NAr fashion to install the 4-amino substituent of **353** in high yield (88%). Chemoselective iron-acetic acid reduction conditions were used again to reduce the nitro group in the presence of the *O*-benzyl providing the 3-aminoquinoline **354** in 78% yield. Subsequent amide formation to **355** (98% yield) followed by condensation in hot propionic acid gave the imidazole **356** in high yield (94%). Removal of the benzyl protecting group to quinolinol **332** was achieved by hydrogenolysis over palladium on charcoal in 92% yield. A minor by-product was formed (4% yield) during this reaction and the structure determined as the ketofuran **364** (Scheme 44).

Scheme 44. Proposed mechanism for the formation of ketofuran by-product **364**.

This by-product was expected to have arisen from reductive cleavage of the isoxazole ring;¹⁴⁰ a transformation believed to have occurred during hydrogenolysis of isoxazole-containing molecules previously in this research but without conclusive evidence. In this case, the intermediate enaminone **362** was trapped by the adjacent hydroxyl group at the 8-position giving the intermediate species **363** which upon aromatisation and loss of ammonia gave the ketofuran **364**. This by-product was easily removed by chromatography and the desired quinolinol **332** used for *O*-alkylations to install the 3-methylpyrrolidine and 4-methylpiperidine selectivity enhancing substituents; despite the profound increase in selectivity gained by installing an *N*-ethylpiperazine substituent previously, this group was not considered for incorporation here due to the unacceptably large resulting molecular weight (548 g/mol). The 3-methylpyrrolidine **358** and 4-methylpiperidine **360** target compounds were obtained after deprotection and these were tested in the BRD4 mutant assays (Table 39).

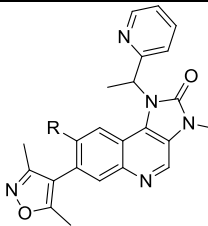
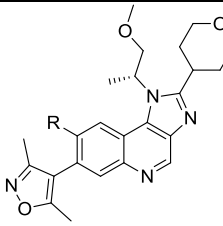
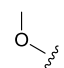
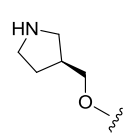
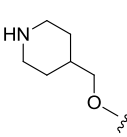
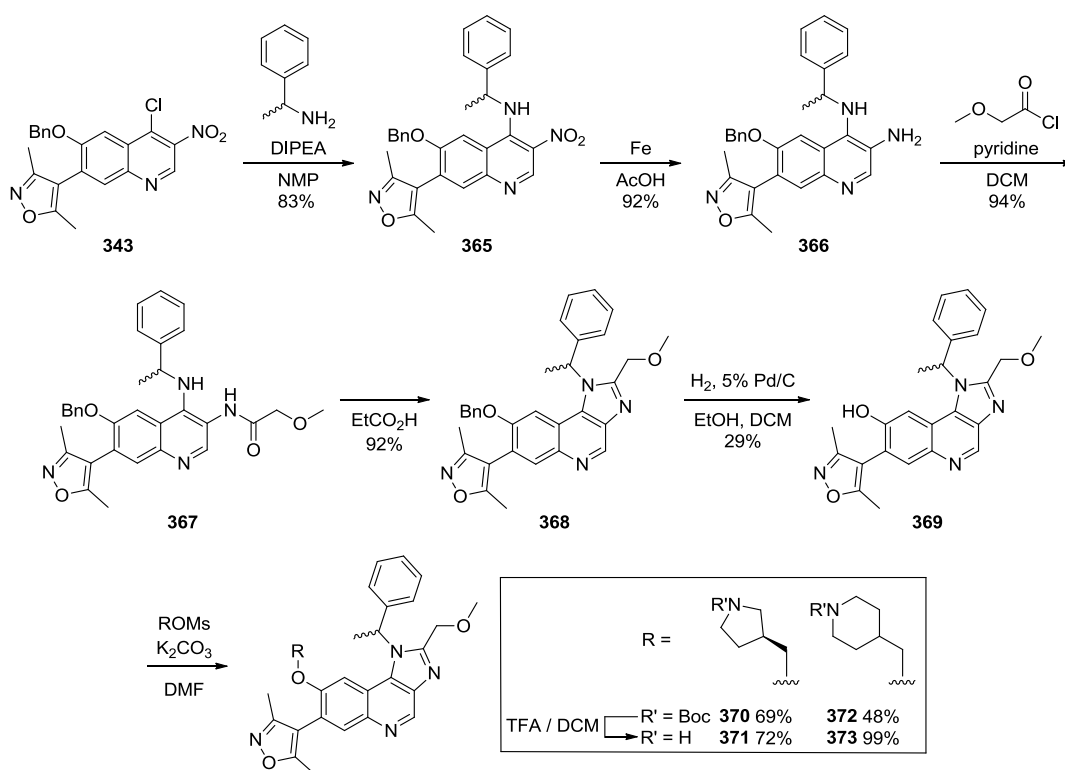
R =			
	Entry	I-BET151	330⁹²
	BRD4 BD1, BD2 pIC₅₀	7.5, 6.5	7.4, 6.9
	BD1–BD2	1.0	0.5
	Entry	313	358
	BRD4 BD1, BD2 pIC₅₀	6.3, 4.6	6.1, 4.5
	BD1–BD2	1.7	1.6
	Entry	322	360
	BRD4 BD1, BD2 pIC₅₀	6.1, 4.4 ^a	5.9, 4.8
	BD1–BD2	1.7	1.1

Table 39. Mutant assay results of 8-substituted variants of a lead imidazolquinoline **330**. ^apIC₅₀ values of <4.3 were determined on two test occasions out of four and were excluded from the reported mean value.

These data confirmed that, similarly to the imidazoquinolinones, appendage of amine substituents to the 8-position of an imidazolquinoline scaffold also improved BD1 selectivity. When compared against the unelaborated 8-OMe imidazolquinoline **330**,⁹² the pyrrolidine **358** increased selectivity 13-fold while the piperidine **360** increased selectivity 4-fold. The considerable selectivity increase observed with pyrrolidine **358** was unexpected as the same transformation in the imidazolinone scaffold (I-BET151 to **313**) only increased selectivity 5-fold. The moderate selectivity increase of piperidine **360** relative to **330**⁹² was more consistent with the 6-fold increase observed with the imidazoquinolinones (I-BET151 to **322**). These data demonstrated that subtle alteration of the quinoline scaffold affected the BRD4 domain selectivity. Unfortunately, the trend for reduced BD1 activity upon appendage of a basic amine found with the imidazoquinolinones, was also evident with the imidazolquinoline derivatives.

As predicted, these molecules did not exhibit the desired selectivity or activity required to warrant progression into the phenotypic assays. However, this work was important to determine if the domain-selectivity of a lead molecule could be improved easily and established the generality of the selectivity substituent incorporation strategy. Attention then turned to the preparation of analogues of the phenethylimidazolquinoline **331** which, in addition to increasing domain selectivity, were also expected to provide BD1 activity comparable to established pan-BET inhibitors.

In this exploration, selectivity substituents were incorporated using the same sequence of reactions already described in the preparation of domain-selective variants of 1-methoxypropan-2-ylimidazolquinoline **330** (Scheme 45). Again, the *N*-ethylpiperazine selectivity enhancing substituent was not considered for incorporation here due to the high molecular weight incurred. Concerned with the possibility that the benzylic centre may racemise during the synthetic sequence (as observed when preparing derivatives of the imidazoquinolinone I-BET151), racemic 1-phenylethanamine was incorporated in this initial exploration to give the diastereomeric mixture **371** and the racemate **373** of the imidazolquinolines; the racemate 8-methoxyimidazolquinoline **374** (Table 40) had been synthesised previously within our laboratories¹⁰² allowing SAR comparisons to be made. If interesting results were achieved with these mixtures, a homochiral synthesis would then be carried out with racemic or diastereomeric analogues available as analytical standards to determine if racemisation had occurred.



Scheme 45. Synthesis of 1-phenethylimidazolquinoline analogues.

Substitution reaction of 4-chloro-3-nitroquinoline **343** with (\pm)-1-phenylethanamine to **365** was accomplished in high yield (83%) and was followed by reduction of the nitro group to give the amine **366** in 92% yield. Reaction with 2-methoxyacetyl chloride formed the amide **367** in 94% yield and imidazole ring formation to **368** proceeded smoothly (92% yield). Selective removal of the *O*-benzyl over the *N*- α -methylbenzyl *via* hydrogenolysis was

achieved albeit in low yield (29%). Extended reaction times were required when conducted using either an H-Cube flow reactor or in batch mode under atmospheric hydrogen. In order to progress quinolinol **369** through to alkylation chemistry quickly, multiple purifications were conducted on incomplete reaction mixtures in-between runs, which was thought to have contributed to the poor yield. No reductive cleavage of the isoxazole ring or loss of the *N*- α -methylbenzyl was observed in the reaction mixtures by LCMS. Alkylation of quinolinol **369** with the appropriate mesylates followed by treatment with TFA gave the desired target molecules **371** and **373**. Screening results of these compounds in the mutant BRD4 assays are shown in Table 40.

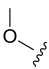
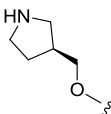
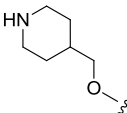
R =		I-BET151	374 ¹⁰²
	Entry BRD4 BD1, BD2 pIC₅₀	7.5, 6.5	7.8, 7.0
	BD1–BD2	1.0	0.8
	Entry BRD4 BD1, BD2 pIC₅₀	313 6.3, 4.6	371 7.1, 5.0
	BD1–BD2	1.7	2.1
	Entry BRD4 BD1, BD2 pIC₅₀	322 6.1, 4.4 ^a	373 6.8, 5.0
	BD1–BD2	1.7	1.8

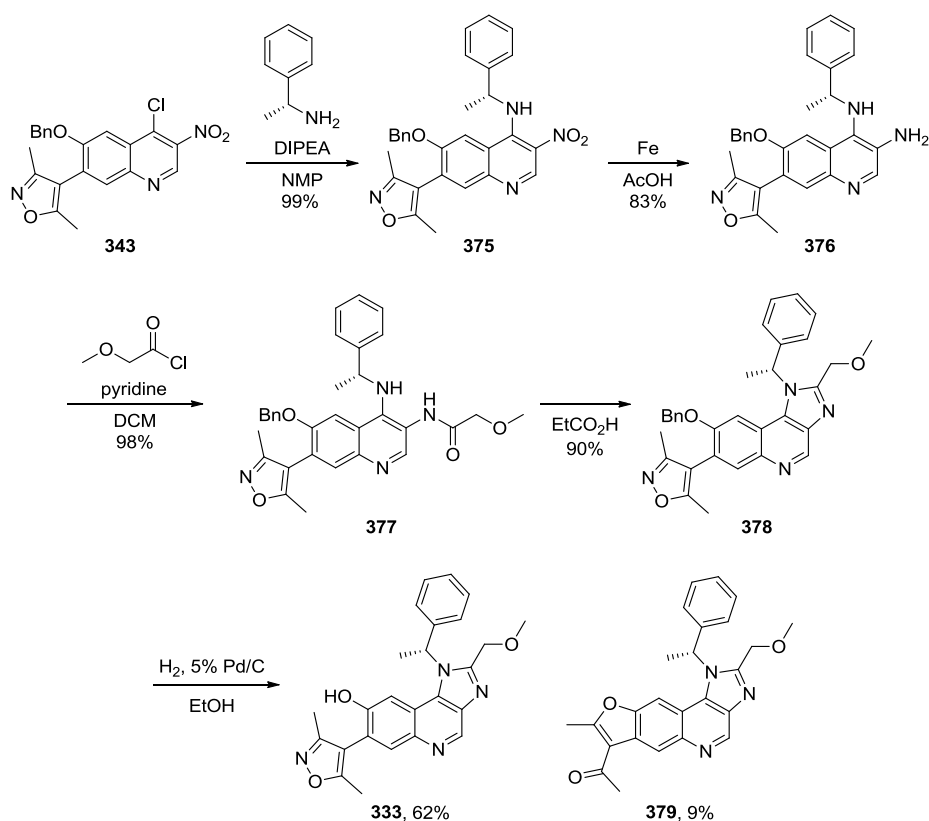
Table 40. Biological results of 8-substituted congeners of BD1 potent imidazolquinoline **374**. ^apIC₅₀ values of <4.3 were determined on two test occasions out of four and were excluded from the reported mean value.

As expected, these data demonstrated that appendage of amine substituents at the 8-position of the imidazolquinoline lowered activity. However, the extent of this reduction was less for the imidazolquinoline analogues compared to the imidazoquinolinone compounds. For example, only 5-fold reduced BRD4 BD1 activity was observed for the 8-pyrrolidin-3-ylmethoxy imidazolquinoline **371** compared to methoxy imidazolquinoline **374**,¹⁰² whereas 16-fold reduced BRD4 BD1 activity was observed for 8-pyrrolidin-3-ylmethoxy imidazoquinolinone **313** compared to methoxy imidazolquinoline I-BET151. In terms of selectivity, pyrrolidine imidazolquinoline **371** displayed 126-fold preferential binding to BRD4 BD1 over BRD4 BD2. SAR generated previously showed that a piperidin-

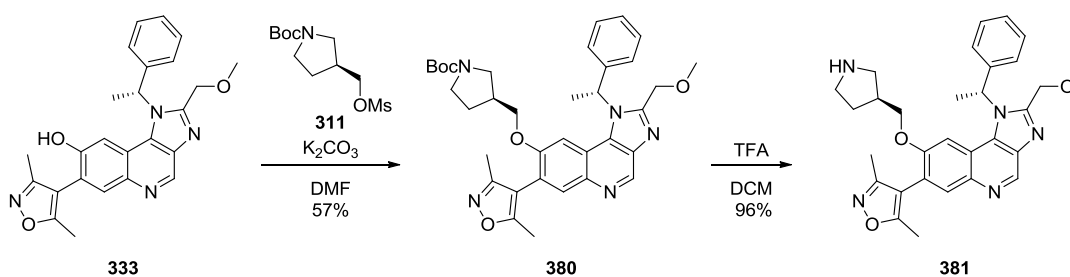
4-ylmethoxy group appended to the 8-position of an imidazoquinolinone reduced BRD4 BD1 activity compared to a pyrrolidin-3-ylmethoxy group (**322** versus **313**) but retained a 50-fold selectivity margin over BRD4 BD2. In the case of the imidazolquinolines, a reduction in BRD4 BD1 activity was also observed upon the pyrrolidine to piperidine transformation (**371** to **373**), but instead of maintaining a selectivity margin, a notable selectivity decrease was observed. These data once again highlighted the distinct subtle SAR trends with each isoxazole quinoline scaffold.

Results for the mixture of diastereoisomers **371** and the racemate **373** demonstrated that higher BRD4 BD1 potency was achieved by appending a selectivity enhancing group onto a more potent starting methoxyquinoline. Although greater BRD4 BD1 potency was achieved with piperidine **373**, the desired 100 nM target was not quite achieved, nor was the desired 100-fold selectivity over BRD4 BD2. Data for the pyrrolidine **371** were much more encouraging with a BRD4 BD1 $IC_{50} = 79$ nM and 126-fold selectivity being achieved. This compound was the most selective isoxazole quinoline synthesised to date and, therefore, further chemistry was conducted to obtain a single diastereoisomer for further studies.

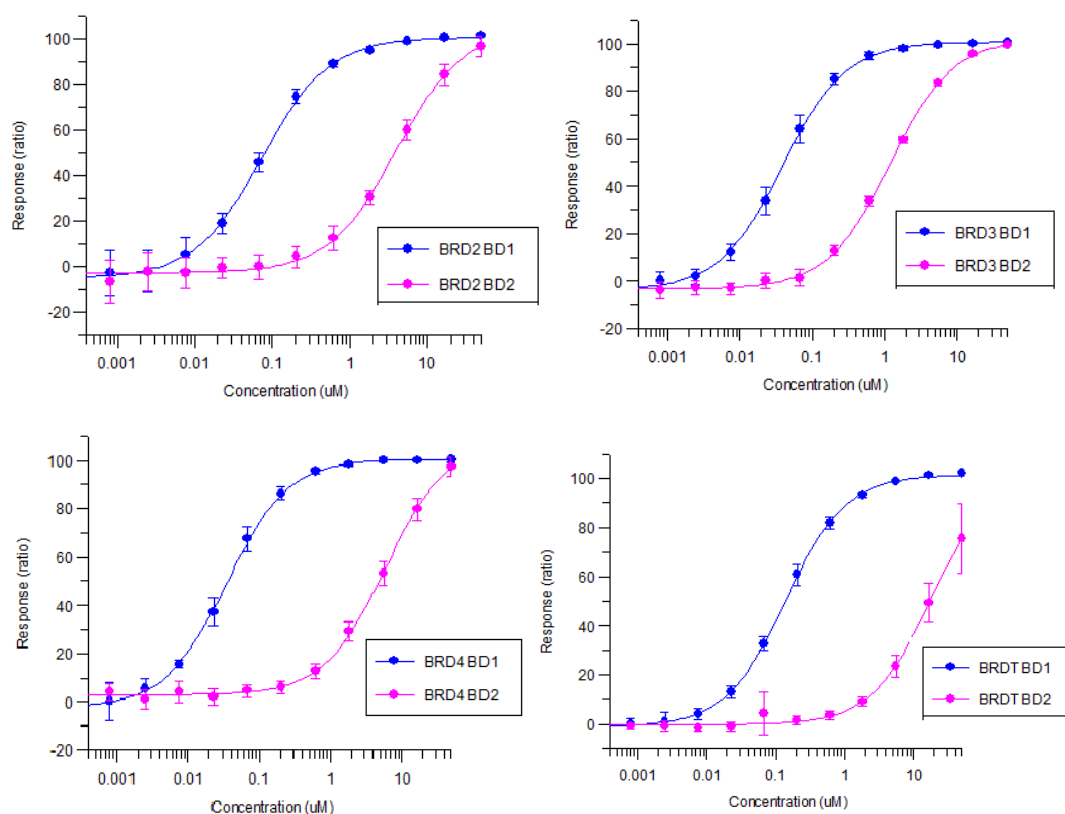
Previous SAR had shown that *R*-stereochemistry at the benzylic centre of imidazoquinolinone BET inhibitors was preferred for activity.⁶³ Therefore, it was postulated that the more active isomers of **371** and **373** should also contain an *R*-configuration at the benzylic positions. A homochiral synthesis was prosecuted to confirm this assignment starting with (*R*)-1-phenylethylamine (>99% e.e.) and 4-chloro-3-nitroquinoline **343** (Scheme 46).

Scheme 46. Homochiral synthesis of intermediate imidazolquinolinol **333**.

The homochiral synthesis proceeded smoothly with yields broadly consistent with the racemic synthesis. In this case though, a minor amount of reductive ring cleavage was observed in the last stage but the by-product (**379**) was easily separated by flash column chromatography. Pleasingly, the desired quinolinol intermediate **333** was obtained in 45% overall yield from 4-chloro-3-nitroquinoline **343**. With this intermediate in hand, the synthesis of a single diastereoisomer was undertaken (Scheme 47).

Scheme 47. Synthesis of single diastereoisomer **381**.

Reaction of quinolinol **333** with mesylate **311** proceeded in 57% yield to give the alkylation product **380**. Deprotection of this material gave the single enantiomer **381** which was then screened in the BET mutant assays with results displayed in Figure 84.



	pIC_{50}		
	BD1	BD2	BD1–BD2
BRD2	7.1	5.4	1.7
BRD3	7.4	5.9	1.5
BRD4	7.5	5.2	2.3
BRDT	6.9	4.8	2.1

Figure 84. Dose response curves and resulting pIC_{50} values for methylpyrrolidine **381** in BET mutant assays.

It was evident from the BRD4 assay data that the single enantiomer **381** had enhanced activity and selectivity compared to the diastereomeric mixture **371**. Remarkably high selectivity (200-fold) for BRD4 BD1 over BRD4 BD2 was determined and this strong preference for BD1-binding was replicated in the other BET family members, albeit at reduced levels compared to BRD4. Notably high BRD4 BD1 activity ($pIC_{50} = 7.5$) was also found for this compound, especially when considering the previously established SAR trend of reduced potency when appending a selectivity enhancing substituent.

At 200-fold BD1 selectivity in BRD4, methylpyrrolidine **381** was the most selective isoxazole quinoline synthesised within this programme of research and exceeded the desired

level of BD1 activity. In order to rationalise the BD1 selectivity, a high resolution X-ray crystal structure of methylpyrrolidine **381** bound to BRD4 BD1 was obtained⁸⁹ (Figure 85).

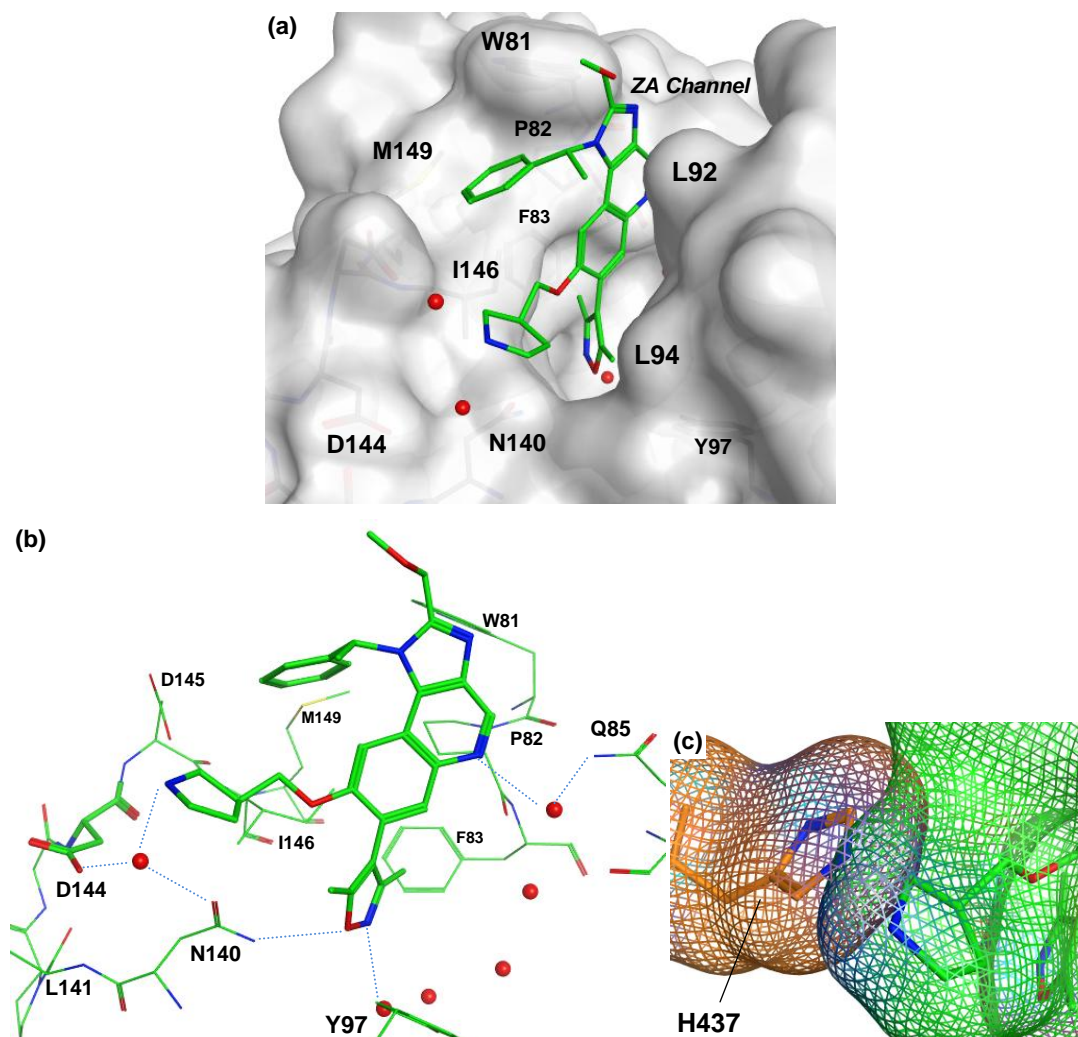


Figure 85. (a) Molecular surface representation of imidazolquinoline **381** (carbon = green) in BRD4 BD1. (b) Interactions of the methylpyrrolidine **381** with BRD4 BD1 (carbon = green). (c) Overlay of apo BRD4 BD2 crystal structure¹⁰ (carbon = orange, pdb 2OUO) onto the BRD4 BD1–imidazolquinoline **381** (carbon = green) complex; solvent and BRD4 BD1 protein were omitted for clarity and molecular surfaces applied.

This revealed a binding mode similar to the imidazoquinolinones discussed previously in this section: hydrogen bond interactions of the 3,5-dimethylisoxazole moiety to Asn140 and the water network at the base of the binding site, occupation of the WPF shelf by the (*R*)-1-phenylethyl substituent, and a through-water interaction of the quinoline nitrogen to Gln85 (Figure 85a and b). The 3-methylpyrrolidine was positioned in the region of Asp144 and, similar to the structures of the BD1-selective imidazoquinolinones obtained previously in this programme of research, the protonated amine interacted with the water molecule bridging Asp144 and Asn140. Superposition of this structure with BRD4 BD2 revealed that

a steric and dipole clash with His437 would result upon binding in this bromodomain, hence offering an explanation for the selectivity for BD1 domains over BD2 (Figure 85c).

Before this compound could be used as an *in vitro* probe molecule for assessment in phenotypic assays, further experiments with this compound were necessary. Firstly, as the phenotypic assays were conducted in whole cells, insight into the cellular permeability was required. Data from an artificial membrane permeability assay (see Appendix)¹⁴¹ revealed that a suitable level of permeability (87 nm/sec) was achieved and, therefore, provided confidence that facile partitioning into the intracellular compartment would not be a limiting factor in phenotypic assays. In addition, determination of the wider bromodomain selectivity of imidazolquinoline **381** was required to ensure any phenotypic response could be attributed only to binding of the first bromodomains of the BET family. This was carried out using BROMOscan technology (see Appendix) to generate dissociation constants for 34 different bromodomain constructs resulting in the selectivity profile shown in Table 41.

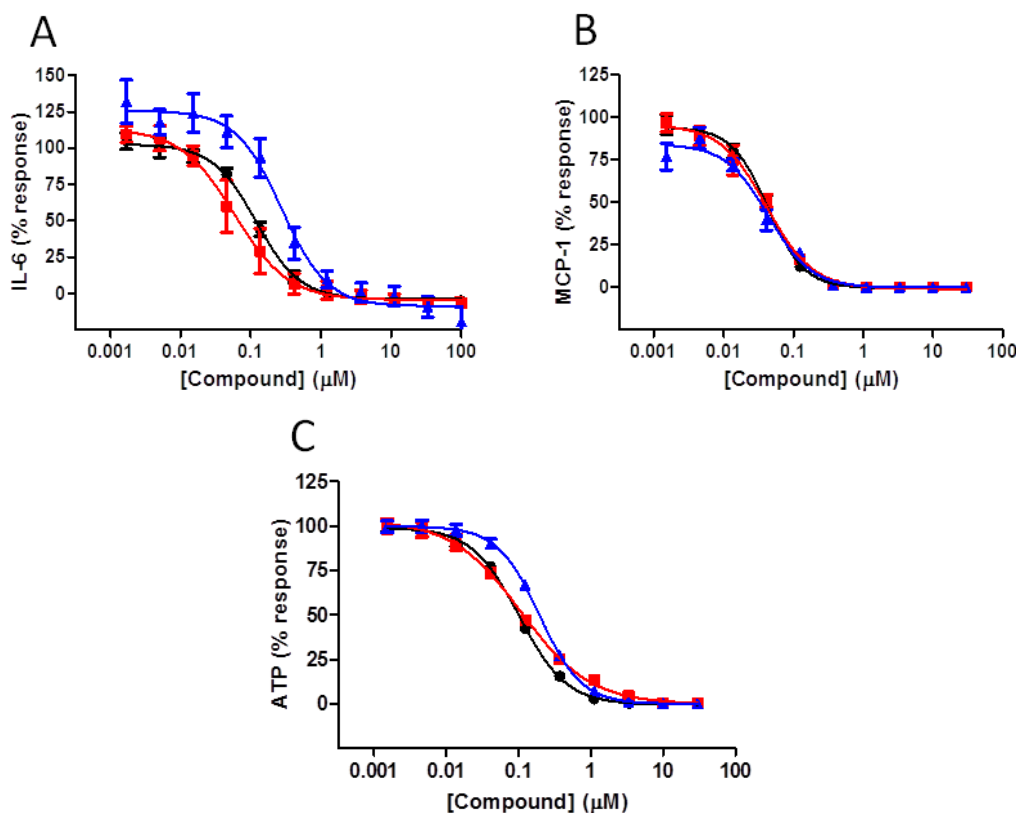
Bromodomain	K_D (nM)	Bromodomain	K_D (nM)
ATAD2A	>30000	BRPF1	15000
ATAD2B	25000	BRPF3	>30000
BAZ2A	>30000	CECR2	>30000
BAZ2B	>30000	CREBBP	3800
BRD1	>30000	EP300	5700
BRD2 BD1	13	FALZ	>30000
BRD2 BD2	840	GCN5L2	>30000
BRD3 BD1	5	PBRM1(2)	29000
BRD3 BD2	310	PBRM1(5)	>30000
BRD4 BD1	5.9	PCAF	33000
BRD4 BD1 & 2	100	SMARCA2	>30000
BRD4 BD2	670	TAF1(2)	>30000
BRD4 (full length, short isoform)	11	TAF1L(2)	>30000
BRD7	>30000	TRIM24 (bromodomain)	>30000
BRD9	>30000	TRIM24 (bromodomain &PHD)	>30000
BRDT BD1	18	TRIM33 (bromodomain &PHD)	>30000
BRDT BD2	5400	WDR9(2)	>30000

Table 41. Bromodomain selectivity profile of imidazolquinoline **381**.

Consistent with data obtained in the mutant FRET assays, imidazolquinoline **381** displayed selective binding within the BET family (K_D 5–18 nM at BD1 and 310–5400 nM at BD2). Specifically, a 200-fold difference between the BD1 and BD2 domains of BRD4 was observed. These data also confirmed the specificity of this compound for the BET family with negligible binding detected at all other bromodomains tested and, as a result, indicated that any phenotypic response driven by imidazolquinoline **381** could be attributed to binding of the first bromodomains of BET only. These data, taken together with the mutant FRET and artificial membrane permeability data, demonstrated that imidazolquinoline **381** met the *in vitro* probe criteria and, therefore, assessment in phenotypic assays was carried out.

In order to establish any difference in phenotype upon BD1 binding compared to pan-selective binding, the BD1-selective BET inhibitor imidazolquinoline **381** was tested alongside GW841819X, the BET inhibitor determined previously within this research programme to be non-selective in the BET mutant FRET assays (Section 3.1). In addition, I-BET151 was also screened in these assays as an intermediary control to evaluate the impact of moderate BD1-selective inhibition.

Firstly, experiments were conducted in human PBMCs to assess the impact upon inhibition of pro-inflammatory cytokine production. As discussed in the introduction of this thesis, studies from our own laboratories have demonstrated the ability of pan-BET inhibitors to inhibit pro-inflammatory cytokine production.^{47,63,64,67,72,74,79,80} These anti-inflammatory properties are now becoming a hallmark of pan-BET inhibition with other labs reporting similar observations with alternative molecules.^{75,82,83} As such, GW841819X, I-BET151 and imidazolquinoline **381** were dosed in varying concentrations into LPS-stimulated human PBMCs and the inhibition of the pro-inflammatory cytokines IL-6 and monocyte chemoattractant protein-1 (MCP-1) measured (Figure 86a and b).¹⁴²



	Compound	IL-6 pIC ₅₀	MCP-1 pIC ₅₀	MV-4-11 pIC ₅₀
▲	GW841819X	6.5	7.3	6.7
●	I-BET151	6.9	7.4	7.0
■	381	7.2	7.4	7.0

Figure 86. Phenotypic data comparing pan-BET inhibitor GW841819X, BD1-biased inhibitor I-BET151 and BD1-selective inhibitor **381**. Inhibition of (a) IL-6 and (b) MCP-1 production in LPS-induced human PBMCs. (c) Growth inhibition of MV-4-11 cells.

These data showed that, in a similar manner to GW841819X and I-BET151, the BD1-selective inhibitor **381** potently suppressed both IL-6 and MCP-1 production. Interestingly, for inhibition of IL-6, notably greater activity was observed for the BD1-selective probe **381** (pIC₅₀ = 7.2) over GW841819X and I-BET151 (pIC₅₀ = 6.5 and 6.9, respectively), whereas for inhibition of MCP-1, data between the three compounds was in closer accordance (pIC₅₀ = 7.3–7.4). Overall, these data demonstrated that the anti-inflammatory phenotype characteristic of pan-BET inhibition was retained upon selective BD1-inhibition.

Several studies were highlighted in the introduction of this thesis detailing the antiproliferative effects of the BET inhibitors I-BET151,⁶⁶ (+)-JQ1²⁵ and, dimethylisoxazoles (**S**)-**78** and **79**⁶⁹ in AML. Therefore, the BD1-selective inhibitor **381** was assessed in MV-4-11 AML cells alongside GW841819X and I-BET151 to determine if selective inhibition of BD1 resulted in similar effects to pan-inhibition or moderate BD1-selective

inhibition. Upon treatment of these cells over a three day period, the BD1-selective probe **381** was found to potently suppress cell growth with a pIC_{50} of 7.0 (Figure 86c).¹⁴³ This value was in close accordance with those obtained for GW841819X and I-BET151 (6.7 and 7.0, respectively), suggesting that efficacy in MV-4-11 cells is mediated through the BD1 domains.

Taken together, these data in human PBMCs and MV-4-11 cells showed that the anti-inflammatory and antiproliferative phenotype characteristic of pan-BET inhibition was retained upon selective inhibition of BD1 domains.

This is the first insight gained into the phenotype resulting from selective BET inhibition using a small molecule and provides the research community with an investigational tool for assessing the wider phenotype of selective BD1 inhibition. Furthermore, having demonstrated that optimisation of selectivity for individual bromodomains within BET can be accomplished through structure-based design, the development of the BD1 probe **381** detailed here provides a platform for future endeavours in the development of other selective BET inhibitors.

3.8. Conclusions

The BET family of BCPs containing eight individual bromodomains are implicated in a diverse range of biological effects. A small number of investigations into the roles of the individual bromodomains within BET have indicated that they exhibit discrete biological functions. However, these studies typically involved deletion of sections of protein or truncation, and, as a result, may have affected the gross behaviour of the protein when the function of the individual bromodomains were studied. Therefore, in the research detailed here, a small molecule probe approach was undertaken to selectively bind to individual bromodomains and deconvolute the biological response upon pan-BET inhibition.

To date, small molecule inhibitors of BET proteins typically bind all eight bromodomains of the family with similar affinity and, consequently, elicit broad biological effects. Further understanding of this biological response has been hampered by the lack of suitably selective inhibitors but this research has begun to address this issue by generating several dimethylisoxazole quinoline probe molecules which were selective for the first bromodomain of the BET family. Through a structure-based and data-driven design approach, compounds displaying high BD1 activity with excellent selectivity over BD2 were discovered.

An extensive understanding of the behaviour of non-selective BET inhibitors was fundamental to the chemistry strategy in order to produce selective compounds quickly. An analysis of the amino acid sequence revealed a number of residue variations between the bromodomain modules and suggested that selectivity for either domain was achievable. Examination of the X-ray crystal structure of I-BET151 bound to BRD4 BD1 identified two vectors to probe an Asp/His residue difference with functionality designed to selectively interact with one amino acid over the other. An SAR analysis was completed at one of these vectors, the imidazoquinolinone 8-position, to determine that an *O*-linkage atom was favoured for activity.

An initial study with various *O*-alkyl substituents was designed to sterically clash with His residues of BD2 to afford BD1 selective compounds. Disappointingly, these substituents did not improve selectivity and were found to be detrimental for BD1 activity. More success was achieved with heteroatom-containing pendant groups where up to 25-fold selectivity for BD1 was established, but attempts to bias the selectivity towards BD2 failed. Data for these heteroatom-containing substituents provided initial evidence that BD1 selectivity could be optimised and supported the structure-based approach taken to achieve the programme objectives.

In parallel to modifications at the imidazoquinolinone 8-position, a brief exploration of the pyridine 6-position was conducted as this vector was also directed towards the Asp/His residue difference. Disappointingly, appending various chemical functionalities at this position did not result in enhanced selectivity and efforts were re-focused on the imidazoquinolinone 8-position.

Building on the initial success of flexible heteroatom-containing chains at the imidazoquinolinone 8-position, a rigidification strategy was implemented to enhance BD1 potency and selectivity over BD2. Several interesting molecules resulted from this effort including the 40-fold selective cyclobutylamine **289** and the 50-fold selective methylpyrrolidine **313**. An X-ray crystal structure of the former compound in BRD4 BD1 revealed a through-water interaction of the primary amine to Asp144, and a steric and dipole clash with His437 as rationale for preferential binding to BD1.

Despite the positive impact of the rigidification strategy upon domain selectivity, the target level of 100-fold was still not achieved and, therefore, a focused exploration around the cyclobutylamine **289** was conducted. These minor modifications did not improve selectivity over BD2 but inspiration was taken from the thienopyridone series of BD1 selective compounds from within our laboratories. Imidazoquinolinone-thienopyridone hybrid molecules were designed and synthesised, and resulted in the piperazine **326** which

was the first dimethylisoxazole imidazoquinolinone to exhibit 100-fold BD1 selectivity. X-ray crystallography was again used to rationalise the domain selectivity of two hybrid molecules.

An unfortunate feature of the SAR generated within this research was that BD1 activity decreased when appending selectivity enhancing substituents at the imidazoquinolinone 8-position. To overcome this obstacle, an SAR analysis was conducted on all dimethylisoxazole quinolines to seek out a more active scaffold. As a result of this analysis, chemistry efforts were repositioned from the imidazoquinolinone scaffold onto the more potent imidazolquinoline scaffold. An attempt to enhance the selectivity of a lead imidazolquinoline (compound **330**⁹²) was unsuccessful and highlighted the sensitive nature of SAR with respect to scaffold modifications. Pleasingly, efforts to improve the selectivity of imidazolquinoline **331**¹⁰² were more successful. Appendage of a methylpyrrolidine group onto the 8-position of this molecule resulted in imidazolquinoline **381**, and testing of this compound in the BRD4 mutant FRET assays resulted in BD1 selectivity of 200-fold; the preference for BD1 binding was replicated in the rest of the BET family members. A crystal structure of imidazolquinoline **381** bound to BRD4 BD1 revealed a binding mode similar to other BD1 selective molecules produced throughout this research and corroborated the through-water interaction of the pendant amine to Asp144, and a clash with His437 in BRD4 BD2, as the basis for domain selectivity. Assessment of imidazolquinoline **381** in a panel of bromodomains confirmed the high selectivity for the BET family of BCPs and, specifically, for their first bromodomains at similar levels of selectivity determined in the mutant FRET assays. After establishing suitably high cell permeability in an artificial membrane permeability assay, imidazolquinoline **381** was selected as a probe molecule for assessment in cellular assays alongside a pan-BET inhibitor, and a BD1-biased inhibitor, to evaluate any differences in phenotype. Results from these studies demonstrated that that selective inhibition of BD1 retains the anti-inflammatory and antiproliferative phenotype characteristic of pan-BET inhibition.

These studies provide the first disclosure of the development of a potent BD1 selective inhibitor and demonstrated structure-based design as a successful approach in optimisation of domain selectivity. Although an anti-inflammatory and antiproliferative phenotype was established with imidazolquinoline **381** in this work, the scope of its utility can be significantly expanded by its assessment in other cell systems by the research community. In addition, due to the increasing interest in the research community for the development of inhibitors selective for a subset of bromodomains with the BET family, this work provides a valuable platform for future endeavours in this specific area.

4. Experimental

4.1. General

All reagents and solvents were obtained from commercial suppliers and used without further purification.

Thin layer chromatography was carried out using Polygram[®] silica plates coated with fluorescent indicator UV₂₅₄. This was analysed using a Spectroline[®] ENF-260C/FE lamp.

Flash column chromatography was carried out using an automated Biotage[®] SP4 system with SNAP silica cartridges or an automated Combiflash[®] Companion[®] system with Redisep[®] silica cartridges.

Optical rotations were measured using a Jasco P-1030 polarimeter.

Melting points were measured using a Stuart SMP40 automatic melting point apparatus.

IR spectra were obtained on a Perkin Elmer Spectrum 1 machine.

¹H NMR spectra were recorded on any of the following: Bruker AV-400 spectrometer at 400 MHz, Bruker AV-600 spectrometer at 600 MHz, Bruker DPX-250 spectrometer at 250 MHz, Varian INOVA spectrometer at 300 MHz.

¹³C NMR spectra were recorded on a Bruker AV-400 spectrometer at 100 MHz or a Bruker AV-600 spectrometer at 150 MHz.

¹⁹F NMR spectra were recorded on a Bruker DPX-400 spectrometer at 376 MHz.

Chemical shifts are reported in ppm. Coupling constants are reported in Hz and refer to ³J_{H-H} and, if observed, ⁴J_{H-H} interactions.

Liquid chromatography mass spectra were carried out using any of the three methods below:

Formic A LCMS was performed on a Waters Acquity UPLC instrument equipped with a BEH column (50 mm x 2.1 mm, 1.7 μm packing diameter). Gradient elution was carried out at 40 °C with the mobile phases as (A) water containing 0.1% volume/volume (v/v) formic acid and (B) acetonitrile containing 0.1% (v/v) formic acid. The conditions for the gradient

elution were initially 1% B, increasing linearly to 97% B over 1.5 min, remaining at 97% B for 0.4 min then increasing to 100% B over 0.1 min. The flow rate was 1 mL/min. The UV detection was a summed signal from wavelength of 210 nm to 350 nm. MS analysis was carried out on a Waters micromass ZQ MS using alternate-scan positive and negative electrospray.

Formic B LCMS was performed on an Agilent 1200 Series HPLC instrument equipped with a HALO C18 column (50 mm x 4.6 mm, 2.7 µm packing diameter). Gradient elution was carried out at 40 °C with the mobile phases as (A) water containing 0.1% (v/v) formic acid and (B) acetonitrile containing 0.1% (v/v) formic acid. The conditions for the gradient elution were initially 5% B for 1 min, increasing linearly to 95% B over 1.01 min and remaining at 95% B for 0.49 min. The flow rate was 1.8 mL/min. The UV detection was a summed signal at wavelength of 210 nm and 254 nm. MS analysis was carried out on an Agilent 6110 MS using positive electrospray.

HpH LCMS was performed on a Waters Acquity UPLC instrument equipped with a BEH column (50 mm x 2.1 mm, 1.7 µm packing diameter). Gradient elution was carried out at 40 °C with the mobile phases as (A) 10 mM ammonium bicarbonate in water solution, adjusted to pH 10 with 0.88 ammonia solution and (B) acetonitrile. The conditions for the gradient elution were initially 1% B, increasing linearly to 97% B over 1.5 min, remaining at 97% B for 0.4 min then increasing to 100% B over 0.1 min. The flow rate was 1 mL/min. The UV detection was a summed signal from wavelength of 210 nm to 350 nm. MS analysis was carried out on a Waters micromass ZQ MS using alternate-scan positive and negative electrospray.

Mass-Directed Autopreparative HPLC (MDAP) methodology was carried out using a Waters ZQ MS using alternate-scan positive and negative electrospray using any of the three LC methods below:

Method Formic The LC separation was conducted on either a Sunfire C18 column (100 mm x 19 mm, 5 µm packing diameter) at 20 mL/min flow rate or a Sunfire C18 column (150 mm x 30 mm, 5 µm packing diameter) at 40 mL/min flow rate. Gradient elution was carried out at ambient temperature, with the mobile phases as (A) water containing 0.1% (v/v) formic acid and (B) acetonitrile containing 0.1% (v/v) formic acid. The UV detection was a summed signal from wavelength of 210 nm to 350 nm.

Method HpH The LC separation was conducted on either an Xbridge C18 column (100 mm x 19 mm, 5 µm packing diameter) at 20 mL/min flow rate or an Xbridge C18 column (150 mm x 30 mm, 5 µm packing diameter) at 40 mL/min flow rate. Gradient elution was carried out at ambient temperature, with the mobile phases as (A) 10 mM ammonium bicarbonate in water solution, adjusted to pH 10 with 0.88 ammonia solution and (B) acetonitrile. The UV detection was a summed signal from wavelength of 210 nm to 350 nm.

Method TFA The LC separation was conducted on a Sunfire C18 column (150 mm x 30 mm, 5 µm packing diameter) at 40 mL/min flow rate. Gradient elution was carried out at ambient temperature, with the mobile phases as (A) water containing 0.1% (v/v) TFA and (B) acetonitrile containing 0.1% (v/v) TFA. The UV detection was a summed signal from wavelength of 210 nm to 350 nm. (Only positive electrospray ionisation was used in this method).

Liquid chromatography high resolution mass spectra were recorded on a Micromass Q-ToF Ultima hybrid quadrupole time-of-flight mass spectrometer. An Agilent 1100 Liquid Chromatograph equipped with a Phenomenex Luna C18(2) reversed phase column (100 mm x 2.1 mm, 3 µm packing diameter) was used to achieve separation. Gradient elution was carried out with the mobile phases as (A) water containing 0.1% (v/v) formic acid and (B) acetonitrile containing 0.1% (v/v) formic acid. The conditions for the gradient elution were initially 5% B, increasing linearly to 100% B over 6 min, remaining at 100% B for 2.5 min then decreasing linearly to 5% B over 1 min followed by an equilibration period of 2.5 min prior to the next injection. The flow rate was 0.5 mL/min, temperature controlled at 35 °C with an injection volume of between 2 to 5 µL. All samples were diluted with DMSO (99.9%) prior to analysis.

Hydrophobic frit cartridges by ISOLUTE® contain a frit which is selectively permeable to organic solutions. These are separated from aqueous phase under gravity. Various cartridge sizes were used.

SCX-2 cartridges by ISOLUTE® contain a silica (50 µm) based sorbent with a chemically bonded propylsulfonic acid group. Various cartridge sizes were used for catch and release and scavenging SPE protocols.

Aminopropyl cartridges by ISOLUTE® contain a silica (50 µm) based sorbent with a chemically bonded aminopropyl group. Various cartridge sizes were used for catch and release and scavenging SPE protocols.

4.2. Notes on NMR Spectra

As mentioned in Section 3.1.1, the additional BET activity observed with incorporation of benzylic methyl groups in the imidazoquinolinones (and by extension to the imidazolquinolines) was possibly through the reduction of conformational freedom arising from restricted rotation about the N1-benzylic carbon bond. This was corroborated by NMR analysis of these series of molecules where broad signals were observed when experiments were conducted at room temperature. An example of this is shown in the ¹H NMR spectrum of imidazoquinolinone **237** (Figure 87a).

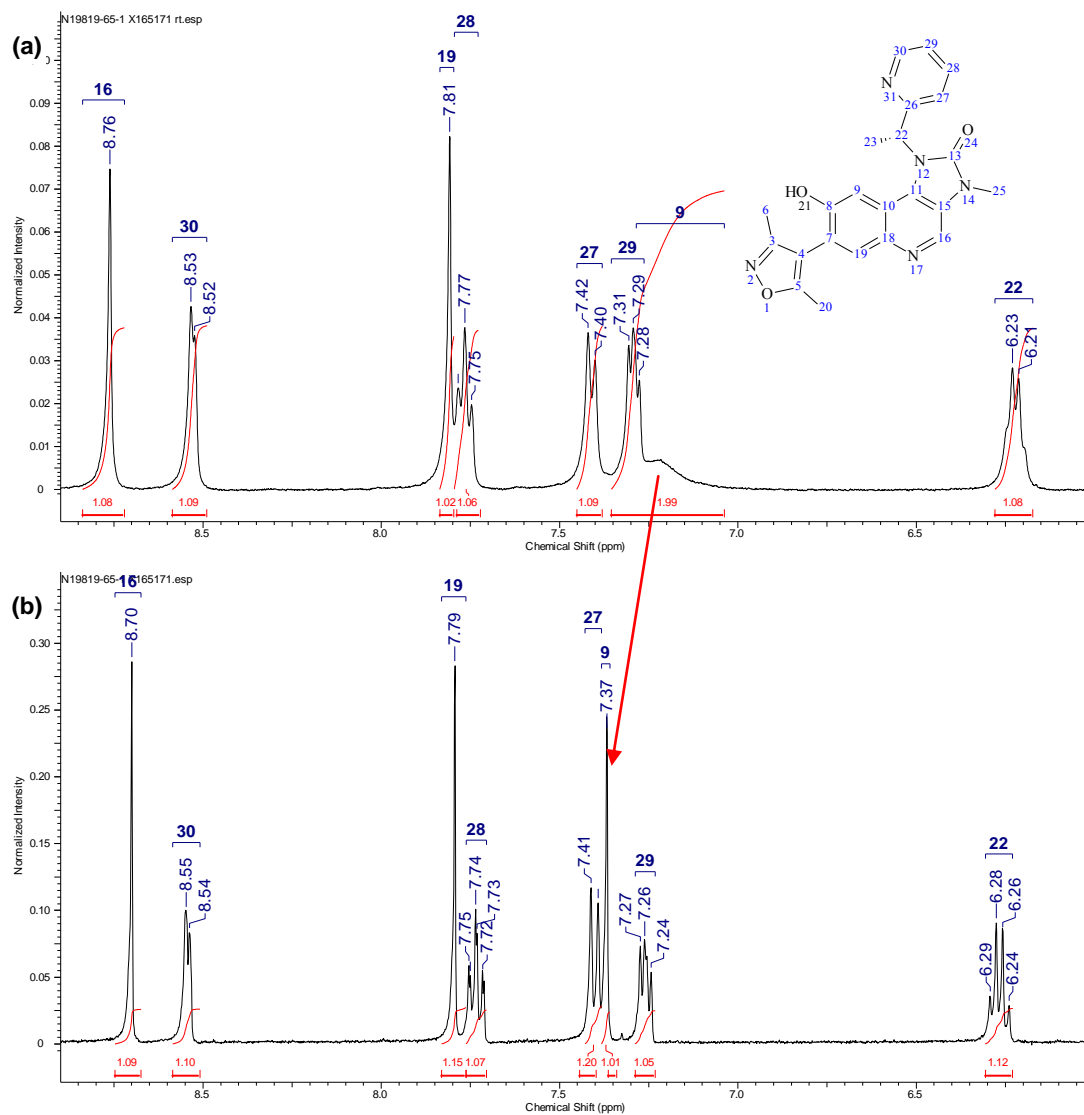


Figure 87. ¹H NMR of imidazoquinolinone **237** at (a) 303 K and (b) 393 K.

Poor signal resolution was observed at 303 K with the benzylic methine (C9) signal particularly affected due to its proximity to the rotationally-restricted bond axis. Increasing the temperature to 393 K using a variable temperature experiment resulted in greater signal resolution (Figure 87b). The majority of imidazoquinolinone and imidazolquinoline ^1H NMR spectra were therefore conducted at this higher temperature.

As ^{13}C NMR spectra were generally carried out at room temperature, broad signals were again observed. Resonance frequencies for both C9 and C22 generally appeared as broad signals and were often barely detectable; an illustrated example is the spectrum for imidazoquinolinone **237** shown in Figure 88.

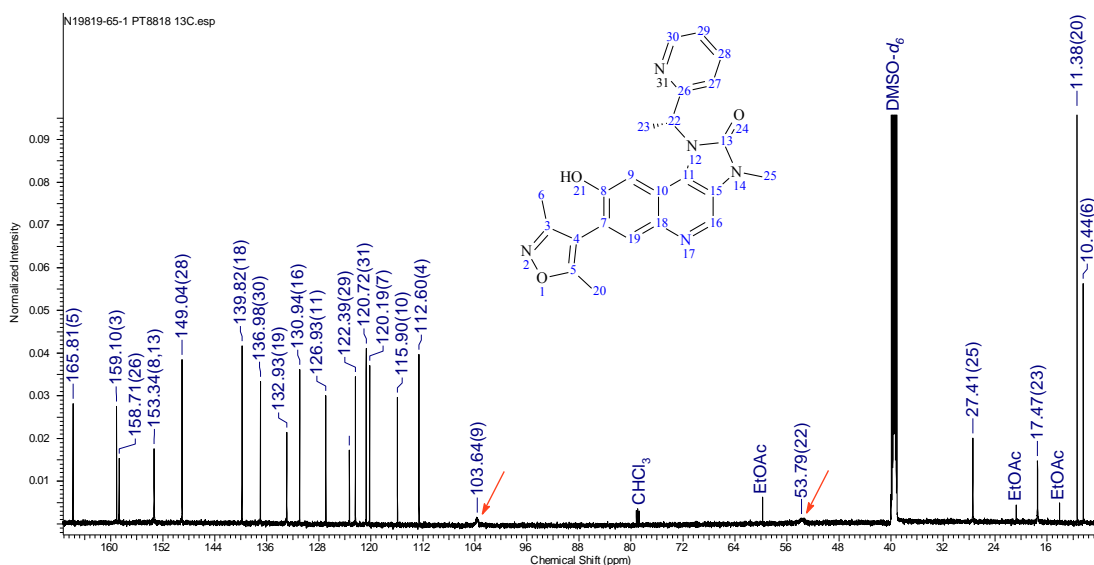
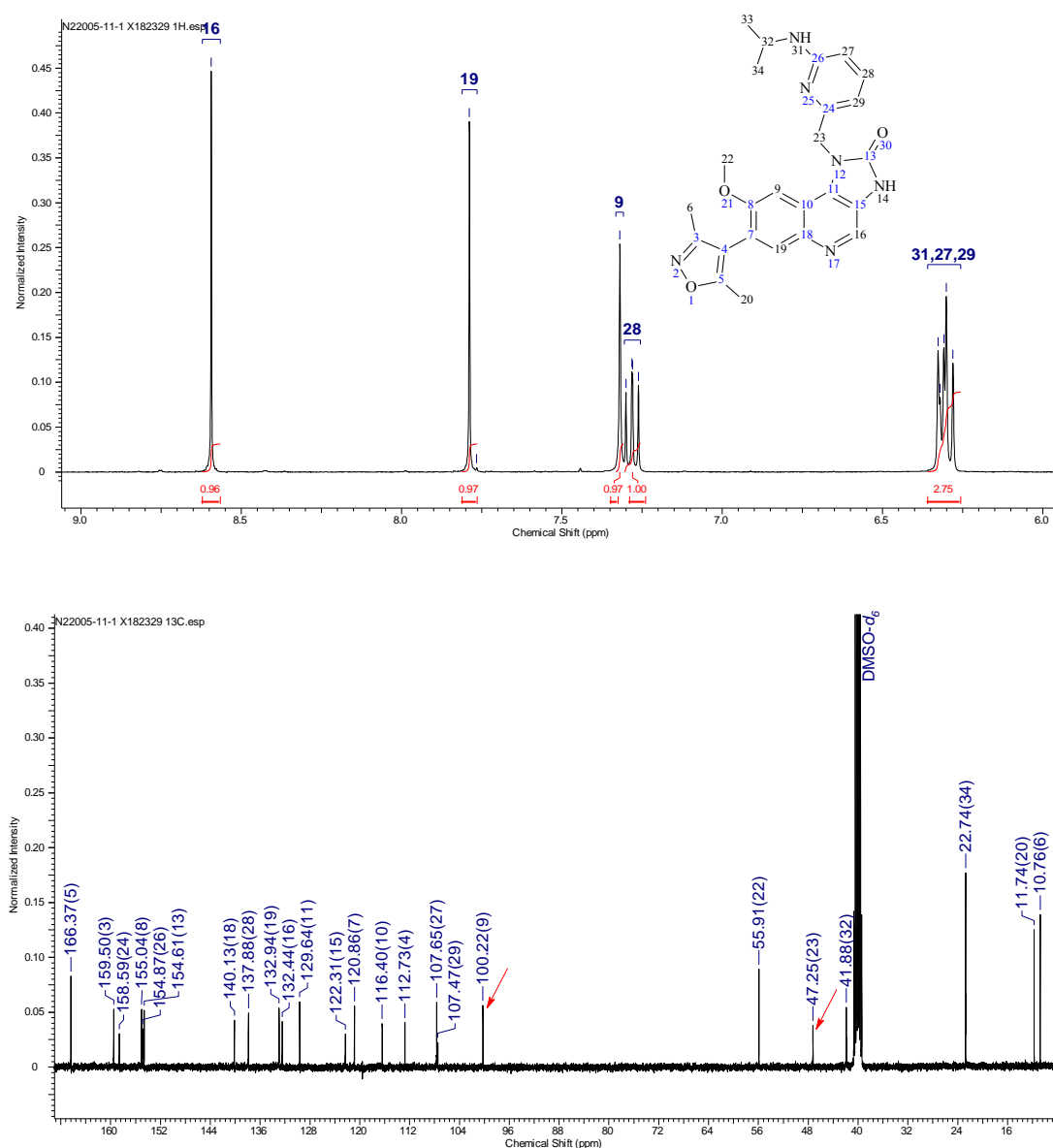


Figure 88. ^{13}C NMR Spectrum for imidazoquinolinone **237**.

The rotationally-restricting nature of the benzylic methyl group was evident when comparing NMR spectra with those of the imidazoquinolinones synthesised in Section 3.3 which lacked the methyl substituent. For example, in the ^1H NMR spectrum of pyridine-2-ylmethyl **280d** (Figure 89a), the H9 signal appeared as a well resolved singlet while in the ^{13}C NMR spectrum (Figure 89b), both the C9 and C23 signals were clearly visible which was in contrast to analogues containing a benzylic methyl substituent.

Figure 89. (a) ^1H NMR and (b) ^{13}C NMR spectra of imidazoquinolinone **280d**.

Another feature of the ^1H NMR spectra were the especially low field chemical shifts of the benzylic methine signals. For example, in the spectra of imidazoquinolinone **237** and imidazolquinoline **333**, H22 resonated at 6.27 ppm and 6.51 ppm, respectively (Figure 90). These signals were significantly downfield of the corresponding signal reported for 1-(1-phenylethyl)-1*H*-imidazole **387** (H6, 5.27 ppm),¹⁴⁴ indicating that the quinoline ring exerted a significant anisotropic deshielding effect.

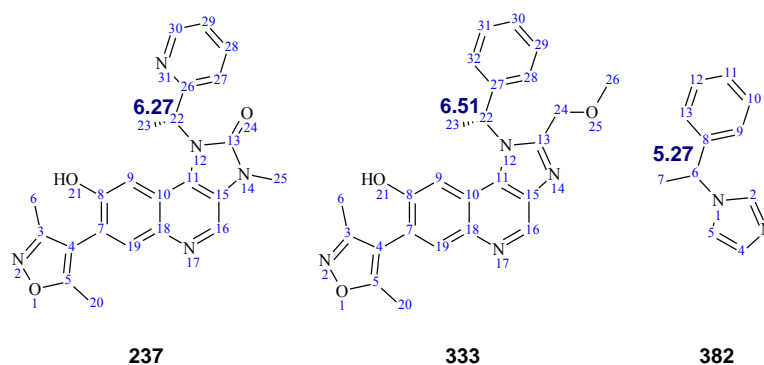
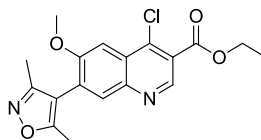


Figure 90. Comparison of chemical shifts of benzylic methine signals.

4.3. Synthetic Procedures and Compound Characterisation

Ethyl 4-chloro-7-(3,5-dimethyl-4-isoxazolyl)-6-(methoxy)-3-quinolinecarboxylate



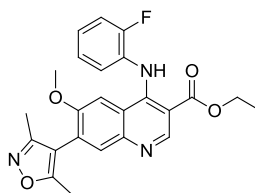
155

A solution of ethyl 7-(3,5-dimethyl-4-isoxazolyl)-6-(methoxy)-4-oxo-1,4-dihydro-3-quinolinecarboxylate **154** (1.91 g, 5.58 mmol) in thionyl chloride (8 mL, 110 mmol) was stirred at 85 °C under nitrogen for 3.5 h. The reaction was allowed to cool to ambient temperature and twice co-evaporated with toluene and DCM under vacuum. The resulting solid was triturated with ether to give the title compound as a brown solid (2.0 g, 5.03 mmol, 90%).

LCMS (formic A): m/z 361, 363 [(M + H)⁺]; Rt: 1.18 min; 72% purity by peak area.

¹H NMR (400 MHz, DMSO-*d*₆): δ 9.05 (s, 1 H), 8.07 (s, 1 H), 7.69 (s, 1 H), 4.43 (q, $J = 7.1$ Hz, 2 H), 4.01 (s, 3 H), 2.35 (s, 3 H), 2.14 (s, 3 H), 1.39 (t, $J = 7.1$ Hz, 3 H).

Ethyl 7-(3,5-dimethylisoxazol-4-yl)-4-[(2-fluorophenyl)amino]-6-methoxyquinoline-3-carboxylate

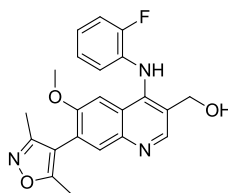
**156**

A mixture of ethyl 4-chloro-7-(3,5-dimethyl-4-isoxazolyl)-6-(methoxy)-3-quinolinecarboxylate **155** (1.98 g, 5.49 mmol) and 2-fluoroaniline (0.636 mL, 6.59 mmol) in anhydrous 1,4-dioxane (40 mL) was stirred at 110 °C under nitrogen for 1 h. The reaction mixture was allowed to cool to r.t. and evaporated *in vacuo*. The residue was loaded in DCM (5 mL) and purified on a 100 g silica cartridge using a gradient of 0–20% MeOH in DCM over 12 column volumes. The appropriate fractions were combined and the solvent removed by rotary evaporation to give the title compound as a light brown solid (1.8 g, 4.13 mmol, 75%).

LCMS (formic A): m/z 436 [(M + H)⁺]; Rt: 0.93 min; 97% purity by peak area.

¹H NMR (400 MHz, DMSO-*d*₆): δ 9.74 (br s, 1 H), 8.85 (s, 1 H), 7.86 (s, 1 H), 7.56 (s, 1 H), 7.40–7.29 (m, 1 H), 7.27–7.14 (m, 3 H), 4.01 (q, $J = 7.1$ Hz, 2 H), 3.67 (s, 3 H), 2.34 (s, 3 H), 2.13 (s, 3 H), 1.20 (t, $J = 7.1$ Hz, 3 H).

{7-(3,5-Dimethylisoxazol-4-yl)-4-[(2-fluorophenyl)amino]-6-methoxyquinolin-3-yl}methanol

**157**

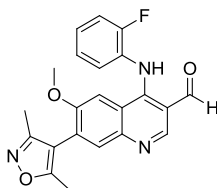
A 3-necked round bottomed flask was dried using a hot air gun and allowed to cool under nitrogen. The flask was charged with ethyl 7-(3,5-dimethyl-4-isoxazolyl)-4-[(2-fluorophenyl)amino]-6-(methoxy)-3-quinolinecarboxylate **156** (1.78 g, 4.09 mmol) followed by anhydrous DCM (50 mL) and the solution evacuated under vacuum and purged with nitrogen three times. The stirred solution was cooled in a dry ice-acetone bath to –72 °C (internal) and DIBAL-H (25 wt.% in toluene, 11.5 mL, 20.24 mmol) added dropwise

maintaining the internal temperature below $-65\text{ }^{\circ}\text{C}$. The reaction was continued to stir in the bath and allowed to warm to r.t. over 2.5 h. The reaction mixture was treated with sat. Rochelle salt (aq) (50 mL) and stirred at r.t. for 1 h. The organic layer was separated and the aqueous phase extracted with DCM (2 x 20 mL). The organics were combined, passed through a hydrophobic frit and the solvent removed under vacuum. The foam was re-evaporated twice with ether then dried under high vacuum (-765 mmHg) to give the crude product. The crude solid was loaded in DCM (5 mL) and purified on a 100 g silica cartridge using a gradient of 0–15% MeOH in DCM over 10 column volumes. The appropriate fractions were combined and the solvent removed by rotary evaporation. The solid was triturated with cyclohexane to give the title compound as a yellow solid (1.39 g, 3.53 mmol, 86%).

LCMS (formic A): m/z 394 $[(M + H)^+]$; Rt: 0.76 min; 100% purity by peak area.

$^1\text{H NMR}$ (400 MHz, CDCl_3): δ 8.47 (s, 1 H), 7.82 (s, 1 H), 7.56 (br s, 1 H), 7.22–7.11 (m, 1 H), 7.04–6.98 (m, 1 H), 6.98–6.86 (m, 2 H), 6.67–6.57 (m, 1 H), 4.85 (s, 2 H), 3.54 (s, 3 H), 3.02 (br s, 1 H), 2.35 (s, 3 H), 2.18 (s, 3 H).

7-(3,5-Dimethylisoxazol-4-yl)-4-[(2-fluorophenyl)amino]-6-methoxyquinoline-3-carbaldehyde



158

A mixture of [7-(3,5-dimethyl-4-isoxazolyl)-4-[(2-fluorophenyl)amino]-6-(methoxy)-3-quinolinyl]methanol **157** (946 mg, 2.405 mmol) and manganese dioxide (4 g, 46.0 mmol) was suspended in anhydrous DCM (5 mL) and stirred at $50\text{ }^{\circ}\text{C}$ for 5 h. The reaction mixture was allowed to cool to r.t. and filtered through Celite[®]. The filtrate was evaporated under vacuum then dissolved in DCM (2 mL) and purified on a 100 g silica cartridge using a gradient of 0–100% EtOAc in DCM over 12 column volumes. The appropriate fractions were combined and the solvent removed by rotary evaporation to give the title compound as a yellow foam (450 mg, 1.15 mmol, 48%).

m.p.: $149\text{ }^{\circ}\text{C}$.

IR (solid) ν (cm^{-1}): 2841, 2754, 1650, 1569, 1504, 1471, 1436, 1221, 774, 727.

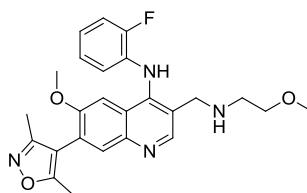
LCMS (formic A): m/z 392 $[(M + H)^+]$; Rt: 0.82 min; 98% purity by peak area.

HRMS (ESI): M + H calcd for C₂₂H₁₉FN₃O₃ 392.1410, found 392.1410.

¹H NMR (400 MHz, CDCl₃): δ 11.19 (br s, 1 H), 10.10 (s, 1 H), 8.77 (s, 1 H), 7.77 (s, 1 H), 7.40–7.19 (m, 4 H), 6.95 (s, 1 H), 3.30 (s, 3 H), 2.34 (s, 3 H), 2.18 (s, 3 H).

¹³C NMR (100 MHz, CDCl₃): δ 193.4, 166.8, 159.5, 157.0 (d, ¹J_{C-F} = 250.1 Hz), 154.2, 153.5, 151.3, 146.0, 132.6, 128.8 (d, ²J_{C-F} = 11.8 Hz), 128.0 (d, ³J_{C-F} = 7.1 Hz), 127.2, 127.1, 124.8 (d, ³J_{C-F} = 3.9 Hz), 118.6, 116.8 (d, ²J_{C-F} = 18.9 Hz), 112.5, 112.2, 104.2, 54.8, 11.9, 10.8.

7-(3,5-Dimethylisoxazol-4-yl)-N-(2-fluorophenyl)-6-methoxy-3-[[2-methoxyethyl]amino]methyl}quinolin-4-amine



159a

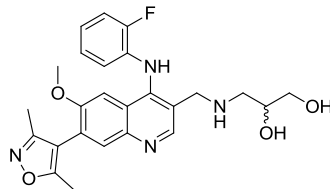
A mixture of 7-(3,5-dimethyl-4-isoxazolyl)-4-[(2-fluorophenyl)amino]-6-(methoxy)-3-quinolinecarbaldehyde **158** (37 mg, 0.095 mmol) and 2-methoxyethylamine (0.012 mL, 0.142 mmol) in DCM (2 mL) in a stoppered flask was stirred at r.t. for 5 min. Sodium triacetoxyborohydride (30 mg, 0.142 mmol) was added and the mixture stirred for 1 h. The reaction mixture was treated with sodium borohydride (5 mg, 0.132 mmol) and left to stir for 1 h. The reaction mixture was treated with sodium borohydride (15 mg, 0.396 mmol) and left to stir for 2 h. The reaction mixture was quenched by the addition of 0.5 M HCl (aq) and the mixture stirred for 5 min. The organic layer was separated, passed through a hydrophobic frit and evaporated under a stream of nitrogen. The residue was dissolved in MeOH (0.5 mL) and applied to a MeOH preconditioned 1 g SCX-2 cartridge. The cartridge was washed with MeOH (5 mL) then with 2 M ammonia in MeOH solution (5 mL). The basic wash was evaporated under a stream of nitrogen to give a yellow gum which was then purified by MDAP using Method Formic. The appropriate fractions were combined and the solvent removed by rotary evaporation. The resulting solid was dissolved in DCM (0.5 mL) and applied to a MeOH preconditioned 0.5 g aminopropyl cartridge. The cartridge was washed with MeOH (5 mL) and the solvent evaporated under a stream of nitrogen to give the title compound as a yellow gum (20 mg, 0.044 mmol, 47%).

LCMS (formic A): *m/z* 451 [(M + H)⁺]; Rt: 0.65 min; 85% purity by peak area.

¹H NMR (400 MHz, CDCl₃): δ 9.38 (s, 1 H), 8.57 (s, 1 H), 7.82 (s, 1 H), 7.15 (ddd, *J* = 11.2, 8.0, 1.5 Hz, 1 H), 7.00 (s, 1 H), 6.97–6.91 (m, 1 H), 6.90–6.83 (m, 1 H), 6.68–6.59 (m, 1 H),

4.04 (d, $J = 5.6$ Hz, 2 H), 3.57 (t, $J = 5.0$ Hz, 2 H), 3.54 (s, 3 H), 3.38 (s, 3 H), 2.89–2.82 (m, 2 H), 2.37 (s, 3 H), 2.21 (s, 3 H), 1.93 (tt, $J = 6.3, 6.3$ Hz, 1 H).

(±)-3-[[7-(3,5-Dimethylisoxazol-4-yl)-4-[(2-fluorophenyl)amino]-6-methoxyquinolin-3-yl]methyl]amino}propane-1,2-diol



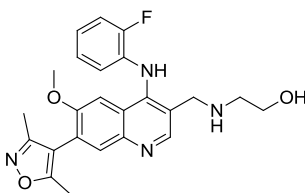
159b

To 7-(3,5-dimethyl-4-isoxazolyl)-4-[(2-fluorophenyl)amino]-6-(methoxy)-3-quinolinecarbaldehyde **158** (45 mg, 0.115 mmol) in anhydrous DCM (1 mL) was added (±)-2,2-dimethyl-1,3-dioxolane-4-methanamine (23 μ L, 0.161 mmol). The mixture was stirred at r.t. under nitrogen for 30 min then sodium triacetoxyborohydride (97 mg, 0.458 mmol) was added. After stirring for 16 h, the reaction mixture was treated with sat. NaHCO₃ (aq) (1 mL) and stirred for 1 h. The organic layer was separated and passed through a hydrophobic frit and the solvent removed under a nitrogen stream. The residue was dissolved in THF (0.75 mL) and treated with 2 M HCl (aq) (0.75 mL) and the mixture stirred at r.t. for 16 h in a stoppered vessel. The reaction mixture was basified to pH 14 with 2 M NaOH (aq) and extracted with EtOAc (2 x 2 mL). The organics were combined, passed through a hydrophobic frit and the solvent removed under a stream of nitrogen. The residue was purified by MDAP using Method HpH. The appropriate fractions were combined and the solvent evaporated under a stream of nitrogen. The gum was dissolved in 1,4-dioxane (0.5 mL) and the solvent removed upon freeze drying. The impure material was purified by MDAP using Method HpH. The appropriate fractions were combined and the solvent removed upon freeze drying to give the title compound white solid (8 mg, 0.017 mmol, 13%).

LCMS (formic A): m/z 467 [(M + H)⁺]; Rt: 0.60 min; 92% purity by peak area.

¹H NMR (400 MHz, CDCl₃): δ 8.58 (s, 1 H), 7.83 (s, 1 H), 7.16 (dd, $J = 10.7, 8.7$ Hz, 1 H), 7.00 (s, 1 H), 6.98–6.92 (m, 1 H), 6.92–6.84 (m, 1 H), 6.62 (t, $J = 7.8$ Hz, 1 H), 4.05 (s, 2 H), 3.97–3.89 (m, 1 H), 3.81–3.72 (m, 1 H), 3.69–3.61 (m, 1 H), 3.55 (s, 3 H), 2.87–2.74 (m, 2 H), 2.37 (s, 3 H), 2.21 (s, 3 H). 2 x NH and 2 x OH signals not resolved.

2-[[7-(3,5-Dimethylisoxazol-4-yl)-4-[(2-fluorophenyl)amino]-6-methoxyquinolin-3-yl]methyl]amino}ethanol



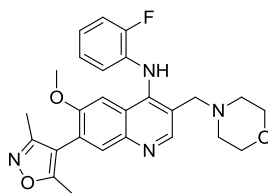
159c

To 7-(3,5-dimethyl-4-isoxazolyl)-4-[(2-fluorophenyl)amino]-6-(methoxy)-3-quinolinecarbaldehyde **158** (45 mg, 0.115 mmol) in anhydrous DCM (1 mL) was added ethanolamine (10 μ L, 0.161 mmol). The mixture was stirred at r.t. under nitrogen for 30 min then sodium triacetoxyborohydride (97 mg, 0.458 mmol) was added. After stirring for 16 h, the reaction mixture was treated with sat. NaHCO₃ (aq) (1 mL) and stirred for 1 h. The organic layer was separated and passed through a hydrophobic frit and the solvent removed under a nitrogen stream. The residue was purified by MDAP using Method Formic. The appropriate fractions were combined and the solvent evaporated under a stream of nitrogen. The gum was dissolved in MeOH (0.5 mL) and applied to a MeOH preconditioned 0.5 g aminopropyl cartridge. The cartridge was washed with MeOH (4 mL) and the solvent evaporated under a stream of nitrogen. The gum was dissolved in 1,4-dioxane (0.5 mL) and the solvent removed upon freeze drying. The impure material was further purified by MDAP using Method HpH. The appropriate fraction was freeze dried to give the title compound as a white solid (6 mg, 0.013 mmol, 10%).

LCMS (formic A): m/z 437 [(M + H)⁺]; Rt: 0.57 min; 100% purity by peak area.

¹H NMR (400 MHz, CDCl₃): δ 9.19 (s, 1 H), 8.58 (s, 1 H), 7.83 (s, 1 H), 7.21–7.11 (m, 1 H), 7.00 (s, 1 H), 6.98–6.91 (m, 1 H), 6.91–6.83 (m, 1 H), 6.67–6.57 (m, 1 H), 4.07 (s, 2 H), 3.81 (t, J = 5.0 Hz, 2 H), 3.55 (s, 3 H), 2.88 (t, J = 5.1 Hz, 2 H), 2.37 (s, 3 H), 2.21 (s, 3 H). *NH* and *OH* signals not resolved.

7-(3,5-Dimethylisoxazol-4-yl)-N-(2-fluorophenyl)-6-methoxy-3-(morpholinomethyl)quinolin-4-amine



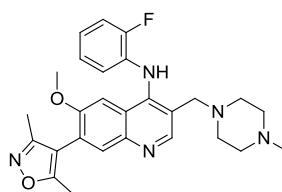
159d

A mixture of 7-(3,5-dimethyl-4-isoxazolyl)-4-[(2-fluorophenyl)amino]-6-(methoxy)-3-quinolinecarbaldehyde **158** (75 mg, 0.192 mmol) and morpholine (0.025 mL, 0.287 mmol) in anhydrous DCM (1 mL) was stirred in a stoppered vessel at r.t. for 0.5 h. Sodium triacetoxyborohydride (162 mg, 0.766 mmol) was added and the reaction mixture allowed to stir for 17 h. The reaction mixture was washed with 0.5 M HCl (aq) (1 mL), the organic layer separated and passed through a hydrophobic frit. The solvent was removed under a stream of nitrogen and the residue purified by MDAP using Method HpH. The appropriate fractions were combined and the solvent evaporated *in vacuo*. The gum was dissolved in 1,4-dioxane and the solvent removed upon freeze drying. The solid was dried in a vacuum pistol to give the title compound as a yellow powder (66 mg, 0.14 mmol, 75%).

LCMS (formic A): m/z 463 $[(M + H)^+]$; Rt: 0.84 min; 98% purity.

^1H NMR (400 MHz, CDCl_3): δ 9.37 (br s, 1 H), 8.53 (s, 1 H), 7.84 (s, 1 H), 7.23–7.12 (m, 1 H), 7.02 (s, 1 H), 7.00–6.93 (m, 1 H), 6.93–6.85 (m, 1 H), 6.70–6.63 (m, 1 H), 3.79 (t, $J = 4.3$ Hz, 4 H), 3.76 (s, 2 H), 3.56 (s, 3 H), 2.56 (br s, 4 H), 2.37 (s, 3 H), 2.22 (s, 3 H).

7-(3,5-Dimethylisoxazol-4-yl)-N-(2-fluorophenyl)-6-methoxy-3-[(4-methylpiperazin-1-yl)methyl]quinolin-4-amine



159e

To 7-(3,5-dimethyl-4-isoxazolyl)-4-[(2-fluorophenyl)amino]-6-(methoxy)-3-quinolinecarbaldehyde **158** (45 mg, 0.115 mmol) in anhydrous DCM (1 mL) was added *N*-methylpiperazine (19 μL , 0.161 mmol). The mixture was stirred at r.t. under nitrogen for 30 min then sodium triacetoxyborohydride (97 mg, 0.458 mmol) was added. After stirring for 16 h, the reaction mixture was treated with sat. NaHCO_3 (aq) (1 mL) and stirred for 1 h. The

organic layer was separated and passed through a hydrophobic frit and the solvent removed under a nitrogen stream. The residue was purified by MDAP using Method HpH. The appropriate fractions were combined and the solvent evaporated under a stream of nitrogen. The gum was dissolved in 1,4-dioxane (0.5 mL) and the solvent removed upon freeze drying to give the title compound as a white solid (33 mg, 0.069 mmol, 56%).

m.p.: 165 °C.

IR (solid) ν (cm⁻¹): 2935, 2795, 1617, 1562, 1508, 1453, 1420, 1219, 755

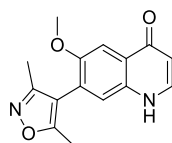
LCMS (formic A): m/z 476 [(M + H)⁺]; Rt: 0.61 min; 99% purity by peak area.

HRMS (ESI): M + H calcd for C₂₇H₃₁FN₅O₂ 476.2462, found 476.2457.

¹H NMR (400 MHz, CDCl₃): δ 9.36 (br s, 1 H), 8.53 (s, 1 H), 7.84 (s, 1 H), 7.20–7.12 (m, 1 H), 7.02 (s, 1 H), 6.99–6.92 (m, 1 H), 6.92–6.84 (m, 1 H), 6.69–6.62 (m, 1 H), 3.76 (s, 2 H), 3.56 (s, 3 H), 2.81–2.42 (m, 8 H), 2.37 (s, 3 H), 2.37 (s, 3 H), 2.21 (s, 3 H).

¹³C NMR (100 MHz, CDCl₃): δ 166.5, 159.7, 154.5, 153.1 (d, ¹J_{C-F} = 243.0 Hz), 149.8, 145.3, 145.1, 132.7, 131.9 (d, ²J_{C-F} = 11.0 Hz), 124.5, 123.8 (2 C), 122.6, 120.9 (2 C), 120.3, 118.0, 115.5 (d, ²J_{C-F} = 18.0 Hz), 112.6, 102.9, 59.0, 55.3, 55.1, 52.4, 45.8, 11.8, 10.8.

7-(3,5-Dimethylisoxazol-4-yl)-6-methoxyquinolin-4(1H)-one



170

To stirring diphenylether (50 mL, 315 mmol) at 260 °C (internal) was added 7-(3,5-dimethylisoxazol-4-yl)-6-methoxy-4-oxo-1,4-dihydroquinoline-3-carboxylic acid **169** (7.0 g, 22.27 mmol) portion-wise and the mixture left to stir for 30 min. The reaction mixture was allowed to cool to r.t. and diluted with ether. The mixture was filtered and the solid washed with ether then dried in a vacuum oven. The solid was suspended in MeOH and filtered. The filtrate was preadsorbed onto Florisil and purified on a 100 g silica cartridge using a gradient of 0–15% MeOH in DCM over 10 column volumes. The appropriate fractions were combined and the solvent removed by rotary evaporation to give batch 1 of the title compound as a pale yellow solid (979 mg, 3.62 mmol, 16%).

LCMS (formic A): m/z 271 [(M + H)⁺]; Rt: 0.64 min; 100% purity by peak area.

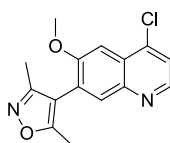
¹H NMR (400 MHz, DMSO-*d*₆): δ 11.75 (br s, 1 H), 7.90 (d, J = 7.3 Hz, 1 H), 7.62 (s, 1 H), 7.43 (s, 1 H), 6.04 (d, J = 7.3 Hz, 1 H), 3.86 (s, 3 H), 2.32 (s, 3 H), 2.12 (s, 3 H).

The ethereal filtrate was evaporated under vacuum and the mixture diluted with cyclohexane. A brown sticky tar formed on the inside of the vessel and the liquid was decanted. The tar was dissolved in DCM (10 mL) and applied to 2 x 100 g silica cartridges and purified using a gradient of 0–15% MeOH in DCM over 14 column volumes. The appropriate fractions were combined and the solvent removed by rotary evaporation to give batch 2 of the title compound as a light brown solid (2.5 g, 9.25 mmol, 42%).

LCMS (formic A): m/z 271 [(M + H)⁺]; Rt: 0.62 min; 95% purity by peak area.

¹H NMR (400 MHz, DMSO-*d*₆): δ 7.90 (d, J = 7.3 Hz, 1 H), 7.62 (s, 1 H), 7.43 (s, 1 H), 6.04 (d, J = 7.3 Hz, 1 H), 3.86 (s, 3 H), 2.31 (s, 3 H), 2.11 (s, 3 H). NH signal not resolved.

4-(4-Chloro-6-methoxyquinolin-7-yl)-3,5-dimethylisoxazole



171

To a round bottomed flask charged with 7-(3,5-dimethyl-4-isoxazolyl)-6-(methoxy)-4-quinolinol **170** (3.1 g, 11.47 mmol) was added phosphorus oxychloride (25 mL, 268 mmol) and the mixture stirred under nitrogen at 105 °C for 1 h. The reaction mixture was allowed to cool to ambient temperature, evaporated under vacuum and the gum azeotropeed twice with toluene (20 mL). The gum was dissolved in DCM (30 mL) and washed with 1 M NaOH (aq) (3 x 30 mL). The organic layer was passed through a hydrophobic frit and the solvent removed under vacuum to give the title compound as a dark green solid (3.15 g, 10.91 mmol, 95%).

m.p.: 161 °C.

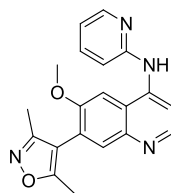
IR (solid) ν (cm⁻¹): 1618, 1579, 1550, 1484, 1416, 1225, 743.

LCMS (formic A): m/z 289, 291 [(M + H)⁺]; Rt: 1.05 min; 94% purity by peak area.

HRMS (ESI): M + H calcd for C₁₅H₁₄ClN₂O₂ 289.0744, found 289.0751.

¹H NMR (400 MHz, CDCl₃): δ 8.68 (d, J = 4.6 Hz, 1 H), 7.90 (s, 1 H), 7.54 (s, 1 H), 7.51 (d, J = 4.6 Hz, 1 H), 4.00 (s, 3 H), 2.37 (s, 3 H), 2.22 (s, 3 H).

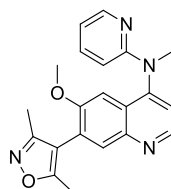
¹³C NMR (100 MHz, CDCl₃): δ 166.6, 159.6, 156.7, 147.9, 144.7, 140.8, 132.7, 127.4, 125.8, 121.7, 112.3, 101.8, 55.9, 11.7, 10.8.

7-(3,5-Dimethylisoxazol-4-yl)-6-methoxy-N-(pyridin-2-yl)quinolin-4-amine**172**

A 0.5–2.0 mL microwave vessel was charged with a magnetic stirrer bar, tris(dibenzylideneacetone)dipalladium(0) (10 mg, 10.92 μ mol), sodium *tert*-butoxide (20 mg, 0.208 mmol), 2-dicyclohexylphosphino-2'-(*N,N*-dimethylamino)biphenyl (8 mg, 0.020 mmol), 2-aminopyridine (20 mg, 0.213 mmol), 4-chloro-7-(3,5-dimethyl-4-isoxazolyl)-6-(methoxy)quinoline **171** (40 mg, 0.139 mmol) and anhydrous 1,4-dioxane (1.5 mL). The vessel was sealed and the mixture heated at 140 °C for 20 min in a Biotage I60 microwave (Fixed hold time [FHT]: on, absorbance: normal, cooling: off). The reaction mixture was evaporated *in vacuo* and the residue partitioned between EtOAc (3 mL) and water (3 mL). The organic layer was separated and the aqueous layer extracted with EtOAc (2 x 3 mL). The organic extracts were combined, passed through a hydrophobic frit and the solvent removed under vacuum. The residue was purified by MDAP using Method HpH. The appropriate fractions were combined and the solvent removed by rotary evaporation. The gum was solidified upon addition of ether and scratching with a spatula. The solvent was removed under a stream of nitrogen and the solid dried in a vacuum oven to give the title compound as a white solid (30 mg, 0.087 mmol, 63%).

LCMS (formic A): m/z 347 [(M + H)⁺]; Rt: 0.67 min; 100% purity by peak area.

¹H NMR (400 MHz, CDCl₃): δ 8.67 (d, J = 5.2 Hz, 1 H), 8.38 (dd, J = 4.9, 1.0 Hz, 1 H), 7.87 (s, 1 H), 7.73–7.67 (m, 1 H), 7.64 (d, J = 5.2 Hz, 1 H), 7.26 (s, 1 H), 7.24 (d, J = 8.3 Hz, 1 H), 7.19 (s, 1 H), 7.02–6.94 (m, 1 H), 3.94 (s, 3 H), 2.37 (s, 3 H), 2.22 (s, 3 H).

7-(3,5-Dimethylisoxazol-4-yl)-6-methoxy-N-methyl-N-(pyridin-2-yl)quinolin-4-amine**173**

A 0.5–2.0 mL microwave vessel was charged with a magnetic stirrer bar, tris(dibenzylideneacetone)dipalladium(0) (17 mg, 0.019 mmol), sodium *tert*-butoxide (37

mg, 0.385 mmol), 2-dicyclohexylphosphino-2'-(*N,N*-dimethylamino)biphenyl (15 mg, 0.038 mmol), *N*-methyl-2-pyridinamine (0.040 mL, 0.390 mmol), 4-chloro-7-(3,5-dimethyl-4-isoxazolyl)-6-(methoxy)quinoline **171** (75 mg, 0.260 mmol) and 1,4-dioxane (0.75 mL). The vessel was sealed and the mixture heated at 125 °C for 15 min in a Biotage I60 microwave (FHT: on, absorbance: normal, cooling: off). To the reaction mixture was added water (3 mL) and the mixture extracted with EtOAc (2 x 3 mL). The organic extracts were combined and passed through a hydrophobic frit. The solvent was evaporated under vacuum and the residue purified by MDAP using Method HpH. The appropriate fractions were combined and the solvent removed by rotary evaporation to give the title compound as a light brown foam (16 mg, 0.044 mmol, 17%).

m.p.: 130 °C.

IR (solid) ν (cm⁻¹): 1558, 1582, 1486, 1414, 1220, 774.

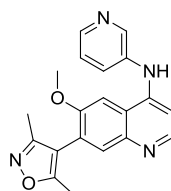
LCMS (formic A): m/z 361 [(M + H)⁺]; Rt: 0.67 min; 99% purity by peak area.

HRMS (ESI): M + H calcd for C₂₁H₂₁N₄O₂ 361.1659, found 361.1660.

¹H NMR (400 MHz, CDCl₃): δ 8.84 (d, J = 4.6 Hz, 1 H), 8.34–8.29 (m, 1 H), 7.93 (s, 1 H), 7.38 (ddd, J = 8.7, 7.0, 1.7 Hz, 1 H), 7.33 (d, J = 4.6 Hz, 1 H), 7.07 (s, 1 H), 6.74 (ddd, J = 7.0, 5.0, 0.8 Hz, 1 H), 6.34 (d, J = 8.7 Hz, 1 H), 3.72 (s, 3 H), 3.62 (s, 3 H), 2.37 (s, 3 H), 2.22 (s, 3 H).

¹³C NMR (100 MHz, CDCl₃): δ 166.5, 159.6, 158.5, 156.0, 150.7, 149.2, 148.1, 145.7, 137.1, 132.8, 126.6, 125.2, 119.0, 114.6, 112.5, 110.1, 101.3, 55.6, 38.7, 11.7, 10.8.

7-(3,5-Dimethylisoxazol-4-yl)-6-methoxy-*N*-(pyridin-3-yl)quinolin-4-amine



174

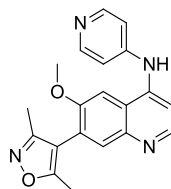
A 0.5–2.0 mL microwave vessel was charged with a magnetic stirrer bar, tris(dibenzylideneacetone)dipalladium(0) (9 mg, 9.83 μ mol), sodium *tert*-butoxide (28 mg, 0.291 mmol), 2-dicyclohexylphosphino-2'-(*N,N*-dimethylamino)biphenyl (11 mg, 0.028 mmol), 3-aminopyridine (22 mg, 0.234 mmol), 4-chloro-7-(3,5-dimethyl-4-isoxazolyl)-6-(methoxy)quinoline **171** (55 mg, 0.190 mmol) and anhydrous 1,4-dioxane (2 mL). The vessel was sealed and the mixture heated at 125 °C for 15 min in a Biotage I60 microwave (FHT: on, absorbance: normal, cooling: off). The reaction mixture was evaporated *in vacuo* and the residue partitioned between EtOAc (3 mL) and water (3 mL). The organic layer was

separated and the aqueous extracted with EtOAc (2 x 3 mL). The organic extracts were combined, passed through a hydrophobic frit and the solvent removed under vacuum. The residue was purified by MDAP using Method HpH. The appropriate fractions were combined and the solvent removed by rotary evaporation. The gum was solidified upon addition of ether and scratching with a spatula. The solvent was removed under a stream of nitrogen and the solid dried in a vacuum oven to give the title compound as a white solid (38 mg, 0.11 mmol, 58%).

LCMS (formic A): m/z 347 [(M + H)⁺]; Rt: 0.58 min; 100% purity by peak area.

¹H NMR (400 MHz, CDCl₃): δ 8.61 (d, J = 2.5 Hz, 1 H), 8.51 (d, J = 5.3 Hz, 1 H), 8.42 (dd, J = 4.8, 1.0 Hz, 1 H), 7.84 (s, 1 H), 7.70 (ddd, J = 8.2, 2.5, 1.0 Hz, 1 H), 7.48 (s, 1 H), 7.35 (dd, J = 8.2, 4.8 Hz, 1 H), 7.00 (d, J = 5.3 Hz, 1 H), 3.86 (s, 3 H), 2.31 (s, 3 H), 2.16 (s, 3 H). NH signal not resolved.

7-(3,5-Dimethylisoxazol-4-yl)-6-methoxy-N-(pyridin-4-yl)quinolin-4-amine



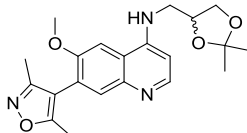
175

A 0.5–2.0 mL microwave vessel was charged with a magnetic stirrer bar, tris(dibenzylideneacetone)dipalladium(0) (8 mg, 8.74 μ mol), sodium *tert*-butoxide (25 mg, 0.260 mmol), 2-dicyclohexylphosphino-2'-(*N,N*-dimethylamino)biphenyl (10 mg, 0.025 mmol), 4-aminopyridine (20 mg, 0.213 mmol), 4-chloro-7-(3,5-dimethyl-4-isoxazolyl)-6-(methoxy)quinoline **171** (50 mg, 0.173 mmol) and anhydrous 1,4-dioxane (1.5 mL). The vessel was sealed and the mixture heated at 125 °C for 15 min in a Biotage I60 microwave (FHT: on, absorbance: normal, cooling: off). The reaction mixture was evaporated *in vacuo* and the residue partitioned between EtOAc (3 mL) and water (3 mL). The organic layer was separated and the aqueous extracted with EtOAc (2 x 3 mL). The organic extracts were combined, passed through a hydrophobic frit and the solvent removed under vacuum. The residue was purified by MDAP using Method HpH. The appropriate fractions were combined and the solvent removed by rotary evaporation. The gum was solidified upon addition of ether and scratching with a spatula. The solvent was removed under a stream of nitrogen and the solid dried in a vacuum oven to give the title compound as a white solid (39 mg, 0.113 mmol, 65%).

LCMS (formic A): m/z 347 $[(M + H)^+]$; Rt: 0.47 min; 100% purity by peak area.

$^1\text{H NMR}$ (400 MHz, CDCl_3): δ 8.70 (d, $J = 5.1$ Hz, 1 H), 8.48 (d, $J = 6.3$ Hz, 2 H), 7.89 (s, 1 H), 7.39 (d, $J = 5.1$ Hz, 1 H), 7.24 (s, 1 H), 7.08 (d, $J = 6.3$ Hz, 2 H), 6.85 (s, 1 H), 3.89 (s, 3 H), 2.36 (s, 3 H), 2.21 (s, 3 H).

(±)-*N*-[(2,2-Dimethyl-1,3-dioxolan-4-yl)methyl]-7-(3,5-dimethylisoxazol-4-yl)-6-methoxyquinolin-4-amine

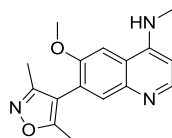


193

A 2.0–5.0 mL microwave vessel was charged with a magnetic stirrer bar, 4-chloro-7-(3,5-dimethyl-4-isoxazolyl)-6-(methoxy)quinoline **171** (500 mg, 1.732 mmol), tris(dibenzylideneacetone)dipalladium(0) (79 mg, 0.087 mmol), sodium *tert*-butoxide (250 mg, 2.60 mmol), 2-dicyclohexylphosphino-2'-(*N,N*-dimethylamino)biphenyl (102 mg, 0.260 mmol), anhydrous 1,4-dioxane (4.5 mL) and (±)-2,2-dimethyl-1,3-dioxolane-4-methanamine (0.269 mL, 2.078 mmol). The vessel was sealed and the mixture heated at 125 °C for 19 min in a Biotage I60 microwave (FHT: off, absorbance: normal, cooling: off). Further sodium *tert*-butoxide (250 mg, 2.60 mmol) was added to the reaction mixture and the mixture heated at 125 °C for 15 min in a Biotage I60 microwave (FHT: off, absorbance: normal, cooling: off). The reaction mixture was diluted with water (10 mL) and the mixture extracted with EtOAc (2 x 10 mL). The organic extracts were combined, passed through a hydrophobic frit and the solvent evaporated *in vacuo*. The residue was loaded in DCM (4 mL) and purified on a 100 g silica cartridge using a gradient of 0–15% MeOH in DCM over 10 column volumes. The appropriate fractions were combined and the solvent removed by rotary evaporation. The gum was re-evaporated from ether to give the title compound as a dark brown foam (235 mg, 0.613 mmol, 35%).

LCMS (formic A): m/z 384 $[(M + H)^+]$; Rt: 0.70 min; 94% purity by peak area.

$^1\text{H NMR}$ (400 MHz, CDCl_3): δ 8.48 (d, $J = 5.4$ Hz, 1 H), 7.84–7.77 (m, 1 H), 7.15 (s, 1 H), 6.49 (d, $J = 5.4$ Hz, 1 H), 5.62 (br s, 1 H), 4.63–4.54 (m, 1 H), 4.21 (dd, $J = 8.5, 6.4$ Hz, 1 H), 3.98–3.90 (m, 4 H), 3.63–3.54 (m, 1 H), 3.51–3.38 (m, 1 H), 2.35 (s, 3 H), 2.20 (s, 3 H), 1.55 (s, 3 H), 1.43 (s, 3 H).

7-(3,5-Dimethylisoxazol-4-yl)-6-methoxy-N-methylquinolin-4-amine**197**

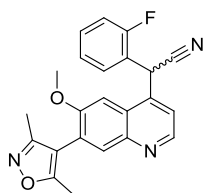
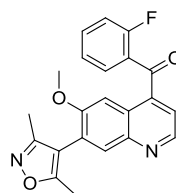
A 2.0–5.0 mL microwave vessel was charged with 4-chloro-7-(3,5-dimethyl-4-isoxazolyl)-6-(methoxy)quinoline **171** (400 mg, 1.385 mmol), a magnetic stirrer bar, sodium *tert*-butoxide (266 mg, 2.77 mmol), 2-dicyclohexylphosphino-2'-(*N,N*-dimethylamino)biphenyl (82 mg, 0.208 mmol), tris(dibenzylideneacetone)dipalladium(0) (63.4 mg, 0.069 mmol) and methylamine (2 M solution in THF, 5 mL, 10.00 mmol). The vessel was sealed and heated in a Biotage I60 microwave at 125 °C for 20 min (FHT: on, cooling: off, absorbance: normal). The reaction mixture was diluted with EtOAc (10 mL) and washed with brine (2 x 10 mL). The organic layer was passed through a hydrophobic frit and the solvent evaporated under vacuum. The residue was loaded in DCM (5 mL) and purified on a 100 g silica cartridge using a gradient of 0–15% MeOH (containing 20% 2 M ammonia in MeOH solution) in DCM over 10 column volumes. The appropriate fractions were combined and the solvent evaporated *in vacuo* to give the title compound as a light brown solid (226 mg, 0.80 mmol, 58%).

LCMS (formic A): m/z 284 [(M + H)⁺]; Rt: 0.59 min; 96% purity by peak area.

¹H NMR (400 MHz, CDCl₃): δ 8.50 (d, J = 5.3 Hz, 1 H), 7.78 (s, 1 H), 7.11 (s, 1 H), 6.47 (d, J = 5.5 Hz, 1 H), 5.38 (br s, 1 H), 3.91 (s, 3 H), 3.10 (d, J = 5.0 Hz, 3 H), 2.34 (s, 3 H), 2.19 (s, 3 H).

(±)-2-[7-(3,5-Dimethylisoxazol-4-yl)-6-methoxyquinolin-4-yl]-2-(2-fluorophenyl)acetonitrile and

[7-(3,5-dimethylisoxazol-4-yl)-6-methoxyquinolin-4-yl](2-fluorophenyl)methanone

**204****205**

A 0.5–2.0 mL microwave vessel was charged with a magnetic stirrer bar, tetrakis(triphenylphosphine)palladium(0) (80 mg, 0.069 mmol), potassium *tert*-butoxide (200 mg, 1.782 mmol), 4-chloro-7-(3,5-dimethyl-4-isoxazolyl)-6-(methoxy)quinoline **171**

(100 mg, 0.346 mmol), anhydrous DME (0.5 mL) and *o*-fluorophenylacetonitrile (80 μ L, 0.627 mmol). The mixture was heated in a Biotage I60 microwave at 125 °C for 15 min (FHT: on, absorbance: normal, cooling: off). The reaction mixture was diluted with brine (5 mL) and extracted with EtOAc (2 x 5 mL). The organic extracts were combined and passed through a hydrophobic frit. The solvent was removed under vacuum and the residue loaded in DCM (2 mL) and purified on a 25 g silica cartridge using a gradient of 0–10% MeOH in DCM over 10 column volumes. The appropriate fractions were combined and the solvent evaporated *in vacuo*. The residue was purified by MDAP using Method Formic. Fraction 1 was evaporated *in vacuo* to give 2-(7-(3,5-dimethylisoxazol-4-yl)-6-methoxyquinolin-4-yl)-2-(2-fluorophenyl)acetonitrile **204** as a yellow gum (27 mg, 0.070 mmol, 20%).

LCMS (formic A): m/z 388 [(M + H)⁺]; Rt: 1.09 min; 100% purity by peak area.

¹H NMR (400 MHz, CDCl₃): δ 8.87 (d, J = 4.5 Hz, 1 H), 7.93 (s, 1 H), 7.62 (d, J = 4.5 Hz, 1 H), 7.47–7.37 (m, 2 H), 7.25–7.16 (m, 3 H), 6.05 (s, 1 H), 3.88 (s, 3 H), 2.34 (s, 3 H), 2.21–2.16 (m, 3 H).

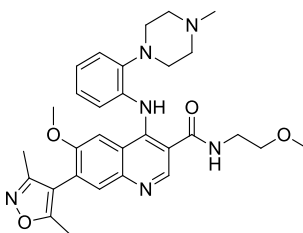
Fraction 2 was evaporated *in vacuo* to give [7-(3,5-dimethylisoxazol-4-yl)-6-methoxyquinolin-4-yl](2-fluorophenyl)methanone **205** as a yellow gum (7 mg, 0.019 mmol, 5%).

LCMS (formic A): m/z 377 [(M + H)⁺]; Rt: 1.11 min; 95% purity by peak area.

¹H NMR (400 MHz, CDCl₃): δ 8.89 (d, J = 4.3 Hz, 1 H), 7.97 (s, 1 H), 7.84–7.78 (m, 1 H), 7.74 (s, 1 H), 7.71–7.60 (m, 1 H), 7.44 (d, J = 4.3 Hz, 1 H), 7.36 (t, J = 7.6 Hz, 1 H), 7.23–7.11 (m, 1 H), 3.88 (s, 3 H), 2.39 (s, 3 H), 2.24 (s, 3 H).

¹³C NMR (100 MHz, CDCl₃): δ 194.0, 166.7, 161.5, 159.7, 157.2, 147.0, 144.8 (2 C), 144.6, 141.3, 135.2, 132.1, 131.6, 126.4, 125.2, 125.0, 121.5, 117.0, 112.3, 102.3, 55.1, 11.2, 10.3.

7-(3,5-Dimethylisoxazol-4-yl)-6-methoxy-N-(2-methoxyethyl)-4-[[2-(4-methylpiperazin-1-yl)phenyl]amino}quinoline-3-carboxamide



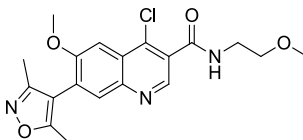
220

A microwave vessel was charged with [2-(4-methyl-1-piperazinyl)phenyl]amine hydrochloride (120 mg, 0.527 mmol), and a stirrer bar followed by 4-chloro-7-(3,5-dimethyl-4-isoxazolyl)-6-(methoxy)-N-[2-(methoxy)ethyl]-3-quinolinecarboxamide **221** (50 mg, 0.128 mmol), then NMP (0.1 mL) was added. The vessel was sealed and the mixture was heated at 180 °C for 20 min in a CEM microwave (FHT: on, cooling: off, Power 300 W, ramp time 1 min). The reaction mixture was diluted with MeOH (3 mL) and applied to a MeOH preconditioned 2 g SCX-2 cartridge. The cartridge was washed with MeOH (10 mL) followed by 2 M ammonia in MeOH solution (10 mL). Both washes were combined and evaporated under vacuum. The residue was purified by MDAP using Method HpH. The appropriate fractions were combined and evaporated under a stream of nitrogen to give the title compound as a yellow gum (8 mg, 0.015 mmol, 11%).

LCMS (formic A): m/z 545 $[(M + H)^+]$; Rt: 0.59 min; 99% purity by peak area.

$^1\text{H NMR}$ (400 MHz, CDCl_3): δ 9.93 (s, 1 H), 8.82 (s, 1 H), 7.77 (s, 1 H), 7.13–7.08 (m, 1 H), 7.07–7.01 (m, 2 H), 6.99–6.93 (m, 1 H), 6.86 (d, $J = 7.8$ Hz, 1 H), 6.78 (t, $J = 5.1$ Hz, 1 H), 3.71–3.65 (m, 2 H), 3.59–3.54 (m, 2 H), 3.41 (s, 3 H), 3.37 (s, 3 H), 3.06 (br s, 4 H), 2.48 (br s, 4 H), 2.35 (s, 3 H), 2.31 (s, 3 H), 2.20 - 2.17 (m, 3 H).

4-Chloro-7-(3,5-dimethylisoxazol-4-yl)-6-methoxy-N-(2-methoxyethyl)quinoline-3-carboxamide



221

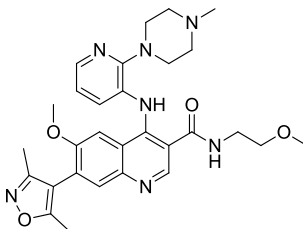
A mixture of 7-(3,5-dimethylisoxazol-4-yl)-6-methoxy-4-oxo-1,4-dihydroquinoline-3-carboxylic acid **169** (3 g, 9.55 mmol) and phosphorus oxychloride (40 ml, 429 mmol) was stirred under nitrogen at 100 °C for 1 h. The reaction mixture was allowed to cool to r.t. and azeotroped with toluene (2 x 50 mL) to give the crude acid chloride (3.5 g) as a brown gum.

A stirred mixture of the crude acid chloride in DCM (50 mL) was cooled in an ice-water bath. Triethylamine (1.5 mL, 10.76 mmol) was added followed by 2-methoxyethylamine (1 mL, 11.61 mmol) and the mixture allowed to stir for 20 min under nitrogen. The flask was removed from the ice-water bath and allowed to warm to r.t. overnight. The reaction mixture was washed with 0.5 M NaOH (aq) (100 mL), followed by 0.5 M HCl (aq) (100 mL), then water (100 mL). The organic layer was passed through a hydrophobic frit and the solvent was evaporated under vacuum. The crude material was loaded in DCM (10 mL) and purified on a 100 g silica cartridge using a gradient of 0–10% MeOH (containing 20% 2 M ammonia in MeOH solution) in DCM over 10 column volumes. The appropriate fractions were combined and the solvent evaporated *in vacuo* to give the title compound as a light yellow solid (1.75 g, 4.49 mmol, 47%).

LCMS (formic A): m/z 390, 392 [(M + H)⁺]; Rt: 0.84 min; 94% purity by peak area.

¹H NMR (400 MHz, DMSO-*d*₆): δ 8.85 (s, 1 H), 8.71 (s, 1 H), 8.02 (s, 1 H), 7.62 (s, 1 H), 4.01 (s, 3 H), 3.56–3.45 (m, 4 H), 3.32 (s, 3 H), 2.35 (s, 3 H), 2.15 (s, 3 H).

7-(3,5-Dimethylisoxazol-4-yl)-6-methoxy-N-(2-methoxyethyl)-4-[(2-(4-methylpiperazin-1-yl)pyridin-3-yl)amino]quinoline-3-carboxamide



228

A 0.5–2.0 mL microwave vessel was charged with potassium orthophosphate (82 mg, 0.385 mmol), a magnetic stirrer bar, tris(dibenzylideneacetone)dipalladium(0) (23 mg, 0.025 mmol), 2-dicyclohexylphosphino-2'-(*N,N*-dimethylamino)biphenyl (20 mg, 0.051 mmol), 2-(4-methyl-1-piperazinyl)-3-pyridinamine **225** (250 mg, 1.300 mmol) and 4-chloro-7-(3,5-dimethyl-4-isoxazolyl)-6-(methoxy)-*N*-[2-(methoxy)ethyl]-3-quinolinecarboxamide **221** (125 mg, 0.321 mmol). The vessel was sealed and heated in a Biotage I60 microwave at 125 °C for 1 h (FHT: on, cooling: off, absorbance: normal). The reaction mixture was applied to a MeOH preconditioned 2 g SCX-2 cartridge which was then washed with MeOH (10 mL) followed by 2 M ammonia in MeOH solution (10 mL). Both the MeOH and basic washes were combined and evaporated under vacuum. The residue was purified by MDAP using Method Formic. The appropriate fractions were combined and the solvent removed by rotary

evaporation. The gum was dissolved in 1,4-dioxane and the solvent removed upon freeze drying to give the title compound as a yellow solid (24 mg, 0.044 mmol, 14%).

m.p.: 106–109 °C.

IR (solid) ν (cm⁻¹): 2933, 2932, 1633, 1584, 1560, 1420, 1224, 794, 770.

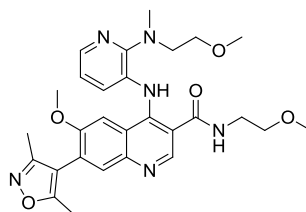
LCMS (formic A): m/z 546 [(M + H)⁺]; Rt: 0.51 min; 99% purity by peak area.

HRMS (ESI): M + H calcd for C₂₉H₃₆N₇O₄ 546.2823, found 546.2806.

¹H NMR (400 MHz, CDCl₃): δ 10.07 (s, 1 H), 8.82 (s, 1 H), 8.10–8.02 (m, 1 H), 7.80 (s, 1 H), 7.04 (d, J = 7.8 Hz, 1 H), 6.95 (s, 1 H), 6.88–6.76 (m, 2 H), 3.75–3.66 (m, 2 H), 3.65–3.57 (m, 2 H), 3.44 (s, 3 H), 3.41 (s, 3 H), 2.64–2.45 (m, 4 H), 2.35 (s, 3 H), 2.34 (s, 3 H), 2.19 (s, 3 H), 2.06–1.86 (m, 4 H).

¹³C NMR (100 MHz, DMSO-*d*₆): δ 167.8, 166.6, 159.5, 154.5 (2 C), 147.4, 146.2, 145.3, 142.5, 132.7, 130.6, 127.8, 125.8, 121.2, 117.3, 113.4, 112.2, 103.6, 70.9, 58.9, 55.1 (3 C), 48.4 (2 C), 46.0, 39.7, 11.8, 10.8.

7-(3,5-Dimethylisoxazol-4-yl)-6-methoxy-N-(2-methoxyethyl)-4-({2-[(2-methoxyethyl)(methyl)amino]pyridin-3-yl}amino)quinoline-3-carboxamide



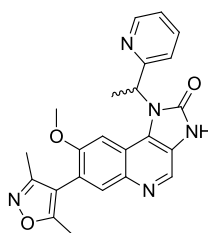
229

A microwave vessel was charged with *N*²-methyl-*N*²-[2-(methoxy)ethyl]-2,3-pyridinediamine **226** (88 mg, 0.486 mmol) and a stirrer bar followed by 4-chloro-7-(3,5-dimethyl-4-isoxazolyl)-6-(methoxy)-*N*-[2-(methoxy)ethyl]-3-quinolinecarboxamide **221** (50 mg, 0.128 mmol). The vessel was sealed and the mixture was heated at 180 °C for 20 min in a CEM microwave (FHT: on, cooling: off, Power 300 W, ramp time 1 min). The reaction mixture was diluted with DCM (5 mL) and applied to a 25 g silica cartridge. Attempted purification using a gradient of 0–15% MeOH (containing 20% 2 M ammonia in MeOH solution) in DCM over 10 column volumes gave no separation. The appropriate fractions were combined and the solvent evaporated *in vacuo*. The residue was purified by MDAP using Method HpH. The appropriate fractions were combined and the solvent evaporated *in vacuo* to give the title compound as a dark brown gum (25 mg, 0.047 mmol, 37%).

LCMS (formic A): m/z 535 $[(M + H)^+]$; Rt: 0.70 min; 96% purity by peak area.

^1H NMR (400 MHz, CDCl_3): δ 9.53 (s, 1 H), 8.89 (s, 1 H), 8.00 (dd, $J = 4.8, 1.5$ Hz, 1 H), 7.85–7.79 (m, 1 H), 7.14 (s, 1 H), 6.97 (dd, $J = 7.8, 1.3$ Hz, 1 H), 6.92 (t, $J = 5.2$ Hz, 1 H), 6.76 (dd, $J = 7.8, 4.8$ Hz, 1 H), 3.69–3.64 (m, 2 H), 3.64–3.60 (m, 2 H), 3.60–3.55 (m, 5 H), 3.53–3.48 (m, 2 H), 3.32 (s, 3 H), 3.28 (s, 3 H), 3.06 (s, 3 H), 2.36 (s, 3 H), 2.20 (s, 3 H).

(±)-7-(3,5-Dimethylisoxazol-4-yl)-8-methoxy-1-[1-(pyridin-2-yl)ethyl]-1H-imidazo[4,5-c]quinolin-2(3H)-one



231

A mixture of 7-(3,5-dimethylisoxazol-4-yl)-6-methoxy-4-{{1-(pyridin-2-yl)ethyl}amino}quinoline-3-carboxamide **240** (1.89 g, 4.53 mmol) and potassium hydroxide (0.330 g, 5.89 mmol) in MeOH (20 mL) was stirred in an open vessel at 0 °C. Iodobenzene diacetate (1.750 g, 5.43 mmol) was added in small portions over 5 min and the mixture stirred for 1.5 h. The reaction mixture was evaporated *in vacuo* and the residue diluted with water (50 mL). The mixture was extracted with DCM (2 x 50 mL), the organic extracts combined and passed through a hydrophobic frit. The solvent was removed *in vacuo* and the residue dissolved in DCM (10 mL). The solution was applied to a 100 g silica cartridge and purified using a gradient of 0–10% 2 M ammonia in methanol/DCM to give the title compound as a light yellow powder (1.64 g, 3.95 mmol, 87%).

m.p.: 167 °C.

IR (solid) ν (cm^{-1}): 2933, 1704, 1621, 1588, 1470, 1430, 1221, 1079, 1033, 751.

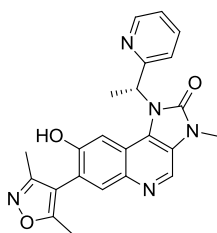
LCMS (formic A): m/z 416 $[(M + H)^+]$; Rt: 0.68 min; 100% purity by peak area.

HRMS (ESI): $M + H$ calcd for $\text{C}_{23}\text{H}_{22}\text{N}_5\text{O}_3$ 416.1717, found 416.1708.

^1H NMR (400 MHz, $\text{DMSO}-d_6$): Variable temperature (393 K) δ 11.29 (br s, 1 H), 8.64–8.60 (m, 2 H), 7.78–7.77 (m, 1 H), 7.79–7.74 (m, 1 H), 7.43 (d, $J = 7.8$ Hz, 1 H), 7.32 (dd, $J = 7.0, 4.8$ Hz, 1 H), 7.01 (s, 1 H), 6.30 (q, $J = 7.2$ Hz, 1 H), 3.59 (s, 3 H), 2.27 (s, 3 H), 2.09 (d, $J = 7.2$ Hz, 3 H), 2.07 (s, 3 H).

^{13}C NMR (100 MHz, CDCl_3): δ 166.4, 159.7, 159.4, 155.9, 155.6, 149.5, 140.7, 137.3, 133.2, 132.6, 128.9, 122.8, 122.4, 121.9, 121.4, 116.2, 112.4, 101.3, 55.8, 53.4, 17.8, 11.7, 10.8.

7-(3,5-Dimethylisoxazol-4-yl)-8-hydroxy-3-methyl-1-[(R)-1-(pyridin-2-yl)ethyl]-1H-imidazo[4,5-c]quinolin-2(3H)-one



237

To 7-(3,5-dimethylisoxazol-4-yl)-8-methoxy-3-methyl-1-[1-(pyridin-2-yl)ethyl]-1H-imidazo[4,5-c]quinolin-2(3H)-one **238** (3.63 g, 8.45 mmol) in DCE (75 mL) was added tribromoborane (8.0 mL, 85 mmol) dropwise. A thick precipitate formed and after addition was complete, the reaction was stirred at 90 °C under nitrogen for 3.5 h. The reaction was cooled in an ice-bath and carefully quenched with 10% EtOH in DCM (75 mL) and then MeOH (75 mL). After stirring for 20 min, the solvent was removed *in vacuo*. The solid-foam mixture was suspended in EtOAc (200 mL) and sonicated for 10 min. To the mixture was added sat. Na₂CO₃ (aq) (200 mL) and the biphasic mixture stirred vigorously for 10 min. The organic layer was separated and left to stand for 5 min during which time a precipitate formed. The solid was isolated by vacuum filtration and the filtrate dried (MgSO₄). The dried filtrate was evaporated *in vacuo* and the resulting solid triturated with ether (50 mL). This solid was combined with the previous solid precipitate to give the title compound as an off-white solid (2.96 g, 7.12 mmol, 84%).

76% e.e. determined by HPLC analysis on a Chiralpak® ID (250 mm x 4.6 mm, 5 µm packing diameter) column. An isocratic system of 50% EtOH in heptane with a flow rate of 1 mL/min was used at r.t. The UV detection was performed at 215 nm. Peak 1 Rt: 8.18 min, 12% peak area; Peak 2 Rt: 11.46 min, 88% peak area.

$[\alpha]_D^{21} -25$ (c 0.5, CHCl₃/MeOH [4:1]).

m.p.: 287 °C (decomp.).

IR (solid) ν (cm⁻¹): 2923, 2531, 1720, 1620, 1588, 1410, 1216, 1036, 747.

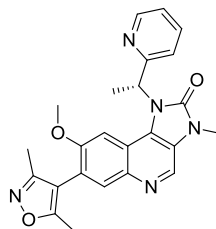
LCMS (formic A): m/z 416 [(M + H)⁺]; Rt: 0.62 min; 99% purity by peak area.

HRMS (ESI): M + H calcd for C₂₃H₂₂N₅O₃ 416.1723, found 416.1711.

¹H NMR (400 MHz, DMSO-*d*₆): Variable temperature (393 K) δ 8.70 (s, 1 H), 8.54 (d, *J* = 4.8 Hz, 1 H), 7.79 (s, 1 H), 7.76–7.70 (m, 1 H), 7.40 (d, *J* = 7.8 Hz, 1 H), 7.37 (s, 1 H), 7.26 (dd, *J* = 7.4, 4.8 Hz, 1H), 6.27 (q, *J* = 7.2 Hz, 1 H), 3.54 (s, 3 H), 2.31 (s, 3 H), 2.14 (s, 3 H), 2.12 (d, *J* = 7.2 Hz, 3 H). OH signal not resolved.

^{13}C NMR (150 MHz, $\text{DMSO-}d_6$): δ 165.8, 159.1, 158.7, 153.3 (2 C), 149.0, 139.8, 137.0, 132.9, 130.9, 126.9, 123.3, 122.4, 120.7, 120.2, 115.9, 112.6, 103.6, 53.8, 27.4, 17.5, 11.4, 10.4.

7-(3,5-Dimethylisoxazol-4-yl)-8-methoxy-3-methyl-1-[(R)-1-(pyridin-2-yl)ethyl]-1H-imidazo[4,5-c]quinolin-2(3H)-one



238

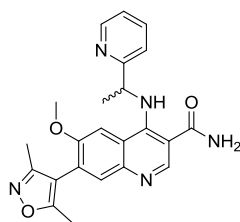
A solution of 7-(3,5-dimethylisoxazol-4-yl)-8-methoxy-1-[(R)-1-(pyridin-2-yl)ethyl]-1H-imidazo[4,5-c]quinolin-2(3H)-one (I-BET151, 4.0 g, 9.63 mmol, %e.e. = 88) in anhydrous NMP (30 mL) under nitrogen at r.t., was treated with sodium hydride (60% dispersion in mineral oil, 0.50 g, 12.5 mmol) and the resulting brown solution was stirred for 20 min. Methyl iodide (0.66 mL, 10.6 mmol) was then added and the mixture stirred for 5 h. The reaction mixture was diluted with brine (50 mL) and extracted with EtOAc (50 mL). The organic layer was washed with water (4 x 50 mL) then passed through a hydrophobic frit. The solvent was evaporated *in vacuo* to give the title compound as a cream foam (3.63 g, 8.45 mmol, 88%).

76% e.e. determined by HPLC analysis on a Chiralpak[®] AD (250 mm x 4.6 mm, 10 μm packing diameter) column. An isocratic system of 40% EtOH in heptane with a flow rate of 1 mL/min was used at r.t. The UV detection was performed at 215 nm. Peak 1 Rt: 11.35 min, 12% peak area; Peak 2 Rt: 16.57 min, 88% peak area.

LCMS (formic A): m/z 430 $[(\text{M} + \text{H})^+]$; Rt: 0.75 min; 99% purity by peak area.

^1H NMR (400 MHz, $\text{DMSO-}d_6$): Variable temperature (353 K) δ 8.82 (s, 1 H), 8.61 (d, $J = 4.8$ Hz, 1 H), 7.81 (s, 1 H), 7.80–7.74 (m, 1 H), 7.44 (d, $J = 8.1$ Hz, 1 H), 7.33 (dd, $J = 7.3, 4.8$ Hz, 1 H), 6.94 (s, 1 H), 6.33 (q, $J = 7.2$ Hz, 1 H), 3.62 (s, 3 H), 3.55 (s, 3 H), 2.26 (s, 3 H), 2.07 (d, $J = 7.2$ Hz, 3 H), 2.06 (s, 3 H).

(±)-7-(3,5-Dimethylisoxazol-4-yl)-6-methoxy-4-[[1-(pyridin-2-yl)ethyl]amino]quinoline-3-carboxamide



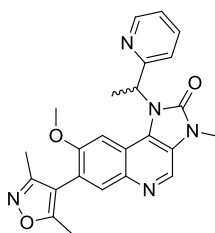
240

A solution of 4-chloro-7-(3,5-dimethylisoxazol-4-yl)-6-methoxyquinoline-3-carboxamide **239** (2.0 g, 6.03 mmol) in anhydrous NMP (9 mL) was treated with DIPEA (3.16 mL, 18.09 mmol) and 1-(pyridin-2-yl)ethanamine (0.88 g, 7.20 mmol). The mixture was stirred at 120 °C for 16 h. The reaction mixture was allowed to cool to r.t and applied to a MeOH preconditioned 70 g SCX-2 cartridge. The cartridge was washed with CHCl₃ (150 mL), MeOH (150 mL) and 2 M ammonia in MeOH (150 mL). The ammonia in MeOH wash was evaporated *in vacuo*, the residue dissolved in EtOAc (50 mL) and washed with water (3 x 50 mL). The organic layer was passed through a hydrophobic frit and the solvent removed *in vacuo*. The residue was dissolved in DCM (5 mL), the solution applied to a 100 g silica cartridge and purified using a gradient of 0–12% 2 M ammonia in MeOH/DCM over 12 column volumes. The appropriate fractions were combined and the solvent evaporated *in vacuo* to give the title compound as a beige foam (1.89 g, 4.53 mmol, 75%).

LCMS (formic A): m/z 418 [(M + H)⁺]; Rt: 0.64 min; 100% purity by peak area.

¹H NMR (400 MHz, CDCl₃): δ 9.47 (d, J = 8.1 Hz, 1 H), 8.74 (s, 1 H), 8.62 (d, J = 4.8 Hz, 1 H), 7.77–7.72 (m, 1 H), 7.69 (s, 1 H), 7.66 (d, J = 7.8 Hz, 1 H), 7.35 (s, 1 H), 7.24 (dd, J = 7.4, 4.8 Hz, 1 H), 6.64–5.68 (m, 2 H), 5.38 (dq, J = 8.1, 6.8 Hz, 1 H), 3.52 (s, 3 H), 2.33 (s, 3 H), 2.17 (s, 3 H), 1.74 (d, J = 6.8 Hz, 3 H).

(±)-7-(3,5-Dimethylisoxazol-4-yl)-8-methoxy-3-methyl-1-[1-(pyridin-2-yl)ethyl]-1*H*-imidazo[4,5-*c*]quinolin-2(3*H*)-one



241

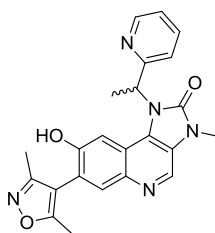
A solution of 7-(3,5-dimethylisoxazol-4-yl)-8-methoxy-1-[1-(pyridin-2-yl)ethyl]-1*H*-imidazo[4,5-*c*]quinolin-2(3*H*)-one **231** (0.5 g, 1.204 mmol) in anhydrous NMP (4 mL) under nitrogen at r.t., was treated with sodium hydride (60% dispersion in mineral oil, 0.072 g, 1.805 mmol) and the resulting brown solution stirred for 20 min. Methyl iodide (0.083 mL, 1.324 mmol) was then added and the mixture stirred for 5 h. The reaction mixture was diluted with brine (10 mL) which was then extracted with EtOAc (10 mL). The organic layer was washed with water (4 x 10 mL) then passed through a hydrophobic frit. The solvent was evaporated under vacuum and the residue dissolved in MeOH (4 mL). The solution was applied to a MeOH preconditioned 10 g SCX-2 cartridge which was then washed with MeOH (60 mL) followed by 2 M ammonia in MeOH solution (60 mL). The basic wash was evaporated under vacuum. The resulting solid was loaded in DCM (5 mL) and purified on a 100 g silica cartridge using a gradient of 0–10% MeOH in DCM over 12 column volumes. The appropriate fractions were combined and the solvent removed by rotary evaporation to give the title compound as an off-white solid (433 mg, 1.008 mmol, 84%).

0% e.e. determined by HPLC analysis on a Chiralpak[®] AD (250 mm x 4.6 mm, 10 μm packing diameter) column. An isocratic system of 40% EtOH in heptane with a flow rate of 1 mL/min was used at r.t. The UV detection was performed at 215 nm. Peak 1 Rt: 11.20 min, 50% peak area; Peak 2 Rt: 16.58 min; 50% peak area.

LCMS (formic A): *m/z* 430 [(M + H)⁺]; Rt: 0.72 min; 100% purity by peak area.

¹H NMR (400 MHz, DMSO-*d*₆): Variable temperature (393 K) δ 8.80 (s, 1 H), 8.61 (d, *J* = 4.8 Hz, 1 H), 7.81 (s, 1 H), 7.80–7.74 (m, 1 H), 7.45 (d, *J* = 8.1 Hz, 1 H), 7.32 (dd, *J* = 7.4, 4.8 Hz, 1 H), 7.05 (s, 1 H), 6.34 (q, *J* = 7.2 Hz, 1 H), 3.62 (s, 3 H), 3.60 (s, 3 H), 2.27 (s, 3 H), 2.10 (d, *J* = 7.2 Hz, 3 H), 2.07 (s, 3 H).

(±)-7-(3,5-Dimethylisoxazol-4-yl)-8-hydroxy-3-methyl-1-[1-(pyridin-2-yl)ethyl]-1H-imidazo[4,5-c]quinolin-2(3H)-one



242

To a solution of 7-(3,5-dimethylisoxazol-4-yl)-6-methoxy-4-((1-(pyridin-2-yl)ethyl)amino)quinoline-3-carboxamide **241** (1.89 g, 4.53 mmol) in MeOH (20 mL) was added potassium hydroxide (0.330 g, 5.89 mmol) and the mixture stirred in an open vessel at 0 °C. Iodobenzene diacetate (1.750 g, 5.43 mmol) was added in small portions over 5 min and the mixture stirred for 1.5 h. The reaction mixture was evaporated *in vacuo* and the residue diluted with water (50 mL). The mixture was extracted with DCM (2 x 50 mL), the organic extracts combined and passed through a hydrophobic frit. The solvent was removed *in vacuo* and the residue dissolved in DCM (10 mL). The solution was applied to a 100 g silica cartridge and purified using a gradient of 0–10% 2 M ammonia in methanol/DCM to give the title compound as a light yellow powder (1.64 g, 3.95 mmol, 87%).

6% e.e. determined by HPLC analysis on a Chiralpak® ID (250 mm x 4.6 mm, 5 µm packing diameter) column. An isocratic system of 50% EtOH in heptane with a flow rate of 1 mL/min was used at r.t. The UV detection was performed at 215 nm. Peak 1 Rt: 8.24 min, 53% peak area; Peak 2 Rt: 11.97 min, 47% peak area.

mp: 167 °C.

IR (solid) ν (cm⁻¹): 2925, 2530, 1720, 1619, 1588, 1410, 1216, 1035, 748.

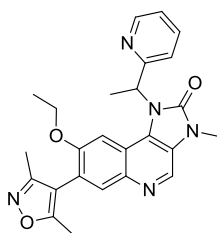
LCMS (formic A): m/z 416 [(M + H)⁺]; Rt: 0.68 min; 100% purity by peak area.

HRMS (ESI): M + H calcd for C₂₃H₂₂N₅O₃ 416.1717, found 416.1708.

¹H NMR (400 MHz, DMSO-*d*₆): Variable temperature (393 K) 11.29 (br s., 1 H), 8.64–8.60 (m, 2 H), 7.78–7.77 (m, 1 H), 7.79–7.74 (m, 1 H), 7.43 (d, J = 7.8 Hz, 1 H), 7.32 (dd, J = 7.0, 4.8 Hz, 1 H), 7.01 (s, 1 H), 6.30 (q, J = 7.2 Hz, 1 H), 3.59 (s, 3 H), 2.27 (s, 3 H), 2.09 (d, J = 7.2 Hz, 3 H), 2.07 (s, 3 H).

¹³C NMR (100 MHz, CDCl₃): δ 166.4, 159.7, 159.4, 155.9, 155.6, 149.5, 140.7, 137.3, 133.2, 132.6, 128.9, 122.8, 122.4, 121.9, 121.4, 116.2, 112.4, 101.3, 55.8, 53.4, 17.8, 11.7, 10.8.

7-(3,5-Dimethylisoxazol-4-yl)-8-ethoxy-3-methyl-1-[1-(pyridin-2-yl)ethyl]-1H-imidazo[4,5-c]quinolin-2(3H)-one



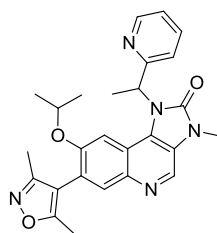
243

A mixture of 7-(3,5-dimethylisoxazol-4-yl)-8-hydroxy-3-methyl-1-[(*R*)-1-(pyridin-2-yl)ethyl]-1H-imidazo[4,5-*c*]quinolin-2(3H)-one **237** (45 mg, 0.108 mmol) and potassium carbonate (18 mg, 0.130 mmol) was suspended in anhydrous DMF (0.8 mL) and treated with bromoethane (10 μ L, 0.134 mmol). The mixture was stirred under nitrogen at 100 °C for 18 h. Further bromoethane (20 μ L, 0.268 mmol) was added and the mixture stirred under nitrogen at 100 °C for 3 h. The reaction mixture was allowed to cool to r.t., diluted with MeOH (0.2 mL) and filtered. The solution was purified by MDAP using Method HpH. The appropriate fractions were combined and the solvent evaporated under a nitrogen stream to give the title compound as a light brown solid (24 mg, 0.054 mmol, 50%).

LCMS (formic A): m/z 444 [(M + H)⁺]; Rt: 0.80 min; 99% purity by peak area.

¹H NMR (400 MHz, DMSO-*d*₆): Variable temperature (393 K) δ 8.79 (s, 1 H), 8.62 (d, *J* = 4.8 Hz, 1 H), 7.81 (s, 1 H), 7.80–7.75 (m, 1 H), 7.45 (d, *J* = 8.1 Hz, 1 H), 7.33 (dd, *J* = 7.3, 4.8 Hz, 1 H), 7.02 (s, 1 H), 6.32 (q, *J* = 7.2 Hz, 1 H), 3.89 (dq, *J* = 9.9, 6.9 Hz, 1 H), 3.66 (dq, *J* = 9.9, 6.9 Hz, 1 H), 3.64–3.56 (m, 3 H), 3.26–3.20 (m, 3 H), 2.28 (s, 3 H), 2.10–2.08 (m, 3 H), 2.08 (d, *J* = 7.2 Hz, 3 H), 1.25 (t, *J* = 6.9 Hz, 3 H).

7-(3,5-Dimethylisoxazol-4-yl)-8-isopropoxy-3-methyl-1-[1-(pyridin-2-yl)ethyl]-1H-imidazo[4,5-c]quinolin-2(3H)-one



244

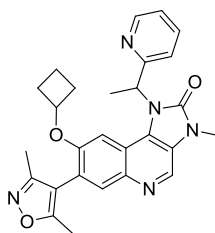
A mixture of 7-(3,5-dimethylisoxazol-4-yl)-8-hydroxy-3-methyl-1-[(*R*)-1-(pyridin-2-yl)ethyl]-1H-imidazo[4,5-*c*]quinolin-2(3H)-one **237** (45 mg, 0.108 mmol) and potassium carbonate (18 mg, 0.130 mmol) was suspended in anhydrous DMF (0.8 mL) and treated with

2-iodopropane (0.013 mL, 0.130 mmol). The mixture was stirred under nitrogen at 100 °C for 18 h. Further 2-iodopropane (0.026 mL, 0.260 mmol) was added and the mixture stirred under nitrogen at 100 °C for 3 h. The reaction mixture was allowed to cool to r.t., diluted with MeOH (0.2 mL) and filtered. The solution was purified by MDAP using Method HpH. The appropriate fractions were combined and the solvent evaporated under a nitrogen stream to give the title compound as a light brown solid (30 mg, 0.066 mmol, 61%).

LCMS (HpH): m/z 458 [(M + H)⁺]; Rt: 1.02 min; 100% purity by peak area.

¹H NMR (400 MHz, DMSO-*d*₆): Variable temperature (393 K) δ 8.79 (s, 1 H), 8.62 (d, J = 4.8 Hz, 1 H), 7.82 (s, 1 H), 7.80–7.75 (m, 1 H), 7.45 (d, J = 8.1 Hz, 1 H), 7.33 (dd, J = 7.3, 4.8 Hz, 1 H), 7.05 (s, 1 H), 6.31 (q, J = 7.2 Hz, 1 H), 4.18 (spt, J = 6.0 Hz, 1 H), 3.61 (s, 3 H), 2.31–2.24 (m, 3 H), 2.10–2.08 (m, 3 H), 2.09 (d, J = 7.2 Hz, 3 H), 1.21 (d, J = 6.0 Hz, 3 H), 1.06 (d, J = 6.0 Hz, 3 H).

8-Cyclobutoxy-7-(3,5-dimethylisoxazol-4-yl)-3-methyl-1-[1-(pyridin-2-yl)ethyl]-1H-imidazo[4,5-*c*]quinolin-2(3H)-one



245

A mixture of 7-(3,5-dimethylisoxazol-4-yl)-8-hydroxy-3-methyl-1-[(*R*)-1-(pyridin-2-yl)ethyl]-1H-imidazo[4,5-*c*]quinolin-2(3H)-one **237** (45 mg, 0.108 mmol) and potassium carbonate (18 mg, 0.130 mmol) was suspended in anhydrous DMF (0.8 mL) and treated with bromocyclobutane (0.012 mL, 0.130 mmol). The mixture was stirred under nitrogen at 100 °C for 18 h. The reaction mixture was allowed to cool to room temperature, diluted with MeOH (0.2 mL) and filtered. The solution was purified by MDAP using Method HpH. The appropriate fractions were combined and the solvent evaporated under stream of nitrogen to give the title compound as a light brown solid (21 mg, 0.045 mmol, 41%).

m.p.: 138 °C.

IR (solid) ν (cm⁻¹): 2939, 1705, 1620, 1580, 1490, 1454, 1213, 748.

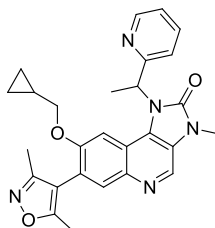
LCMS (HpH): m/z 470 [(M + H)⁺]; Rt: 1.07 min; 100% purity by peak area.

HRMS (ESI): M + H calcd for C₂₇H₂₈N₅O₃ 470.2187, found 470.2172.

^1H NMR (400 MHz, $\text{DMSO}-d_6$): Variable temperature (393 K) δ 8.80 (s, 1H), 8.67 (d, $J = 4.8$ Hz, 1 H), 7.84 (s, 1 H), 7.82–7.76 (m, 1 H), 7.44 (d, $J = 8.1$ Hz, 1 H), 7.36 (dd, $J = 7.3, 4.8$ Hz, 1 H), 6.89 (s, 1 H), 6.30 (q, $J = 7.2$ Hz, 1 H), 4.22 (quin, $J = 6.8$ Hz, 1 H), 3.61 (s, 3 H), 2.49–2.40 (m, 1 H), 2.33–2.27 (m, 3 H), 2.24–2.14 (m, 1 H), 2.12 (s, 3 H), 2.09 (d, $J = 7.2$ Hz, 3 H), 1.98–1.87 (m, 2 H), 1.87–1.77 (m, 1 H), 1.73–1.61 (m, 1 H).

^{13}C NMR (100 MHz, CDCl_3): δ 166.3, 159.6, (2 C), 154.4, 153.4, 149.4, 140.5, 137.2, 133.0, 129.9, 128.5, 123.9, 122.6, 121.2 (2 C), 115.9, 112.5, 102.2, 71.6, 30.4, 29.8, 27.9, 17.7, 13.4, 11.9, 11.0. Benzylic signal not observed.

8-(Cyclopropylmethoxy)-7-(3,5-dimethylisoxazol-4-yl)-3-methyl-1-[1-(pyridin-2-yl)ethyl]-1H-imidazo[4,5-c]quinolin-2(3H)-one



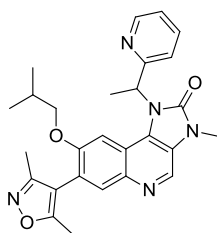
246

A mixture of 7-(3,5-dimethylisoxazol-4-yl)-8-hydroxy-3-methyl-1-[(*R*)-1-(pyridin-2-yl)ethyl]-1H-imidazo[4,5-*c*]quinolin-2(3H)-one **237** (50 mg, 0.12 mmol), potassium carbonate (43 mg, 0.31 mmol) and (bromomethyl)cyclopropane (0.014 mL, 0.14 mmol) was suspended in anhydrous DMF (2.5 mL) and stirred under nitrogen at 100 °C for 16 h. The reaction mixture was allowed to cool to r.t. and evaporated *in vacuo*. The crude material was purified by MDAP using Method HpH. The appropriate fractions were combined and the solvent removed by rotary evaporation to give the title compound as a light brown foam (38 mg, 0.08 mmol, 64%).

LCMS (formic A): m/z 470 $[(M + H)^+]$; Rt: 0.88 min; 98% purity by peak area.

^1H NMR (400 MHz, $\text{DMSO}-d_6$): δ 8.95–8.91 (m, 1 H), 8.76–8.69 (m, 1 H), 7.94 (s, 1 H), 7.93–7.86 (m, 1 H), 7.61–7.54 (m, 1 H), 7.49–7.41 (m, 1 H), 7.13 (s, 1 H), 6.44 (q, $J = 7.3$ Hz, 1 H), 3.89–3.81 (m, 1 H), 3.56–3.49 (m, 1 H), 2.43 (s, 3 H), 2.24 (s, 3 H), 2.20 (d, $J = 7.1$ Hz, 3 H), 1.27–1.18 (m, 1 H), 0.73–0.67 (m, 2 H), 0.44–0.33 (m, 2 H). NCH_3 signal obscured by water. Broad signals observed due to restricted rotation.

7-(3,5-Dimethylisoxazol-4-yl)-8-isobutoxy-3-methyl-1-[1-(pyridin-2-yl)ethyl]-1H-imidazo[4,5-c]quinolin-2(3H)-one



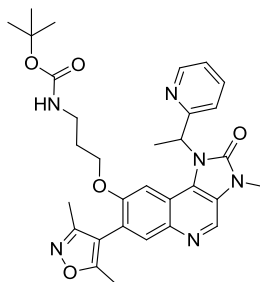
247

A mixture of 7-(3,5-dimethylisoxazol-4-yl)-8-hydroxy-3-methyl-1-[(*R*)-1-(pyridin-2-yl)ethyl]-1H-imidazo[4,5-*c*]quinolin-2(3H)-one **237** (50 mg, 0.12 mmol), potassium carbonate (43 mg, 0.31 mmol) and 1-bromo-2-methylpropane (0.016 mL, 0.15 mmol) was suspended in anhydrous DMF (2.5 mL) and stirred under nitrogen at 100 °C for 3 h. The reaction mixture was allowed to cool to r.t. and evaporated *in vacuo*. The crude material was purified by MDAP using Method HpH. The appropriate fractions were combined and the solvent removed by rotary evaporation to give the title compound as a light brown glass (38 mg, 0.08 mmol, 63%).

LCMS (formic A): m/z 472 [(M + H)⁺]; Rt: 0.92 min; 100% purity by peak area.

¹H NMR (400 MHz, CDCl₃): δ 8.71–8.62 (m, 2 H), 7.85 (s, 1 H), 7.68–7.59 (m, 1 H), 7.34 (br s, 1 H), 7.25–7.21 (m, 1 H), 6.85 (br s, 1 H), 6.44 (q, $J = 6.6$ Hz, 1 H), 3.70 (s, 3 H), 3.58–3.51 (m, 1 H), 3.03 (br s, 1 H), 2.29 (s, 3 H), 2.16–2.11 (m, 6 H), 2.01–1.89 (m, 1 H), 0.95 (d, $J = 6.7$ Hz, 3 H), 0.91 (d, $J = 6.7$ Hz, 3 H). Broad signals observed due to restricted rotation.

***tert*-Butyl [3-({7-(3,5-dimethylisoxazol-4-yl)-3-methyl-2-oxo-1-[1-(pyridin-2-yl)ethyl]-2,3-dihydro-1H-imidazo[4,5-*c*]quinolin-8-yl}oxy)propyl]carbamate**



248

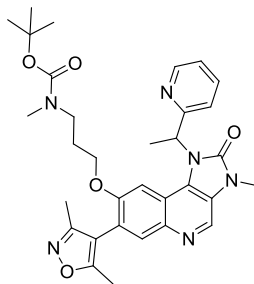
A mixture of 7-(3,5-dimethylisoxazol-4-yl)-8-hydroxy-3-methyl-1-[(*R*)-1-(pyridin-2-yl)ethyl]-1H-imidazo[4,5-*c*]quinolin-2(3H)-one **237** (145 mg, 0.349 mmol) and potassium carbonate (60 mg, 0.349 mmol) in DMF (5 mL) and treated with *tert*-butyl (3-

bromopropyl)carbamate (102 mg, 0.428 mmol). The mixture was stirred under nitrogen at 100 °C for 2.5 h and then allowed to cool to r.t. EtOAc (10 mL) was added and washed with 10% LiCl (aq) (10 mL). The aqueous layer was extracted with EtOAc (10 mL), the organic layers combined and washed with 10% LiCl (aq) (10 mL). The aqueous layer was extracted with EtOAc (10 mL), the organic layers combined and passed through a hydrophobic frit. The solvent was removed by rotary evaporation. The residue was dissolved in MeOH (1.0 mL) and loaded onto a MeOH preconditioned 5 g SCX-2 cartridge. The cartridge was washed with MeOH (30 mL) and 2 M ammonia in MeOH solution (30 mL). The basic wash was evaporated *in vacuo* and the residue purified by MDAP using Method HpH. The appropriate fractions were combined and the solvent removed by rotary evaporation to give the title compound as a brown gum (172 mg, 0.300 mmol, 86%).

LCMS (HpH) m/z 573 [(M + H)⁺]; Rt: 1.07 min; 100% purity by peak area.

¹H NMR (400 MHz, DMSO-*d*₆): Variable temperature (393 K) δ 8.76 (s, 1 H), 8.58 (d, J = 4.8 Hz, 1 H), 7.77 (s, 1 H), 7.77–7.72 (m, 1 H), 7.43 (d, J = 8.1 Hz, 1 H), 7.29 (dd, J = 7.3, 4.8 Hz, 1 H), 7.01 (s, 1 H), 6.29 (q, J = 7.3 Hz, 1 H), 6.22 (br s, 1 H), 3.83 (dt, J = 9.9, 6.3 Hz, 1 H), 3.58 (s, 3 H), 3.56 (dt, J = 9.9, 6.3 Hz, 1 H), 2.99 (t, J = 6.3 Hz, 1 H), 2.98 (t, J = 6.3 Hz, 1 H), 2.25 (s, 3 H), 2.05 (s, 3 H), 2.05 (d, J = 7.3 Hz, 3 H), 1.77 (quin, J = 6.3, 6.3 Hz, 2 H), 1.38 (s, 9 H).

***tert*-Butyl [3-({7-(3,5-dimethylisoxazol-4-yl)-3-methyl-2-oxo-1-[1-(pyridin-2-yl)ethyl]-2,3-dihydro-1*H*-imidazo[4,5-*c*]quinolin-8-yl}oxy)propyl](methyl)carbamate**



249

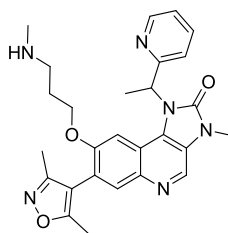
A solution of *tert*-butyl [3-({7-(3,5-dimethylisoxazol-4-yl)-3-methyl-2-oxo-1-[1-(pyridin-2-yl)ethyl]-2,3-dihydro-1*H*-imidazo[4,5-*c*]quinolin-8-yl}oxy)propyl]carbamate **248** (153 mg, 0.267 mmol) in anhydrous NMP (1 mL) under nitrogen was treated with sodium hydride (60% dispersion in mineral oil, 15 mg, 0.374 mmol) and the mixture stirred at r.t. for 20 min. Methyl iodide (0.018 mL, 0.294 mmol) was added and the mixture was left to stir for 17 h. The mixture was treated with sodium hydride (60% dispersion in mineral oil, 15 mg) and stirred for 20 min before methyl iodide (0.009 mL, 0.147 mmol) was added. After

4.5 h stirring, water (8 mL) was added. The mixture was extracted with EtOAc (2 x 10 mL), the extracts combined and passed through a hydrophobic frit. The solvent was removed by rotary evaporation and the residue purified by MDAP using Method HpH. The appropriate fractions were combined and the solvent removed by rotary evaporation to give the title compound as a yellow solid (34 mg, 0.058 mmol, 22%).

LCMS (HpH): m/z 587 [(M + H)⁺]; Rt: 1.13 min; 100% purity by peak area.

¹H NMR (400 MHz, DMSO-*d*₆): Variable temperature (393 K) δ 8.77 (s, 1 H), 8.58 (d, *J* = 4.8 Hz, 1 H), 7.78 (s, 1 H), 7.77–7.70 (m, 1 H), 7.42 (d, *J* = 8.1 Hz, 1 H), 7.29 (dd, *J* = 7.3, 4.8 Hz, 1 H), 7.02 (s, 1 H), 6.29 (q, *J* = 7.3 Hz, 1 H), 3.82 (dt, *J* = 9.9, 6.1 Hz, 1 H), 3.58 (s, 3 H), 3.55 (dt, *J* = 9.9, 6.1 Hz, 1 H), 3.17 (t, *J* = 6.9 Hz, 1 H), 3.17 (t, *J* = 6.9 Hz, 1 H), 2.70 (s, 3 H), 2.25 (s, 3 H), 2.06 (s, 3 H), 2.05 (d, *J* = 7.3 Hz, 3 H), 1.88–1.79 (m, 2 H), 1.34 (s, 9 H).

7-(3,5-Dimethylisoxazol-4-yl)-3-methyl-8-[3-(methylamino)propoxy]-1-[1-(pyridin-2-yl)ethyl]-1*H*-imidazo[4,5-*c*]quinolin-2(3*H*)-one



250

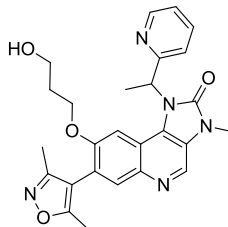
A solution of *tert*-butyl [3-({7-(3,5-dimethylisoxazol-4-yl)-3-methyl-2-oxo-1-[1-(pyridin-2-yl)ethyl]-2,3-dihydro-1*H*-imidazo[4,5-*c*]quinolin-8-yl}oxy)propyl](methyl)-carbamate **249** (23 mg, 0.039 mmol) in 1,4-dioxane (0.5 mL) was treated with 4 M HCl in 1,4-dioxane solution (0.5 mL, 0.039 mmol) and the mixture stirred at r.t. for 2 h in a stoppered vessel. The reaction mixture was evaporated under a stream of nitrogen and the residue was dissolved in MeOH (0.5 mL). The solution was applied to a MeOH preconditioned 2 g SCX-2 cartridge. The cartridge was washed with MeOH (16 mL) followed by 2 M ammonia in MeOH solution (16 mL). The basic wash was evaporated under vacuum to give a light brown oil which solidified upon standing (19 mg, 0.039 mmol, 100%).

LCMS (HpH): m/z 487 [(M + H)⁺]; Rt: 0.77 min; 97% purity by peak area.

¹H NMR (400 MHz, DMSO-*d*₆): Variable temperature (393 K) δ 8.76 (s, 1 H), 8.59 (d, *J* = 4.8 Hz, 1 H), 7.78 (s, 1 H), 7.77–7.71 (m, 1 H), 7.41 (d, *J* = 8.1 Hz, 1 H), 7.29 (dd, *J* = 7.3,

4.8 Hz, 1 H), 7.02 (s, 1 H), 6.29 (q, $J = 7.3$ Hz, 1 H), 3.86 (dt, $J = 9.7, 6.4$ Hz, 1 H), 3.58 (s, 3 H), 3.63–3.57 (m, 1 H), 2.52 (t, $J = 6.7$ Hz, 2 H), 2.29 (s, 3 H), 2.24 (s, 3 H), 2.05 (s, 3 H), 2.05 (d, $J = 7.1$ Hz, 3 H), 1.74 (tt, $J = 6.7, 6.4$ Hz, 2 H). *NH* signal not resolved.

7-(3,5-Dimethylisoxazol-4-yl)-8-(3-hydroxypropoxy)-3-methyl-1-[1-(pyridin-2-yl)ethyl]-1*H*-imidazo[4,5-*c*]quinolin-2(3*H*)-one



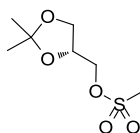
255

A solution of 7-(3,5-dimethylisoxazol-4-yl)-8-hydroxy-3-methyl-1-[(*R*)-1-(pyridin-2-yl)ethyl]-1*H*-imidazo[4,5-*c*]quinolin-2(3*H*)-one **237** (270 mg, 0.65 mmol) in anhydrous DMF (4.5 mL) was dispensed evenly between 6 x vessels each containing potassium carbonate (18 mg, 0.13 mmol). To one of these vessels was added 3-bromo-1-propanol (11 μ L, 0.13 mmol) and the mixture stirred under nitrogen at 100 °C for 16 h. The reaction mixture was evaporated under a stream of nitrogen and the crude material purified by MDAP using Method HpH. The appropriate fractions were combined and the solvent removed by rotary evaporation to give the title compound as a light brown foam (23 mg, 0.05 mmol, 45%).

LCMS (formic A): m/z 474 [(*M* + *H*)⁺]; Rt: 0.64 min; 100% purity by peak area.

¹H NMR (400 MHz, CDCl₃): δ 8.70–8.63 (m, 2 H), 7.82 (s, 1 H), 7.63 (t, $J = 7.3$ Hz, 1 H), 7.44–7.30 (m, 1 H), 7.28–7.21 (m, 1 H), 7.19–6.76 (m, 1 H), 6.44 (d, $J = 7.1$ Hz, 1 H), 4.07–3.93 (m, 1 H), 3.78–3.71 (m, 2 H), 3.70 (s, 3 H), 3.60 (br s, 1 H), 2.30 (s, 3 H), 2.18–2.10 (m, 6 H), 2.01–1.90 (m, 2 H), 1.81 (br s, 1 H). Broad signals observed due to restricted rotation.

(*R*)-(2,2-Dimethyl-1,3-dioxolan-4-yl)methyl methanesulfonate



252

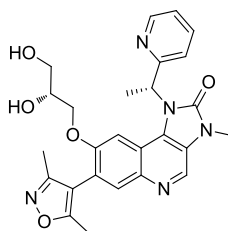
A stirred solution of (*R*)-(2,2-dimethyl-1,3-dioxolan-4-yl)methanol (0.42 mL, 3.40 mmol) and triethylamine (1.2 mL, 8.61 mmol) in DCM (6 mL) at 0 °C was treated with methanesulfonyl chloride (0.32 mL, 4.11 mmol). The mixture was stirred under nitrogen for

10 min and then allowed to warm to r.t. over 20 h. The reaction mixture was diluted with EtOAc (10 mL) and the solution washed with brine (10 mL). The aqueous layer was extracted with EtOAc (10 mL), the organic layers combined and washed with sat. NaHCO₃ (aq) (5 mL) then with brine/water (1:1, 2 x 5 mL). The organic layer was passed through a hydrophobic frit and the solvent removed by rotary evaporation. The residue was loaded in DCM (2 mL) and purified on a 25 g silica cartridge using a gradient of 0–100% EtOAc in cyclohexane over 12 column volumes. The appropriate fractions were combined and the solvent removed by rotary evaporation to give the title compound as a colourless oil (688 mg, 3.27 mmol, 96%).

¹H NMR (400 MHz, CDCl₃): δ 4.37 (m, 1 H), 4.23 (d, *J* = 5.2 Hz, 2 H), 4.11 (dd, *J* = 8.8 Hz, 6.5 Hz, 1 H), 3.83 (dd, *J* = 8.8 Hz, 5.5 Hz, 1 H), 3.06 (s, 3 H), 1.45 (s, 3 H), 1.37 (s, 3 H).

The ¹H NMR was in agreement with that reported in the literature.¹⁴⁵

8-[(*R*)-2,3-Dihydroxypropoxy]-7-(3,5-dimethylisoxazol-4-yl)-3-methyl-1-[(*R*)-1-(pyridin-2-yl)ethyl]-1*H*-imidazo[4,5-*c*]quinolin-2(3*H*)-one



256

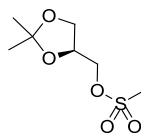
A mixture of 7-(3,5-dimethylisoxazol-4-yl)-8-hydroxy-3-methyl-1-[(*R*)-1-(pyridin-2-yl)ethyl]-1*H*-imidazo[4,5-*c*]quinolin-2(3*H*)-one **237** (100 mg, 0.241 mmol), (*R*)-(2,2-dimethyl-1,3-dioxolan-4-yl)methyl methanesulfonate **252** (123 mg, 0.585 mmol) and potassium carbonate (48 mg, 0.347 mmol) in DMF (2 mL) was stirred at 100 °C under nitrogen for 15 h. EtOAc (10 mL) was added to the reaction mixture which was washed with 10% LiCl (aq) (10 mL). The aqueous layer was extracted with EtOAc (10 mL), the organic layers combined and passed through a hydrophobic frit. The solvent removed by rotary evaporation and the residue was dissolved in the minimum volume of MeOH. The solution was applied to a MeOH preconditioned 5 g SCX-2 cartridge. The cartridge was washed with MeOH (30 mL) followed by 2 M ammonia in MeOH solution (30 mL). The basic wash was evaporated *in vacuo* to give a light brown gum. The gum was dissolved in MeOH (1.5 mL) and 4 M HCl in 1,4-dioxane solution (1 mL, 0.241 mmol) added. The mixture was left to stir at r.t. for 1.5 h. The reaction mixture was evaporated by rotary evaporation and the crude product was dissolved in 1:1 DMSO:MeOH and purified by MDAP using Method HpH.

Product was not collected and so the waste was evaporated. The residue was dissolved in 1:1 DMSO:MeOH and the mixture purified by MDAP using Method HpH. The appropriate fractions were combined and the solvent was removed by rotary evaporation to give the title compound as a light brown oil which solidified upon standing (65 mg, 0.133 mmol, 55%).

LCMS (HpH): m/z 490 [(M + H)⁺]; Rt: 0.73 min; 100% purity by peak area.

¹H NMR (400 MHz, DMSO-*d*₆): Variable temperature (393 K) δ 8.76 (s, 1 H), 8.60 (d, J = 4.8 Hz, 1 H), 7.77 (s, 1 H), 7.76–7.71 (m, 1 H), 7.42 (d, J = 8.1 Hz, 1 H), 7.28 (dd, J = 7.3, 4.8 Hz, 1 H), 7.06 (s, 1 H), 6.30 (q, J = 7.3 Hz, 1 H), 4.35 (d, J = 4.8 Hz, 1 H), 4.13 (t, J = 5.2 Hz, 1 H), 3.86 (dd, J = 9.9, 4.2 Hz, 1 H), 3.74 (dddd, J = 5.8, 5.5, 4.8, 4.2 Hz, 1 H), 3.58 (s, 3 H), 3.50 (dd, J = 9.9, 5.8 Hz, 1 H), 3.39 (dd, J = 5.5, 5.2 Hz, 2 H), 2.26 (s, 3 H), 2.07 (s, 3 H), 2.05 (d, J = 7.3 Hz, 3 H). Only a single diastereoisomer was observed.

(S)-(2,2-Dimethyl-1,3-dioxolan-4-yl)methyl methanesulfonate



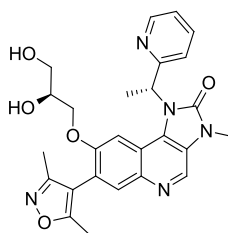
253

A stirred solution of (*S*)-(2,2-dimethyl-1,3-dioxolan-4-yl)methanol (0.43 mL, 3.46 mmol) and triethylamine (1.2 mL, 8.64 mmol) in DCM (6 mL) at 0 °C was treated with methanesulfonyl chloride (0.32 mL, 4.11 mmol). The mixture was stirred under nitrogen for 10 min and then allowed to warm to r.t. over 4 h. The reaction mixture was diluted with EtOAc (10 mL) and the solution washed with brine (10 mL). The aqueous layer was extracted with EtOAc (10 mL), the organic layers combined and washed with sat. NaHCO₃ (aq) (5 mL) then with brine/water (1:1, 2 x 5 mL). The organic layer was passed through a hydrophobic frit and the solvent removed by rotary evaporation. The residue was loaded in DCM (2 mL) and purified on a 25 g silica cartridge using a gradient of 0–100% EtOAc in cyclohexane over 12 column volumes. The appropriate fractions were combined and the solvent removed by rotary evaporation to give the title compound as a colourless oil (645 mg, 3.07 mmol, 89%).

¹H NMR (400 MHz, CDCl₃): δ 4.37 (m, 1 H), 4.23 (d, J = 5.2 Hz, 2 H), 4.11 (dd, J = 8.8 Hz, 6.5 Hz, 1 H), 3.83 (dd, J = 8.8 Hz, 5.5 Hz, 1 H), 3.06 (s, 3 H), 1.45 (s, 3 H), 1.37 (s, 3 H).

The ¹H NMR was identical to that of the enantiomer, compound **252**.¹⁴⁵

8-[(S)-2,3-Dihydroxypropoxy]-7-(3,5-dimethylisoxazol-4-yl)-3-methyl-1-[(R)-1-(pyridin-2-yl)ethyl]-1H-imidazo[4,5-c]quinolin-2(3H)-one



257

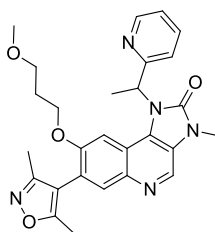
A mixture of 7-(3,5-dimethylisoxazol-4-yl)-8-hydroxy-3-methyl-1-[(R)-1-(pyridin-2-yl)ethyl]-1H-imidazo[4,5-c]quinolin-2(3H)-one **237** (100 mg, 0.241 mmol), (S)-(2,2-dimethyl-1,3-dioxolan-4-yl)methyl methanesulfonate **253** (67 mg, 0.319 mmol) and potassium carbonate (46 mg, 0.333 mmol) in DMF (2 mL) was stirred at 100 °C under nitrogen for 5.5 h. Further (S)-(2,2-dimethyl-1,3-dioxolan-4-yl)methyl methanesulfonate **253** (51 mg) in DMF (0.5 mL) was added and the mixture was stirred at 100 °C under nitrogen for 16.5 h. The reaction mixture was diluted with EtOAc (15 mL) then washed with 10% LiCl (aq) (10 mL). The aqueous layer was extracted with EtOAc (10 mL) and the combined organic layers were passed through a hydrophobic frit. The solvent was removed by rotary evaporation and the residue dissolved in MeOH. The solution was applied to a MeOH preconditioned 5 g SCX-2 cartridge which was then washed with MeOH (30 mL) followed by 2 M ammonia in MeOH solution (30 mL). The basic wash was evaporated *in vacuo*, the residue dissolved in MeOH (3 mL) and 4 M HCl in 1,4-dioxane solution (1 mL, 0.241 mmol) added. The mixture was left to stir at r.t. for 3 h. The reaction mixture was diluted with DCM (10 mL) and washed with brine (10 mL). The aqueous layer was washed with DCM (10 mL), basicified to pH = 14 by the addition of 2 M NaOH (aq) and washed with DCM (10 mL). The aqueous layer was applied to a MeOH preconditioned 5 g SCX-2 cartridge which was then washed with MeOH (30 mL) followed by 2 M ammonia in MeOH solution (30 mL). The basic wash was combined with all organic extracts (after drying through hydrophobic frits) and the solvent removed by rotary evaporation. The residue was dissolved in a 1:1 mixture of DCM:MeOH and filtered. The filtrate was concentrated *in vacuo* and the residue purified by MDAP using Method HpH. The appropriate fractions were combined and dried under a stream of nitrogen. The sample was dissolved in EtOH (1 mL) and heptane (1 mL). One injection was made onto a Chiralcel® OD-H column (250 mm x 30 mm, 5 µm packing diameter). An isocratic system of 10% EtOH in heptane with a flow rate of 40 mL/min was used at r.t. The UV detection was performed at 240 nm. The appropriate

fractions were combined and evaporated *in vacuo* to give the title compound (25 mg, 0.051 mmol, 21%).

LCMS (HpH): m/z 490 [(M + H)⁺]; Rt: 0.73 min; 100% purity by peak area.

¹H NMR (400 MHz, DMSO-*d*₆): Variable temperature (393 K) δ 8.76 (s, 1 H), 8.60 (d, J = 4.8 Hz, 1 H), 7.77 (s, 1 H), 7.76–7.71 (m, 1 H), 7.42 (d, J = 8.1 Hz, 1 H), 7.28 (dd, J = 7.3, 4.8 Hz, 1 H), 7.05 (s, 1 H), 6.30 (q, J = 7.3 Hz, 1 H), 4.37 (d, J = 4.8 Hz, 1 H), 4.13 (t, J = 5.2 Hz, 1 H), 3.78 (dd, J = 9.5, 5.7 Hz, 1 H), 3.76–3.69 (m, 1 H), 3.58 (s, 3 H), 3.57–3.54 (m, 1 H), 3.41–3.36 (m, 2 H), 2.26 (s, 3 H), 2.07 (s, 3 H), 2.05 (d, J = 7.3 Hz, 3 H). Only a single diastereoisomer was observed.

7-(3,5-Dimethylisoxazol-4-yl)-8-(3-methoxypropoxy)-3-methyl-1-[1-(pyridin-2-yl)ethyl]-1*H*-imidazo[4,5-*c*]quinolin-2(3*H*)-one



258

A solution of 7-(3,5-dimethylisoxazol-4-yl)-8-hydroxy-3-methyl-1-[(*R*)-1-(pyridin-2-yl)ethyl]-1*H*-imidazo[4,5-*c*]quinolin-2(3*H*)-one **237** (270 mg, 0.65 mmol) in anhydrous DMF (4.5 mL) was dispensed evenly between 6 x vessels each containing potassium carbonate (18 mg, 0.13 mmol). To one of these vessels was added 1-bromo-3-methoxypropane **254** (20 mg, 0.13 mmol) and the mixture stirred under nitrogen at 100 °C for 16 h. The reaction mixture was evaporated under a stream of nitrogen and the crude material purified by MDAP using Method Formic. The appropriate fractions were combined and the solvent removed by rotary evaporation to give the title compound as an off-white solid (26 mg, 0.05 mmol, 49%).

m.p.: 110–112 °C.

IR (solid) ν (cm⁻¹): 2930, 1704, 1621, 1579, 1453 1216, 1036, 748.

LCMS (formic A): m/z 488 [(M + H)⁺]; Rt: 0.79 min; 100% purity by peak area.

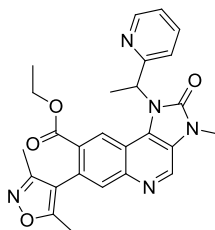
HRMS (ESI): M + H calcd for C₂₇H₃₀N₅O₄ 488.2292, found 488.2289.

¹H NMR (400 MHz, CDCl₃): δ 8.70–8.62 (m, 2 H), 7.82 (s, 1 H), 7.67–7.57 (m, 1 H), 7.35 (br s, 1 H), 7.23 (dd, J = 7.3, 5.1 Hz, 1 H), 6.93 (br s, 1 H), 6.50–6.37 (m, 1 H), 3.95–3.84 (m, 1 H), 3.70 (s, 3 H), 3.46–3.39 (m, 2 H), 3.34 (s, 3 H), 3.41 (br s, 1 H), 2.30 (s, 3 H), 2.15

(s, 3 H), 2.13 (d, $J = 7.3$ Hz, 3 H), 1.99–1.90 (m, 2 H). Broad signals observed due to restricted rotation.

^{13}C NMR (100 MHz, $\text{DMSO-}d_6$): δ 166.2, 154.9, 154.5, 149.4, 140.9, 137.2, 133.2, 130.4, 128.2, 123.9, 122.6, 122.0, 121.4, 115.9, 112.5, 101.9, 68.9, 65.7, 58.7, 53.8, 29.4, 27.9, 11.7, 10.8.

Ethyl 7-(3,5-dimethylisoxazol-4-yl)-3-methyl-2-oxo-1-[1-(pyridin-2-yl)ethyl]-2,3-dihydro-1H-imidazo[4,5-c]quinoline-8-carboxylate



266

A 100 mL 3-necked flask was charged with palladium diacetate (15 mg, 0.07 mmol), 1,3-bis(diphenylphosphino)propane (27 mg, 0.07 mmol), 7-(3,5-dimethylisoxazol-4-yl)-3-methyl-2-oxo-1-[1-(pyridin-2-yl)ethyl]-2,3-dihydro-1H-imidazo[4,5-c]quinolin-8-yl trifluoromethanesulfonate **265** (500 mg, 0.91 mmol), anhydrous DMF (10 mL), EtOH (8 mL, 137 mmol) and triethylamine (0.28 mL, 2.01 mmol). The flask was fitted with a reflux condenser and the apparatus purged with CO gas. A balloon of CO gas was fitted to the top of the condenser and the mixture stirred at 70 °C for 3 h. The reaction mixture was evaporated *in vacuo* and the resulting gum dissolved in EtOAc (10 mL). The organic layer was washed with 10% LiCl (aq) (10 mL) and then water (2 x 10 mL). The organic layer was passed through a hydrophobic frit and the solvent evaporated *in vacuo*. The crude material was purified on a 100 g silica cartridge using a gradient of 0–15% MeOH in DCM over 12 column volumes. The appropriate fractions were combined and the solvent evaporated *in vacuo* to give the title compound as a light yellow foam (430 mg, 0.91 mmol, 100%).

m.p.: 90–92 °C.

IR (solid) ν (cm^{-1}): 2983, 1707, 1575, 1432, 1251, 1097, 1035, 748.

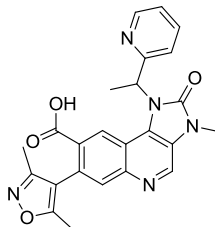
LCMS (formic A): m/z 472 [(M + H) $^+$]; Rt: 0.87 min; 94% purity by peak area.

HRMS (ESI): M + H calcd for $\text{C}_{26}\text{H}_{26}\text{N}_5\text{O}_4$ 472.1979, found 472.1972.

^1H NMR (400 MHz, $\text{DMSO-}d_6$): δ 9.12 (s, 1 H), 8.54 (d, $J = 4.8$ Hz, 1 H), 8.15 (br s, 1 H), 7.91 (s, 1 H), 7.78 (dd, $J = 7.8, 7.3$ Hz, 1 H), 7.47 (d, $J = 7.8$ Hz, 1 H), 7.31 (dd, $J = 7.3, 4.8$ Hz, 1 H), 6.33 (q, $J = 7.3$ Hz, 1 H), 4.19–4.05 (m, 2 H), 3.30 (s, 3 H), 2.20 (s, 3 H), 2.05 (d, $J = 7.3$ Hz, 3 H), 1.96 (s, 3 H), 1.18 (t, $J = 7.1$ Hz, 3 H).

^{13}C NMR (100 MHz, $\text{DMSO-}d_6$): δ 164.6, 163.3, 158.2, 158.5, 153.6, 149.2, 145.0, 137.3, 135.8, 133.7, 133.5, 129.0, 126.5, 126.3, 124.2, 122.6, 120.9, 115.2, 113.4, 60.9, 54.9, 27.8, 17.1, 13.8, 10.9, 10.0.

7-(3,5-Dimethylisoxazol-4-yl)-3-methyl-2-oxo-1-[1-(pyridin-2-yl)ethyl]-2,3-dihydro-1H-imidazo[4,5-c]quinoline-8-carboxylic acid



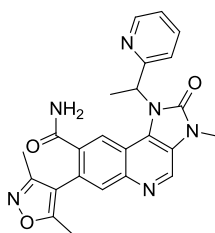
267

A solution of ethyl 7-(3,5-dimethylisoxazol-4-yl)-3-methyl-2-oxo-1-[1-(pyridin-2-yl)ethyl]-2,3-dihydro-1H-imidazo[4,5-c]quinoline-8-carboxylate **266** (300 mg, 0.64 mmol) in EtOH (2 mL) was treated with 2 M NaOH (aq) (0.33 mL, 0.66 mmol) and the reaction mixture stirred at r.t. for 15 h. Further 2 M NaOH (aq) (0.150 mL) was added and the mixture stirred at 50 °C for 3 h. The reaction mixture was evaporated *in vacuo* and the crude material purified by MDAP using Method Formic. The appropriate fractions were combined and the solvent removed by rotary evaporation to give the title compound (0.5 mol ratio formic acid salt) as an off-white solid (191 mg, 0.41 mmol, 64%).

LCMS (formic A): m/z 444 $[(M + H)^+]$; Rt: 0.61 min; 99% purity by peak area.

^1H NMR (400 MHz, $\text{DMSO-}d_6$): Variable temperature (353 K) δ 9.04 (s, 1 H), 8.52 (d, $J = 4.8$ Hz, 1 H), 8.30 (s, 1 H), 8.14 (s, 0.5 H), 7.85 (s, 1 H), 7.74 (dd, $J = 7.8, 7.3$ Hz, 1 H), 7.44 (d, $J = 7.8$ Hz, 1 H), 7.28 (dd, $J = 7.3, 4.8$ Hz, 1 H), 6.33 (q, $J = 7.3$ Hz, 1 H), 3.63 (s, 3 H), 2.21 (s, 3 H), 2.07 (d, $J = 7.3$ Hz, 3 H), 1.99 (s, 3 H).

7-(3,5-Dimethylisoxazol-4-yl)-3-methyl-2-oxo-1-[1-(pyridin-2-yl)ethyl]-2,3-dihydro-1H-imidazo[4,5-c]quinoline-8-carboxamide



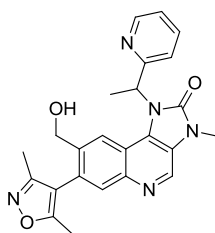
268

A mixture of 7-(3,5-dimethylisoxazol-4-yl)-3-methyl-2-oxo-1-[1-(pyridin-2-yl)ethyl]-2,3-dihydro-1H-imidazo[4,5-c]quinoline-8-carboxylic acid **267** (36 mg, 0.08 mmol) and HATU (40 mg, 0.11 mmol) was suspended in anhydrous DMF (0.5 mL) and DIPEA (0.043 mL, 0.24 mmol) added. A solution formed which was allowed to stand in a stoppered vessel at r.t. for 15 min. Ammonia in 1,4-dioxane solution (0.5 M, 1.0 mL, 0.50 mmol) was added to the reaction mixture and left to stand for 1 h. The reaction mixture was partially evaporated under a stream of nitrogen (until ~0.5 mL was remaining) and purified by MDAP using Method Formic. The appropriate fractions were combined and the solvent evaporated *in vacuo*. The residue was dissolved in MeOH (0.5 mL) and was applied to a MeOH preconditioned 0.5 g NH₂ cartridge. The cartridge was washed with MeOH (3 mL), and the solvent evaporated under a stream of nitrogen to give the title compound as an off-white solid (17 mg, 0.04 mmol, 47%).

LCMS (formic A): m/z 443 [(M + H)⁺]; Rt: 0.54 min; 100% purity by peak area.

¹H NMR (400 MHz, DMSO-*d*₆): δ 9.03 (s, 1 H), 8.53 (d, J = 4.8 Hz, 1 H), 7.87 (s, 1 H), 7.91 (br s, 1 H), 7.77 (dd, J = 7.8, 7.3 Hz, 1 H), 7.54 (br s, 1 H), 7.46 (d, J = 7.8 Hz, 1 H), 7.34–7.24 (m, 2 H), 6.36 (q, J = 7.3 Hz, 1 H), 3.60 (s, 3 H), 2.25 (s, 3 H), 2.07 (s, 3 H), 2.07 (d, J = 7.3 Hz, 3 H).

7-(3,5-Dimethylisoxazol-4-yl)-8-(hydroxymethyl)-3-methyl-1-[1-(pyridin-2-yl)ethyl]-1H-imidazo[4,5-c]quinolin-2(3H)-one



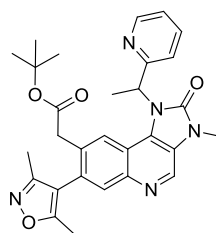
269

A vacuum oven dried 25 mL 3-necked flask under nitrogen was charged with a solution of ethyl 7-(3,5-dimethylisoxazol-4-yl)-3-methyl-2-oxo-1-[1-(pyridin-2-yl)ethyl]-2,3-dihydro-1H-imidazo[4,5-c]quinoline-8-carboxylate **266** (40 mg, 0.09 mmol) in anhydrous THF (1 mL) and the flask evacuated and purged with nitrogen (x 3). The solution was cooled to $-78\text{ }^{\circ}\text{C}$ and DIBAL-H (1 M solution in DCM, 0.13 mL, 0.13 mmol) was added dropwise. The reaction was stirred at this temperature for 30 min then allowed to warm to r.t. over 1 h. The reaction mixture was cooled to $-78\text{ }^{\circ}\text{C}$ and further DIBAL-H (1 M solution in DCM, 0.39 mL, 0.39 mmol) was added dropwise. The reaction mixture was stirred at this temperature for 30 min then allowed to warm to r.t. over 1 h. The reaction mixture was quenched by the addition of sat. Rochelle's salt (aq) (5 mL). The mixture was diluted with EtOAc (5 mL) and the layers allowed to separate. The organic layer was washed with water (2 x 5 mL), separated and passed through a hydrophobic frit. The solvent was evaporated under reduced pressure and the crude material purified by MDAP using Method Formic. The appropriate fractions were combined and the solvent removed by rotary evaporation. The residue was dissolved in MeOH (0.5 mL) and applied to a MeOH preconditioned 0.5 g SCX-2 cartridge. The cartridge was washed with MeOH (3 mL) followed by 2 M ammonia in MeOH solution (3 mL). The basic wash was evaporated under a stream of nitrogen to give the title compound as a light yellow gum (11 mg, 0.03 mmol, 30%).

LCMS (formic A): m/z 430 $[(M + H)^+]$; Rt: 0.58 min; 99% purity by peak area.

^1H NMR (400 MHz, DMSO- d_6): Variable temperature (353 K) δ 8.92 (s, 1 H), 8.54 (d, $J = 4.8$ Hz, 1 H), 7.94 (s, 1 H), 7.77 (s, 1 H), 7.76–7.72 (m, 1 H), 7.44 (d, $J = 8.1$ Hz, 1 H), 7.27 (dd, $J = 7.4, 4.8$ Hz, 1 H), 6.35 (q, $J = 7.2$ Hz, 1 H), 4.26 (d, $J = 13.6$ Hz, 1 H), 4.20 (d, $J = 13.6$ Hz, 1 H), 3.59 (s, 3 H), 2.20 (s, 3 H), 2.08 (d, $J = 7.2$ Hz, 3 H), 2.00 (s, 3 H). OH signal not resolved.

***tert*-Butyl 2-{7-(3,5-dimethylisoxazol-4-yl)-3-methyl-2-oxo-1-[1-(pyridin-2-yl)ethyl]-2,3-dihydro-1*H*-imidazo[4,5-*c*]quinolin-8-yl}acetate**



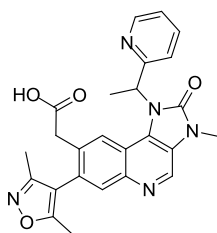
270

To a mixture of 7-(3,5-dimethylisoxazol-4-yl)-3-methyl-2-oxo-1-[1-(pyridin-2-yl)ethyl]-2,3-dihydro-1*H*-imidazo[4,5-*c*]quinolin-8-yl trifluoromethanesulfonate **265** (250 mg, 0.457 mmol) and palladium tetrakis (53 mg, 0.046 mmol) in a sealed vessel under nitrogen was added anhydrous NMP (0.5 mL) and [2-(*tert*-butoxy)-2-oxoethyl]zinc(II) chloride (0.5 M solution in THF, 2.5 mL, 1.250 mmol). The mixture was heated in a Biotage I60 microwave at 90 °C for 20 min (FHT: on, absorbance: high, cooling: off). The reaction mixture was diluted with sat. NH₄Cl (aq) (2 mL) and extracted with EtOAc (3 x 2 mL). The organic extracts were combined and passed through a hydrophobic frit. The solvent was removed *in vacuo*, the residue loaded in DCM (2 mL) and purified on a 100 g silica cartridge using a gradient of 0–100% acetone in cyclohexane over 12 column volumes. The appropriate fractions were combined and the solvent removed by rotary evaporation. The solid was purified by MDAP using Method HpH. The appropriate fractions were combined and the solvent removed by rotary evaporation to give the title compound as an off-white solid (39 mg, 0.076 mmol, 17%).

LCMS (formic A): m/z 514 [(M + H)⁺]; Rt: 0.91 min; 100% purity by peak area.

¹H NMR (400 MHz, DMSO-*d*₆): Variable temperature (393 K) 8.92 (s, 1 H), 8.56 (d, *J* = 4.8 Hz, 1 H), 7.81 (s, 1 H), 7.78 (s, 1 H), 7.77–7.72 (m, 1 H), 7.44 (d, *J* = 7.8 Hz, 1 H), 7.27 (dd, *J* = 7.8, 4.8 Hz, 1 H), 6.35 (q, *J* = 7.2 Hz, 1 H), 3.60 (s, 3 H), 3.36 (br s, 2 H), 2.20 (s, 3 H), 2.08 (d, *J* = 7.2 Hz, 3 H), 2.01 (s, 3 H), 1.32 (s, 9 H).

2-{7-(3,5-Dimethylisoxazol-4-yl)-3-methyl-2-oxo-1-[1-(pyridin-2-yl)ethyl]-2,3-dihydro-1H-imidazo[4,5-c]quinolin-8-yl}acetic acid



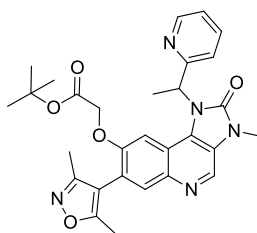
271

A solution of *tert*-butyl 2-{7-(3,5-dimethylisoxazol-4-yl)-3-methyl-2-oxo-1-[1-(pyridin-2-yl)ethyl]-2,3-dihydro-1H-imidazo[4,5-c]quinolin-8-yl}acetate **270** (35 mg, 0.068 mmol) in DCM (0.5 mL) was treated with TFA (0.5 mL, 6.49 mmol) and the mixture left to stand at r.t. in a stoppered vessel for 36 h. The reaction mixture was evaporated under a stream of nitrogen and was purified by MDAP using Method TFA. The appropriate fractions were combined and the solvent evaporated under a stream of nitrogen. The solid was dissolved in MeOH (0.5 mL) and applied to MeOH preconditioned 0.5 g SCX-2 cartridge. The cartridge was washed with MeOH (3 mL) followed by 2 M ammonia in MeOH solution (3 mL). The basic wash was evaporated under a stream of nitrogen to give the title compound as an off white solid (11 mg, 0.024 mmol, 35%).

LCMS (formic A): m/z 458 [(M + H)⁺]; Rt: 0.59 min; 97% purity by peak area.

¹H NMR (400 MHz, DMSO-*d*₆): Variable temperature (393 K) δ 8.94–8.88 (m, 1 H), 8.56 (d, J = 4.8 Hz, 1 H), 7.81–7.77 (m, 2 H), 7.77–7.71 (m, 1 H), 7.44 (d, J = 8.1 Hz, 1 H), 7.27 (dd, J = 7.3, 4.8 Hz, 1 H), 6.35 (q, J = 7.2 Hz, 1 H), 3.60 (s, 3 H), 3.42–3.30 (m, 2 H), 2.19 (s, 3 H), 2.08 (d, J = 7.2 Hz, 3 H), 2.00 (s, 3 H).

***tert*-Butyl 2-({7-(3,5-dimethylisoxazol-4-yl)-3-methyl-2-oxo-1-[1-(pyridin-2-yl)ethyl]-2,3-dihydro-1H-imidazo[4,5-c]quinolin-8-yl}oxy)acetate**



272

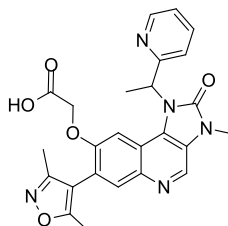
A mixture of 7-(3,5-dimethylisoxazol-4-yl)-8-hydroxy-3-methyl-1-[(*R*)-1-(pyridin-2-yl)ethyl]-1H-imidazo[4,5-c]quinolin-2(3H)-one **237** (60 mg, 0.14 mmol) and potassium carbonate (24 mg, 0.17 mmol) was suspended in anhydrous DMF (1 mL) and treated with

tert-butyl bromoacetate (0.026 mL, 0.17 mmol). The mixture was stirred under nitrogen at 100 °C for 5 h. The reaction mixture was allowed to cool to r.t. and partially evaporated under a stream of nitrogen (~ 0.9 mL remaining). The mixture was filtered and purified by MDAP using Method Formic. The appropriate fractions were combined and the solvent removed by rotary evaporation. The solid was dissolved in MeOH (0.5 mL) and applied to a MeOH preconditioned 1 g SCX-2 cartridge. The cartridge was washed with MeOH (3 mL) followed by 2 M ammonia in MeOH solution (3 mL). The basic wash was evaporated under a stream of nitrogen to give the title compound as a light brown solid (37 mg, 0.07 mmol, 48%).

LCMS (formic A): m/z 530 [(M + H)⁺]; Rt: 0.96 min; 100% purity by peak area.

¹H NMR (400 MHz, DMSO-*d*₆): Variable temperature (393 K) δ 8.80 (s, 1 H), 8.62 (d, *J* = 4.8 Hz, 1 H), 7.85 (s, 1 H), 7.80–7.74 (m, 1 H), 7.46 (d, *J* = 8.1 Hz, 1 H), 7.33 (dd, *J* = 7.3, 4.8 Hz, 1 H), 7.15 (s, 1 H), 6.29 (q, *J* = 7.2 Hz, 1 H), 4.43–4.31 (m, 2 H), 3.59 (s, 3 H), 2.30 (s, 3 H), 2.13 (s, 3 H), 2.06 (d, *J* = 7.2 Hz, 3 H), 1.47 (s, 9 H).

2-({7-(3,5-Dimethylisoxazol-4-yl)-3-methyl-2-oxo-1-[1-(pyridin-2-yl)ethyl]-2,3-dihydro-1*H*-imidazo[4,5-*c*]quinolin-8-yl}oxy)acetic acid



273

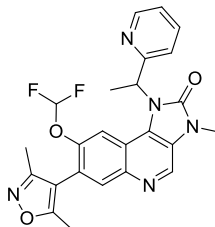
A solution of *tert*-butyl 2-({7-(3,5-dimethylisoxazol-4-yl)-3-methyl-2-oxo-1-[1-(pyridin-2-yl)ethyl]-2,3-dihydro-1*H*-imidazo[4,5-*c*]quinolin-8-yl}oxy)acetate **272** (29 mg, 0.06 mmol) in DCM (0.75 mL) was treated with TFA (0.5 mL, 6.49 mmol) and left to stand in a stoppered vessel for 2 h. The reaction mixture was evaporated *in vacuo*. The solid was dissolved in MeOH (0.5 mL) and applied to MeOH preconditioned 0.5 g SCX-2 cartridge. The cartridge was washed with MeOH (3 mL) followed by 2 M ammonia in MeOH solution (3 mL). The basic wash was evaporated under a stream of nitrogen to give the title compound as an off-white solid (15 mg, 0.032 mmol, 58%).

LCMS (formic A): m/z 474 [(M + H)⁺]; Rt: 0.61 min; 94% purity by peak area.

¹H NMR (400 MHz, DMSO-*d*₆): Variable temperature (393 K) 8.79 (s, 1 H), 8.60 (d, *J* = 4.8 Hz, 1 H), 7.83 (s, 1 H), 7.80–7.73 (m, 1 H), 7.46 (d, *J* = 8.1 Hz, 1 H), 7.30 (dd, *J* = 7.3, 4.8

Hz, 1H), 7.15 (s, 1 H), 6.31 (q, $J = 7.2$ Hz, 1 H), 4.44–4.34 (m, 2 H), 3.60 (s, 3 H), 2.31 (s, 3 H), 2.14 (s, 3 H), 2.07 (d, $J = 7.2$ Hz, 3 H). CO_2H signal not resolved.

8-(Difluoromethoxy)-7-(3,5-dimethylisoxazol-4-yl)-3-methyl-1-[1-(pyridin-2-yl)ethyl]-1H-imidazo[4,5-c]quinolin-2(3H)-one

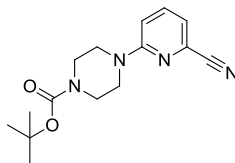


274

A stirred solution of 7-(3,5-dimethylisoxazol-4-yl)-8-hydroxy-3-methyl-1-[(*R*)-1-(pyridin-2-yl)ethyl]-1H-imidazo[4,5-*c*]quinolin-2(3H)-one **237** (100 mg, 0.24 mmol) and potassium hydroxide (270 mg, 4.81 mmol) in acetonitrile (1 mL) and water (1 mL) was cooled to -78 °C and treated with diethyl (bromodifluoromethyl)phosphonate (0.171 mL, 0.96 mmol). The mixture was allowed to warm to r.t. over 3 h. The reaction mixture was diluted with brine (10 mL) and extracted with EtOAc (2 x 10 mL). The organic layers were combined, passed through a hydrophobic frit and the solvent evaporated *in vacuo*. The crude material was purified on a 50 g silica cartridge using a gradient of 0–15% MeOH in DCM over 10 column volumes. The appropriate fractions were combined and the solvent evaporated *in vacuo*. The crude material was purified by MDAP using Method Formic. The appropriate fractions were combined and the solvent removed by rotary evaporation. The residue was dissolved in MeOH (0.5 mL) and applied to a MeOH preconditioned 0.5 g NH_2 cartridge. The cartridge was washed with MeOH (3 mL) and the solvent removed under a stream of nitrogen to give the title compound as an off-white solid (15 mg, 0.03 mmol, 13%).

LCMS (formic A): m/z 466 [$(\text{M} + \text{H})^+$]; Rt: 0.89 min; 100% purity by peak area.

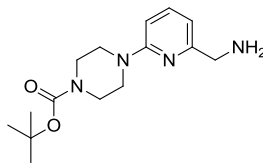
^1H NMR (400 MHz, CDCl_3): δ 8.77 (s, 1 H), 8.65 (dd, $J = 4.8, 1.6$ Hz, 1 H), 7.94 (s, 1 H), 7.66 (ddd, $J = 7.6, 7.4, 1.6$ Hz, 1 H), 7.50 (br s, 1 H), 7.38 (d, $J = 7.6$ Hz, 1 H), 7.24 (dd, $J = 7.4, 4.8$ Hz, 1 H), 6.43 (q, $J = 7.2$ Hz, 1 H), 6.30 (t, $J = 7.3$ Hz, 1 H), 3.71 (s, 3 H), 2.32 (s, 3 H), 2.18 (s, 3 H), 2.12 (d, $J = 7.2$ Hz, 3 H).

***tert*-Butyl 4-(6-cyanopyridin-2-yl)piperazine-1-carboxylate****277a**

A mixture of 6-chloropicolinonitrile **275** (1 g, 7.22 mmol), potassium carbonate (1.3 g, 9.41 mmol) and *tert*-butyl 1-piperazinecarboxylate (1.7 g, 9.13 mmol) was suspended in anhydrous DMF (15 mL) and stirred under nitrogen at 100 °C for 15 h. The reaction mixture was allowed to cool to r.t., diluted with EtOAc (50 mL) and washed sequentially with water (2 x 50 mL) and 10% LiCl (aq) (50 mL). The organic layer was separated, passed through a hydrophobic frit and the solvent evaporated *in vacuo*. The crude material was purified on a 100 g silica cartridge using a gradient of 0–100% EtOAc in cyclohexane over 10 column volumes. The appropriate fractions were combined and the solvent removed by rotary evaporation to give the title compound as a white solid (1.75 g, 6.07 mmol, 84%).

LCMS (formic A): m/z 289 [(M + H)⁺]; Rt: 1.13 min; 97% purity by peak area.

¹H NMR (400 MHz, CDCl₃): δ 7.53 (dd, J = 8.8, 7.1 Hz, 1 H), 6.99 (d, J = 7.1 Hz, 1 H), 6.81 (d, J = 8.8 Hz, 1 H), 3.61–3.51 (m, 8 H), 1.49 (s, 9 H).

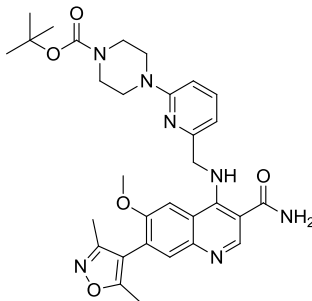
***tert*-Butyl 4-[6-(aminomethyl)pyridin-2-yl]piperazine-1-carboxylate****278a**

A solution of *tert*-butyl 4-(6-cyanopyridin-2-yl)piperazine-1-carboxylate **277a** (1.72 g, 5.96 mmol) in MeOH (80 mL) was hydrogenated over 5% Pd/C (CatCart 30) at 70 °C using an H-cube (50 bar, 1 mL/min flow rate). The eluent was evaporated *in vacuo* and the oil dissolved in MeOH (10 mL). The solution was applied to a MeOH preconditioned 70 g SCX-2 cartridge. The cartridge was washed with MeOH (200 mL) followed by 2 M ammonia in MeOH solution (200 mL). The basic wash was evaporated *in vacuo* and the oil purified on a 100 g silica cartridge using a gradient of 0–15% 2 M ammonia/MeOH in DCM over 10 column volumes. The appropriate fractions were combined and the solvent removed by rotary evaporation to give the title compound as a yellow oil (607 mg, 2.08 mmol, 35%).

LCMS (formic A): m/z 293 [(M + H)⁺]; Rt: 0.67 min; 92% purity by peak area.

^1H NMR (400 MHz, CDCl_3): δ 7.45 (dd, $J = 8.4, 7.2$ Hz, 1 H), 6.58 (d, $J = 7.1$ Hz, 1 H), 6.50 (d, $J = 8.6$ Hz, 1 H), 3.80 (s, 2 H), 3.54 (s, 8 H), 1.49 (s, 9 H). NH_2 signal not resolved.

***tert*-Butyl 4-[6-([3-carbamoyl-7-(3,5-dimethylisoxazol-4-yl)-6-methoxyquinolin-4-yl]amino)methyl]pyridin-2-yl]piperazine-1-carboxylate**



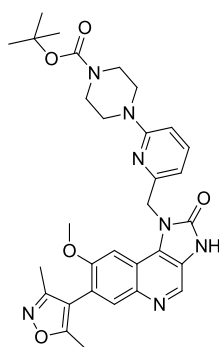
279a

A mixture of *tert*-butyl 4-[6-(aminomethyl)pyridin-2-yl]piperazine-1-carboxylate **278a** (190 mg, 0.65 mmol) and 4-chloro-7-(3,5-dimethylisoxazol-4-yl)-6-methoxyquinoline-3-carboxamide **239** (200 mg, 0.60 mmol) in anhydrous NMP (2 mL) and DIPEA (125 μL , 0.72 mmol) was stirred at 100 $^\circ\text{C}$ under nitrogen for 15 h. The reaction mixture was allowed to cool to r.t. and applied to a MeOH preconditioned 5 g SCX-2 cartridge. The cartridge was washed with MeOH (30 mL) followed by 2 M ammonia in MeOH solution (30 mL). The basic wash was evaporated *in vacuo* and the crude material purified on a 100 g silica cartridge using a gradient of 0–15% 2 M ammonia/MeOH in DCM over 10 column volumes. The appropriate fractions were combined and the solvent removed by rotary evaporation to give the title compound as a yellow gum (240 mg, 0.41 mmol, 68%).

LCMS (formic A): m/z 588 $[(\text{M} + \text{H})^+]$; Rt: 0.98 min; 93% purity by peak area.

^1H NMR (400 MHz, CDCl_3): δ 9.57 (t, $J = 6.1$ Hz, 1 H), 8.67 (s, 1 H), 7.71 (s, 1 H), 7.52 (dd, $J = 8.6, 7.1$ Hz, 1 H), 7.48 (s, 1 H), 6.84 (d, $J = 7.1$ Hz, 1 H), 6.56 (d, $J = 8.6$ Hz, 1 H), 5.90 (br s, 2 H), 4.89 (d, $J = 6.1$ Hz, 2 H), 3.62 (s, 3 H), 3.61–3.51 (m, 8 H), 2.34 (s, 3 H), 2.19 (s, 3 H), 1.49 (s, 9 H).

***tert*-Butyl 4-(6-([7-(3,5-dimethylisoxazol-4-yl)-8-methoxy-2-oxo-2,3-dihydro-1*H*-imidazo[4,5-*c*]quinolin-1-yl)methyl)pyridin-2-yl)piperazine-1-carboxylate**



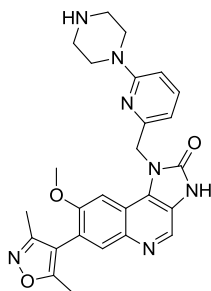
280a

A solution of *tert*-butyl 4-[6-([3-carbamoyl-7-(3,5-dimethylisoxazol-4-yl)-6-methoxyquinolin-4-yl]amino)methyl]pyridin-2-yl]piperazine-1-carboxylate **279a** (235 mg, 0.40 mmol) in MeOH (4 mL) was treated with potassium hydroxide (34 mg, 0.61 mmol) followed by iodobenzene diacetate (167 mg, 0.52 mmol). The mixture was stirred at r.t. in a stoppered vessel for 15 h. The reaction mixture was evaporated *in vacuo* and the resulting gum purified by MDAP using Method HpH. The appropriate fractions were combined and the solvent removed by rotary evaporation to give the title compound as a yellow gum (154 mg, 0.26 mmol, 66%).

LCMS (HpH): m/z 586 [(M + H)⁺]; Rt: 1.09 min; 100% purity by peak area.

¹H NMR (400 MHz, CDCl₃): δ 8.74 (s, 1 H), 7.85 (s, 1 H), 7.50–7.40 (m, 1 H), 7.30–7.28 (m, 1 H), 6.57–6.53 (m, 2 H), 5.57 (s, 2 H), 3.64 (s, 3 H), 3.45 (s, 8 H), 2.32 (s, 3 H), 2.16 (s, 3 H), 1.48 (s, 9 H). NH signal not resolved.

7-(3,5-Dimethylisoxazol-4-yl)-8-methoxy-1-[[6-(piperazin-1-yl)pyridin-2-yl]methyl]-1*H*-imidazo[4,5-*c*]quinolin-2(3*H*)-one



281a

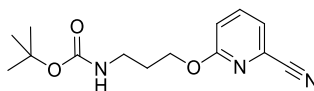
A solution of *tert*-butyl 4-(6-([7-(3,5-dimethylisoxazol-4-yl)-8-methoxy-2-oxo-2,3-dihydro-1*H*-imidazo[4,5-*c*]quinolin-1-yl)methyl)pyridin-2-yl)piperazine-1-carboxylate **280a**

(100 mg, 0.17 mmol) was dissolved in DCM (1.5 mL) and treated with TFA (0.75 mL, 9.73 mmol). The mixture was allowed to stand in a stoppered vessel at r.t. for 2 h. The reaction mixture was evaporated *in vacuo* and the crude material purified by MDAP using Method HpH. The appropriate fractions were combined and the solvent removed by rotary evaporation to give the title compound as a white solid (48 mg, 0.10 mmol, 58%).

LCMS (formic A): m/z 486 $[(M + H)^+]$; Rt: 0.57 min; 100% purity by peak area.

^1H NMR (400 MHz, DMSO- d_6): δ 8.60 (s, 1 H), 7.79 (s, 1 H), 7.46 (dd, $J = 8.6, 7.3$ Hz, 1 H), 7.29 (s, 1 H), 6.65 (d, $J = 8.6$ Hz, 1 H), 6.47 (d, $J = 7.3$ Hz, 1 H), 5.44 (s, 2 H), 3.65 (s, 3 H), 3.26–3.20 (m, 4 H), 2.64–2.57 (m, 4 H), 2.27 (s, 3 H), 2.06 (s, 3 H). Imidazoquinolinone and piperazine NH signals not resolved.

***tert*-Butyl {3-[(6-cyanopyridin-2-yl)oxy]propyl}carbamate**

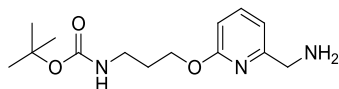


277b

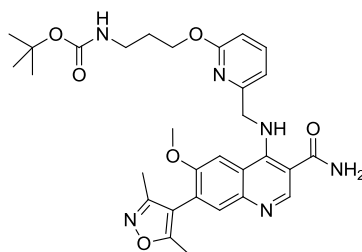
A stirred solution of *tert*-butyl (3-hydroxypropyl)carbamate (1.48 mL, 8.67 mmol) in NMP (15 mL) was treated with sodium hydride (60% dispersion in mineral oil, 0.35 g, 8.63 mmol) and the mixture stirred under nitrogen at 0 °C for 20 min. 6-Chloropicolinonitrile **275** (1.01 g, 7.25 mmol) was added and the mixture stirred at 60 °C for 18 h. The reaction was allowed to cool to r.t. and water (40 mL) added. The mixture was extracted with diethyl ether (40 mL), the phases separated and the organic phase washed with water (2 x 40 mL). The organic phase was dried with magnesium sulfate, filtered through a hydrophobic frit and the solvent evaporated *in vacuo*. The sample was dissolved in DCM and purified on a 50 g silica cartridge using a gradient of 0–25% EtOAc in cyclohexane. The appropriate fractions were combined and the solvent removed by rotary evaporation to give the title compound as a pale yellow gum (296 mg, 1.01 mmol, 14%).

LCMS (formic A): m/z 278 $[(M + H)^+]$; Rt: 1.04 min; 98% purity by peak area.

^1H NMR (400 MHz, CDCl₃): δ 7.65 (dd, $J = 8.6, 7.3$ Hz, 1 H), 7.29 (d, $J = 7.3$ Hz, 1 H), 6.95 (d, $J = 8.6$ Hz, 1 H), 4.69 (d, $J = 4.5$ Hz, 1 H), 4.40 (t, $J = 6.2$ Hz, 2 H), 3.33–3.24 (m, 2 H), 2.01–1.92 (m, 2 H), 1.43 (s, 9 H).

***tert*-Butyl (3-[[6-(aminomethyl)pyridin-2-yl]oxy]propyl)carbamate****278b**

A solution of *tert*-butyl {3-[[6-(aminomethyl)pyridin-2-yl]oxy]propyl}carbamate **277b** (296 mg, 1.066 mmol) in MeOH (22 mL) was hydrogenated over 10% Pd/C (CatCart 30) at 70 °C using an H-cube (50 bar, 1 mL/min flow rate). The eluent was evaporated *in vacuo* to give the title compound as a yellow gum (302 mg) which was used without purification in the next step.

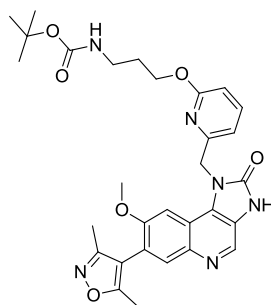
***tert*-Butyl (3-[[6-({[3-carbamoyl-7-(3,5-dimethylisoxazol-4-yl)-6-methoxyquinolin-4-yl]amino)methyl]pyridin-2-yl]oxy]propyl)carbamate****279b**

A mixture of *tert*-butyl (3-[[6-(aminomethyl)pyridin-2-yl]oxy]propyl)carbamate **278b** (299 mg, 1.061 mmol) and 4-chloro-7-(3,5-dimethylisoxazol-4-yl)-6-methoxyquinoline-3-carboxamide **239** (290 mg, 0.874 mmol) in anhydrous NMP (3 mL) and DIPEA (0.168 mL, 0.962 mmol) was stirred at 100 °C under nitrogen for 3.5 h. The reaction mixture was allowed to cool to r.t. and applied to a MeOH preconditioned 5 g SCX-2 cartridge. The cartridge was washed with MeOH (30 mL) followed by 2 M ammonia in MeOH solution (30 mL). The washes were combined and evaporated *in vacuo* to and the residue purified on a 100 g silica cartridge using 100% EtOAc. The appropriate fractions were combined and the solvent removed by rotary evaporation to give the title compound as a yellow glass (80 mg, 0.131 mmol, 15%).

LCMS (HpH): m/z 577 [(M + H)⁺]; Rt: 1.08 min; 100% purity by peak area.

¹H NMR (400 MHz, DMSO-*d*₆): δ 9.04 (br s, 1 H), 8.69 (s, 1 H), 7.70–7.62 (m, 3 H), 7.36 (br s, 2 H), 7.04 (d, J = 7.1 Hz, 1 H), 6.66 (d, J = 8.3 Hz, 1 H), 6.30 (br s, 1 H), 4.88 (d, J = 5.8 Hz, 2 H), 4.31 (t, J = 6.6 Hz, 2 H), 3.80 (s, 3 H), 3.09 (td, J = 6.3, 6.0 Hz, 2 H), 2.32 (s, 3 H), 2.13 (s, 3 H), 1.85 (tt, J = 6.6, 6.3 Hz, 2 H), 1.38 (s, 9 H).

***tert*-Butyl {3-[(6-[[7-(3,5-dimethylisoxazol-4-yl)-8-methoxy-2-oxo-2,3-dihydro-1*H*-imidazo[4,5-*c*]quinolin-1-yl]methyl]pyridin-2-yl)oxy]propyl}carbamate**



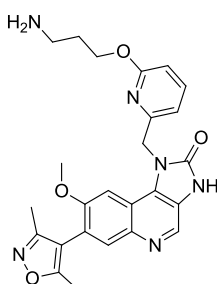
280b

A solution of *tert*-butyl (3-[[6-([3-carbamoyl-7-(3,5-dimethylisoxazol-4-yl)-6-methoxyquinolin-4-yl]amino)methyl]pyridin-2-yl]oxy)propyl)carbamate **279b** (78 mg, 0.138 mmol) in MeOH (1.2 mL) was treated with potassium hydroxide (12 mg, 0.219 mmol) followed by iodobenzene diacetate (58 mg, 0.181 mmol). The mixture was stirred at r.t. in a stoppered vessel for 1 h. The reaction mixture was evaporated under a stream of nitrogen and the residue purified by MDAP using Method HpH. The appropriate fractions were combined and the solvent evaporated under a stream of nitrogen to give the title compound as a yellow glass (60 mg, 0.099 mmol, 72%).

LCMS (HpH): m/z 575 [(M + H)⁺]; Rt: 1.05 min; 100% purity by peak area.

¹H NMR (400 MHz, CDCl₃): δ 9.85 (br s, 1 H), 8.73 (s, 1 H), 7.85 (s, 1 H), 7.54 (dd, $J = 8.1, 7.2$ Hz, 1 H), 7.22 (s, 1 H), 6.82 (d, $J = 7.2$ Hz, 1 H), 6.62 (d, $J = 8.1$ Hz, 1 H), 5.61 (s, 2 H), 4.80 (br s, 1 H), 4.15 (t, $J = 6.8$ Hz, 2 H), 3.66 (s, 3 H), 3.20 (td, $J = 6.8, 6.0$ Hz, 2 H), 2.31 (s, 3 H), 2.16 (s, 3 H), 1.83 (tt, $J = 6.8, 6.8$ Hz, 2 H), 1.47 (s, 9 H).

1-[[6-(3-Aminopropoxy)pyridin-2-yl]methyl]-7-(3,5-dimethylisoxazol-4-yl)-8-methoxy-1*H*-imidazo[4,5-*c*]quinolin-2(3*H*)-one



281b

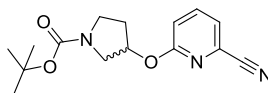
4 M HCl in 1,4-dioxane solution (1.5 mL, 6.00 mmol) was added to *tert*-butyl {3-[(6-[[7-(3,5-dimethylisoxazol-4-yl)-8-methoxy-2-oxo-2,3-dihydro-1*H*-imidazo[4,5-*c*]quinolin-

1-yl)methyl}pyridin-2-yl)oxy]propyl}carbamate **280b** (60 mg, 0.104 mmol) and the resulting mixture stirred in a stoppered vessel at r.t. for 3.25 h. The solvent was evaporated under a stream of nitrogen and the residue purified by MDAP using Method HpH. The appropriate fractions were combined and the solvent evaporated under a stream of nitrogen to give the title compound as a yellow glass (37 mg, 0.073 mmol, 71%).

LCMS (HpH): m/z 475 [(M + H)⁺]; Rt: 0.74 min; 100% purity by peak area.

¹H NMR (400 MHz, CDCl₃): δ 8.74 (s, 1 H), 7.85 (s, 1 H), 7.54 (dd, J = 8.1, 7.2 Hz, 1 H), 7.24 (s, 1 H), 6.82 (d, J = 7.2 Hz, 1 H), 6.64 (d, J = 8.1 Hz, 1 H), 5.62 (s, 2 H), 4.20 (t, J = 6.4 Hz, 2 H), 3.65 (s, 3 H), 2.79 (t, J = 6.8 Hz, 2 H), 2.32 (s, 3 H), 2.16 (s, 3 H), 1.79 (tt, J = 6.8, 6.4 Hz, 2 H). Imidazoquinolinone and amine NH signals not resolved.

(±)-tert-Butyl 3-[(6-cyanopyridin-2-yl)oxy]pyrrolidine-1-carboxylate



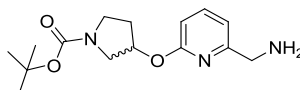
277c

A mixture of (±)-tert-butyl 3-hydroxypyrrolidine-1-carboxylate (810 mg, 4.33 mmol) and sodium hydride (60% dispersion in mineral oil, 289 mg, 7.22 mmol) in DMF (10 mL) was stirred at r.t. for 30 min then 6-chloropicolinonitrile **275** (500 mg, 3.61 mmol) added. The mixture was stirred for 3 h and quenched with sat. NH₄Cl (aq) (100 mL). The mixture was extracted with EtOAc (2 x 100 mL), the organic extracts combined and washed with brine (2 x 100 mL). The organic layer was evaporated *in vacuo* and the residue purified by silica gel chromatography (petroleum ether:EtOAc = 2:1) to give the title compound as a yellow oil (500 mg, 1.73 mmol, 48%).

LCMS (formic B): m/z 234 [(M - ^tBu)⁺]; Rt: 1.64 min; 100% purity by peak area.

¹H NMR (300 MHz, CDCl₃): δ 7.68 (dd, J = 8.4, 7.2 Hz, 1 H), 7.31 (d, J = 7.2 Hz, 1 H), 6.95 (d, J = 8.4 Hz, 1 H), 5.61–5.53 (m, 1 H), 3.71–3.43 (m, 4 H), 2.20–2.11 (m, 2 H), 1.49–1.44 (m, 9 H).

(±)-tert-Butyl 3-[(6-(aminomethyl)pyridin-2-yl)oxy]pyrrolidine-1-carboxylate



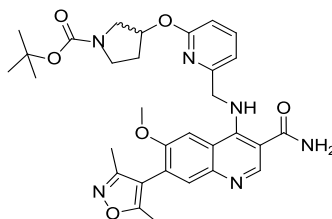
278c

A mixture of (±)-tert-butyl 3-[(6-cyanopyridin-2-yl)oxy]pyrrolidine-1-carboxylate **277c** (500 mg, 1.73 mmol) and RaNi (50 mg) in MeOH (30 mL) was degassed with H₂ for 5

min. The reaction mixture was stirred under an atmosphere of H₂ at r.t overnight and filtered. The filtrate was concentrated *in vacuo* and the residue purified by silica gel chromatography (DCM:MeOH = 10:1) to obtain the title compound as a yellow oil (350 mg, 1.19 mmol). The crude material was used without further purification in the next step.

LCMS (formic B): *m/z* 294 [(M + H)⁺]; Rt: 1.22 min; 100% purity by peak area.

(±)-*tert*-Butyl 3-{{[6-{{[3-carbamoyl-7-(3,5-dimethylisoxazol-4-yl)-6-methoxyquinolin-4-yl]amino}methyl]pyridin-2-yl]oxy}pyrrolidine-1-carboxylate



279c

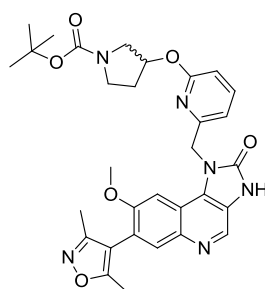
Batch 1: A mixture of 4-chloro-7-(3,5-dimethylisoxazol-4-yl)-6-methoxyquinoline-3-carboxamide **239** (20 mg, 0.060 mmol), (±)-*tert*-butyl 3-{{[6-(aminomethyl)pyridin-2-yl]oxy}pyrrolidine-1-carboxylate **278c** (22 mg, 0.075 mmol) and DIPEA (0.021 mL, 0.121 mmol) in NMP (2 mL) was stirred at 100 °C overnight. The reaction mixture was purified by preparative TLC (DCM:MeOH = 10:1) to give the title compound as a yellow solid (16 mg, 0.027 mmol). The crude material was used without further purification in the next step.

LCMS (formic B): *m/z* 589 [(M + H)⁺]; Rt: 1.40 min; 100% purity by peak area.

Batch 2: A mixture of 4-chloro-7-(3,5-dimethylisoxazol-4-yl)-6-methoxyquinoline-3-carboxamide **239** (30 mg, 0.1 mmol), (±)-*tert*-butyl 3-{{[6-(aminomethyl)pyridin-2-yl]oxy}pyrrolidine-1-carboxylate **278c** (36 mg, 0.123 mmol) and DIPEA (0.026 mL, 0.2 mmol) in NMP (2 mL) was heated at 150 °C for 8 h. The reaction mixture was purified by preparative TLC (DCM:MeOH = 10:1) to give the title compound as a yellow solid (36 mg, 0.06 mmol). The crude material was used without further purification in the next step.

LCMS (formic B): *m/z* 589 [(M + H)⁺]; Rt: 1.37 min; 100% purity by peak area.

(±)-tert-Butyl 3-[(6-([7-(3,5-dimethylisoxazol-4-yl)-8-methoxy-2-oxo-2,3-dihydro-1H-imidazo[4,5-c]quinolin-1-yl)methyl]pyridin-2-yl)oxy]pyrrolidine-1-carboxylate



280c

Batch 1: A mixture of (±)-tert-butyl 3-[[6-([3-carbamoyl-7-(3,5-dimethylisoxazol-4-yl)-6-methoxyquinolin-4-yl]amino)methyl]pyridin-2-yl]oxy]pyrrolidine-1-carboxylate **279c** (16 mg, 0.027 mmol) and KOH (4 mg, 0.054 mmol) in MeOH (2 mL) was stirred at r.t. for 30 min and iodobenzene diacetate (10 mg, 0.061 mmol) added. The reaction was stirred at r.t. overnight.

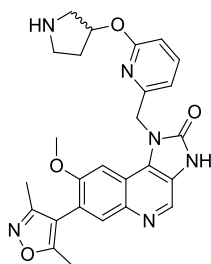
Batch 2: A mixture of (±)-tert-butyl 3-[[6-([3-carbamoyl-7-(3,5-dimethylisoxazol-4-yl)-6-methoxyquinolin-4-yl]amino)methyl]pyridin-2-yl]oxy]pyrrolidine-1-carboxylate **279c** (36 mg, 0.061 mmol) and KOH (8 mg, 0.12 mmol) in MeOH (4 mL) was stirred at r.t. for 30 min and iodobenzene diacetate (20 mg, 0.061 mmol) added. The reaction was stirred at r.t. overnight.

Both reaction mixture batches were combined and the solvent was removed *in vacuo*. The residue purified by preparative TLC (petroleum ether:EtOAc = 1:1) to give the title compound as a yellow solid (40 mg, 0.068 mmol, 77%).

LCMS (formic B): m/z 587 [(M + H)⁺]; Rt: 1.40 min; 100% purity by peak area.

¹H NMR (300 MHz, MeOD): δ 8.64 (s, 1 H), 7.81 (s, 1 H), 7.68 (dd, $J = 8.2, 7.3$ Hz, 1 H), 7.40–7.31 (m, 1 H), 7.12–7.01 (m, 1 H), 6.66 (d, $J = 8.2$ Hz, 1 H), 5.69 (br s, 2 H), 5.02–4.93 (m, 1 H), 3.76–3.67 (m, 3 H), 3.29–3.23 (m, 2 H), 3.19–3.12 (m, 2 H), 2.30 (s, 3 H), 2.12 (s, 3 H), 1.78–1.66 (m, 2 H), 1.45–1.34 (m, 9 H). Broad signals observed due to restricted rotation.

(±)-7-(3,5-Dimethylisoxazol-4-yl)-8-methoxy-1-[[6-(pyrrolidin-3-yloxy)pyridin-2-yl]methyl]-1*H*-imidazo[4,5-*c*]quinolin-2(3*H*)-one hydrochloride



281c

Batch 1: HCl (g) was bubbled through a solution of (±)-*tert*-butyl 3-[[6-[[7-(3,5-dimethylisoxazol-4-yl)-8-methoxy-2-oxo-2,3-dihydro-1*H*-imidazo[4,5-*c*]quinolin-1-yl]methyl]pyridin-2-yl]oxy]pyrrolidine-1-carboxylate **280c** (10 mg, 0.017 mmol) in DCM (2 mL) for 15 min. The reaction mixture was stirred at r.t. for 1 h.

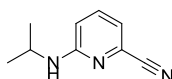
Batch 2: HCl (g) was bubbled through a solution of (±)-*tert*-butyl 3-[[6-[[7-(3,5-dimethylisoxazol-4-yl)-8-methoxy-2-oxo-2,3-dihydro-1*H*-imidazo[4,5-*c*]quinolin-1-yl]methyl]pyridin-2-yl]oxy]pyrrolidine-1-carboxylate **280c** (30 mg, 0.051 mmol) in DCM (5 mL) for 15 min. The reaction mixture was stirred at r.t. for 1 h.

Both reaction mixture batches were combined and the solvent was removed *in vacuo* to give the title compound as a yellow solid (35 mg, 0.067 mmol, 98%).

LCMS (formic B): m/z 587 [(M + H)⁺]; Rt: 1.40 min; 100% purity by peak area.

¹H NMR (300 MHz, DMSO-*d*₆): δ 8.98 (s, 1 H), 8.10 (s, 1 H), 7.86 (dd, *J* = 8.2, 7.3 Hz, 1 H), 7.39 (s, 1 H), 7.28 (d, *J* = 7.3 Hz, 1 H), 6.80 (d, *J* = 8.2 Hz, 1 H), 5.80 (br s, 2 H), 5.06–5.00 (m, 1 H), 3.74 (s, 3 H), 3.25–3.15 (m, 2 H), 3.11–2.97 (m, 2 H), 2.35 (s, 3 H), 2.14 (s, 3 H), 1.91–1.81 (m, 2 H). *NH* signals not resolved.

6-(Isopropylamino)picolinonitrile



277d

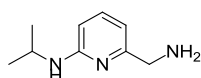
A mixture of 6-chloropicolinonitrile **275** (1 g, 7.22 mmol), potassium carbonate (1.3 g, 9.41 mmol) and isopropylamine (0.738 mL, 8.66 mmol) was suspended in anhydrous DMF (15 mL) and stirred under nitrogen at 100 °C for 25 h. The mixture was allowed to cool to r.t., diluted with EtOAc (50 mL) and washed sequentially with water (2 x 50 mL) and 10% LiCl (aq) (50 mL). The organic layer was separated, dried through a hydrophobic frit and the solvent evaporated *in vacuo*. The resulting solid was dissolved in DCM (5 mL), the solution

loaded onto a 100 g silica cartridge and purified using a gradient of 0–40% EtOAc in cyclohexane over 10 column volumes. The appropriate fractions were combined and the solvent removed by rotary evaporation. The solid was dissolved in DCM (5 mL) and the solution purified on a 100 g silica cartridge using 100% DCM over 10 column volumes. The appropriate fractions were combined and the solvent removed by rotary evaporation to give the title compound as a yellow oil (201 mg, 1.18 mmol, 16%).

LCMS (formic A): m/z 162 [(M + H)⁺]; Rt: 0.93 min; 98% purity by peak area.

¹H NMR (400 MHz, CDCl₃): δ 7.42 (dd, J = 8.6, 7.3 Hz, 1 H), 6.92 (d, J = 7.3 Hz, 1 H), 6.51 (d, J = 8.6 Hz, 1 H), 4.55 (br s, 1 H), 4.03–3.90 (m, 1 H), 1.23 (d, J = 6.4 Hz, 6 H).

6-(Aminomethyl)-*N*-isopropylpyridin-2-amine



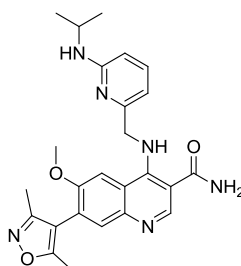
278d

A stirred solution of 6-(isopropylamino)picolinonitrile **277d** (226 mg, 1.402 mmol) in THF (2 mL) under nitrogen was treated with 1 M borane in THF solution (4.21 mL, 4.21 mmol) at 0 °C. After 10 min at 0 °C, the reaction was heated to 55 °C for 16 h. After allowing to cool to r.t., the reaction was quenched by addition of a mixture of 0.5 M HCl (aq) (25 mL) and ice-water (25 mL) and left to stir for 3 h. The mixture was basified to pH = 11 by addition of 2 M NaOH (aq) solution and the aqueous layer extracted with DCM (2 x 20 mL). The organic extracts were combined, passed through a hydrophobic frit and the solvent removed by rotary evaporation to give the title compound as a yellow oil (119 mg, 0.605 mmol, 43%).

LCMS (HpH): m/z 166 [(M + H)⁺]; Rt: 0.74 min; 84% purity by peak area.

¹H NMR (400 MHz, CDCl₃): δ 7.42–7.32 (m, 1 H), 6.49 (d, J = 7.3 Hz, 1 H), 6.22 (d, J = 8.1 Hz, 1 H), 4.37 (br s, 1 H), 3.90–3.80 (m, 1 H), 3.75 (s, 2 H), 1.92 (br s, 2 H), 1.23 (d, J = 6.3 Hz, 6 H).

7-(3,5-Dimethylisoxazol-4-yl)-4-([6-(isopropylamino)pyridin-2-yl]methyl)amino)-6-methoxyquinoline-3-carboxamide

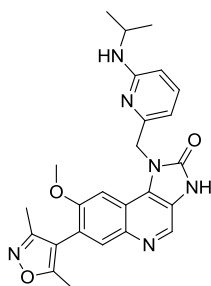


279d

A mixture of 6-(aminomethyl)-*N*-isopropylpyridin-2-amine **278d** (113 mg, 0.684 mmol) and 4-chloro-7-(3,5-dimethylisoxazol-4-yl)-6-methoxyquinoline-3-carboxamide **239** (229 mg, 0.690 mmol) was dissolved in anhydrous NMP (2 mL) and treated with DIPEA (0.143 mL, 0.821 mmol). The mixture was stirred at 100 °C for 15 h under nitrogen. The reaction mixture was applied to a MeOH preconditioned 5 g SCX-2 cartridge which was then washed with MeOH (60 mL) followed by 2 M ammonia in MeOH solution (60 mL). The basic wash was evaporated *in vacuo* and the crude material purified on a 100 g silica cartridge using a gradient of 0–15% 2 M ammonia/MeOH in DCM over 10 column volumes. The appropriate fractions were combined and the solvent removed by rotary evaporation to give the title compound as a brown solid (102 mg). The crude material was used without further purification in the next step.

LCMS (HpH): m/z 461 [(M + H)⁺]; Rt: 1.06 min; 79% purity by peak area.

7-(3,5-Dimethylisoxazol-4-yl)-1-([6-(isopropylamino)pyridin-2-yl]methyl)-8-methoxy-1*H*-imidazo[4,5-*c*]quinolin-2(3*H*)-one



280d

A solution of 7-(3,5-dimethylisoxazol-4-yl)-4-([6-(isopropylamino)pyridin-2-yl]methyl)amino)-6-methoxyquinoline-3-carboxamide **279d** (102 mg, 0.221 mmol) in MeOH (4 mL) was treated with potassium hydroxide (20 mg, 0.356 mmol) and iodobenzene diacetate (96 mg, 0.298 mmol) and the mixture stirred at r.t. for 15 h in a stoppered flask.

The reaction mixture was evaporated by rotary evaporation and the residue was purified by MDAP using Method HpH. The appropriate fractions were combined and the solvent removed by rotary evaporation to give the title compound as a yellow solid (51 mg, 0.111 mmol, 50%).

m.p.: 180–182 °C.

IR (solid) ν (cm⁻¹): 3527, 3326, 2963, 1712, 1601, 1577, 1518, 1475, 1225, 732.

LCMS (HpH): m/z 459 [(M + H)⁺]; Rt: 1.04 min; 100% purity by peak area.

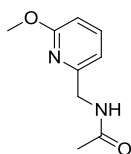
HRMS (ESI): M + H calcd for C₂₅H₂₇N₆O₃ 459.2139, found 459.2134.

¹H NMR (400 MHz, CDCl₃): δ 10.10 (br s, 1 H), 8.67 (s, 1 H), 7.77 (s, 1 H), 7.30–7.24 (m, 2 H), 6.36 (d, J = 7.3 Hz, 1 H), 6.19 (d, J = 8.1 Hz, 1 H), 5.45 (s, 2 H), 4.31 (d, J = 8.1 Hz, 1 H), 3.78–3.68 (dsep, J = 8.1, 6.3 Hz, 1 H), 3.62 (s, 3 H), 2.25 (s, 3 H), 2.10 (s, 3 H), 1.09 (d, J = 6.3 Hz, 6 H).

¹H NMR (400 MHz, DMSO-*d*₆): δ 11.59 (br s, 1 H), 8.59 (s, 1 H), 7.81–7.76 (m, 1 H), 7.32 (s, 1 H), 7.30–7.25 (m, 1 H), 6.34–6.27 (m, 3 H), 5.40 (s, 2 H), 3.74–3.64 (m, 4 H), 2.27 (s, 3 H), 2.07 (s, 3 H), 0.91 (d, J = 6.4 Hz, 6 H).

¹³C NMR (100 MHz, DMSO-*d*₆): δ 166.4, 159.5, 158.6, 155.0, 154.9, 154.6, 140.1, 137.9, 132.9, 132.4, 129.6, 122.3, 120.9, 116.4, 112.7, 107.7, 107.5, 100.2, 55.9, 47.3, 41.9, 22.7 (2 C), 11.7, 10.8.

***N*-[(6-Methoxypyridin-2-yl)methyl]acetamide**

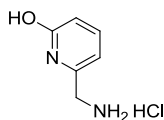


277e

A mixture of 6-methoxypicolonitrile **276** (500 mg, 3.73 mmol) in acetic anhydride (10 mL) was hydrogenated over 10% Pd/C (50 mg) at r.t. and atmospheric pressure for 3 h. The reaction mixture was filtered and the filtrate concentrated *in vacuo*. The residue was purified by silica gel chromatography (petroleum ether:EtOAc = 2:1) to obtain the title compound as a yellow oil (460 mg, 2.55 mmol, 68%).

LCMS (formic B): m/z 181 [(M + H)⁺]; Rt: 1.15 min; 100% purity by peak area.

¹H NMR (300 MHz, CDCl₃): δ 7.55 (dd, J = 8.3, 7.3 Hz, 1 H), 6.83 (d, J = 7.3 Hz, 1 H), 6.64 (d, J = 8.3 Hz, 1 H), 6.54 (br s, 1 H), 4.48 (d, J = 5.1 Hz, 2 H), 3.95 (s, 3 H), 2.07 (s, 3 H).

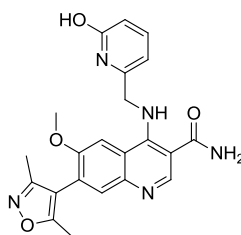
6-(Aminomethyl)pyridin-2-ol hydrochloride**278e**

A mixture of *N*-[(6-methoxypyridin-2-yl)methyl]acetamide **277e** (460 mg, 2.55 mmol) in 6 M HCl (aq) (30 mL) was stirred at reflux for 36 h. The solvent was removed under vacuum to give the title compound as a yellow solid (500 mg) which was used without further purification in the next step.

LCMS (formic B): m/z 125 [(M + H)⁺]; Rt: 0.32 min; 100% purity by peak area.

¹H NMR (300 MHz, DMSO-*d*₆ + D₂O): δ 7.53 (dd, $J = 9.0, 7.0$ Hz, 1 H), 6.46 (d, $J = 7.0$ Hz, 1 H), 6.44 (d, $J = 9.0$ Hz, 1 H), 3.93 (s, 2 H).

7-(3,5-Dimethylisoxazol-4-yl)-4-[(6-hydroxypyridin-2-yl)methyl]amino}-6-methoxyquinoline-3-carboxamide

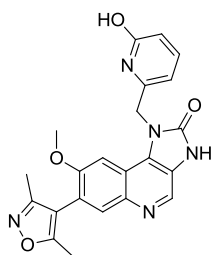
**279e**

A mixture of 4-chloro-7-(3,5-dimethylisoxazol-4-yl)-6-methoxyquinoline-3-carboxamide **239** (50 mg, 0.151 mmol), 6-(aminomethyl)pyridin-2-ol hydrochloride **278e** (40 mg) and DIPEA (0.054 mL, 0.302 mmol) in NMP (2 mL) was heated at 100 °C for 5 h. The reaction mixture was purified by preparative TLC (DCM:MeOH = 5:1) to give the title compound as a yellow solid (40 mg, 0.095 mmol, 63%).

LCMS (formic B): m/z 420 [(M + H)⁺]; Rt: 1.10 min; 100% purity by peak area.

¹H NMR (300 MHz, CD₃OD): δ 8.61 (s, 1 H), 7.73 (s, 1 H), 7.69 (s, 1 H), 7.55 (dd, $J = 9.2, 6.8$ Hz, 1 H), 6.49–6.42 (m, 2 H), 4.81 (s, 2 H), 3.90 (s, 3 H), 2.36 (s, 3 H), 2.18 (s, 3 H).

7-(3,5-Dimethylisoxazol-4-yl)-1-[(6-hydroxypyridin-2-yl)methyl]-8-methoxy-1H-imidazo[4,5-c]quinolin-2(3H)-one



280e

Batch 1: A mixture of 7-(3,5-dimethylisoxazol-4-yl)-4-[[[(6-hydroxypyridin-2-yl)methyl]amino]-6-methoxyquinoline-3-carboxamide **279e** (16 mg, 0.038 mmol) and KOH (5 mg, 0.089 mmol) in MeOH (2 mL) was stirred at r.t. for 30 min and iodobenzene diacetate (13 mg, 0.040 mmol) added. The reaction was stirred at r.t. overnight.

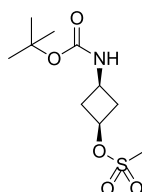
Batch 2: A mixture of 7-(3,5-dimethylisoxazol-4-yl)-4-[[[(6-hydroxypyridin-2-yl)methyl]amino]-6-methoxyquinoline-3-carboxamide **279e** (20 mg, 0.048 mmol) and KOH (6 mg, 0.095 mmol) in MeOH (3 mL) was stirred at r.t. for 30 min and iodobenzene diacetate (16 mg, 0.049 mmol) added. The reaction was stirred at r.t. overnight.

Both reaction mixture batches were combined and the solvent was removed *in vacuo*. The residue purified by preparative TLC (petroleum ether:EtOAc = 1:1) to give the title compound as a yellow solid (28 mg, 0.067 mmol, 78%)

LCMS (formic B): m/z 418 [(M + H)⁺]; Rt: 1.14 min; 98% purity by peak area.

¹H NMR (300 MHz, CD₃OD): δ 8.65 (s, 1 H), 7.84 (s, 1 H), 7.48 (dd, J = 8.9, 6.9 Hz, 1 H), 7.16 (s, 1 H), 6.48 (d, J = 8.9 Hz, 1 H), 6.13 (d, J = 6.9 Hz, 1 H), 5.53 (s, 2 H), 3.77 (s, 3 H), 2.31 (s, 3 H), 2.14 (s, 3 H).

***cis*-3-[(*tert*-Butoxycarbonyl)amino]cyclobutyl methanesulfonate**



283

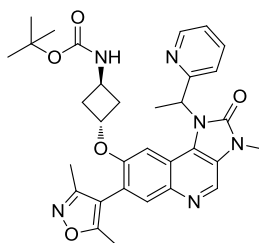
A solution of *tert*-butyl (*cis*-3-hydroxycyclobutyl)carbamate **282** (150 mg, 0.80 mmol) and triethylamine (0.167 mL, 1.20 mmol) in DCM (3 mL) under nitrogen was cooled to 0 °C and methanesulfonyl chloride (0.075 mL, 0.96 mmol) added dropwise. The mixture was stirred at 0 °C for 10 min, allowed to warm to r.t., and stirred for 3 h. Water (10 mL) was

added to the reaction mixture which was extracted with DCM (2 x 10 mL). The combined organic layers were passed through a hydrophobic frit and the solvent evaporated *in vacuo*. The crude material was purified on a 25 g silica cartridge using a gradient of 0–15% MeOH in DCM over 10 column volumes. The appropriate fractions were combined and the solvent removed by rotary evaporation to give the title compound as a white solid (205 mg, 0.77 mmol, 96%).

¹H NMR (400 MHz, CDCl₃): δ 4.71 (quin, *J* = 7.1 Hz, 1 H), 4.69 (br s, 1 H), 3.82 (br s, 1 H), 2.98 (s, 3 H), 2.95–2.86 (m, 2 H), 2.24–2.13 (m, 2 H), 1.44 (s, 9 H).

The ¹H NMR was in agreement with that reported in the literature.¹⁴⁶

***tert*-Butyl [trans-3-({7-(3,5-dimethyl-4-isoxazolyl)-3-methyl-2-oxo-1-[(1*R*)-1-(2-pyridinyl)ethyl]-2,3-dihydro-1*H*-imidazo[4,5-*c*]quinolin-8-yl}oxy)cyclobutyl]carbamate**



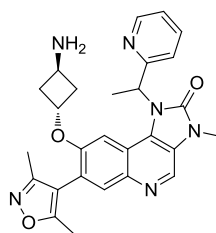
284

A mixture of *cis*-3-[(*tert*-butoxycarbonyl)amino]cyclobutyl methanesulfonate **283** (63 mg, 0.24 mmol), potassium carbonate (36 mg, 0.26 mmol) and 7-(3,5-dimethylisoxazol-4-yl)-8-hydroxy-3-methyl-1-[(*R*)-1-(pyridin-2-yl)ethyl]-1*H*-imidazo[4,5-*c*]quinolin-2(3*H*)-one **237** (90 mg, 0.22 mmol) was suspended in anhydrous DMF (1 mL) and stirred under nitrogen at r.t. overnight. The temperature was raised to 100 °C and the reaction left to stir for 6 h. The reaction mixture was allowed to cool to r.t. and filtered. The filtrate was purified by MDAP using Method HpH. The appropriate fractions were combined and the solvent removed by rotary evaporation to give the title compound as a light brown gum (84 mg, 0.14 mmol, 66%).

LCMS (formic A): *m/z* 585 [(*M* + *H*)⁺]; Rt: 0.93 min; 100% purity by peak area.

¹H NMR (400 MHz, DMSO-*d*₆): Variable temperature (393 K) δ 8.77 (s, 1 H), 8.65 (d, *J* = 4.8 Hz, 1 H), 7.81 (s, 1 H), 7.78–7.70 (m, 1 H), 7.39 (d, *J* = 7.8 Hz, 1 H), 7.30 (dd, *J* = 7.8, 4.8 Hz, 1 H), 6.80 (s, 1 H), 6.69 (d, *J* = 5.6 Hz, 1 H), 6.26 (q, *J* = 7.3 Hz, 1 H), 4.36–4.27 (m, 1 H), 4.06–3.95 (m, 1 H), 3.57 (s, 3 H), 2.51–2.42 (m, 1 H), 2.27 (s, 3 H), 2.32–2.08 (m, 3 H), 2.09 (s, 3 H), 2.05 (d, *J* = 7.3 Hz, 3 H), 1.41 (s, 9 H).

8-(*trans*-3-Aminocyclobutoxy)-7-(3,5-dimethylisoxazol-4-yl)-3-methyl-1-[1-(pyridin-2-yl)ethyl]-1*H*-imidazo[4,5-*c*]quinolin-2(3*H*)-one



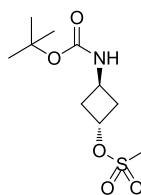
285

A solution of *tert*-butyl [*trans*-3-({7-(3,5-dimethylisoxazol-4-yl)-3-methyl-2-oxo-1-[1-(pyridin-2-yl)ethyl]-2,3-dihydro-1*H*-imidazo[4,5-*c*]quinolin-8-yl}oxy)cyclobutyl]carbamate **284** (75 mg, 0.13 mmol) in DCM (1.5 mL) was treated with TFA (0.5 mL, 6.49 mmol). The mixture was allowed to stand in a stoppered vessel at r.t. for 2 h. The reaction mixture was evaporated under a stream of nitrogen and the crude material purified by MDAP using Method HpH. The appropriate fractions were combined and the solvent removed by rotary evaporation to give the title compound as an off-white solid (48 mg, 0.10 mmol, 77%).

LCMS (formic A): m/z 485 [(M + H)⁺]; Rt: 0.52 min; 100% purity by peak area.

¹H NMR (400 MHz, DMSO-*d*₆): Variable temperature (393 K) δ 8.76 (s, 1 H) 8.68 (d, J = 4.8 Hz, 1 H), 7.80 (s, 1 H), 7.78–7.71 (m, 1 H), 7.40 (d, J = 7.8 Hz, 1 H), 7.31 (dd, J = 7.8, 4.8 Hz, 1 H), 6.81 (s, 1 H), 6.27 (q, J = 7.3 Hz, 1 H), 4.38–4.31 (m, 1 H), 3.58 (s, 3 H), 3.56–3.49 (m, 1 H), 2.27 (s, 3 H), 2.18–2.13 (m, 2 H), 2.08 (s, 3 H), 2.06 (d, J = 7.3 Hz, 3 H), 2.12–2.03 (m, 1 H), 1.99–1.91 (m, 1 H), 1.73 (br s, 2 H).

***trans*-3-[(*tert*-Butoxycarbonyl)amino]cyclobutyl methanesulfonate**



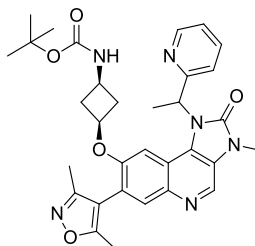
287

A solution of *tert*-butyl (*trans*-3-hydroxycyclobutyl)carbamate **286** (400 mg, 2.14 mmol) in DCM (8 mL) was added triethylamine (0.234 mL, 1.69 mmol) and the mixture cooled to 0 °C under a nitrogen atmosphere. Methanesulfonyl chloride (0.208 mL, 2.67 mmol) was added dropwise and the mixture stirred 0 °C for 10 min. The reaction was allowed to warm to r.t. and stirred for 3 h. Water (10 mL) was added and the mixture extracted with DCM (2 x 10 mL). The combined organic extracts were passed through a hydrophobic frit and the solvent evaporated *in vacuo*. The crude material was purified on a

25 g silica cartridge using a gradient of 0–15% MeOH in DCM over 10 column volumes. The appropriate fractions were combined and the solvent removed by rotary evaporation to give the title compound as a white solid (544 mg, 2.05 mmol, 96%).

¹H NMR (400 MHz, CDCl₃): δ 5.17 (m, 1 H), 4.69 (br s, 1 H), 4.26 (br s, 1 H), 2.99 (s, 3 H), 2.73–2.62 (m, 2 H), 2.49–2.36 (m, 2 H), 1.44 (s, 9 H).

***tert*-Butyl [cis-3-({7-(3,5-dimethylisoxazol-4-yl)-3-methyl-2-oxo-1-[1-(pyridin-2-yl)ethyl]-2,3-dihydro-1*H*-imidazo[4,5-*c*]quinolin-8-yl}oxy)cyclobutyl]carbamate**



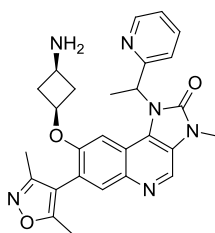
288

A mixture of *trans*-3-[(*tert*-butoxycarbonyl)amino]cyclobutyl methanesulfonate **287** (281 mg, 1.06 mmol), potassium carbonate (160 mg, 1.16 mmol) and 7-(3,5-dimethylisoxazol-4-yl)-8-hydroxy-3-methyl-1-[(*R*)-1-(pyridin-2-yl)ethyl]-1*H*-imidazo[4,5-*c*]quinolin-2(3*H*)-one **237** (400 mg, 0.96 mmol) was suspended in anhydrous DMF (4 mL) and stirred under nitrogen at 100 °C for 6 h. The reaction mixture was allowed to cool to r.t. and diluted with brine (20 mL). The mixture was extracted with DCM (2 x 20 mL), the organic layers combined and passed through a hydrophobic frit. The solvent was removed *in vacuo* to give a brown oil. The oil was dissolved in MeOH (5 mL) and applied to a MeOH preconditioned 50 g SCX-2 cartridge. The cartridge was washed with MeOH (200 mL) followed by 2 M ammonia in MeOH solution (200 mL). The basic wash was evaporated *in vacuo* to give a brown gum. The crude material was purified by MDAP using Method Formic. The appropriate fractions were combined and the solvent removed by rotary evaporation to give the title compound as a white solid (233 mg, 0.40 mmol, 41%).

LCMS (formic A): *m/z* 585 [(M + H)⁺]; Rt: 0.96 min; 100% purity by peak area.

¹H NMR (400 MHz, DMSO-*d*₆): Variable temperature (393 K) δ 8.77 (s, 1 H), 8.63 (d, *J* = 4.8 Hz, 1 H), 7.80 (s, 1 H), 7.79–7.72 (m, 1 H), 7.42 (d, *J* = 7.8 Hz, 1 H), 7.33 (dd, *J* = 7.8, 4.8 Hz, 1 H), 6.89 (s, 1 H), 6.64 (d, *J* = 6.3 Hz, 1 H), 6.27 (q, *J* = 7.2 Hz, 1 H), 3.92–3.83 (m, 1 H), 3.70–3.60 (m, 1 H), 3.58 (s, 3 H), 2.82–2.72 (m, 1 H), 2.54–2.44 (m, 1 H), 2.27 (s, 3 H), 2.09 (s, 3 H), 2.06 (d, *J* = 7.2 Hz, 3 H), 1.94–1.84 (m, 2 H), 1.40 (s, 9 H).

8-(*cis*-3-Aminocyclobutoxy)-7-(3,5-dimethylisoxazol-4-yl)-3-methyl-1-[1-(pyridin-2-yl)ethyl]-1*H*-imidazo[4,5-*c*]quinolin-2(3*H*)-one



289

A solution of *tert*-butyl [*cis*-3-({7-(3,5-dimethylisoxazol-4-yl)-3-methyl-2-oxo-1-[1-(pyridin-2-yl)ethyl]-2,3-dihydro-1*H*-imidazo[4,5-*c*]quinolin-8-yl}oxy)cyclobutyl]carbamate **288** (229 mg, 0.39 mmol) in DCM (6 mL) was treated with TFA (2 mL, 26.0 mmol). The mixture was allowed to stand in a stoppered vessel at r.t. for 2 h. The reaction mixture was evaporated under a stream of nitrogen and the residue dissolved in MeOH (2 mL). The solution was applied to a MeOH preconditioned 5 g SCX-2 cartridge. The cartridge was washed with MeOH (30 mL) followed by 2 M ammonia in MeOH solution (30 mL). The basic wash was evaporated under a stream of nitrogen to give the title compound as an off-white solid (178 mg, 0.37 mmol, 94%).

m.p.: 158–160 °C.

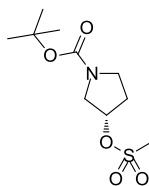
IR (solid) ν (cm⁻¹): 3363, 2981, 2934, 1702, 1619, 1581, 1490, 1453, 1432, 1215, 1035, 772, 748.

LCMS (formic A): m/z 485 [(M + H)⁺]; Rt: 0.52 min; 100% purity by peak area.

HRMS (ESI): M + H calcd for C₂₇H₂₉N₆O₃ 485.2301, found 485.2292.

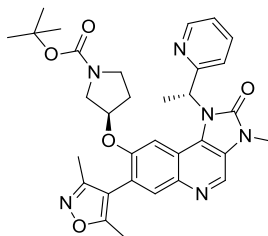
¹H NMR (400 MHz, DMSO-*d*₆): Variable temperature (393 K) δ 8.77 (s, 1 H), 8.62 (d, *J* = 4.8 Hz, 1 H), 7.80 (s, 1 H), 7.78–7.71 (m, 1 H), 7.41 (d, *J* = 7.8 Hz, 1 H), 7.32 (dd, *J* = 7.8, 4.8 Hz, 1 H), 6.87 (s, 1 H), 6.27 (q, *J* = 7.3 Hz, 1 H), 3.83–3.75 (m, 1 H), 3.58 (s, 3 H), 3.09–3.00 (m, 1 H), 2.80–2.71 (m, 1 H), 2.52–2.44 (m, 1 H), 2.27 (s, 3 H), 2.09 (s, 3 H), 2.06 (d, *J* = 7.3 Hz, 3 H), 1.65–1.54 (m, 2 H). NH₂ signal not resolved.

¹³C NMR (150 MHz, DMSO-*d*₆): δ 166.0, 159.1, 158.9, 153.7, 152.4, 149.3, 140.1, 137.5, 133.1, 131.6, 127.1, 124.0, 122.8, 120.8, 120.6, 115.2, 112.1, 101.6, 64.7, 52.7, 41.2, 40.4, 39.7, 27.7, 17.5, 11.5, 10.5.

(S)-tert-Butyl 3-[(methylsulfonyl)oxy]pyrrolidine-1-carboxylate**291**

A stirred solution of (*S*)-*tert*-butyl 3-hydroxypyrrolidine-1-carboxylate **290** (500 mg, 2.67 mmol) and triethylamine (0.931 mL, 6.68 mmol) in DCM (6 mL) at 0 °C was treated with methanesulfonyl chloride (0.250 mL, 3.20 mmol). The mixture was stirred under nitrogen for 10 min and allowed to warm to r.t. over 2 h. The reaction was diluted with DCM (10 mL) and washed with brine (15 mL). The aqueous layer was extracted with DCM (10 mL), the organic layers combined and passed through a hydrophobic frit. The solvent was removed by rotary evaporation and the crude material purified on a 25 g silica cartridge using a gradient of 0–15% MeOH in DCM over 10 column volumes. The appropriate fractions were combined and the solvent was removed by rotary evaporation to give the title compound as a light yellow oil (691 mg, 2.60 mmol, 98%).

¹H NMR (400 MHz, CDCl₃): δ 5.28–5.23 (m, 1 H), 3.75–3.41 (m, 4 H), 3.04 (s, 3 H), 2.37–2.08 (m, 2 H), 1.45 (s, 9 H).

(3R)-tert-Butyl 3-({7-(3,5-dimethylisoxazol-4-yl)-3-methyl-2-oxo-1-[(R)-1-(pyridin-2-yl)ethyl]-2,3-dihydro-1H-imidazo[4,5-c]quinolin-8-yl}oxy)pyrrolidine-1-carboxylate**292**

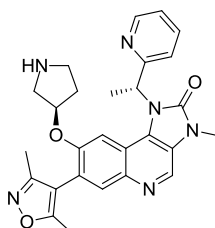
To a vessel containing (*S*)-*tert*-butyl 3-[(methylsulfonyl)oxy]pyrrolidine-1-carboxylate **291** (89 mg, 0.34 mmol) was added potassium carbonate (47 mg, 0.34 mmol) and 7-(3,5-dimethylisoxazol-4-yl)-8-hydroxy-3-methyl-1-[(*R*)-1-(pyridin-2-yl)ethyl]-1*H*-imidazo[4,5-*c*]quinolin-2(3*H*)-one **237** (103 mg, 0.25 mmol). DMF (2 mL) was added and the mixture stirred under nitrogen at 100 °C for 4 h. EtOAc (10 mL) was added to the reaction mixture which was then washed with brine (10 mL). The aqueous layer was extracted with EtOAc (10 mL), the organic layers combined and passed through a hydrophobic frit. The solvent was removed by rotary evaporation and the crude material purified on a 25 g silica cartridge

using a gradient of 0–15% MeOH in DCM over 10 column volumes. The appropriate fractions were combined and the solvent removed by rotary evaporation. The sample was dissolved in EtOH (3 mL) and heptane (3 mL). Fifteen injections were made onto a Chiralpak® IA column (250 mm x 30 mm, 5 µm packing diameter). An isocratic system of 15% EtOH in heptane with a flow rate of 40 mL/min was used at r.t. The UV detection was performed at 215 nm. The appropriate fractions were combined and evaporated *in vacuo* to give the title compound (49 mg, 0.08 mmol, 34%).

LCMS (HpH): m/z 585 [(M + H)⁺]; Rt: 1.11 min; 100% purity by peak area.

¹H NMR (400 MHz, DMSO-*d*₆): Variable temperature (393 K) δ 8.79 (s, 1 H), 8.60 (d, *J* = 4.8 Hz, 1 H), 7.81 (s, 1 H), 7.78–7.72 (m, 1 H), 7.44 (d, *J* = 7.8 Hz, 1 H), 7.30 (dd, *J* = 7.3, 4.8 Hz, 1 H), 7.09 (s, 1 H), 6.29 (q, *J* = 7.3 Hz, 1 H), 4.55–4.50 (m, 1 H), 3.58 (s, 3 H), 3.38–3.29 (m, 2 H), 3.19–3.11 (m, 2 H), 2.22 (s, 3 H), 2.17–2.08 (m, 1 H), 2.06 (d, *J* = 7.3 Hz, 3 H), 2.02 (s, 3 H), 1.98–1.89 (m, 1 H), 1.39 (s, 9 H). Only a single diastereoisomer was observed.

7-(3,5-Dimethylisoxazol-4-yl)-3-methyl-1-[(*R*)-1-(pyridin-2-yl)ethyl]-8-[(*R*)-pyrrolidin-3-yloxy]-1*H*-imidazo[4,5-*c*]quinolin-2(3*H*)-one



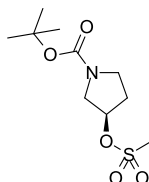
293

A solution of (*3R*)-*tert*-butyl 3-({7-(3,5-dimethylisoxazol-4-yl)-3-methyl-2-oxo-1-[1-(pyridin-2-yl)ethyl]-2,3-dihydro-1*H*-imidazo[4,5-*c*]quinolin-8-yl}oxy)pyrrolidine-1-carboxylate **292** (45 mg, 0.08 mmol) in 1,4-dioxane (0.5 mL) was treated with 4 M HCl in 1,4-dioxane solution (0.5 mL, 16.46 mmol). The mixture was left to stir at r.t. for 2 h. The reaction mixture was evaporated under a stream of nitrogen and the solid dissolved in MeOH. The solution was applied to a MeOH preconditioned 2 g SCX-2 cartridge which was then washed with MeOH (12 mL) followed by 2 M ammonia in MeOH solution (12 mL). The basic wash was evaporated by rotary evaporation to give the title compound as a light brown solid (31 mg, 0.06 mmol, 83%).

LCMS (HpH): m/z 485 [(M + H)⁺]; Rt: 0.75 min; 100% purity by peak area.

^1H NMR (400 MHz, $\text{DMSO-}d_6$): Variable temperature (393 K) δ 8.77 (s, 1 H), 8.60 (d, $J = 4.8$ Hz, 1 H), 7.80 (s, 1 H), 7.78–7.72 (m, 1 H), 7.41 (d, $J = 7.8$ Hz, 1 H), 7.30 (dd, $J = 7.3, 4.8$ Hz, 1 H), 7.04 (s, 1 H), 6.29 (q, $J = 7.3$ Hz, 1 H), 4.42–4.35 (m, 1 H), 3.58 (s, 3 H), 2.98–2.92 (m, 2 H), 2.68–2.62 (m, 1 H), 2.24 (s, 3 H), 2.07 (d, $J = 7.3$ Hz, 3 H), 2.05 (s, 3 H), 2.05–1.99 (m, 1 H), 1.72–1.64 (m, 1 H). One pyrrolidine proton signal obscured by water. NH signal not resolved. Only a single diastereoisomer was observed.

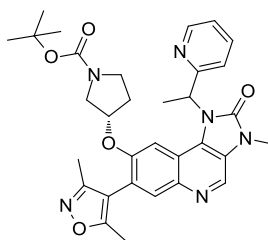
(*R*)-*tert*-Butyl 3-[(methylsulfonyl)oxy]pyrrolidine-1-carboxylate



295

A stirred solution of (*R*)-*tert*-butyl 3-hydroxypyrrolidine-1-carboxylate **294** (481 mg, 2.57 mmol) and triethylamine (0.931 mL, 6.68 mmol) in DCM (6 mL) at 0 °C was treated with methanesulfonyl chloride (0.250 mL, 3.20 mmol). The mixture was stirred under nitrogen for 10 min and allowed to warm to r.t. over 1 h. The reaction was diluted with DCM (10 mL) and washed with water (10 mL). The aqueous layer was extracted with DCM (10 mL), the organic layers combined and passed through a hydrophobic frit. The solvent was removed by rotary evaporation and the crude material purified on a 25 g silica cartridge using a gradient of 0–15% MeOH in DCM over 10 column volumes. The appropriate fractions were combined and the solvent was removed by rotary evaporation to give the title compound as a light yellow oil (651 mg, 2.45 mmol, 96%).

^1H NMR (400 MHz, CDCl_3): δ 5.28–5.23 (m, 1 H), 3.75–3.41 (m, 4 H), 3.04 (s, 3 H), 2.37–2.08 (m, 2 H), 1.45 (s, 9 H).

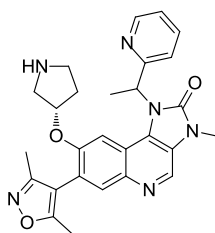
(3S)-tert-Butyl 3-({7-(3,5-dimethylisoxazol-4-yl)-3-methyl-2-oxo-1-[1-(pyridin-2-yl)ethyl]-2,3-dihydro-1H-imidazo[4,5-c]quinolin-8-yl}oxy)pyrrolidine-1-carboxylate**296**

To a vessel containing (*R*)-*tert*-butyl 3-[(methylsulfonyl)oxy]pyrrolidine-1-carboxylate **295** (82 mg, 0.31 mmol) was added potassium carbonate (43 mg, 0.31 mmol) and 7-(3,5-dimethylisoxazol-4-yl)-8-hydroxy-3-methyl-1-[(*R*)-1-(pyridin-2-yl)ethyl]-1*H*-imidazo[4,5-*c*]quinolin-2(3*H*)-one **237** (100 mg, 0.24 mmol). DMF (2 mL) was added and the mixture stirred under nitrogen and at 100 °C for 5 h. EtOAc (10 mL) was added to the reaction mixture which was then washed with brine (10 mL). The aqueous layer was extracted with EtOAc, the organic layers combined and passed through a hydrophobic frit. The solvent was removed by rotary evaporation and the crude product dissolved in DCM (4 mL) and purified on a 25 g silica cartridge using a gradient of 0–15% MeOH in DCM over 10 column volumes. The appropriate fractions were combined and the solvent removed by rotary evaporation. The crude material was purified by MDAP using Method Formic. The appropriate fractions were combined and the solvent removed by rotary evaporation to give the title compound as an off-white solid (99 mg, 0.17 mmol, 70%).

LCMS (formic A): m/z 585 [(M + H)⁺]; Rt: 0.96 min; 100% purity by peak area.

¹H NMR (400 MHz, DMSO-*d*₆): Variable temperature (393 K) δ 8.80 (s, 1 H), 8.60 (d, *J* = 4.8 Hz, 1 H), 7.82 (s, 1 H), 7.79–7.73 (m, 1 H), 7.45 (d, *J* = 7.3 Hz, 1 H), 7.31 (dd, *J* = 7.3, 4.8 Hz, 1 H), 7.06 (s, 1 H), 6.30 (q, *J* = 7.3 Hz, 1 H), 4.47 (m, 1 H), 3.59 (s, 3 H), 3.58–3.52 (m, 1 H), 3.39–3.30 (m, 2 H), 3.19–3.11 (m, 1 H), 2.22 (s, 3 H), 2.06 (d, *J* = 7.3 Hz, 3 H), 2.02 (s, 3 H), 2.01–1.94 (m, 1 H), 1.82–1.73 (m, 1 H), 1.42 (s, 1.3 H), 1.39 (s, 7.7 H). A 85:15 mixture of diastereoisomers present.

7-(3,5-Dimethylisoxazol-4-yl)-3-methyl-1-[1-(pyridin-2-yl)ethyl]-8-[(S)-pyrrolidin-3-yloxy]-1*H*-imidazo[4,5-*c*]quinolin-2(3*H*)-one



297

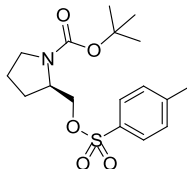
A solution of (3*S*)-*tert*-butyl 3-({7-(3,5-dimethylisoxazol-4-yl)-3-methyl-2-oxo-1-[1-(pyridin-2-yl)ethyl]-2,3-dihydro-1*H*-imidazo[4,5-*c*]quinolin-8-yl}oxy)pyrrolidine-1-carboxylate **296** (103 mg, 0.18 mmol) in anhydrous 1,4-dioxane (0.5 mL) was treated with 4 M HCl in 1,4-dioxane solution (0.5 mL, 16.46 mmol) and the mixture allowed to stand in a stoppered vessel for 2 h. The reaction mixture was evaporated under a stream of nitrogen and the solid dissolved in MeOH. The solution was applied to a MeOH preconditioned 2 g SCX-2 cartridge. The cartridge was washed with MeOH (20 mL) followed by 2 M ammonia in MeOH solution (20 mL). The basic wash was evaporated by rotary evaporation. Starting material still remained so the residue was dissolved in anhydrous 1,4-dioxane (0.5 mL) and 4 M HCl in 1,4-dioxane solution (0.5 mL, 16.46 mmol) and the mixture left to stir overnight in a stoppered vessel. The reaction mixture was evaporated under a stream of nitrogen and the solid was dissolved in the minimum volume of MeOH. The solution was applied to a MeOH preconditioned 2 g SCX-2 cartridge which was then washed with MeOH (20 mL) followed by 2 M ammonia in MeOH solution (20 mL). The basic wash was evaporated by rotary evaporation and the crude material purified by MDAP conducted on an Xbridge BEH Shield RP18 column (150 mm x 19 mm, 5 μ m packing diameter) at 20 mL/min flow rate. Gradient elution was carried out at ambient temperature, with the mobile phases as (A) water containing 0.1% (v/v) formic acid and (B) acetonitrile containing 0.1% (v/v) formic acid. The UV detection was a summed signal from wavelength of 210 nm to 400 nm. The appropriate fractions were combined and dried under a stream of nitrogen and the crude material purified on a 10 g silica cartridge using a gradient of 0–20% 2 M ammonia/MeOH in DCM over 15 column volumes. The appropriate fractions were combined and evaporated *in vacuo* to give the title compound as a colourless oil (10 mg, 0.02 mmol, 12%).

LCMS (formic A): m/z 485 [(M + H)⁺]; Rt: 0.52 min; 100% purity by peak area.

¹H NMR (400 MHz, DMSO-*d*₆): Variable temperature (393 K) δ 8.77 (s, 1 H), 8.60 (d, J = 4.8 Hz, 1 H), 7.79 (s, 1 H), 7.77–7.71 (m, 1 H), 7.41 (d, J = 7.3 Hz, 1 H), 7.31 (dd, J = 7.3,

4.8 Hz, 1 H), 7.01 (s, 1 H), 6.29 (q, $J = 7.3$ Hz, 1 H), 4.37 (m, 1 H), 3.58 (s, 3 H), 3.21–3.15 (m, 0.15 H), 3.13–3.07 (m, 0.85 H), 2.80–2.62 (m, 3 H), 2.24 (s, 2.6 H), 2.19 (s, 0.4 H), 2.10–2.02 (m, 5.1 H), 2.01 (s, 0.9 H), 1.82–1.71 (m, 1 H), 1.55–1.47 (m, 1 H). A 85:15 mixture of diastereoisomers present.

(*R*)-tert-Butyl 2-[(methylsulfonyl)oxy]methylpyrrolidine-1-carboxylate



299

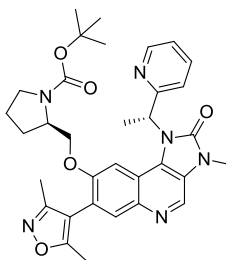
A stirred solution of (*R*)-tert-butyl 2-(hydroxymethyl)pyrrolidine-1-carboxylate **298** (496 mg, 2.46 mmol) and triethylamine (0.86 mL, 6.16 mmol) in DCM (6 mL) at 0 °C was treated with 4-methylbenzene-1-sulfonyl chloride (564 mg, 2.96 mmol) followed by 4-dimethylpyridine (DMAP) (33 mg, 0.27 mmol). The mixture was stirred under nitrogen for 10 min and allowed to warm to r.t. over 4 h. Further 4-methylbenzene-1-sulfonyl chloride (55 mg, 0.29 mmol) was added to the vessel and the mixture stirred for 1 h. The reaction was diluted with DCM (10 mL) and washed with water (10 mL). The aqueous layer was extracted with DCM (10 mL), the organic layers combined and passed through a hydrophobic frit. The solvent was removed by rotary evaporation and the crude material purified on a 25 g silica cartridge using a gradient of 0–15% MeOH in DCM over 10 column volumes. The appropriate fractions were combined and the solvent removed by rotary evaporation to give the title compound as a light yellow oil (759 mg, 2.14 mmol, 87%).

LCMS (formic A): m/z 356 [(M + H)⁺]; Rt: 1.22 min; 100% purity by peak area.

¹H NMR (400 MHz, CDCl₃): δ 7.77 (d, $J = 8.1$ Hz, 2 H), 7.34 (d, $J = 8.1$ Hz, 2 H), 4.11–3.87 (m, 3 H), 3.29 (d, $J = 6.3$ Hz, 2 H), 2.44 (s, 3 H), 2.03–1.72 (m, 4 H), 1.38 (s, 9 H).

The ¹H NMR was in agreement with that reported in the literature.¹⁴⁷

(2*R*)-tert-Butyl 2-[(7-(3,5-dimethylisoxazol-4-yl)-3-methyl-2-oxo-1-[(*R*)-1-(pyridin-2-yl)ethyl]-2,3-dihydro-1*H*-imidazo[4,5-*c*]quinolin-8-yl)oxy)methyl]pyrrolidine-1-carboxylate



300

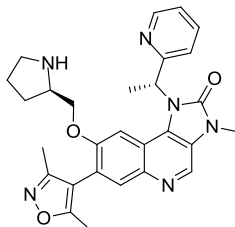
To a vessel containing (*R*)-*tert*-butyl 2-[(tosyloxy)methyl]pyrrolidine-1-carboxylate **299** (116 mg, 0.33 mmol) in DMF (4 mL) was added potassium carbonate (43 mg, 0.31 mmol) followed by 7-(3,5-dimethylisoxazol-4-yl)-8-hydroxy-3-methyl-1-[(*R*)-1-(pyridin-2-yl)ethyl]-1*H*-imidazo[4,5-*c*]quinolin-2(3*H*)-one **237** (103 mg, 0.25 mmol). The mixture was stirred under nitrogen at 100 °C for 20 h. EtOAc (10 mL) was added to the reaction mixture which was then washed with brine (10 mL). The aqueous layer was extracted with EtOAc (10 mL), the organic layers were combined then passed through a hydrophobic frit. The solvent was removed by rotary evaporation and the residue dissolved in the minimum volume of MeOH. The solution was applied to a MeOH preconditioned 5 g SCX-2 cartridge which was then washed with MeOH (45 mL) followed by 2 M ammonia in MeOH solution (45 mL). The basic wash was evaporated *in vacuo* and the crude material purified on a 25 g silica cartridge using a gradient of 0–15% MeOH in DCM over 10 column volumes. The appropriate fractions were combined and the solvent removed by rotary evaporation. The crude material was purified by MDAP using Method Formic. The appropriate fractions were combined and the solvent removed by rotary evaporation. The sample was dissolved in EtOH (1 mL) and heptane (1 mL). One injection was made onto a Chiralcel® OD-H column (250 mm x 30 mm, 5 µm packing diameter). An isocratic system of 10% EtOH in heptane with a flow rate of 40 mL/min was used at r.t. The UV detection was performed at 240 nm. The appropriate fractions were combined and evaporated *in vacuo* to give the title compound (22 mg, 0.03 mmol, 15%).

LCMS (formic A): m/z 599 [(M + H)⁺]; Rt: 1.00 min; 100% purity by peak area.

¹H NMR (400 MHz, DMSO-*d*₆): Variable temperature (393 K) δ 8.77 (s, 1 H), 8.56 (d, *J* = 4.8 Hz, 1 H), 7.78 (s, 1 H), 7.76–7.70 (m, 1 H), 7.42 (d, *J* = 7.8 Hz, 1 H), 7.27 (dd, *J* = 7.8, 4.8 Hz, 1 H), 7.05 (s, 1 H), 6.30 (q, *J* = 7.3 Hz, 1 H), 3.97–3.90 (m, 2 H), 3.58 (s, 3 H), 3.57–3.48 (m, 1 H), 3.32–3.24 (m, 1 H), 3.11–3.03 (m, 1 H), 2.22 (s, 3 H), 2.04 (d, *J* = 7.3 Hz, 3

H), 2.02 (s, 3 H), 1.98–1.84 (m, 1 H), 1.71–1.57 (m, 3 H), 1.38 (s, 9 H). Only a single diastereoisomer was observed.

7-(3,5-Dimethylisoxazol-4-yl)-3-methyl-1-[(*R*)-1-(pyridin-2-yl)ethyl]-8-[(*R*)-pyrrolidin-2-ylmethoxy]-1*H*-imidazo[4,5-*c*]quinolin-2(3*H*)-one

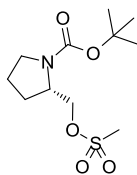


301

A solution of (*2R*)-*tert*-butyl 2-[(7-(3,5-dimethylisoxazol-4-yl)-3-methyl-2-oxo-1-[1-(pyridin-2-yl)ethyl]-2,3-dihydro-1*H*-imidazo[4,5-*c*]quinolin-8-yl]oxymethyl]pyrrolidine-1-carboxylate **300** (17 mg, 0.03 mmol) in 1,4-dioxane (0.3 mL) was treated with 4 M HCl in 1,4-dioxane solution (0.2 mL, 6.58 mmol) and the mixture left to stir at r.t. for 2 h. The solvent was evaporated under a stream of nitrogen and the residue dissolved in MeOH (0.5 mL). The solution was applied to a MeOH preconditioned 2 g SCX-2 cartridge which was washed with MeOH (10 mL) followed by 2 M ammonia in MeOH solution (10 mL). The basic washes were combined and the solvent was removed by rotary evaporation to give the title compound as a colourless gum (11 mg, 0.02 mmol, 78%).

LCMS (HpH): m/z 499 [(M + H)⁺]; Rt: 0.86 min; 95% purity by peak area.

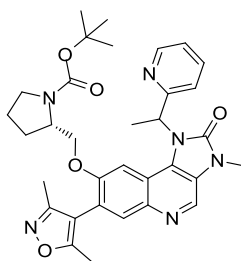
¹H NMR (400 MHz, DMSO-*d*₆): Variable temperature (393 K) δ 8.77 (s, 1 H), 8.59 (d, J = 4.8 Hz, 1 H), 7.78 (s, 1 H), 7.78–7.72 (m, 1 H), 7.42 (d, J = 7.8 Hz, 1 H), 7.30 (dd, J = 7.3, 4.8 Hz, 1 H), 7.03 (s, 1 H), 6.29 (q, J = 7.1 Hz, 1 H), 3.74–3.68 (m, 1 H), 3.58 (s, 3 H), 3.47–3.41 (m, 1 H), 3.41–3.33 (m, 1 H), 2.84–2.79 (m, 2 H), 2.25 (s, 3 H), 2.06 (s, 3 H), 2.05 (d, J = 7.1 Hz, 3 H), 1.87–1.77 (m, 1 H), 1.71–1.62 (m, 2 H), 1.43–1.34 (m, 1 H). NH signal not resolved. Only a single diastereoisomer was observed.

(S)-tert-Butyl 2-[[methylsulfonyl]oxy]methylpyrrolidine-1-carboxylate**303**

A solution of (*S*)-*tert*-butyl 2-(hydroxymethyl)pyrrolidine-1-carboxylate **302** (163 mg, 0.81 mmol) and triethylamine (0.140 mL, 1.01 mmol) in DCM (3 mL) under nitrogen was cooled to 0 °C and methanesulfonyl chloride (0.082 mL, 1.05 mmol) added. The mixture was stirred at 0 °C for 10 min, allowed to warm to r.t., and then stirred for 2 h. Water (10 mL) was added to the reaction mixture which was then extracted with DCM (2 x 10 mL). The combined organic extracts were passed through a hydrophobic frit and the solvent evaporated *in vacuo*. The crude material was purified on a 25 g silica cartridge using a gradient of 0–10% MeOH in DCM over 10 column volumes. The appropriate fractions were combined and the solvent removed by rotary evaporation to give the title compound as a colourless oil (155 mg, 0.56 mmol, 69%).

¹H NMR (400 MHz, CDCl₃): δ 4.38–3.95 (m, 3 H), 3.49–3.27 (m, 2 H), 3.00 (s, 3 H), 2.12–1.73 (m, 4 H), 1.48 (s, 9 H).

(2S)-tert-Butyl 2-[(7-(3,5-dimethylisoxazol-4-yl)-3-methyl-2-oxo-1-[1-(pyridin-2-yl)ethyl]-2,3-dihydro-1H-imidazo[4,5-c]quinolin-8-yl)oxy]methyl]pyrrolidine-1-carboxylate

**304**

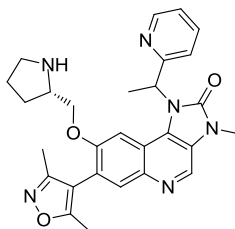
A mixture of (*S*)-*tert*-butyl 2-[[methylsulfonyl]oxy]methylpyrrolidine-1-carboxylate **303** (37 mg, 0.13 mmol), potassium carbonate (20 mg, 0.15 mmol) and 7-(3,5-dimethylisoxazol-4-yl)-8-hydroxy-3-methyl-1-[(*R*)-1-(pyridin-2-yl)ethyl]-1*H*-imidazo[4,5-*c*]quinolin-2(3*H*)-one **237** (50 mg, 0.12 mmol) was suspended in anhydrous DMF (0.5 mL) and stirred under nitrogen at 100 °C for 2 h. The temperature was raised to 120 °C and the reaction stirred for 1.5 h. Potassium carbonate (20 mg, 0.15 mmol) and a solution of (*S*)-*tert*-

butyl 2-[[[(methylsulfonyl)oxy]methyl]pyrrolidine-1-carboxylate (37 mg, 0.13 mmol) in anhydrous DMF (0.4 mL) was added and the reaction stirred at 120 °C for 15 h. The reaction mixture was allowed to cool to r.t. and diluted with MeOH (0.1 mL). The mixture was filtered and purified by MDAP using Method HpH. The appropriate fractions were combined and the solvent removed by rotary evaporation to give the title compound as an off-white solid (26 mg, 0.04 mmol, 36%).

LCMS (formic A): m/z 599 $[(M + H)^+]$; Rt: 1.01 min; 100% purity by peak area.

^1H NMR (400 MHz, DMSO- d_6): Variable temperature (393 K) δ 8.77 (s, 1 H), 8.56 (d, $J = 4.8$ Hz, 1 H), 7.78 (s, 1 H), 7.76–7.68 (m, 1 H), 7.43 (d, $J = 7.8$ Hz, 0.13 H), 7.40 (d, $J = 7.8$ Hz, 0.87 H), 7.28 (dd, $J = 7.3, 4.8$ Hz, 1 H), 7.05 (s, 0.13 H), 7.02 (s, 0.87 H), 6.30 (q, $J = 7.1$ Hz, 1 H), 3.99–3.87 (m, 2 H), 3.58 (s, 3 H), 3.55–3.52 (m, 0.13 H), 3.49–3.41 (m, 0.87 H), 3.33–3.24 (m, 1 H), 3.16–3.09 (m, 0.87 H), 3.09–3.03 (m, 0.13 H), 2.24 (s, 0.36 H), 2.22 (s, 2.64 H), 2.06–2.02 (m, 6 H), 1.95–1.83 (m, 1 H), 1.74–1.53 (m, 3 H), 1.41 (s, 9 H). A 87:13 mixture of diastereoisomers present.

7-(3,5-Dimethylisoxazol-4-yl)-3-methyl-1-[1-(pyridin-2-yl)ethyl]-8-[(*S*)-pyrrolidin-2-ylmethoxy]-1*H*-imidazo[4,5-*c*]quinolin-2(3*H*)-one



305

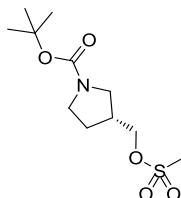
A solution of (*2S*)-*tert*-butyl 2-[[({7-(3,5-dimethylisoxazol-4-yl)-3-methyl-2-oxo-1-[1-(pyridin-2-yl)ethyl]-2,3-dihydro-1*H*-imidazo[4,5-*c*]quinolin-8-yl}oxy)methyl]pyrrolidine-1-carboxylate **304** (22 mg, 0.04 mmol) was dissolved in DCM (0.5 mL) and treated with TFA (0.5 mL, 6.49 mmol). The mixture was allowed to stand in a stoppered vessel at r.t. for 1.5 h. The reaction mixture was evaporated under a stream of nitrogen and the resulting gum dissolved in MeOH (0.5 mL). The solution was applied to a MeOH preconditioned 1 g SCX-2 cartridge which was then washed with MeOH (6 mL) followed by 2 M ammonia in MeOH solution (6 mL). The basic wash was evaporated under a stream of nitrogen and the crude material purified by MDAP conducted on an Atlantis T3 C18 column (150 mm x 19 mm, 5 μm packing diameter) at 20 mL/min flow rate. Gradient elution was carried out at ambient temperature, with the mobile phases as (A) water containing 0.1% (v/v) formic acid and (B) MeOH. The UV detection was a summed signal from wavelength of 210 nm to 400 nm. The

appropriate fractions were combined and dried under a stream of nitrogen. The crude material was purified on a 10 g silica cartridge using a gradient of 0–10% 2 M ammonia/MeOH in DCM over 10 column volumes. The appropriate fractions were combined and evaporated *in vacuo* to give the title compound as a white solid (8 mg, 0.02 mmol, 44%). A 87:13 mixture of diastereoisomers present.

LCMS (formic A): m/z 499 $[(M + H)^+]$; Rt: 0.56 min; 100% purity by peak area.

^1H NMR (400 MHz, DMSO- d_6): Variable temperature (393 K) δ 8.77 (s, 1 H), 8.61 (d, $J = 4.8$ Hz, 1 H), 7.80 (s, 1 H), 7.78–7.72 (m, 1 H), 7.44 (d, $J = 7.8$ Hz, 1 H), 7.31 (dd, $J = 7.3, 4.8$ Hz, 1 H), 7.08 (s, 0.87 H), 7.03 (s, 0.13 H), 6.32 (q, $J = 7.1$ Hz, 1 H), 3.76–3.66 (m, 1 H), 3.60 (s, 3 H), 3.49–3.45 (m, 0.13 H), 3.45–3.36 (m, 0.87 H), 3.36–3.24 (m, 1 H), 2.86–2.81 (m, 2 H), 2.26 (s, 3 H), 2.09 (s, 3 H), 2.08 (d, $J = 7.1$ Hz, 3 H), 1.84–1.71 (m, 1 H), 1.71–1.60 (m, 2 H), 1.42–1.27 (m, 1 H). NH signal not resolved.

(*R*)-*tert*-Butyl 3-[(methylsulfonyl)oxy]methylpyrrolidine-1-carboxylate



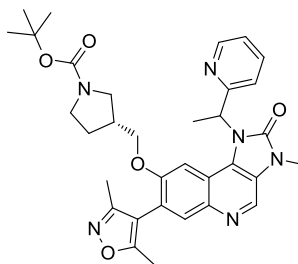
307

A solution of (*R*)-*tert*-butyl 3-(hydroxymethyl)pyrrolidine-1-carboxylate **306** (162 mg, 0.81 mmol) and triethylamine (0.14 mL, 1.01 mmol) in DCM (3 mL) under nitrogen was cooled to 0 °C and methanesulfonyl chloride (0.08 mL, 1.03 mmol) added dropwise. The mixture was stirred at 0 °C for 10 min, allowed to warm to r.t., and then stirred for 2 h. Water (10 mL) was added to the reaction mixture which was then extracted with DCM (2 x 10 mL). The combined organic extracts were passed through a hydrophobic frit and the solvent evaporated *in vacuo*. The crude material was purified on a 25 g silica cartridge using a gradient of 0–10% MeOH in DCM over 10 column volumes. The appropriate fractions were combined and the solvent removed by rotary evaporation to give the title compound as a colourless oil (204 mg, 0.73 mmol, 91%).

^1H NMR (400 MHz, CDCl₃): δ 4.28–4.11 (m, 2 H), 3.62–3.09 (m, 4 H), 3.03 (s, 3 H), 2.70–2.56 (m, 1 H), 2.11–1.99 (m, 1 H), 1.73 (br s, 1 H), 1.46 (s, 9 H).

The ^1H NMR was in agreement with that reported in the literature.¹⁴⁸

(3*R*)-tert-Butyl 3-[(7-(3,5-dimethylisoxazol-4-yl)-3-methyl-2-oxo-1-[1-(pyridin-2-yl)ethyl]-2,3-dihydro-1*H*-imidazo[4,5-*c*]quinolin-8-yl)oxy)methyl]pyrrolidine-1-carboxylate



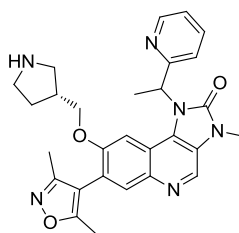
308

A mixture of (*R*)-*tert*-butyl 3-[(methylsulfonyl)oxy]methyl]pyrrolidine-1-carboxylate **307** (52 mg, 0.19 mmol), potassium carbonate (28 mg, 0.20 mmol) and 7-(3,5-dimethylisoxazol-4-yl)-8-hydroxy-3-methyl-1-[(*R*)-1-(pyridin-2-yl)ethyl]-1*H*-imidazo[4,5-*c*]quinolin-2(3*H*)-one **237** (70 mg, 0.17 mmol) was suspended in anhydrous DMF (0.8 mL) and stirred under nitrogen at 45 °C for 16 h. The reaction temperature was raised to 100 °C and left to stir for 3.5 h. The reaction mixture was allowed to cool to r.t. and diluted with MeOH (0.2 mL). The mixture was filtered and purified by MDAP using Method Formic. The appropriate fractions were combined and the solvent removed by rotary evaporation to give the title compound as a dark brown gum (79 mg, 0.13 mmol, 78%).

LCMS (formic A): m/z 599 [(M + H)⁺]; Rt: 0.98 min; 100% purity by peak area.

¹H NMR (400 MHz, DMSO-*d*₆): Variable temperature (393 K) δ 8.81 (s, 1 H), 8.59 (d, J = 4.8 Hz, 1 H), 7.82 (s, 1 H), 7.80–7.73 (m, 1 H), 7.46 (d, J = 7.8 Hz, 1 H), 7.32 (dd, J = 7.3, 4.8 Hz, 1 H), 7.03 (s, 0.15 H), 7.01 (s, 0.85 H), 6.32 (q, J = 7.1 Hz, 1 H), 3.81 (dd, J = 9.6, 6.1 Hz, 0.15 H), 3.76 (dd, J = 9.5, 7.2 Hz, 0.85 H), 3.62 (s, 3 H), 3.51–3.42 (m, 1 H), 3.42–3.35 (m, 1 H), 3.35–3.22 (m, 2 H), 3.03–2.98 (m, 1 H), 2.55–2.47 (m, 1 H), 2.26 (s, 3 H), 2.07 (s, 3 H), 2.07 (d, J = 7.1 Hz, 3 H), 1.99–1.88 (m, 1 H), 1.64–1.53 (m, 1 H), 1.45 (s, 9 H). A 85:15 mixture of diastereoisomers present.

7-(3,5-Dimethylisoxazol-4-yl)-3-methyl-1-[1-(pyridin-2-yl)ethyl]-8-[(R)-pyrrolidin-3-ylmethoxy]-1H-imidazo[4,5-c]quinolin-2(3H)-one



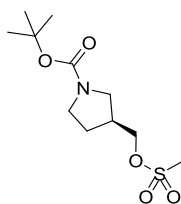
309

A solution of (3*R*)-*tert*-butyl 3-[(7-(3,5-dimethylisoxazol-4-yl)-3-methyl-2-oxo-1-[1-(pyridin-2-yl)ethyl]-2,3-dihydro-1*H*-imidazo[4,5-*c*]quinolin-8-yl)oxy)methyl]pyrrolidine-1-carboxylate **308** (73 mg, 0.12 mmol) was dissolved in DCM (1.5 mL) and treated with TFA (0.5 mL, 6.49 mmol). The mixture was allowed to stand in a stoppered vessel at r.t. for 2 h. The reaction mixture was evaporated *in vacuo* and the crude material purified by MDAP using Method HpH. The appropriate fractions were combined and the solvent removed by rotary evaporation to give the title compound as a white solid (44 mg, 0.09 mmol, 72%).

LCMS (formic A): m/z 499 [(M + H)⁺]; Rt: 0.53 min; 100% purity by peak area.

¹H NMR (400 MHz, DMSO-*d*₆): Variable temperature (393 K) δ 8.77 (s, 1 H), 8.58 (d, $J = 4.8$ Hz, 1 H), 7.78 (s, 1 H), 7.77–7.72 (m, 1 H), 7.42 (d, $J = 7.3$ Hz, 1 H), 7.30 (dd, $J = 7.3, 4.8$ Hz, 1 H), 6.99 (s, 1 H), 6.29 (q, $J = 7.3$ Hz, 1 H), 3.74 (dd, $J = 9.8, 3.2$ Hz, 0.15 H), 3.69 (dd, $J = 9.6, 6.3$ Hz, 0.85 H), 3.59 (s, 3 H), 3.46–3.37 (m, 1 H), 2.84–2.78 (m, 2 H), 2.53–2.49 (m, 1 H), 2.38–2.27 (m, 1 H), 2.24 (s, 3 H), 2.04 (s, 3 H), 2.05 (d, $J = 7.3$ Hz, 3 H), 1.84–1.74 (m, 1 H), 1.40–1.28 (m, 1 H). One pyrrolidine proton signal obscured by water. *NH* signal not resolved. A 85:15 mixture of diastereoisomers present.

(S)-*tert*-Butyl 3-[(methylsulfonyl)oxy]methylpyrrolidine-1-carboxylate



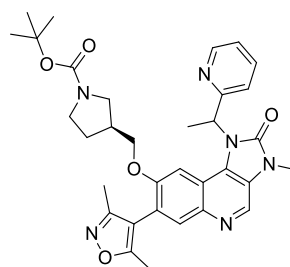
311

A solution of (*S*)-*tert*-butyl 3-(hydroxymethyl)pyrrolidine-1-carboxylate **310** (174 mg, 0.87 mmol) and triethylamine (0.150 mL, 1.08 mmol) in DCM (3 mL) under nitrogen was cooled to 0 °C and methanesulfonyl chloride (0.086 mL, 1.10 mmol) added dropwise. The mixture was stirred at 0 °C for 10 min, allowed to warm to r.t., and then stirred for 2 h. Water

(10 mL) was added to the reaction mixture which was then extracted with DCM (2 x 10 mL). The combined organic extracts were passed through a hydrophobic frit and the solvent evaporated *in vacuo*. The crude material was purified on a 25 g silica cartridge using a gradient of 0–10% MeOH in DCM over 10 column volumes. The appropriate fractions were combined and the solvent removed by rotary evaporation to give the title compound as a colourless oil (219 mg, 0.78 mmol, 91%).

¹H NMR (400 MHz, CDCl₃): δ 4.28–4.11 (m, 2 H), 3.62–3.09 (m, 4 H), 3.03 (s, 3 H), 2.70–2.56 (m, 1 H), 2.11–1.99 (m, 1 H), 1.73 (br s, 1 H), 1.46 (s, 9 H).

(3*S*)-*tert*-Butyl 3-[(7-(3,5-dimethylisoxazol-4-yl)-3-methyl-2-oxo-1-[1-(pyridin-2-yl)ethyl]-2,3-dihydro-1*H*-imidazo[4,5-*c*]quinolin-8-yl)oxy)methyl]pyrrolidine-1-carboxylate



312

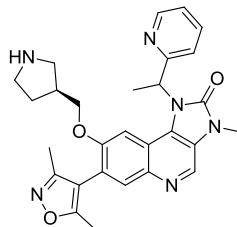
A mixture of (*S*)-*tert*-butyl 3-[(methylsulfonyl)oxy]methyl]pyrrolidine-1-carboxylate **311** (37 mg, 0.13 mmol), potassium carbonate (20 mg, 0.14 mmol) and 7-(3,5-dimethylisoxazol-4-yl)-8-hydroxy-3-methyl-1-[(*R*)-1-(pyridin-2-yl)ethyl]-1*H*-imidazo[4,5-*c*]quinolin-2(3*H*)-one **237** (50 mg, 0.12 mmol) was suspended in anhydrous DMF (0.5 mL) and stirred under nitrogen at 100 °C for 4 h. The reaction mixture was allowed to cool to r.t. and diluted with MeOH (0.5 mL). The mixture was filtered and was purified by MDAP using Method HpH. The appropriate fractions were combined and the solvent removed by rotary evaporation to give the title compound as a colourless gum (49 mg, 0.08 mmol, 68%).

LCMS (formic A): *m/z* 599 [(M + H)⁺]; Rt: 0.94 min; 100% purity by peak area.

¹H NMR (400 MHz, DMSO-*d*₆): Variable temperature (393 K) δ 8.77 (s, 1 H), 8.57 (d, *J* = 4.8 Hz, 1 H), 7.79 (s, 1 H), 7.76–7.70 (m, 1 H), 7.42 (d, *J* = 7.8 Hz, 1 H), 7.29 (dd, *J* = 7.3, 4.8 Hz, 1 H), 7.02 (s, 0.85 H), 7.00 (s, 0.15 H), 6.29 (q, *J* = 7.1 Hz, 1 H), 3.79 (dd, *J* = 9.6, 6.3 Hz, 0.85 H), 3.73 (dd, *J* = 9.6, 7.0 Hz, 0.15 H), 3.59 (s, 3 H), 3.45–3.39 (m, 1 H), 3.37–3.28 (m, 2 H), 3.26–3.19 (m, 1 H), 2.94 (dd, *J* = 10.9, 6.8 Hz, 1 H), 2.52–2.44 (m, 1 H), 2.23

(s, 3 H), 2.05 (d, $J = 7.1$ Hz, 3 H), 2.04 (s, 3 H), 1.98–1.87 (m, 1 H), 1.62–1.52 (m, 1 H), 1.41 (s, 9 H). A 85:15 mixture of diastereoisomers present.

7-(3,5-Dimethylisoxazol-4-yl)-3-methyl-1-[1-(pyridin-2-yl)ethyl]-8-[(*S*)-pyrrolidin-3-ylmethoxy]-1*H*-imidazo[4,5-*c*]quinolin-2(3*H*)-one



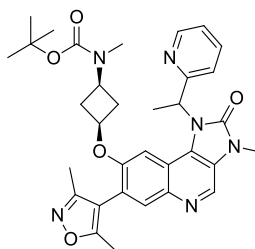
313

A solution of (*3S*)-*tert*-butyl 3-[(7-(3,5-dimethylisoxazol-4-yl)-3-methyl-2-oxo-1-[1-(pyridin-2-yl)ethyl]-2,3-dihydro-1*H*-imidazo[4,5-*c*]quinolin-8-yl]oxymethyl]pyrrolidine-1-carboxylate **312** (39 mg, 0.07 mmol) was dissolved in DCM (0.6 mL) and treated with TFA (0.3 mL, 3.89 mmol). The mixture was allowed to stand in a stoppered vessel at r.t. for 2 h. The reaction mixture was evaporated under a stream of nitrogen and the gum dissolved in MeOH (0.5 mL). The solution was applied to a MeOH preconditioned 1 g SCX-2 cartridge which was then washed with MeOH (6 mL) followed by 2 M ammonia in MeOH solution (6 mL). The basic wash was evaporated under a stream of nitrogen to give the title compound as a white solid (28 mg, 0.06 mmol, 86%).

LCMS (formic A): m/z 499 [(M + H)⁺]; Rt: 0.53 min; 100% purity by peak area.

¹H NMR (400 MHz, DMSO-*d*₆): Variable temperature (393 K) δ 8.77 (s, 1 H), 8.58 (d, $J = 4.8$ Hz, 1 H), 7.78 (s, 1 H), 7.77–7.71 (m, 1 H), 7.42 (d, $J = 7.8$ Hz, 1 H), 7.30 (dd, $J = 7.3, 4.8$ Hz, 1 H), 6.98 (s, 1 H), 6.29 (q, $J = 7.1$ Hz, 1 H), 3.74–3.65 (m, 1 H), 3.59 (s, 3 H), 3.40–3.34 (m, 1 H), 2.79–2.70 (m, 4 H), 2.42 (dd, $J = 10.6, 6.3$ Hz, 1 H), 2.34–2.25 (m, 1 H), 2.24 (s, 3 H), 2.04 (s, 3 H), 2.05 (d, $J = 7.1$ Hz, 3 H), 1.82–1.71 (m, 1 H), 1.36–1.26 (m, 1 H). One pyrrolidine proton signal obscured by water. NH signal not resolved. A estimated 85:15 mixture of diastereoisomers present; signal overlap prevented accurate ratio determination.

***tert*-Butyl [cis-3-({7-(3,5-dimethylisoxazol-4-yl)-3-methyl-2-oxo-1-[1-(pyridin-2-yl)ethyl]-2,3-dihydro-1*H*-imidazo[4,5-*c*]quinolin-8-yl}oxy)cyclobutyl](methyl)carbamate**



315

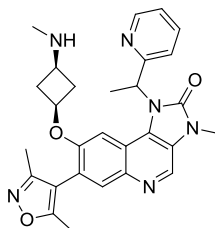
A slurry of sodium hydride (60% dispersion in mineral oil, 20 mg, 0.500 mmol) in anhydrous THF (0.5 mL) under nitrogen was cooled in an ice-water bath and iodomethane (30 μ L, 0.482 mmol) added. A solution of *trans*-3-[(*tert*-butoxycarbonyl)amino]cyclobutyl methanesulfonate **287** (100 mg, 0.377 mmol) in anhydrous THF (1.5 mL) was added and the mixture stirred in the ice-water bath for 5 min then at r.t. for 18 h. The reaction mixture was quenched by the addition of water and the mixture extracted with EtOAc (2 x 5 mL). The organic extracts were combined, passed through a hydrophobic frit and the solvent evaporated under vacuum. The gum was loaded in DCM (2 mL) and purified on a 25 g silica cartridge using a gradient of 0–15% MeOH in DCM over 10 column volumes. The appropriate fractions were combined and the solvent removed by rotary evaporation to give crude *cis*-3-[(*tert*-butoxycarbonyl)(methyl)amino]cyclobutyl methanesulfonate as a clear gum (70 mg) which was used without further purification in the next step.

A mixture of crude *trans*-3-[(*tert*-butoxycarbonyl)(methyl)amino]cyclobutyl methanesulfonate (70 mg), potassium carbonate (40 mg, 0.289 mmol) and 7-(3,5-dimethylisoxazol-4-yl)-8-hydroxy-3-methyl-1-[(*R*)-1-(pyridin-2-yl)ethyl]-1*H*-imidazo[4,5-*c*]quinolin-2(3*H*)-one **237** (100 mg, 0.241 mmol) was suspended in anhydrous DMF (0.8 mL) and stirred under nitrogen at 100 °C for 6 h. The reaction mixture was diluted with MeOH (0.2 mL), filtered, and purified by MDAP using Method Formic. The appropriate fractions were combined and the solvent removed by rotary evaporation. The residue was dissolved in MeOH (0.5 mL) and applied to a MeOH preconditioned 1 g SCX-2 cartridge. The cartridge was washed with MeOH (6 mL) followed by 2 M ammonia in MeOH solution (6 mL) and the basic wash was evaporated under a stream of nitrogen. The sample was purified on a Chiralcel[®] OD-H column (250 mm x 30 mm, 5 μ m packing diameter). An isocratic system of 25% IPA in EtOH with a flow rate of 40 mL/min was used at r.t. The UV detection was performed at 240 nm. The appropriate fractions were combined and evaporated *in vacuo* to give the title compound as a white solid (22 mg, 0.037 mmol, 10%).

LCMS (formic A): m/z 599 $[(M + H)^+]$; Rt: 1.01 min; 100% purity by peak area.

^1H NMR (400 MHz, $\text{DMSO-}d_6$): Variable temperature (393 K) δ 8.77 (s, 1 H), 8.65 (d, $J = 4.8$ Hz, 1 H), 7.82 (s, 1 H), 7.80–7.73 (m, 1 H), 7.43 (d, $J = 7.8$ Hz, 1 H), 7.33 (dd, $J = 7.8, 4.8$ Hz, 1 H), 6.92 (s, 1 H), 6.27 (q, $J = 7.2$ Hz, 1 H), 4.05–3.95 (m, 1 H), 3.95–3.86 (m, 1 H), 3.58 (s, 3 H), 2.70 (s, 3 H), 2.77–2.68 (m, 1 H), 2.47–2.40 (m, 1 H), 2.27 (s, 3 H), 2.09 (s, 3 H), 2.06 (d, $J = 7.2$ Hz, 3 H), 2.04–1.97 (m, 2 H), 1.42 (s, 9 H).

7-(3,5-Dimethylisoxazol-4-yl)-3-methyl-8-[*cis*-3-(methylamino)cyclobutoxy]-1-[1-(pyridin-2-yl)ethyl]-1*H*-imidazo[4,5-*c*]quinolin-2(3*H*)-one



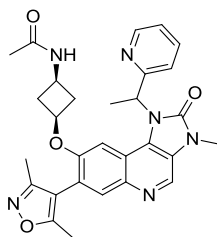
316

A solution of *tert*-butyl [cis-3-({7-(3,5-dimethylisoxazol-4-yl)-3-methyl-2-oxo-1-[1-(pyridin-2-yl)ethyl]-2,3-dihydro-1*H*-imidazo[4,5-*c*]quinolin-8-yl}oxy)cyclobutyl](methyl)-carbamate **315** (19 mg, 0.032 mmol) in DCM (0.75 mL) was treated with TFA (0.25 mL, 3.24 mmol). The mixture was allowed to stand in a stoppered vessel at r.t. for 2 h and then evaporated under a stream of nitrogen. The residue was dissolved in MeOH (0.5 mL) and applied to a MeOH preconditioned 0.5 g SCX-2 cartridge. The cartridge was washed with MeOH (5 mL) followed by 2 M ammonia in MeOH solution (5 mL). The basic wash was evaporated under a stream of nitrogen to give the title compound as a white solid (11 mg, 0.022 mmol, 70%).

LCMS (formic A): m/z 499 $[(M + H)^+]$; Rt: 0.53 min; 100% purity by peak area.

^1H NMR (400 MHz, $\text{DMSO-}d_6$): Variable temperature (393 K) δ 8.77 (s, 1 H), 8.63 (d, $J = 4.8$ Hz, 1 H), 7.80 (s, 1 H), 7.78–7.72 (m, 1 H), 7.41 (d, $J = 7.8$ Hz, 1 H), 7.32 (dd, $J = 7.8, 4.8$ Hz, 1 H), 6.88 (s, 1 H), 6.27 (q, $J = 7.2$ Hz, 1 H), 3.96–3.84 (m, 1 H), 3.58 (s, 3 H), 2.75–2.65 (m, 1 H), 2.45–2.35 (m, 1 H), 2.27 (s, 3 H), 2.22 (s, 3 H), 2.08 (s, 3 H), 2.06 (d, $J = 7.2$ Hz, 3 H), 1.64–1.55 (m, 2 H). *NH* signal not resolved. 1 x Cyclobutyl signal obscured by DMSO.

***N*-[*cis*-3-({7-(3,5-Dimethylisoxazol-4-yl)-3-methyl-2-oxo-1-[1-(pyridin-2-yl)ethyl]-2,3-dihydro-1*H*-imidazo[4,5-*c*]quinolin-8-yl}oxy)cyclobutyl]acetamide**



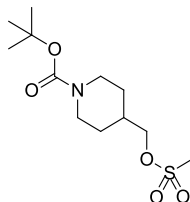
317

A solution of 8-(*cis*-3-aminocyclobutoxy)-7-(3,5-dimethylisoxazol-4-yl)-3-methyl-1-[1-(pyridin-2-yl)ethyl]-1*H*-imidazo[4,5-*c*]quinolin-2(3*H*)-one **289** (20 mg, 0.041 mmol) was dissolved in DCM (0.4 mL) and treated with triethylamine (9 μ L, 0.065 mmol) in DCM (0.1 mL). A solution of acetyl chloride (4 μ L, 0.056 mmol) in DCM (0.1 mL) was then added and the mixture allowed to stand at r.t. for 3 h. The reaction mixture was diluted with DCM (1 mL) washed with water (2 x 2 mL) then passed through a hydrophobic frit. The solvent was evaporated under a stream of nitrogen and the residue dissolved in DCM (0.5 mL). The solution was applied to a 10 g silica cartridge and purified using a gradient of 0–20% MeOH in DCM over 10 column volumes. The appropriate fractions were combined and the solvent removed by rotary evaporation to give the title compound as an off-white solid (17 mg, 0.031 mmol, 76%).

LCMS (formic A): m/z 527 [(M + H)⁺]; Rt: 0.65 min; 100% purity by peak area.

¹H NMR (400 MHz, DMSO-*d*₆): Variable temperature (393 K) δ 8.77 (s, 1 H), 8.64 (d, J = 4.8 Hz, 1 H), 7.81 (s, 1 H), 7.79–7.73 (m, 1 H), 7.67 (br s, 1 H), 7.43 (d, J = 7.8 Hz, 1 H), 7.33 (dd, J = 7.8, 4.8 Hz, 1 H), 6.90 (s, 1 H), 6.27 (q, J = 7.1 Hz, 1 H), 3.98–3.85 (m, 2 H), 3.58 (s, 3 H), 2.85–2.75 (m, 1 H), 2.58–2.50 (m, 1 H), 2.27 (s, 3 H), 2.09 (s, 3 H), 2.06 (d, J = 7.1 Hz, 3 H), 1.91–1.81 (m, 2 H), 1.78 (s, 3 H).

***tert*-Butyl 4-[[*(methylsulfonyl)oxy*]methyl]piperidine-1-carboxylate**



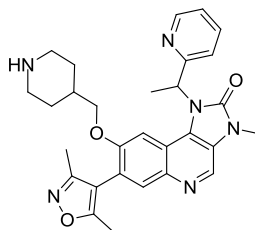
321

A stirred solution of *tert*-butyl 4-(hydroxymethyl)piperidine-1-carboxylate **320** (310 mg, 1.440 mmol) and triethylamine (0.26 mL, 1.865 mmol) in DCM (3 mL) at 0 °C was

treated with methanesulfonyl chloride (0.13 mL, 1.668 mmol). The mixture was stirred for 1 h under nitrogen and then sat. NaHCO₃ (aq) (10 mL) was added. The aqueous layer was separated and extracted with DCM (10 mL). The organic layers were combined and washed with sat. NaHCO₃ (aq) (10 mL). The organic layer was separated, passed through a hydrophobic frit and the solvent evaporated under vacuum to give the title compound as a yellow oil (386 mg, 1.316 mmol, 91%).

¹H NMR (400 MHz, CDCl₃): δ 4.23–4.10 (m, 2 H), 4.10–4.04 (m, 2 H), 3.01 (s, 3 H), 2.78–2.65 (m, 2 H), 1.98–1.86 (m, 1 H), 1.79–1.69 (m, 2 H), 1.46 (br s, 9 H), 1.31–1.15 (m, 2 H). The ¹H NMR was in agreement with that reported in the literature.¹⁴⁹

7-(3,5-Dimethylisoxazol-4-yl)-3-methyl-8-(piperidin-4-ylmethoxy)-1-[1-(pyridin-2-yl)ethyl]-1H-imidazo[4,5-c]quinolin-2(3H)-one



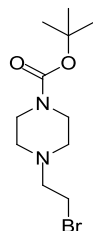
322

A mixture of 7-(3,5-dimethylisoxazol-4-yl)-8-hydroxy-3-methyl-1-[(*R*)-1-(pyridin-2-yl)ethyl]-1H-imidazo[4,5-*c*]quinolin-2(3H)-one **237** (63 mg, 0.152 mmol), *tert*-butyl 4-[[[(methylsulfonyl)oxy]methyl]piperidine-1-carboxylate **321** (59 mg, 0.201 mmol) and potassium carbonate (34 mg, 0.246 mmol) in DMF (1.5 mL) was stirred under nitrogen at 100 °C and for 2.5 h. The reaction mixture was allowed to cool to r.t., diluted with EtOAc (8 mL) and washed with brine (8 mL). The aqueous layer was separated and extracted with EtOAc (8 mL), the organic layers combined and passed through a hydrophobic frit. The solvent was removed by rotary evaporation and the residue dissolved in MeOH (1 mL). The solution was applied to a MeOH preconditioned 2 g SCX-2 cartridge. The cartridge was washed with MeOH (10 mL) followed by 2 M ammonia in MeOH solution (10 mL). The basic wash was evaporated *in vacuo* and the residue dissolved in 1,4-dioxane (0.7 mL). To the solution was added 4 M HCl in 1,4-dioxane solution (0.5 mL, 0.152 mmol) and the mixture left to stir at r.t. for 1 h. The reaction was concentrated under a stream of nitrogen and the residue purified by MDAP using Method HpH. The appropriate fractions were combined and the solvent removed by rotary evaporation to give the title compound as a green solid (53 mg, 0.103 mmol, 68%).

LCMS (HpH): m/z 513 [(M + H)⁺]; Rt: 0.78 min; 100% purity by peak area.

¹H NMR (400 MHz, DMSO-*d*₆): Variable temperature (393 K) δ 8.77 (s, 1 H), 8.58 (d, J = 4.8 Hz, 1 H), 7.77 (s, 1 H), 7.77–7.71 (m, 1 H), 7.41 (d, J = 7.8 Hz, 1 H), 7.31 (dd, J = 7.8, 4.8 Hz, 1 H), 6.97 (s, 1 H), 6.29 (q, J = 7.3 Hz, 1 H), 3.64–3.60 (m, 1 H), 3.59 (s, 3 H), 3.28 (dd, J = 9.4, 6.8 Hz, 1 H), 2.96–2.89 (m, 2 H), 2.46–2.41 (m, 1 H), 2.23 (s, 3 H), 2.05 (d, J = 7.3 Hz, 3 H), 2.03 (s, 3 H), 1.77–1.65 (m, 1 H), 1.57–1.47 (m, 2 H), 1.13–0.99 (m, 2 H). One piperidine proton signal obscured by DMSO. NH signal not resolved.

***tert*-Butyl 4-(2-bromoethyl)piperazine-1-carboxylate**



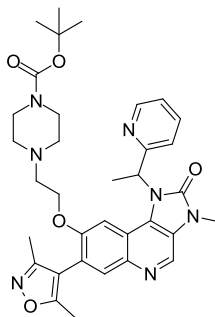
324

tert-Butyl 4-(2-hydroxyethyl)piperazine-1-carboxylate **323** (1.15 g, 4.99 mmol) was dissolved in anhydrous THF (20 mL) and carbon tetrabromide (1.82 g, 5.49 mmol) added. A solution of triphenylphosphine (1.44 g, 5.49 mmol) in anhydrous THF (5 mL) was added dropwise over 1 h. The mixture was stirred at r.t. for 4 h, then left to stand for 56 h. Isohexane (10 mL) was added to the mixture, which was then washed sequentially with sat. NaHCO₃ (aq) (2 x 5 mL), water (5 mL), and brine (5 mL). The organic phase was passed through a hydrophobic frit and evaporated *in vacuo*. The resulting oil was dissolved in DCM (5 mL) and purified on a 100 g silica cartridge using a gradient of 0–100% EtOAc in cyclohexane over 10 column volumes. The appropriate fractions were combined and the solvent removed by rotary evaporation to give the title compound as an off-white solid (954 mg, 3.25 mmol, 65%).

¹H NMR (400 MHz, CDCl₃): δ 3.47–3.39 (m, 6 H), 2.79 (t, J = 7.2 Hz, 2 H), 2.45 (t, J = 5.2 Hz, 4 H), 1.46 (s, 9 H).

The ¹H NMR was in agreement with that reported in the literature.¹⁵⁰

***tert*-Butyl 4-[2-({7-(3,5-dimethylisoxazol-4-yl)-3-methyl-2-oxo-1-[1-(pyridin-2-yl)ethyl]-2,3-dihydro-1*H*-imidazo[4,5-*c*]quinolin-8-yl}oxy)ethyl]piperazine-1-carboxylate**

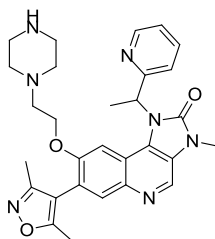
**325**

A mixture of *tert*-butyl 4-(2-bromoethyl)piperazine-1-carboxylate **324** (50 mg, 0.171 mmol), potassium carbonate (25 mg, 0.181 mmol) and 7-(3,5-dimethylisoxazol-4-yl)-8-hydroxy-3-methyl-1-[(*R*)-1-(pyridin-2-yl)ethyl]-1*H*-imidazo[4,5-*c*]quinolin-2(3*H*)-one **237** (60 mg, 0.144 mmol) was suspended in anhydrous DMF (0.8 mL) and stirred under nitrogen at 75 °C for 16 h. The reaction mixture was allowed to cool to r.t., diluted with MeOH (0.2 mL) and purified by MDAP using Method Formic. The appropriate fractions were combined and the solvent removed by rotary evaporation to give the title compound as a white foam (63 mg, 0.100 mmol, 70%).

LCMS (formic A): m/z 628 [(M + H)⁺]; Rt: 0.69 min; 100% purity by peak area.

¹H NMR (400 MHz, DMSO-*d*₆): Variable temperature (393 K) δ 8.77 (s, 1 H), 8.59 (d, J = 4.8 Hz, 1 H), 7.79 (s, 1 H), 7.77–7.69 (m, 1 H), 7.42 (d, J = 7.8 Hz, 1 H), 7.30 (dd, J = 7.8, 4.8 Hz, 1 H), 7.02 (s, 1 H), 6.30 (q, J = 7.2 Hz, 1 H), 3.94–3.86 (m, 1 H), 3.66–3.59 (m, 1 H), 3.59 (s, 3 H), 3.28 (t, J = 5.1 Hz, 4 H), 2.63 (t, J = 5.7 Hz, 2 H), 2.35–2.30 (m, 4 H), 2.25 (s, 3 H), 2.06 (s, 3 H), 2.05 (d, J = 7.2 Hz, 3 H), 1.40 (s, 9 H).

7-(3,5-Dimethylisoxazol-4-yl)-3-methyl-8-[2-(piperazin-1-yl)ethoxy]-1-[1-(pyridin-2-yl)ethyl]-1*H*-imidazo[4,5-*c*]quinolin-2(3*H*)-one

**326**

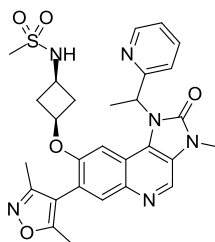
A solution of *tert*-butyl 4-[2-({7-(3,5-dimethylisoxazol-4-yl)-3-methyl-2-oxo-1-[1-(pyridin-2-yl)ethyl]-2,3-dihydro-1*H*-imidazo[4,5-*c*]quinolin-8-yl}oxy)ethyl]piperazine-1-

carboxylate **325** (53 mg, 0.084 mmol) in DCM (0.7 mL) was treated with TFA (0.3 mL, 3.89 mmol). The mixture was allowed to stand in a stoppered vessel at r.t. for 1.5 h. The reaction mixture was evaporated under a stream of nitrogen and the residue dissolved in MeOH (0.5 mL). The solution was applied to a MeOH preconditioned 1 g SCX-2 cartridge. The cartridge was washed with MeOH (5 mL) followed by 2 M ammonia in MeOH solution (5 mL). The basic wash was evaporated under a stream of nitrogen to give the title compound as an off-white solid (37 mg, 0.070 mmol, 83%).

LCMS (HpH): m/z 528 $[(M + H)^+]$; Rt: 0.76 min; 100% purity by peak area.

^1H NMR (400 MHz, DMSO- d_6): Variable temperature (393 K), δ 8.76 (s, 1 H), 8.59 (d, $J = 4.8$ Hz, 1 H), 7.78 (s, 1 H), 7.77–7.71 (m, 1 H), 7.42 (d, $J = 7.8$ Hz, 1 H), 7.29 (dd, $J = 7.8, 4.8$ Hz, 1 H), 7.01 (s, 1 H), 6.30 (q, $J = 7.2$ Hz, 1 H), 3.91–3.84 (m, 1 H), 3.65–3.58 (m, 1 H), 3.59 (s, 3 H), 2.72–2.65 (m, 4 H), 2.56 (t, $J = 5.8$ Hz, 2 H), 2.33–2.27 (m, 4 H), 2.25 (s, 3 H), 2.07 (s, 3 H), 2.05 (d, $J = 7.2$ Hz, 3 H). NH signal not resolved.

***N*-[*cis*-3-({7-(3,5-dimethylisoxazol-4-yl)-3-methyl-2-oxo-1-[1-(pyridin-2-yl)ethyl]-2,3-dihydro-1*H*-imidazo[4,5-*c*]quinolin-8-yl}oxy)cyclobutyl]methanesulfonamide**



327

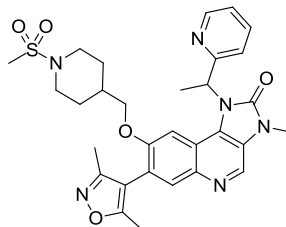
A solution of 8-(*cis*-3-aminocyclobutoxy)-7-(3,5-dimethylisoxazol-4-yl)-3-methyl-1-[1-(pyridin-2-yl)ethyl]-1*H*-imidazo[4,5-*c*]quinolin-2(3*H*)-one **289** (30 mg, 0.062 mmol) and DIPEA (11 μL , 0.062 mmol) in DCM (1 mL) was treated with methanesulfonyl chloride (5 μL , 0.068 mmol) and the mixture stirred at r.t. for 3 h. The solvent was evaporated under a stream of nitrogen and the residue purified by MDAP using Method Formic. The appropriate fractions were combined and the solvent evaporated *in vacuo* to give the title compound as a white solid (29 mg, 0.051 mmol, 82%).

LCMS (formic A): m/z 563 $[(M + H)^+]$; Rt: 0.71 min; 100% purity by peak area.

^1H NMR (400 MHz, DMSO- d_6): Variable temperature (393 K) δ 8.83 (s, 1 H), 8.67 (d, $J = 4.8$ Hz, 1 H), 7.86 (s, 1 H), 7.83–7.76 (m, 1 H), 7.47 (d, $J = 7.8$ Hz, 1 H), 7.36 (dd, $J = 7.8, 4.8$ Hz, 1 H), 7.12 (br s, 1 H), 6.95 (s, 1 H), 6.31 (q, $J = 7.1$ Hz, 1 H), 4.03–3.95 (m, 1 H),

3.61 (s, 3 H), 3.58–3.50 (m, 1 H), 3.23 (s, 3 H), 2.93–2.84 (m, 1 H), 2.66–2.57 (m, 1 H), 2.31 (s, 3 H), 2.12 (s, 3 H), 2.10 (d, $J = 7.1$ Hz, 3 H), 2.02–1.94 (m, 2 H).

7-(3,5-Dimethylisoxazol-4-yl)-3-methyl-8-[[1-(methanesulfonyl)piperidin-4-yl]methoxy]-1-[1-(pyridin-2-yl)ethyl]-1*H*-imidazo[4,5-*c*]quinolin-2(3*H*)-one



328

A solution of 7-(3,5-dimethylisoxazol-4-yl)-3-methyl-8-(piperidin-4-ylmethoxy)-1-[1-(pyridin-2-yl)ethyl]-1*H*-imidazo[4,5-*c*]quinolin-2(3*H*)-one **322** (27 mg, 0.053 mmol) in anhydrous DCM (0.25 mL) and pyridine (0.125 mL) was treated with methanesulfonyl chloride (5 μ L, 0.064 mmol) and the mixture allowed to stir at r.t. in a stoppered vessel for 1 h. Further methanesulfonyl chloride (5 μ L, 0.064 mmol) was added and left for 1 h. Further methanesulfonyl chloride (25 μ L, 0.32 mmol) was added and left for 5 h. The reaction mixture was evaporated under a stream of nitrogen and the residue dissolved in DCM (1 mL). The organic layer was washed with water (1 mL), passed through a hydrophobic frit and the solvent removed under a stream of nitrogen. The residue was purified by MDAP using Method Formic. The appropriate fraction was evaporated *in vacuo* and the residue dissolved in MeOH (0.5 mL). The solution was applied to a MeOH preconditioned 0.5 g NH₂ cartridge which was then washed with MeOH (3 mL). The solvent was evaporated under a stream of nitrogen to give the title compound as a white solid (23 mg, 0.039 mmol, 74%).

m.p.: 151 °C.

IR (solid) ν (cm⁻¹): 2926, 1703, 1621, 1581, 1453, 1326, 1215, 1144, 1037, 774.

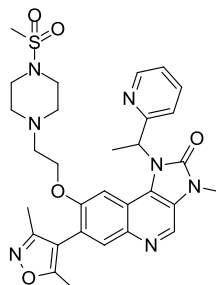
LCMS (formic A): m/z 591 [(M + H)⁺]; Rt: 0.76 min; 100% purity by peak area.

HRMS (ESI): M + H calcd for C₃₀H₃₅N₆O₅S 591.2384, found 591.2375.

¹H NMR (400 MHz, DMSO-*d*₆): Variable temperature (393 K) δ 8.78 (s, 1 H), 8.59 (d, $J = 4.8$ Hz, 1 H), 7.78 (s, 1 H), 7.78–7.72 (m, 1 H), 7.43 (d, $J = 7.8$ Hz, 1 H), 7.32 (dd, $J = 7.8, 4.8$ Hz, 1 H), 6.99 (s, 1 H), 6.29 (q, $J = 7.2$ Hz, 1 H), 3.69 (dd, $J = 9.6, 6.3$ Hz, 1 H), 3.59 (s, 3 H), 3.63–3.56 (m, 2 H), 3.35 (dd, $J = 9.6, 6.3$ Hz, 1 H), 2.80 (s, 3 H), 2.77–2.69 (m, 2 H), 2.24 (s, 3 H), 2.05 (d, $J = 7.2$ Hz, 3 H), 2.04 (s, 3 H), 1.86–1.74 (m, 1 H), 1.74–1.64 (m, 2 H), 1.31–1.17 (m, 2 H).

^{13}C NMR (150 MHz, $\text{DMSO-}d_6$): δ 166.1, 159.6 (2 C), 154.6, 154.5, 149.4, 141.0, 137.3, 133.6, 130.7 (2 C), 124.0, 122.7, 121.8, 121.5, 115.9, 112.5, 102.0, 72.7, 45.7, 45.7, 35.5, 34.9, 28.8, 28.6, 27.9, 17.8, 11.6, 10.8. Benzylic ^{13}C signal not observed.

7-(3,5-Dimethylisoxazol-4-yl)-3-methyl-8-{2-[4-(methanesulfonyl)piperazin-1-yl]ethoxy}-1-[1-(pyridin-2-yl)ethyl]-1H-imidazo[4,5-c]quinolin-2(3H)-one



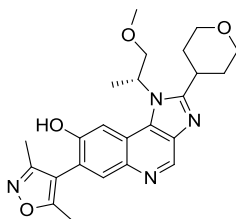
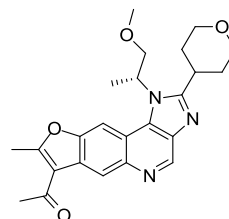
329

A solution of 7-(3,5-dimethylisoxazol-4-yl)-3-methyl-8-[2-(piperazin-1-yl)ethoxy]-1-[1-(pyridin-2-yl)ethyl]-1H-imidazo[4,5-c]quinolin-2(3H)-one **326** (20 mg, 0.038 mmol) in anhydrous DCM (0.25 mL) and pyridine (0.125 mL) was treated with methanesulfonyl chloride (3.5 μL , 0.05 mmol) and the mixture allowed to stir at r.t. in a stoppered vessel for 1 h. The reaction mixture was evaporated under a stream of nitrogen and the residue dissolved in DCM (1 mL). The organic layer was washed with water (1 mL), passed through a hydrophobic frit and the solvent removed under a stream of nitrogen. The residue was purified by MDAP using Method Formic. The appropriate fraction was evaporated *in vacuo* and the residue dissolved in MeOH (0.5 mL). The solution was applied to a MeOH preconditioned 0.5 g NH_2 cartridge which was then washed with MeOH (3 mL). The solvent was evaporated under a stream of nitrogen to give the title compound as a colourless gum (13 mg, 0.02 mmol, 57%).

LCMS (formic A): m/z 606 $[(\text{M} + \text{H})^+]$; Rt: 0.57 min; 100% purity by peak area.

^1H NMR (400 MHz, $\text{DMSO-}d_6$): Variable temperature (393 K) δ 8.77 (s, 1 H), 8.60 (d, $J = 4.8$ Hz, 1 H), 7.79 (s, 1 H), 7.78–7.72 (m, 1 H), 7.42 (d, $J = 7.8$ Hz, 1 H), 7.31 (dd, $J = 7.8, 4.8$ Hz, 1 H), 7.02 (s, 1 H), 6.30 (q, $J = 7.2$ Hz, 1 H), 3.94–3.86 (m, 1 H), 3.66–3.60 (m, 1 H), 3.59 (s, 3 H), 3.13–3.06 (m, 4 H), 2.82 (s, 3 H), 2.68 (t, $J = 5.7$ Hz, 2 H), 2.25 (s, 3 H), 2.07 (s, 3 H), 2.06 (d, $J = 7.2$ Hz, 3 H). 4 x piperazine signals obscured by DMSO.

(3,5-Dimethylisoxazol-4-yl)-1-[(*R*)-1-methoxypropan-2-yl]-2-(tetrahydro-2*H*-pyran-4-yl)-1*H*-imidazo[4,5-*c*]quinolin-8-ol and (*R*)-1-[1-(1-methoxypropan-2-yl)-8-methyl-2-(tetrahydro-2*H*-pyran-4-yl)-1*H*-furo[2,3-*g*]imidazo[4,5-*c*]quinolin-7-yl]ethanone

**332****364**

A solution of 4-{8-(benzyloxy)-1-[(*R*)-1-methoxypropan-2-yl]-2-(tetrahydro-2*H*-pyran-4-yl)-1*H*-imidazo[4,5-*c*]quinolin-7-yl}-3,5-dimethylisoxazole **356** (1.17 g, 2.22 mmol) in EtOH (5 mL) was hydrogenated over 5% Pd/C (100 mg) at r.t. and atmospheric pressure for 24 h. The reaction mixture was filtered through Celite, which was then washed with EtOH (30 mL) and the filtrate evaporated *in vacuo*. The resulting gum was dissolved in DCM (5 mL) and purified on a 100 g silica cartridge using a gradient of 0–20% MeOH in DCM over 12 column volumes. The appropriate fractions were combined and the solvent removed by rotary evaporation to give:

7-(3,5-dimethylisoxazol-4-yl)-1-[(*R*)-1-methoxypropan-2-yl]-2-(tetrahydro-2*H*-pyran-4-yl)-1*H*-imidazo[4,5-*c*]quinolin-8-ol **332** as a light yellow gum (891 mg, 2.041 mmol, 92%).

LCMS (formic A): m/z 437 [(M + H)⁺]; Rt: 0.60 min; 100% purity by peak area.

¹H NMR (400 MHz, DMSO-*d*₆): Variable temperature (393 K) δ 9.83 (br s, 1 H), 8.92 (s, 1 H), 7.89 (s, 1 H), 7.80 (s, 1 H), 5.38–5.24 (m, 1 H), 4.12–4.04 (m, 1 H), 4.03–3.92 (m, 2 H), 3.63–3.52 (m, 3 H), 3.40 (tt, $J = 10.9, 4.0$ Hz, 1 H), 3.23 (s, 3 H), 2.33 (s, 3 H), 2.17 (s, 3 H), 2.11–1.97 (m, 2 H), 1.96–1.81 (m, 2 H), 1.77 (d, $J = 7.3$ Hz, 3 H).

and a crude by-product which was purified twice by MDAP using Method HpH. The appropriate fractions were combined and the solvent evaporated under a stream of nitrogen to give (*R*)-1-[1-(1-methoxypropan-2-yl)-8-methyl-2-(tetrahydro-2*H*-pyran-4-yl)-1*H*-furo[2,3-*g*]imidazo[4,5-*c*]quinolin-7-yl]ethanone **364** as a light brown solid (39 mg, 0.093 mmol, 4%).

$[\alpha]_D^{21} +2.2$ (c 0.5, CHCl₃).

m.p.: 180–182 °C.

IR (solid) ν (cm^{-1}): 3379, 2951, 2837, 1655, 1570, 1524, 1370, 1106.

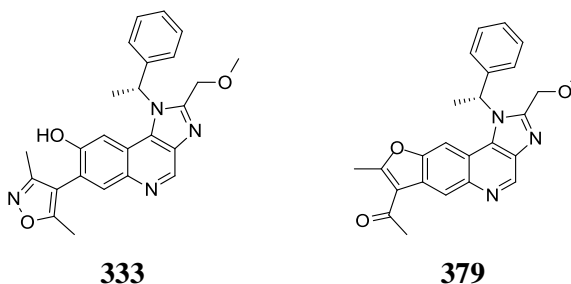
LCMS (formic A): m/z 422 $[(M + H)^+]$; Rt: 0.66 min; 100% purity by peak area.

HRMS (ESI): $M + H$ calcd for $\text{C}_{24}\text{H}_{28}\text{N}_3\text{O}_4$ 422.2074, found 422.2075.

^1H NMR (400 MHz, $\text{DMSO-}d_6$): Variable temperature (393 K) δ 9.11 (s, 1 H), 8.73 (s, 1 H), 8.42 (s, 1 H), 5.56–5.43 (m, 1 H), 4.13–4.04 (m, 1 H), 4.04–3.94 (m, 3 H), 3.64–3.52 (m, 2 H), 3.44 (tt, $J = 11.0, 3.9$ Hz, 1 H), 3.21 (s, 3 H), 2.86 (s, 3 H), 2.69 (s, 3 H), 2.12–2.00 (m, 2 H), 1.95–1.83 (m, 2 H), 1.77 (d, $J = 7.1$ Hz, 3 H).

^{13}C NMR (100 MHz, $\text{DMSO-}d_6$): δ 192.6, 164.8, 158.1, 150.9, 143.5, 141.7, 135.6, 132.7, 125.6, 122.1, 116.3, 114.5, 100.9, 73.9, 66.1 (2 C), 57.9, 51.8, 33.8, 31.9, 31.7, 30.0, 16.9, 14.5.

7-(3,5-Dimethylisoxazol-4-yl)-2-(methoxymethyl)-1-[(*R*)-1-phenylethyl]-1*H*-imidazo[4,5-*c*]quinolin-8-ol and (*R*)-1-{2-(methoxymethyl)-8-methyl-1-(1-phenylethyl)-1*H*-furo[2,3-*g*]imidazo[4,5-*c*]quinolin-7-yl}ethanone



A solution of 4-{8-(benzyloxy)-2-(methoxymethyl)-1-[(*R*)-1-phenylethyl]-1*H*-imidazo[4,5-*c*]quinolin-7-yl}-3,5-dimethylisoxazole **378** (1.81 g, 3.49 mmol) in EtOH (20 mL) was hydrogenated over 5% Pd/C (180 mg) at r.t. and atmospheric pressure for 15 h. The reaction mixture was filtered through Celite and the cake washed with EtOH (50 mL). The filtrate was evaporated under vacuum and the residue dissolved in EtOH (40 mL). The solution was hydrogenated over 5% Pd/C (360 mg) at r.t. and atmospheric pressure for 20 h. The reaction mixture was filtered through Celite and the cake washed with EtOH (50 mL). The filtrate was evaporated under vacuum and the residue dissolved in DCM (8 mL). The solution was loaded onto a 220 g silica cartridge and purified using a gradient of 0–15% MeOH in DCM over 10 column volumes. The appropriate fractions were combined and the solvent removed by rotary evaporation to give an off-white solid which was purified by MDAP using Method HpH. The appropriate fractions were combined and the solvent removed by rotary evaporation to give 7-(3,5-dimethylisoxazol-4-yl)-2-(methoxymethyl)-1-[(*R*)-1-phenylethyl]-1*H*-imidazo[4,5-*c*]quinolin-8-ol **333** as a light yellow solid (923 mg, 2.154 mmol, 62%).

LCMS (formic A): m/z 429 $[(M + H)^+]$; Rt: 0.72 min; 96% purity by peak area.

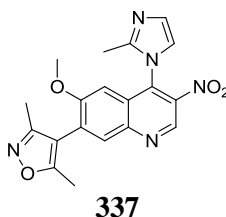
^1H NMR (400 MHz, DMSO- d_6): Variable temperature (393 K) δ 9.50 (br s, 1 H), 9.04 (s, 1 H), 7.89 (s, 1 H), 7.45–7.23 (m, 6 H), 6.51 (q, $J = 7.1$ Hz, 1 H), 4.69 (d, $J = 12.9$ Hz, 1 H), 4.62 (d, $J = 12.9$ Hz, 1 H), 3.33 (s, 3 H), 2.31 (s, 3 H), 2.17 (d, $J = 7.1$ Hz, 3 H), 2.14 (s, 3 H).

The appropriate fractions were combined and the solvent removed by rotary evaporation to give (*R*)-1-{2-(methoxymethyl)-8-methyl-1-(1-phenylethyl)-1*H*-furo[2,3-*g*]imidazo[4,5-*c*]-quinolin-7-yl}ethanone **379** as a light yellow foam (129 mg, 0.312 mmol, 9%).

LCMS (formic A): m/z 414 $[(M + H)^+]$; Rt: 0.81 min; 96% purity by peak area.

^1H NMR (400 MHz, DMSO- d_6): Variable temperature (393 K) δ 9.24 (s, 1 H), 8.71 (s, 1 H), 7.70 (s, 1 H), 7.44–7.36 (m, 2 H), 7.36–7.25 (m, 3 H), 6.57 (q, $J = 7.1$ Hz, 1 H), 4.82 (s, 2 H), 3.38 (s, 3 H), 2.79 (s, 3 H), 2.67 (s, 3 H), 2.13 (d, $J = 7.1$ Hz, 3 H).

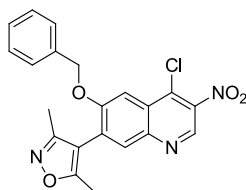
4-[6-Methoxy-4-(2-methyl-1*H*-imidazol-1-yl)-3-nitroquinolin-7-yl]-3,5-dimethylisoxazole



A mixture of 4-(4-chloro-6-methoxy-3-nitroquinolin-7-yl)-3,5-dimethylisoxazole **334** (250 mg, 0.749 mmol) and 2-methyl-1*H*-imidazole (154 mg, 1.873 mmol) in anhydrous 1,4-dioxane (3.0 mL) was heated in a 0.5–2.0 mL sealed vessel in a Biotage I60 microwave at 120 °C for 30 min (absorbance: normal; FHT: on; cooling: off). The reaction mixture was diluted with EtOAc (15 mL) and washed with water (15 mL). The aqueous layer was extracted with EtOAc (15 mL), the organic layers combined and passed through a hydrophobic frit. The solvent was removed under vacuum and the residue loaded in DCM (5 mL) and purified on a 50 g silica cartridge using a gradient of 0–10% MeOH in DCM over 10 column volumes. The appropriate fractions were combined and the solvent removed by rotary evaporation to give the title compound as a yellow foam (284 mg, 0.749 mmol, 100%).

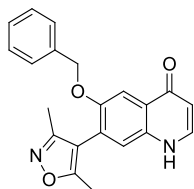
LCMS (formic A): m/z 380 $[(M + H)^+]$; Rt: 0.68 min; 100% purity by peak area.

^1H NMR (400 MHz, CDCl₃): δ 9.36 (s, 1 H), 8.07 (s, 1 H), 7.27 (d, $J = 1.5$ Hz, 1 H), 7.04 (s, $J = 1.5$ Hz, 1 H), 6.60 (s, 1 H), 3.79 (s, 3 H), 2.39 (s, 3 H), 2.23 (s, 3 H), 2.22 (s, 3 H).

4-[6-(Benzyloxy)-4-chloro-3-nitroquinolin-7-yl]-3,5-dimethylisoxazole**343**

To 6-(benzyloxy)-7-(3,5-dimethylisoxazol-4-yl)-3-nitroquinolin-4(1*H*)-one **352** (3.53 g, 9.02 mmol) was added phosphorus oxychloride (20 mL, 215 mmol) and the suspension stirred at 100 °C under nitrogen for 1 h. The reaction mixture was allowed to cool to r.t. and evaporated under vacuum. Toluene (20 mL) was added and the mixture evaporated. The residue was dissolved in DCM (25 mL) and sat. NaHCO₃ (aq) (25 mL) was added. The mixture was stirred vigorously for 30 min and the organic layer separated. The aqueous layer was extracted with DCM (25 mL), the organics combined and passed through a hydrophobic frit. The solvent was removed under vacuum and the resulting solid triturated with cyclohexane:diethylether (8:2) (40 mL). The solid was dried *in vacuo* to give the title compound as a light brown solid (3.54 g, 8.64 mmol, 96%).

m.p.: 230–232 °C.

IR (solid) ν (cm⁻¹): 3130, 1619, 1556, 1526, 1420, 1381, 1331, 1227, 1023, 739.LCMS (formic A): m/z 410, 412 [(M + H)⁺]; Rt: 1.32 min; 98% purity by peak area.HRMS (ESI): M + H calcd for C₂₁H₁₇³⁵ClN₃O₄ 410.0902, found 410.0897.¹H NMR (400 MHz, CDCl₃): δ 9.16 (s, 1 H), 8.01 (s, 1 H), 7.82 (s, 1 H), 7.47–7.33 (m, 5 H), 5.32 (s, 2 H), 2.37 (s, 3 H), 2.23 (s, 3 H).¹³C NMR (100 MHz, CDCl₃): δ 167.1, 159.3, 157.3, 144.9, 142.6, 141.7, 135.0, 134.2, 133.0, 129.2, 128.9 (2 C), 128.7, 127.4 (2 C), 126.7, 111.7, 104.7, 71.3, 12.0, 10.9.**6-(Benzyloxy)-7-(3,5-dimethylisoxazol-4-yl)quinolin-4(1*H*)-one****344**

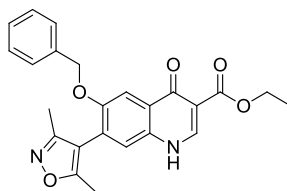
Diphenyl ether (70 mL) was heated with stirring to 260 °C (internal) using an isomantle (set to level 10, then maintained at level 8). Solid 6-(benzyloxy)-7-(3,5-dimethylisoxazol-4-yl)-4-oxo-1,4-dihydroquinoline-3-carboxylic acid **351** (7.2 g, 18.44

mmol) was added in one portion followed by diphenyl ether (10 mL). The mixture stirred for 20 min. The reaction was allowed to cool to r.t. and the solution applied to a 330 g silica cartridge with DCM (20 mL). The mixture was purified using a gradient of 0–20% MeOH in DCM over 10 column volumes. The appropriate fractions were combined and the solvent removed by rotary evaporation to give the title compound as a brown solid (5.7 g, 16.46 mmol, 89%).

LCMS (formic A): m/z 347 $[(M + H)^+]$; Rt: 0.83 min; 89% purity by peak area.

$^1\text{H NMR}$ (400 MHz, $\text{DMSO-}d_6$): δ 11.72 (br s, 1 H), 7.92–7.86 (m, 1 H), 7.75 (s, 1 H), 7.44 (s, 1 H), 7.41–7.29 (m, 5 H), 6.03 (d, $J = 7.2$ Hz, 1 H), 5.21 (s, 2 H), 2.29 (s, 3 H), 2.11 (s, 3 H).

Ethyl 6-(benzyloxy)-7-(3,5-dimethylisoxazol-4-yl)-4-oxo-1,4-dihydroquinoline-3-carboxylate

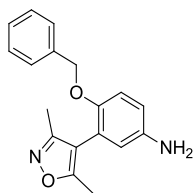


345

Diphenyl ether (75 mL) was heated with stirring to 260 °C (internal) using an isomantle (set to level 10, then maintained at level 8). Solid diethyl 2-({[4-(benzyloxy)-3-(3,5-dimethylisoxazol-4-yl)phenyl]amino}methylene)malonate **350** (9.6 g, 20.67 mmol) was added in portions, followed by diphenyl ether (10 mL). The mixture was stirred for 20 min. The mixture was allowed to cool to r.t. and diluted with DCM (20 mL). The solution was loaded onto a 330 g silica cartridge and purified using a gradient of 0–20% MeOH in DCM over 10 column volumes. The appropriate fractions were combined and the solvent removed by rotary evaporation to give the title compound as a light brown solid (7.8 g, 18.64 mmol, 90%).

LCMS (formic A): m/z 419 $[(M + H)^+]$; Rt: 0.93 min; 85% purity by peak area. 9% Decarboxylated material present.

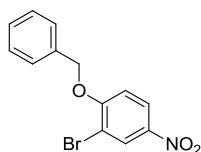
$^1\text{H NMR}$ (400 MHz, $\text{DMSO-}d_6$): δ 12.27 (br s, 1 H), 8.55 (s, 1 H), 7.82 (s, 1 H), 7.53 (s, 1 H), 7.40–7.29 (m, 5 H), 5.24 (s, 2 H), 4.22 (q, $J = 7.1$ Hz, 2 H), 2.30 (s, 3 H), 2.10 (s, 3 H), 1.29 (t, $J = 7.1$ Hz, 3 H).

4-(Benzyloxy)-3-(3,5-dimethylisoxazol-4-yl)aniline**346**

A mixture of 4-[2-(benzyloxy)-5-nitrophenyl]-3,5-dimethylisoxazole **349** (9.2 g, 28.4 mmol), iron powder (6.0 g, 107 mmol) and ammonium chloride (12 g, 224 mmol) was suspended in EtOH (400 mL) and water (100 mL) and stirred at r.t for 15 h. The reaction mixture was filtered through a pad of Celite and the cake washed with EtOH. The filtrate was evaporated under vacuum and the residue partitioned between EtOAc (150 mL) and water (150 mL). The organic layer was separated, washed with further water (100 mL) and dried over MgSO₄. The solvent was removed under vacuum to give the title compound as a dark brown oil (8.2 g, 27.9 mmol, 98%).

LCMS (formic A): *m/z* 295 [(M + H)⁺]; Rt: 0.75 min; 85% purity by peak area. 10% starting material remains.

¹H NMR (400 MHz, CDCl₃): δ 7.37–7.25 (m, 3 H), 7.25–7.20 (m, 2 H), 6.91 (d, *J* = 8.6 Hz, 1 H), 6.69 (dd, *J* = 8.6, 2.9 Hz, 1 H), 6.51 (d, *J* = 2.9 Hz, 1 H), 4.92 (s, 2 H), 3.53 (br s, 2 H), 2.29 (s, 3 H), 2.18 (s, 3 H).

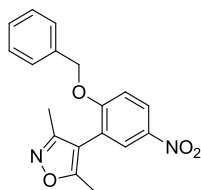
1-(Benzyloxy)-2-bromo-4-nitrobenzene**348**

To a slurry of sodium hydride (60% dispersion in mineral oil, 2.8 g, 70.0 mmol) and DMA (60 mL) was added benzyl alcohol (4.75 mL, 45.7 mmol) dropwise with stirring under nitrogen. The mixture was stirred for 2 h at r.t. and then cooled to 0 °C. 2-Bromo-1-fluoro-4-nitrobenzene **347** (11 g, 50.0 mmol) was added to the cooled solution and stirred for 1 h. The reaction mixture was poured onto sat. NH₄Cl (aq) (80 mL) and stirred for 10 min, filtered and washed with water. The solid was triturated with diethyl ether (25 mL) and filtered to give the title compound as a tan solid (11.25 g, 36.5 mmol, 73%).

LCMS (formic A): poor ionisation; Rt: 1.30 min; 100% purity by peak area.

^1H NMR (400 MHz, DMSO- d_6): δ 8.45 (d, J = 2.8 Hz, 1 H), 8.28 (dd, J = 9.1, 2.8 Hz, 1 H), 7.53–7.47 (m, 2 H), 7.47–7.40 (m, 3 H), 7.40–7.34 (m, 1 H), 5.39 (s, 2 H).

4-[2-(Benzyloxy)-5-nitrophenyl]-3,5-dimethylisoxazole



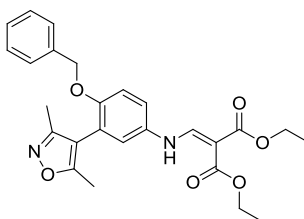
349

Nitrogen was bubbled through a mixture of 1-(benzyloxy)-2-bromo-4-nitrobenzene **348** (10.73 g, 34.8 mmol), cesium carbonate (23 g, 70.6 mmol), DME (100 mL) and water (40 mL) for 30 min. (3,5-Dimethylisoxazol-4-yl)boronic acid (9.75 g, 69.2 mmol) and PEPPSITM-IPr catalyst (0.6 g, 0.883 mmol) was added and the mixture stirred at 90 °C for 5 h under nitrogen. The reaction was allowed to cool to r.t. then EtOAc (150 mL) and water (75 mL) added. The layers were separated and the organic layer washed with 10% Na₂SO₃ (aq) (75 mL) followed by brine (75 mL). The organic layer was dried over MgSO₄, filtered and concentrated under reduced pressure. The resulting solid was triturated with diethyl ether (50 mL), filtered and washed with cyclohexane (100 mL). The solid was dried in a vacuum oven to give the title compound as a light brown solid (9.72 g, 30.0 mmol, 86%).

LCMS (formic A): m/z 325 [(M + H)⁺]; Rt: 1.19 min; 100% purity by peak area.

^1H NMR (400 MHz, CDCl₃): δ 8.26 (dd, J = 9.1, 2.8 Hz, 1 H), 8.07 (d, J = 2.8 Hz, 1 H), 7.41–7.31 (m, 3 H), 7.30–7.25 (m, 2 H), 7.13 (d, J = 9.1 Hz, 1 H), 5.19 (s, 2 H), 2.30 (s, 3 H), 2.16 (s, 3 H).

Diethyl 2-([4-(benzyloxy)-3-(3,5-dimethylisoxazol-4-yl)phenyl]amino)methylene)malonate



350

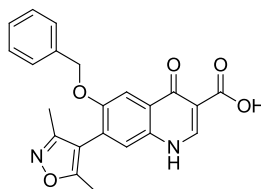
A mixture of 4-(benzyloxy)-3-(3,5-dimethylisoxazol-4-yl)aniline **346** (8.2 g, 27.9 mmol) and diethyl 2-(ethoxymethylene)malonate (5.6 mL, 28.0 mmol) was stirred at 130 °C for 1 h. The brown oil was concentrated under reduced pressure. The residue was loaded in

DCM (20 mL) and purified on a 330 g silica cartridge using a gradient of 0–100% EtOAc in DCM over 10 column volumes. The appropriate fractions were combined and the solvent removed by rotary evaporation. The resulting solid was triturated with cyclohexane, filtered and dried in a vacuum oven to give the title compound as a light brown solid (9.6 g, 20.67 mmol, 74%).

LCMS (formic A): m/z 465 $[(M + H)^+]$; Rt: 1.30 min; 100% purity by peak area.

$^1\text{H NMR}$ (400 MHz, CDCl_3): δ 11.02 (d, $J = 13.5$ Hz, 1 H), 8.44 (d, $J = 13.5$ Hz, 1 H), 7.40–7.24 (m, 5 H), 7.15 (dd, $J = 8.8, 2.9$ Hz, 1 H), 7.07 (d, $J = 8.8$ Hz, 1 H), 6.94 (d, $J = 2.9$ Hz, 1 H), 5.06 (s, 2 H), 4.32 (q, $J = 7.1$ Hz, 2 H), 4.26 (q, $J = 7.1$ Hz, 2 H), 2.31 (s, 3 H), 2.18 (s, 3 H), 1.40 (t, $J = 7.1$ Hz, 3 H), 1.34 (t, $J = 7.1$ Hz, 3 H).

6-(Benzyloxy)-7-(3,5-dimethylisoxazol-4-yl)-4-oxo-1,4-dihydroquinoline-3-carboxylic acid

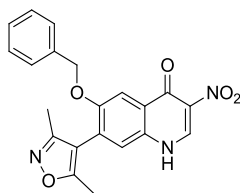


351

To ethyl 6-(benzyloxy)-7-(3,5-dimethylisoxazol-4-yl)-4-oxo-1,4-dihydroquinoline-3-carboxylate **345** (7.8 g, 18.64 mmol) was added EtOH (50 mL) and 2 M NaOH (aq) (30 mL, 60.0 mmol) and the mixture stirred at 95 °C for 3 h. The reaction was allowed to cool to r.t. and the volatiles evaporated under vacuum. The remaining mixture was acidified to pH = 1 with 12.5% HCl (aq) (~30 mL) and the resulting precipitate isolated by vacuum filtration. The solid was washed with water (200 mL) and diethylether (50 mL), and then dried in a vacuum oven overnight to give the title compound as an off-white solid (7.2 g, 18.44 mmol, 99%).

LCMS (formic A): m/z 391 $[(M + H)^+]$; Rt: 1.00 min; 82% purity by peak area. 10% Decarboxylated material present.

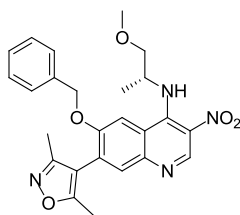
$^1\text{H NMR}$ (400 MHz, $\text{DMSO}-d_6$): δ 15.64 (br s, 1 H), 8.85 (s, 1 H), 7.90 (s, 1 H), 7.76 (s, 1 H), 7.43–7.30 (m, 5 H), 5.31 (s, 2 H), 2.31 (s, 3 H), 2.12 (s, 3 H).

6-(Benzyloxy)-7-(3,5-dimethylisoxazol-4-yl)-3-nitroquinolin-4(1H)-one**352**

To a 500 mL round bottomed flask containing 6-(benzyloxy)-7-(3,5-dimethylisoxazol-4-yl)quinolin-4(1H)-one **344** (5.7 g, 16.46 mmol) was added propionic acid (75 mL, 1002 mmol) followed by 70% nitric acid (1.6 mL, 35.8 mmol). A suspension formed which was stirred at 100 °C for 1.5 h. The reaction mixture was allowed to cool to r.t., filtered under vacuum and washed with cyclohexane (100 mL). The solid was dried in a vacuum oven to give the title compound as a tan solid (3.7 g, 9.45 mmol, 57%).

LCMS (formic A): m/z 392 [(M + H)⁺]; Rt: 0.94 min; 98% purity by peak area.

¹H NMR (400 MHz, DMSO-*d*₆): δ 12.97 (br s, 1 H), 9.18 (s, 1 H), 7.91 (s, 1 H), 7.63 (s, 1 H), 7.42–7.29 (m, 5 H), 5.29 (s, 2 H), 2.30 (s, 3 H), 2.11 (s, 3 H).

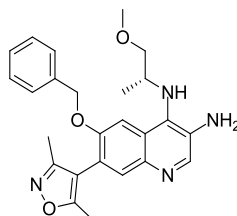
6-(Benzyloxy)-7-(3,5-dimethylisoxazol-4-yl)-N-[(R)-1-methoxypropan-2-yl]-3-nitroquinolin-4-amine**353**

A solution of 4-[6-(benzyloxy)-4-chloro-3-nitroquinolin-7-yl]-3,5-dimethylisoxazole **343** (1.75 g, 4.27 mmol) in anhydrous NMP (10 mL) was treated with DIPEA (2.2 mL, 12.60 mmol) followed by (*R*)-1-methoxypropan-2-amine hydrochloride (0.60 g, 4.78 mmol). The mixture was stirred at r.t. for 3 h then diluted with water (25 mL) and extracted with EtOAc (2 x 30 mL). The combined organic extracts were washed with brine (30 mL), passed through a hydrophobic frit and evaporated *in vacuo*. The gum was loaded in DCM (5 mL) and purified on a 100 g silica cartridge using a gradient of 0–100% EtOAc in DCM over 12 column volumes. The appropriate fractions were combined and the solvent removed by rotary evaporation. A mixture of cyclohexane (8:2) (10 mL) was added to the gum and evaporated, and the process repeated. The resulting bright yellow foam was dried under high vacuum to give the title compound (1.73 g, 3.74 mmol, 88%).

LCMS (formic A): m/z 463 $[(M + H)^+]$; Rt: 1.18 min; 97% purity by peak area.

^1H NMR (400 MHz, CDCl_3): δ 9.30 (s, 1 H), 8.93 (d, $J = 9.5$ Hz, 1 H), 7.86 (s, 1 H), 7.83 (s, 1 H), 7.43–7.30 (m, 5 H), 5.30–5.17 (m, 2 H), 4.37–4.24 (m, 1 H), 3.54–3.44 (m, 2 H), 3.43 (s, 3 H), 2.38 (s, 3 H), 2.26 (s, 3 H), 1.32 (d, $J = 6.6$ Hz, 3 H).

6-(Benzyloxy)-7-(3,5-dimethylisoxazol-4-yl)- N^4 -[(*R*)-1-methoxypropan-2-yl]quinoline-3,4-diamine



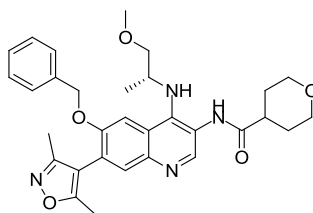
354

Iron powder (1.93 g, 34.6 mmol) was added to a solution of 6-(benzyloxy)-7-(3,5-dimethylisoxazol-4-yl)- N^4 -[(*R*)-1-methoxypropan-2-yl]-3-nitroquinolin-4-amine **353** (1.60 g, 3.46 mmol) in acetic acid (12 mL) and the mixture stirred at r.t. for 6 h. Further iron powder (1.93 g, 34.6 mmol) was added, and the reaction stirred for 2 h. The mixture was diluted with EtOAc (100 mL) and stirred for 30 min. The mixture was filtered through Celite and the filtrate diluted with 5 M NaOH (aq) (100 mL). The organic layer was separated, washed with sat. NaHCO_3 (aq) (100 mL), passed through a hydrophobic frit and evaporated *in vacuo*. The residue was loaded in DCM (5 mL) and purified on a 100 g silica cartridge using a gradient of 0–10% 2 M ammonia/MeOH in DCM over 10 column volumes. The appropriate fractions were combined and the solvent removed by rotary evaporation to give the title compound as a light brown solid (1.16 g, 2.68 mmol, 78%).

LCMS (formic A): m/z 433 $[(M + H)^+]$; Rt: 0.87 min; 95% purity by peak area.

^1H NMR (400 MHz, CDCl_3): δ 8.40 (s, 1 H), 7.74 (s, 1 H), 7.42–7.30 (m, 6 H), 5.26–5.17 (m, 2 H), 4.11 (s, 2 H), 3.59–3.50 (m, 1 H), 3.46 (s, 3 H), 3.40 (dd, $J = 9.3, 2.0$ Hz, 1 H), 3.29 (dd, $J = 9.3, 4.2$ Hz, 1 H), 2.36 (s, 3 H), 2.23 (s, 3 H), 1.26 (d, $J = 6.4$ Hz, 3 H). *NH* signal not resolved.

***N*-[6-(benzyloxy)-7-(3,5-dimethylisoxazol-4-yl)-4-[[*(R)*-1-methoxypropan-2-yl]amino}quinolin-3-yl]tetrahydro-2*H*-pyran-4-carboxamide**



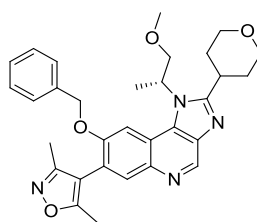
355

6-(Benzyloxy)-7-(3,5-dimethylisoxazol-4-yl)-*N*⁴-[[*(R)*-1-methoxypropan-2-yl]quinoline-3,4-diamine **354** (1.13 g, 2.61 mmol) was dissolved in a mixture of DCM (10 mL) and pyridine (0.50 mL, 6.18 mmol) and stirred for 10 min at r.t. The solution was cooled to 0 °C then tetrahydro-2*H*-pyran-4-carbonyl chloride (0.43 g, 2.89 mmol) was added. The solution was stirred at 0 °C for 10 min then allowed to warm to r.t. over 2 h. Further tetrahydro-2*H*-pyran-4-carbonyl chloride (0.05 g, 0.337 mmol) was added and the mixture stirred for 1 h. The reaction mixture was diluted with DCM (15 mL) and washed with water (2 x 25 mL). The organic layer was passed through a hydrophobic frit and the solvent evaporated *in vacuo*. The foam was loaded in DCM (5 mL) and purified on a 100 g silica cartridge using a gradient of 0–15% MeOH in DCM over 10 column volumes. The appropriate fractions were combined and the solvent removed by rotary evaporation. The residue was dissolved in MeOH (5 mL) and was applied to a MeOH preconditioned 20 g SCX-2 cartridge. The cartridge was washed with MeOH (60 mL) followed by 2 M ammonia in MeOH solution (60 mL). The basic wash was evaporated *in vacuo* to give the title compound as a light brown foam (1.40 g, 2.57 mmol, 98%).

LCMS (formic A): *m/z* 545 [(M + H)⁺]; Rt: 0.85 min; 96% purity by peak area.

¹H NMR (400 MHz, CDCl₃): δ 9.30 (s, 1 H), 8.34 (s, 1 H), 7.87–7.83 (m, 1 H), 7.42–7.30 (m, 7 H), 5.28–5.17 (m, 2 H), 4.13 (d, *J* = 10.8 Hz, 2 H), 3.50 (s, 3 H), 3.58–3.43 (m, 4 H), 3.29 (dd, *J* = 9.5, 5.9 Hz, 1 H), 2.64 (s, 1 H), 2.36 (s, 3 H), 2.24 (s, 3 H), 2.08–1.89 (m, 4 H), 1.22 (d, *J* = 6.6 Hz, 3 H).

4-{8-(Benzyloxy)-1-[(R)-1-methoxypropan-2-yl]-2-(tetrahydro-2H-pyran-4-yl)-1H-imidazo[4,5-c]quinolin-7-yl}-3,5-dimethylisoxazole



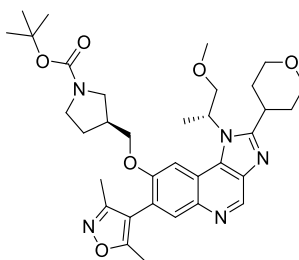
356

A solution of *N*-[6-(benzyloxy)-7-(3,5-dimethylisoxazol-4-yl)-4-{[(*R*)-1-methoxypropan-2-yl]amino}quinolin-3-yl]tetrahydro-2*H*-pyran-4-carboxamide **355** (1.36 g, 2.497 mmol) in propionic acid (7 mL, 94 mmol) was stirred at 140 °C for 3 h. The reaction mixture was allowed to cool to r.t. and evaporated *in vacuo*. The oil was dissolved in DCM (25 mL) and washed with 1 M NaOH (aq) (25 mL). The aqueous layer was extracted with DCM (25 mL), the organic layers combined and dried over MgSO₄ to give the title compound as a yellow gum (1.24 g, 2.36 mmol, 94%).

LCMS (formic A): *m/z* 527 [(M + H)⁺]; Rt: 0.90 min; 97% purity by peak area.

¹H NMR (400 MHz, DMSO-*d*₆): Variable temperature (393 K) δ 9.00 (s, 1 H), 7.98 (s, 1 H), 7.72 (s, 1 H), 7.42–7.34 (m, 4 H), 7.34–7.27 (m, 1 H), 5.32 (s, 2 H), 5.31–5.23 (m, 1 H), 4.03–3.95 (m, 2 H), 3.93 (d, *J* = 9.6 Hz, 1 H), 3.79 (dd, *J* = 10.4, 4.3 Hz, 1 H), 3.61–3.50 (m, 2 H), 3.44–3.32 (m, 1 H), 3.17 (s, 3 H), 2.31 (s, 3 H), 2.14 (s, 3 H), 2.12–1.95 (m, 2 H), 1.94–1.79 (m, 2 H), 1.65 (d, *J* = 7.3 Hz, 3 H).

(3*S*)-tert-Butyl 3-({[7-(3,5-dimethylisoxazol-4-yl)-1-[(*R*)-1-methoxypropan-2-yl]-2-(tetrahydro-2*H*-pyran-4-yl)-1*H*-imidazo[4,5-*c*]quinolin-8-yl]oxy)methyl}pyrrolidine-1-carboxylate



357

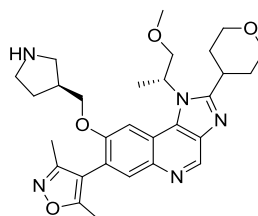
A mixture of 7-(3,5-dimethylisoxazol-4-yl)-1-[(*R*)-1-methoxypropan-2-yl]-2-(tetrahydro-2*H*-pyran-4-yl)-1*H*-imidazo[4,5-*c*]quinolin-8-ol **332** (100 mg, 0.229 mmol), potassium carbonate (45 mg, 0.326 mmol) and (*S*)-*tert*-butyl 3-[(methylsulfonyl)oxy]methyl}pyrrolidine-1-carboxylate **311** (72 mg, 0.258 mmol) was stirred at 100 °C under

nitrogen for 3 h. The reaction mixture was allowed to cool to r.t. and diluted with MeOH (0.2 mL). The mixture was filtered and purified by MDAP using Method HpH. The appropriate fractions were combined and the solvent evaporated under a stream of nitrogen and the brown gum freeze dried from 1,4-dioxane to give the title compound as an off white solid (81 mg, 0.131 mmol, 57%).

LCMS (formic A): m/z 620 $[(M + H)^+]$; Rt: 0.93 min; 100% purity by peak area.

^1H NMR (400 MHz, DMSO- d_6): Variable Temperature (393 K) δ 9.01 (s, 1 H), 7.96 (s, 1 H), 7.74 (s, 1 H), 5.47–5.33 (m, 1 H), 4.20–3.96 (m, 6 H), 3.58–3.55 (m, 2 H), 3.49–3.39 (m, 2 H), 3.37–3.29 (m, 1 H), 3.26 (s, 3 H), 3.28–3.19 (m, 1 H), 3.07 (dd, $J = 10.9, 7.1$ Hz, 1 H), 2.69–2.58 (m, 1 H), 2.31 (s, 3 H), 2.13 (s, 3 H), 2.11–1.82 (m, 5 H), 1.78 (d, $J = 7.3$ Hz, 3 H), 1.73–1.62 (m, 1 H), 1.40 (s, 9 H).

4-{1-[(*R*)-1-Methoxypropan-2-yl]-8-[(*S*)-pyrrolidin-3-ylmethoxy]-2-(tetrahydro-2*H*-pyran-4-yl)-1*H*-imidazo[4,5-*c*]quinolin-7-yl}-3,5-dimethylisoxazole



358

A solution of (3*S*)-*tert*-butyl 3-([7-(3,5-dimethylisoxazol-4-yl)-1-[(*R*)-1-methoxypropan-2-yl]-2-(tetrahydro-2*H*-pyran-4-yl)-1*H*-imidazo[4,5-*c*]quinolin-8-yl]oxy)methylpyrrolidine-1-carboxylate **357** (76 mg, 0.123 mmol) was dissolved in DCM (1 mL) and treated with TFA (0.25 mL, 3.24 mmol). The mixture was allowed to stand in a stoppered vessel at r.t. for 1.5 h. The reaction mixture was evaporated under a stream of nitrogen and the residue dissolved in MeOH. The solution was applied to a MeOH preconditioned 1 g SCX-2 cartridge. The cartridge was washed with MeOH (5 mL) followed by 2 M ammonia in MeOH solution (5 mL). The basic wash was evaporated under a stream of nitrogen to give the title compound as a off-white solid (50 mg, 0.096 mmol, 78%).

$[\alpha]_D^{23} -7.5$ (c 0.5, CHCl_3).

m.p.: 94 °C.

IR (solid) ν (cm^{-1}): 3383, 2931, 1619, 1505, 1418, 1367, 1212, 1106.

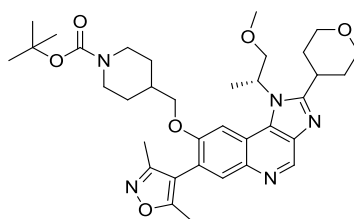
LCMS (formic A): m/z 520 $[(M + H)^+]$; Rt: 0.51 min; 100% purity by peak area.

HRMS (ESI): $M + H$ calcd for $\text{C}_{29}\text{H}_{38}\text{N}_5\text{O}_4$ 520.2918, found 520.2900.

^1H NMR (400 MHz, $\text{DMSO-}d_6$): Variable temperature (393 K) δ 9.00 (s, 1 H), 7.95 (s, 1 H), 7.73 (s, 1 H), 5.47–5.33 (m, 1 H), 4.12–4.05 (m, 3 H), 4.04–3.95 (m, 3 H), 3.65–3.53 (m, 2 H), 3.43 (tt, $J = 11.0, 3.9$ Hz, 1 H), 3.26 (s, 3 H), 2.62–2.53 (m, 1 H), 2.47–2.41 (m, 1 H), 2.31 (s, 3 H), 2.13 (s, 3 H), 2.12–1.97 (m, 2 H), 1.97–1.80 (m, 3 H), 1.78 (d, $J = 7.3$ Hz, 3 H), 1.46–1.35 (m, 1 H). 3 x alkyl protons obscured by water. NH signal not resolved.

^{13}C NMR (100 MHz, CDCl_3): δ 166.2, 159.7, 158.3, 154.7, 143.9, 140.4, 138.1, 134.3, 132.7, 120.8, 117.9, 112.5, 103.5, 74.9, 71.8, 67.7, 67.5, 59.3, 52.0, 50.2, 46.7, 38.6, 34.6, 32.0, 31.5, 29.3, 18.0, 11.7, 10.8.

***tert*-Butyl 4-([7-(3,5-dimethylisoxazol-4-yl)-1-[(*R*)-1-methoxypropan-2-yl]-2-(tetrahydro-2*H*-pyran-4-yl)-1*H*-imidazo[4,5-*c*]quinolin-8-yl]oxy)methyl)piperidine-1-carboxylate**



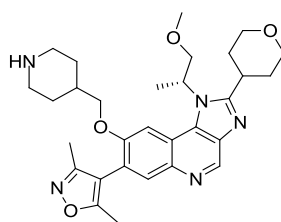
359

A mixture of 7-(3,5-dimethylisoxazol-4-yl)-1-[(*R*)-1-methoxypropan-2-yl]-2-(tetrahydro-2*H*-pyran-4-yl)-1*H*-imidazo[4,5-*c*]quinolin-8-ol **332** (100 mg, 0.229 mmol), potassium carbonate (45 mg, 0.326 mmol) and *tert*-butyl 4-[(methylsulfonyl)oxy]methyl)piperidine-1-carboxylate **321** (75 mg, 0.256 mmol) was stirred at 100 °C under nitrogen for 5.5 h. The reaction mixture was allowed to cool to r.t. and diluted with MeOH (0.2 mL). The mixture was filtered and purified by MDAP using Method HpH. The appropriate fractions were combined and the solvent evaporated under a stream of nitrogen and the brown gum freeze dried from 1,4-dioxane to give the title compound as an off white solid (70 mg, 0.110 mmol, 48%).

LCMS (formic A): m/z 634 $[(M + H)^+]$; Rt: 0.99 min; 100% purity by peak area.

^1H NMR (400 MHz, $\text{DMSO-}d_6$): Variable Temperature (393 K) δ 9.01 (s, 1 H), 7.95 (s, 1 H), 7.73 (s, 1 H), 5.46–5.35 (m, 1 H), 4.14–3.88 (m, 8 H), 3.64–3.53 (m, 2 H), 3.43 (tt, $J = 11.0, 3.9$ Hz, 1 H), 3.26 (s, 3 H), 2.81–2.69 (m, 2 H), 2.31 (s, 3 H), 2.12 (s, 3 H), 2.11–1.82 (m, 5 H), 1.78 (d, $J = 7.3$ Hz, 3 H), 1.71–1.63 (m, 2 H), 1.40 (s, 9 H), 1.26–1.13 (m, 2 H).

4-{1-[(*R*)-1-Methoxypropan-2-yl]-8-(piperidin-4-ylmethoxy)-2-(tetrahydro-2*H*-pyran-4-yl)-1*H*-imidazo[4,5-*c*]quinolin-7-yl}-3,5-dimethylisoxazole



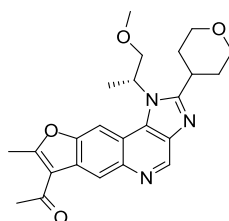
360

A solution of *tert*-butyl 4-({[7-(3,5-dimethylisoxazol-4-yl)-1-[(*R*)-1-methoxypropan-2-yl]-2-(tetrahydro-2*H*-pyran-4-yl)-1*H*-imidazo[4,5-*c*]quinolin-8-yl]oxy}methyl)piperidine-1-carboxylate **359** (65 mg, 0.103 mmol) was dissolved in DCM (1 mL) and treated with TFA (0.25 mL, 3.24 mmol). The mixture was allowed to stand in a stoppered vessel at r.t. for 1.5 h. The reaction mixture was evaporated under a stream of nitrogen and the residue dissolved in MeOH. The solution was applied to a MeOH preconditioned 1 g SCX-2 cartridge. The cartridge was washed with MeOH (5 mL) followed by 2 M ammonia in MeOH solution (5 mL). The basic wash was evaporated under a stream of nitrogen to give the title compound as a off white solid (44 mg, 0.082 mmol, 80%).

LCMS (formic A): m/z 534 [(M + H)⁺]; Rt: 0.52 min; 100% purity by peak area.

¹H NMR (400 MHz, DMSO-*d*₆): Variable temperature (393 K) δ 9.00 (s, 1 H), 7.94 (s, 1 H), 7.73 (s, 1 H), 5.46–5.32 (m, 1 H), 4.11–4.05 (m, 1 H), 4.04–3.95 (m, 5 H), 3.63–3.53 (m, 2 H), 3.43 (tt, $J = 11.0, 3.9$ Hz, 1 H), 3.26 (s, 3 H), 2.97–2.91 (m, 2 H), 2.52–2.44 (m, 2 H), 2.30 (s, 3 H), 2.12 (s, 3 H), 2.10–1.98 (m, 2 H), 1.95–1.83 (m, 3 H), 1.78 (d, $J = 7.3$ Hz, 3 H), 1.65–1.57 (m, 2 H), 1.25–1.08 (m, 2 H). *NH* signal not resolved.

***R*-1-[1-(1-Methoxypropan-2-yl)-8-methyl-2-(tetrahydro-2*H*-pyran-4-yl)-1*H*-furo[2,3-*g*]imidazo[4,5-*c*]quinolin-7-yl]ethanone**

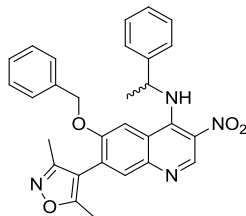


364

(*R*)-1-[1-(1-Methoxypropan-2-yl)-8-methyl-2-(tetrahydro-2*H*-pyran-4-yl)-1*H*-furo[2,3-*g*]imidazo[4,5-*c*]quinolin-7-yl]ethanone **364** was isolated as a by-product in the

synthesis of **332**. Please refer to the experimental relating to the preparation of **332** for characterisation data of **364**.

(±)-6-(Benzyloxy)-7-(3,5-dimethylisoxazol-4-yl)-3-nitro-N-(1-phenylethyl)quinolin-4-amine



365

A solution of 4-[6-(benzyloxy)-4-chloro-3-nitroquinolin-7-yl]-3,5-dimethylisoxazole **343** (1.628 g, 3.97 mmol) in anhydrous NMP (10 mL) was treated with DIPEA (1.73 mL, 9.91 mmol) followed by (±)-1-phenylethylamine (0.564 mL, 4.37 mmol). The reaction mixture was stirred under nitrogen at r.t. for 3.5 h. The reaction was diluted with water (20 mL) and brine (5 mL) and extracted with EtOAc (40 mL). A yellow precipitate formed between the layers and was retained in the separating funnel. The aqueous layer was extracted once more with EtOAc (40 mL) and the organic layers were combined then passed through a hydrophobic frit. The solvent was removed by rotary evaporation. The precipitate from the separating funnel was dissolved in DCM (50 mL) and combined with the residue from the evaporated EtOAc extractions. The solution was washed with brine (20 mL) and the organic layer passed through a hydrophobic frit. The solvent was removed by rotary evaporation and the resulting oil solidified upon standing. EtOAc was added and the suspension filtered to give batch 1 of the title compound as a yellow solid (843 mg, 1.705 mmol, 43%).

LCMS (formic A): m/z 495 [(M + H)⁺]; Rt: 1.34 min; 100% purity by peak area.

¹H NMR (400 MHz, CDCl₃): δ 9.61 (d, J = 7.8 Hz, 1 H), 9.34 (s, 1 H), 7.77 (s, 1 H), 7.58–7.54 (m, 2 H), 7.51–7.45 (m, 3 H), 7.42–7.36 (m, 1 H), 7.35–7.28 (m, 3 H), 7.06–7.02 (m, 2 H), 5.38 (dq, J = 7.8, 6.7, Hz, 1 H), 4.53 (d, J = 11.8 Hz, 1 H), 4.14 (d, J = 11.8 Hz, 1 H), 2.27 (s, 3 H), 2.14 (s, 3 H), 1.76 (d, J = 6.7 Hz, 3 H).

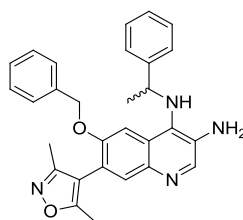
The filtrate was diluted with EtOAc (50 mL) and washed with water (45 mL). The aqueous layer was extracted with EtOAc (2 x 50 mL), the organic layers combined and passed through a hydrophobic frit. The solvent was removed by rotary evaporation, leaving a gum.

The gum was azeotroped with cyclohexane and the resulting solid dried in a vacuum oven to give batch 2 of the title compound as a brown solid (794 mg, 1.606 mmol, 40%).

LCMS (formic A): m/z 495 [(M + H)⁺]; Rt: 1.34 min; 91% purity by peak area.

¹H NMR (400 MHz, CDCl₃): δ 9.61 (d, J = 7.6 Hz, 1 H), 9.34 (s, 1 H), 7.77 (s, 1 H), 7.58–7.54 (m, 2 H), 7.51–7.45 (m, 3 H), 7.42–7.36 (m, 1 H), 7.36–7.27 (m, 3 H), 7.06–7.02 (m, 2 H), 5.39 (dq, J = 7.8, 6.7 Hz, 1 H), 4.53 (d, J = 11.8 Hz, 1 H), 4.14 (d, J = 11.8 Hz, 1 H), 2.27 (s, 3 H), 2.14 (s, 3 H), 1.76 (d, J = 6.7 Hz, 3 H).

(±)-6-(Benzyloxy)-7-(3,5-dimethylisoxazol-4-yl)-N⁴-(1-phenylethyl)quinoline-3,4-diamine



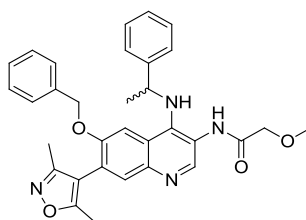
366

Iron powder (1.88 g, 33.7 mmol) was added to a solution of (±)-6-(benzyloxy)-7-(3,5-dimethylisoxazol-4-yl)-3-nitro-*N*-(1-phenylethyl)quinolin-4-amine **365** (1.63 g, 3.30 mmol) in acetic acid (15 mL). The mixture was stirred at r.t. for 1.5 h. EtOAc (100 mL) was added to the flask and the mixture was left to stir for 1 h. The mixture was filtered through Celite and washed with 5 M NaOH (aq) (100 mL). The organic layer was separated and washed with a mixture of sat. NaHCO₃ (aq) (100 mL) and brine (20 mL), and passed through a hydrophobic frit. The solvent was removed by rotary evaporation to give the title compound as a light brown foam (1.41 g, 3.04 mmol, 92%).

LCMS (formic A): m/z 465 [(M + H)⁺]; Rt: 0.96 min; 95% purity by peak area.

¹H NMR (400 MHz, CDCl₃): δ 8.36 (s, 1 H), 7.71 (s, 1 H), 7.39–7.21 (m, 10 H), 6.97 (s, 1 H), 5.00–4.90 (m, 2 H), 4.49 (q, J = 6.7 Hz, 1 H), 3.67 (br s, 2 H), 3.53 (br s, 1 H), 2.31 (s, 3 H), 2.19 (s, 3 H), 1.59 (d, J = 6.7 Hz, 3 H).

(±)-*N*-{6-(Benzyloxy)-7-(3,5-dimethylisoxazol-4-yl)-4-[(1-phenylethyl)amino]quinolin-3-yl}-2-methoxyacetamide



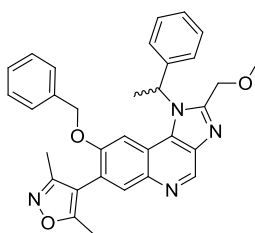
367

A solution of (±)-6-(benzyloxy)-7-(3,5-dimethylisoxazol-4-yl)-*N*⁴-(1-phenylethyl)quinoline-3,4-diamine **366** (1.41 g, 3.04 mmol) and pyridine (0.540 mL, 6.68 mmol) in DCM (15 mL) under nitrogen at r.t. was stirred for 10 min. 2-Methoxyacetyl chloride (0.32 mL, 3.50 mmol) was added and the reaction mixture stirred for 1.5 h. The mixture was washed with water (2 x 10 mL) and the organic layer passed through a hydrophobic frit. The solvent was removed by rotary evaporation to give the title compound as a light brown foam (1.53 g, 2.84 mmol, 94%).

LCMS (formic A): *m/z* 537 [(M + H)⁺]; Rt: 0.91 min; 100% purity by peak area.

¹H NMR (400 MHz, CDCl₃): δ 8.77 (s, 1 H), 8.23 (s, 1 H), 7.80 (s, 1 H), 7.38–7.27 (m, 9 H), 7.25–7.18 (m, 3 H), 4.90–4.82 (m, 2 H), 4.61 (q, *J* = 6.8 Hz, 1 H), 4.08 (s, 2 H), 3.52 (s, 3 H), 2.32 (s, 3 H), 2.19 (s, 3 H), 1.59 (d, *J* = 6.8 Hz, 3 H).

(±)-4-[8-(Benzyloxy)-2-(methoxymethyl)-1-(1-phenylethyl)-1*H*-imidazo[4,5-*c*]quinolin-7-yl]-3,5-dimethylisoxazole



368

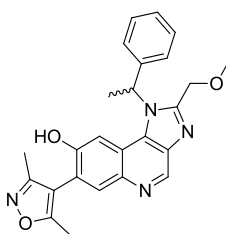
A solution of (±)-*N*-{6-(benzyloxy)-7-(3,5-dimethylisoxazol-4-yl)-4-[(1-phenylethyl)amino]quinolin-3-yl}-2-methoxyacetamide **367** (1.5 g, 2.80 mmol) in propionic acid (4 mL, 53.5 mmol) was heated at 140 °C under nitrogen for 3 h. The solvent was removed *in vacuo*, the residue dissolved in DCM (15 mL) and washed with 1 M NaOH (aq) (15 mL). The aqueous layer was extracted with DCM (15 mL), the organic layers combined and passed through a hydrophobic frit. The solvent was removed by rotary evaporation, the foam loaded in DCM and purified on a 100 g silica cartridge using a gradient of 0–15%

MeOH in DCM over 12 column volumes. The appropriate fractions were combined and the solvent removed by rotary evaporation to give the title compound as a light brown foam (1.33 g, 2.56 mmol, 92%).

LCMS (formic A): m/z 519 [(M + H)⁺]; Rt: 1.06 min; 96% purity by peak area.

¹H NMR (400 MHz, DMSO-*d*₆): Variable temperature (393 K) δ 9.12 (s, 1 H), 7.93 (s, 1 H), 7.43–7.27 (m, 8 H), 7.21–7.17 (m, 2 H), 7.05 (s, 1 H), 6.44 (q, $J = 7.1$ Hz, 1 H), 4.84–4.82 (m, 2 H), 4.77 (d, $J = 11.9$ Hz, 1 H), 4.38 (d, $J = 11.9$ Hz, 1 H), 3.37 (s, 3 H), 2.21 (s, 3 H), 2.04–2.00 (m, 6 H).

(±)-7-(3,5-Dimethylisoxazol-4-yl)-2-(methoxymethyl)-1-(1-phenylethyl)-1H-imidazo[4,5-*c*]quinolin-8-ol



369

Starting material (±)-4-[8-(benzyloxy)-2-(methoxymethyl)-1-(1-phenylethyl)-1H-imidazo[4,5-*c*]quinolin-7-yl]-3,5-dimethylisoxazole **368** (1.2 g, 2.31 mmol) was split into two batches (batch 1 and batch 2).

Batch 1: A solution of (±)-4-[8-(benzyloxy)-2-(methoxymethyl)-1-(1-phenylethyl)-1H-imidazo[4,5-*c*]quinolin-7-yl]-3,5-dimethylisoxazole **368** (600 mg, 1.157 mmol) in EtOH (15 mL) and (DCM) (9 mL) was hydrogenated over 5% Pd/C (CatCart 30) at 25 °C using an H-cube (full H₂ mode, 1 mL/min flow rate). The eluent was evaporated *in vacuo* and the residue was dissolved in a mixture of EtOH (15 mL) and DCM (9 mL). The solution was hydrogenated over 5% Pd/C (CatCart 30) at 25 °C using an H-cube (full H₂ mode, 1 mL/min flow rate). The eluent was evaporated *in vacuo* and the residue loaded in DCM and purified on a 100 g silica cartridge using a gradient of 0–15% MeOH in DCM over 12 column volumes. The appropriate fractions were combined and the solvent was removed by rotary evaporation to give the title compound as a white solid (105 mg, 0.245 mmol, 11%).

LCMS (formic A): m/z 429 [(M + H)⁺]; Rt: 0.73 min; 97% purity by peak area.

¹H NMR (400 MHz, DMSO-*d*₆): Variable temperature (393 K) δ 9.47 (br s, 1 H), 9.00 (s, 1 H), 7.86 (s, 1 H), 7.41–7.20 (m, 6 H), 6.48 (q, $J = 7.1$ Hz, 1 H), 4.66 (d, $J = 12.9$ Hz, 1 H),

4.58 (d, $J = 12.9$ Hz, 1 H), 3.30 (s, 3 H), 2.28 (s, 3 H), 2.14 (d, $J = 7.1$ Hz, 3 H), 2.10 (s, 3 H).

Starting material **368** was recovered (217 mg) and used in the batch 2 reaction.

Batch 2: The second batch of (\pm)-4-[8-(benzyloxy)-2-(methoxymethyl)-1-(1-phenylethyl)-1*H*-imidazo[4,5-*c*]quinolin-7-yl]-3,5-dimethylisoxazole **368** (600 mg, 1.157 mmol) was combined with the recovered starting material **368** from the batch 1 reaction (217 mg) and dissolved in a mixture of EtOH (20 mL) and DCM (10 mL). The solution was hydrogenated over 5% Pd/C (CatCart 30) at 25 °C using an H-cube (full H₂ mode, 1 mL/min flow rate). The eluent was subjected to a second pass through an H-Cube at 30 °C. The eluent was evaporated *in vacuo* leaving a light yellow foam (615 mg) as a mixture of SM and product (~2:3). This was split into two batches (batch 2A and batch 2B).

Batch 2A was purified by MDAP using Method HpH. The appropriate fractions were combined and the solvent was removed by rotary evaporation to give the title compound as an orange solid (43 mg, 0.100 mmol, 9%).

LCMS (formic A): m/z 429 [(M + H)⁺]; Rt: 0.73 min; 95% purity by peak area.

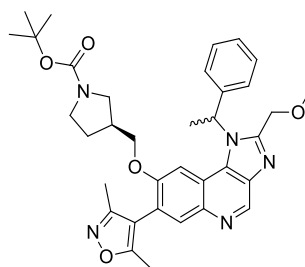
¹H NMR (400 MHz, DMSO-*d*₆): Variable temperature (393 K) δ 9.52 (br s, 1 H), 9.07 (s, 1 H), 7.90 (s, 1 H), 7.46–7.23 (m, 6 H), 6.52 (q, $J = 7.1$ Hz, 1 H), 4.69 (d, $J = 12.9$ Hz, 1 H), 4.62 (d, $J = 12.9$ Hz, 1 H), 3.33 (s, 3 H), 2.31 (s, 3 H), 2.17 (d, $J = 7.1$ Hz, 3 H), 2.13 (s, 3 H).

Batch 2B was dissolved in a mixture of EtOH (30 mL) and DCM (3 mL) and was hydrogenated over 5% Pd/C (40 mg) at r.t. and atmospheric pressure for 7 d. The reaction mixture was filtered through Celite, which was then washed with EtOH and the filtrate evaporated *in vacuo*. The residue was dissolved in a mixture of EtOH (30 mL) and DCM (3 mL) and was hydrogenated over 5% Pd/C (40 mg) at r.t. and atmospheric pressure for 24 h. The reaction mixture was filtered through Celite, which was then washed with EtOH and the filtrate evaporated *in vacuo*. The residue was purified by MDAP using Method HpH. The appropriate fractions were combined and the solvent evaporated *in vacuo* to give the title compound as a beige solid (92 mg, 0.215 mmol, 9%).

LCMS (formic A): m/z 429 [(M + H)⁺]; Rt: 0.72 min; 96% purity by peak area.

^1H NMR (400 MHz, $\text{DMSO-}d_6$): Variable temperature (393 K) δ 9.46 (br s, 1 H), 9.00 (s, 1 H), 7.86 (s, 1 H), 7.39–7.21 (m, 6 H), 6.48 (q, $J = 7.1$ Hz, 1 H), 4.66 (d, $J = 12.9$ Hz, 1 H), 4.58 (d, $J = 12.9$ Hz, 1 H), 3.30 (s, 3 H), 2.28 (s, 3 H), 2.14 (d, $J = 7.1$ Hz, 3 H), 2.11 (s, 3 H).

(3S)-tert-Butyl 3-([7-(3,5-dimethylisoxazol-4-yl)-2-(methoxymethyl)-1-(1-phenylethyl)-1H-imidazo[4,5-c]quinolin-8-yl]oxy)methylpyrrolidine-1-carboxylate (Diastereomeric Mixture)



370

A mixture of (\pm)-7-(3,5-dimethylisoxazol-4-yl)-2-(methoxymethyl)-1-(1-phenylethyl)-1H-imidazo[4,5-c]quinolin-8-ol **369** (100 mg, 0.233 mmol), (*S*)-tert-butyl 3-[[methylsulfonyl]oxy)methyl]pyrrolidine-1-carboxylate **310** (82 mg, 0.294 mmol) and potassium carbonate (46 mg, 0.333 mmol) in anhydrous DMF (2 mL) was heated under nitrogen at 100 °C for 1.5 h. The reaction mixture was allowed to cool, diluted with EtOAc (10 mL) and washed with 10% LiCl (aq) (10 mL) followed by water (10 mL). The organic layer was passed through a hydrophobic frit and the solvent was removed by rotary evaporation. The residue was purified by MDAP using Method HpH. The appropriate fractions were combined and the solvent removed by rotary evaporation to give the title compound (a mixture of diastereoisomers) as an off-white foam (98 mg, 0.160 mmol, 69%).

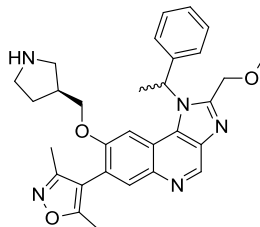
49:51 d.r. by HPLC analysis on a Chiralpak[®] AD (250 mm x 4.6 mm, 10 μm packing diameter) column. An isocratic system of 15% EtOH (containing 0.2% isopropylamine) in heptane with a flow rate of 1 mL/min was used at r.t. The UV detection was performed at 215 nm. Peak 1 Rt: 13.94 min, 49% peak area; Peak 2 Rt: 17.14 min, 51% peak area.

LCMS (HpH): m/z 612 [(M + H)⁺]; Rt: 1.24 min; 100% purity by peak area.

^1H NMR (400 MHz, $\text{DMSO-}d_6$): Variable temperature (393 K) δ 9.11 (s, 1 H), 7.89 (s, 1 H), 7.40–7.34 (m, 2 H), 7.34–7.27 (m, 3 H), 6.89 (s, 0.5 H), 6.88 (s, 0.5 H), 6.45 (q, $J = 7.1$ Hz, 1 H), 4.91–4.82 (m, 2 H), 3.67 (dd, $J = 9.3, 6.4$ Hz, 0.5 H), 3.63 (dd, $J = 9.3, 7.1$ Hz, 0.5 H), 3.37 (s, 3 H), 3.35–3.27 (m, 2 H), 3.27–3.18 (m, 1 H), 3.13–3.05 (m, 1 H), 2.99–2.87 (m, 1

H), 2.45–2.36 (m, 1 H), 2.23 (s, 3 H), 2.07 (d, $J = 7.1$ Hz, 3 H), 2.04 (s, 3 H), 1.95–1.82 (m, 1 H), 1.60–1.47 (m, 1 H), 1.43 (s, 4.5 H), 1.42 (s, 4.5 H).

4-{2-(Methoxymethyl)-1-(1-phenylethyl)-8-[(*S*)-pyrrolidin-3-ylmethoxy]-1*H*-imidazo[4,5-*c*]quinolin-7-yl}-3,5-dimethylisoxazole (Diastereomeric Mixture)



371

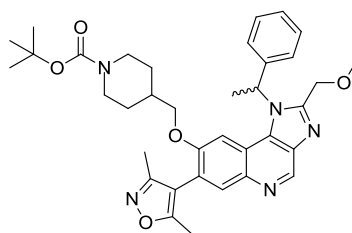
A solution of (3*S*)-*tert*-butyl 3-({[7-(3,5-dimethylisoxazol-4-yl)-2-(methoxymethyl)-1-(1-phenylethyl)-1*H*-imidazo[4,5-*c*]quinolin-8-yl]oxy}methyl)pyrrolidine-1-carboxylate (a mixture of diastereoisomers) **370** (30 mg, 0.049 mmol) in DCM (0.3 mL) was treated with TFA (0.2 mL, 2.60 mmol). The solution was allowed to stand in a stoppered vessel at r.t. for 2 h then concentrated under a stream of nitrogen. The residue was purified by MDAP using Method HpH. The appropriate fractions were combined and the solvent was removed by rotary evaporation to give the title compound (a mixture of diastereoisomers) as a white foam (18 mg, 0.035 mmol, 72%).

2% d.e. determined by HPLC analysis on a Chiralpak[®] AD column (250 mm x 4.6 mm, 10 μ m packing diameter), elution with 20% EtOH in heptane containing 0.1% isopropylamine, flow rate 1 mL/min, UV detection at 235 nm. Peak 1 Rt: 9.77 min, 49% peak area; Peak 2 Rt: 12.59 min, 51% peak area.

LCMS (HpH): m/z 512 [(M + H)⁺]; Rt: 0.83 min; 100% purity by peak area.

¹H NMR (400 MHz, DMSO-*d*₆): Variable temperature (393 K) δ 9.14 (s, 1 H), 7.93 (s, 1 H), 7.45–7.38 (m, 2 H), 7.38–7.30 (m, 3 H), 6.95 (s, 1 H), 6.49 (q, $J = 7.1$ Hz, 1 H), 4.92–4.84 (m, 2 H), 3.74 (dd, $J = 9.3, 6.3$ Hz, 0.5 H), 3.69 (dd, $J = 9.3, 7.8$ Hz, 0.5 H), 3.41 (s, 3 H), 3.27–3.04 (m, 4 H), 2.75–2.62 (m, 1 H), 2.49–2.42 (m, 1 H), 2.27 (s, 3 H), 2.11 (d, $J = 7.1$ Hz, 3 H), 2.07 (s, 3 H), 2.03–1.90 (m, 1 H), 1.59–1.47 (m, 1 H). NH signal not resolved.

(±)-*tert*-Butyl 4-([7-(3,5-dimethylisoxazol-4-yl)-2-(methoxymethyl)-1-(1-phenylethyl)-1*H*-imidazo[4,5-*c*]quinolin-8-yl]oxy)methyl)piperidine-1-carboxylate



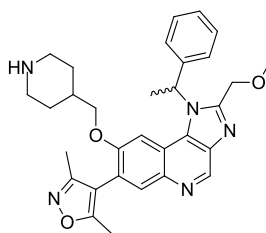
372

A mixture of (±)-7-(3,5-dimethylisoxazol-4-yl)-2-(methoxymethyl)-1-(1-phenylethyl)-1*H*-imidazo[4,5-*c*]quinolin-8-ol **369** (30 mg, 0.070 mmol), *tert*-butyl 4-[[[(methylsulfonyl)oxy]methyl]piperidine-1-carboxylate **321** (26 mg, 0.089 mmol) and potassium carbonate (14 mg, 0.101 mmol) in anhydrous DMF (1.5 mL) was heated at 100 °C under nitrogen for 16 h. The reaction mixture was diluted with EtOAc (10 mL) and washed with 10% LiCl (aq) (10 mL) followed by water (10 mL). The organic layer was passed through a hydrophobic frit and the solvent removed by rotary evaporation. The residue was purified by MDAP using Method HpH. The appropriate fractions were combined and the solvent removed by rotary evaporation to give the title compound as an off-white foam (21 mg, 0.034 mmol, 48%).

LCMS (HpH): m/z 626 [(M + H)⁺]; Rt: 1.30 min; 95% purity by peak area.

¹H NMR (400 MHz, DMSO-*d*₆): Variable temperature (393 K) δ 9.13 (s, 1 H), 7.91 (s, 1 H), 7.44–7.37 (m, 2 H), 7.37–7.29 (m, 3 H), 6.92 (s, 1 H), 6.47 (q, $J = 7.1$ Hz, 1 H), 4.94–4.84 (m, 2 H), 3.98–3.88 (m, 2 H), 3.58 (dd, $J = 9.2, 6.4$ Hz, 1 H), 3.40 (s, 3 H), 3.06 (dd, $J = 9.2, 6.4$ Hz, 1 H), 2.80–2.71 (m, 2 H), 2.26 (s, 3 H), 2.11 (d, $J = 7.1$ Hz, 3 H), 2.06 (s, 3 H), 1.85–1.74 (m, 1 H), 1.62–1.51 (m, 2 H), 1.45 (s, 9 H), 1.15–1.00 (m, 2 H).

(±)-4-[2-(Methoxymethyl)-1-(1-phenylethyl)-8-(piperidin-4-ylmethoxy)-1*H*-imidazo[4,5-*c*]quinolin-7-yl]-3,5-dimethylisoxazole



373

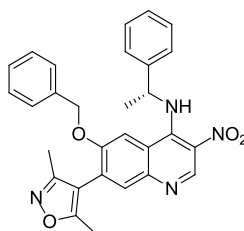
A solution of (±)-*tert*-butyl 4-([7-(3,5-dimethylisoxazol-4-yl)-2-(methoxymethyl)-1-(1-phenylethyl)-1*H*-imidazo[4,5-*c*]quinolin-8-yl]oxy)methyl)piperidine-1-carboxylate **372** (18 mg, 0.029 mmol) in DCM (0.3 mL) was treated with TFA (0.2 mL, 2.60 mmol). The

solution was allowed to stand at r.t. in a stoppered vessel for 1.5 h. The reaction mixture was concentrated under a stream of nitrogen and the residue dissolved in MeOH. The solution was applied to a MeOH preconditioned 1 g SCX-2 cartridge which was then washed with MeOH (10 mL) followed by 2 M ammonia in MeOH solution (10 mL). The basic wash was evaporated *in vacuo* to give the title compound as an off-white solid (15 mg, 0.029 mmol, 99%).

LCMS (HpH): m/z 526 [(M + H)⁺]; Rt: 0.85 min; 97% purity by peak area.

¹H NMR (400 MHz, DMSO-*d*₆): Variable temperature (393 K) δ 9.13 (s, 1 H), 7.91 (s, 1 H), 7.44–7.38 (m, 2 H), 7.38–7.29 (m, 3 H), 6.92 (s, 1 H), 6.48 (q, $J = 7.1$ Hz, 1 H), 4.94–4.85 (m, 2 H), 3.59–3.52 (m, 1 H), 3.41 (s, 3 H), 3.09–2.96 (m, 3 H), 2.62–2.53 (m, 2 H), 2.26 (s, 3 H), 2.11 (d, $J = 7.1$ Hz, 3 H), 2.08–2.05 (m, 3 H), 1.79–1.66 (m, 1 H), 1.62–1.51 (m, 2 H), 1.22–1.07 (m, 2 H).

6-(Benzyloxy)-7-(3,5-dimethylisoxazol-4-yl)-3-nitro-N-[(R)-1-phenylethyl]quinolin-4-amine



375

(*R*)-1-Phenylethanamine was purchased from Sigma Aldrich and >99% e.e. determined by HPLC analysis on a Chiralcel[®] OD-H (250 mm x 4.6 mm, 5 μ m packing diameter) column. An isocratic system of 2% EtOH (containing 0.1% isopropylamine) in heptane with a flow rate of 1 mL/min was used at r.t. The UV detection was performed at 254 nm. Rt: 9.65 min, 100% peak area.

(\pm)-1-Phenylethanamine was purchased from Sigma Aldrich and used as the chiral HPLC standard. Peak 1 Rt: 9.90 min, 50% peak area; Peak 2 Rt: 11.24 min, 50% peak area.

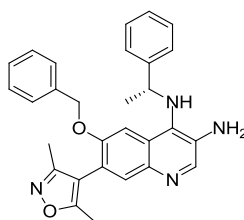
A solution of 4-[6-(benzyloxy)-4-chloro-3-nitroquinolin-7-yl]-3,5-dimethylisoxazole **343** (5 g, 12.20 mmol) in anhydrous NMP (25 mL) was treated with DIPEA (4.26 mL, 24.40 mmol) followed by (*R*)-1-phenylethanamine (1.712 mL, 13.42 mmol). The solution was stirred under nitrogen at r.t. for 2.5 h. The reaction mixture was diluted with water (50 mL) and extracted with EtOAc (75 mL). The organic layer was washed with 10% LiCl (aq) (2 x 50 mL) followed by water (50 mL) and passed through a hydrophobic frit. The solvent was

removed *in vacuo* and dried in the vacuum oven to give the title compound as a yellow foam (5.96 g, 12.05 mmol, 99%).

LCMS (formic A): m/z 495 [(M + H)⁺]; Rt: 1.31 min; 100% purity by peak area.

¹H NMR (400 MHz, CDCl₃): δ 9.54 (d, J = 7.8 Hz, 1 H), 9.27 (s, 1 H), 7.70 (s, 1 H), 7.53–7.46 (m, 2 H), 7.44–7.37 (m, 3 H), 7.36–7.29 (m, 1 H), 7.28–7.21 (m, 3 H), 7.00–6.95 (m, 2 H), 5.32 (dq, J = 7.8, 6.7 Hz, 1 H), 4.46 (d, J = 11.8 Hz, 1 H), 4.07 (d, J = 11.8 Hz, 1 H), 2.20 (s, 3 H), 2.07 (s, 3 H), 1.69 (d, J = 6.7 Hz, 3 H).

6-(Benzyloxy)-7-(3,5-dimethylisoxazol-4-yl)-N^d-[(R)-1-phenylethyl]quinoline-3,4-diamine



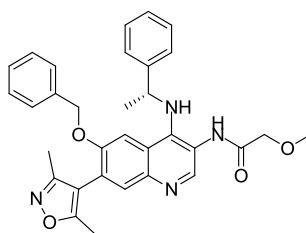
376

Iron powder (5.36 g, 96 mmol) was added to a solution of 6-(benzyloxy)-7-(3,5-dimethylisoxazol-4-yl)-3-nitro-*N*-[(*R*)-1-phenylethyl]quinolin-4-amine **375** (5.93 g, 11.99 mmol) in acetic acid (50 mL). The mixture was stirred in an open vessel at r.t. for 1 h. EtOAc (50 mL) was added to the flask and the mixture stirred for 1 h. The mixture was filtered through a Celite cartridge which was washed with further EtOAc (100 mL). The filtrate was washed with 0.5 M NaOH (aq) (2 x 100 mL) and water (100 mL). The organic layer was separated and passed through a hydrophobic frit. The solvent was removed by rotary evaporation to give a light brown foam (5.9 g). The foam was dissolved in MeOH (10 mL) and applied to a MeOH preconditioned 50 g NH₂ cartridge. The cartridge was washed with MeOH (160 mL) and the solvent evaporated under vacuum to give the title compound as a light brown foam (4.62 g, 9.94 mmol, 83%).

LCMS (formic A): m/z 465 [(M + H)⁺]; Rt: 0.99 min; 95% purity by peak area.

¹H NMR (400 MHz, CDCl₃): δ 8.38 (s, 1 H), 7.73 (s, 1 H), 7.41–7.25 (m, 10 H), 6.99 (s, 1 H), 5.02–4.93 (m, 2 H), 4.52 (q, J = 6.7 Hz, 1 H), 3.69 (br s, 2 H), 3.56 (br s, 1 H), 2.34 (s, 3 H), 2.21 (s, 3 H), 1.61 (d, J = 6.7 Hz, 3 H).

***N*-[6-(Benzyloxy)-7-(3,5-dimethylisoxazol-4-yl)-4-{{(R)-1-phenylethyl}amino}quinolin-3-yl]-2-methoxyacetamide**



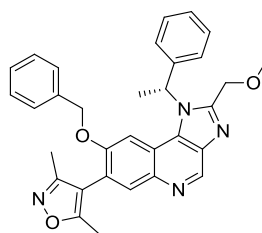
377

A solution of 6-(benzyloxy)-7-(3,5-dimethylisoxazol-4-yl)-*N*⁴-[(*R*)-1-phenylethyl]quinoline-3,4-diamine **376** (1.89 g, 4.07 mmol) and pyridine (0.50 mL, 6.18 mmol) in DCM (20 mL) was cooled to 0 °C and 2-methoxyacetyl chloride (0.41 mL, 4.48 mmol) added. The mixture was stirred under nitrogen at 0 °C for 10 min and allowed to warm to r.t. over 3.5 h. The reaction mixture was washed sequentially with 0.5 M HCl (aq) (20 mL) and water (2 x 20 mL). The organic layer was separated, passed through a hydrophobic frit and the solvent removed by rotary evaporation to give the title compound as a light brown foam (2.14 g, 3.99 mmol, 98%).

LCMS (formic A): *m/z* 537 [(M + H)⁺]; Rt: 0.91 min; 100% purity by peak area.

¹H NMR (400 MHz, CDCl₃): δ 8.80 (s, 1 H), 8.25 (s, 1 H), 7.82 (s, 1 H), 7.40–7.29 (m, 8 H), 7.26–7.21 (m, 3 H), 4.92–4.85 (m, 2 H), 4.62 (dq, *J* = 8.6, 6.8 Hz, 1 H), 4.27 (d, *J* = 8.6 Hz, 1 H), 4.10 (s, 2H), 3.53 (s, 3 H), 2.34 (s, 3 H), 2.21 (s, 3 H), 1.61 (d, *J* = 6.8 Hz, 3 H).

4-{8-(Benzyloxy)-2-(methoxymethyl)-1-[(*R*)-1-phenylethyl]-1*H*-imidazo[4,5-*c*]quinolin-7-yl}-3,5-dimethylisoxazole



378

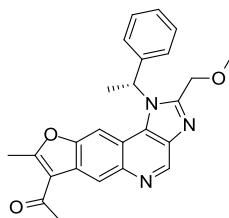
A solution of *N*-(6-(benzyloxy)-7-(3,5-dimethylisoxazol-4-yl)-4-{{(R)-1-phenylethyl}amino}quinolin-3-yl)-2-methoxyacetamide **377** (2.14 g, 3.99 mmol) in propionic acid (6.0 mL, 80 mmol) was stirred at 140 °C under nitrogen for 2 h. The reaction mixture was allowed to cool to r.t. and the solvent removed *in vacuo*. The residue was dissolved in DCM (25 mL) and washed with 1 M NaOH (aq) (25 mL). The aqueous layer was extracted with DCM (25 mL), the organic layers combined and passed through a

hydrophobic frit. The solvent was removed by rotary evaporation, the foam dissolved in DCM (5 mL) and purified on a 100 g silica cartridge using a gradient of 0–15% MeOH in DCM over 12 column volumes. The appropriate fractions were combined and the solvent was removed by rotary evaporation to give the title compound as a light brown foam (1.87 g, 3.61 mmol, 90%).

LCMS (formic A): m/z 519 $[(M + H)^+]$; Rt: 1.08 min; 96% purity by peak area.

^1H NMR (400 MHz, DMSO- d_6): Variable temperature (393 K) δ 9.15 (s, 1 H), 7.96 (s, 1 H), 7.46–7.30 (m, 8 H), 7.24–7.20 (m, 2 H), 7.09 (s, 1 H), 6.47 (q, $J = 7.1$ Hz, 1 H), 4.88–4.85 (m, 2 H), 4.80 (d, $J = 11.9$ Hz, 1 H), 4.41 (d, $J = 11.9$ Hz, 1 H), 3.40 (s, 3 H), 2.24 (s, 3 H), 2.07–2.03 (m, 6 H).

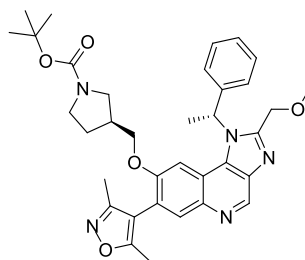
(R)-1-{2-(Methoxymethyl)-8-methyl-1-(1-phenylethyl)-1H-furo[2,3-g]imidazo[4,5-c]quinolin-7-yl}ethanone



379

(R)-1-{2-(methoxymethyl)-8-methyl-1-(1-phenylethyl)-1H-furo[2,3-g]imidazo[4,5-c]quinolin-7-yl}ethanone **379** was isolated as a by-product in the synthesis of **333**. Please refer to the experimental relating to the preparation of **333** for characterisation data of **379**.

(3S)-tert-Butyl 3-[(7-(3,5-dimethylisoxazol-4-yl)-2-(methoxymethyl)-1-[(R)-1-phenylethyl]-1H-imidazo[4,5-c]quinolin-8-yl)oxy)methyl]pyrrolidine-1-carboxylate



380

A mixture of 7-(3,5-dimethylisoxazol-4-yl)-2-(methoxymethyl)-1-[(R)-1-phenylethyl]-1H-imidazo[4,5-c]quinolin-8-ol **333** (233 mg, 0.544 mmol), potassium carbonate (107 mg, 0.778 mmol) and (S)-tert-butyl 3-[(methylsulfonyl)oxy)methyl]pyrrolidine-1-carboxylate **311** (190 mg, 0.680 mmol) was stirred at 100 °C under nitrogen for 3 h. The reaction mixture

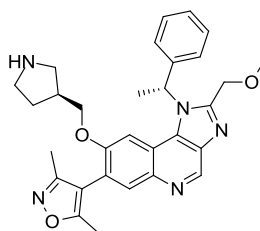
was allowed to cool to r.t., diluted with 10% LiCl (aq) (10 mL) and extracted with EtOAc (3 x 10 mL). The organic extracts were combined and passed through a hydrophobic frit. The solvent was removed by rotary evaporation and the residue purified by MDAP using Method HpH. The appropriate fractions were combined and the solvent evaporated *in vacuo* to give the title compound as an off-white solid (191 mg, 0.312 mmol, 57%).

LCMS (formic A): m/z 612 $[(M + H)^+]$; Rt: 1.08 min; 100% purity by peak area.

HRMS (ESI): M + H calcd for $C_{35}H_{42}N_5O_5$ 612.3181, found 612.3170.

1H NMR (400 MHz, DMSO- d_6): Variable temperature (373 K) δ 9.15 (s, 1 H), 7.93 (s, 1 H), 7.44–7.38 (m, 2 H), 7.37–7.31 (m, 3 H), 6.92 (s, 1 H), 6.49 (q, $J = 7.0$ Hz, 1 H), 4.91 (ABq, $\Delta\delta_{AB} = 0.04$, $J_{AB} = 12.9$ Hz, 2 H), 3.71 (dd, $J = 9.4, 6.4$ Hz, 1 H), 3.41 (s, 3 H), 3.39–3.25 (m, 3 H), 3.13–3.07 (m, 1 H), 2.93–2.91 (m, 1 H), 2.49–2.41 (m, 1 H), 2.27 (s, 3 H), 2.11 (d, $J = 7.0$ Hz, 3 H), 2.08 (s, 3 H), 2.00–1.89 (m, 1 H), 1.65–1.54 (m, 1 H), 1.46 (s, 9 H).

4-{2-(Methoxymethyl)-1-[(R)-1-phenylethyl]-8-[(S)-pyrrolidin-3-ylmethoxy]-1H-imidazo[4,5-c]quinolin-7-yl}-3,5-dimethylisoxazole



381

A solution of (3S)-*tert*-butyl 3-[(7-(3,5-dimethylisoxazol-4-yl)-2-(methoxymethyl)-1-[(R)-1-phenylethyl]-1H-imidazo[4,5-c]quinolin-8-yl)oxy)methyl]pyrrolidine-1-carboxylate **380** (186 mg, 0.304 mmol) in anhydrous 1,4-dioxane (2 mL) was treated with 4 M HCl in 1,4-dioxane (2 mL, 8.00 mmol) and the mixture allowed to stand in a stoppered vessel for 1 h. The reaction mixture was evaporated *in vacuo* and the solid dissolved in MeOH (2 mL). The solution was applied to a MeOH preconditioned 5 g SCX-2 cartridge which was then washed with MeOH (30 mL) followed by 2 M ammonia in MeOH solution (30 mL). The basic wash was evaporated *in vacuo* to give the title compound as an off-white solid (150 mg, 0.293 mmol, 96% yield).

>99% d.e. determined by HPLC analysis on a Chiralpak® AD column (250 mm x 4.6 mm, 10 μ m packing diameter), elution with 20% EtOH in heptane containing 0.1% isopropylamine, flow rate 1 mL/min, UV detection at 235 nm. Rt: 12.08 min, 100% peak area.

$[\alpha]_{\text{D}}^{21} -27$ (c 0.5, CHCl_3).

IR (solid) ν (cm^{-1}): 2929, 1618, 1495, 1444, 1393, 1367, 1215, 1095.

m.p.: 130–132 °C.

LCMS (formic A): m/z 512 $[(\text{M} + \text{H})^+]$; Rt: 0.59 min; 100% purity by peak area.

HRMS (ESI): $\text{M} + \text{H}$ calcd for $\text{C}_{30}\text{H}_{34}\text{N}_5\text{O}_3$ 512.2656, found 512.2650.

^1H NMR (400 MHz, $\text{DMSO}-d_6$): Variable temperature (393 K) δ 9.13 (s, 1 H), 7.92 (s, 1 H), 7.44–7.37 (m, 2 H), 7.37–7.29 (m, 3 H), 6.95 (s, 1 H), 6.48 (q, $J = 7.0$ Hz, 1 H), 4.89 (ABq, 2 H, $\Delta\delta_{\text{AB}} = 0.03$, $J_{\text{AB}} = 13.0$ Hz), 3.65 (dd, $J = 9.3, 6.3$ Hz, 1 H), 3.41 (s, 3 H), 3.19–3.12 (m, 1 H), 2.92–2.81 (m, 3 H), 2.44 (dd, $J = 10.6, 6.0$ Hz, 1 H), 2.34–2.22 (m, 4 H), 2.11 (d, $J = 7.0$ Hz, 3 H), 2.07 (s, 3 H), 1.85–1.74 (m, 1 H), 1.40–1.29 (m, 1 H), *NH* not resolved.

^{13}C NMR (100 MHz, $\text{DMSO}-d_6$, 393 K): δ 165.2, 158.3, 153.9, 151.8, 142.7, 139.7, 139.6, 137.1, 132.5, 132.4, 128.6 (2C), 127.0, 125.1 (2C), 120.2, 117.4, 111.8, 104.1, 71.3, 66.8, 57.5, 54.1, 49.4, 45.6, 38.1, 28.5, 18.7, 10.6, 9.5.

4.4. Racemisation Study

A mixture of 7-(3,5-dimethylisoxazol-4-yl)-8-hydroxy-3-methyl-1-[(*R*)-1-(pyridin-2-yl)ethyl]-1*H*-imidazo[4,5-*c*]quinolin-2(3*H*)-one **237** (76% e.e., 10 mg, 0.024 mmol) and potassium carbonate (5 mg, 0.036 mmol) was suspended in anhydrous DMF (0.25 mL) and stirred under nitrogen at 100 °C for 24 h. The reaction mixture was allowed to cool to r.t. and filtered. The filtrate was evaporated under a stream of nitrogen to give 7-(3,5-dimethylisoxazol-4-yl)-8-hydroxy-3-methyl-1-[(*R*)-1-(pyridin-2-yl)ethyl]-1*H*-imidazo[4,5-*c*]quinolin-2(3*H*)-one **237** (10 mg, 0.024 mmol, 100% recovery).

An enantiomeric composition of 74% e.e. was determined by HPLC analysis on a Chiralpak[®] ID (250 mm x 4.6 mm, 5 μm packing diameter) column. An isocratic system of 50% EtOH in heptane with a flow rate of 1 mL/min was used at r.t. The UV detection was performed at 215 nm.

LCMS (formic A): m/z 416 $[(\text{M} + \text{H})^+]$; Rt: 0.60 min; 92% purity by peak area.

4.5. Computational Procedures

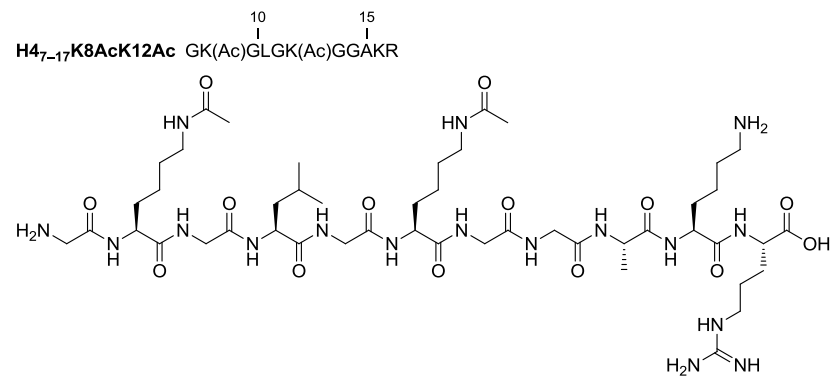
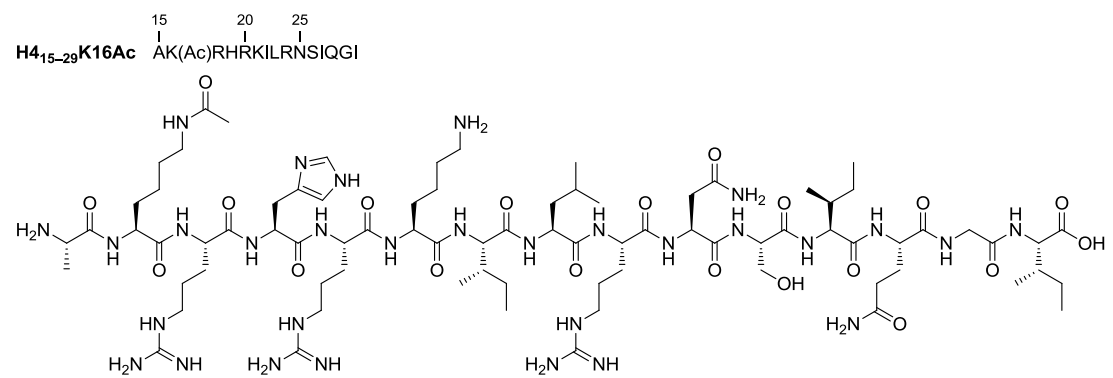
Dihedral scan of 3,5-dimethyl-4-(quinolin-7-yl)isoxazole and 4-(6-methoxyquinolin-7-yl)-3,5-dimethylisoxazole

A conformational analysis of was carried out in MacroModel (version 9.8) in Schrodinger Suite 2010 from Schrodinger LLC. The structures were first minimised and

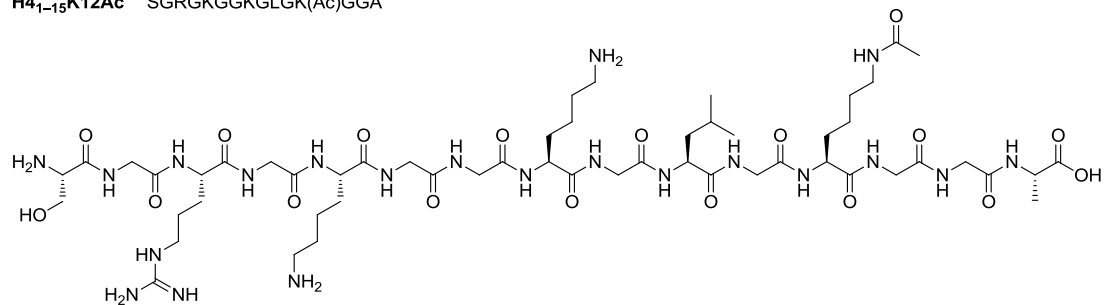
coordinate scans performed on the dihedral angle between the dimethylisoxazole and quinoline rings. The OPLS2005 force field was used with water as solvent with a PRCG minimisation procedure. The maximum iterations option was set to 5000 with a convergence threshold of 0.005. The relative energies in kcal/mol of each minimised conformer were plotted against the dihedral angle for each structure.

5. Appendix

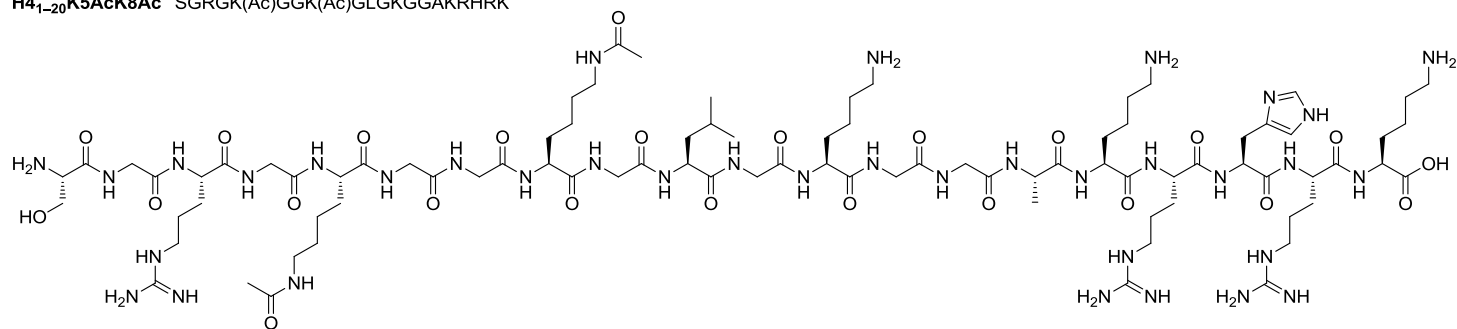
5.1. Structures of Histone Peptides



H4₁₋₁₅K12Ac 1 5 10 15
SGRGKGGKGLGK(Ac)GGA



H4₁₋₂₀K5AcK8Ac 1 5 10 15 20
SGRGK(Ac)GGK(Ac)GLGKGGAKRHRK



5.2. BET WT FP Assays

Assay Principle

Biochemical FP assays previously reported by our laboratories,⁴⁴ were used during the lead optimisation research programme detailed in Section 2 of this thesis. These assays utilised a derivative of I-BET762 **383** as the fluorescent ligand which binds to the BET proteins (Figure 91).

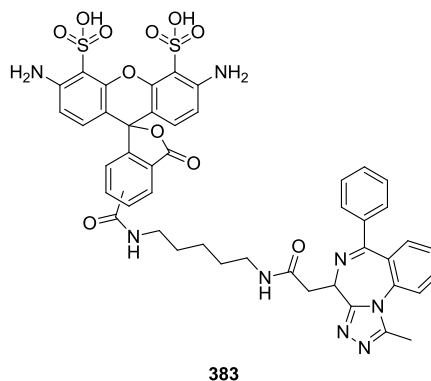


Figure 91. Fluorophore-tagged BzD **383**.

When excited with polarized light, unbound ligand emits largely depolarized light during the fluorescence lifetime due to rapid rotation of the molecule in solution. Bound ligand is immobilised enough to emit more of the light in the same plane in which it was excited. The increase in FP is calculated from a weighted average of fluorescence intensity in the parallel and perpendicular planes. BET inhibitors will compete with the fluorescent ligand and cause a decrease in FP signal. By using solutions of compound in DMSO at different concentrations, dose-response curves were generated and the concentration of compound inducing 50% inhibition of fluoro-ligand binding resulted in IC_{50} values. These assays utilised WT protein constructs containing both BD1 and BD2 of BRD2, 3 and 4, and this methodology was used as a primary screen to generate SAR in the first programme of work in this thesis. The FP assays were discontinued nearing the end of the research conducted in Section 2 and were replaced with HTRF assays which are described on the next page.

Assay Procedure

All components were dissolved in buffer composition of 50 mM HEPES pH 7.4, 150 mM NaCl and 0.5 mM CHAPS with final concentrations of 75 nM BET protein (BRD2 (1–473), BRD3 (1–435) or BRD4 (1–477)) and 5 nM fluorescent ligand **383**. 10 μ L of this mixture was added using a micro multidrop to wells containing 100 nL of various concentrations of test compound or DMSO vehicle (1% final) in a Greiner 384 well Black

low volume microtitre plate and equilibrated in dark for 60 min at r.t. Fluorescence polarisation was read using an Envision plate reader (excitation = 485 nm, emission = 530 nm; dichroic = 505 nm). All data was normalized to the mean of 16 high and 16 low control wells on each plate. A four parameter curve fit of the following form was then applied: $y = a + ((b - a) / (1 + (10^x / 10^c)^d))$ Where 'a' is the minimum, 'b' is the Hill slope, 'c' is the pIC₅₀ and 'd' is the maximum.

5.3. *BET WT HTRF Assays*

Assay Principle

HTRF was used to measure binding of a biotinylated tetraacetylated histone H4 peptide to BET protein. The protein:protein interaction is detected through binding of the allophycocyanin (APC)-labelled anti-6His antibody to 6His-tagged protein. Europium cryptate labelled streptavidin binds the biotin in the H4 peptide resulting in FRET between the two fluorophores when in close proximity upon excitation at 317 nm. Fluorescent emission by APC at 665 nm correlates with the amount of protein:protein binding. BET inhibitors will compete with the peptide ligand and cause a decrease in fluorescence signal. By using solutions of compound in DMSO at different concentrations, dose-response curves were generated and the concentration of compound inducing 50% inhibition of peptide binding resulted in IC₅₀ values.

For only dimethylisoxazole quinoline **228**, was HTRF data reported and, through using the line of best fit for compounds tested in both BRD4 HTRF and WT FP assays ($y = -0.31 + (0.92x)$ where $y = \text{WT FP}$ and $x = \text{HTRF}$, r^2 value = 0.79), the expected HTRF pIC₅₀ was calculated as 5.9.

Assay Procedure

BET protein was diluted to a concentration sufficient to yield a robust signal of at least 3:1 signal:background (~100 nM FAC), into an aliquot of assay buffer (50 mM HEPES, 50 mM NaCl, 0.5 mM CHAPs, pH 7.4, r.t.). The addition of 2x Kd of an H4 peptide (~300 nM FAC) was made and the mixture left in the dark for 1 h at r.t. The protein-H4 solution was dispensed (8 µL/well, medium speed) using a Multidrop combi, to a black low volume Greiner 384-well plate containing concentration response curves of compound (50 nL/well). This was then left to incubate for 1 h, in the dark at r.t. Detection reagents were prepared 15 min prior to use by diluting the Streptavidin-Eu (10 nM FAC) and XL-665 (50 nM FAC) into detection buffer (50 mM HEPES, 50 mM NaCl, 0.5 mM CHAPs, 150 mM KF, pH 7.4,

r.t.) then added to the assay plate (2 μL /well), followed by a further 1 h incubation. The plates were read on the Envision reader and the donor and acceptor counts were determined. From this, the ratio of acceptor/donor was calculated (excitation = 317 nm, emission donor = 615 nm, emission acceptor = 665 nm) and used for data analysis. All data was normalized to the robust mean of 16 high (DMSO) and 16 low control wells on each plate. $y = ((a - d) / (1 + (x / c)^b)) + d$ where 'a' is the minimum, 'b' is the Hill slope, 'c' is the pIC_{50} and 'd' is the maximum.

5.4. Solubility Measurements by CLND

Assay Principle

In the programme of work detailed in Section 2, aqueous solubility was approximated from a high throughput DMSO precipitative solubility assay method. After filtration of a precipitate, CLND was used to determine the solution concentration from which the solubility was derived. In general, values of $<50 \mu\text{g/mL}$ were considered poor, values in the range $50\text{--}100 \mu\text{g/mL}$ moderate, and those $>100 \mu\text{g/mL}$ good. The CLND assay was used to filter compounds for progression into solubility measurements from solid.

Assay Procedure

A 5 μL aliquot of a 10 mM solution of compound in DMSO was added to 95 μL aqueous phosphate buffer (pH 7.4) and equilibrated at r.t. for 1 h. The mixture was filtered through a Millipore Multiscreen HTS-PCF filter plate and the filtrate analysed by suitably calibrated flow injection CLND. The standard error of the CLND solubility determination is 30 μM , the upper limit of the solubility is 500 μM .

5.5. Solubility Measurements from Solid

Assay Principle

A lower throughput solubility screen using compound from solid was used to more accurately determine aqueous solubility and suitability of compounds for *i.v.* administration in Section 2 of this thesis. Solubility was determined at both pH 5.0 and 7.0 using visual inspection and HPLC analysis.

Assay Procedure

Britton–Robinson aqueous buffer (pH 5.0 and/or 7.0, 0.1 mL) was added to 1 mg solid compound and after agitation and sonication, the sample was visually inspected to determine

a solubility >10,000 µg/mL. If undissolved compound remained, the sample was diluted with 0.1 mL buffer and, after agitation and sonication, the sample was visually inspected to determine a solubility >5000 µg/mL. If undissolved compound remained, the sample was diluted with 0.8 mL buffer and after agitation and sonication, the sample was visually inspected to determine a solubility >1000 µg/mL. If undissolved compound remained, 0.1 mL of the sample was diluted with 0.9 mL 50% acetonitrile in water and the solution analysed by HPLC (with comparison to a standard) to determine a solubility in the range of 0–1000 µg/mL. Note that instead of a 10 mg/mL starting concentration, a 5 mg/mL starting concentration was sometimes used.

5.6. *hERG Inhibition*

Assay Principle

Inhibition of hERG activity was determined using patch clamp electrophysiology assays. An individual cell of a cell line expressing the hERG ion channel is sealed, or ‘clamped’, by a hollow glass micropipette containing an electrode and electrolyte. The area of cell surface, or ‘patch’, sealed by the pipette often contains a single hERG ion channel and after addition of test compound to the electrolyte, inhibition of current measured. A hERG IonWorks Quattro electrophysiology assay was used in Section 2 of this thesis but this assay was discontinued towards the latter end of this research and replaced with a hERG Ionworks Barracuda assay – only compound **228** was tested in the latter assay. Data between the two assays were considered interchangeable.

Assay Procedure (hERG Quattro)

Chinese hamster ovary cells stably expressing hERG were cultured in M1 DMEM Hams with F12, supplemented with 10% FBS and 400 µg/mL geneticin. Cells were thawed in T175 flasks at 6–8 million cells per T175 flask, maintained at 37 °C in a humidified environment containing 5% CO₂ for 3–4 h and transferred to a 30 °C incubator containing 5% CO₂ and incubated for another 72 h before assaying. On day of assay, cells which were over 80% confluence were used. Media were removed and cells were washed with warm PBS (without magnesium and calcium) two times. 5 mL pre-warmed Versene was added for 6 min, followed by addition of 10 mL of warm M1 media. The suspension was placed into a 15 mL centrifuge tube and spun for 2 min at 1K rpm. The supernatant was removed and cells were re-suspended in 5 mL of warm M1 media and incubated for 5 min for the cells to recover. After 5 min the cells the suspension was centrifuged at 1K rpm for 2 min, the pellet

re-suspended to a cell concentration of 4–5 million cells/mL and that solution was added to the IonWorks.

All currents were recorded before and after the addition of compound using a Molecular Devices IonWorks Quattro automated electrophysiology instrument in Population Patch-Clamp mode. The KCl intracellular solution contained the following: 140 mM KCl, 1 mM MgCl₂, 1 mM CaCl₂, 20 mM HEPES, pH 7.3 with KOH. Amphotericin-B solution was prepared as 50 mg/mL stock solution in DMSO and diluted to a final working concentration of 0.1 mg/mL in intracellular solution. The external solution was D-PBS (-). The voltage pulse protocol applied pre- and post- compound addition was as follows: hERG currents were activated by 4 sec depolarising pulse to +40 mV from a holding potential of –80 mV. The cells were then repolarised to –50 mV to generate large outward tail currents for 5 sec.

Ionworks recordings are population patch measurements in which the average of the current across many cells is determined. Hence the word observation is used for a single concentration response curve. There could be several observations on a certain day. Data were normalised to the high and low controls. Low controls were wells in which 50 µM Quinidine was added for the hERG blocker assay. High controls were wells in which only 1% DMSO was added for the hERG assay. The normalised data were analysed by using ActivityBase software. The amount of tonic block is calculated from peak (maximum tail current value). This value is amplitude of the peak tail current minus the steady state average value obtained at –50 mV holding potential before the first voltage step to +40 mV. For all channels: Concentration response data were derived using a four parameter concentration effect curve fitting procedure. pIC₅₀ values and Hill coefficients were determined from these inhibition curves.

Assay Procedure (hERG Barracuda)

Chinese hamster ovary cells stably expressing hERG were cultured in DMEM F12 Hams medium, supplemented with 10% FBS and 400 µg/ml Geneticin. Frozen cells were thawed in T175 asks at 6–8 x 10⁶ cells per ask, maintained at 37 °C in a humidified environment containing 5% CO₂ for 3–4 h and then transferred to a 30 °C incubator containing 5% CO₂ and incubated for a further 72 h prior to assay. Cells with a confluence of over 80% were harvested by washing twice with warm PBS (without magnesium and calcium) and incubating at 37 °C with 5 mL pre-warmed Versene for 6 min, followed by addition of 10 mL of warm culture medium. The resulting suspension was transferred to a 15 mL centrifuge tube and spun for 2 min at 1300 rpm. The supernatant was removed and cells were re-suspended in 5 mL of warm culture medium and incubated at 37 °C for a further 5

min. The suspension was then centrifuged for 2 min at 1300 rpm, the supernatant discarded and the pellet re-suspended to a cell concentration of $4\text{--}5 \times 10^6$ cells/ml. This suspension was transferred to the IonWorks Barracuda.

hERG currents were recorded before and after the addition of compound using a Molecular Devices IonWorks Barracuda automated electrophysiology instrument in Population Patch-Clamp mode. The KCl intracellular solution contained the following: 140 mM KCl, 1 mM MgCl_2 , 1 mM CaCl_2 , 20 mM HEPES, pH 7.3 with KOH. Amphotericin-B solution was prepared as 50 mg/mL stock solution in DMSO and diluted to a final working concentration of 0.1 mg/mL in intracellular solution. The external solution was D-PBS(-). The voltage pulse protocol applied pre- and post- compound addition was as follows: hERG currents were activated by a 5500 msec depolarising pulse to +20 mV from a holding potential of -80 mV. The cells were then repolarised to -50 mV for 1000 msec to generate large outward tail currents.

Recordings are population patch measurements in which the average of the current across many cells is determined. Hence the word 'observation' is used for a single concentration response curve. There could be several observations on a certain day.

Data were normalised to high and low controls. Low control wells contained 50 μM Quinidine and high control wells contained equivalent quantities of DMSO. The normalised data were analysed by using ActivityBase software. The amount of tonic block was calculated from the peak tail current (the maximum amplitude of the tail current obtained after the voltage step to -50 mV). Concentration response data were derived using a four parameter logistic fitting procedure. pIC_{50} values were determined from these inhibition curves.

5.7. ChromLogD and ChromLogP Measurements

Assay Principle

An important parameter discussed in the programme of research contained within Section 3 of this thesis is lipophilicity. Measurements of lipophilicity were conducted using a LCMS method termed chromLogD. Values were derived from chromatographic hydrophobicity index (CHI) LogD^{151} obtained from the retention time of a compound on three C18 columns using an increasing gradient of acetonitrile in three different aqueous mobile phases (pH 2.0, 7.4 and 10.5). This allowed determination of chromLogP (hydrophobicity of the neutral form) which was taken as the highest chromLogD value in

any of the three buffers. In general, chromLogD values at pH 7.4 were reported throughout Section 2 of this thesis to best approximate physiological conditions.

Assay Procedure

LCMS was performed on a Waters early candidate profiling (ECP) four-way MUX system equipped with a Luna C18(2) column (50 mm x 3 mm). Gradient elution was carried out with the mobile phases as (A) aqueous solution and (B) acetonitrile. Aqueous phases used were pH 2.0 phosphoric acid/or formic acid solution, ammonium acetate solution adjusted to pH 7.4 and ammonium acetate solution adjusted to pH 10.5 with ammonia solution. The conditions for the gradient elution were initially 0% B, increasing linearly to 100% B over 2.5 min, remaining at 100% B for 3.0 min then decreasing to 0% B over 0.2 min. The flow rate was 1 mL/min. CHI values were derived directly from retention time by using a calibration line obtained for standard compounds. The CHI value approximates to the volume % organic concentration when the compound elutes and is linearly transformed into chromlogD by least-squares fitting experimental CHI values to calculated logP values for over 20K research compounds using the following formula: $\text{chromlogD} = 0.0857 \text{ CHI} - 2.00$.

5.8. Inhibition of IL-6 Production in LPS-Stimulated Human WB

Assay Principle

A human whole blood assay was conducted in the first research programme contained within this thesis and, unlike isolated PBMCs, provided a model to study compounds in a system where cell-cell or cell-protein interactions occur – effects that may take place *in vivo*. Stimulation of blood with LPS elicited an immune response through the release of pro-inflammatory cytokines and upon treatment with compound at different concentrations, MesoScale Discovery (MSD) plates coated with a labelled antibody were used to capture IL-6. Electrochemiluminescence detection determined cytokine levels and IC₅₀ values were determined.

Assay Procedure

Whole blood was taken from healthy volunteers. All donors provided written informed consent for use of their samples and the collection, and use of the samples received Institutional Review Board approval. Blood/well (140 µL) were added to 96 well plates containing prediluted test compounds to achieve a range of final assay concentrations (1.69

nM–30 μ M) in 0.7% DMSO. 0.7% DMSO was also tested as a vehicle control, along with an assay positive standard. Test compounds were incubated for 30 min before the addition of 10 μ L of 2.8 μ g/mL LPS (Sigma). Assay plates were then incubated at 37 °C, 5% CO₂ overnight.

140 μ L of Dulbecco's PBS (Invitrogen) was added to each well, mixed and the plates centrifuged for 10 min at 2500 rpm. 100 μ L of cell supernatants were then removed from the assay plate and analysed for IL-6 using MSD single plex plates in accordance with the manufacturer's instructions. Plates were read on an MSD Sector Imager 6000 and pg/ml values were back-calculated to standard curves using MSD Discovery Workbench software v4.0.11. IL-6 data were then normalised to the assay positive and negative controls using curve fitting packages within Microsoft Excel.

5.9. Mutant FRET Assays

Assay Principle

To determine the domain selectivity of a probe molecule in Section 3 of this thesis, assays allowing measurement of compound binding to a single bromodomains of the BET proteins were used. In previous studies with the bromodomain of PCAF, site-directed mutagenesis of the conserved tyrosine residue with an alanine residue was shown to abrogate acetylated histone peptide binding.¹² Coupled with the crystallographic information discussed in the introduction of this thesis, mutation of the key tyrosine amino acids would disrupt the interactions essential for KAc recognition and in this programme of study, these findings were extended to prevent small molecule binding. Thus, BET protein constructs containing tyrosine/alanine substitutions were generated¹⁵² to distinguish selective binding of a compound to either BD1 or BD2 (Table 42).

Mutant Protein	Shorthand Description
BRD2 (1–473) Y386A	BRD2 BD1
BRD2 (1–473) Y113A	BRD2 BD2
BRD3 (1–435) Y348	BRD3 BD1
BRD3 (1–435) Y73A	BRD3 BD2
BRD4 (1–477) Y390A	BRD4 BD1
BRD4 (1–477) Y97A	BRD4 BD2
BRDT (1–397) Y309A	BRDT BD1
BRDT (1–397) Y66A	BRDT BD2

Table 42. Details of mutant constructs used for BET BD1 and BD2 FRET assays.

As an example, the BRD4 Y390A mutant abrogated binding at the KAc recognition site at BD2 while the BRD4 Y97A mutant prevented binding at the KAc recognition site at BD1.

FP technology was first employed in all the BET mutant assays and this data was used for SAR determination and optimisation.¹⁵³ Midway through the programme, the assays were reconfigured in FRET format¹⁵³ to increase the tight binding limit compared to the FP assays, allowing IC₅₀ determination up to 5 nM and this data was reported throughout Section 3 of the thesis. For only imidazoquinolinone **281a**, was FP data reported and through using the line of best fit for compounds tested in both BRD4 BD1 assays ($y = -1.20 + (1.19x)$ where $y = \text{FRET}$ and $x = \text{FP}$, r^2 value = 0.76), the expected FRET pIC₅₀ was calculated as 5.6. For cyclobutylamine **289**, the first two test occasions in the BRD4 FP assays resulted in 100-fold selectivity (BD1 and BD2 pIC₅₀s = 6.7 and 4.7, respectively) but this narrowed upon subsequent retesting to a mean selectivity of 50-fold (BD1 pIC₅₀ = 6.5, BD2 pIC₅₀ = 4.8) – data obtained in BRD4 FRET assays were in close accordance (BD1 pIC₅₀ = 6.6 and BD2 pIC₅₀ = 5.0, selectivity = 40-fold).

In the mutant FRET assays, an Alexa Fluor 647 tagged derivative of I-BET762 (**384**, Figure 92) functioned as the ligand and FRET acceptor. This ligand bound to the bromodomain of each mutant construct, and with wild type protein, with similarly high affinities while significantly lowered affinities were measured for double mutant constructs and, therefore, confirmed that this approach was suitable for selectivity measurements.¹⁵³

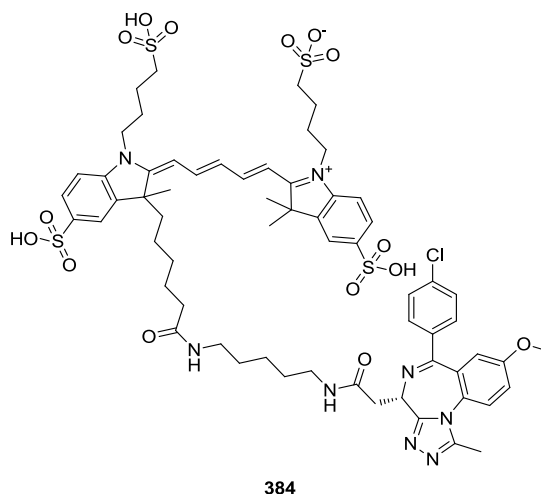


Figure 92. Fluorophore tagged derivative of I-BET762 **384** used in the mutant FRET assays.

A 6His purification tag at the *N*-terminal of the protein acted as the epitope for an anti-6His Europium chelate, which functioned as a donor in the FRET pair. Binding of the fluoroligand to a bromodomain was detected by laser excitation of the Eu chelate at 337 nm.

This caused energy transfer to the Alexa Fluor tag and the resulting emission at 665 nm was measured. Displacement of the fluorescent ligand by small molecules reduced the FRET signal to varying extents depending on their affinity. When conducted at different concentrations of small molecule, a dose-response curve was generated and an IC₅₀ value determined.

The BRD4 mutant assays were conducted regularly and were used for SAR screening and compound profiling. The other BET mutant assays were used only for periodic assessment as these were expected to show similar potency and selectivity due to the high homology between each of the BET proteins and the similar residue variations between BD1 and BD2.

Assay Procedure

Compounds were screened against *N*-terminal 6His-tagged single mutant tandem bromodomain proteins in a dose-response format using an Alexa Fluor 647 derivative of I-BET762 (**384**). Compounds were titrated from 10 mM in 100% DMSO and 100 nL transferred to a low volume black 384 well micro titre plate using a Labcyte Echo 555. A Thermo Scientific Multidrop Micro were used to dispense 5 µL of 10 nM protein in 50 mM HEPES, 50 mM NaCl and 1 mM CHAPS, pH 7.4, in the presence of 50 nM compound **384** (~*K_d* concentration for the interaction between all BET single mutant tandem bromodomain proteins and **384**, with the exception of BRDT Y66A, which used 200 nM). After equilibrating for 1 h in the dark at r.t., the bromodomain protein:fluorescent ligand interaction was detected using TR-FRET following a 5 µL addition of 1.5 nM europium chelate labelled anti-6His antibody (Perkin Elmer, W1024, AD0111) in assay buffer. Time resolved fluorescence (TRF) was then detected on a TRF laser equipped Perkin Elmer Envision multimode plate reader (excitation = 337 nm; emission 1 = 615 nm; emission 2 = 665 nm; dual wavelength bias dichroic = 400 nm, 630 nm). TR-FRET ratio was calculated using the following equation: Ratio = ((Acceptor fluorescence at 665 nm) / (Donor fluorescence at 615 nm)) * 1000. TR-FRET ratio data was normalised to a mean of 16 replicates per micro titre plate of both 10 µM I-BET151 and 1% DMSO controls and IC₅₀ values determined for each of the compounds tested by fitting the fluorescence ratio data to a four parameter model: $y = a + ((b - a) / (1 + (10^x / 10^c)^d))$ where 'a' is the minimum, 'b' is the Hill slope, 'c' is the IC₅₀ and 'd' is the maximum.

5.10. AMP Assay

Assay Principle

The ability of a compound to permeate a cell membrane was estimated using an artificial membrane assay. An artificial lipid membrane comprised of egg-lecthucin is formed on a filter plate and test compound in buffer applied to the donor side of the plate. After 3 h, the concentration of the compound in the donor and the acceptor compartments is measured and the rate of permeation calculated.

Assay Procedure

An artificial membrane was prepared by addition of 1.8% phosphatidylcholine and 1% cholesterol decane solution (3.5 μ L) to a polycarbonate filter plate and evaporation. The membrane was hydrated by addition of pH 7.4 phosphate buffer containing 0.5% hydroxypropylcyclodextrin to the donor side (250 μ L) and receiver side (100 μ L) and the plate shaken for 45 min. A 10 mM solution of test compound in DMSO (2.5 μ L) was added to the donor side and the plate incubated at r.t. for 3 h. The sample concentration in both the donor and acceptor compartments was determined by HPLC and rate of permeation calculated. Values >200 nm/sec were considered high, values in the range 50–200 nm/sec were considered moderate and values <50 nm/sec were considered low.

5.11. qPCR Bromodomain Binding Assay Panel

Assay Principle

Bromodomain selectivity profiling was conducted using BROMOscan technology by DiscoverX Corp. BROMOscan uses the same assay technology as KINOMEScan a detailed description of which has been previously reported.¹⁵⁴ Here, binding of compound to a particular bromodomain displaced an immobilised ligand and reduced the amount of DNA-tagged bromodomain captured on the solid support. When compared to a solvent control, the precise quantity of bromodomain captured was determined using ultra-sensitive quantitative polymerase chain reaction (qPCR), which detected the DNA tag on the bromodomain. Dissociation constants for 34 different bromodomain constructs were calculated after measuring the quantity of captured bromodomain at different compound concentrations.

Assay Procedure

T7 phage strains displaying bromodomains were grown in parallel in 24-well blocks in an *E. coli* host derived from the BL21 strain. *E. coli* were grown to log-phase and infected

with T7 phage from a frozen stock (multiplicity of infection = 0.4) and incubated with shaking at 32 °C until lysis (90–150 min). The lysates were centrifuged (5,000 x g) and filtered (0.2 µm) to remove cell debris. Streptavidin-coated magnetic beads were treated with biotinylated small molecule or acetylated peptide ligands for 30 min at r.t. to generate affinity resins for bromodomain assays. The liganded beads were blocked with excess biotin and washed with blocking buffer (SeaBlock (Pierce), 1% BSA, 0.05% Tween 20, 1 mM DTT) to remove unbound ligand and to reduce non-specific phage binding. Binding reactions were assembled by combining bromodomains, liganded affinity beads, and test compounds in 1 x binding buffer (17% SeaBlock, 0.33x PBS, 0.04% Tween 20, 0.02% BSA, 0.004% Sodium azide, 7.4 mM DTT). Test compounds were prepared as 1000X stocks in 100% DMSO and subsequently diluted 1:10 in monoethylene glycol (MEG) to create stocks at 100X the screening concentration (resulting stock solution is 10% DMSO/90% MEG). The compounds were then diluted directly into the assays such that the final concentration of DMSO and MEG were 0.1% and 0.9%, respectively. All reactions were performed in polystyrene 96-well plates in a final volume of 0.135 mL. The assay plates were incubated at room temperature with shaking for 1 h and the affinity beads were washed with wash buffer (1x PBS, 0.05% Tween 20). The beads were then re-suspended in elution buffer (1x PBS, 0.05% Tween 20, 2 µM nonbiotinylated affinity ligand) and incubated at room temperature with shaking for 30 min. The bromodomain concentration in the eluates was measured by qPCR.

An 11-point 3-fold serial dilution of each test compound was prepared in 100% DMSO at 1000x final test concentration. This serial is then diluted to 100x in ethylene glycol and subsequently diluted to 1x in the assay (final DMSO concentration = 0.1%, Ethylene glycol concentration = 0.9%). Most Kds were determined using a compound top concentration = 10,000 nM. If the initial Kd determined was <0.169 nM (the lowest concentration tested), the measurement was repeated with a serial dilution starting at a lower top concentration. A Kd value reported as 40,000 nM indicates that the Kd was determined to be >10,000 nM.

Binding constants (Kds) were calculated with a standard dose-response curve using the Hill equation:

$$Response = Background + \frac{Signal - Background}{1 + (Kd^{Hill\ Slope} / Dose^{Hill\ Slope})}$$

The Hill Slope was set to -1. Curves were fitted using a non-linear least square fit with the Levenberg-Marquardt algorithm.

5.12. Inhibition of IL-6 Production in LPS-Stimulated Human PBMCs

Assay Principle

PBMCs are blood cells important in the immune system and assays using PBMCs were conducted in the second research programme contained within this thesis. Stimulation of human PBMCs with LPS elicited an immune response through the release of pro-inflammatory cytokines and upon treatment with compound at different concentrations, MSD plates coated with a labelled antibody were used to capture IL-6 and MCP-1. Electrochemiluminescence detection determined cytokine levels and IC₅₀ values were determined.

Assay Procedure (IL-6)

Blood containing 15% v/v ACD-A anticoagulant (Baxter Healthcare) was collected and 30 mL poured into 50 mL Leucosep tubes (Greiner Bio-one) pre-filled with Ficoll. The tubes were centrifuged for 15 min at 800 x g at r.t. The enriched cell fractions from each Leucosep tube were pooled in a 500 mL centrifuge tube. The pooled fractions were centrifuged at room temperature for 10 min at 400 x g, and the supernatant discarded. The cell pellet was resuspended in 40 mL PBS and the cells counted on a haematology analyser (Sysmex). The cells were centrifuged at 300 x g for 10 min at r.t., the supernatant discarded, and the cell pellet resuspended in freezing medium (90% heat-inactivated FBS, 10% DMSO) to make a final concentration of 4 x 10⁷ cells/mL. The cells were aliquoted and cryopreserved. Compound plates containing 0.5 µL test sample in 1% DMSO were prepared (two replicates on account of PBMC donor variability). PBMCs were thawed from frozen stocks and resuspended in warm media (500 mL DMEM, 50 mL Heat Inactivated Australian Foetal Bovine Serum, 5 mL Penicillin/Streptomycin, 5 mL Glutamax) at a concentration of 2 x 10⁵ cells/mL. 1 ng/mL LPS was added then 50 µL added to each well of the compound plates. The seeded plates were then lidded and placed in the humidified primary cell incubator for 18–24 hours at 37 °C, 5% CO₂.

10 µL of cell supernatant was placed in a low-profile 384-well MSD plate pre-coated with human IL-6 capture antibody. The plates were sealed and placed on a shaker at 600 rpm for 2 h at r.t. A 1% solution of MSD Blocker A (MesoScale Discovery, USA) was prepared by dissolving solid Blocker A in Phosphate buffered saline (Invitrogen, UK). This was used to dilute the anti-human IL-6 antibody labelled with MSD SULFO-TAGTM reagent to 1 µg/mL. 10 µL of the antibody solution was then added to each well of the MSD plates. The plates were then re-sealed and shaken for another 2 h before washing 3 times with PBS. 35

µL of 2X MSD Read Buffer T (stock 4X MSD Read Buffer T was diluted 50:50 with de-ionised water) was then added to each well and the plates read on the MSD Sector Imager 6000.

Assay Procedure (MCP-1)

Blood containing 15% v/v ACD-A anticoagulant (Baxter Healthcare) was collected and 30 mL poured into 50 mL Leucosep tubes (Greiner Bio-one) pre-filled with Ficoll. The tubes were centrifuged for 15 min at 800 x g (r.t.). The enriched cell fractions from each Leucosep tube were pooled in a 500 mL centrifuge tube. The pooled fractions were centrifuged at room temperature for 10 min at 400 x g, and the supernatant discarded. The cell pellet was resuspended in 40 mL PBS and the cells counted on a Nucleocounter (Chemometec). The cells were centrifuged at 300 x g for 10 min at r.t., the supernatant discarded, and the cell pellet resuspended in freezing medium (90% heat-inactivated FBS, 10% DMSO) to make a final concentration of 4×10^7 cells/mL. The cells were aliquoted and cryopreserved using a controlled-rate freezer (Planer). Compound plates containing 0.5 µL test sample in 100% DMSO were prepared (two replicates on account of PBMC donor variability). PBMCs were thawed from frozen stocks and resuspended in warm media (500 mL RPMI, 50 mL Heat Inactivated Australian Foetal Bovine Serum, 5 mL Penicillin/Streptomycin, 5 mL Glutamax) at a concentration of 0.32×10^6 cells/mL. 10 µL of lipopolysaccharide (1ng/mL final assay concentration) was added to each well of the compound plates. The seeded plates were then lidded and placed in the humidified primary cell incubator for 18–24 h at 37 °C, 5% CO₂.

20 µL of cell supernatant was placed in a 96-well MSD plate pre-coated with human MCP-1 capture antibody. The plates were sealed and placed on a shaker at 600 rpm for 2 h at r.t. 20 µL of Anti-human MCP-1 antibody labelled with MSD SULFO-TAGTM reagent is added to each well of the MSD plate (stock 50X was diluted 1:50 with Diluent 100, final assay concentration is 1 µg/mL). The plates were then re-sealed and shaken for 1 h before washing with PBS. 150 µL of 2X MSD Read Buffer T (stock 4X MSD Read Buffer T was diluted 50:50 with de-ionised water) was then added to each well and the plates read on the MSD Sector Imager 6000.

5.13. MV-4-11 Growth Inhibition Assay

Assay Principle

MV-4-11 cells are an AML cell line and the ability of compounds to suppress their growth as a model for leukemia treatment was assessed in Section 3 of this thesis. After treatment of these cells with compound, the the number of viable cells were determined by addition of a reagent (Cell Titre Glo solution) which induces cell lysis and generates a luminescent signal that is proportional to the amount of ATP present – a marker for the presence of metabolically active cells.

Assay Procedure

MV-4-11 cells were maintained in IMDM media (Invitrogen) supplemented with 10% (v/v) FCS (Hyclone) and 5 mM glutamine (Invitrogen). Cells were plated in a volume of 90 μ L (10,000 cells per well) into 96-well plates (Greiner Microclear) in growth media containing penicillin/streptomycin solution (Invitrogen) and cultured overnight at 37 °C, 5% CO₂. Prior to addition of compounds, one plate of each cell type was removed from the incubator and equilibrated at r.t. for 1 h before assaying for ATP content by the addition of an equal volume of Cell Titre Glo solution (Promega). Luminescence was then measured using a Perkin Elmer Envision 2104 Multilabel reader in order to determine the zero time-point value.

10 μ L of 10x final assay concentrations of test compounds were added to the cell plates. A range of final compound concentrations (1.52 nM – 30 μ M) containing 0.5% DMSO in an assay medium were used. Plates were cultured for a further 72 h at 37 °C, 5% CO₂, and ATP levels were assayed, as described above. Cell titre glo data at 72 h were expressed as the percentage of the zero time point value, and then further normalized using GraphPadPrism (v5). IC₅₀ values were generated by nonlinear regression of the normalized t=0 data from three independent experiments using GraphPadPrism (v5).

6. References

- ¹ Wain, H. M.; Bruford, E. A.; Lovering, R. C.; Lush, M. J.; Wright, M. W.; Povey, S. *Genomics* **2002**, *79*, 464–470.
- ² Arrowsmith, C. H.; Bountra, C.; Fish, P. V.; Lee, K.; Schapira, M. *Nat. Rev. Drug Discovery* **2012**, *11*, 384–400.
- ³ Kouzarides, T. *Cell* **2007**, *128*, 693–705.
- ⁴ *Introduction to Genetic Analysis*, Griffiths, A. J. F.; Wessler, S. R.; Lewontin, R. C.; Carroll, S. B.; 9th edition; W.H. Freeman and Company: New York, **2008**.
- ⁵ Marmorstein, R.; Trievel, R. C. *Biochim. Biophys. Acta* **2009**, *1789*, 58–68.
- ⁶ Fuchs, S. M.; Larabee, R. N.; Strahl, B. D. *Biochim. Biophys. Acta* **2009**, *1789*, 26–36.
- ⁷ Taverna, S. D.; Li, H.; Ruthenburg, A. J.; Allis, C. D.; Patel, D. J. *Nature Struct. Mol. Biol.* **2007**, *14*, 1025–1040.
- ⁸ Haynes, S. R.; Dollard, C.; Winston, F.; Beck, S.; Trowsdale, J.; Dawid, I. B. *Nucleic Acids Res.* **1992**, *20*, 2603.
- ⁹ Choudhary, C.; Kumar, C.; Gnad, F.; Nielsen, M. L.; Rehman, M.; Walther, T. C.; Olsen, J. V.; Mann, M. *Science* **2009**, *325*, 834–840.
- ¹⁰ Filippakopoulos, P.; Picaud, S.; Mangos, M.; Keates, T.; Lambert, J.-P.; Barsyte-Lovejoy, D.; Felletar, I.; Volkmer, R.; Müller, S.; Pawson, T.; Gingras, A.-C.; Arrowsmith, C. H.; Knapp, S. *Cell* **2012**, *149*, 214–231.
- ¹¹ Bamborough, P. (GlaxoSmithKline) *Personal communication*.
- ¹² Dhalluin, C.; Carlson, J. E.; Zeng, L.; He, C.; Aggarwal, A. K.; Zhou, M. M. *Nature* **1999**, *399*, 491–496.
- ¹³ Owen, D. J.; Ornaghi, P.; Yang, J.-C.; Lowe, N.; Evans, P. R.; Ballario, P.; Neuhaus, D.; Filetici, P.; Travers, A. A. *EMBO J.* **2000**, *19*, 6141–6149.
- ¹⁴ See Appendix for chemical structure.
- ¹⁵ Zeng, L.; Zhou, M. M. *FEBS Lett.* **2002**, *513*, 124–128.
- ¹⁶ Yap, K. L.; Zhou, M. M. *Crit. Rev. Biochem. Mol. Biol.* **2010**, *45*, 488–505.
- ¹⁷ Vollmuth, F.; Geyer, M. *Angew. Chem. Int. Ed. Engl.* **2010**, *49*, 6768–6772.
- ¹⁸ Vidler, L. R.; Brown, N.; Knapp, S.; Hoelder, S. *J. Med. Chem.* **2012**, *55*, 7346–7359.
- ¹⁹ Peterlin, B. M.; Price, D. H. *Mol. Cell* **2006**, *23*, 297–305.
- ²⁰ Dey, A.; Nishiyama, A.; Karpova, T.; McNally, J.; Ozato, K. *Mol. Biol. Cell* **2009**, *20*, 4899–4909.
- ²¹ Yang, Z.; He, N.; Zhou, Q. *Mol. Cell. Biol.* **2008**, *28*, 967–976.

- ²² LeRoy, G.; Rickards, B.; Flint, S. J. *Mol. Cell.* **2008**, *30*, 51–60.
- ²³ French, C. A.; Miyoshi, I.; Kubonishi, I.; Grier, H. E.; Perez-Atayde, A. R.; Fletcher, J. A. *Cancer Res.* **2003**, *63*, 304–307.
- ²⁴ French, C. A.; Ramirez, C. L.; Kolmakova, J.; Hickman, T. T.; Cameron, M. J.; Thyne, M. E.; Kutok, J. L.; Toretsky, J. A.; Tadavarthy, A. K.; Kees, U. R.; Fletcher, J. A.; Aster, J. C. *Oncogene* **2008**, *27*, 2237–2242.
- ²⁵ Zuber, J.; Shi, J.; Wang, E.; Rappaport, A. R.; Herrmann, H.; Sison, E. A.; Magoon, D.; Qi, J.; Blatt, K.; Wunderlich, M.; Taylor, M. J.; Johns, C.; Chicas, A.; Mulloy, J. C.; Kogan, S. C.; Brown, P.; Valent, P.; Bradner, J. E.; Lowe, S. W.; Vakoc, C. R. *Nature* **2011**, *478*, 524–528.
- ²⁶ Crawford, N. P. S.; Alsarraj, J.; Lukes, L.; Walker, R. C.; Officewala, J. S.; Yang, H. H.; Lee, M. P.; Ozato, K.; Hunter, K. W. *Proc. Natl. Acad. Sci. U.S.A.* **2008**, *105*, 6380–6385.
- ²⁷ Greenwald, R. J.; Tumang, J. R.; Sinha, A.; Currier, N.; Cardiff, R. D.; Rothstein, T. L.; Faller, D. V.; Denis, G. V. *Blood* **2004**, *103*, 1475–1484.
- ²⁸ Mahdi, H.; Fisher, B. A.; Kallberg, H.; Plant, D.; Malmstrom, V.; Ronnelid, J.; Charles, P.; Ding, B.; Alfredsson, L.; Padyukov, L.; Symmons, D. P.; Venables, P. J.; Klareskog, L.; Lundberg, K. *Nat. Genet.* **2009**, *41*, 1319–1324.
- ²⁹ Hargreaves, D. C.; Horng, T.; Medzhitov, R. *Cell* **2009**, *138*, 129–145.
- ³⁰ Huang, B.; Yang, X. D.; Zhou, M. M.; Ozato, K.; Chen, L. F. *Mol. Cell. Biol.* **2009**, *29*, 1375–1387.
- ³¹ McBride, A. A.; McPhillips, M. G.; Oliveira, J. G. *Trends Microbiol.* **2004**, *12*, 527–529.
- ³² Wu, S. Y.; Chiang, C. M. *J. Biol. Chem.* **2007**, *282*, 13141–13145.
- ³³ Weidner-Glunde, M.; Ottinger, M.; Schulz, T. F. *Front. Biosci.* **2010**, *15*, 537–549.
- ³⁴ Nakamura, Y.; Umehara, T.; Nakano, K.; Jang, M. K.; Shirouzu, M.; Morita, S.; Uda-Tochio, H.; Hamana, H.; Terada, T.; Adachi, N.; Matsumoto, T.; Tanaka, A.; Horikoshi, M.; Ozato, K.; Padmanabhan, B.; Yokoyama, S. *J. Biol. Chem.* **2007**, *282*, 4193–4201.
- ³⁵ Padmanabhan, B.; Yokoyama, S. *The Protein Data Bank*. (<http://www.rcsb.org/pdb/>) accession code 2DVV, accessed Jan 2014.
- ³⁶ Muller, S.; Filippakopoulos, P.; Knapp, S. *Expert Rev. Mol. Med.* **2011**, *13*, e29.
- ³⁷ Chung, C.-w. *Prog. Med. Chem.* **2012**, *51*, 1–55.
- ³⁸ Hewings, D. S.; Rooney, T. P. C.; Jennings, L. E.; Hay, D. A.; Schofield, C. J.; Brennan, P. E.; Knapp, S.; Conway, S. J. *J. Med. Chem.* **2012**, *55*, 9393–9413.
- ³⁹ Conway, S. J. *ACS Med. Chem. Lett.* **2012**, *3*, 691–694.
- ⁴⁰ Furdas, S. D.; Carlino, L.; Sippl, W.; Jung, M. *Med. Chem. Commun.* **2012**, *3*, 123–134.

- ⁴¹ Brennan, P.; Filippakopoulos, P.; Knapp, S. *Drug Discovery Today: Ther. Strategies*. **2012**, *9*, e101–e110.
- ⁴² Chung, C.-w.; Tough, D. F. *Drug Discovery Today: Ther. Strategies*, **2012**, *9*, e111–e120.
- ⁴³ Prinjha, R. K.; Witherington, J.; Lee, K. *Trends Pharmacol. Sci.* **2012**, *33*, 146–153.
- ⁴⁴ Chung, C.-w.; Coste, H.; White, J. H.; Mirguet, O.; Wilde, J.; Gosmini, R. L.; Delves, C.; Magny, S. M.; Woodward, R.; Hughes, S. A.; Boursier, E. V.; Flynn, H.; Bouillot, A. M.; Bamborough, P.; Brusq, J.-M. G.; Gellibert, F. J.; Jones, E. J.; Riou, A. M.; Homes, P.; Martin, S. L.; Uings, I. J.; Toum, J.; Clément, C. A.; Boullay, A.-B.; Grimley, R. L.; Blandel, F. M.; Prinjha, R. K.; Lee, K.; Kirilovsky, J.; Nicodème, E. *J. Med. Chem.* **2011**, *54*, 3827–3838.
- ⁴⁵ Mirguet, O.; Gosmini, R.; Toum, J.; Clément, C. A.; Barnathan, M.; Brusq, J.-M.; Mordaunt, J. E.; Grimes, R. M.; Crowe, M.; Pineau, O.; Ajakane, M.; Daugan, A.; Jeffrey, P.; Cutler, L.; Haynes, A. C.; Smithers, N. N.; Chung, C.-w.; Bamborough, P.; Uings, I. J.; Lewis, A.; Witherington, J.; Parr, N.; Prinjha, R. K.; Nicodème, E. *J. Med. Chem.* **2013**, *56*, 7501–7515.
- ⁴⁶ Umehara, T.; Nakamura, Y.; Jang, M. K.; Nakano, K.; Tanaka, A.; Ozato, K.; Padmanabhan, B.; Yokoyama, S. *J. Biol. Chem.* **2010**, *285*, 7610–7618.
- ⁴⁷ Nicodème, E.; Jeffrey, K. L.; Schaefer, U.; Beinke, S.; Dewell, S.; Chung, C.-w.; Chandwani, R.; Marazzi, I.; Wilson, P.; Coste, H.; White, J.; Kirilovsky, J.; Rice, C. M.; Lora, J. M.; Prinjha, R. K.; Lee, K.; Tarakhovsky, A. *Nature* **2010**, *468*, 1119–1123.
- ⁴⁸ GlaxoSmithKline. Protocol Summary for 115521. http://www.gsk-clinicalstudyregister.com/protocol_detail.jsp?protocolId=115521&studyId=8CA80D1C-BFAC-4309-9EA7-9F65BC8197A2&compound=115521&type=GSK+Study+ID&letterange=All accessed Jan 2014.
- ⁴⁹ Filippakopoulos, P.; Qi, J.; Picaud, S.; Shen, Y.; Smith, W. B.; Fedorov, O.; Morse, E. M.; Keates, T.; Hickman, T. T.; Felletar, I.; Philpott, M.; Munro, S.; McKeown, M. R.; Wang, Y.; Christie, A. L.; West, N.; Cameron, M. J.; Schwartz, B.; Heightman, T. D.; La Thangue, N.; French, C. A.; Wiest, O.; Kung, A. L.; Knapp, S.; Bradner, J. E. *Nature* **2010**, *468*, 1067–1073.
- ⁵⁰ Miyoshi, S.; Ooike, S.; Iwata, K.; Hikawa, H.; Sugahara, K. PCT/JP2008/073864 (WO/2009/084693), 2009.
- ⁵¹ Delmore, J. E.; Issa, G. C.; Lemieux, M. E.; Rahl, P. B.; Shi, J.; Jacobs, H. M.; Kastritis, E.; Gilpatrick, T.; Paranal, R. M.; Qi, J.; Chesi, M.; Schinzel, A. C.; McKeown, M. R.;

- Heffernan, T. P.; Vakoc, C. R.; Bergsagel, P. L.; Ghobrial, I. M.; Richardson, P. G.; Young, R. A.; Hahn, W. C.; Anderson, K. C.; Kung, A. L.; Bradner, J. E.; Mitsiades, C. S. *Cell* **2011**, *146*, 904–917.
- ⁵² Mertz, J. A.; Conery, A. R.; Bryant, B. M.; Sandy, P.; Balasubramanian, S.; Mele, D. A.; Bergeron, L.; Sims, R. J. *Proc. Natl. Acad. Sci. USA* **2011**, *108*, 16669–16674.
- ⁵³ Ott, C. J.; Kopp, N.; Bird, L.; Paranal, R. M.; Qi, J.; Bowman, T.; Rodig, S. J.; Kung, A. L.; Bradner, J. E.; Weinstock, D. M. *Blood* **2012**, *120*, 2843–2852.
- ⁵⁴ Zou, Z.; Huang, B.; Wu, X.; Zhang, H.; Qi, J.; Bradner, J. E.; Nair, S.; Chen, L.-F. *Oncogene* **2014**, *33*, 2395–2404.
- ⁵⁵ Zhang, G.; Liu, R.; Zhong, Y.; Plotnikov, A. N.; Zhang, W.; Zeng, L.; Rusinova, E.; Gerona-Nevarro, G.; Moshkina, N.; Joshua, J.; Chuang, P. Y.; Ohlmeyer, M.; He, J. C.; Zhou, M.-M. *J. Biol. Chem.* **2012**, *287*, 28840–28851. Note that a methyl ester analogue of (+)-JQ1, and not (+)-JQ1 itself, was used in this study.
- ⁵⁶ Zhu, J.; Gaiha, G. D.; John, S. P.; Pertel, T.; Chin, C. R.; Gao, G.; Qu, H.; Walker, B. D.; Elledge, S. J.; Brass, A. L. *Cell Rep.* **2012**, *2*, 807–816.
- ⁵⁷ Banerjee, C.; Archin, N.; Michaels, D.; Belkina, A. C.; Denis, G. V.; Bradner, J. E.; Sebastiani, P.; Margolis, D. M.; Montano, M. *J. Leukoc. Biol.* **2012**, *92*, 1147–1154.
- ⁵⁸ Belkina, A. C.; Nikolajczyk, B. S.; Denis, G. V. *J. Immunol.* **2013**, *190*, 3670–3678.
- ⁵⁹ Tang, X.; Peng, R.; Phillips, J. E.; Deguzman, J.; Ren, Y.; Apparsundaram, S.; Luo, R.; Bauer, C. M. T.; Fuentes, M. E.; DeMartino, J. A.; Tyagi, G.; Garrido, R.; Hogaboam, C. M.; Denton, C. P.; Holmes, A. M.; Kitson, C.; Stevenson, C. S.; Budd, D. C. *Am. J. Pathol.* **2013**, *183*, 470–479.
- ⁶⁰ Matzuk, M. M.; McKeown, M. R.; Filippakopoulos, P.; Li, Q.; Ma, L.; Agno, J. E.; Lemieux, M. E.; Picaud, S.; Yu, R. N.; Qi, J.; Knapp, S.; Bradner, J. E. *Cell* **2012**, *150*, 673–684.
- ⁶¹ Filippakopoulos, P.; Picaud, S.; Fedorov, O.; Keller, M.; Wrobel, M.; Morgenstern, O.; Bracher, F.; Knapp, S. *Bioorg. Med. Chem.* **2012**, *20*, 1878–1886.
- ⁶² Gehling, V. S.; Hewitt, M. C.; Vaswani, R. G.; Leblanc, Y.; Côté, A.; Nasveschuk, C. G.; Taylor, A. M.; Harmange, J.-C.; Audia, J. E.; Pardo, E.; Joshi, S.; Sandy, P.; Mertz, J. A.; Sims III, R. J.; Bergeron, L.; Bryant, B. M.; Bellon, S.; Poy, F.; Jayaram, H.; Sankaranarayanan, R.; Yellapantula, S.; Srinivasamurthy, N. B.; Birudukota, S.; Albrecht, B. K. *ACS Med. Chem. Lett.* **2013**, *4*, 835–840.
- ⁶³ Mirguet, O.; Lamotte, Y.; Donche, F.; Toum, J.; Gellibert, F.; Bouillot, A.; Gosmini, R.; Nguyen, V. L.; Delannée, D.; Seal, J.; Blandel, F.; Boullay, A. B.; Boursier, E.; Martin, S.;

Brusq, J. M.; Krysa, G.; Riou, A.; Tellier, R.; Costaz, A.; Huet, P.; Dudit, Y.; Trottet, L.; Nicodème, E. *Bioorg. Med. Chem. Lett.* **2012**, *22*, 2963–2967.

⁶⁴ Seal, J.; Lamotte, Y.; Donche, F.; Bouillot, A.; Mirguet, O.; Gellibert, F.; Nicodème, E.; Krysa, G.; Kirilovsky, J.; Beinke, S.; McCleary, S.; Rioja, I.; Bamborough, P.; Chung, C.-w.; Gordon, L.; Lewis, T.; Walker, A. L.; Cutler, L.; Lugo, D.; Wilson, D. M.; Witherington, J.; Lee, K.; Prinjha, R. K. *Bioorg. Med. Chem. Lett.* **2012**, *22*, 2968–2972.

⁶⁵ Note that the numbering of the amino acid sequence in the pdb file 4ALG was inconsistent with other BRD2 BD1 structures deposited in the protein data bank (accessible from <http://www.rcsb.org/pdb>). Corrected numbering (46 higher) was used in the text and figures when referring to pdb 4ALG.

⁶⁶ Dawson, M. A.; Prinjha R. K.; Dittman, A.; Giotopoulos, G.; Bantscheff, M.; Chan, W. I.; Robson, S. C.; Chung, C.-w.; Hopf, C.; Savitski, M. M.; Huthmacher, C.; Gudgin, E.; Lugo, D.; Beinke, S.; Chapman, T. D.; Roberts, E. J.; Soden, P. E.; Auger, K. R.; Mirguet, O.; Doehner, K.; Delwel, R.; Burnett, A. K.; Jeffrey, P.; Drewes, G.; Lee, K.; Huntly, B. J. P.; Kouzarides, T. *Nature* **2011**, *478*, 529–533.

⁶⁷ Mirguet, O.; Lamotte, Y.; Chung, C.-w.; Bamborough, P.; Delannée, D.; Bouillot, A.; Gellibert, F.; Krysa, G.; Lewis, T.; Witherington, J.; Huet, P.; Dudit, Y.; Trottet, L.; Nicodème, E. *ChemMedChem* **2014**, *9*, 580–589.

⁶⁸ Hewings, D. S.; Wang, M.; Philpott, M.; Fedorov, O.; Uttakar, S.; Filippakopoulos, P.; Picaud, S.; Vuppasetty, C.; Marsden, B.; Knapp, S.; Conway, S. J.; Heightman, T. D. *J. Med. Chem.* **2011**, *54*, 6761–6770.

⁶⁹ Hewings, D. S.; Fedorov, O.; Filippakopoulos, P.; Martin, S.; Picaud, S.; Tumber, A.; Wells, C.; Olcina, M. M.; Freeman, C.; Gill, A.; Ritchie, A. J.; Sheppard, D. W.; Russell, A. J.; Hammond, E. M.; Knapp, S.; Brennan, P. E.; Conway, S. J. *J. Med. Chem.* **2013**, *56*, 3217–3227.

⁷⁰ Hay, D.; Fedorov, O.; Filippakopoulos, P.; Martin, S.; Philpott, M.; Picaud, S.; Hewings, D. S.; Uttakar, S.; Heightman, T. D.; Conway, S. J.; Knapp, S.; Brennan, P. E. *Med. Chem. Commun.* **2013**, *4*, 140–144.

⁷¹ Calculated using the equation: LE = pIC₅₀ x 1.4 (kcal/mol) ÷ heavy atom count.

⁷² Bamborough, P.; Diallo, H.; Goodacre, J. D.; Gordon, L.; Lewis, A.; Seal, J. T.; Wilson, D. M.; Woodrow, M. D.; Chung, C.-w. *J. Med. Chem.* **2012**, *55*, 587–596.

⁷³ Moriniere, J.; Rousseaux, S.; Steuerwald, U.; Soler-Lopez, M.; Curtet, S.; Vitte, A. L.; Govin, J.; Gaucher, J.; Sadoul, K.; Hart, D. J.; Krijgsveld, J.; Khochbin, S.; Muller, C. W.; Petosa, C. *Nature* **2009**, *461*, 664–668.

- ⁷⁴ Chung, C.-w.; Dean, A. W.; Woolven, J. M.; Bamborough, P. *J. Med. Chem.* **2012**, *55*, 576–586.
- ⁷⁵ Fish, P. V.; Filippakopoulos, P.; Bish, G.; Brennan, P. E.; Bunnage, M. E.; Cook, A. S.; Federov, O.; Gerstenberger, B. S.; Jones, H.; Knapp, S.; Marsden, B. B.; Nocka, K. K.; Owen, D. R.; Philpott, M. M.; Picaud, S.; Primiano, M. J.; Ralph, M. J.; Sciammetta, N. N.; Trzupsek, J. D. *J. Med. Chem.* **2012**, *55*, 9831–9837.
- ⁷⁶ Zhao, L.; Cao, D.; Chen, T.; Wang, Y.; Miao, Z.; Xu, Y.; Chen, W.; Wang, X.; Li, Y.; Du, Z.; Xiong, B.; Li, J.; Xu, C.; Zhang, N.; He, J.; Shen, K. *J. Med. Chem.* **2013**, *56*, 3833–3851.
- ⁷⁷ Ito, T.; Umehara, T.; Sasaki, K.; Nakamura, Y.; Nishino, N.; Terada, T.; Shirouzu, M.; Padmanabhan, B.; Yokoyama, S.; Ito, A.; Yoshida, M. *Chem. Biol.* **2011**, *18*, 495–507.
- ⁷⁸ Vidler, L. R.; Filippakopoulos, P.; Fedorov, O.; Picaud, S.; Martin, S.; Tomsett, M.; Woodward, H.; Brown, N.; Knapp, S.; Hoelder, S. *J. Med. Chem.* **2013**, *56*, 8073–8088.
- ⁷⁹ Demont, E. H.; Garton, N. S.; Gosmini, R. L.; Hayhow, T. G.; Seal, J.; Wilson, D. M.; Woodrow, M. D. PCT/EP2010/066693 (WO/2011/054841), 2011.
- ⁸⁰ Demont, E. H.; Gosmini, R. L. PCT/EP2010/066701 (WO/2011/054848), 2011.
- ⁸¹ Wyce, A.; Ganji, G.; Smitheman, K. N.; Chung, C.-w.; Korenchuk, S.; Bai, Y.; Barbash, O.; Le, B.; Craggs, P. D.; McCabe, M. T.; Kennedy-Wilson, K. M.; Sanchez, L. V.; Gosmini, R. L.; Parr, N.; McHugh, C. F.; Dhanak, D.; Prinjha, R. K.; Auger, K. R.; Tummino, P. J. *PLoS One* **2013**, *8*, e72967.
- ⁸² Wang, L.; Pratt, J. K.; McDaniel, K. F. PCT/CN2011/002224 (WO/2013/097052), 2013.
- ⁸³ Wang, L.; Pratt, J. K.; McDaniel, K. F.; Dai, Y.; Fidanze, S. D.; Hasvold, L.; Holms, J. H.; Kati, W. M.; Liu, D.; Mantei, R. A.; McClellan, W. J.; Sheppard, G. S.; Wada, C. K. PCT/CN2012/086357 (WO/2013/097601), 2013.
- ⁸⁴ <http://www.resverlogix.com/blog/2013/02/26/the-exciting-new-frontier-of-epigenetics> accessed Jan 2014.
- ⁸⁵ Bailey, D.; Jahagirdar, R.; Gordon, A.; Hafiane, A.; Campbell, S.; Chatur, S.; Wagner, G. S.; Hansen, H. C.; Chiacchia, F. S.; Johansson, J.; Krimbou, L.; Wong, N. C. W.; Genest, J. *J. Am. Coll. Cardiol.* **2010**, *55*, 2580–2589.
- ⁸⁶ Picaud, S.; Wells, C.; Felletar, I.; Brotherton, D.; Martin, S.; Savitsky, P.; Diez-Dacal, B.; Philpott, M.; Bountra, C.; Lingard, H.; Fedorov, O.; Müller, S.; Brennan, P. E.; Knapp, S.; Filippakopoulos, P. *Proc. Natl. Acad. Sci. USA* **2013**, *110*, 19754–19759.
- ⁸⁷ Marshall, J. C.; Reinhart, K. *Surg. Infect.* **2011**, *12*, 1–2.
- ⁸⁸ Riedemann, N. C.; Guo R.-F.; Ward, P. A. *Nature Medicine* **2003**, *9*, 517–524.

- ⁸⁹ Chung, C.-w. (GlaxoSmithKline) *Unpublished results*.
- ⁹⁰ Delannee, D. (GlaxoSmithKline) *Unpublished results*.
- ⁹¹ Lamotte, Y. (GlaxoSmithKline) *Unpublished results*.
- ⁹² Jones, K. (GlaxoSmithKline) *Unpublished results*.
- ⁹³ The commercially available algorithm from www.acdlabs.com was used for aqueous solubility predictions at pH 4.5 (ACD/Labs version 12).
- ⁹⁴ Watson, R. (GlaxoSmithKline) *Unpublished results*.
- ⁹⁵ Diallo, H. (GlaxoSmithKline) *Unpublished results*.
- ⁹⁶ Gleeson, M. P. *J. Med. Chem.* **2008**, *51*, 817–834.
- ⁹⁷ The commercially available algorithm from www.acdlabs.com was used for aqueous solubility predictions at pH 4.5 (ACD/Labs version 11).
- ⁹⁸ Ellis, M. J.; Stevens, M. F. G. *J. Chem. Soc., Perkin Trans. 1* **2001**, 3180–3185.
- ⁹⁹ Boschelli, D. H.; Wang, Y. D.; Ye, F.; Wu, B.; Zhang, N.; Dutia, M.; Powell, D. W.; Wissner, A.; Arndt, K.; Weber, J. M.; Boschelli, F. *J. Med. Chem.* **2001**, *44*, 822–833.
- ¹⁰⁰ Lee, Y.; Parks, D. J.; Lu, T.; Thieu, T. V.; Markotan, T.; Pan, W.; McComsey, D. F.; Milkiewicz, K. L.; Crysler, S. S.; Ninan, N.; Abad, M. C.; Giardino, E. C.; Maryanoff, B. E.; Damiano, B. P.; Player, M. R. *Bioorg. Med. Chem. Lett.* **2008**, *51*, 282–297.
- ¹⁰¹ Toum, J. (GlaxoSmithKline) *Unpublished results*.
- ¹⁰² Donche, F. (GlaxoSmithKline) *Unpublished results*.
- ¹⁰³ Lovering, F.; Bikker, J.; Humblet, C. *J. Med. Chem.* **2009**, *52*, 6752–6756.
- ¹⁰⁴ Willems, H. (GlaxoSmithKline) *Unpublished results*.
- ¹⁰⁵ Satoh, T.; Inoh, J.-i.; Kawamura, Y.; Kawamura, Y.; Miura, M.; Nomura, M. *Bull. Chem. Soc. Jpn.* **1998**, *71*, 2239–2246.
- ¹⁰⁶ Culkin, D. A.; Hartwig, J. F. *Acc. Chem. Res.* **2003**, *36*, 234–245.
- ¹⁰⁷ Culkin, D. A.; Hartwig, J. F. *Organometallics* **2004**, *23*, 3398–3416.
- ¹⁰⁸ Pearson, D. E.; Buehler, C. A. *Chem. Rev.* **1974**, *74*, 45–86.
- ¹⁰⁹ Nishimura, T.; Onoue, T.; Ohe, K.; Uemura, S. *J. Org. Chem.* **1999**, *64*, 6750–6755.
- ¹¹⁰ Selikson, S. J.; Watt, D. S. *J. Org. Chem.* **1975**, *40*, 267–268.
- ¹¹¹ Vaz, R. J.; Li, Y.; Rampe, D. *Prog. Med. Chem.* **2005**, *43*, 1–18 and references therein.
- ¹¹² Waring, M. J.; Johnstone, C. *Bioorg. Med. Chem. Lett.* **2007**, *17*, 1759–1764.
- ¹¹³ Young, R. J.; Green, D. V. S.; Luscombe, C. N.; Hill, A. P. *Drug Discov. Today* **2011**, *16*, 822–830.
- ¹¹⁴ Walker, A. (GlaxoSmithKline) *Unpublished results*.

- ¹¹⁵ Maruyama, T.; Farina, A.; Dey, A.; Cheong, J. H.; Bermudez, V. P.; Tamura, T.; Sciortino, S.; Shuman, J.; Hurwitz, J.; Ozato, K. *Mol. Cell. Biol.* **2002**, *31*, 6509–6520.
- ¹¹⁶ Alsarraj, J.; Walker, R. C.; Webster, J. D.; Geiger, T. R.; Crawford, N. P. S.; Simpson, M. R.; Ozato, K.; Hunter, K. *Cancer Res.* **2011**, *71*, 3121–3131.
- ¹¹⁷ Berkovits, B. D.; Wolgemuth, D. J. *Dev. Biol.* **2011**, *360*, 358–368.
- ¹¹⁸ Wilson, J. W.; Free, S. M. *J. Med. Chem.* **1964**, *7*, 395–399.
- ¹¹⁹ Weininger, D. *J. Chem. Inf. Comput. Sci.* **1988**, *28*, 31–36.
- ¹²⁰ Zondlo, N. J. *Acc. Chem. Res.*, **2013**, *46*, 1039–1049.
- ¹²¹ Using GRID software, MIFs for a water probe at its OPLS-AA forcefield optimised position was calculated. Woolven, J. (GlaxoSmithKline) *Unpublished results*.
- ¹²² Berthelot, M.; Laurence, C.; Safar, M.; Besseau, F. *J. Chem. Soc., Perkin Trans. 2* **1998**, 283–290.
- ¹²³ Laurence, C.; Brameld, K. A.; Graton, J.; Le Questel, J.-Y.; Renault, E. *J. Med. Chem.* **2009**, *52*, 4073–4086.
- ¹²⁴ Hammett, L. P. *J. Am. Chem. Soc.* **1937**, *59*, 96–103.
- ¹²⁵ Mitchell, D. J. (GlaxoSmithKline) *Unpublished results*.
- ¹²⁶ Angelici, G.; Contaldi, S.; Green, S. L.; Tomasini, C. *Org. Biomol. Chem.* **2008**, *6*, 1849–1852.
- ¹²⁷ Note that only a single diastereoisomer was observed by ¹H NMR. See Synthetic Procedures and Compound Characterisation for further details.
- ¹²⁸ Bohm, H. J.; Banner, D.; Bendels, S.; Kansy, M.; Kuhn, B.; Muller, K.; Obst-Sander, U.; Stahl, M. *ChemBioChem* **2004**, *5*, 637–643.
- ¹²⁹ CSD entry codes: VAYHEI, VAYJOU, FUSTES.
- ¹³⁰ Zafrani, Y.; Sod-Moriah, G.; Segali, Y. *Tetrahedron* **2009**, *65*, 5278–5283.
- ¹³¹ Klebe, G.; Böhm, H.-J. *J. Receptor Signal Transduction Res.* **1997**, *17*, 459–473.
- ¹³² Chiral HPLC purification was conducted after the alkylation stage to afford a single diastereoisomer as determined by ¹H NMR. See Synthetic Procedures and Compound Characterisation for further details.
- ¹³³ Note that a mixture of diastereoisomers was observed by ¹H NMR. See Synthetic Procedures and Compound Characterisation for further details.
- ¹³⁴ Bit, R. (GlaxoSmithKline) *Unpublished results*.
- ¹³⁵ Hit compound from GSK Compound Collection *Unpublished results*.
- ¹³⁶ Implemented using Tibco Spotfire v3.2 (<http://spotfire.tibco.com/en/discover-spotfire/who-uses-spotfire/by-industry/life-sciences-pe.aspx>).

- ¹³⁷ Campbell, I. B.; Erdmann, N.; Mills, G. (GlaxoSmithKline) *Unpublished results*.
- ¹³⁸ Hartung, W. H.; Simonoff, R. *Org. React.* **1953**, *VII*, 263–326.
- ¹³⁹ Gould, R. G.; Jacobs, W. A. *J. Am. Chem. Soc.* **1939**, *61*, 2890–2895.
- ¹⁴⁰ Casnati, G.; Quilico, A.; Ricca, A.; Finzi, P. V. *Tetrahedron. Lett.* **1966**, *7*, 233–238.
- ¹⁴¹ Wabuye, M. (GlaxoSmithKline) *Unpublished results*.
- ¹⁴² Lewis, T.; Karamshi, B. (GlaxoSmithKline) *Unpublished results*.
- ¹⁴³ Soden, P. E. (GlaxoSmithKline) *Unpublished results*.
- ¹⁴⁴ Konishi, P. H.; Ueda, T.; Muto, T.; Manabe, K. *Org. Lett.* **2012**, *14*, 4722–4725.
- ¹⁴⁵ Kim, H. S.; Barak, D.; Harden, T. K.; Boyer, J. L.; Jacobson, K. A. *J. Med. Chem.* **2001**, *44*, 3092–3108.
- ¹⁴⁶ Radchenko, D. S.; Pavlenko, S. O.; Grygorenko, O. O.; Volochnyuk, D. M.; Shishkina, S. V.; Shishkin, O. V.; Komarov, I. V. *J. Org. Chem.* **2010**, *75*, 5941–5952.
- ¹⁴⁷ Bartoli, G.; Bosco, M.; Dalpozzo, R.; Giuliani, A.; Marcantoni, E.; Mecozzi, T.; Sambri, L.; Torregiani, E. *J. Org. Chem.* **2002**, *67*, 9111–9114.
- ¹⁴⁸ Sternfeld, F.; Guiblin, A. R.; Jelley, R. A.; Matassa, V. G.; Reeve, A. J.; Hunt, P. A.; Beer, M. S.; Heald, A.; Stanton, J. A.; Sohal, B.; Watt, A. P.; Street, L. J. *J. Med. Chem.* **1999**, *42*, 677–690.
- ¹⁴⁹ Zampieri, D.; Mamolo, M. G.; Laurini, E.; Zanette, C.; Florio, C.; Collina, S.; Rossi, D.; Azzolina, O.; Vio, L. *Eur. J. Med. Chem.* **2009**, *44*, 124–130.
- ¹⁵⁰ Baraldi, P. G.; Romagnoli, R.; Del, C. N. M.; Perretti, M.; Paul, C. M. J.; Ferrario, M.; Govoni, M.; Benedini, F.; Ongini, F. *J. Med. Chem.* **2004**, *47*, 711–719.
- ¹⁵¹ Valkó, K.; Bevan, C.; Reynolds, D. *Anal. Chem.* **1997**, *69*, 2022–2029.
- ¹⁵² Barrett, N. (GlaxoSmithKline) *Unpublished results*.
- ¹⁵³ Craggs, P.; Bingham, R.; Gordon, L. (GlaxoSmithKline) *Unpublished results*.
- ¹⁵⁴ Fabian, M. A.; Biggs, W. H., III; Treiber, D. K.; Atteridge, C. E.; Azimioara, M. D.; Benedetti, M. G.; Carter, T. A.; Ciceri, P.; Edeen, P. T.; Floyd, M.; Ford, J. M.; Galvin, M.; Gerlach, J. L.; Grotzfeld, R. M.; Herrgard, S.; Insko, D. E.; Insko, M. A.; Lai, A. G.; Lélias, J. M.; Mehta, S. A.; Milanov, Z. V.; Velasco, A. M.; Wodicka, L. M.; Patel, H. K.; Zarrinkar, P. P.; Lockhart, D. J. *Nat. Biotechnol.* **2005**, *23*, 329–336.